CONTENTS

Page

INTENTIONALLY LEFT BLANK

TABLES

INTENTIONALLY LEFT BLANK

FIGURES

FIGURES (Continued)

FIGURES (Continued)

FIGURES (Continued)

FIGURES (Continued)

FIGURES (Continued)

FIGURES (Continued)

FIGURES (Continued)

Page

FIGURES (Continued)

FIGURES (Continued)

FIGURES (Continued)

FIGURES (Continued)

FIGURES (Continued)

FIGURES (Continued)

FIGURES (Continued)

Page

FIGURES (Continued)

2.4 DEMONSTRATION OF COMPLIANCE WITH THE POSTCLOSURE PUBLIC HEALTH AND ENVIRONMENTAL STANDARDS

The purpose of this section is to demonstrate compliance with postclosure public health and environmental standards specified in proposed 10 CFR 63.303 (70 FR 53313). Proposed 10 CFR 63.303 states as follows:

> (a) Compliance is based upon the arithmetic mean of the projected doses from DOE performance assessments for the period within 10,000 years after disposal for:
>
> (1) § 63.311(a)(1); and
>
> (2) §§ 63.321(b)(1) and 63.331, if performance assessment is used to demonstrate compliance with either or both of these sections.
>
> (b) Compliance is based upon the median of the projected doses from DOE's performance assessments for the period after 10,000 years of disposal and through the period of geologic stability for:
>
> (1) § 63.311(a)(2); and
>
> (2) § 63.321(b)(2), if performance assessment is used to demonstrate compliance.

As discussed in proposed 10 CFR 63.303, there are three quantitative public health requirements for demonstrating postclosure compliance and safety: (1) the individual protection standard after permanent closure in the absence of human intrusion, defined at proposed 10 CFR 63.311; (2) the individual protection standard for human intrusion, defined at proposed 10 CFR 63.321; and (3) the separate standards for protection of groundwater, defined at 10 CFR 63.331. The two individual protection standards apply to the 10,000 year and post-10,000-year time frames (the period of geologic stability up to 1 million years after permanent closure), whereas the groundwater protection standard only applies to the first 10,000 years after permanent closure of the repository. All three standards are addressed in this section in the preceding order.

Consistent with the limits on performance assessment at proposed 10 CFR 63.342, separate performance assessments have been prepared for each of the three quantitative standards. As used throughout this section, "performance assessment" refers both in a general sense to the full suite of information used to develop the compliance analyses, including the evaluation and screening of potentially relevant features, events, and processes (FEPs) (described in Section 2.2) and the development of models from available data for specific processes (Section 2.3), and in a narrower sense, to the individual analyses conducted with the total system model to satisfy the specific requirements of the three different postclosure standards. The term "total system performance assessment," or "TSPA," is also used throughout this section and refers more narrowly to the model, analyses, and codes used to estimate overall performance. "TSPA model" refers to the computational tool (which is a suite of coupled software codes and associated pre- and post-processors), and associated input files, used to conduct the analyses needed to satisfy the performance objectives established in 10 CFR 63.113 and the three performance assessments required by proposed 10 CFR 63.342.

In this introductory subsection, the quantitative standards for individual protection are used to illustrate the basic concepts underlying the performance assessments that the U.S. Department of Energy (DOE) must address. Proposed 10 CFR 63.311 requires:

> (a) DOE must demonstrate, using performance assessment, that there is a reasonable expectation that the reasonably maximally exposed individual receives no more than the following annual dose from releases from the undisturbed Yucca Mountain disposal system:
>
> (1) 0.15 mSv (15 mrem) for 10,000 years following disposal; and
>
> (2) 3.5 mSv (350 mrem) after 10,000 years, but within the period of geologic stability.
>
> (b) DOE's performance assessment must include all potential environmental pathways of radionuclide transport and exposure.

As required in proposed 10 CFR 63.303, compliance with these requirements shall be based on the mean of projected doses for the period within 10,000 years after disposal and on the median of projected doses during the period of geologic stability after 10,000 years (i.e., until 1,000,000 years after permanent closure). Demonstration of compliance with this standard requires appropriate consideration of three concepts introduced in proposed 10 CFR 63.311(a): performance assessment, reasonable expectation, and the reasonably maximally exposed individual (RMEI). The first two concepts, performance assessment and reasonable expectation, share a common focus on risk. As stated in NUREG-1804, Section 2.2.1, "The U.S. Department of Energy performance assessment is a systematic analysis that answers the risk triplet questions: what can happen; how likely is it to happen; and what are the consequences." To understand how risk information is applied within the performance assessment, it is important to first consider the U.S. Nuclear Regulatory Commission (NRC) definition of performance assessment.

Application of Risk Information in the Performance Assessment—The NRC defines performance assessment at 10 CFR 63.2 as modified in proposed 10 CFR 63.2 (70 FR 55313):

> Performance assessment means an analysis that:
>
> (1) Identifies the features, events, processes (except human intrusion), and sequences of events and processes (except human intrusion) that might affect the Yucca Mountain disposal system and their probabilities of occurring;

> (2) Examines the effects of those features, events, processes and sequences of events and processes upon the performance of the Yucca Mountain disposal system; and
>
> (3) Estimates the dose incurred by the reasonably maximally exposed individual, including the associated uncertainties, as a result of releases caused by all significant features, events, processes, and sequences of events and processes, weighted by their probability of occurrence.

This definition of performance assessment directly incorporates the questions of the risk triplet. Specifically, the 10 CFR 63.2 reference to "Identifies features, events, processes" corresponds to the first of the risk triplet questions and "Identifies… their probabilities of occurring" corresponds to the second of the risk triplet questions. Similarly, the 10 CFR 63.2 reference to "Examines the effects of those features, events, processes" and "Estimates the dose incurred by the reasonably maximally exposed individual" correspond to the third risk triplet question.

The role of risk information in the performance assessment is stated in NUREG-1804, Section 2.2.1:

> Because the performance assessment encompasses such a broad range of issues, the staff needs to use risk information throughout the review process. Using risk information will ensure the review focuses on those items most important to waste isolation.
>
> Section 2.2.1 requires the staff to apply risk information throughout the review of the performance assessment. First, the staff reviews the barriers important to waste isolation in Section 2.2.1.1. The U.S. Department of Energy must identify the important barriers (engineered and natural) of the performance assessment, describe each barrier's capability, and provide the technical basis for that capability. This risk information describes the U.S. Department of Energy understanding of each barrier's capability to prevent or substantially delay the movement of water or radioactive materials. Staff review of the U.S. Department of Energy performance assessment-first the barrier analysis and later the rest of the performance assessment-considers risk insights from previous performance assessments conducted for the Yucca Mountain site, detailed process modeling efforts, laboratory and field experiments, and natural analog studies. …The emphasis placed on particular parts of the staff review will change based on changes to the risk insights….

Section 2.1 (Tables 2.1-1, 2.1-2, 2.1-3, and 2.1-4) provides risk information regarding the FEPs that have been evaluated for inclusion in the TSPA. The FEPs marked "Processes and Characteristics that are Important to the Capability of the Barrier" are those considered to be most important to the capability of the barriers to prevent or reduce the rate of movement of water or radionuclides from the repository to the accessible environment, or to prevent or substantially reduce the rate of radionuclide release from the waste. The entire set of FEPs evaluated for consideration in the TSPA is identified in Section 2.2, Table 2.2-1.

Reasonable expectation is defined by the NRC at 10 CFR 63.304 as follows:

> Reasonable expectation means that the Commission is satisfied that compliance will be achieved based upon the full record before it. Characteristics of reasonable expectation include that it:
>
> (1) Requires less than absolute proof because absolute proof is impossible to attain for disposal due to the uncertainty of projecting long-term performance;
>
> (2) Accounts for the inherently greater uncertainties in making long-term projections of the performance of the Yucca Mountain disposal system;
>
> (3) Does not exclude important parameters from assessments and analyses simply because they are difficult to precisely quantify to a high degree of confidence; and
>
> (4) Focuses performance assessments and analyses on the full range of defensible and reasonable parameter distributions rather than only upon extreme physical situations and parameter values.

This principle of reasonable expectation is applied in the context of the risk triplet and in the context of using a risk-informed approach to demonstrating public health and safety. In particular, FEPs that are judged to be very unlikely to occur or to have insignificant effects on consequence are omitted from the performance assessment, as described in Section 2.2. Conservative models and assumptions are, in many cases, used to evaluate FEPs for exclusion from the TSPA and are also used in the treatment of some of the components of the TSPA, as described in the various parts of Section 2.3. NRC guidance on the use of conservatism in this context is set forth in NUREG-1804, Section 2.2.1:

> In many regulatory applications, a conservative approach can be used to decrease the need to collect additional information or to justify a simplified modeling approach. Conservative estimates for the dose to the reasonably maximally exposed individual may be used to demonstrate that the proposed repository meets U.S. Nuclear Regulatory Commission regulations and provides adequate protection of public health and safety…The total system performance assessment is a complex analysis with many parameters, and the U.S. Department of Energy may use conservative assumptions to simplify its approaches and data collection needs. However, a technical basis that supports the selection of models and parameter ranges or distributions must be provided. The staff evaluation of the adequacy of technical bases supporting models and parameter ranges or distributions will consider whether the approach results in calculated doses that would overestimate, rather than underestimate, the dose to the reasonably maximally exposed individual. …

Conservatisms in the TSPA model are described in Section 2.4.2.3.2.3.2.4, including discussions of the most important conservatisms from a risk-informed perspective. The known risk-significant nonconservatisms, based on various reviews of the TSPA model and its precursors (Section 2.4.2.3.2.3.4), were addressed during revision of the underlying submodels that comprise the TSPA model, to help ensure that the resulting dose is not underestimated. The combined effect of risk-significant conservatisms on the dose to the RMEI is addressed with the Performance Margin Analysis (PMA), which in conjunction with various other analyses, is used to build confidence in the TSPA model (Section 2.4.2.3.2.3). Additional risk insights regarding the important FEPs and parameters in the TSPA are provided in Section 2.4.2.3.3, which describes the results of a series of analyses on the sensitivity of the annual dose curve to various abstractions and parameters.

Uncertainty in the analyses and dose calculations could be considered a "fourth" question in addition to the risk triplet, stated as follows:

> (iv) What is the uncertainty (or equivalently, how much confidence can be placed) in the answers to the first three questions of the risk triplet?

The importance of this fourth question is acknowledged in the 10 CFR 63.2 definition of performance assessment, which says that a "performance assessment means an analysis that...estimates the dose incurred by the reasonably maximally exposed individual, including the associated uncertainties...." In addition, the 10 CFR 63.304 definition of reasonable expectation implicitly refers to this fourth question in the statements: "Accounts for the inherently greater uncertainties in making long-term projections..." and "Focuses performance assessments and analyses on the full range of defensible and reasonable parameter distributions..." Analysis of uncertainty is also described as one of the seven requirements for performance assessment at proposed 10 CFR 63.114(a)(2): "Any performance assessment used to demonstrate compliance with 10 CFR 63.113 for 10,000 years after disposal must...account for uncertainties and variabilities in parameter values, for 10,000 years after disposal, and provide for the technical basis for parameter ranges, probability distributions, or bounding values used in the performance assessment." How uncertainty is folded into the conceptual structure of the TSPA analyses, and how the fourth question is answered for component models, is explained in the relevant sections of Section 2.3, and in more detail with respect to TSPA in Sections 2.4.1 and 2.4.2, which show how the computational structure of the TSPA model is built around separation of uncertainties into two key types: aleatory (irreducible) and epistemic (reducible).

Types of Uncertainty Considered in the TSPA—Uncertainties are inherent in projections into the future of the geologic and environmental conditions surrounding the Yucca Mountain repository (see, for example, "Effects of Uncertainty" in the proposed U.S. Environmental Protection Agency (EPA) rule, 40 CFR Part 197, at 70 FR 49014). Because of these intrinsic uncertainties, estimates of future doses to the RMEI are also uncertain. Assessment of total system performance during the period of geologic stability must take these uncertainties into account. In addition, the discussion of the quantitative estimates of this performance (e.g., estimates of mean annual dose) will include information regarding the impacts of these uncertainties on those estimates—see Section 2.4.2.2.1, which addresses NUREG-1804, Section 2.2.1.4.1.3, Acceptance Criterion 2(2), and Section 2.4.2.3.3, which addresses NUREG-1804, Section 2.2.1.4.1.3, Acceptance Criterion 3(3).

The TSPA separates quantitative uncertainty in model inputs into two categories: aleatory uncertainty and epistemic uncertainty. Aleatory uncertainty primarily refers to the inherent uncertainty regarding the timing and magnitude of future events that could affect the repository and the impact of these events on repository performance. Because aleatory uncertainty cannot be reduced by the acquisition of additional data or knowledge, this kind of uncertainty is also referred to as irreducible uncertainty. Examples of aleatory uncertainty considered in the TSPA include the time and amplitude of seismic ground motion events, the occurrence of igneous events, and the location and number of early failures of waste packages and drip shields due to undetected manufacturing or emplacement defects.

The other important type of uncertainty is called epistemic uncertainty and stems from a lack of knowledge about a parameter or a probability distribution that is believed to be fixed (or deterministic). Sources of epistemic uncertainties include incomplete data, estimates based upon expert judgment, and measurement errors. Unlike aleatory uncertainty, epistemic uncertainty is potentially reducible with additional data and knowledge. In the TSPA model, epistemic quantities are generally inputs to specific submodels, with the submodels having been developed to use single values for these quantities. A particular epistemic quantity can be a parameter that characterizes a probability distribution (e.g., the mean value of the fracture permeability distribution used to calculate drift seepage), a field of values selected from alternative sets (e.g., the flow field in the unsaturated zone), or a measured parameter that characterizes a physical-chemical process (e.g., the temperature dependency of general corrosion of Alloy 22 (UNS N06022) or the unsaturated-zone fracture frequency).

Definition of the RMEI—The final concept mentioned above with respect to proposed 10 CFR 63.311 is the concept of the RMEI, which is defined at 10 CFR 63.312:

> The reasonably maximally exposed individual is a hypothetical person who meets the following criteria:
>
> (a) Lives in the accessible environment above the highest concentration of radionuclides in the plume of contamination;
>
> (b) Has a diet and living style representative of the people who now reside in the Town of Amargosa Valley, Nevada. DOE must use projections based upon surveys of the people residing in the Town of Amargosa Valley, Nevada, to determine their current diets and living styles and use the mean values of these factors in the assessments conducted for [proposed 10 CFR] 63.311 and [proposed 10 CFR] 63.321;
>
> (c) Uses well water with average concentrations of radionuclides based on an annual water demand of 3,000 acre-feet;
>
> (d) Drinks 2 liters of water per day from wells drilled into the ground water at the location specified in paragraph (a) of this section; and
>
> (e) Is an adult with metabolic and physiological considerations consistent with present knowledge of adults.

The accessible environment above the highest concentration of radionuclides in the plume of contamination mentioned in 10 CFR 63.312, or the point of compliance for calculating dose with respect to the postclosure individual protection, human intrusion, and groundwater protection standards, is based on the definition of the controlled area in 10 CFR 63.302. Consistent with the regulatory definition at 10 CFR 63.302, the DOE has defined the southern boundary of the controlled area as extending to 36° 40′ 13.6661″ north latitude, approximately 18 km from the repository footprint in the predominant direction of groundwater flow (GI Section 1.1).

Organization of Section 2.4—Results and analyses in Section 2.4 are derived in large part from *Total System Performance Assessment Model/Analysis for the License Application* (SNL 2008a). Section 2.4 is arranged to correspond to the acceptance criteria and their associated subcriteria in the three subsections of NUREG-1804, Section 2.2.1.4. However, Section 2.4 contains four, rather than three, major subsections because the first subsection, Section 2.4.1, summarizes the TSPA method and approach and the structure of the TSPA model, which provides the context for the detailed quantitative demonstration of compliance with postclosure public health and environmental standards described in the next three sections. Section 2.4.1 also provides a high-level summary of the TSPA results for all three applicable public and environmental health standards. Section 2.4.2 addresses quantitative requirements relating to the postclosure individual protection standard contained in proposed 10 CFR 63.311 by demonstrating the ability of the repository to limit radiological exposures to the RMEI for the period after permanent repository closure. Section 2.4.3 addresses quantitative requirements relating to the individual protection standard for human intrusion in proposed 10 CFR 63.321 by demonstrating the ability of the repository to limit radiological exposure to the RMEI for the period after permanent closure in the event of human intrusion into the Engineered Barrier System (EBS). Lastly, Section 2.4.4 addresses the quantitative requirements relating to the separate standards for the protection of groundwater contained in 10 CFR 63.331 by demonstrating the ability of the repository to limit releases of radionuclides into the accessible environment.

The information provided in this section is cross-referenced below to the corresponding current or proposed regulatory requirements and applicable acceptance criteria from NUREG-1804.

SAR Section	Information Category	Proposed 10 CFR Part 63 Reference	NUREG-1804 Reference
2.4	Demonstration of Compliance with the Postclosure Public Health and Environmental Standards	63.21(c)(11)[a] 63.21(c)(12)[a] 63.21(c)(13)[a] 63.21(c)(15)[a] 63.113[a] 63.114 63.303 63.305 63.311 63.312[a] 63.321 63.322[a] 63.331[a] 63.332[a] 63.342	Section 2.2.1.2.1.3: Acceptance Criterion 3 Section 2.2.1.3.1.3: Acceptance Criterion 1(2) Section 2.2.1.3.2.3: Acceptance Criterion 1(3) Section 2.2.1.3.3.3: Acceptance Criterion 1(2) Acceptance Criterion 1(5) Acceptance Criterion 1(7) Section 2.2.1.3.4.3: Acceptance Criterion 1(2) Section 2.2.1.3.5.3: Acceptance Criterion 1(3) Section 2.2.1.3.6.3: Acceptance Criterion 1(3) Section 2.2.1.3.7.3: Acceptance Criterion 1(3) Section 2.2.1.3.8.3: Acceptance Criterion 1(3) Section 2.2.1.3.9.3: Acceptance Criterion 1(3) Section 2.2.1.3.14.3: Acceptance Criterion 1(3) Section 2.2.1.4.1.3: Acceptance Criterion 1 Acceptance Criterion 2 Acceptance Criterion 3 Section 2.2.1.4.2.3: Acceptance Criterion 1 Acceptance Criterion 2 Acceptance Criterion 3 Section 2.2.1.4.3.3: Acceptance Criterion 1 Acceptance Criterion 2 Acceptance Criterion 3
2.4.1	Total System Performance Assessment Model and Summary of Results	63.303 63.113[a] 63.114 63.311 63.321 63.331[a] 63.342	Not applicable

SAR Section	Information Category	Proposed 10 CFR Part 63 Reference	NUREG-1804 Reference
2.4.2	Demonstration of Compliance with the Postclosure Individual Protection Standard	63.21(c)(11)[a] 63.21(c)(15)[a] 63.113(b)[a] 63.114 63.303 63.305 63.311 63.312[a] 63.342	Section 2.2.1.2.1.3: Acceptance Criterion 3 Section 2.2.1.3.1.3: Acceptance Criterion 1(2) Section 2.2.1.3.2.3: Acceptance Criterion 1(3) Section 2.2.1.3.3.3: Acceptance Criterion 1(2) Acceptance Criterion 1(5) Acceptance Criterion 1(7) Section 2.2.1.3.4.3: Acceptance Criterion 1(2) Section 2.2.1.3.5.3: Acceptance Criterion 1(3) Section 2.2.1.3.6.3: Acceptance Criterion 1(3) Section 2.2.1.3.7.3: Acceptance Criterion 1(3) Section 2.2.1.3.8.3: Acceptance Criterion 1(3) Section 2.2.1.3.9.3: Acceptance Criterion 1(3) Section 2.2.1.3.14.3: Acceptance Criterion 1(3) Section 2.2.1.4.1.3: Acceptance Criterion 1 Acceptance Criterion 2 Acceptance Criterion 3
2.4.3	Demonstration of Compliance with the Individual Protection Standard for Human Intrusion	63.21(c)(13)[a] 63.21(c)(15)[a] 63.113(d)[a] 63.114 63.303 63.321 63.322[a] 63.342	Section 2.2.1.4.2.3: Acceptance Criterion 1 Acceptance Criterion 2 Acceptance Criterion 3
2.4.4	Analysis of Repository Performance that Demonstrates Compliance with the Separate Standards for the Protection of Groundwater	63.21(c)(12)[a] 63.113(c)[a] 63.114 63.303 63.331[a] 63.332[a] 63.342	Section 2.2.1.4.3.3: Acceptance Criterion 1 Acceptance Criterion 2 Acceptance Criterion 3

NOTE: [a]Not changed by the proposed rule.

2.4.1 Total System Performance Assessment Model and Summary of Results

This section briefly summarizes the method and approach of the DOE performance assessment, including a description of the scenario classes, major components and associated submodels of the TSPA model, and an introduction to the modeling cases that are used to compute the annual dose

(SNL 2008a). It also briefly summarizes the quantitative results of the performance assessment. More detail on scenario classes and modeling cases may be found in Sections 2.2 and 2.4.2.1. Also, detailed information about the abstractions that form the basis of the TSPA model components and submodels is described in Section 2.3. Details about the implementation of the various abstractions for the TSPA model components and submodels, as well as the flow of information and coupling between model components and submodels, may be found in Section 2.4.2.3.2.1. A short discussion at the end of this section introduces the TSPA computational structure, including the rationale for separation of aleatory and epistemic uncertainties. This section concludes with a summary of the results of the performance assessment, which demonstrates compliance with the applicable postclosure public health and environmental standards at proposed 10 CFR 63.311, proposed 63.321, and 63.331.

2.4.1.1 TSPA Method and Approach

The TSPA model incorporates and integrates models describing the characteristics, features and processes associated with the three barriers (Upper Natural Barrier, EBS, and Lower Natural Barrier). Sections 2.1.1 and 2.1.2 contain a description of these three barriers, and a summary of the associated features and processes. Section 2.3 provides a much more in-depth description of the various physical phenomena, thermal-hydrologic-chemical-mechanical couplings, and modeling abstractions for these features and processes (as well as the likely and unlikely disruptive events associated with the Yucca Mountain site). The TSPA approach combines these underlying abstractions in such a way that it incorporates the estimated ranges of uncertainty in the parameter distributions, model abstractions, and disruptive events and then propagates this uncertainty into estimates of the annual dose.

The TSPA model was built expressly to evaluate the Yucca Mountain repository system in accordance with the requirements of proposed 10 CFR Part 63. The first step in building the model, consistent with the definition of performance assessment in proposed 10 CFR 63.2 and requirements in proposed 10 CFR 63.114(a)(4) to (6), is to identify the FEPs that could be important to repository performance. As specified in the proposed 10 CFR 63.342, the performance assessments for the human intrusion and groundwater protection standards do not include consideration of unlikely FEPs (those with a greater than one chance in 10,000 of occurring in 10,000 years but less than a one chance in 10 of occurring in 10,000 years). However, the performance assessment for the individual protection standard includes both likely and unlikely FEPs, and only excludes very unlikely FEPs (those with less than one chance in 10,000 of occurring in 10,000 years) or those with low consequence (proposed 10 CFR 63.114(a)(4) to (6)). Furthermore, the TSPA model and associated performance assessment described in this section expressly follow the requirements in proposed 10 CFR 63.342(c) by projecting the continued effects of the 10,000-year screened-in FEPs through the period of geologic stability (up to 1,000,000 years after permanent closure), and including the effects of seismic events, igneous events, climate change, and general corrosion beyond 10,000 years.

The TSPA is built upon FEPs that have been identified and screened in accordance with the requirements in proposed 10 CFR 63.114(a)(4) to (6). FEPs are included or excluded based upon the three screening criteria described in Section 2.2.1.2: low probability (proposed 10 CFR 63.342(a)), low consequence (proposed 10 CFR 63.114(a)(5)), and regulation. Each screening decision is supported by a technically sound screening justification, as described in detail in *Features, Events,* *and Processes for the Total System Performance Assessment: Methods* (SNL 2008b) and *Features, Events, and Processes for the Total System Performance Assessment: Analyses* (SNL 2008c). The FEPs screening methodology is summarized in Section 2.2.1, and the FEPs screening decisions (i.e., inclusion or exclusion), along with a brief description of each FEP, can be found in Table 2.2-5. Summaries of the technical basis and justification for each included FEP screening decision can be found in the FEPs inclusion tables of each Section 2.3 subsection (e.g., Table 2.3.1-1) and in Section 2.2 (i.e., Table 2.2-4) for "system" FEPs.

2.4.1.2 Scenario Classes and Modeling Cases

As introduced in Section 2.2, the TSPA calculates the total annual dose as the sum of the annual doses attributable to the nominal scenario class, the early failure scenario class, and the two disruptive event scenario classes (the igneous scenario class and the seismic scenario class). Computation of the dose attributable to each scenario class relies on the separation of each disruptive-event scenario class (as well as the early failure scenario class) into two modeling cases, each of which is built around a more narrowly defined event occurrence. For example, the volcanic eruption modeling case calculates the contribution to the total annual dose from the set of futures within the broader igneous scenario class that have one or more atmospheric eruptions occurring in them. The six modeling cases associated with the aforementioned event scenario classes are as follows: igneous intrusion, volcanic eruption, seismic ground motion, seismic fault displacement, early-failure of waste packages, and early-failure of drip shields. In addition, a seventh modeling case describes performance in the absence of disruptive or early failure events, and is called the nominal modeling case.

2.4.1.2.1 Nominal Scenario Class

The nominal scenario class in the TSPA describes the future performance of the repository system in the absence of any disruptive or early failure events (i.e., no igneous events, no seismic events, and no early waste package or drip shield failures). It represents the set of possible futures with radionuclide releases from the EBS arising from nominal waste package and drip shield degradation processes (e.g., corrosion processes such as general corrosion, localized corrosion, and stress corrosion cracking) but no degradation from disruptive events (i.e., igneous or seismic events) or early failure events. The nominal scenario class in the TSPA model is represented by only a single modeling case that considers these nominal degradation processes of the waste packages and drip shields, as well as all of the other included FEPs listed in Table 2.2-5 that are not associated with disruptive or early-failure events. Radionuclides released from the emplacement drifts in the nominal scenario class may be transported to the saturated zone by the groundwater percolating through the unsaturated zone below the repository, and then transported to the accessible environment by water flowing in the saturated zone. The annual dose to the RMEI in the nominal scenario class includes FEPs associated with the biosphere and incorporates the important effects and system perturbations caused by climate change and repository thermal evolution, and changes in repository system thermal characteristics that are projected to occur over the period of geologic stability (1,000,000 years).

The general structure or architecture of the TSPA model is built around the FEPs that comprise the nominal scenario class. The description of this architecture is linked to the set of eight principal model components discussed below (SNL 2008a, Section 6.1.4), with each model component being comprised of one or more submodels. Model components and submodels each represent some subset of FEPs associated with one or more of the three barriers. A submodel can be either a detailed process model developed, tested, and validated in a supporting document, a simple or detailed abstraction of the process model, an abstraction of the process model results, or a direct process model input (e.g., a lookup table or distribution of values). Model components are generally comprised of a collection of submodels (i.e., process models, analyses, or abstractions) that together represent a key component of the repository system. TSPA model components and submodels are specifically chosen because they provide a useful framework for discussing and reviewing the integration aspects of the TSPA model, as well as discussing the flow of information among modules of the TSPA code (Section 2.4.2.3.2.1).

The TSPA model for the nominal scenario class explicitly includes the following eight principal model components, shown in Figure 2.4-1:

- Unsaturated Zone Flow, which describes fluid flow through the unsaturated welded and nonwelded tuffs above and below the repository

- EBS Environment, which describes the coupled thermal-hydrologic-chemical processes in the environment surrounding and within the engineered elements of the repository

- Waste Package and Drip Shield Degradation, which describes the responses of these engineered features to heat, humidity, seepage, and the geochemical environment of the EBS

- Waste Form Degradation and Mobilization, which describes the degradation and dissolution of the waste forms and the mobilization of radionuclides into the liquid phase that forms inside the waste packages and EBS

- EBS Flow and Transport, which describes the flow of water and the transport of radionuclides within and from the EBS to the unsaturated zone below the repository

- Unsaturated Zone Transport, which describes the transport of radionuclides through the unsaturated zone below the repository to the water table at the top of the saturated zone

- Saturated Zone Flow and Transport, which describes water flow and radionuclide transport through volcanic tuff and alluvium in the saturated zone to the location of the RMEI

- Biosphere, which describes the biologic uptake of radionuclides, including inhalation, ingestion, and water consumption by humans at the location of the RMEI.

Each model component is itself a system of dynamic calculations performed by one or more submodels. These model components form the basis for the representation of the three barriers that comprise the Yucca Mountain system (i.e., the Upper Natural Barrier, the EBS, and the Lower Natural Barrier (Section 2.1)), and their contribution to waste isolation as calculated by the TSPA model. As indicated in Figure 2.4-1, these same model components and associated FEPs also form the basis of the other scenario classes and modeling cases (with the exception of the volcanic eruption modeling case), but with the addition of those FEPs related to early failures and disruptive activity.

Submodels of the eight principal model components are shown in Figure 2.4-2, in the rows of boxes below the first row. Figure 2.4-2 also depicts the types of events considered in the disruptive-event and early-failure scenario classes. The nominal, early failure, igneous, and seismic scenario classes use many of the same submodels and parameters, with differences primarily related to the drip shield and waste package damage submodels. The technical bases for the process models, abstractions, and included FEPs that support the TSPA model components and submodels are discussed in Section 2.3.

Table 2.4-1 maps the principal model components of the TSPA model from Figure 2.4-2 to the subsection in Section 2.3 where the technical bases for the supporting process model, abstractions, and included FEPs are described. Additionally, the process model, analysis, or abstraction that feeds each submodel is listed in Table 2.4-1. As discussed and described in the introduction to Section 2.3, the structure of the model abstractions presented in Section 2.3 is a modification of that provided in NUREG-1804. The differences are discussed in the introduction to Section 2.3. Table 2.3-1 maps the NUREG model abstraction areas to the TSPA model components and submodels shown in Table 2.4-1.

Although Section 2.3 provides in-depth descriptions of each model component and submodel, and Section 2.4.2.3.2.1 provides a detailed summary of their implementation in the TSPA model, it is useful here to provide a brief introduction to the various submodels and their relationship to the three barriers.

Upper Natural Barrier—The Upper Natural Barrier is represented in the TSPA in the unsaturated zone flow model component, which incorporates spatial and temporal variability and uncertainty.

The Upper Natural Barrier consists of (1) surface topography and surficial soils, and (2) the unsaturated zone above the repository. The unsaturated zone flow model component of the TSPA integrates five processes that contribute to flow in the unsaturated zone: climate, infiltration, site-scale unsaturated zone flow, drift seepage, and drift-wall condensation (Sections 2.3.1, 2.3.2, 2.3.3, and 2.3.5). The unsaturated zone flow model component defines the temporal and spatial distribution of water flow from the ground surface through the unsaturated tuffs above and below the repository horizon and the temporal and spatial distribution of seepage into the waste emplacement drifts and condensation on the drift walls, driven by the early thermal perturbation from the waste heat. Water at the repository horizon is derived from precipitation in the form of rainfall and snow at the land surface above the repository, infiltration below surficial soils, and percolation through the unsaturated zone above the repository. A set of flow fields defining liquid flux and velocity fields as a function of space and time were developed as input to various submodels representing flow and transport processes in the EBS and Lower Natural Barriers. Long-term temporal variability is included in the TSPA model by calculating flow fields specific to successive climate states: present-day, monsoon, and glacial-transition. Flow fields for the period beyond 10,000 years after disposal are based on specifications regarding deep percolation rates provided in proposed 10 CFR 63.342(c)(2).

Engineered Barrier System—The representation of the EBS includes the EBS environment, waste package and drip shield degradation, waste form degradation and mobilization, and EBS flow and transport model components.

The EBS environment model component includes the thermal-hydrologic environment in the unsaturated-zone host rock surrounding the emplacement drifts, as well as the thermal-hydrologic environment and chemical environment within the emplacement drifts, as discussed in Section 2.3.5. These environments are important to repository performance because they help determine the degradation rates of the EBS components, the mass of mobilized radionuclides, and the degree of transport of radionuclides and fluids through the emplacement drifts and into the unsaturated zone below the repository. Water percolating into the repository environment will be affected by heat from the emplaced waste, and the resulting hydrologic and geochemical processes will determine the chemical environment of the EBS.

The waste packages and drip shields are the primary engineered components of the EBS (Section 2.3.6). The waste package and drip shield degradation model component describes the degradation of the waste packages and drip shields as a function of time, environment, and repository location. The waste package and drip shield degradation model component simulates general corrosion of the waste packages and drip shields, stress corrosion cracking of the waste packages, microbially influenced corrosion of the waste package outer surface, and the possibility of localized corrosion of the waste package outer surface.

The waste form degradation and mobilization model component simulates the degradation of commercial spent nuclear fuel (SNF), DOE SNF, and high-level radioactive waste (HLW) glass waste and the subsequent dissolution of their radionuclide inventories into the liquid phase present in the degraded waste. Section 2.3.7 describes this mobilization of radionuclide mass as either dissolved species or as attached to colloidal particles. The waste form degradation and mobilization model component accounts for in-package water chemistry; matrix degradation rates for commercial SNF, DOE SNF, and HLW glass waste forms; radionuclide solubilities; and the types and concentrations of waste-form, groundwater, and iron oxyhydroxide colloids.

The EBS flow and transport model component calculates the rate of radionuclide release from the EBS to the unsaturated zone, which is determined by seepage into the emplacement drifts, condensation on the drift walls, waste package and drip shield degradation, the presence of water films on in-package internals, waste-form degradation, and the thermal-hydrologic environment of the EBS (Section 2.3.7). The EBS flow and transport model component simulates the rate of water flow through the EBS, diffusive and advective transport of dissolved radionuclides, sorption, and colloid-facilitated transport.

The implementation of the EBS representation in the TSPA model involves discretization of the submodels by waste type, percolation subregion, and seepage environment (Figure 2.4-3). The first level of discretization is by waste type. The TSPA model considers two types of waste packages: commercial SNF and codisposal waste packages. Codisposal waste packages contain both DOE SNF and HLW glass. Within the TSPA model, discretization by waste type is handled explicitly by implementing different GoldSim source terms to perform the fuel-type-specific calculations (GoldSim Technology Group 2007a, Chapter 5). The second level of discretization is by percolation subregion. The magnitude of infiltration varies spatially across the land surface above the repository footprint and percolation flux varies spatially at the repository level. This spatial variability is captured in a CDF of percolation flux values (SNL 2008d, Section 6.2.12.1[a]). This CDF provides the basis for the TSPA model representation of five percolation subregions, which represent the variation of liquid flux (seepage) into the drifts (Section 2.3.3) and its influence on advective transport of radionuclides. The third level of discretization is by seeping environment (i.e., drift seepage with or without drift-wall condensate). The commercial SNF and codisposal waste packages in each percolation subregion are identified as either having seepage above each waste package location or not. The foregoing three levels of discretization result in 20 environments in the TSPA model (two fuel types × five percolation subregions × two seepage conditions) that are used to represent all of the waste packages in the repository. (Note: As shown in Figure 2.4-3, there is also an additional level of discretization in the TSPA model related to the potential occurrence of localized corrosion of the waste package, which produces 30 actual environments in the GoldSim Model file. However, because of the low impact to performance of localized corrosion, as described later in Section 2.4.2.3.2.1.5, these environments are not required in the main TSPA simulations (SNL 2008a, Appendix O).)

Lower Natural Barrier—The Lower Natural Barrier consists of two natural features: (1) the unsaturated zone below the repository horizon; and (2) the saturated zone beneath the repository that extends to the accessible environment, approximately 18 km downgradient of the repository.

The unsaturated zone transport model component describes the migration of radionuclides through the unsaturated zone to the water table. Consistent with the unsaturated zone flow model component, the conceptual model for unsaturated zone transport simulates coupled advective and diffusive transport through fracture and matrix continua using a dual continuum approach (Section 2.3.8). The unsaturated zone transport model component simulates advective, dispersive, and diffusive transport; sorption in the matrix continuum; colloid retardation; radioactive decay and ingrowth; and changes in water table elevation. Changes in climate are represented by a set of steady state flow fields representing the three climate states during the first 10,000 years and a deep percolation flux distribution specified at proposed 10 CFR 63.342(c)(2) to represent climate change in the post-10,000-year period.

The saturated zone flow and transport model component simulates the transport of radionuclides from their introduction at the water table below the repository to the accessible environment located approximately 18 km downgradient from the Yucca Mountain repository. Radionuclides are transported through the saturated zone either in the dissolved phase or sorbed reversibly or irreversibly to colloids. The saturated zone flow and transport model component simulates advection, dispersion, and diffusion in fractures; matrix diffusion; colloid retardation and filtration; sorption; and radioactive decay and ingrowth (Section 2.3.9). Climate change is represented by the use of set of flux multipliers applied to the present-day saturated-zone specific discharge, to simulate the increased groundwater specific discharge during future climates, including the effects of climate change on saturated-zone specific discharge during the post-10,000-year period.

The biosphere model component, although not a feature of the Lower Natural Barrier as defined in Section 2.1, is an important component of the TSPA model. In the TSPA, this model component simulates potential pathways of radionuclide transport in the biosphere and the resulting exposure of the RMEI to radionuclides released from the repository after closure (Section 2.3.10). The TSPA model includes two mechanisms of radionuclide release to the biosphere: (1) release through the saturated zone via groundwater pumping; and (2) release through the air by ash dispersal from a volcanic eruption.

2.4.1.2.2 Early Failure Scenario Class

The early failure scenario class estimates the contribution to mean annual dose attributable to early failure of waste packages or drip shields. An early failure is defined as the through-wall penetration of a waste package or drip shield due to manufacturing or handling-induced defects at a time earlier than would be predicted by mechanistic degradation models for a defect-free waste package or drip shield. The FEPs and models associated with the potential for early failure (which is modeled as failure at emplacement) of either waste packages or drip shields are described in Section 2.3.6. As described in Section 2.3.6, various potential manufacturing and handling defects that could result in early-failed waste packages or drip shields have been identified, such as weld flaws and improper heat treatment. These defects were assessed for probability of occurrence and consequences for postclosure performance (SNL 2007a). The occurrence of an undetected defect is assumed to result in early failure; hence, the probability distribution for the rate of occurrence of undetected defects is equivalent to a probability distribution for the rate of early failures. Both major types of uncertainty, aleatory and epistemic, are represented in the failure distributions for early waste package failures and early drip shield failures (Section 2.4.2.3.2.1.12.1).

The early failure scenario class consists of two modeling cases: the drip shield early failure modeling case and waste package early failure modeling case. In the drip shield early failure modeling case, complete failure of the drip shield is assumed to occur. Also, as a bounding assumption, the waste package under an early-failed drip shield is assumed to experience localized corrosion over its entire surface as soon as seepage contacts the waste package, since the area of the Alloy 22 waste package that is contacted by seepage is potentially subject to localized corrosion (Section 2.3.6.4). Because the drip shield early failure modeling case contributes only negligibly to total dose, as will be seen below in Section 2.4.2.2.1, this bounding assumption is justified. In the waste package early failure modeling case, an early-failed waste package is considered breached from the beginning of the simulation, and its entire surface area is considered degraded. General corrosion of the drip shields due to nominal corrosion processes (Section 2.3.6.8.1) is also included in the waste package early failure modeling case. This indicates that advective transport of radionuclides can occur after drip shield failure, which happens on average at about 300,000 years after permanent closure (Figure 2.1-8).

Other than the changes to the waste package and drip shield degradation model component described above, the two modeling cases in the early failure scenario class have the same framework as the nominal scenario class modeling case, and are based on the same modeling components and submodels as are used in the nominal scenario class. That is, the framework includes the TSPA model components that evaluate the mobilization of radionuclides exposed to seeping water, radionuclide releases from the EBS, transport in the unsaturated zone down to the water table, and transport in the saturated zone to the accessible environment. The relationships between the TSPA model components for the early failure scenario class are illustrated on Figure 2.4-4.

2.4.1.2.3 Igneous Scenario Class

The FEPs and models associated with potential igneous activity in the vicinity of Yucca Mountain are described in Section 2.3.11. The igneous scenario class in the TSPA includes all screened-in FEPs related to igneous activity (SNL 2008b). Yucca Mountain is in a region that has had volcanic activity in the geologic past, and, although there is a very low probability of recurrence of igneous activity affecting the repository, the mean probability is slightly greater than 1 in 10,000 in 10,000 years (BSC 2004a, Table 7-1). Accordingly, based on the probability requirements in proposed 10 CFR 63.342, igneous activity is examined with the TSPA model.

A probabilistic volcanic hazard analysis (PVHA) was performed to assess the volcanic hazard at Yucca Mountain. For the PVHA, an expert panel was convened in 1995 to review pertinent data relating to volcanism at Yucca Mountain and, based on these data, to quantify both the annual probability and associated uncertainty of a volcanic event intersecting a proposed repository sited at Yucca Mountain (BSC 2004a, Section 6.1).

The contribution to mean annual dose attributable to the igneous scenario class is addressed by two modeling cases: the igneous intrusion modeling case (Section 2.3.11.3) and the volcanic eruption modeling case (Section 2.3.11.4). In both modeling cases, magma propagates upward through the Earth’s crust in fluid-driven cracks (dikes). The igneous intrusion modeling case considers the intersection of repository drifts by one or more dikes, and the subsequent damage to waste packages, which allows radionuclides to be released and transported to the groundwater. The volcanic eruption modeling case considers an eruptive conduit that forms when a portion of the intruding dike begins to widen, creating a conduit through one of the emplacement drifts, and thereby allowing magma flow to the surface, with subsequent atmospheric dispersal of ash and entrained waste.

In the igneous intrusion modeling case, magma from a dike(s) that intersects one or more repository drifts is assumed to engulf all drip shields and waste packages in the repository, rendering them incapable of protecting their contents. In that case, the waste packages no longer act to prevent or slow the rate of transport, allowing radionuclides to move downward through the unsaturated zone to the water table, and then to the accessible environment by groundwater flow in the saturated zone. The TSPA model components needed to estimate annual dose in the igneous intrusion modeling case are shown on Figure 2.4-5. Modifications to these components for the igneous scenario class are indicated by the bulleted items on the figure. The effects of igneous events occurring more than 10,000 years after disposal are taken into account with respect to EBS model components, as required by the NRC proposed rule, 10 CFR 63.342, but not with respect to the natural system components, since the effect of igneous processes on the Lower Natural Barrier have been determined to be of low consequence and therefore are excluded from the TSPA (Table 2.2-5).

In the volcanic eruption modeling case, magma erupts into the atmosphere. For most futures within the eruption modeling case, the conduit that brings magma to the surface does not intersect an emplacement drift and, therefore, does not entrain waste into the erupted tephra. For those futures where an eruptive conduit(s) intersects an emplacement drift, the waste packages located within the conduit cross-sectional area are assumed to fail. The rising magma entrains radionuclide waste particles and a portion of the erupting stream becomes a buoyant, convecting column that is ejected into the atmosphere. The associated tephra plume is transported downwind and the particles in the plume are dispersed and eventually deposited on the land surface. The contaminated soil, including tephra, is then subject to redistribution by sedimentary processes. The TSPA model components needed to estimate mean annual dose in the volcanic eruption modeling case are shown on Figure 2.4-6. Because radionuclide transport is via atmospheric dispersal and ash redistribution, rather than groundwater transport, the model components for this modeling case are different from the other six modeling cases.

2.4.1.2.4 Seismic Scenario Class

The FEPs and models associated with potential seismic activity in the vicinity of Yucca Mountain are described in Section 2.3.4. The seismic scenario class describes the future performance of the repository system in the event of seismic activity that could disrupt the repository system, and it represents the direct effects of vibratory ground motion and fault displacement associated with seismic activity. The most important direct effects that are considered are the seismic consequences to drip shield and waste package integrity because damage to or failure of these components has the potential to initiate or increase releases of radionuclides by forming new diffusive or advective transport pathways. Indirect effects of seismic activity are also considered in this scenario class, including drift collapse and the resulting changes in seepage and drift wall condensation and in the EBS thermal environment.

The probability of occurrence of seismic events is expressed in terms of a mean annual exceedance frequency. Probabilistic seismic hazard analysis (PSHA) was performed to assess the seismic hazards of vibratory ground motion and fault displacement at Yucca Mountain. *Probabilistic Seismic Hazard Analyses for Fault Displacement and Vibratory Ground Motion at Yucca Mountain, Nevada* (CRWMS M&O 1998) used an expert elicitation process to determine the annual probability with which various levels of ground motion will be exceeded at Yucca Mountain (Section 2.2.2.1). The results of the PSHA process provided hazard curves for a reference rock outcrop that were then modified to account for the effects of the local, site-specific geology of Yucca Mountain on the ground motions using a ground motion site-response model (Section 2.3.4.3.2). The output of the site-response model was used to produce acceleration and velocity time histories for the range of possible ground motions considered in the TSPA (Section 2.3.4.3.2). A separate analysis was performed to determine a reasonable bound to peak horizontal ground velocity at the waste emplacement level, taking into account geologic observations of historical maximum strain levels observable in repository rocks at Yucca Mountain (Section 2.3.4.3.3). The fault displacement analysis is derived directly from the PSHA for fault displacement (Section 2.2.2.1). This analysis used an expert elicitation process to determine how the annual probability of exceedance for fault displacement at the surface varies as a function of the size of the displacement. The results also apply to the waste emplacement level and are used directly in the seismic consequence abstraction. The seismic scenario class for the TSPA uses only the mean hazard curve for the peak ground velocity (PGV) associated with either strong ground motion or fault displacement. The use of the mean hazard curve is conservative relative to the median hazard curve, because it typically lies above the 80th percentile of the distribution of hazard curves, so the mean is dominated by the larger values of the distribution (SNL 2008a, Section 6.6.1.2).

The seismic scenario class estimates the contribution to mean annual dose attributable to seismic activity by means of two modeling cases. The first modeling case includes those waste packages and drip shields that fail due to the ground motion damage associated with the seismic event and is denoted as the seismic ground motion modeling case. Because nominal corrosion processes have the potential to alter the repository's susceptibility to damage during a seismic ground motion event, the seismic ground motion modeling case includes these nominal corrosion processes when calculating consequences. The second modeling case includes only those waste packages and drip shields that fail due to fault displacement damage and it is denoted as the seismic fault displacement modeling case.

The model components and submodels of the TSPA model for the seismic scenario class are shown on Figure 2.4-7. The two modeling cases have the same framework as the nominal scenario class modeling case. That is, the framework includes the TSPA model components to evaluate the mobilization of radionuclides exposed to seeping water, released from the EBS, transported in the unsaturated zone, and transported in the saturated zone from the repository to the accessible environment. Modifications to these model components for the seismic scenario class are indicated by the bulleted items on the figure. The effects of seismic events for the post-10,000 year period after closure are taken into account with respect to EBS model components, as required by proposed 10 CFR 63.342, but not with respect to the natural system components, since the effect of seismic processes on the Lower Natural Barrier have been determined to be of low consequence and therefore are excluded from the TSPA (Section 2.2).

2.4.1.3 TSPA Computational Structure

As detailed in Section 2.4.2.1, at the highest level the TSPA model computational structure is built around the separation of aleatory (inherent or irreducible) and epistemic ("lack of knowledge" or reducible) uncertainty, which results in a nested loop structure for computing the dose for each modeling case, as well as the total dose from all modeling cases. A brief introduction to these two types of uncertainty was given in the introductory section of Section 2.4, above.

Computational Methodology—The TSPA model computes mean annual dose by integrating over both aleatory and epistemic uncertainty. Several slightly different computational strategies are used to compute the expectation over aleatory uncertainty. For example, the computational strategy for the seismic ground motion modeling case calculations for 10,000 years is illustrated schematically in Figure 2.4-8. First, in the outer loop, a sample (specifically, a Latin hypercube sample of size 300) of the epistemic parameters is generated, and one sample element out of the 300 samples is chosen, represented by the notation $\mathbf{e}$. Based on this chosen sampling of parameter values, $\mathbf{e}$, the inner loop is then executed a certain number of times, for different values of the aleatory parameters (denoted by $\mathbf{a}$), which are different for each modeling case. The purpose of the inner loop is to derive an "expectation" or average dose over aleatory uncertainty for each epistemic sample element $\mathbf{e}$. This expectation over aleatory uncertainty is the expected dose over multiple repository futures, each of which represents a different event sequence, conditional on the epistemic realization $\mathbf{e}$.

In most modeling cases, numerical integration (quadrature) is used to determine the expectation over aleatory uncertainty as a function of time, based on annual dose curves for specified values of event occurrence times and other aleatory variables. This is an analytical technique that does not require the use of a sampling methodology. For example, as illustrated schematically in Figure 2.4-8 for the 10,000-year seismic ground motion modeling case, 30 annual dose curves are produced for a combination of 6 event occurrence times and 5 possible damage areas. These are then integrated in two steps, to first give annual doses for specific event occurrence times but integrated over damage area, and secondly to give "expected annual dose" integrated over all aleatory uncertainty (in this case, event time and damage area). In contrast, the 1,000,000-year seismic ground motion modeling case employs a Monte Carlo sampling of aleatory parameters in the inner loop because of the large number of aleatory parameters and the complexity of submodel interactions. An expectation is then calculated over the finite set of annual dose curves corresponding to this Monte Carlo sampling of aleatory uncertainty. Also, the volcanic eruption modeling case employs a combination of Latin hypercube sampling and numerical integration in the inner aleatory loop for similar reasons. The expectation over aleatory uncertainty as a function of time (derived by quadrature and/or Monte Carlo sampling), for a given realization of the epistemically uncertain parameters, produces what is termed here an "expected annual dose curve." There are expected annual dose curves for each radionuclide and for the sum of all radionuclides. (Note: Aleatory uncertainty is not explicitly included in the calculation of the distribution of expected annual dose curves for the nominal modeling case. This will be explained in more detail in Section 2.4.2.1.5.)

The above process is repeated 300 times (the size of the Latin hypercube sample of epistemic parameters used in the TSPA). This produces a set of 300 expected annual dose curves, which represent the distribution of doses at each time τ based on epistemic uncertainty. To reiterate, each of the expected annual dose curves is an expectation over aleatory (irreducible or stochastic) uncertainty, which has effectively averaged out the aleatory variability (uncertainty attributable to random occurrences), such as the type and location of the intersected waste package or the random timing of igneous and seismic events in all possible futures.

The computational strategy illustrated schematically in Figure 2.4-8 is for a single modeling case. To compute the distribution of expected annual dose curves over all modeling cases (i.e., the distribution of total expected annual dose curves), the strategy shown in Figure 2.4-8 is repeated for each modeling case. This produces the set of 300 expected annual dose curves for each modeling case. These 300 projected annual dose histories for each modeling case are then summed across the six modeling cases, for corresponding elements in the epistemic sample, to give a distribution of 300 total expected annual dose histories. This methodology is illustrated in Figure 2.4-9 for scenario classes, but it is the same for the individual modeling cases that comprise the scenario classes.

As indicated in Figure 2.4-8, a variety of statistical measures are derived from (or superimposed on) the expected annual dose plots, including the mean, median, and 5th and 95th percentile curves. The mean annual dose curve or history is plotted as a red curve and computed by taking the arithmetic average or expectation of the 300 expected annual dose values at each time τ along the curves. Similarly, the median dose curve, plotted as a blue curve, is constructed by sorting the 300 expected values from lowest to highest at each time τ, and then averaging the two middle values. Curves for the 5th and 95th percentiles are also plotted to illustrate the uncertainty in the expected annual dose histories; 90% (or 270 of the 300 epistemic realizations) of the projected dose histories fall between these two percentile curves. For the first 10,000-year period after closure of the repository, as required by proposed 10 CFR 63.303 and 63.311, the actual "annual dose curve" referred to in Section 2.2.1.4 of NUREG-1804 is calculated to be the aforementioned arithmetic mean annual dose curve, while for post-10,000-year compliance, the median annual dose curve is calculated to determine compliance with the individual protection and human intrusion standards. The actual single value compliance metric in proposed 10 CFR 63.303 and proposed 10 CFR 63.311 (either 15 mrem/yr for 10,000-year compliance or 350 mrem/yr for post-10,000-year compliance) is either the maximum of the mean curve before 10,000 years or the maximum of the median curve after 10,000 years.

Within the TSPA computational structure a different calculational methodology is used to demonstrate compliance over the two periods of interest for the seismic ground motion modeling case (i.e., over the first 10,000 years after permanent closure and for the period from 10,000 years to 1,000,000 years after closure). Because of the rare occurrence of certain types of seismic consequences in the first 10,000 years, TSPA analyses have shown that it is unnecessary to include some seismic damage mechanisms in the total 10,000-year dose, since they make a negligible contribution to the dose from this modeling case (SNL 2008a, Section 7.3.2.6.1.3). For example, the failure of commercial SNF waste packages by seismic ground motion events is too rare in the first 10,000 years to significantly impact the expected dose for the seismic ground motion modeling case. Thus, only codisposal waste package failures contribute significantly to the expected annual dose of the seismic ground motion modeling case in the first 10,000 years after closure. However, for the post-10,000-year period, these various rare seismic consequences combined with the complex couplings between general corrosion and seismic degradation processes preclude the use of some of the simplifying techniques that can be applied for the 10,000-year seismic ground motion computations (SNL 2008a, Section 7.3.2.6.1.3). This necessitates the use of a Monte Carlo sampling method for the aleatory expectation in the post-10,000-year period, as mentioned above, rather than the numerical integration techniques. (Section 2.4.2.2.2.3 provides a complete listing of the rare seismic consequences that have a negligible effect on the 10,000-year annual dose.)

TSPA GoldSim Model File—The process models and model abstractions comprising the TSPA model are linked together in the GoldSim Model File, which is the object-oriented input file for the GoldSim software program. GoldSim is a system simulator that integrates all the submodels, codes, and abstractions together into a coherent structure that allows for the calculation of system response for a given random sampling of uncertain input variables. It includes a Monte Carlo looping structure that allows for multiple realizations of the inputs and outputs with one single execution of the program. GoldSim produces the realizations and associated annual dose curves in the inner computation loop of Figure 2.4-8.

Submodels are coupled into GoldSim by a variety of methods, from most complex to least complex, as follows:

- External function calls to detailed process software codes, such as the unsaturated-zone transport software, FEHM V. 2.24, or the waste-package degradation software, WAPDEG V. 4.07. These external subroutines are referred to as dynamically linked libraries (DLLs).

- Cell Elements in GoldSim that are basically equilibrium batch reactors, which when linked in series, provide a finite-difference description of radionuclide transport through selected parts of the repository system (such as the EBS); and Pipe Pathway Elements in GoldSim that simulate radionuclide transport using an analytical Laplace transform solution for flow and transport (such as the 1-D saturated-zone flow and transport submodel).

- Response surfaces, which take the form of multidimensional tables, representing the results of modeling with detailed process models that are run before running the TSPA model (e.g., inputs to the EBS environment model component, such as temperature and relative humidity of the waste package, which are derived from the multiscale thermal-hydrologic process model).

- Functional representations of a submodel directly built into the GoldSim code, such as waste form degradation models.

Much of the computational work for the TSPA model is done using separate software codes whose results are integrated within the GoldSim software as the aforementioned response surfaces, DLLs, lookup tables, and input distributions. For example, the unsaturated zone flow fields are computed using the software code Transport of Unsaturated Groundwater and Heat V1.6 (TOUGH2 V. 1.6). This is a three-dimensional, finite-volume numerical simulator, representing the entire unsaturated-zone model domain for the dual permeability site-scale unsaturated zone flow process model (SNL 2007b). Details of the calculation results using detailed process models are presented in the subsections of Section 2.3. Results of these detailed process-level calculations are provided to the TSPA model as multi-dimensional tables that are read into GoldSim at run time. Examples of these multi-dimensional tables include: (1) liquid flux and velocity fields for the unsaturated zone as a function of time, location, and infiltration flux; and (2) temperature and relative humidity of the waste package as a function of time and location within the repository.

EXDOC_LA—Once the GoldSim realizations are completed, the software code EXDOC_LA V 2.0 is used to calculate the expected annual dose curves for each of the modeling cases. Its overall purpose is to integrate over aleatory uncertainty to produce the expected annual dose histories, and to produce the summary metrics, such as the mean and median dose curves, shown in Figure 2.4-8. The GoldSim runs provide input to these expected dose calculations performed by EXDOC_LA V 2.0. In particular, the doses from GoldSim are integrated over the aleatory uncertainty, for fixed values of the epistemic parameters, to calculate an expected annual dose history, conditional on one epistemic element. This operation is repeated by EXDOC_LA for each epistemic sample, to obtain the entire suite of expected annual dose histories, described above. Statistics (i.e., mean, median, and percentiles) are calculated for these results. In order to produce representative output to be used as input to the EXDOC_LA V 2.0 calculations, the TSPA model in GoldSim is configured with separate sampling of epistemic and aleatory quantities. (Note: EXDOC_LA does not compute expected annual dose for the nominal modeling case because this quantity is computed by GoldSim itself, through its coupling to the waste package degradation software, WAPDEG.)

2.4.1.4 Summary of TSPA Model

In summary, the TSPA model is an integral part of the evaluation of the performance of the repository. This model incorporates the included FEPs (as described in Section 2.2), integrates the model abstractions used to describe these FEPs (as described in Section 2.3), and propagates the uncertainty and variability of parameters associated with these model abstractions to evaluate a range of possible beneficial and potentially adverse effects on repository performance. The performance measures evaluated in the TSPA model are the total mean (or median) annual dose to the RMEI (i.e., the individual protection standards in proposed 10 CFR 63.303, proposed 10 CFR 63.311, and proposed 10 CFR 63.321) and the level of radioactivity in the representative volume of groundwater (i.e., the groundwater protection standard in 10 CFR 63.331). The projection of these performance measures through time accounts for the uncertainties in data, parameters, and models identified in Section 2.3. The propagation of uncertainty results in distributions of both projected doses and projected levels of radioactivity in the groundwater. Although compliance is based on the total mean (or median) of the distributions of estimated expected annual doses and radioactivity (proposed 10 CFR 63.303), the development of these dose distributions aids in understanding the evolution of the repository system and the associated repository barriers (Section 2.4.2.3.3).

The TSPA model, in addition to being the quantitative tool for evaluating compliance with the postclosure performance standards presented in Sections 2.4.2, 2.4.3, and 2.4.4, is also the tool used to comply with the provisions in 10 CFR 63.115(b), which requires that uncertainties be taken into account in the modeling and behavior of barriers, and to address Acceptance Criterion 2(3) of Section 2.2.1.1.3 of NUREG-1804, which states that the capabilities of the barriers should be consistent with the TSPA. These evaluations have been presented in Section 2.1.2 for each of the three barriers: the Upper Natural Barrier, the EBS, and the Lower Natural Barrier. Complete details about the TSPA model, the TSPA method and approach, the TSPA computational structure, the scenario classes, and the TSPA results, validation, and analyses are described in *Total System Performance Assessment Model/Analysis for the License Application* (SNL 2008a).

2.4.1.5 Summary of TSPA Model Results

This section provides a brief summary of the results of the TSPA model calculations (Tables 2.4-2, 2.4-3, and 2.4-4), which shows that the estimated total mean and median annual doses and radioactivity are less than the levels required by proposed 10 CFR 63.303, proposed 10 CFR 63.311, proposed 10 CFR 63.321, and 10 CFR 63.331. The expected annual dose curves and activity curves that form the basis of the results in Tables 2.4-2, 2.4-3, and 2.4-4 are shown in Figure 2.4-10 for individual protection, Figure 2.4-11 for human intrusion, and Figures 2.4-12, 2.4-13, and 2.4-14 for groundwater protection.

2.4.2 Demonstration of Compliance with the Postclosure Individual Protection Standard

[NUREG-1804, Section 2.2.1.2.1.3: AC 3; Section 2.2.1.3.1.3: AC 1(2);
Section 2.2.1.3.2.3: AC 1(3); Section 2.2.1.3.3.3: AC 1(2), (5), (7);
Section 2.2.1.3.4.3: AC 1(2); Section 2.2.1.3.5.3: AC 1(3); Section 2.2.1.3.6.3: AC 1(3);
Section 2.2.1.3.7.3: AC 1(3); Section 2.2.1.3.8.3: AC 1(3); Section 2.2.1.3.9.3: AC 1(3);
Section 2.2.1.3.14.3: AC 1(3); Section 2.2.1.4.1.3: AC 1, AC 2, AC 3]

Section 2.4.2 provides information that addresses specific regulatory acceptance criteria contained in Section 2.2.1.4.1.3 of NUREG-1804. The information presented in this section also addresses performance objectives contained in 10 CFR 63.113(b) and proposed 10 CFR 63.311(a) relating to requirements for performance assessment at proposed 10 CFR 63.114(a) and (b) for the repository after permanent closure. The final dose results from the TSPA analyses for the individual protection standard are shown in Table 2.4-2.

2.4.2.1 Scenario Classes and Modeling Cases Used in the Calculation of Annual Dose *[NUREG-1804, Section 2.2.1.2.1.3: AC 3; Section 2.2.1.4.1.3: AC 1]*

A scenario is a well-defined, connected sequence of events and processes that describes a possible future of the repository system. A scenario class is a set of related scenarios that share sufficient similarities that they can usefully be aggregated for the purposes of screening and/or analysis. The objective of scenario class development for the TSPA (Section 2.2) is to define scenario classes that can be quantitatively analyzed while maintaining comprehensive coverage of the range of possible future states of the repository (SNL 2008a, Section 6.1.1). As discussed in Section 2.2.1, the identification and screening of FEPs for Yucca Mountain has resulted in four primary scenario classes in the TSPA analysis: nominal, early failure, igneous, and seismic.

This section focuses in detail on Steps 3 through 5 of the FEPs and scenario analysis process, as defined in Section 2.2.1, with emphasis on Step 5, which is the implementation of the scenario classes in the computational modeling for the TSPA. All FEPs screened in during the formal identification and screening for Step 1 and Step 2 are used for TSPA scenario class development and are incorporated into the retained scenario classes. For the purpose of scenario class formation (Step 3), features and processes generally are present in all possible repository futures. In contrast, the retained events (early failure, igneous, and seismic) may or may not occur (in the specified time span) in every future of the repository system. For this reason, scenario classes are distinguished by the retained events, while the features and processes are generally applicable across all scenario classes.

The primary purpose of Section 2.4.2.1 is to address Acceptance Criterion 1 of NUREG-1804, Section 2.2.1.4.1.3, "Scenarios Used in the Calculation of Annual Dose as a Function of Time Are Adequate:"

1. The annual dose as a function of time includes all scenario classes that have been determined to be sufficiently probable, or to have a sufficient effect on overall performance that they could not be screened from the total system performance assessment analyses; and

2. The calculation of the annual dose curve appropriately sums the contribution of each of the disruptive event scenario classes. The contribution to the annual dose from each scenario class calculation properly accounts for the effects that the time of occurrence of the disruptive events comprising the scenario class has on the consequences. The annual probability of occurrence of the events used to calculate the contribution to the annual dose is consistent with the results of the scenario analysis. The probabilities of occurrence of all scenario classes, included in calculating the annual dose curve, sum to one.

A secondary purpose of Section 2.4.2.1 is to address Acceptance Criterion 3 of NUREG-1804, Section 2.2.1.2.1.3, "Formation of Scenario Classes Using the Reduced Set of Events is Adequate:"

1. Scenario classes are mutually exclusive and complete, clearly documented, and technically acceptable.

This section first reviews the treatment of uncertainty in the TSPA model (Section 2.4.2.1.1), which is important to the computational methodology, and then discusses the calculation of the total mean and total median annual dose (Section 2.4.2.1.2), which are the quantities compared to the regulatory limits specified in 10 CFR 63.311. Next, this section describes how events and scenario classes are defined and used in the evaluation of total mean and total median annual dose (Section 2.4.2.1.3). This section then introduces an important additivity assumption for the calculation of total annual dose, that the dose resulting from a combination of events is the sum of the separate doses resulting from each of those events (Section 2.4.2.1.4). The use of modeling cases, which subdivide scenario classes for the purposes of computation, is then summarized, and calculations performed for each modeling case are outlined (Section 2.4.2.1.5). Next is a discussion of the probabilities of the event or scenario classes (Section 2.4.2.1.6), followed by a discussion that describes the amount of overestimation resulting from the application of the additivity assumption (Section 2.4.2.1.7). Finally, this section concludes with a summary of how the acceptance criteria listed above are addressed (Section 2.4.2.1.8).

2.4.2.1.1 Treatment of Aleatory and Epistemic Uncertainty

Section 2.4.1 introduced the four scenario classes for the TSPA model, which are formed from the event classes (Section 2.2.1.3.1). In order to indicate how the total annual dose curve is estimated from these scenario classes, it is necessary to first review how aleatory and epistemic uncertainties are defined and treated in the TSPA model.

In the TSPA model aleatory uncertainty is characterized by a set $\mathcal{A}$ of vectors $\mathbf{a}$, in which each vector $\mathbf{a} \in \mathcal{A}$ represents a possible future of the repository, and each element of the aleatory vector is a random variable that represents a specific property of the future $\mathbf{a}$ (e.g., number of waste package early failures, igneous event times, seismic event times). The elements of $\mathbf{a}$ vary among the scenario classes, as indicated in Table 2.4-5. Similarly, epistemic uncertainty is characterized by a set $\mathcal{E}$ of vectors $\mathbf{e}$ where each element of the vector $\mathbf{e}$ is a random variable that characterizes an uncertain model parameter (e.g., igneous occurrence rate, probability of early waste package failure, uncertainty in radionuclide solubility). Major categories of uncertainties characterized by $\mathbf{e}$ are indicated in Table 2.4-6. Mathematical descriptions of the vectors $\mathbf{a}$ and $\mathbf{e}$, the sets $\mathcal{A}$ and $\mathcal{E}$, and their corresponding probability spaces are provided in Appendix J, Sections J4.1 and J4.4, of *Total System Performance Assessment Model/Analysis for the License Application* (SNL 2008a).

The individual elements of $\mathbf{e}$ are described by probability distributions which conceptually leads to a density function $d_E(\mathbf{e})$ for $\mathcal{E}$. Similarly, the individual elements of the aleatory vector $\mathbf{a} \in \mathcal{A}$ are also described by probability distributions. However, the distributions for several of these elements are dependent on elements of the epistemic vector $\mathbf{e}$. Thus, the density function of the aleatory vector is expressed conditionally as $d_A(\mathbf{a}|\mathbf{e})$ to signify the dependence of $\mathbf{a}$ on $\mathbf{e}$.

In the TSPA model, elements of the aleatory vector $\mathbf{a}$ are those random variables associated with events and their consequences. Therefore, the aleatory vector is represented as $\mathbf{a} = (\mathbf{a}_S, \mathbf{a}_I, \mathbf{a}_{EF})$, where $\mathbf{a}_S$ denotes the vector elements of $\mathbf{a}$ that describe seismic events, $\mathbf{a}_I$ denotes the vector elements of $\mathbf{a}$ that describe igneous events, and $\mathbf{a}_{EF}$ denotes the vector elements of $\mathbf{a}$ that describe early-failure events. The three types of events are assumed to be independent of each other, which allows the aleatory density function to be written as the product of individual event density functions (i.e, $d_A(\mathbf{a}|\mathbf{e}) = d_S(\mathbf{a}_S|\mathbf{e})d_I(\mathbf{a}_I|\mathbf{e})d_{EF}(\mathbf{a}_{EF}|\mathbf{e})$). This partitioning of the elements of $\mathbf{a}$ is indicated in Table 2.4-5, which also indicates aleatory uncertainty associated with the nominal scenario class. However, this aleatory uncertainty in the nominal scenario class is not explicitly represented in the TSPA computational methodology, as described in Section 2.4.2.1.5.1.

2.4.2.1.2 Calculation of Total Mean and Median Annual Dose

The total annual dose at any time for a given future or realization is designated as a function of the epistemic and aleatory vectors, $D(\tau|\mathbf{a},\mathbf{e})$, and is dependent on time as indicated, as well as many other (nonstochastic) quantities (i.e., the number of emplaced waste packages, the probability that an eruptive conduit intersects the repository, etc.). The word "total" is used to indicate that total annual dose is the sum of contributions to annual dose from all scenario classes. The expected value of total annual dose conditional on epistemic uncertainty, $\bar{D}(\tau|\mathbf{e})$, where the expectation is taken over aleatory uncertainty, is defined as:

$$\bar{D}(\tau|\mathbf{e}) = \int_{\mathcal{A}} D(\tau|\mathbf{a},\mathbf{e})\, d_A(\mathbf{a}|\mathbf{e})\, dA \qquad \text{(Eq. 2.4-1)}$$

For convenience, this section uses the less cumbersome term "total expected annual dose" to refer to $\bar{D}(\tau|\mathbf{e})$; however, it is important to remember that this expectation is conditional on the epistemic vector. In particular, the TSPA model estimates total expected annual dose $\bar{D}(\tau|\mathbf{e}_i)$ for each vector $\mathbf{e}_i, i = 1, \ldots, N_E$, in a Latin hypercube sample of the epistemic parameters.

The total mean annual dose is defined as the expected value of annual dose, where the expectation is taken over both aleatory and epistemic uncertainty:

$$\begin{aligned}\bar{\bar{D}}(\tau) &= \int_{\mathcal{E}}\left(\int_{\mathcal{A}} D(\tau|\mathbf{a},\mathbf{e})\, d_A(\mathbf{a}|\mathbf{e})\, dA\right) d_E(\mathbf{e})\, dE \\ &= \int_{\mathcal{E}} \bar{D}(\tau|\mathbf{e})\, d_E(\mathbf{e})\, dE\end{aligned} \qquad \text{(Eq. 2.4-2)}$$

The TSPA calculation estimates the total mean annual dose using the sample mean of the estimates of the total expected annual dose $\bar{D}(\tau|\mathbf{e}_i), i = 1, \ldots, N_E$:

$$\bar{\bar{D}}(\tau) \cong \frac{1}{N_E}\sum_{i=1}^{N_E} \bar{D}(\tau|\mathbf{e}_i) \qquad \text{(Eq. 2.4-3)}$$

Total median annual dose, $Q_{E,0.5}[\bar{D}(\tau|\mathbf{e})]$, is the median of the distribution of total expected annual dose $\bar{D}(\tau|\mathbf{e})$ and is estimated as the sample median of the estimates of the total expected annual dose $\bar{D}(\tau|\mathbf{e}_i)$, $i = 1, \ldots, N_E$.

As specified in the proposed revision to 10 CFR 63.303 (70 FR 53313), total mean annual dose $\bar{\bar{D}}(\tau)$ is the quantity to be compared to the regulatory limit specified in proposed 10 CFR 63.311 for the period within 10,000 years after permanent closure, and total median annual dose $Q_{E,0.5}[\bar{D}(\tau|\mathbf{e})]$ is the quantity to be compared to the regulatory limit specified in proposed 10 CFR 63.311 for the post-10,000-year period after permanent closure. The calculation of total mean annual dose and total median annual dose is described in further detail in Appendix J, Sections J.4 and J.9 of *Total System Performance Assessment Model/Analysis for the License Application* (SNL 2008a), which presents the computational approach to the calculation of total mean and total median annual dose.

The primary reason for separating aleatory and epistemic uncertainty in the TSPA model is to enable the performance assessment to represent the uncertainty in the estimates of repository performance, as requested by the NRC and as incorporated in several acceptance criteria in NUREG-1804. Acceptance Criterion 2 of NUREG-1804, Section 2.2.1.4.1.3, contains an expectation that:

> 2. The annual dose curve includes confidence intervals (e.g., 95th and 5th percentile) to represent the uncertainty in dose calculations;

and Acceptance Criterion 3 of the same section contains an expectation that:

> 3. The estimate of the uncertainty in the performance assessment results is consistent with the model and parameter uncertainty.

By separating aleatory and epistemic uncertainty, it is possible to obtain estimates of expected dose, as well as assessments of the uncertainty in these estimates. The assessments of the uncertainty in expected dose allow meaningful statements to be made about the confidence that these estimates comply with the limits specified in the regulations.

The separation of aleatory and epistemic uncertainty greatly facilitates the performance of sensitivity analyses, such as those summarized in Sections 2.4.2.3.3 and 2.4.3.4.3, which address Acceptance Criterion 3(3), Sections 2.2.1.4.1.3 and 2.2.1.4.2.3, of NUREG-1804, respectively. Such sensitivity analyses provide important insights into system behavior and enable a demonstration that performance assessment results are consistent with parameter uncertainty.

The calculation of total mean and median annual dose requires computation of two intermediate quantities: total annual dose $D(\tau|\mathbf{a},\mathbf{e})$ and total expected annual dose $\bar{D}(\tau|\mathbf{e})$. Calculation of these quantities relies on definitions of event and scenario classes, which are discussed next. Section 2.4.2.1.4 then describes the calculation of these intermediate quantities.

2.4.2.1.3 Event and Scenario Classes

There are three types of events that are included in the TSPA calculations (Section 2.2), namely early failures, seismic events and igneous events. Of the three event types, two correspond to future disruptive events, namely seismic or igneous disruptions. These two types of futures are characterized by the type of disruption or damage caused to the EBS components—in particular, the waste packages, drip shields, and/or emplacement drifts. Impacts to either the Upper or Lower Natural Barriers are screened out. A third type of event, which is designated by its own scenario class, is an early failure event. This event represents the failure of one or more waste packages and/or drip shields at the time of closure of the repository. The grouping of repository futures into scenario classes based on seismic and igneous events is consistent with the requirements of proposed 10 CFR 63.342, which requires the DOE to consider the effects of seismic and igneous damage to the drift and waste packages.

In NUREG-1804 (glossary), a scenario is defined as:

> ...a well-defined, connected sequence of features, events, and processes that can be thought of as an outline of a possible future condition of the potential repository system. Scenarios can be undisturbed, in which case the performance would be the expected, or nominal, behavior for the system. Scenarios can also be disturbed, if altered by disruptive events such as human intrusion or natural phenomena such as volcanism or nuclear criticality.

Thus, by this definition, each possible future of the repository can be thought of as a scenario. However, because the term "scenario" has many other meanings in a variety of contexts, the term "scenario" will not be used in Section 2.4 to refer to a repository future. It will only occasionally be used to define certain subsets of FEPs appearing in a repository future, such as the infiltration FEPs (i.e., the "infiltration scenario"), the biosphere exposure FEPs (i.e., "the exposure scenario"), or the thermal characteristics of the host rock. Instead, the reference to a repository future will always be in terms of its specific aleatory and epistemic characteristics, $(\mathbf{a}, \mathbf{e})$. A scenario or future also corresponds to what is usually referred to as an elementary event in the standard terminology of probability theory.

In NUREG-1804 (glossary), a scenario class is defined as:

> ...a set of related scenarios sharing sufficient similarities that they can usefully be aggregated for the purposes of screening or analysis. The number and breadth of scenario classes depend on the resolution at which scenarios have been defined. Coarsely defined scenarios result in fewer, broad scenario classes, whereas narrowly defined scenarios result in many narrow scenario classes. Scenario classes (and scenarios) should be aggregated at the coarsest level at which a technically sound argument can be made while still retaining adequate detail for the purposes of the analysis.

Thus, a scenario class in the TSPA will designate a special subset or group of repository futures sharing common characteristics—in particular, a common type of event. A scenario class corresponds to what is usually referred to as an event in the standard terminology of probability theory. However, as used in Section 2.4, the term "event" always refers to a physical event modeled in the TSPA.

In 10 CFR 63.102(j) an event class is defined to consist "…of all possible specific initiating events that are caused by a common natural process (e.g., the event class for seismicity includes the range of credible earthquakes for the Yucca Mountain site)." For the purposes of analyses, event classes need not be limited to aggregation of initiating events by a common natural process; event classes can be the aggregation of initiating events by any common characteristic. For example, early waste package failures and early drip shield failures are aggregated into the early failure event class. Event classes are the most basic type of scenario class, with common characteristics that can be usefully aggregated for the purposes of screening or analysis.

An event class is thus a specific type of scenario class that is defined by the inclusion (or exclusion) of particular event types. There are four event classes that are included in the TSPA. There are three event classes that include all futures related to distinct types of event occurrences: early failure, igneous, and seismic. Additionally, one event class (the nominal event class) comprises the set of futures with no igneous, seismic, or early-failure occurrences. It should also be noted that event classes allow further division into more narrowly defined subsets referred to as modeling cases (Section 2.4.2.1.5), which are useful in the TSPA computational scheme (e.g., the two igneous modeling cases, intrusion and eruption, are based on the fact that the set of futures corresponding to the igneous event class can have igneous intrusion with or without a volcanic eruption intersecting the repository drifts). Figure 2.4-15 illustrates the four event classes.

Scenario classes corresponding to each event class can be formally defined in terms of elements of the aleatory vector $\mathbf{a}$. The mathematical structure of this vector (SNL 2008a, Appendix J, Section J4.4) includes terms that count the number of events that occur in a future $\mathbf{a}$, and allow formal definition of the scenario class corresponding to each event class listed above. These terms are the number of early failures (*nEW* for waste packages and *nED* for drip shields), number of igneous events (*nII*), and the number of seismic events (*nSG* for ground motion events and *nSF* for fault displacement events). These elements of $\mathbf{a}$ are used to define three subsets of $\mathcal{A}$ corresponding to the occurrence of each class of event, and one subset of $\mathcal{A}$ in which no events occur:

- **Early-failure scenario class** $\mathcal{A}_E = \{\mathbf{a}\text{: } nEW \geq 1 \text{ or } nED \geq 1\}$: The set of futures each of which includes one or more early failures (i.e., one or more early-failed waste packages and/or one or more early-failed drip shields)

- **Igneous scenario class** $\mathcal{A}_I = \{\mathbf{a}\text{: } nII \geq 1\}$: The set of futures each of which includes one or more igneous events

- **Seismic scenario class** $\mathcal{A}_S = \{\mathbf{a}\text{: } nSG \geq 1 \text{ or } nSF \geq 1\}$: The set of futures each of which includes one or more seismic events (ground motion or fault displacement)

- **Nominal scenario class** $\mathcal{A}_N = \{\mathbf{a}\text{:} nEW = nED = nII = nSG = nSF = 0\}$: The set of futures in which no early failures or events (seismic or igneous) occur.

The nominal scenario class should not be confused with the occurrence of nominal processes (e.g., corrosion processes, such as general corrosion, localized corrosion, and stress corrosion cracking). Nominal processes occur in all futures of the repository, and in all scenario classes, and thus contribute to total annual dose for all futures. In contrast, the nominal scenario class represents repository behavior for futures in which nominal processes are the only cause of damage or degradation to the EBS.

Although the events that define the early failure, seismic and igneous scenario classes are independent of each other, the resulting three scenario classes are not mutually exclusive because a future may include more than one type of event. For example, it is possible to conceive of a repository future in which an early failure occurs and a seismic event occurs; thus, this future is an element of both $\mathcal{A}_E$ and $\mathcal{A}_S$. Thus, the scenario classes shown in Figure 2.4-15 overlap.

Due to the complexity of $D(\tau|\mathbf{a}, \mathbf{e})$, evaluation of the integral in Equation 2.4-1 requires that the set of all futures $\mathcal{A}$ be divided into subsets, for which the integral can be numerically evaluated. Accordingly, the four scenario classes are used to divide the full set of repository futures $\mathcal{A}$ into eight subsets that are mutually exclusive, termed disjoint scenario classes. The partitioning of $\mathcal{A}$ into mutually exclusive subsets is intentional in order to demonstrate how the calculation of total annual dose satisfies Acceptance Criterion 3 of NUREG-1804, Section 2.2.1.2.1.3.

The disjoint scenario classes are based on the intersections of the scenario classes defined above. For n independent event types there are 2^n disjoint scenario classes (e.g., in the case of $n = 3$ for the igneous, seismic, and early failure event types, there are $2^3 = 8$ disjoint scenario classes). Of the eight disjoint scenario classes, seven include futures with one or more of the three types of events (igneous, seismic, or early-failure), and the eighth is the complement of the union of the other seven and is synonymous with the nominal scenario class. It is the set of futures with no event occurrences. Figure 2.4-16 illustrates the set of repository futures partitioned into the eight disjoint scenario classes or subsets. All of the disjoint scenario classes include nominal processes:

- **Early-failure disjoint scenario class**, S_{EF}: The set of futures that includes early-failure events (i.e., one or more early-failed waste packages and/or one or more early-failed drip shields), but no seismic or igneous events.

- **Igneous disjoint scenario class**, S_I: The set of futures each of which includes igneous events, but no seismic or early-failure events.

- **Early-failure/Igneous disjoint scenario class**, S_{EF+I}: The set of futures that includes igneous events and early-failure events, but no seismic events.

- **Seismic disjoint scenario class**, S_S: The set of futures each of which includes seismic events, but no igneous or early-failure events.

- **Early-failure/Seismic disjoint scenario class**, S_{EF+S}: The set of futures that includes seismic events and early-failure events, but no igneous events.

- **Igneous/Seismic disjoint scenario class**, S_{I+S}: The set of futures that includes seismic events and igneous events, but no early failures.

- **Early-failure/Igneous/Seismic disjoint scenario class**, S_{EF+I+S}: The set of futures that includes seismic events and igneous events and early-failure events.

- **Nominal disjoint scenario class**, S_N: The set of futures in which no events occur (i.e., no seismic events, no igneous events, and no early failure events).

The nominal disjoint scenario class excludes the occurrence of any events, and thus does not depend on any of the aleatory uncertainties that describe events. The nominal disjoint scenario class does address other types of aleatory uncertainty (e.g., describing the time, location and extent of damage to waste packages caused by corrosion processes). However, these are implicitly included in the calculation of annual dose, and are therefore not indicated explicitly in the following discussion. The nominal disjoint scenario class and the nominal scenario class are identical.

The eight sets of futures defined above partition the set of all futures of the repository into a collection of disjoint sets. Because the union of the eight sets equals all of $\mathcal{A}$, and the eight sets are disjoint, the probabilities associated with each of the eight sets sum exactly to one, as contemplated by Acceptance Criterion 1(2) in NUREG-1804, Section 2.2.1.4.1.3. These eight mutually exclusive sets form the basis for the evaluation of total expected annual dose, as described in the next section.

2.4.2.1.4 Total Expected Annual Dose Approximations

The total expected annual dose $\bar{D}(\tau|\mathbf{e})$ is defined by Equation 2.4-1 as the expectation over aleatory uncertainty of total annual dose $D(\tau|\mathbf{a},\mathbf{e})$. The following sections outline how this expectation is evaluated. To evaluate total expected annual dose, total annual dose is first approximated as the sum of contributions to total annual dose from each type of event. In particular, the annual dose, arising from the future behavior of all processes occurring in a given future, is separated into several parts representing the incremental or additional dose caused by a particular class of events, e.g., the incremental or additional dose arising from the occurrence of early failures. Next, the expectation over aleatory uncertainty of this approximation to total annual dose is expressed as a sum of integrals over each of the eight disjoint scenario classes. Finally, the terms in this sum are aggregated into integrals of the additional dose terms over each of the four primary scenario classes, as a means of simplifying the calculation of total expected annual dose.

Total Annual Dose Approximation for the First 10,000-Years—For an arbitrary future $\mathbf{a}$ and a given epistemic realization $\mathbf{e}$, the total annual dose for the first 10,000 years after disposal is approximated as the sum of dose resulting from nominal processes and additional dose resulting from events (SNL 2008a, Eq. 6.1.2 1):

$$D(\tau|\mathbf{a},\mathbf{e}) \cong D_N(\tau|\mathbf{e}) + D_S(\tau|\mathbf{a},\mathbf{e}) + D_I(\tau|\mathbf{a},\mathbf{e}) + D_{EF}(\tau|\mathbf{a},\mathbf{e}) \qquad \text{(Eq. 2.4-4)}$$

where

$D_N(\tau\vert\mathbf{e})$	dose (mrem/yr) at time τ resulting from nominal processes
$D_{EF}(\tau\vert\mathbf{a},\mathbf{e})$	additional dose (mrem/yr) at time τ resulting from any early failures occurring in the future $\mathbf{a}$
$D_I(\tau\vert\mathbf{a},\mathbf{e})$	additional dose (mrem/yr) at time τ resulting from any igneous events occurring in the future $\mathbf{a}$
$D_S(\tau\vert\mathbf{a},\mathbf{e})$	additional dose (mrem/yr) at time τ resulting from any seismic events occurring in the future $\mathbf{a}$.

Because the aleatory variables described by $\mathbf{a}$ involve only the occurrence of events and early failures, $D_N(\tau|\mathbf{e})$ does not depend on $\mathbf{a}$.

The approximation in Equation 2.4-4 relies on the simplifying assumption that the dose resulting from a combination of events is the sum of the doses resulting from each separate event. For example, this simplifying assumption, referred to as the additivity assumption, allows the TSPA model to approximate the dose from a future involving a combination of events, such as a seismic event followed by an igneous intrusion, as the sum of the doses calculated by considering the seismic event and the igneous event separately. Effectively, this assumption implies that the consequences of different classes of events (e.g., igneous and seismic) are not synergistic; thus, it is also referred to as the no-synergisms assumption. In general, this method of approximation affects the TSPA results in a conservative fashion, by overestimating the total expected annual dose. This assumption is justified in more detail in Section 2.4.2.1.7, which describes the amount of overestimation resulting from the application of this additivity assumption for each of the eight disjoint subsets.

Next, the integral in Equation 2.4-1 is separated into a sum of eight integrals over the separate disjoint sets $\{S_{EF}, S_I, S_S, S_{EF+I}, S_{EF+S}, S_{I+S}, S_{EF+I+S}, S_N\}$:

$$
\begin{aligned}
\bar{D}(\tau\,|\,\mathbf{e}) &= \int_{\mathcal{A}} D(\tau\,|\,\mathbf{a},\mathbf{e})\,d_A(\mathbf{a}\,|\,\mathbf{e})\,dA \\
&= \int_{\bigcup\limits_J S_J} D(\tau\,|\,\mathbf{a},\mathbf{e})\,d_A(\mathbf{a}\,|\,\mathbf{e})\,dA \\
&= \int_{S_N} D(\tau\,|\,\mathbf{a},\mathbf{e})\,d_A(\mathbf{a}\,|\,\mathbf{e})\,dA + \int_{S_{EF}} D(\tau\,|\,\mathbf{a},\mathbf{e})\,d_A(\mathbf{a}\,|\,\mathbf{e})\,dA \\
&\quad + \int_{S_I} D(\tau\,|\,\mathbf{a},\mathbf{e})\,d_A(\mathbf{a}\,|\,\mathbf{e})\,dA + \int_{S_S} D(\tau\,|\,\mathbf{a},\mathbf{e})\,d_A(\mathbf{a}\,|\,\mathbf{e})\,dA \\
&\quad + \int_{S_{EF+I}} D(\tau\,|\,\mathbf{a},\mathbf{e})\,d_A(\mathbf{a}\,|\,\mathbf{e})\,dA + \int_{S_{EF+S}} D(\tau\,|\,\mathbf{a},\mathbf{e})\,d_A(\mathbf{a}\,|\,\mathbf{e})\,dA \\
&\quad + \int_{S_{I+S}} D(\tau\,|\,\mathbf{a},\mathbf{e})\,d_A(\mathbf{a}\,|\,\mathbf{e})\,dA + \int_{S_{EF+I+S}} D(\tau\,|\,\mathbf{a},\mathbf{e})\,d_A(\mathbf{a}\,|\,\mathbf{e})\,dA
\end{aligned}
$$

(Eq. 2.4-5)

where, for convenience in the presentation, $J = 1,2,\ldots,8$ is introduced as an index to the collection $\{S_J\}$ of the eight disjoint sets $\{S_{EF}, S_I, S_S, S_{EF+I}, S_{EF+S}, S_{I+S}, S_{EF+I+S}, S_N\}$.

Equation 2.4-4 and Equation 2.4-5 are combined to obtain:

$$
\begin{aligned}
\bar{D}(\tau|\mathbf{e}) &= \int_{\bigcup_J S_J} D(\tau\,|\,\mathbf{a},\mathbf{e})\, d_A(\mathbf{a}\,|\,\mathbf{e})\, dA \\
&\cong \int_{\bigcup_J S_J} \left(D_N(\tau\,|\,\mathbf{e}) + D_{EF}(\tau\,|\,\mathbf{a},\mathbf{e}) + D_I(\tau\,|\,\mathbf{a},\mathbf{e}) + D_S(\tau\,|\,\mathbf{a},\mathbf{e})\right) d_A(\mathbf{a}\,|\,\mathbf{e})\, dA \\
&\cong \int_{\bigcup_J S_J} D_N(\tau\,|\,\mathbf{e})\, d_A(\mathbf{a}\,|\,\mathbf{e})\, dA + \int_{\bigcup_J S_J} D_{EF}(\tau\,|\,\mathbf{a},\mathbf{e})\, d_A(\mathbf{a}\,|\,\mathbf{e})\, dA \\
&\quad + \int_{\bigcup_J S_J} D_I(\tau\,|\,\mathbf{a},\mathbf{e})\, d_A(\mathbf{a}\,|\,\mathbf{e})\, dA + \int_{\bigcup_J S_J} D_S(\tau\,|\,\mathbf{a},\mathbf{e})\, d_A(\mathbf{a}\,|\,\mathbf{e})\, dA
\end{aligned}
$$

(Eq. 2.4-6)

Consider first the integral involving $D_{EF}(\tau|\mathbf{a}, \mathbf{e})$. If a future $\mathbf{a}$ does not include any early failure events, there is no additional dose that can result from early failure. Thus, the quantity $D_{EF}(\tau|\mathbf{a}, \mathbf{e})$ is zero for any future $\mathbf{a}$ that does not include any early failure events. Using this observation, the term in Equation 2.4-6 that involves $D_{EF}(\tau|\mathbf{a}, \mathbf{e})$ is expanded as:

$$
\begin{aligned}
\int_{\bigcup_J S_J} D_{EF}(\tau\,|\,\mathbf{a},\mathbf{e})\, d_A(\mathbf{a})\, dA &= \sum_J \int_{S_J} D_{EF}(\tau\,|\,\mathbf{a},\mathbf{e})\, d_A(\mathbf{a}\,|\,\mathbf{e})\, dA \\
&= \int_{S_{EF}} D_{EF}(\tau\,|\,\mathbf{a},\mathbf{e})\, d_A(\mathbf{a}\,|\,\mathbf{e})\, dA + \int_{S_{EF+I}} D_{EF}(\tau\,|\,\mathbf{a},\mathbf{e})\, d_A(\mathbf{a}\,|\,\mathbf{e})\, dA \\
&\quad + \int_{S_{EF+S}} D_{EF}(\tau\,|\,\mathbf{a},\mathbf{e})\, d_A(\mathbf{a}\,|\,\mathbf{e})\, dA + \int_{S_{EF+I+S}} D_{EF}(\tau\,|\,\mathbf{a},\mathbf{e})\, d_A(\mathbf{a}\,|\,\mathbf{e})\, dA
\end{aligned}
$$

(Eq. 2.4-7)

because $D_{EF}(\tau|\mathbf{a}, \mathbf{e})$ is zero on each of the sets $\{S_I, S_S, S_{I+S}, S_N\}$. Finally, by using the definitions of the early-failure scenario class, $\mathcal{A}_E$, and the eight disjoint scenario sets, $\{S_{EF}, S_I, S_S, S_{EF+I}, S_{EF+S},$

S_{I+S}, S_{EF+I+S}, $S_N\}$, the scenario class $\mathcal{A}_E$ is expressed as a union of disjoint scenario sets, $\mathcal{A}_E = S_{EF} \cup S_{EF+I} \cup S_{EF+S} \cup S_{EF+I+S}$. Equation 2.4-7 becomes:

$$\begin{aligned}
&\int_{S_{EF}} D_{EF}(\tau \mid \mathbf{a},\mathbf{e})\, d_A(\mathbf{a} \mid \mathbf{e})\, dA + \int_{S_{EF+I}} D_{EF}(\tau \mid \mathbf{a},\mathbf{e})\, d_A(\mathbf{a} \mid \mathbf{e})\, dA \\
&\quad + \int_{S_{EF+S}} D_{EF}(\tau \mid \mathbf{a},\mathbf{e})\, d_A(\mathbf{a} \mid \mathbf{e})\, dA + \int_{S_{EF+I+S}} D_{EF}(\tau \mid \mathbf{a},\mathbf{e})\, d_A(\mathbf{a} \mid \mathbf{e})\, dA \\
&\qquad = \int_{S_{EF} \cup S_{EF+I} \cup S_{EF+S} \cup S_{EF+I+S}} D_{EF}(\tau \mid \mathbf{a},\mathbf{e})\, d_A(\mathbf{a} \mid \mathbf{e})\, dA \\
&\qquad = \int_{\mathcal{A}_E} D_{EF}(\tau \mid \mathbf{a},\mathbf{e})\, d_A(\mathbf{a} \mid \mathbf{e})\, dA \\
&\qquad = \bar{D}_{EF}(\tau \mid \mathbf{e})
\end{aligned}$$

(Eq. 2.4-8)

where $\bar{D}_{EF}(\tau|\mathbf{e})$ is the contribution to total expected annual dose attributable to early failures. Similar sequences of operations lead to the following expressions for the contributions to total expected annual dose from igneous events, $\bar{D}_I(\tau|\mathbf{e})$, and from seismic events, $\bar{D}_S(\tau|\mathbf{e})$:

$$\bar{D}_I(\tau|\mathbf{e}) = \int_{\mathcal{A}_I} D_I(\tau|\mathbf{a}, \mathbf{e})\, d_A(\mathbf{a}|\mathbf{e})\, dA \qquad \text{(Eq. 2.4-9)}$$

$$\bar{D}_S(\tau|\mathbf{e}) = \int_{\mathcal{A}_S} D_S(\tau|\mathbf{a}, \mathbf{e})\, d_A(\mathbf{a}|\mathbf{e})\, dA \qquad \text{(Eq. 2.4-10)}$$

where

$\mathcal{A}_I = S_I \cup S_{EF+I} \cup S_{I+S} \cup S_{EF+I+S}$	is the igneous scenario class.
$\bar{D}_I(\tau\|\mathbf{e})$	is the contribution to total expected annual dose due to igneous events.
$\mathcal{A}_S = S_S \cup S_{EF+S} \cup S_{I+S} \cup S_{EF+I+S}$	is the seismic scenario class.
$\bar{D}_S(\tau\|\mathbf{e})$	is the contribution to total expected annual dose due to seismic events.

The final quantity required for calculation of total expected annual dose is the expected value of the dose at time τ resulting from nominal processes, $D_N(\tau|\mathbf{e})$. Nominal processes describe waste package and drip shield degradation processes occurring at all times (as well as the other screened-in nominal thermal, hydrologic, mechanical, and chemical processes), regardless of igneous, seismic, or early-failure occurrence. Consequently, these processes occur in all futures of the repository. The contribution to total dose attributed to these processes is approximated by the dose $D_N(\tau|\mathbf{e})$ for the nominal scenario class (i.e., for the set of futures which include no events). Because the nominal scenario class excludes the occurrence of any events, the quantity $D_N(\tau|\mathbf{e})$ does not depend on any of the aleatory uncertainties described by $\mathbf{a}$.

Finally, using the results of Equation 2.4-8 through Equation 2.4-10, Equation 2.4-6 can be written as

$$\begin{aligned}
\bar{D}(\tau\,|\,\mathbf{e}) &= \int_{\bigcup_J S_J} D_N(\tau\,|\,\mathbf{a},\mathbf{e})\,d_A(\mathbf{a}\,|\,\mathbf{e})\,dA + \int_{\bigcup_J S_J} D_{EF}(\tau\,|\,\mathbf{a},\mathbf{e})\,d_A(\mathbf{a}\,|\,\mathbf{e})\,dA \\
&\quad + \int_{\bigcup_J S_J} D_I(\tau\,|\,\mathbf{a},\mathbf{e})\,d_A(\mathbf{a}\,|\,\mathbf{e})\,dA + \int_{\bigcup_J S_J} D_S(\tau\,|\,\mathbf{a},\mathbf{e})\,d_A(\mathbf{a}\,|\,\mathbf{e})\,dA \\
&\cong \int_{\mathcal{A}} D_N(\tau\,|\,\mathbf{a},\mathbf{e})\,d_A(\mathbf{a}\,|\,\mathbf{e})\,dA + \int_{\mathcal{A}_{EF}} D_{EF}(\tau\,|\,\mathbf{a},\mathbf{e})\,d_A(\mathbf{a}\,|\,\mathbf{e})\,dA \\
&\quad + \int_{\mathcal{A}_I} D_I(\tau\,|\,\mathbf{a},\mathbf{e})\,d_A(\mathbf{a}\,|\,\mathbf{e})\,dA + \int_{\mathcal{A}_S} D_S(\tau\,|\,\mathbf{a},\mathbf{e})\,d_A(\mathbf{a}\,|\,\mathbf{e})\,dA \\
&\cong D_N(\tau\,|\,\mathbf{e}) + \bar{D}_{EF}(\tau\,|\,\mathbf{e}) + \bar{D}_I(\tau\,|\,\mathbf{e}) + \bar{D}_S(\tau\,|\,\mathbf{e})
\end{aligned}$$

(Eq. 2.4-11)

The preceding expectation process is illustrated schematically in Figure 2.4-9 (also Figure 2.4-8).

In summary, the total expected annual dose for the first 10,000 years is approximated as the sum of the expected annual doses for the four scenario classes:

$$\bar{D}(\tau|\mathbf{e}) \cong D_N(\tau|\mathbf{e}) + \bar{D}_{EF}(\tau|\mathbf{e}) + \bar{D}_I(\tau|\mathbf{e}) + \bar{D}_S(\tau|\mathbf{e})$$ (Eq. 2.4-12)

The TSPA model does not use the disjoint scenario classes explicitly in the calculation of expected annual dose. Rather, as described in *Total System Performance Assessment Model/Analysis for the License Application* (SNL 2008a, Section 6.1.2.4), the expected annual dose for each of the four scenario classes (i.e., $D_N(\tau|\mathbf{e})$, $\bar{D}_{EF}(\tau|\mathbf{e})$, $\bar{D}_S(\tau|\mathbf{e})$, and $\bar{D}_I(\tau|\mathbf{e})$) is computed by integrating annual dose over the given scenario class ($\mathcal{A}_N$, $\mathcal{A}_{EF}$, $\mathcal{A}_S$, or $\mathcal{A}_I$) to obtain the quantities identified in Equation 2.4-12. As implemented in the GoldSim and EXDOC_LA software, calculation of expected annual dose is evaluated by means of modeling cases (Section 2.4.2.1.5) which further subdivide each of the scenario classes for a more computationally efficient implementation. *Total System Performance Assessment Model/Analysis for the License Application* (SNL 2008a, Section 6.1.2.4 and Appendix J) describes in further detail the calculation of each term in Equation 2.4-12.

Equation 2.4-12 can also be obtained directly from the expectation over aleatory uncertainty ($E_{\mathcal{A}}$) of the total annual dose defined in Equation 2.4-4:

$$\begin{aligned}\bar{D}(\tau|\mathbf{e}) &= E_{\mathcal{A}}[D(\tau|\mathbf{a},\mathbf{e})]\\ &\cong E_{\mathcal{A}}[D_N(\tau|\mathbf{e}) + D_{EF}(\tau|\mathbf{a},\mathbf{e}) + D_I(\tau|\mathbf{a},\mathbf{e}) + D_S(\tau|\mathbf{a},\mathbf{e})]\\ &\cong D_N(\tau|\mathbf{e}) + \bar{D}_{EF}(\tau|\mathbf{e}) + \bar{D}_I(\tau|\mathbf{e}) + \bar{D}_S(\tau|\mathbf{e})\end{aligned} \qquad \text{(Eq. 2.4-13)}$$

However, the development of Equation 2.4-12 by means of disjoint scenario classes explicitly demonstrates how the TSPA addresses Acceptance Criterion 1(2) in NUREG-1804, Section 2.2.1.4.1.3.

Total Annual Dose Approximation for the Post-10,000 Year Period—Total annual dose is approximated by Equation 2.4-4 for the 10,000-year period after disposal. However, for the post-10,000-year period calculations, a different approximation is required because of the interactions of nominal and seismic processes and the relatively high probability that seismic damage occurs (Section 2.4.2.1.6). For these reasons it is not practical to separate the contributions to total annual dose from nominal processes and seismic events.

Consequently, for the post-10,000-year period, total annual dose at time τ is approximated as:

$$D(\tau|\mathbf{a},\mathbf{e}) \cong D_{N+S}(\tau|\mathbf{a},\mathbf{e}) + D_{EF}(\tau|\mathbf{a},\mathbf{e}) + D_I(\tau|\mathbf{a},\mathbf{e}) \qquad \text{(Eq. 2.4-14)}$$

where

$D_{N+S}(\tau\|\mathbf{a},\mathbf{e})$	dose (mrem/yr) at time τ resulting from the combined effect of nominal processes and seismic events occurring in the future $\mathbf{a}$
$D_{EF}(\tau\|\mathbf{a},\mathbf{e})$	additional dose (mrem/yr) at time τ resulting from any early failures occurring in the future $\mathbf{a}$
$D_I(\tau\|\mathbf{a},\mathbf{e})$	additional dose (mrem/yr) at time τ resulting from any igneous events occurring in the future $\mathbf{a}$

Because futures involving seismic events are not differentiated from futures involving nominal processes, the set of eight disjoint scenario classes collapses to four ($2^2 = 4$) disjoint scenario classes for the post-10,000-year dose calculation (Figure 2.4-17; SNL 2008a, Section 8.1.1). Additional discussion regarding the validity of the total annual dose approximation for the post-10,000-year period is given in Section 2.4.2.1.7.4.

The sequence of operations outlined in Equations 2.4-5 through 2.4-11 is applied to the total annual dose approximation for the post-10,000-year period (Equation 2.4-14) to obtain the total expected annual dose for the post-10,000-year period based on disjoint sets in terms of the nondisjoint scenario classes:

$$\overline{D}(\tau|\mathbf{e}) \cong \overline{D}_{N+S}(\tau|\mathbf{e}) + \overline{D}_{I}(\tau|\mathbf{e}) + \overline{D}_{EF}(\tau|\mathbf{e}) \qquad \text{(Eq. 2.4-15)}$$

Analogous to the first 10,000-year period, the total expected annual dose can be written as the sum of the expected annual dose for three scenario classes defined by three event classes: the combination of nominal processes and seismic events, early failures, and igneous events (SNL 2008a, Section 8.1.1). As implemented in the GoldSim and EXDOC_LA software, calculation of expected annual dose is evaluated by means of modeling cases (Section 2.4.2.1.5) which further subdivide each of the scenario classes for a more computationally efficient implementation. *Total System Performance Assessment Model/Analysis for the License Application* (SNL 2008a, Section 6.1.2.4 and Appendix J) describes in further detail the calculation of each term in Equation 2.4-15.

2.4.2.1.5 Modeling Cases

For the purpose of estimating expected annual dose, each of the scenario classes is further divided into smaller scenario classes, each of which represents the dose resulting from the occurrence of a particular type of event. For convenience, these scenario classes are termed “modeling cases” to distinguish them from the four scenario classes defined for each of the four event classes. In calculating Equations 2.4-12 and 2.4-15, the terms on the right-hand side are subdivided, because each scenario class includes two distinct types of event occurrences whose sets of futures are subsets of the parent scenario class:

- **Early-failure Scenario Class**—Early-failed waste packages (EW) and early-failed drip shields (ED)
- **Igneous Scenario Class**—Igneous intrusions (II) events and volcanic eruptions (VE)
- **Seismic Scenario Class**—Seismic ground motion (GM) events and fault displacement (FD) events.

Modeling cases are based on this set of six types of event occurrences, which in turn describe specific modes of waste package degradation or radionuclide transport. As shown in *Total System Performance Assessment Model/Analysis for the License Application* (SNL 2008a, Sections J4.4 and J4.5), it is possible to construct a set of nondisjoint scenario classes around the aforementioned six types of distinct event occurrences, similar to the construction shown in Section 2.4.2.1.3, and to express the total expected dose as the sum of the expected dose for each of these six scenario classes and the nominal scenario class. Thus, for the purposes of this discussion on modeling cases, the calculation of additional dose for the three parent scenario classes is understood to be subdivided into two sets of calculations for each parent scenario class.

While the dose for the nominal scenario class consists of only one term, the other terms in Equation 2.4-12 are each the sum of two terms representing the dose for the corresponding modeling cases within the scenario class. Specifically, the expected additional annual doses for the 10,000 year period after disposal for the early failure, igneous, and seismic scenario classes, given $\mathbf{e}$, are computed as:

$$\bar{D}_{EF}(\tau|\mathbf{e}) \cong \bar{D}_{EW}(\tau|\mathbf{e}) + \bar{D}_{ED}(\tau|\mathbf{e}) \qquad \text{(Eq. 2.4-16)}$$

$$\bar{D}_{I}(\tau|\mathbf{e}) \cong \bar{D}_{II}(\tau|\mathbf{e}) + \bar{D}_{VE}(\tau|\mathbf{e}) \qquad \text{(Eq. 2.4-17)}$$

$$\bar{D}_{S}(\tau|\mathbf{e}) \cong \bar{D}_{SG}(\tau|\mathbf{e}) + \bar{D}_{SF}(\tau|\mathbf{e}) \qquad \text{(Eq. 2.4-18)}$$

where the terms $\bar{D}_{EW}(\tau|\mathbf{e})$ and $\bar{D}_{ED}(\tau|\mathbf{e})$ are the expected annual dose estimates for the waste package and drip shield early failure modeling cases, respectively; $\bar{D}_{II}(\tau|\mathbf{e})$ and $\bar{D}_{VE}(\tau|\mathbf{e})$ are the expected annual dose estimates for the igneous intrusion and volcanic eruption modeling cases, respectively; and $\bar{D}_{SG}(\tau|\mathbf{e})$ and $\bar{D}_{SF}(\tau|\mathbf{e})$ are the expected annual dose estimates for the seismic ground motion and fault displacement modeling cases, respectively. Combining these three equations with Equation 2.4-12, produces the total expected annual dose estimate for 10,000 years:

$$\bar{D}(\tau|\mathbf{e}) \cong \bar{D}_{N}(\tau|\mathbf{e}) + \bar{D}_{EW}(\tau|\mathbf{e}) + \bar{D}_{ED}(\tau|\mathbf{e}) + \bar{D}_{II}(\tau|\mathbf{e}) + \bar{D}_{VE}(\tau|\mathbf{e}) + \bar{D}_{SG}(\tau|\mathbf{e}) + \bar{D}_{SF}(\tau|\mathbf{e}) \qquad \text{(Eq. 2.4-19)}$$

For the post-10,000-year period, the nominal and the seismic scenario classes are combined, and the expected annual dose for this combined scenario class is computed as (compare to Equation 2.4-18):

$$\bar{D}_{N+S}(\tau|\mathbf{e}) = \bar{D}_{N+SG}(\tau|\mathbf{e}) + \bar{D}_{SF}(\tau|\mathbf{e}) \qquad \text{(Eq. 2.4-20)}$$

where $\bar{D}_{N+SG}(\tau|\mathbf{e})$ is the expected annual dose at time τ resulting from the combined effect of nominal and seismic ground motion processes. Thus, combining Equations 2.4-15, 2.4-16, 2.4-17, and 2.4-20, gives the approximation for total expected annual dose for the post-10,000-year period:

$$\bar{D}(\tau|\mathbf{e}) \cong \bar{D}_{EW}(\tau|\mathbf{e}) + \bar{D}_{ED}(\tau|\mathbf{e}) + \bar{D}_{II}(\tau|\mathbf{e}) + \bar{D}_{VE}(\tau|\mathbf{e}) + \bar{D}_{N+SG}(\tau|\mathbf{e}) + \bar{D}_{SF}(\tau|\mathbf{e}) \qquad \text{(Eq. 2.4-21)}$$

As previously described, the nominal processes and seismic ground motion events are combined into one modeling case because the seismic ground motion consequences abstraction (SNL 2007c) takes into account the increased susceptibility to seismic damage as a result of corrosion-induced thinning of the waste package outer barrier, drip shield plate, and drip shield framework (Sections 2.3.4.5.1.3.6 and 2.4.2.3.2.1.12.3).

Equations 2.4-19 and 2.4-21, which are used to calculate the total expected annual dose, show that this calculation "appropriately sums the contribution of each of the disruptive event scenario classes," as described in Acceptance Criterion 1(2) of NUREG-1804, Section 2.2.1.4.1.3.

2.4.2.1.5.1 Nominal Scenario Class

The nominal scenario class includes one modeling case, the nominal modeling case. This modeling case estimates the dose resulting from nominal processes, primarily corrosion of the waste package and drip shield material. Although there is no aleatory uncertainty in the nominal modeling case related to the occurrence of events, conceptually, the time, location and degree of damage to each waste package that fails by nominal corrosion processes are aleatory uncertainties that could be described by adding appropriate elements to the vector for aleatory uncertainty, $\mathbf{a}$. These aleatory quantities are not explicitly represented in the TSPA model in the same manner as aleatory quantities related to early failures or events. Rather, the aleatory uncertainty pertaining to nominal processes is addressed through a number of averaging operations within submodels that determine time, location and degree of damage occurring by corrosion processes. *Total System Performance Assessment Model/Analysis for the License Application* (SNL 2008a, Section 6.3.5) describes these submodels and outlines the averaging operations that account for the aleatory uncertainty in these submodels (SNL 2008a, Appendix N). The nominal modeling case computes the expectation over aleatory uncertainty of the annual dose directly by means of these averaging operations.

The annual dose for the nominal modeling case, $D_N(\tau|\mathbf{e})$, is calculated both for the first 10,000 years after disposal and for the post-10,000-year period by the GoldSim component of the TSPA model. However, as described above, for estimating total expected annual dose for the post-10,000-year period, $D_N(\tau|\mathbf{e})$ is not used directly in Equation 2.4-21. Instead, as described in Section 2.4.2.1.5.4, the dose due to nominal processes is calculated as part of the seismic ground motion modeling case. *Total System Performance Assessment Model /Analysis for the License Application* (SNL 2008a, Section 6.1.2.4 and Section J5) provides more details of the evaluation of $D_N(\tau|\mathbf{e})$.

2.4.2.1.5.2 Early Failure Scenario Class

The early failure scenario class includes two modeling cases: the waste package early failure modeling case (EW) and the drip shield early failure modeling case (ED). Because the two types of early failure events are independent, the expected annual dose for the early failure scenario class is equal to the sum of the expected annual doses from its constituent modeling cases, as given by Equation 2.4-16. (Futures with both types of early failures contribute negligibly to the total dose.)

Waste Package Early Failure Modeling Case—The waste package early failure modeling case estimates the dose resulting from the occurrence of waste package early failures. The aleatory uncertainties in this modeling case are the number of waste package early failures, the type of each waste package having early failure, and the location of each early failed waste package.

For each realization $\mathbf{e}$ of epistemically uncertain parameters, the expected annual dose $\bar{D}_{EW}(\tau|\mathbf{e})$ is calculated by:

$$\bar{D}_{EW}(\tau|\mathbf{e}) = \sum_{r=1}^{2}\sum_{s=1}^{5}\sum_{t=0}^{1} nWP\, pW(\mathbf{e})\, fWT_r\, fBN_s\, pDRP_{rst}(\mathbf{e})\, D_{EW}(\tau|[1,r,s,t]\mathbf{e})$$

(Eq. 2.4-22)

where

$$pDRP_{rst}(\mathbf{e}) = \begin{cases} 1 - fDRP_{rs}(\mathbf{e}) \text{ if } t = 0 \\ fDRP_{rs}(\mathbf{e}) \text{ if } t = 1 \end{cases}$$

and

nWP	number of emplaced waste packages in the repository
$pW(\mathbf{e})$	probability of a randomly chosen waste package having early failure (element of $\mathbf{e}$)
fWT_r	fraction of waste packages of type r (commercial SNF or codisposal)
fBN_s	fraction of waste packages that are in percolation subregion s
$fDRP_{rs}(\mathbf{e})$	fraction of waste packages of type r in percolation subregion s that experience seeping ($t = 1$) or non-seeping ($t = 0$) conditions (function of elements of $\mathbf{e}$)
$D_{EW}(\tau\|[1,r,s,t]\mathbf{e})$	dose at time τ that results from early failure of one waste package of type r in percolation subregion s with seeping ($t = 1$) or non-seeping ($t = 0$) conditions.

The GoldSim component of the TSPA model calculates the quantity $D_{EW}(\tau|[1,r,s,t]\mathbf{e})$, and the EXDOC_LA component computes the sum indicated in Equation 2.4-22. *Total System Performance Assessment Model/Analysis for the License Application* (SNL 2008a, Sections 6.1.2.4 and J6.2) provides more details of Equation 2.4-22.

Drip Shield Early Failure Modeling Case—The drip shield early failure modeling case estimates the dose resulting from the occurrence of drip shield early failures. The aleatory uncertainties in this modeling case are the number of early drip shield failures, the type of waste package located beneath each early failed drip shield, and the location of each early-failed drip shield.

The calculation of expected annual dose for the drip shield early failure modeling case is similar to Equation 2.4-22 for expected annual dose for the waste package early failure modeling case. Failure of a drip shield allows seepage waters, if present, to contact the underlying waste package. The TSPA model assumes that localized corrosion occurs on any waste package under an early failed drip shield in a location with seepage, and that no waste package failure occurs under other early-failed drip shields (Section 2.4.2.3.2.1.12.1). Thus, only early-failed drip shields in locations with seeping conditions contribute to the expected annual dose (Section 2.4.2.3.2.1.12.1). For each realization $\mathbf{e}$ of epistemically uncertain parameters, the expected annual dose $\bar{D}_{ED}(\tau|\mathbf{e})$ is calculated by:

$$\bar{D}_{ED}(\tau|\mathbf{e}) = \sum_{r=1}^{2}\sum_{s=1}^{5} nWP\; pD(\mathbf{e})\; fWT_r\; fBN_{rs}\; fDRP_s(\mathbf{e})\; D_{ED}\,(\tau|[1, r, s]\mathbf{e}) \qquad \text{(Eq. 2.4-23)}$$

nWP	number of emplaced waste packages in the repository
$pD(\mathbf{e})$	probability of a randomly chosen drip shield having early failure (element of $\mathbf{e}$)
fWT_r	fraction of waste packages of type r (commercial SNF or codisposal)
fBN_s	fraction of waste packages that are in percolation subregion s
$fDRP_{rs}(\mathbf{e})$	fraction of waste packages of type r in percolation subregion s that experience seeping conditions (function of elements of $\mathbf{e}$)
$D_{ED}\,(\tau|[1, r, s]\mathbf{e})$	dose at time τ that results from early failure of one drip shield over a waste package of type r in percolation subregion s with seeping conditions.

The GoldSim component of the TSPA model calculates the quantity; the EXDOC_LA component computes the sum indicated in Equation 2.4-23. *Total System Performance Assessment Model/Analysis for the License Application* (SNL 2008a, Sections 6.1.2.4 and J6.3) provides more details of Equation 2.4-23.

2.4.2.1.5.3 Igneous Scenario Class

The igneous scenario class includes two modeling cases: the igneous intrusion modeling case (II) and the volcanic eruption modeling case (VE). Although the occurrences of intrusion and eruption are not independent (Section 2.4.2.3.2.1.12.2), the dose transport pathways of an intrusion and an eruption are independent, because an eruption results in radionuclide transport through the atmosphere, whereas an intrusion results in radionuclide transport through the groundwater pathway. For the igneous scenario class, the expected annual dose is given in Equation 2.4-17.

Igneous Intrusion Modeling Case—The igneous intrusion modeling case calculates the dose resulting from groundwater transport of radionuclides resulting from an igneous intrusion into the repository. The occurrence time of the igneous event is the single aleatory random variable in the igneous intrusion modeling case. The TSPA assumes that an igneous intrusion completely compromises all waste packages; thus, the extent of damage is not treated as uncertain.

For each realization $\mathbf{e}$ of the epistemically uncertain parameters, the expected annual dose $\bar{D}_{II}(\tau|\mathbf{e})$ at time τ is approximated by:

$$\bar{D}_{II}(\tau|\mathbf{e}) = \int_0^{\tau} D_{II}(\tau|[1,t],\mathbf{e})\lambda_I(\mathbf{e})dt \qquad \text{(Eq. 2.4-24)}$$

where $D_{II}(\tau|[1,t],\mathbf{e})$ is the dose at time τ from one igneous intrusion event occurring at time τ, and $\lambda_I(\mathbf{e})$ is the sampled value for the annual frequency of igneous events. The quantity $D_{II}(\tau|[1,t],\mathbf{e})$ is computed using the GoldSim component of the TSPA model, and the integral over igneous occurrences is approximated by a quadrature technique implemented in the EXDOC_LA component of the TSPA model. For more details of Equation 2.4-24, see *Total System Performance Assessment Model/Analysis for the License Application* (SNL 2008a, Sections 6.1.2.4 and J7.2).

Nominal corrosion processes are included in the igneous intrusion model for calculation of dose in the post-10,000-year period. However, the calculation of $D_{II}(\tau|[1,t],\mathbf{e})$ does not accumulate the dose from radionuclides released by corrosion processes prior to the igneous intrusion to avoid counting these radionuclides twice in the calculation of total mean annual dose in Equation 2.4-21. This dose is accounted for as part of the nominal modeling case for the first 10,000 years after closure, and as part of the seismic ground motion modeling case for the post-10,000-year period.

Volcanic Eruption Modeling Case—The volcanic eruption modeling case estimates the annual dose resulting from eruptions, which are a subset of the igneous events. The aleatory uncertainties in this modeling case include:

- Number of eruptive events
- Time of each eruptive event
- Number of waste packages affected in each event
- Fraction of waste package content that is ejected into the atmosphere in each event
- Eruptive power, eruptive velocity, duration, wind speed, and wind direction for each eruptive event.

For each realization $\mathbf{e}$ of the epistemically uncertain parameters, the expected annual dose $\overline{D}_{VE}(\tau|\mathbf{e})$ at time τ is formally calculated by:

$$\overline{D}_{VE}(\tau|\mathbf{e}) = pE\lambda_I(\mathbf{e})\overline{N}_{VE}\overline{F}\int_0^{\tau}\left[\int_{U_{VE}} D_{VE}(\tau|[1, t, 1, \mathbf{u}], \mathbf{e})d_u(\mathbf{u})dU\right]dt \qquad \text{(Eq. 2.4-25)}$$

where

pE	probability that an igneous event has eruptive conduits that intersect the emplaced waste, $(0.28) \cdot (0.2968) = 0.083$ (Section 2.3.11.4.2.1)
$\lambda_I(\mathbf{e})$	epistemic uncertain frequency of igneous events
$\overline{N}_{VE}$	mean number of waste packages affected by eruptive conduits
$\overline{F}$	mean fraction of waste package content ejected into the atmosphere
U_{VE}	vector space of all values of eruptive power, eruptive velocity, duration, wind speed, and wind direction
$\mathbf{u}$	vector of values sampled from the distributions eruptive power, eruptive velocity, duration, wind speed, and wind direction
$d_u(\mathbf{u})$	probability density function (pdf) on U_{VE} formed from the individual probability distributions for eruptive power, eruptive velocity, duration, wind speed, and wind direction
$D_{VE}(\tau\|[1, t, 1, \mathbf{u}], \mathbf{e})$	dose at time τ from one eruption occurring at time t, which affects all of the content of one waste package, with eruptive power, eruptive velocity, duration, wind speed, and wind direction described by $\mathbf{u}$.

The quantity $D_{VE}(\tau|[1, t, 1, \mathbf{u}], \mathbf{e})$ is computed using the GoldSim component of the TSPA model. Due to the relatively large number of aleatory uncertainties described by the vector $\mathbf{u}$, the integral over U_{VE} is calculated by means of a Monte Carlo method, using a Latin hypercube sample from the vector space U_{VE}. The integral over the igneous occurrence time is calculated by a quadrature technique. These integrals are evaluated using the EXDOC_LA component of the TSPA model. For more details of Equation 2.4-25, see *Total System Performance Assessment Model/Analysis for the License Application* (SNL 2008a, Sections 6.1.2.4 and J7.3).

2.4.2.1.5.4 Seismic Scenario Class

The seismic scenario class includes two modeling cases: the seismic ground motion modeling case (SG), and the seismic fault displacement modeling case (SF). For the seismic scenario class, the expected annual dose for the first 10,000 years is approximated with Equation 2.4-18 using Equations 2.4-26 and 2.4-28 below. For the post 10,000 year period the approximation in Equation 2.4-20 results from the combination of Equations 2.4-27 and 2.4-28.

Seismic Ground Motion Modeling Case (First 10,000 Years)—The seismic ground motion modeling case calculates annual dose from radionuclides released from the EBS due to damage to waste packages resulting from vibratory ground motion. As discussed in more detail in Section 2.4.2.2.2.3, for the first 10,000 years, the consequences of seismic ground motion events can be approximated by examining only the occurrence of stress corrosion cracking damage to codisposal waste packages with the drip shield intact and without rockfall, and without considering thinning of the waste package outer barrier due to corrosion processes (SNL 2008a, Section 7.3.2). This does not represent any changes to FEPs screening but, rather, a TSPA simplification based on TSPA consequence analyses that have shown that other damage mechanisms are insignificant in the first 10,000 years.

The aleatory uncertainties in the seismic ground motion modeling case for 10,000 years include:

- Number of seismic events that cause stress corrosion cracking damage to co-disposal waste packages
- Occurrence time of each damaging seismic event
- Waste package surface area damaged by each damaging seismic event.

For a vector $\mathbf{e}$ of epistemically uncertain parameters, the expected annual dose is approximated by:

$$
\begin{aligned}
\bar{D}_{SG}(\tau \mid \mathbf{e}) = & \int_0^{\tau} \left(\lambda_1(\mathbf{e}) \exp\left(-\lambda_1(\mathbf{e}) t\right) \left(\int_0^{D} D_{SG}\left(\tau \mid [1, t, A], \mathbf{e}\right) d_{A1}(A \mid \mathbf{e})\, dA \right) \right) dt \\
& + \int_0^{\tau} \left(\lambda_1(\mathbf{e}) \exp\left(-\lambda_1(\mathbf{e}) t\right) \left(\int_t^{\tau} \int_0^{D} D_{SG}\left(\tau \mid [1, s, B], \mathbf{e}\right) d_{A2}(B \mid \mathbf{e}) \lambda_2(\mathbf{e})\, dB\, ds \right) \right) dt
\end{aligned}
$$

(Eq. 2.4-26)

where

$\lambda_1(\mathbf{e})$	frequency of seismic ground motion events that cause stress corrosion cracking damage to codisposal waste packages with intact internals

$\lambda_2(\mathbf{e})$	frequency of seismic ground motion events that cause stress corrosion cracking damage to codisposal waste packages with degraded internals
$d_{A1}(A\|\mathbf{e})$	density function for damage area occurring on codisposal waste packages with intact internals from seismic events that cause damage, defined on the domain [0, *D*], where *D* is the surface area of the waste package
$d_{A2}(B\|\mathbf{e})$	density function for damage area occurring on codisposal waste packages with degraded internals from seismic events that cause damage, defined on the domain [0, *D*], where *D* is the surface area of the waste package
$D_{SG}(\tau\|[1, t, A], \mathbf{e})$	dose at time τ resulting from one seismic ground motion event occurring at time *t* that causes damaged area equal to *A*

Two occurrence frequencies and damage density functions are used in Equation 2.4-26 because there are different probability models for the occurrence and the extent of damage depending on whether the internals of the waste package are intact or degraded (SNL 2007c). The calculation of expected annual dose in Equation 2.4-26 accounts for the possibility that more than one damaging event occurs in the future of the repository, using the conservative assumption that the annual dose from a sequence of seismic events causing cumulative damage to waste packages is reasonably approximated by the sum of the annual dose resulting from the individual events. This assumption of additivity in seismic consequences is discussed in Section 2.4.2.1.7 (SNL 2008a, Section J8.3).

The quantity $D_{SG}(\tau|[1, t, A], \mathbf{e})$ is calculated by the Goldsim component of the TSPA model. The integrals in Equation 2.4-26 are approximated by employing quadrature techniques implemented in the EXDOC_LA component of the TSPA model. For more details of Equation 2.4-26, including the derivation of the occurrence frequencies and damage density functions from the seismic hazard curve and the seismic consequence abstraction, see *Total System Performance Assessment Model/Analysis for the License Application* (SNL 2008a, Sections 6.1.2.4.4, J8.3, J8.4, and J8.5).

Seismic Ground Motion Modeling Case (Post-10,000 Year-Period)—Section 2.3.4 outlines a probabilistic model for effects on the EBS due to seismic ground motion events and provides different probability models for (SNL 2007c):

- The probability and extent of stress corrosion cracking damage to codisposal and commercial SNF waste packages
- The probability and extent of rupture and puncture of codisposal and commercial SNF waste packages
- The probability and extent of rockfall in the lithophysal and nonlithophysal zones
- The state of the drip shield and its supporting framework as a function of time.

The model also accounts for the change in susceptibility (i.e., probability) of each EBS component to damage, and, if damage occurs, the extent of damage. As mentioned at the beginning of this section, for the post-10,000-year period after permanent closure, this full seismic consequence abstraction (SNL 2007c) is used, including the effects of corrosion processes on EBS components and the dose resulting from corrosion processes.

The aleatory uncertainties in the seismic ground motion modeling case for 1,000,000 years include:

- The number of seismic events
- The time of each seismic event
- The amount of rockfall in the lithophysal zone caused by each seismic event (see Section 2.4.2.3.2.1.12.3, which discusses the use of the lithophysal rubble abstraction in both lithophysal and nonlithophysal rock)
- The effect of drift collapse on the structure and function of drip shields at the time of each seismic event
- The occurrence and extent of stress corrosion cracking damage to each type of waste package (codisposal and commercial SNF) for each seismic event
- The occurrence and extent of rupture and/or puncture of the outer barrier for each type of waste package (codisposal and commercial SNF) for each seismic event.

Because of the complexity of the post-10,000-year seismic consequence abstraction, the hundreds of seismic events that could occur in the long-term future of the repository, as well as the failure of waste packages and drip shields by nominal corrosion processes, a Monte Carlo technique is used to estimate expected annual dose given epistemic uncertainty in the post-10,000-year period for the seismic ground motion modeling case:

$$\bar{D}_{N+SG}(\tau|\mathbf{e}) \cong \frac{1}{N_A} \sum_{j=1}^{N_A} D_{N+SG}(\tau|\mathbf{a}_j, \mathbf{e}) \qquad \text{(Eq. 2.4-27)}$$

where

$\mathbf{a}_j,\ j = 1, \ldots, N_A$	random sample of size N_A for aleatory quantities (listed above)
$D_{N+SG}(\tau\|\mathbf{a}_j, \mathbf{e})$	annual dose at time τ from combined effects of seismic events and nominal corrosion processes described by elements of $\mathbf{a}_j$ and $\mathbf{e}$.

The quantity $D_{N+SG}(\tau|\mathbf{a}_j, \mathbf{e})$ is computed by the GoldSim component of the TSPA model, and the averaging indicated in Equation 2.4-27 is done with the EXDOC_LA component. For more details of Equation 2.4-27, see *Total System Performance Assessment Model/Analysis for the License Application* (SNL 2008a, Sections 6.1.2.4.4 and J8.3).

Seismic Fault Displacement Modeling Case—The seismic fault displacement modeling case computes annual dose from radionuclides released from the EBS due to damage caused by fault displacements. The aleatory uncertainties included in this modeling case are:

- Number of fault displacement events affecting each type of waste package (commercial SNF or codisposal)
- Occurrence time of each fault displacement event
- Number of waste packages of each type (commercial SNF or codisposal) damaged by each fault displacement event
- Damaged area in the Alloy 22 outer barrier of each waste package type by each fault displacement event.

When a fault displacement event occurs, the drip shield above the affected waste packages is assumed to be ruptured by the event.

The calculation of expected annual dose for fault displacements, $\bar{D}_{SF}(\tau|\mathbf{e})$, does not explicitly treat the aleatory uncertainty for the location of each affected waste package. Instead, to reduce computational requirements, $\bar{D}_{SF}(\tau|\mathbf{e})$ is approximated by modeling 100 waste packages of each type, placed proportionally into the percolation subregions and, within each subregion, into seeping or non-seeping locations. Results are calculated for each set of 100 waste packages and then scaled to the expected number of packages affected by a fault displacement event. This technique efficiently calculates the expected annual dose considering the uncertainty in the locations and the types of waste packages affected by fault displacement.

For each realization $\mathbf{e}$ of epistemically uncertain parameters, the expected annual dose $\bar{D}_{SF}(\tau|\mathbf{e})$ at time τ is calculated by:

$$\bar{D}_{SF}(\tau|\mathbf{e}) \cong \sum_{r=1}^{2} [\bar{N}_r \lambda_{Fr}/100]\left[\int_0^{\tau}\left(\int_0^{D_r} D_{SFr}(\tau|[1, t, 100, A], \mathbf{e})\, d_{Ar}(A)\, dA\right)dt\right] \qquad \text{(Eq. 2.4-28)}$$

where

λ_{Fr}	frequency of fault displacement events that cause damage to waste packages of type r
$\bar{N}_r$	expected number of waste packages of type r (commercial SNF or codisposal) damaged by one fault displacement event

$d_{A_r}(A)$	density function for damage area on waste packages of type r from a fault displacement, defined over domain $[0, A_r]$, where A_r is the cross-sectional area of a waste package of type r
$D_{SFr}(\tau \| [1, t, 100, A], \mathbf{e})$	dose at time τ resulting from one fault displacement occurring at time t, which damages 100 waste packages of type r, causing area opened equal to A on each waste package of type r.

The GoldSim component of the TSPA model computes the quantity $D_{SFr}(\tau|[1, t, 100, A], \mathbf{e})$, and the two integrals in Equation 2.4-28 are approximated using quadrature techniques implemented in the EXDOC_LA component. For more details of Equation 2.4-28, see *Total System Performance Assessment Model/Analysis for the License Application* (SNL 2008a, Sections 6.1.2.4.4 and J8.6).

2.4.2.1.6 Scenario Class Probabilities

Because each scenario class is a subset of the probability space describing aleatory uncertainty, from a mathematical perspective (SNL 2008a, Appendix J, Section J4.4) a probability can be computed for each scenario class. However, because of the dependence of several elements of the aleatory vector $\mathbf{a}$ on elements of the epistemic vector $\mathbf{e}$, the calculation of the probability for a scenario class is also dependent on the epistemic vector $\mathbf{e}$. In addition, because seismic and igneous events are modeled as occurring randomly in time, the probability of these scenario classes also depends on the time interval being considered.

For a given time interval and a given epistemic vector $\mathbf{e}$, the probability of a scenario class $\mathcal{A}_J$ conditional on the epistemic vector $\mathbf{e}$ is calculated by integrating the density function $d_A(\mathbf{a}|\mathbf{e})$ over the scenario class of interest:

$$p_A(\mathcal{A}_J|\mathbf{e}) = \int_{\mathcal{A}_J} d_A(\mathbf{a}|\mathbf{e}) d_A \tag{Eq. 2.4-29}$$

The mean probability of each scenario class $p_A(\mathcal{A}_J)$ can then be calculated by integrating $p_A(\mathcal{A}_J|\mathbf{e})$ over epistemic uncertainty.

Intuitive definitions of these mean probabilities are

$p_A(\mathcal{A}_E)$ = probability of one or more early failures (either waste package or drip shield),
$p_A(\mathcal{A}_I)$ = probability of one or more igneous events,
$p_A(\mathcal{A}_S)$ = probability of one or more seismic events,
$p_A(\mathcal{A}_N)$ = probability of no early failures, igneous events or seismic events

The following sections provide values for the mean probabilities of each scenario class, as well as the mean probabilities for the events represented by each scenario class.

Early Failure Scenario Class—Because early failure is considered independently for each waste package and drip shield (SNL 2008a, Section 6.4), the number of waste package and drip shield early failures is described by binomial distributions. However, because the probability of early failure of a randomly chosen waste package or drip shield is small (SNL 2008a, Table 6.4-2), the number of early failures can be reasonably approximated by a Poisson distribution:

$$\begin{aligned} p_A(\mathcal{A}_E|\mathbf{e}) &= \int_{\mathcal{A}_J} d_A(\mathbf{a}|\mathbf{e})d_A \\ &\cong 1 - \exp[-nWP(pW(\mathbf{e}) + pD(\mathbf{e}))] \end{aligned} \qquad \text{(Eq. 2.4-30)}$$

where $nWP = 11{,}629$ (i.e., 3,416 codisposal and 8,213 commercial waste packages) is the number of individual waste packages and drip shields represented in the TSPA model, and $pW(\mathbf{e})$ and $pD(\mathbf{e})$ are the probabilities of early failure for a randomly chosen waste package or drip shield, respectively (SNL 2008a, Appendix J, Section J6.5).

The mean probability for the early-failure scenario class $p_A(\mathcal{A}_E)$ is evaluated to be 0.45, which is the mean probability that one or more early failures of waste packages or drip shields occur. Considering the types of early failure separately, the mean probability of one or more early waste package failures is 0.44, and the mean probability of one or more early drip shield failures is 0.017 (SNL 2008a, Section 8.2.2).

Igneous Scenario Class—The igneous scenario class considers the occurrence of igneous events. Each igneous event involves a magmatic intrusion of the repository; some igneous events also involve eruptive conduits that intersect emplaced waste. The number of igneous events occurring in an interval of time is described by a Poisson distribution with an epistemically uncertain rate $\lambda_I(\mathbf{e})$/yr. Thus, considering a time interval of length T, the probability of the igneous scenario class $\mathcal{A}_I$ conditional on the epistemic vector $\mathbf{e}$ (SNL 2008a, Appendix J, Section J7.5) is given by:

$$p_A(\mathcal{A}_I|T, \mathbf{e}) = 1 - \exp(-\lambda_I(\mathbf{e})T) \qquad \text{(Eq. 2.4-31)}$$

The mean probability of the igneous scenario class $p_A(\mathcal{A}_I)$ is estimated to be 1.7×10^{-4} for 10,000 years, and 1.7×10^{-2} for one million years (SNL 2008a, Table 6.5-2).

Every igneous event involves an intrusion into the repository by a magmatic dike; hence the mean probability of the occurrence of an igneous intrusion event is the same as the mean probability of the igneous scenario class (i.e., 1.7×10^{-8}). As described in Section 2.3.11.4.2, only a fraction (0.083) of these events also involve an eruptive conduit that intersects emplaced waste (SNL 2008a, Section 6.5.2.2). Therefore, the mean probability of a volcanic eruption is $(0.083) \times (1.7 \times 10^{-4}) = 1.4 \times 10^{-5}$ for 10,000 years, and 1.4×10^{-3} for 1,000,000 years.

Seismic Scenario Class—The seismic scenario class represents the occurrence of two types of seismic events: ground motion and fault displacement. Each type of event is modeled to occur independently and is described by a Poisson process. Not every ground motion event included in the seismic scenario class causes damage to waste packages and drip shields (Section 2.3.4). Consequently, the rate for the Poisson process describing ground motion events is the rate of occurrence of ground motion events with potential to cause damage to waste packages and drip shields. For the purpose of calculating a probability for the seismic scenario class, this rate is approximated as $\lambda_{mx} = 4.287 \times 10^{-4}$ per year, corresponding to the frequency of events with PGV exceeding 0.219 m/s (SNL 2008a, Appendix J, Section J8.8). The rate of occurrence of fault displacement events is $\lambda_{SF} = 2.5 \times 10^{-7}$ per year, which is the frequency of fault displacement events with potential to cause damage to waste packages (Table 2.3.4-59).

Considering a time interval of length T, the probability of the seismic scenario class $\mathcal{A}_S$ is (SNL 2008a, Appendix J, Section J8.8):

$$\begin{aligned} p_A(\mathcal{A}_S|T) &= 1 - \exp(-(\lambda_{mx} + \lambda_{SF})T) \\ &\cong 1 - \exp(-(4.29 \times 10^{-4})T) \end{aligned} \qquad \text{(Eq. 2.4-32)}$$

The probability of the seismic scenario class $p_A(\mathcal{A}_S)$ is estimated to be 0.99 for 10,000 years, and 1.00 for one million years. It is important to note that this probability (0.99) is the probability of seismic events with potential to cause damage. The probability that damage occurs is much smaller, as is discussed next.

Further insight into the outcomes associated with the seismic scenario class can be gained by considering the probability of damage resulting from seismic events. These probabilities should not be confused with the probability of occurrence of seismic events with potential to cause damage. The probability that a seismic event causes damage depends on additional uncertainties, such as the PGV of the seismic event, the state of the waste packages and drip shields at the time of the event, and the epistemic uncertainty in residual stress threshold for Alloy 22. Section 2.3.4 describes the probability models developed to describe the effects of seismic events; Section 2.4.2.3.2.1.12.3 summarizes the implementation of these models in the TSPA model.

Because seismic damage results from seismic events which are modeled by a Poisson process, the occurrence of different modes of damage is also described by a Poisson process, with appropriate rate terms. The following quantities illustrate the probabilities of occurrence of seismic events resulting in several of the different modes of damage associated with the occurrence of a potentially damaging seismic event:

- Mean probability of seismic events before 10,000 years which cause damage to intact codisposal waste packages with outer barrier at least 23 mm in thickness: 0.070

- Mean probability of seismic events before 10,000 years which cause damage to intact commercial SNF waste packages with outer barrier at least 23 mm in thickness 5.2×10^{-5}.

Additional information about the effect of seismic events on waste packages and drip shields is provided in Figures 2.1-11 through 2.1-17.

Nominal Scenario Class—The nominal scenario class represents futures in which no early failures and no igneous or seismic events occur. Consequently, the mean probability of the nominal scenario class is

$$p_A(\mathcal{A}_N) = (1 - p_A(\mathcal{A}_E))(1 - p_A(\mathcal{A}_I))(1 - p_A(\mathcal{A}_S)) \quad \text{(Eq. 2.4-33)}$$

Using the values for $p_A(\mathcal{A}_E)$, $p_A(\mathcal{A}_I)$, and $p_A(\mathcal{A}_S)$ provided above, the mean probability of the nominal scenario class is 0.0055 for 10,000 years and essentially 0 for 1,000,000 years.

As described in Section 2.4.2.1.3, the probabilities of the scenario classes, $p_A(\mathcal{A}_E)$, $p_A(\mathcal{A}_I)$, and $p_A(\mathcal{A}_S)$ should not be expected to add to 1.0, since they are not disjoint. However, the probabilities of the eight disjoint scenario classes, which form the basis for the total annual dose calculation, described in Section 2.4.2.1.4, do add to 1.0 because union of the eight disjoint scenario classes is the entire aleatory probability space.

2.4.2.1.7 Overestimation in Annual Dose Arising from the Additivity Assumption

As outlined in Section 2.4.2.1.4, the calculation of total annual dose as the sum of annual dose from each of the four primary scenario classes relies on the simplifying assumption that the occurrence of an early failure or other event has no effect on the consequences of a later event. This additivity or no-synergisms assumption allows the TSPA model to approximate the dose from a future involving a combination of events, such as a seismic event followed by an igneous intrusion, as the sum of the dose from the seismic event and the dose from the igneous event (plus the dose due to nominal processes). The appropriateness of this assumption depends on both scenario class probability and the expected doses to the RMEI that result from the futures associated with individual scenario classes. However, in general, this method of approximation affects the TSPA model results by overestimating the resulting dose. Table 2.4-7 summarizes the effect of each combination of events on the calculation of total mean annual dose. These effects are discussed below (SNL 2008a, Sections 6.1.2.3 and J10).

2.4.2.1.7.1 Intersection of Nominal Scenario Class with Other Scenario Classes

During the period before 10,000 years, the corrosion processes included in the nominal scenario class have no consequences that affect the consequences of any early failure or disruptive event. Thus, no combinations of the nominal scenario class with other scenario classes are relevant before 10,000 years.

During the post-10,000-year period after permanent closure, the corrosion processes described by the nominal scenario class affect the consequences of seismic ground motion events, so these processes are included in the seismic ground motion modeling case. As explained in Sections 2.4.2.1.4 and 2.4.2.1.5, the inclusion of these processes means that dose due to nominal processes is combined with the dose due to seismic ground motion events, and this combined quantity is calculated by the seismic ground motion modeling case. The nominal corrosion processes are also accounted for in the igneous intrusion modeling case, but the dose due to corrosion processes before the time of the first intrusion is not included in the dose for the igneous intrusion modeling case. The corrosion processes are included in the simulation so that the inventory remaining in the waste packages at the time of the intrusion is reduced by the radionuclides released due to corrosion processes prior to the intrusion. This is done in the TSPA model in order to avoid counting radionuclides twice in the calculation of total expected annual dose $\overline{D}_I$ (Equation 2.4-21). Nominal corrosion processes are not, however, included in the seismic fault displacement, volcanic eruption, or early failure modeling cases resulting in a small overestimation of radionuclide releases, because the inventory in the waste packages affected by these events is not reduced by the radionuclides released due to corrosion processes prior to the intrusion. The effect of the overestimation on total mean annual dose is small because the number of waste packages impacted by these cases is, at most, two percent.

2.4.2.1.7.2 Intersection of Early-Failure Scenario Class with Other Scenario Classes

The TSPA model assumes all waste package and drip shield early failures occur at repository closure. Further, an early failure cannot follow any disruptive event. In the TSPA, if a disruptive event follows an early failure, the inventory released as a consequence of the disruptive event is estimated without subtracting the inventory released from the waste packages affected by early failure. This assumption is conservative, although its magnitude is small because on average less than 2.49/11,629 = 0.02% of the waste packages are affected previously by early failure (SNL 2008a, Section 6.1.2.3.2), and, as a result, no more than 0.02% (on average) of the inventory is counted twice.

2.4.2.1.7.3 Intersection of Igneous Scenario Class with Other Scenario Classes

The combinations of an igneous intrusion and volcanic eruption with other scenario classes are considered separately (SNL 2008a, Section 6.1.2.3.3).

Igneous Intrusion with Seismic Scenario Class—The TSPA model assumes that all components of the EBS suffer maximum damage from an igneous intrusion event. In other words, after the intrusion, the EBS components (drip shields and waste packages) no longer function to prevent or slow the rate of transport of radionuclides. Since the effects of a seismic event (either vibratory ground motion or fault displacement) are damage to components of the EBS, a seismic event following an igneous intrusion will not have any effect on the repository performance because all waste packages and drip shields would have already been destroyed.

The TSPA model overestimates total dose by not excluding the dose resulting from seismic events occurring after an igneous intrusion. Although this too is a conservative assumption, during 1,000,000 years the average probability of an igneous intrusion is roughly $(1.7 \times 10^{-8}/\text{yr}) \times (10^6\ \text{yr}) = 1.7 \times 10^{-2}$, so the overestimate of dose affects only 2% of the futures considered in the seismic ground motion modeling case.

Volcanic Eruption with Seismic Scenario Class—The TSPA model overestimates total dose by not reducing the inventory that could be released by seismic events by the amount of inventory released by any volcanic eruptions. However, on average an eruptive event affects less than 0.03% of the waste packages, so not more than 0.03% (on average) of the inventory could be counted twice, and the net effect on total mean annual dose of the combination of volcanic eruptions and seismic events is negligible.

Combinations of Igneous Intrusions with Volcanic Eruptions—The TSPA model overestimates total dose by not reducing the inventory that could be released by intrusions or eruptions by the amount of inventory released by any preceding igneous event. However, on average an eruptive event affects less than 0.03% of the waste packages, so the effect on total mean annual dose of an eruptive event preceding other igneous events is negligible (SNL 2008a, Section 6.1.2.3.3). The TSPA Model accounts for multiple igneous intrusion events and for multiple volcanic eruption events in the calculation of total mean annual dose.

2.4.2.1.7.4 Intersection of Seismic Scenario Class with Other Scenario Classes

The TSPA model overestimates total expected annual dose by not subtracting the inventory released due to preceding seismic ground motion events from the inventory available at the time of an igneous event (SNL 2008a, Section 6.1.2.3.4). During the 1,000,000 years after disposal, essentially all future states of the repository eventually include releases due to either seismic ground motion damage or nominal corrosion processes; thus, many realizations of the igneous modeling cases overstate releases by the amount of inventory released prior to an intrusion. This interaction is conservative in the sense that the consequences of the igneous modeling cases are always overstated. However, the overestimate in expected annual dose from igneous events is shown to be minor (SNL 2008a, Appendix J, Section J10).

The inventory released from a fault displacement event is not subtracted from the inventory that could be released by a later disruptive event. In addition, the inventory that could be released from waste packages affected by fault displacement is not reduced by releases from any preceding disruptive events. However, a fault displacement affects at most 214/11,629 = 1.8% of the waste packages (SNL 2008a, Section 6.1.2.3.4), so at most 1.8% of the inventory is counted twice, and the net effect on total mean annual dose of the combination of fault displacements, with other disruptive events, is negligible.

Table 2.4-7 summarizes all of the interaction terms discussed in Section 2.4.2.1.7.

2.4.2.1.8 Conclusion

The primary purpose of Section 2.4.2.1 is to address Acceptance Criterion 1 of NUREG-1804, Section 2.2.1.4.1.3, "Scenarios Used in the Calculation of Annual Dose as a Function of Time Are Adequate," and Acceptance Criterion 3 of NUREG-1804, Section 2.2.1.2.1.3, "Formation of Scenario Classes Using the Reduced Set of Events is Adequate." The following discussion summarizes the presentation in Section 2.4.2.1, and indicates where each part of these acceptance criteria is addressed.

Section 2.4.2.1.2 presents the calculation of total mean and median annual dose as a function of time. Section 2.4.2.1.3 describes the event and scenario classes that are included in these calculations, and Section 2.4.2.1.4 outlines the methodology used in the calculations. Together, these sections demonstrate, as requested by Acceptance Criterion 1(1) of NUREG-1804, Section 2.2.1.4.1.3, that "all scenario classes that have been determined to be sufficiently probable, or to have a sufficient effect on overall performance that they could not be screened from the total system performance assessment analyses" are included in the annual dose calculations presented in Section 2.4.2.2.1.

As anticipated by Acceptance Criterion 1(2) of NUREG-1804, Section 2.2.1.4.1.3, Section 2.4.2.1.4 shows how the calculation of the annual dose curve "appropriately sums the contribution of each of the disruptive event scenario classes." Section 2.4.2.1.5 summarizes how the calculation for each scenario class "properly accounts for the effects that the time of occurrence of the disruptive events comprising the scenario class has on the consequences." Section 2.4.2.1.6 presents the calculation of probabilities for each scenario class and Section 2.4.2.2.1 summarizes results and analyses for each scenario class; together, these sections demonstrate that the "annual probability of occurrence of the events used to calculate the contribution to the annual dose is consistent with the results of the scenario analysis." Finally, Section 2.4.2.1.3 shows how the "probabilities of occurrence of all scenario classes, included in calculating the annual dose curve, sum to one."

Formation of scenario classes is described in Section 2.2.1.3 and the results of that analysis are summarized in Section 2.4.2.1.3. The methodology for calculating total expected annual dose, presented in Section 2.4.2.1.4, is based on the set of mutually exclusive scenario classes listed in Section 2.4.2.1.3. Thus, these sections show that the performance assessment results are based on a set of scenario classes that are "mutually exclusive and complete, clearly documented, and technically acceptable."

2.4.2.2 Evaluation of Annual Dose to the RMEI with Respect to the Postclosure Individual Protection Standard

[NUREG-1804, Section 2.2.1.4.1.3: AC 2]

The second of three acceptance criteria in NUREG-1804, Section 2.2.1.4.1.3, requires an adequate demonstration that the annual dose to the RMEI does not exceed the individual protection standards after permanent closure in proposed 10 CFR 63.311. This is demonstrated below. The individual protection standard after permanent closure is defined in proposed 10 CFR 63.311, as follows:

> (a) DOE must demonstrate, using performance assessment, that there is a reasonable expectation that the reasonably maximally exposed individual receives no more than the following annual dose from releases from the undisturbed Yucca Mountain disposal system:
>
> 1. 0.15 mSv (15 mrem) for 10,000 years following disposal; and
>
> 2. 3.5 mSv (350 mrem) after 10,000 years, but within the period of geologic stability.
>
> (b) DOE's performance assessment must include all potential environmental pathways of radionuclide transport and exposure.

As stated in proposed 10 CFR 63.303, compliance with the above numerical requirements is based on the mean of projected doses prior to 10,000 years and on the median of projected doses during the period of geologic stability after 10,000 years (i.e., until 1,000,000 years after permanent closure). Also, the "undisturbed Yucca Mountain disposal system" is not affected by human intrusion. Human intrusion is addressed in Section 2.4.3.

The four specific subcriteria of NUREG-1804, Section 2.2.1.4.1.3, Acceptance Criterion 2 are as follows:

1. A sufficient number of realizations has been obtained, for each scenario class, using the total system performance assessment code, to ensure that the results of the calculations are statistically stable;
2. The annual dose curve includes confidence intervals (e.g., 95th and 5th percentile) to represent the uncertainty in the dose calculations;
3. Repository performance and the performance of individual components or subsystems are consistent and reasonable; and
4. The total system performance assessment results confirm that the repository performance results in annual dose, to the reasonably maximally exposed individual, in any year, during the compliance period, that does not exceed the postclosure individual protection standard.

Section 2.4.2.2.1 addresses Acceptance Criterion 2(2) and Acceptance Criterion 2(4) by showing the dose results (statistical quantiles and major radionuclide contributors) for the seven modeling cases and for the total dose. The annual dose plots, that include 5th and 95th percentile curves for the uncertainty distribution of expected annual doses address Acceptance Criterion 2(2) by indicating the range of uncertainty in the results. Section 2.4.2.2.2 addresses Acceptance Criterion 2(1) by demonstrating statistical stability of the annual dose curves for the seven modeling cases and for the total annual dose, including the confidence intervals for uncertainty in the mean annual dose. Section 2.4.2.2.3 addresses Acceptance Criterion 2(3) by demonstrating consistency between total system and subsystem results.

2.4.2.2.1 Annual Dose to the Reasonably Maximally Exposed Individual

[NUREG-1804, Section 2.2.1.4.1.3: AC 2(2) to (4)]

This section demonstrates that DOE satisfies Acceptance Criterion 2(2) and Acceptance Criterion 2(4) in NUREG-1804, Section 2.2.1.4.1.3. In particular, (1) the mean annual dose to the RMEI for the 10,000-year period after repository closure (proposed 10 CFR 63.303(a)), and the median of the total expected annual dose to the RMEI for the post-10,000-year period ending at 1,000,000 years after disposal, do not exceed the corresponding individual protection standards in proposed 10 CFR 63.311; and (2) the 5th and 95th percentile of the distribution of annual doses indicate the range of uncertainty in the projected annual doses. This section, along with Sections 2.4.2.2.3 and 2.4.2.3.3, also helps to demonstrate that the DOE satisfies Acceptance Criterion 2(3) in NUREG-1804, Section 2.2.1.4.1.3 regarding consistency of total system performance (dose) and subsystem performance. In particular, the following sections explain some of the underlying causes of the shape and magnitude of the total mean annual dose curve through descriptions of the behavior of key processes and submodels, such as release rates, solubilities, waste package degradation, and transport processes. (More in-depth discussion of Acceptance Criterion 2(3) is found in Section 2.4.2.2.3, which discusses details of various single-realization analyses, and also in Section 2.4.2.3.3, which discusses uncertainty propagation in the TSPA model.) In addition to total mean annual dose, the mean annual dose from each of the seven modeling cases that comprise the total mean annual dose curve is shown and explained, including the uncertainty in the distribution of doses for each modeling case.

2.4.2.2.1.1 Quantitative Results for Total Mean or Median Annual Dose

Detailed probabilistic projections of the total annual dose, along with various statistical measures of uncertainty are described in this section. The information will address several questions, including which radionuclides contribute most to the projected annual doses and which scenario classes and processes most influence the projected annual doses. As will be demonstrated below, the numerical limits prescribed in proposed 10 CFR 63.311 are met, with the maximum of the total mean or median annual dose, which is the mean (or median) dose summed over all modeling cases (i.e., all scenario classes) and over all radionuclides, falling well below the statutory limits. A description of which uncertain parameters are most important with respect to uncertainty in total mean annual dose can be found in Section 2.4.2.3.3, which addresses Acceptance Criterion 3(3) in NUREG-1804, Section 2.2.1.4.1.3 regarding uncertainty propagation in the TSPA model.

2.4.2.2.1.1.1 Total Annual Dose, with Associated Uncertainty

The total expected annual dose results computed according to Equations 2.4-19 and 2.4-21 are shown in Figure 2.4-10a for the period within 10,000 years after permanent closure, and Figure 2.4-10b for the post-10,000-year period. The mean, median, and 5th and 95th percentile curves are superimposed on each plot to illustrate the central tendency and uncertainty. The total mean annual dose history, which is plotted as the red curve, is computed by taking the arithmetic average of the 300 expected annual dose values at each time τ along the curves. Similarly, the median dose history, plotted as the blue curve, is constructed by sorting the 300 expected values from lowest to highest at each time τ, and then averaging the two middle values. Curves for the 5th and 95th percentiles are also plotted to illustrate the spread in the expected annual dose histories; 270 of the 300 epistemic realizations of the projected dose histories fall between these two percentile curves. For the 10,000-year period after permanent closure, the maximum mean annual dose to the RMEI is estimated to be about 0.24 mrem, which is below the individual protection limit of 15 mrem. Similarly, the maximum median annual dose for the post-10,000-year period but within the period of geologic stability (1,000,000 years) is estimated to be about 0.96 mrem, which is below the individual protection limit of 350 mrem. Note that the dose for the first 10,000 years of the post-10,000-year dose plot is similar to the 10,000-year dose plot, even though a different time stepping and calculation methodology is used. This provides additional confidence in the two methodologies.

The times of the maximum mean and median doses are shown in Table 2.4-2.

2.4.2.2.1.1.2 Contribution of Modeling Cases to Total Mean Annual Dose

Important risk insights can be gained by disaggregating the total mean annual dose into the mean annual dose contributions from the individual modeling cases, as shown on Figure 2.4-18. From these dose curves, the following general observations can be drawn about the projected postclosure performance:

- Mean annual doses calculated for both the 10,000-year and the post-10,000-year time periods are dominated by dose contributions from the seismic ground motion modeling case (which includes releases caused by nominal corrosion failures) and the igneous intrusion modeling case. (Note: "Failure" of a waste package means a through-wall opening in the Alloy 22 outer barrier, either a crack (which only allows diffusive releases) or a patch (which allows both diffusive and advective releases).)

- Mean annual doses from all other modeling cases for both the 10,000-year and the post-10,000-year time periods comprise on the order of 1% or less of the total mean annual dose for the majority of the simulated time period.

With regard to the first observation, the seismic ground motion modeling case dominates the mean annual dose for 10,000 years after permanent closure, whereas for the post-10,000-year period, the igneous intrusion modeling case and seismic ground motion modeling case provide approximately equal contributions to the total mean annual dose to the RMEI for the last 300,000 years of the time period.

This discussion of the contribution of individual modeling cases to total dose is based on the total mean and the individual modeling case means, even for the post-10,000-year period (when the regulatory metric is the median rather than the mean) because of the mathematical nature of the mean and median. In particular, the sum of the means of the expected annual doses for the individual modeling cases equals the total mean; however, the same cannot be said for the medians; the total median is not the sum of the individual medians. Thus, for the purposes of discussing the influence of the individual modeling case on the total dose, it is more useful and appropriate to discuss means, regardless of the time period. This same rationale also applies in Sections 2.4.2.2.1.1.3 and 2.4.2.2.1.2 in the discussions of the contributions of dose from individual radionuclides to the dose summed over radionuclides, which is also called "total" dose for a given modeling case.

An important clarification regarding the seismic ground motion modeling case is that the releases and annual doses for the 10,000-year time period are only for the damaged codisposal waste packages. As described in Section 2.4.2.2.2.3, the releases from the commercial SNF waste packages contribute only negligibly to the total dose of the seismic ground motion modeling case because of the low consequences of seismic-induced failures of commercial SNF waste packages. Seismic-induced failures of commercial SNF waste packages result in low consequences largely due to the low probability of damage to transportation, aging, and disposal (TAD)-bearing commercial SNF packages in the first 10,000 years (SNL 2008a, Section 7.3.2.6.1.3). The expected damage frequency for TAD-bearing commercial SNF package is calculated to be 5.249×10^{-9} per year, which leads to the probability of failure of 5.249×10^{-5} in 10,000 years.

For most of the postclosure period release of radionuclides from the repository is attributable to effects on EBS components resulting from nominal corrosion processes and from vibratory ground motion and igneous intrusion events. Based on the FEPs screening process (Section 2.2), these two types of disruptive events affect only the EBS barrier. In the case of vibratory ground motion, the important aspects are the occurrence of damage to the waste package (also called waste package failure, which is defined as any through-wall breach in the Alloy 22 outer barrier), the cumulative damage area on the waste packages, and the failure of drip shields. The initial failure and initial damage to waste packages generally results from a relatively large ground motion event. After the waste package is breached, subsequent seismic damage is calculated based on the degraded internals seismic consequence abstraction, whereby small to moderate ground motion events can cause damage, which results in a gradual increase in the number of through-wall stress corrosion cracks in the waste packages (Figures 2.1-13a and 2.1-15a). This accumulation continues up to the time of drip shield plate failure, after which the waste package is modeled to be surrounded by rubble (due to drift degradation), which cushions the waste package from any significant further damage. The stress corrosion cracks release radionuclides to the surrounding host rock through diffusive transport. This mode of transport dominates until patch penetrations of the waste package by general corrosion patches or seismic-induced puncture of the waste packages, after which advective transport also becomes important in seeping environments. General corrosion does not result in patch penetrations until about 500,000 years after repository closure (Figures 2.1-16b and 2.1-17b); however, in the seismic ground motion modeling case there can be a few realizations with seismic ruptures (prior to drip shield plate failure) or punctures (past drip shield plate failure) that allow advective releases much earlier (Figures 2.1-16a and 2.1-17a). In general, the dose attributable to nonsorbing, high solubility radionuclides, such as ^{99}Tc and ^{129}I, is due to the first seismic event, because of their rapid release from the EBS through even small waste-package openings, whereas the dose arising from lower solubility and more highly sorbing actinides, such as ^{242}Pu and ^{237}Np, is proportional to the cumulative waste package opening area, caused by a succession of small to moderate seismic events that follow the first damaging event.

In contrast to the effect of seismic events, in the case of an igneous intrusion into the emplacement drifts, the damage and failure of the waste packages is by a single discrete event that causes complete elimination of the primary contribution of the waste package and drip shield to barrier capability (i.e., isolation from the outside aqueous environment). This results in advection being the dominant release mechanism through all waste packages.

The occurrence of seismic events is described as a Poisson process with the highest annual exceedance frequency, λ_{max}, of potentially damaging events equal to 4.287×10^{-4} per year and the lowest annual exceedance frequency of λ_{min} equal to 10^{-8} per year (SNL 2007c, Section 6.12.2), which is the threshold in proposed 10 CFR 63.342(b) for the occurrence rate of very unlikely events that can be excluded from the performance assessment. Based on these exceedance frequencies from the seismic hazard curve, the expected number of events in any time period T is equal to $(\lambda_{max} - \lambda_{min})T$. Thus, during the first 10,000 years after permanent closure, approximately four potentially damaging events can be expected to occur, compared to approximately 430 potentially damaging events in the 1,000,000-year period after permanent closure (SNL 2008a, Section 6.6.1.3.2). In contrast, the mean annual frequency of a magmatic dike intersecting the repository is estimated to be 1.7×10^{-8} per year (BSC 2004a, Table 7-1), which is just slightly greater than the NRC threshold frequency of 10^{-8} per year for very unlikely events and processes that are excluded from the performance assessment (proposed 10 CFR 63.342(b)), and which leads to an expected number of damaging igneous events equal to about 0.00017 in 10,000 years and 0.017 in 1,000,000 years. Thus, while both igneous and seismic disruptive events are included in the TSPA, seismic events are much more probable, and therefore the focus of much of the subsequent discussion is on seismic consequences. The consequences attributable to igneous events in the TSPA are estimated by assuming that all waste packages and drip shields in the repository are completely destroyed by any dike that intersects the repository. (Note that the expected number of actually damaging seismic events is significantly less than the expected number of potentially damaging seismic events. For example, the expected frequency of damaging seismic events for codisposal packages with intact internals, is equal to 7.48×10^{-6} per year when averaged over all values of the residual stress threshold, which implies that there are less than 0.075 damaging seismic events in 10,000 years. However, this expected number of seismic events is still orders of magnitude more than the expected number (0.00017) of igneous events in 10,000 years.)

Seismically-induced damage of the waste packages is most likely to occur from deformation or denting of the Alloy 22 outer wall (Section 2.3.4.1). These localized areas of deformation or denting develop residual stresses that can cause damage by stress corrosion cracking (which allows only diffusive releases of radionuclides). Rupture or puncture of the Alloy 22 outer wall of a waste package can also occur (which allows advective releases of radionuclides) but only as a result of low probability strong-ground-motion earthquakes (SNL 2008a, Section 7.3.2.6.1.3). The probability of incurring seismic damage as a function of time for codisposal and commercial SNF waste packages is shown on Figure 2.4-19. As shown in Figure 2.4-19, the commercial SNF waste package has a very low probability of failing by events in the first 10,000 years and a low probability of failing for 1,000,000 years. (Note that the expected fraction of waste packages breached is the same as the probability of incurring seismic damage because prior to the breach the failure fraction is zero and following the breach it is one.)

Damage of the waste packages by either nominal degradation processes, such as general corrosion, or by seismic or igneous events, will allow radionuclides to be available for transport out of the EBS. The processes involved in such transport are discussed in Sections 2.1 and 2.3.

A much more in-depth discussion and explanation of the dose projections for each of the seven modeling cases is presented in Section 2.4.2.2.1.2.

2.4.2.2.1.1.3 Radionuclides Important to Postclosure Performance

The contributions of the individual radionuclides to the total mean annual dose are shown on Figure 2.4-20 for 10,000 years and post-10,000 years after disposal. All dose curves on this figure are mean annual dose curves. The radionuclides that dominate the calculation of annual doses typically have a combination of unique characteristics such as: (1) large initial inventory in the nuclear waste, (2) moderate to high solubility, (3) long half-life (e.g., $\geq 10^5$ years), and (4) low sorption. The radionuclides that become important to dose also depend on the time frame considered (i.e., 10,000 years or 1,000,000 years after permanent closure) because of the effect of radionuclide decay and the effect of retardation from sorption along the flow path. Ingrowth of radionuclides via chain decay over a very long period of time can also be an important process that determines the role and importance of radionuclides in the actinium, uranium, neptunium, and thorium decay series (Figure 2.4-21) (SNL 2008a, Section 8.1.1.5[a]).

Important Radionuclides for 10,000-Year Performance—The mean dose curves shown on Figure 2.4-20a, show the principal contributors to the mean annual dose, ranked from highest to lowest, are: ^{99}Tc (half-life 2.13×10^5 years), ^{14}C (half-life 5.72×10^3 years), ^{239}Pu (half-life 2.41×10^4 years), ^{129}I (half-life 1.57×10^7 years), ^{36}Cl (half-life 3.01×10^5 years), ^{240}Pu (half-life 6.56×10^3 years), ^{79}Se (half-life 2.90×10^5 years), and ^{237}Np (half-life 2.14×10^6 years) (SNL

2008a, Table 6.3.9-1[a]). Collectively, these eight radionuclides account for over 99% of the maximum mean annual dose, which occurs at the end of 10,000 years. The single largest contributor is ^{99}Tc, which accounts for about 51% of the maximum mean dose.

The dominant fission products, ^{99}Tc and ^{129}I together with the activation product, ^{14}C, which is treated in the TSPA as having similar mobilization and transport properties as ^{99}Tc, contribute to the mean dose because they are very soluble in water, do not sorb to materials in the engineered system and natural system, and (with the exception of ^{14}C) have long half-lives relative to the 10,000-year time frame. Their release rates are limited only by: (1) the waste-form degradation rate, (2) the rate and extent of water ingress into the waste package, and (3) the relevant mass transport mechanism (i.e., diffusion and/or advection) out of the waste package (SNL 2008a, Section 8.1.1.5[a]). Their nonsorbing nature causes these radionuclides to be transported from the EBS through the Lower Natural Barrier and to the RMEI with no delay by chemical retardation. A description of repository barrier capabilities with respect to ^{99}Tc has previously been presented in Section 2.1. (Note: Although ^{14}C can be expected to have a significant partitioning into the gas and mineral phases, because of the complexity of modeling the associated reactive transport processes and because the ^{14}C inventory is relatively small, ^{14}C is treated as behaving similarly to non-reactive tracers, such as ^{99}Tc and ^{129}I—see excluded FEP 2.2.11.03.0A, Gas transport in geosphere (Table 2.2-1) (SNL 2008c, Section 6).)

Important Radionuclides for Post-10,000-Year Performance—Figure 2.4-20b shows that between 10,000 years and 20,000 years, the dominant radionuclides are the same as those listed for the 10,000-year performance projection, namely, ^{99}Tc, ^{14}C, ^{239}Pu and ^{129}I; however, ^{239}Pu becomes increasingly important with time. Between about 20,000 years until 200,000 years, the radionuclides with largest contributions to total mean annual dose are ^{239}Pu and ^{99}Tc, with ^{242}Pu (half-life 3.75×10^5 years) supplanting ^{99}Tc around 150,000 years to become the second highest dose contributor. Beyond 200,000 years, ^{242}Pu is the largest contributor, with secondary contributions from ^{99}Tc, ^{129}I, ^{237}Np (half-life 2.14×10^6 years), and ^{226}Ra (half-life 1,600 years). The peak of the total mean annual dose occurs at 1,000,000 years; the radionuclides contributing to total mean annual dose, ranked from highest to lowest, are: ^{242}Pu, ^{237}Np, ^{226}Ra, and ^{129}I. These four radionuclides account for about 77% of the total mean annual dose, with ^{242}Pu and ^{237}Np together accounting for about 52% of the total mean annual dose. (Note that the ^{226}Ra mean annual dose curve, which is overlain by the ^{237}Np dose curve for the period from about 300,000 to 700,000 years, represents the sum of ^{226}Ra and ^{210}Pb doses, based on an assumption of secular equilibrium. Thus, a combined biosphere dose conversion factor (BDCF) is used for these two radionuclides, which has a contribution of about 42% from the individual ^{210}Pb BDCF and 58% from the ^{226}Ra BDCF (Figure 2.3.10-11).)

The persistent importance of ^{99}Tc and ^{129}I to total mean annual dose for the post-10,000-year period (Figure 2.4-18) is derived from their contributions to mean annual dose from seismic ground motion modeling case, where commercial SNF waste packages gradually fail by nominal corrosion processes, most commonly by stress corrosion cracking of lid welds (Figures 2.1-13a and 2.1-15a). As these waste packages fail, additional quantities of ^{99}Tc and ^{129}I are released from the EBS, which results in continual releases of these radionuclides from the repository system throughout the 1,000,000 year period. Beyond 20,000 years, two plutonium species, ^{239}Pu and ^{242}Pu, are the dominant contributors to total mean annual dose, with ^{242}Pu supplanting ^{239}Pu at about 200,000 years due to radioactive decay of the latter. The contribution of these two plutonium species to total mean annual dose is due primarily to the igneous intrusion modeling case, where these two species comprise the dominant contributors to mean annual dose and are transported out of the waste package by both advection and diffusion once all waste packages fail following the igneous event. The contribution of ^{237}Np and ^{226}Ra to total mean annual dose is also primarily from the igneous intrusion modeling case. ^{237}Np has a long half-life and undergoes moderate retardation during its transport, while the ^{226}Ra dose, even though ^{226}Ra has a relatively short half life (1,600 years), is sustained through chain decay of the longer lived radionuclides ^{230}Th (half-life 7.54×10^4 years) and ^{234}U (half-life 2.46×10^5 years), which travel with some retardation in the unsaturated zone and saturated zone.

2.4.2.2.1.2 Expected Annual Doses for the Individual Modeling Cases

To clarify and help explain the behavior of the total annual dose projections in the previous section, this section presents the probabilistic dose projections for the seven individual modeling cases. As indicated previously, the distributions of annual dose to the RMEI are based on a summation (Equations 2.4-19 and 2.4-21) of the expected annual doses over the scenario-class modeling cases. The individual scenario-class modeling cases are: (1) nominal; (2) waste package early failure; (3) drip shield early failure; (4) igneous intrusion; (5) volcanic eruption; (6) seismic ground motion; and (7) fault displacement. As stated earlier, for 1,000,000-year calculations the nominal modeling case is not explicitly included in the sum of expected doses from the other six modeling cases because its effects are already embedded in the seismic ground motion modeling case, and to a lesser extent in the igneous intrusion modeling case. Also, as mentioned in the previous section, contributions of modeling cases to the total annual dose, and contributions of individual radionuclides to the total annual dose, are generally described in terms of the mean expected annual dose, even for the post-10,000-year period, because the sum of the means equals the mean of the sum, which is not the case for medians.

As mentioned in the previous section and displayed in Figure 2.4-18, examination of the projected annual doses for the individual modeling cases leads to the following general observations about relative importance of these modeling cases:

- Mean annual doses calculated for both the 10,000-year and the post-10,000-year time periods are dominated by releases from the seismic ground motion and igneous intrusion modeling cases.

- Mean annual doses from all other modeling cases (i.e., waste package early failure, drip shield early failure, seismic fault displacement, and volcanic eruption) for both the 10,000-year and the post-10,000-year time periods comprise on the order of 1% or less of the total mean annual dose.

- Mean annual doses from the drip shield early failure and volcanic eruption cases are least important to the total mean annual dose and comprise on the order of 0.1% or less of the total mean annual dose in the first 10,000 years and on the order of 0.01% or less of the total mean annual dose in the post-10,000-year period.

At the maximum of the total mean annual dose in 10,000 years (which takes place at 10,000 years), the seismic ground motion modeling case contributes about 71% and the igneous intrusion modeling case contributes about 27% of the maximum mean dose. In contrast, for the post-10,000-year period, the seismic ground motion and igneous intrusion modeling cases contribute almost equally to the maximum of the total mean (which occurs at 1,000,000 years) (Figure 2.4-18). A discussion of the causes of this behavior follows.

2.4.2.2.1.2.1 Nominal Modeling Case

The nominal scenario class serves as a "reference system state" from which all other modeling cases are developed and is a representation of the set of possible repository futures when disruptive events and early failures of drip shields and waste packages are excluded. The system behavior for the nominal modeling case is defined in terms of the likely and unlikely included FEPs that describe the evolution of the natural and engineered barriers in the absence of disruptive events and early failure events. The technical discussion for the representation of this nominal scenario class is summarized in Section 2.4.2.3.2.1 and Section 2.1 and discussed in detail in Section 2.3. Characteristics of the nominal scenario class include:

1. Climate changes and attendant changes in net infiltration and percolation in the Upper Natural Barrier

2. Seepage of percolating water into the repository drifts

3. Changes to the water chemistry induced by repository heating

4. Progressive degradation of the engineered barriers by corrosion processes and subsequent partial loss of the waste isolation integrity

5. Accumulation of moisture inside the waste packages, degradation and dissolution of the waste forms, and mobilization of the radionuclides

6. Migration of dissolved and colloidal-phase radionuclides through and out of the EBS Barrier

7. Radionuclide transport through the Lower Natural Barrier and to the accessible environment

8. Water withdrawal and exposure to the RMEI.

The probabilistic projections of annual dose for this modeling case are shown on Figure 2.4-22a. As can be seen from this plot, there are no doses to the RMEI due to nominal processes alone in the 10,000-year period after disposal.

As indicated in Figures 2.1-9a and 2.1-9b, there is only a 5% chance of having a waste package failure due to nominal processes prior to about 170,000 years (i.e., 95% of the possible repository futures have had no waste package failures by nominal processes alone for at least 170,000 years after permanent closure). These initial failures are due to stress corrosion cracking of the closure-lid welds (Figure 2.1-10a). The number of these through-wall cracks per breached waste package gradually increases with time (Figures 2.1-13b and 2.1-15b), leading to an increased area for diffusion through the thin water films adsorbed to the pore walls of the degraded waste form and the corrosion products of the degrading waste package (both the stainless-steel inner vessel and the Alloy 22 outer corrosion barrier). Realizations with waste package failures by general corrosion patches (Section 2.3.6.2.2), which allow both diffusive and advective transport of radionuclides through the Alloy 22 outer corrosion barrier, take much longer to appear, as indicated in Figure 2.1-10b. The surface area affected by through-wall patches increases with time as the waste package outer barrier thins from general corrosion (Figures 2.1-16b and 2.1-17b). (The spatially averaged thickness of the outer corrosion barrier is shown in Figure 2.4-23.) There is only a 5% chance of a general corrosion patch penetration prior to 600,000 years. By 1,000,000 years, approximately 57% of the waste packages are projected to have failed by stress corrosion cracking and about 9% by general corrosion patches (Figure 2.1-10).

Regarding the integrity of the drip shields, Figure 2.1-8 indicates that there is a 5% chance of failure of the drip shields by nominal processes alone prior to 280,000 years but a 95% chance prior to 312,000 years. Thus, the uncertainty regarding the drip shield general corrosion rate has a relatively narrow range. There is no spatial variability regarding drip shield failure in the TSPA, so all drip shields fail concurrently when general corrosion has completely thinned the initial 15 mm-thick titanium drip shield plates (SNL 2007d, Table 4-2). However, drip shield failures occur in the TSPA through a combination of general corrosion thinning and static and dynamic loading caused by rockfall and strong vibratory ground motion in the seismic ground motion modeling case (SNL 2008a, Section 8.1.1.3[a]). This causes the drip shields to fail somewhat earlier than the approximately 300,000-year expected failure time from general corrosion alone. The difference is indicated in Figure 2.4-24.

The TSPA results for the post-10,000-year period indicate that the chance of radiologic exposure to the RMEI is less than 5% before about 160,000 years after closure (Figure 2.4-22a). The maximum median annual dose for this reference modeling case (where only nominal processes are considered) is about 0.3 mrem, occurring about 850,000 years, while the peak mean annual dose is about 0.5 mrem, occurring at about 730,000 years. Two radionuclides dominate the mean annual dose over most of the post-10,000-year performance period. These radionuclides are the highly soluble, long-lived, and mobile radionuclide species ^{129}I and ^{99}Tc. At 1,000,000 years, several other radionuclides contribute to total mean dose, including ^{242}Pu, ^{135}Cs, ^{237}Np, and ^{79}Se, as indicated in Figure 2.4-22b. The mobile radionuclides such as ^{129}I and ^{99}Tc are released quickly by diffusion though stress corrosion cracks once the waste package is breached and their release rate is primarily controlled by the waste package failure rate (Figure 2.1-9). On the other hand, the release of radionuclides such as ^{242}Pu and ^{237}Np out of the waste package is considerably slower and is primarily controlled by imposed dissolved concentration limits (from solubility of controlling mineral phase) and by sorption on the stationary corrosion products inside the waste package (SNL 2008a, Section 7.7.1.5[a]). The dose from ^{242}Pu and ^{237}Np continues to increase with the increasing number and surface area of failed packages by general corrosion patch penetrations (Figures 2.1-10b and 2.1-16b).

Although the individual dose histories on Figure 2.4-22a are labeled as “expected annual dose,” they do not involve an explicit expectation over aleatory uncertainty. However, there is an implicit expectation over the aleatory uncertainty associated with the spatial location of waste packages failed by nominal processes alone, in the sense that each percolation subregion and each waste package type involve a different set of thermal-hydrologic conditions, which produces a different waste package failure curve for each location and type (Section 2.4.2.1.5.1). The uncertainty in expected annual dose is found to result predominantly from the uncertainty in the temperature-dependent coefficient for the general corrosion rate of Alloy 22 (Section 2.4.2.3.3.4) (Note that the several jumps in the annual dose curves at 200,000, 300,000, 500,000, and 700,000 years are due to the temporal discretization used in the waste package degradation code WAPDEG—see Sections 2.4.2.2.3.1 and Sections 2.4.2.3.2.2.2). The stress corrosion crack growth rate is reevaluated at each calculation timestep using the waste package thickness and stress profiles appropriate for the time step. When increases in the growth rate occur, existing cracks may penetrate the remaining thickness rapidly, resulting in several breaches immediately after the timestep. The increase in the number of waste package failures is the cause of the resulting dose increase.

As mentioned previously, it is very important to differentiate the nominal modeling case results from those for other modeling cases. The nominal modeling case projections of annual dose are not to be taken as a representation of compliance with radiation protection limits because the mean annual dose for the nominal modeling case is not summed into the calculation of the total mean annual doses for the post-10,000-year period (Equation 2.4-21). Rather, the effect of nominal drip shield and waste package corrosion processes for the post-10,000-year period are accounted for in the seismic ground motion modeling case (see explanation in Section 2.4.2.1.4). This special nominal modeling case only provides a reference system state that can be compared to the other six modeling cases.

2.4.2.2.1.2.2 Seismic Scenario Class Modeling Cases

As described in Sections 2.4.2.1 and 2.4.2.3.2.1.12.3, the seismic scenario class consists of two modeling cases: (1) the seismic ground motion modeling case and (2) the seismic fault displacement modeling case. These modeling cases take into account the aleatory uncertainty in the timing and number of seismic events and various random effects of seismic events on the integrity of drip shields, waste packages, and emplacement drifts (SNL 2008a, Table 6.6-2). They also include epistemic uncertainties related to several important parameters, including both the residual stress threshold for crack propagation through Alloy 22 and the density of the ensuing crack network for the seismic ground motion case. The probabilistic projections for expected annual doses for the seismic scenario class are based on seismic events with a mean annual exceedance frequency in the range of 4.287×10^{-4} to 10^{-8} per year from the ground-motion hazard curve and a range of 2.5×10^{-7} to 10^{-8} per year from the fault-displacement hazard curve (SNL 2007c, Sections 6.4.3 and 6.11.4).

For the seismic ground motion modeling case for most of the postclosure period (at least until about 600,000 years after closure) the important release pathway for each waste package is the accumulated crack damage induced by vibratory ground motion events (Figures 2.1-13a, 2.1-15a, 2.1-16a, and 2.1-17a). Only diffusive radionuclide releases occur through these cracks. Rarer rupture or puncture events cause patch openings in the waste packages, which allow advective releases, but their contribution to dose is small because of their low probability (SNL 2008a, Section 7.3.2.6.1.3). However, patch failures caused by nominal general corrosion processes become important at about 600,000 years after closure and allow advective transport of radionuclides out of the waste packages. In the seismic fault displacement modeling case, the releases are mainly via advection, due to the failure of the drip shield and the open breach area in the waste package and the fact that about 70% of the waste packages are modeled as being in a seeping environment (SNL 2008a, Table 8.3-5[a] and Table P-2). Thus, the release and transport behavior of the radionuclides in the seismic fault displacement modeling case is expected to be similar to the other two modeling cases that primarily have advective releases, which are the drip shield early failure modeling case and the igneous intrusion modeling case, as described below.

2.4.2.2.1.2.2.1 Seismic Ground Motion Modeling Case

The seismic ground motion modeling case focuses on postclosure performance as a function of EBS disruptions caused by vibratory ground motion. Depending on the timing, sequence, and intensity of the ground motion events, the drip shields could fail by either buckling of the drip shield framework or rupture of the drip shield plates (SNL 2008a, Section 8.2.4.1). Similarly, the waste packages can be damaged by: (1) local tensile strain resulting in stress that exceeds ultimate tensile strength (rupture); (2) deformations creating residual stresses that induce stress corrosion cracking; and (3) lithostatic loading from rockfall that causes a puncture of the outer barrier by the degraded waste package internals (Section 2.4.2.3.2.1.12.3). Drip shields and waste packages are also degraded by nominal corrosion processes (e.g., general corrosion of the waste packages and drip shields and stress corrosion cracking of the waste-package closure lid welds). Drift degradation also results in a significant increase in the fraction of waste packages that encounter seeping conditions, from 40% to 69% based on the increase in the seepage fraction (SNL 2008a, Tables 8.3-3[a] and 8.3-5[a]).

The expected annual dose histories for the seismic ground motion modeling case are shown in Figure 2.4-25 for the (a) 10,000-year period, and (b) post-10,000-year period. The mean, median, and 5th and 95th percentile curves indicate the range and central tendency of the epistemic uncertainty. Each of the 300 expected annual dose curves in this figure is an average over the aleatory uncertainty associated with the seismic ground motion—specifically, the number of future events and the time at which they occur, as well as the EBS damage associated with each event (SNL 2008a, Section 6.1.2.4.4). This figure shows that the maximum mean annual dose for the first 10,000 years after closure is less than 0.2 mrem, while the maximum median expected dose in the 1,000,000-year period after closure is less than 0.5 mrem. The expected annual dose curves for 1,000,000 years are not as smooth as the ones for 10,000 years because of the two different integration methods that are used. In particular, the random sampling of aleatory uncertainty in the 1,000,000-year case is fairly coarse (sample size = 30), but sufficient, as described in Section 2.4.2.2.2.3. However, despite the coarseness of the aleatory integration for 1,000,000 years, the annual dose at 10,000 years in Figure 2.4-25b is approximately the same (equal to about 0.2 mrem) as the dose indicated on Figure 2.4-25a. This is the case even though the integration methods for computing the aleatory expectation (Section 2.4.2.1.5.4) are quite different for the 10,000-year analysis (quadrature) versus the million-year analysis (Monte Carlo sampling) and even though the dose presented in the 10,000-year analysis is strictly due to stress corrosion cracking damage of codisposal waste packages, whereas the million-year analysis includes all possible seismic damage mechanisms in the dose computation (Section 2.4.2.1.5.4). (Also, the numerical timestepping in the GoldSim calculations is coarser in the million-year analysis compared to the 10,000-year analysis.)

The radionuclides that contribute most to the estimate of mean annual dose for this modeling case are presented on Figure 2.4-26. These mean dose curves illustrate that five radionuclides, ^{99}Tc, ^{14}C, ^{129}I, ^{36}Cl, and ^{79}Se, contribute most to the maximum mean annual dose for the 10,000-year time period, while the radionuclides that contribute most to the maximum mean annual dose for the post-10,000 years are ^{242}Pu, ^{129}I, ^{237}Np, ^{135}Cs, and ^{231}Pa (Figure 2.4-26). As previously mentioned, the predominant damage to the codisposal and commercial SNF waste packages are stress corrosion cracks that result in releases from the waste packages by diffusion. Diffusive transport of dissolved radionuclides through the cracks is relatively rapid for high solubility radionuclides such as ^{99}Tc and ^{129}I, which is why they dominate the mean dose curve.

The different shapes of the various radionuclide annual dose curves in Figure 2.4-26b for the 1,000,000-year period, such as ^{129}I versus ^{242}Pu, are the result of a combination of a number of competing processes. For example, the ^{129}I dose curve is relatively flat and stable for the entire 1,000,000-year period, whereas the ^{242}Pu dose curve (as well as the other actinide dose curves) is steadily increasing (although radioactive decay does begin to limit the increase of ^{242}Pu toward the end of the 1,000,000 years, since its half life is about 375,000 years). These two different behaviors reflect the fact that highly soluble radionuclides such as ^{99}Tc and ^{129}I have nearly instantaneous release and depletion from the waste packages and so their releases and doses are controlled by the waste package failure rate. In other words, a relatively constant waste package failure rate (as demonstrated by the slope of the mean curve on Figure 2.1-12a) will produce a relatively flat and constant release and dose for quick-release radionuclides, such as ^{129}I and ^{99}Tc. On the other hand, solubility-limited radionuclides that undergo sorption, such as ^{242}Pu or ^{237}Np, have nearly constant continuous release from all failed waste packages (Figure 2.1-23b). Thus, because the number of commercial SNF waste packages continue to fail by nominal corrosion processes through time, primarily by stress corrosion cracking (Figure 2.1-10a), there is a continually increasing slow release of actinides available for transport in the EBS, such as ^{242}Pu or ^{237}Np. This different release behavior for these two classes of radionuclides is discussed in Section 2.4.2.2.3, which describes in detail the behavior of the repository system for a single future in the seismic ground motion case.

Other factors also contribute to the shape of the individual dose curves. For example, the more sharply rising nature of the ^{242}Pu and ^{237}Np mean dose curves after about 600,000 years is due to a significant increase in the advective breach area of the failed waste packages, which causes a proportional increase in releases of solubility-limited radionuclides, such as ^{242}Pu and ^{237}Np (Figure 2.1-23b). This is associated with the increasing number of packages that have general corrosion patch failures (Figure 2.1-10b) and the increasing expected number of general corrosion patches per failed waste package (Figure 2.1-16b). Comparison of the seismic ground motion dose histories in Figure 2.4-26b with the waste package fractional failure histories in Figures 2.1-12a and 2.1-12c shows that releases from codisposal waste packages dominate doses prior to about 250,000 years, and that the commercial SNF releases arising from a combination of nominal and seismic processes dominate releases later in time. This is because seismic failures of codisposal packages occur early in time, since they lack the structural strength of the TAD-bearing commercial SNF packages (although the seismic codisposal failures generally only result in a very tiny open crack area that allows diffusive transport). More specifically, it is rare for an intact commercial SNF waste package to fail by seismicity; however, as shown in Figures 2.1-9a and 2.1-10a, nominal stress corrosion cracking processes result in through-wall cracks in the lid weld region beginning at about 200,000 years. After a nominal stress corrosion crack penetrates Alloy 22, it is assumed that the inner vessel and the TAD canister degrade rapidly, which causes the commercial SNF package to lose structural strength. At that point it can be damaged more readily (i.e., there is greater probability of damage) by subsequent seismic events, particularly if the drip shield plates are still not failed, resulting in increased area for diffusion. This only has an effect while the drip shield plates are still intact because after drip shield plate failure the applicable seismic abstraction model is the abstraction for a waste package surrounded by rubble (Section 2.4.2.3.2.1.12.3), which is applied regardless of the condition of the waste package internals. The use of the surrounded by rubble abstraction is appropriate because analyses have shown that the drip shields typically fail by rubble loading prior to the time of drip shield failure by corrosion processes. Also, applying the abstraction for degraded internals to waste packages whose internals may still provide some structural strength is considered a bounding approach (SNL 2007c, Section 6.9). Because the rock rubble pins the waste package in place after drip shield plate failure, and therefore reduces the seismic impact and deformation forces encountered by the package, subsequent seismic events cause little damage to the waste package (SNL 2008a, Section 7.7.1.4[a]). This is why the damage curve flattens out beyond about 250,000 years (Figure 2.1-15a). (Only rarely occurring large events can cause damage to a waste package after it is surrounded by rubble (SNL 2008a, Figure 6.6-15)).

As demonstrated in Section 2.4.2.3.3.6, the occurrence of damage to waste packages in the first 200,000 years is strongly affected by the uncertainty in the residual stress threshold for Alloy 22. The probability of waste package damage decreases as the residual stress threshold increases. At later times, the uncertainty in the temperature dependent coefficient for general corrosion rate of Alloy 22 becomes important, indicating the increasing importance of nominal corrosion processes.

2.4.2.2.1.2.2.2 Seismic Fault Displacement Modeling Case

As described in Section 2.4.2.3.2.1.12.3, the expected number of waste package failures that could occur due to fault displacement is less than 1% of the total number of waste packages in the repository (SNL 2008a, Table 6.6-1). The EBS consequences of a fault displacement that occurs in an emplacement drift are a sudden discontinuity in the profile of the drift, which could result in one portion of the drift being displaced vertically or horizontally relative to the adjacent section. Such a discontinuity in the drift could cause shearing of the waste package and drip shield located over the fault if the fault displacement exceeds the available clearance in the EBS (taken to be one-quarter of the outer diameter of the waste package (SNL 2007c, Section 6.11.1.2)).

Fault displacement events are only caused by extremely low frequency, high amplitude seismic events, corresponding to an annual exceedance frequency of less than or equal to 2.5×10^{-7} per year (SNL 2007c, Table 6-67). At greater frequencies no effects of fault displacement are considered in the TSPA. Damaging fault displacement events are considered to cause an open breach area in the waste package and a complete elimination of the drip shield's ability to limit advective flow into the waste package. The drift is also assumed to be collapsed or significantly degraded following the event, allowing a higher seepage rate (SNL 2008a, Section 6.3.3.1.2). Given the complexity of the response of EBS components and the invert to a fault displacement, a simplified failure criterion is applied to determine shear failure in a collapsed drift. If the fault displacement exceeds one-quarter of the outer diameter of the outer corrosion barrier (about 0.4 to 0.5 m), the waste package fails from shear (SNL 2007c, Section 6.11.1.2). The simplified failure criterion is justified by the fact that fault displacement events affect very few waste packages (SNL 2007c, Table 6-87) and are caused only by low frequency seismic events.

The expected mean annual dose histories for the seismic fault displacement modeling case are shown on Figure 2.4-27 for the (a) 10,000-year period, and (b) 1,000,000-year period. The expected annual dose takes into account aleatory uncertainty associated with the number and timing of fault-displacement events and the number and damage area of affected waste packages (SNL 2008a, Section 6.1.2.4.4). The mean, median, and 5th and 95th percentile curves on Figure 2.4-27 show uncertainty in the value of the expected annual dose, taking into account epistemic uncertainty associated with parameters related to nominal processes such as degradation, release, and transport processes. Figure 2.4-27 shows that the maximum mean annual dose from fault displacement for 10,000 years postclosure is less than 0.002 mrem and that the maximum median expected dose for the 1,000,000-year time period is approximately 0.01 mrem.

The individual radionuclide contributions to mean annual dose are shown in the results presented on Figure 2.4-28 for the 10,000 year and post-10,000-year period after closure. The plot for the 10,000-year period shows that ^{99}Tc and ^{129}I dominate the dose for the first 5,000 years after closure and that ^{99}Tc and ^{239}Pu dominate for the subsequent 5,000 years. Figure 2.4-28b shows that ^{239}Pu (half-life equal to 24,100 years) dominates the mean annual doses for the period after 10,000 years and up to about 200,000 years. At 1,000,000 years, the radionuclides contributing most to mean annual dose are ^{242}Pu, ^{237}Np, and ^{226}Ra. The contributions and behavior of the individual radionuclides for this advection-dominated modeling case are similar to the contributions and behavior of other advection-dominated modeling cases, such as the drip shield early failure case and the igneous intrusion case.

As described in Section 2.4.2.3.3.8, during the 10,000 year period after closure the uncertain inputs that (1) influence the rate of water flow (such as the saturated-zone groundwater specific discharge and the infiltration scenario) and (2) affect ^{99}Tc dose (such as the biosphere dose conversion factor for technetium) have the strongest influence on the uncertainty in the expected annual dose. For the post-10,000 year period after closure, the uncertain parameters that influence the rate of water flow continue to remain important, but other uncertain input parameters also become important due to the fact that other radionuclides, such as ^{239}Pu and ^{242}Pu, contribute strongly to the total mean annual dose. For example, the uncertain parameter that influences plutonium solubility is important at late times.

2.4.2.2.1.2.3 Igneous Scenario Class Modeling Cases

The projections for the igneous scenario class demonstrate postclosure performance for unlikely igneous events and processes that could disrupt the EBS. As noted in Section 2.4.2.2.1.1.2, the estimated annual frequency of igneous activity at the repository site is 1.7×10^{-8} per year (BSC 2004a). The TSPA submodel for igneous intrusion EBS damage assumes that all the 3,416 codisposal and 8,213 commercial SNF modeled waste packages and associated drip shields completely fail when exposed to the magma. As previously described, the igneous scenario class consists of two modeling cases: (1) the igneous intrusion modeling case that represents the intersection of one or more magmatic dikes with the emplacement drifts and the ensuing release of radionuclides to the groundwater; and (2) the volcanic eruption modeling case that represents a hypothetical eruptive conduit to the ground surface and the subsequent dispersal of radionuclides to the atmosphere.

2.4.2.2.1.2.3.1 Igneous Intrusion Modeling Case

In this modeling case, a simulated magmatic dike intersects a drift in the geologic repository, causing failure of the waste packages and drip shields (Section 2.4.2.3.2.1.12.2). Radionuclides are then transported out of the EBS primarily by advection, because the drip shield has been compromised and the waste package has lost its integrity to flow. The natural barriers function in the same way as the other modeling cases. As mentioned previously, this modeling case assumes that a dike intersection of any emplacement drift will affect all emplacement drifts via communication along the main drifts and ventilation drifts, causing failure of all waste packages. With drifts assumed to be filled with magma, which then fractures as it cools, the drifts will not act as a capillary barrier. Accordingly, the seepage water flux into a magma-intruded drift is assumed equal to the percolation flux in the overlying host rock (SNL 2008a, Section 8.2.3.1). Both the geometry of the waste form (which is important for diffusive transport) and the formation of corrosion products from degradation of the waste package are assumed to be the same as in the nominal scenario class.

The expected annual dose histories for the igneous intrusion modeling case are shown in Figure 2.4-29 for the (a) 10,000-year period and (b) post-10,000 year period. The mean, median, and 5th and 95th percentile curves indicate the range and central tendency of the epistemic uncertainty. Each of the 300 expected annual dose curves on this figure is calculated by taking an expectation over the aleatory uncertainty associated with the igneous intrusion—specifically, the number of future events and the time at which they occur (SNL 2008a, Section 6.1.2.4.3). Figure 2.4-29 indicates that the maximum mean annual dose for the 10,000 year time period is less than 0.1 mrem and the maximum median dose for the post-10,000-year time period is less than 0.5 mrem.

Figure 2.4-30 shows that ^{99}Tc and ^{129}I dominate the estimate of the mean for the first 4,000 years and ^{239}Pu, ^{99}Tc, ^{240}Pu, and ^{129}I dominate the estimate of the mean for the remainder of the 10,000-year postclosure period. Figure 2.4-30 also indicates that ^{239}Pu, which is transported both in dissolved and colloidal form, dominates the maximum mean annual dose for the first 150,000 years and ^{242}Pu, ^{237}Np, and ^{226}Ra dominate the estimate of the mean for the remainder of the post-10,000-year time period. The behavior of the major radionuclides is similar between the igneous intrusion case and the drip shield early failure case, described later. This is because both cases are dominated by advective transport due to the total failure of the drip shield and waste package. The waste package early failure case, described later, is also similar, but has a greater delay in the rise of importance of ^{239}Pu because diffusive transport (the only mode of transport in the early failure waste package case up to about 300,000 years) combined with sorption is a slower mode of release than advective transport combined with sorption (sorption in the waste package corrosion products). In the igneous intrusion case compared to the other two advection-dominated release cases (drip shield early failure and seismic fault displacement), the in-package uranium solubility is on average higher, because of the occurrence of silica-rich solubility-controlling mineral phases, such as Na-boltwoodite, that are possible due to the availability of dissolved silica from basalt dissolution (SNL 2008a, Section 6.3.7.5.2).

The behavior related to the nature of Poisson processes can be seen in the different shapes of the individual radionuclide mean dose curves on Figure 2.4-30. The ^{129}I dose curve is relatively flat and stable for the entire 1,000,000-year period (and essentially unaffected by radioactive decay because of its long half-life), whereas the dose curves for actinides with long half-lives, such as ^{235}U, ^{238}U, and ^{237}Np (and their decay products) are steadily increasing. These two differing behaviors are a result of the Poisson nature of igneous activity at the repository in which the probability of an igneous event increases linearly through time at a value of $\lambda\tau$ for small $\lambda\tau$ (where λ is the annual occurrence rate, with a mean of 1.7×10^{-8} per year for igneous activity, and τ is the time since closure). This steadily increasing probability has two different manifestations when combined with: (1) nearly instantaneous release (and limited dispersion and delay in the natural system) of a radionuclide such as ^{129}I, and (2) nearly constant continuous release of a solubility-limited radionuclide that undergoes sorption such as ^{235}U or ^{237}Np (SNL 2008a, Section 8.2.3.1[a]). The manifestations are as previously mentioned: a relatively constant expected-value consequence (dose) for the instantaneous release radionuclide and an approximately linearly increasing expected-value consequence (dose) for the constant release radionuclide. (The linear increase of expected dose with time is more obvious on a linear y-axis scale.) The expected dose curve for ^{129}I is not perfectly flat through time, as would be expected for a Poisson process, but rather begins to show a decreasing tendency in mean annual dose beginning about 400,000 years after repository closure. This is because, as mentioned in Section 2.4.2.1.5.3, nominal corrosion processes (e.g., stress corrosion cracking and general corrosion) are included in the igneous intrusion modeling case prior to the occurrence of the event, which leads to some ^{129}I inventory depletion prior to the occurrence of late-time igneous events. The contribution of ^{129}I released prior to the igneous intrusion is not included in the dose curve for the igneous intrusion case (but is instead included in the seismic ground motion modeling case), thereby leading to the decreasing tendency at late times in Figure 2.4-30.

The uncertain input that predominately explains the uncertainty in the expected annual dose is the rate of occurrence of the igneous intrusive event. Other uncertain inputs that are identified as having a lesser effect on expected annual dose are related to those that influence the rate of water flow in the natural system (such as the saturated zone groundwater specific discharge and the infiltration scenario).

2.4.2.2.1.2.3.2 Volcanic Eruption Modeling Case

In this modeling case, the EBS disruption is conceptualized as a volcanic eruptive conduit intersecting an emplacement drift resulting in a portion of the waste dispersed through waste-contaminated tephra in the atmosphere, with attendant deposition of contaminated tephra on the land surface. The performance projections evaluate the post-eruption consequences due to both waste redistributed from upstream in the Fortymile Wash watershed and waste deposited directly at the RMEI location. Waste packages in the direct path of the conduit are assumed to be destroyed and entrained into the eruption, although a certain percentage of the entrained waste (average equal to 70%) is deposited as a scoria cone and lava flows and not dispersed into the atmosphere (Section 2.4.2.3.2.1.12.2). The primary radiologic exposure scenario is the RMEI inhaling contaminated volcanic ash mixed with surface soil.

Every igneous intrusion that rises to within several hundred meters of the land surface can reasonably be assumed to be accompanied by a volcanic eruption somewhere. However, as noted in Section 2.4.2.3.2.1.12.2, probabilistic calculations of the number of waste packages hit by a volcanic conduit indicate that there is about a 72% probability that the conduit will form outside of the repository footprint and not impact any waste packages. In addition, the small conduit diameters relative to drift spacing leads to the result that, of the 28% of conduits that intersect the repository footprint, 70% of these will intersect between drifts and not impact any waste packages. Therefore, the probability of an eruption that intersects waste packages is a factor of 0.28 times 0.297, or 0.083. In the 8.3% of eruptions in which one or more packages are intersected, the expected number hit is about four and the maximum number hit is seven.

The expected annual dose histories for this modeling case are shown on Figure 2.4-31 for the (a) 10,000-year and (b) post-10,000-year periods. The expected dose histories take into account aleatory uncertainty associated with characteristics of the eruption such as the number of waste packages intersected by the eruption, time of the eruption, fraction of waste-form content that is ejected into the atmosphere, eruption power, wind direction, and wind speed (SNL 2008a, Eq. 6.1.2-18). The mean, median, and 5th and 95th percentile curves on Figure 2.4-31 show uncertainty in the value of the expected annual dose, taking into account epistemic uncertainty associated with incomplete knowledge of the frequency of igneous events as well as the eruption properties and the tephra redistribution properties in the Fortymile Wash watershed, such as tephra particle diameter, and fraction of the alluvial fan that represents distributary channels versus interchannel divides, among others (SNL 2008a, Tables 6.5-4 and 6.5-5). Figure 2.4-31 shows that the mean annual dose within 10,000 years postclosure is about 10^{-4} mrem, and is largely uniform for the entire postclosure period. The maximum median annual dose after 10,000 years is less than 6×10^{-5} mrem, occurring at 1,000,000 years.

The radionuclide contributions to the mean annual dose are shown on Figure 2.4-32. Because of potentially rapid atmospheric transport of radionuclides to the location of the RMEI for the volcanic eruption modeling case compared to the igneous intrusion modeling case, radionuclides with short half-lives are able to contribute to the estimate of the mean annual dose at very early times. Examples of three short-lived radionuclides are ^{137}Cs, ^{90}Sr, and ^{238}Pu, which make significant contributions to the dose in the first few hundred years, but their contributions drop off rapidly because of radioactive decay. However, there is a very low probability of this type of dose scenario. For example, based on the mean annual occurrence frequency of 1.7×10^{-8} per year, the chance of an eruption that intersects waste in the first 500 years is (1.7×10^{-8}/yr) (0.083) (500 years), which is equal to about one chance in 1.4 million. At 300 years, ^{241}Am dominates the total, but its contribution rapidly diminishes after about 1,000 years, also due to radioactive decay (its half life is about 433 years—Figure 2.4-21). After 1,000 years, ^{239}Pu and ^{240}Pu become dominant contributors until approximately 100,000 years, then ^{226}Ra and ^{229}Th become the primary contributors for the remainder of the post-10,000-year time period.

The uncertain input that predominately explains the uncertainty in the expected annual dose is the rate of occurrence of the igneous eruptive event (Section 2.4.2.3.3.8). Other uncertain inputs such as those related to long-term inhalation dose, diffusivity of radionuclides in divides of the Fortymile Wash alluvial fan, and inventory mass have relatively smaller effects on expected annual dose.

2.4.2.2.1.2.4 Early Failure Scenario Class Modeling Cases

As described in Sections 2.4.1 and 2.4.2.3.2.1.12.1, drip shield and waste package early failures are attributed to manufacturing and handling defects, such as the presence of undetected weld flaws and improper heat treatment. In the case of a drip shield, these types of defects would diminish its ability to withstand the dynamic and static loadings caused by seismic activity; however, they are treated in the TSPA model as an immediate failure, which means loss of protection for the waste package from impinging seepage or rockfall. Similarly, an improperly heat-treated waste package, for example, would lead to a shorter period of containment for nominal performance and would also be more susceptible to seismic damage. This greater susceptibility to damage would occur over a period of time, perhaps a significant length of time, but it is treated as an immediate failure (loss of isolation from the outer aqueous environment) in the TSPA.

The numbers of failed drip shields and waste packages are simulated in the TSPA model using random Poisson processes with the following characteristics (see SNL 2008a, Sections 6.4.1 and 6.4.2 for an exact definition of the Poisson probability distributions) (SNL 2008a, Section 8.2.2):

- Drip Shield Early Failure
  - Probability of one or more early failures ≅ 0.0166
  - Expected number of early failures ≅ 0.018
  - Expected number of early failures if one or more occur ≅ 1.1
- Waste Package Early Failure
  - Probability of one or more early failure ≅ 0.44
  - Expected number of early failures ≅ 1.1
  - Expected number of early failures if one or more occur ≅ 2.5

The FEPs for these two early failure modeling cases (Section 2.3.6) are the same as those for the nominal modeling case, except for the FEPs specifically related to early failure of the waste package and drip shield. It is important to emphasize that waste packages associated with early failed drip shields are also assumed to be failed in the TSPA model through localized corrosion processes (Section 2.4.2.3.2.1.12.1).

2.4.2.2.1.2.4.1 Drip Shield Early Failure Modeling Case

As indicated above, the expected number of drip shield early failures is estimated to be very small, equal to 0.018 waste-package/drip-shield pairs out of a total number of 11,629 emplaced waste packages, which means that this modeling case must be simulated with importance sampling (i.e., by assuming one early-failed drip shield and associated failed waste package) and then effectively weighting these conditional results by the expected number of early-failed drip shields (SNL 2008a, Section 6.1.2.4.2). With such a small expected number, the contribution of the drip shield early failure modeling case to the total dose will be minimal. As implemented in the TSPA model, the drip shield early failures are accounted for by simply removing the drip shield as a barrier to seepage for a given realization, as well as failing the underlying waste package (SNL 2008a, Section 6.4).

The expected annual dose histories for the drip shield early failure modeling case are shown in Figure 2.4-33 for the (a) 10,000-year period after closure and (b) 1,000,000-year period. The projections for the first 10,000 years show that the maximum mean annual dose is about 3×10^{-4} mrem and occurs at approximately 2,000 years, after which the mean annual dose declines to about 6×10^{-5} mrem at 10,000 years. In the post-10,000-year period, the mean annual dose shows a second peak occurring at about 40,000 years with a value slightly greater than 10^{-4} mrem, but declines thereafter for the entire postclosure period. The first peak at 2,000 years is a result of the step change between the monsoon and the glacial-transition climates, with its accompanying increase in seepage flux and flow through the waste package and invert. The second peak at about 40,000 years is due to increased advective releases of ^{239}Pu caused by the post-10,000-year climate change, whose effect is delayed by retardation in the unsaturated and saturated zones. After about 200,000 years ^{239}Pu has decayed by about eight half-lives, so its importance has diminished and the longer-lived actinides ^{242}Pu and ^{237}Np begin to dominate the mean annual doses. The contributions of the individual radionuclides are shown in Figure 2.4-34, which indicates that the highly soluble and mobile nuclides ^{99}Tc and ^{129}I are the major dose contributors out to about 5,000 years, after which ^{239}Pu becomes important as it is released slowly from the waste packages due to solubility constraints and sorption on the corrosion products. As shown in Figure 2.4-33b, in the post-10,000-year period, the median annual dose reaches a maximum of about 10^{-5} mrem at about 60,000 years.

The uncertainty in the expected annual dose is predominantly due to the uncertain input that quantifies the probability of early failure of the drip shield (Section 2.4.2.3.3.5.1). Other uncertain inputs that are identified as having lesser effects are those related to uncertainty in seepage and in the infiltration scenario.

2.4.2.2.1.2.4.2 Waste Package Early Failure Modeling Case

As indicated above, the expected number of waste package early failures is estimated to be small—equal to 1.1 waste packages out of a total number of 11,629 emplaced waste packages. Although this number is not nearly as small as the number of early failed drip shields, it is still small enough that this modeling case is simulated with importance sampling (i.e., by assuming one early failed waste package per realization) and then weighting these conditional results by the expected number of early failed waste packages (SNL 2008a, Section 6.1.2.4.2). Part of the reason for this is that although there is slightly more than one expected early-failed waste package, it could be either a codisposal or commercial SNF fuel type and would randomly fail in a number of different environments, such as seeping versus nonseeping, and percolation subregions 1 through 5, which means that each of these environments would have an expected number of early failures much less than 1. This aleatory uncertainty is handled by assuming one waste package failure in each different environment and then weighting the results of each environment by its probability of occurrence (SNL 2008a, Eq. 6.1.2-13). With the average number of early failed waste packages being around 1, the contribution of the waste package early failure modeling case to the total dose is small. Thus, as implemented in the TSPA model, the waste package early failure is conservatively conceptualized as if the entire surface area is breached at the time of repository closure (SNL 2008a, Section 6.4).

The expected annual dose histories for the waste package early failure modeling case are shown in Figure 2.4-35 for the (a) 10,000-year period after closure and (b) 1,000,000-year period. For the first 10,000 years after repository closure, the maximum mean annual dose is estimated to be about 4×10^{-3} mrem, occurring just before 10,000 years. This is the time when releases begin to occur from the commercial SNF waste package, due to the increase of the commercial SNF in-package relative humidity above the 95% threshold necessary for the formation of a continuous water film, followed by diffusive releases (Section 2.4.2.3.2.1.8). Prior to that time, the dose is strictly due to releases from early failed codisposal packages. The mean annual dose then reaches a maximum, as a result of commercial SNF releases, at approximately 2×10^{-2} mrem between 10,000 and 15,000 years and thereafter declines until about 300,000 years, at which time the drip shield fails (Figure 2.1-8), allowing advective releases of ^{242}Pu and ^{237}Np, as shown in Figure 2.4-36. This raises the mean annual dose slightly, but not above its earlier peak. The mean annual dose declines thereafter to a level of 10^{-3} mrem at 1,000,000 years. The median annual dose in the post-10,000-year period reaches a maximum of about 6×10^{-3} mrem between 10,000 and 15,000 years (SNL 2008a, Section 8.2.2.2[a]).

The major radionuclides that contribute to the mean annual dose for the waste package early failure modeling case are shown in Figure 2.4-36, which indicates that in the first 10,000 years postclosure, the soluble and mobile radionuclides ^{99}Tc, ^{14}C, and ^{129}I dominate the estimate of mean annual dose. In the post-10,000-year period, after the ^{99}Tc, ^{14}C, and ^{129}I contribution declines, the maximum mean annual dose is dominated by ^{239}Pu up to about 200,000 years (its half life is 24,100 years), after which ^{242}Pu, ^{226}Ra, and ^{237}Np are the primary contributors. As stated in Section 2.4.2.2.1.1.3, the importance of ^{14}C is exaggerated by assumptions about its transport properties (i.e., its lack of interaction with gas and mineral phases).

The uncertainty in the expected annual dose is predominantly due to the uncertain input that quantifies the probability of early failure of the waste package (Section 2.4.2.3.3.5.2). Other uncertain inputs that are identified as having lesser effects are those related to uncertainty in the infiltration scenario and host rock thermal conductivity, both of which affect the time to reach the 95% relative humidity threshold for initiating transport (Section 2.4.2.3.2.1.7).

2.4.2.2.2 Statistical Stability

[NUREG-1804, Section 2.2.1.4.1.3: AC 2(1)]

This section addresses the NUREG-1804, Section 2.2.1.4.1.3, Acceptance Criterion 2(1) for statistical stability of the annual dose curve: “A sufficient number of realizations has been obtained, for each scenario class, using the total system performance assessment code, to ensure that the results of the calculations are statistically stable.” Stability relates to how much variability takes place in the outcome of interest as model results are repeatedly calculated with different samples. As described in Section 2.4.2.1, the four primary scenario classes have been broken into modeling cases for numerical and computational purposes. Therefore, stability for each scenario class is demonstrated by showing stability for each modeling case. Stability is also demonstrated for the total annual dose curve summed over the modeling cases.

2.4.2.2.2.1 Statistical Stability Methodology

The main issue regarding the stability of the TSPA model results is whether enough Monte Carlo realizations (i.e., enough statistical experiments) were performed to adequately estimate the mean and median annual dose. In other words, although there is inherent uncertainty in the mean dose estimates because of: (1) incomplete knowledge about the data and processes (epistemic or reducible uncertainty); and (2) the stochastic nature of some of the event-driven processes (aleatory or irreducible uncertainty), the uncertainty in the mean arising from the finite nature of the numerical estimation technique must be quantified and reduced as much as practically possible. Theoretically, quantification of the numerical or statistical stability of model results involves carrying out multiple model runs with different numbers or sets of realizations, and examining whether or not the computed outcomes converge toward a constant value that would be obtained using an infinite number of realizations.

Several techniques are available to address the TSPA model stability. Each technique relies on a statistical analysis of the model results. The technique used successfully in the certification of the Waste Isolation Pilot Plant transuranic nuclear waste repository is replicated sampling, or repetitions of the same number of realizations for each modeling case but using a different random seed in the Latin hypercube sample, which forces a different sampling of the underlying parameters, albeit with the same stratification. Another method that is employed to illustrate the stability of the TSPA results is the bootstrap method, which is a resampling method described below that relies on the already existing distribution of output (dose) results to generate an uncertainty (or "sampling") distribution for the mean of those results (from which confidence intervals can be derived). Both of these statistical techniques for illustrating the stability of the mean are used here and they not only provide a numerical estimation of confidence intervals, but they also allow visual or graphical comparison of the results and associated confidence intervals, to provide a qualitative assessment of stability. In particular, because there is no exact quantitative assessment of stability, qualitative methods are also important.

As described in Section 2.4.2.1, the TSPA model computes total mean annual dose $\overline{\overline{D}}(\tau)$ at time τ by numerically evaluating

$$\begin{aligned}\overline{\overline{D}}(\tau) &= \mathrm{E}_E[\mathrm{E}_A[D(\tau|\mathbf{a},\mathbf{e})]]\\ &= \int_{\mathcal{E}}\left(\int_{\mathcal{A}} D(\tau|\mathbf{a},\mathbf{e})d_A(\mathbf{a}|\mathbf{e})dA\right)d_E(\mathbf{e})dE\\ &= \int_{\mathcal{E}} \overline{D}(\tau|\mathbf{e})d_E(\mathbf{e})dE\\ &= \mathrm{E}_E[\overline{D}(\tau|\mathbf{e})]\end{aligned} \qquad \text{(Eq. 2.4-34)}$$

where E is the expectation operator, $\mathcal{E}$ is a probability space comprising the epistemic uncertain parameters, $\mathcal{A}$ is a probability space comprising the aleatory uncertainties that describe possible future states of the repository, and $D(\tau|\mathbf{a},\mathbf{e})$ is a function that computes the annual dose at time τ for a given element $\mathbf{e}$ in $\mathcal{E}$, and $\mathbf{a}$ in $\mathcal{A}$. Numerical evaluation of Equation 2.4-34 involves four steps:

1. Selection of values for epistemic parameters $\mathbf{e}$ and aleatory uncertainties $\mathbf{a}$
2. Evaluation of the annual dose, $D(\tau|\mathbf{a},\mathbf{e})$, by numerically solving a complex, coupled system of differential equations describing radionuclide decay, flow, transport, and other physical processes
3. Integration over aleatory uncertainty, carried out either by quadrature or Monte Carlo techniques, depending on the modeling case (SNL 2008a, Section 6.1.2.4)
4. Integration over epistemic uncertainty, conducted by a Monte Carlo technique due to the large number of epistemic parameters that define the probability space $\mathcal{E}$.

These steps are carried out for each of the modeling cases defined in Section 2.4.2.1. The results of the modeling cases are summed to compute mean annual dose, which is the overall measure of repository compliance with the individual protection standard up to 10,000 years postclosure specified in proposed 10 CFR 63.303(a) (70 FR 53313). The process for demonstrating stability for Steps 3 and 4 is summarized in this section, in reverse order.

The integration over epistemic uncertainty employs Latin hypercube sampling (McKay et al. 1979), to sample the distributions of epistemic uncertain parameters. This sampling technique is selected because of the efficient manner in which it stratifies the sampling of values across the range of each uncertain variable, and the stability it provides for uncertainty and sensitivity analysis results in performance assessments of complex systems (McKay et al. 1979; Iman and Helton 1991; Helton 1999). Theoretical results indicate that, under certain conditions, Latin hypercube sampling does indeed exhibit better statistical convergence properties than random sampling (McKay et al. 1979; Stein 1987). However, due to the complexity of the TSPA model, it is not possible to prove theoretically that these conditions are respected. As a result, a practical method of assessing the stability of the results obtained with Latin hypercube sampling is used. In particular, Section 2.4.2.2.2.2 compares mean annual dose and uncertainty in the mean annual dose for three independent Latin hypercube sampling samples, each with a sample size of 300. Using these three independent Latin hypercube sampling samples, confidence intervals are computed. The analysis concludes that the sample size of 300 is adequate to estimate mean annual dose for each modeling case, as well as to estimate total mean annual dose (summed over all modeling cases) (SNL 2008a, Section 7.3.1).

Section 2.4.2.2.2.3 discusses the numerical accuracy and stability of the integration over aleatory uncertainty. These calculations evaluate the expected annual dose for each modeling case using the following equation:

$$\overline{D}(\tau|\mathbf{e}) = \mathrm{E}_A[D(\tau|\mathbf{a},\mathbf{e})] = \int_{\mathcal{A}} D(\tau|\mathbf{a},\mathbf{e})d_A(\mathbf{a}|\mathbf{e})dA \qquad \text{(Eq. 2.4-35)}$$

for each modeling case. As described earlier, the quantity $\overline{D}(\tau|\mathbf{e})$ is called “expected annual dose,” to distinguish it from the mean annual dose defined in Equation 2.4-34 (which is the expectation over both aleatory and epistemic uncertainty), and to avoid cumbersome repetition of the more precise phrase “the expectation over aleatory uncertainty of annual dose conditional on the epistemic parameters.” Expected annual dose is computed either by quadrature techniques or by Monte Carlo techniques, depending on the modeling case; both techniques are implemented in EXDOC_LA V2.0. Section 2.4.2.2.2.3 presents an analysis that concludes that the discretization used for the quadrature techniques is sufficient, and that the sample sizes used for the Monte Carlo techniques are also sufficient (SNL 2008a, Section 7.3.2).

Use of Stability Testing for TSPA Model Validation Activities—The statistical and numerical stability of the TSPA model results is important to validation and confidence building. Also, demonstration of model stability is one of the procedurally required “during-development” activities described below in Section 2.4.2.3.2.3. As discussed next, these stability tests were conducted on a slightly different version of the TSPA model, v5.000, than the one that produced the dose results shown in Section 2.4.2.2.1, v5.005 (SNL 2008a, Section 7.10.3[a]).

As described in Section 2.4.2.3.2.3.4, a key aspect about confidence-building and validation of the TSPA model is the iterative nature of the process. Scientific data and models are updated on a continuous basis, as are software and hardware, as well as underlying process models and abstractions. Independent reviews of the TSPA, both during and after model development, are another factor that can result in various improvements and changes to the TSPA (Section 2.4.2.3.2.3.4). Thus, TSPA methodology, and associated models, has evolved through the years and decisions that are the basis of one particular iteration can be expected to evolve or change for the next iteration. This also occurs on even a shorter time scale within the timeframe of a particular iteration of the TSPA model, particularly given the large number of validation activities and various formal and informal reviews described in Section 2.4.2.3.2. Iterations of the TSPA model within this shorter timescale resulted in two versions used for the performance assessment: v5.000 and v5.005.

Various validation analyses were conducted for both TSPA versions v5.000 and v5.005. The differences between these two versions did not reduce confidence in the validation, even though the model changes between the two versions produced slightly different annual dose curves (Section 2.4.2.3.2). Thus, the annual doses in Section 2.4.2.2.1 were generated with v5.005 of the TSPA model, but many of the validation result plots shown in this Section 2.4.2.2.2 were generated with v5.000 of the TSPA model. Each validation activity for TSPA model v5.000 was reviewed to determine which activities were affected by changes made between TSPA model v5.000 and v5.005. Where validation activities could potentially be affected by model changes, these validation activities were repeated using v5.005 to verify that model changes did not adversely affect the overall validation of the TSPA model (SNL 2008a, Sections 7[a] and 7.3.1.5[a]). Both the v5.000 and v5.005 total mean annual dose curves for 10,000 years and the total median annual dose curves for post-10,000-years are well below the compliance standards in proposed 10 CFR 63.311 and both fall within the bounds of the 5th and 95th percentiles of the distribution of projected doses for either version of the model. Validation activities conducted with both versions include the single-realization analyses presented below in Section 2.4.2.2.3 and the uncertainty/sensitivity analyses presented below in Section 2.4.2.3.3. However, only the v5.005 results are presented for these two types of analyses, since they represent the latest iteration. Replicated sampling to show statistical stability with respect to sample size was conducted only with v5.000; however, a bootstrap analysis to determine the uncertainty in the distribution of the mean was conducted for v5.005. All other validation analyses shown in Section 2.4.2 are from v5.000 of the TSPA model except the verification tests in Section 2.4.2.3.2.2, which are from v4.042 (SNL 2008a, Section 7.2).

Some of the validation analyses that motivated the update from v5.000 to v5.005 included detailed analyses of both probabilistic results and single-realization analyses (Sections 2.4.2.2.3 and 2.4.2.3.3), which indicated that some TSPA implementations of the underlying seismic consequence abstractions were too simplistic in nature (SNL 2008a, Section P3). This led to some changes in the implementation of the seismic ground motion modeling case between v5.000 and v5.005. Other analyses of the v.5.000 TSPA probabilistic results revealed conservatisms in some underlying process models (SNL 2008a, Section P15) that could bias the results to extreme physical situations instead of the full range of defensible parameter distributions, in contrast to the requirements in 10 CFR 63.304. This led to changes in parameter distributions (e.g., longitudinal dispersivity in the 1-D saturated zone flow and transport submodel) that resulted in more defensible parameter values for the v5.005 annual dose results, which form the basis for demonstrating compliance with proposed 10 CFR 63.311, proposed 10 CFR 63.321, and 10 CFR 63.331. Finally, as indicated in Section 2.4.2.2.3, single-realization analyses are necessary, in addition to rigorous verification, implementation, and quality assurance procedures, in order to uncover implementation errors. These single-realization analyses revealed some minor implementation errors in v5.000

(SNL 2008a, Table P-6[a]). An impact assessment of each of the differences between v5.000 and v5.005 (SNL 2008a, Table P-7[a]) indicates that the predicted annual doses are similar, as discussed in Section 2.4.2.3.2.

2.4.2.2.2.2 Statistical Stability for the Epistemic Uncertainty

As discussed above, mean annual dose is calculated as the expected value over both the epistemic uncertainty and the aleatory uncertainty in the estimates of annual dose, $D(\tau|\mathbf{a}, \mathbf{e})$. The expectation of annual dose over aleatory uncertainty is evaluated first, the result of which is termed "expected annual dose." The integral of expected annual dose over epistemic uncertainty is referred to as the "mean annual dose," and is evaluated numerically using a Monte Carlo technique.

This section describes the methodology used to determine statistical stability and to compute the confidence intervals for the mean annual dose. Results are presented for each modeling case and for total mean annual dose (summed over all modeling cases). The analysis concludes that the sample size used in the Monte Carlo technique is adequate to estimate mean annual dose in each modeling case, as well as to estimate the total mean annual dose (SNL 2008a, Section 7.3.1).

As described in Section 2.4.2.1, values for epistemic parameters are selected using a form of Monte Carlo random sampling called Latin hypercube sampling. In the TSPA, the Latin hypercube sampling technique samples 305 epistemically uncertain parameters in the groundwater release pathway (comprising all modeling cases except the volcanic eruption modeling case) and 87 epistemically uncertain parameters in the volcanic eruption modeling case (SNL 2008a, Section 7.3.1.1 and Table K.3-1). The base sample size for the Latin hypercube sampling is 300 for all modeling cases.

A replicated sampling procedure developed in the NRC HLW program at Sandia National Laboratories provides an effective approach to estimating the potential sampling error in quantities derived from Latin hypercube sampling (Iman 1982). With this procedure, the random sample of all (epistemic) uncertain parameters is repeatedly generated with different random seeds (SNL 2008a, Section J4.10). Each sample is used to produce an estimate of the mean annual dose. The ensemble of estimates of the mean annual dose is used to compute an overall mean and standard error. Confidence intervals for the mean annual dose can then be estimated by means of the *t*-distribution. The appropriate value for the number of replicates cannot be known a priori. In practice, a reasonable computational strategy is to start with a small number of replicates (e.g., three to five) and then add additional replicates if additional refinement of the confidence interval is desired.

For the TSPA model, the epistemic stability analysis is conducted by generating three replicates for each modeling case. The mean annual dose and the distribution of uncertainty in the annual dose (e.g., the 5th and 95th percentiles of the 300-realization sample) are compared for the three replicates. The three sample means are used to compute an overall mean and a 95% confidence interval about the overall mean. The confidence interval is displayed as an upper and lower bound. At each point in time, the overall mean annual dose is less than the upper bound of the confidence interval (and greater than the lower bound) with probability 0.95 (i.e., a 95% confidence interval is plotted for each of the cases shown below).

Nominal Modeling Case—Figure 2.4-37a shows the mean annual dose for each of the three replicates of the nominal modeling case, along with the median and the 5th and 95th percentiles of the distribution of uncertainty in the annual dose. The similarity of the median and the 5th and 95th percentiles indicates that the distributions of annual dose are similar in all three replicates. The means differ somewhat before 200,000 years because the mean is being determined by a very few realizations (less than 5%) that have corrosion failures before about 175,000 years (Figure 2.1-9).

Figure 2.4-37b shows the mean annual dose for each of the three replicates, the overall mean, and the upper and lower bounds for the 95% confidence interval about the overall mean. The interval indicates that, with probability 0.975, there is no numerically significant dose from nominal processes before 100,000 years. Between 100,000 years and 300,000 years, when relatively few realizations have corrosion failures, the confidence intervals are wider than after 300,000 years, when corrosion failures are observed in many realizations. However, for most of the 1,000,000-year period, the mean of each replicate is within an order of magnitude of the upper confidence bound and within a factor of 2 at the maximum of the mean, indicating that the true mean annual dose is estimated adequately by each of the three replicates. The similarity evident among the three replicates and the relatively small width of the confidence interval demonstrate that the sample size of 300 is adequate.

As described in Section 2.4.2.1.5.1, because the aleatory uncertain variables in the nominal modeling case are sampled with the epistemic uncertain variables, the expected annual dose is the same as the annual dose calculated directly by GoldSim (i.e., $\bar{D}(\tau|\mathbf{e}) = D(\tau|\mathbf{a}, \mathbf{e})$ in Equation 2.4-35). Consequently, the accuracy of the estimate of mean annual dose for each replicate depends on the size of the Latin hypercube sample used to calculate annual dose. To demonstrate that mean annual dose is numerically stable, the sample size was increased from 300 to 1000.

Increasing the Latin hypercube sampling size to 1,000 did not result in any meaningful differences in the mean annual dose. For the larger sample size, waste package corrosion failures were observed to occur before 100,000 years in six realizations, which did not occur in the smaller Latin hypercube sampling size of 300 (SNL 2008a, Figure 7.3.2-1). Figure 2.4-38 compares the mean, median, 95th percentile and 5th percentile of dose for (1) a Latin hypercube sampling of size 300; and (2) a Latin hypercube sampling of size 1,000. The mean dose for Latin hypercube sampling size of 1,000 is larger at very early times than the mean dose for Latin hypercube sampling size of 300, due to the six realizations with very early corrosion failures. However, at these early times the magnitude of the mean dose for either Latin hypercube sampling size is small ($<10^{-5}$ mrem) compared to the long-term mean dose (~0.4 mrem); thus the differences in mean dose for the two sample sizes are not meaningful. In addition, the uncertainties in expected annual dose (as depicted by the median, 95th, and 5th percentiles) are nearly identical for the two sample sizes. Consequently, the mean dose computed using a Latin hypercube sampling of size 300 is numerically stable.

Early Failure Modeling Cases—Figure 2.4-39a shows the mean annual dose for each of the three replicates of the waste package early failure modeling case for 20,000 years, along with the median and the 5th and 95th percentiles of the distribution of uncertainty in the expected annual dose. Figure 2.4-39b displays the 95% confidence interval for the waste package early failure modeling case for 20,000 years. Similarly to the nominal modeling case, the lower bound of the confidence interval is visually distorted by the logarithmic scale used for displaying dose. However, the similarity evident among the three replicates and the relatively small width of the confidence interval demonstrates that the mean annual dose is estimated with sufficient accuracy with the sample size of 300.

Figure 2.4-40a shows the mean annual dose for each of the three replicates of the waste package early failure modeling case for 1,000,000 years, along with the median and the 5th and 95th percentiles of the distribution of uncertainty in the expected annual dose. Figure 2.4-40b displays the 95% confidence interval for the waste package early failure modeling case for 1,000,000 years. The figures indicate that the sample size for 300 is adequate to estimate the mean annual dose.

Figures 2.4-41 and 2.4-42 display the mean annual dose, along with the median and the 5th and 95th percentiles of expected annual dose, for each of the three replicates of the drip shield early failure modeling case, and the 95% confidence intervals for the drip shield early failure modeling case for both 20,000 years and 1,000,000 years. The figures indicate that the sample size for 300 is adequate for the drip shield early failure modeling cases.

Igneous Modeling Cases—Figure 2.4-43a shows the mean annual dose for each of the three replicates of the igneous intrusion modeling case for 20,000 years, along with the median and the 5th and 95th percentiles of the distribution of uncertainty in the expected annual dose. Figure 2.4-43b displays the 95% confidence interval for this modeling case. The high degree of similarity among replicates and the overall narrow confidence interval indicates that the mean annual dose for this modeling case is accurately estimated and the sample size of 300 is adequate.

Figure 2.4-44a shows the mean annual dose for each of the three replicates of the igneous intrusion modeling case for 1,000,000 years, along with the median and the 5th and 95th percentiles of the distribution of uncertainty in the expected annual dose. Figure 2.4-44b displays the 95% confidence interval for this modeling case. As in the 20,000-year calculation, the high degree of similarity among replicates and the overall narrow confidence interval indicates that the mean annual dose for this modeling case is accurately estimated and the sample size of 300 is adequate.

Figures 2.4-45 and 2.4-46 display the mean annual dose along with the median and the 5th and 95th percentiles of expected annual dose for each of the three replicates of the volcanic eruption modeling case, and the 95% confidence intervals of this modeling case for both 20,000 years and 1,000,000 years. The figures indicate that the sample size of 300 is adequate to estimate mean annual dose for the volcanic eruption modeling cases.

Seismic Modeling Cases—Figure 2.4-47a shows the mean annual dose for each of the three replicates of the seismic ground motion modeling case for 20,000 years, along with the median and the 5th and 95th percentiles of the distribution of uncertainty in the expected annual dose. Figure 2.4-47b displays the 95% confidence interval for this modeling case. The high degree of similarity among replicates and the very narrow confidence interval indicates that the mean annual dose for this modeling case is accurately estimated and the sample size of 300 is adequate.

Figure 2.4-48a shows the mean annual dose for each of the three replicates of the seismic ground motion modeling case for 1,000,000 years, along with the median and the 5th and 95th percentiles of the uncertainty distribution in the expected annual dose. Figure 2.4-48b displays the 95%

confidence interval for this modeling case. Because the seismic ground motion modeling case employs a Monte Carlo integration technique for 1,000,000 years and a quadrature integration technique for 20,000 years (SNL 2008a, Section 6.1.2.4), the 1,000,000-year results are not as smooth as the 20,000 year results. However, the distribution of mean annual dose compares very well among the three replicates, and the confidence interval indicates that the estimate of the mean annual dose is stable (Figure 2.4-48b). Therefore, the sample size of 300 is adequate for estimating mean annual dose in this modeling case.

Figure 2.4-49a shows the mean annual dose for each of the three replicates of the seismic fault displacement modeling case for 20,000 years, along with the median and the 5th and 95th percentiles of the distribution of uncertainty in the expected annual dose. Figure 2.4-49b displays the 95% confidence interval for this modeling case. The high degree of similarity among replicates and the very narrow confidence interval indicates that the sample size of 300 is adequate.

Figure 2.4-50 displays the distributions of mean annual dose and the 95% confidence interval for the seismic fault displacement modeling case for 1,000,000 years. The figure indicates that the sample size of 300 is adequate to estimate mean annual dose for this modeling case.

Total Annual Dose—Total annual dose is computed by summing the results of each modeling case, as described in Section 2.4.2.1. The distribution of uncertainty in total annual dose is first obtained by summing the expected annual doses for each modeling case by epistemic sample element, resulting in one total expected annual dose history for each sample element. The mean of the distribution of total expected annual dose is the total mean annual dose.

The stability of the total mean annual dose is determined, as above, for each modeling case by computing first the distribution of total expected annual dose for each of the three replicated Latin hypercube sampling samples, and then the confidence interval using the total mean annual doses from the three replicates, assuming a *t*-distribution for the sampling distribution of the mean. This is done at every time τ in the various dose histories. Figure 2.4-51a shows the total mean annual dose for the three replicates for 20,000 years, along with the median and the 5th and 95th percentiles of the distribution of uncertainty in the total expected annual dose. Figure 2.4-51b displays the 95% confidence interval for total mean annual dose for 20,000 years. The high degree of similarity among replicates, the very narrow confidence interval, and the large separation between the confidence interval and the regulatory limit relative to the width of the confidence interval indicates that the total mean annual dose is estimated with sufficient accuracy. Therefore, the sample size of 300 is adequate.

Figure 2.4-52 displays the distributions of total mean annual dose, and the 95% confidence interval for total mean annual dose for 1,000,000 years. The figure indicates that the sample size of 300 is adequate.

Stability of the Total Dose Using the Bootstrap Method—As indicated at the beginning of this section, another statistical technique is employed to show the stability of the v5.005 TSPA model. Bootstrap simulation is a numerical procedure for simulating the sampling distribution of any statistic of interest (e.g., mean dose) and estimating its mean and standard deviation, as well as the corresponding confidence intervals (Cullen and Frey 1999). Given a data set of sample size *n*, the general approach in bootstrap simulation is to perform *r* replications of the data set by randomly drawing, with replacement, n values from the empirical cumulative distribution function. The statistic of interest is calculated for each new data set, yielding a bootstrap distribution of the statistic. The fundamental assumption here is that the observed data are representative of the underlying population. This assumption is justified by the replicated sampling analysis performed with results from TSPA version v5.000. By resampling observations from the observed data, the process of sampling observations from the population is mimicked. Furthermore, confidence intervals for the statistic of interest can be readily obtained from the r values that form an approximation of its sampling distribution.

To estimate the variability of the mean annual dose of the TSPA model v5.005, the bootstrap method is applied to the single replicate of the total dose (of size 300), shown in Figure 2.4-10. One thousand samples of size 300 were drawn with replacement from the original set of 300 realizations, at each time τ. These 1,000 samples created a sampling distribution of the total mean annual dose, from which the 95% confidence interval could be generated. Figure 2.4-53a shows the 95% confidence interval for the total mean annual dose for the first 20,000 years for v5.000 of the TSPA model (using the bootstrap method), while Figure 2.4-53b shows the 95% confidence interval for total mean annual dose for the first 20,000 years for v5.005 of the TSPA model (using the bootstrap method). Figure 2.4-54a shows the 95% confidence interval for total mean annual dose for the 1,000,000-year postclosure period for v5.000 of the TSPA model, while Figure 2.4-54b shows the 95% confidence interval for total mean annual dose for the 1,000,000-year postclosure period for v5.005 of the TSPA model. Figures 2.4-53 and 2.4-54 show relatively narrow confidence intervals, indicating that the sample size of 300 is sufficient to estimate the mean annual dose. When compared to Figures 2.4-51b and 2.4-52b, which are confidence intervals based on applying the t-distribution to the three v5.000 replicates, the confidence interval bands from both statistical methods are similar. Therefore, the results of TSPA v5.005 are statistically stable.

2.4.2.2.2.3 Statistical Stability for the Aleatory Uncertainty and Numerical Accuracy of the Expected Dose Integration

The TSPA model calculates an expected annual dose curve, $\bar{D}(\tau|\mathbf{e})$, for each epistemic realization. As described above, the term "expected annual dose" refers to the expectation of dose over aleatory uncertainty, but this is conditional on epistemic uncertainty. In general, the calculation for expected annual dose involves numerical evaluation of one or more integrals (SNL 2008a, Section 6.1.2.4). Because each modeling case addresses different aleatory uncertainties, the methods of calculating expected annual dose differ for each modeling case. Also, in general, the numerical methods can differ for 10,000 years versus 1,000,000 years. This is particularly true for the seismic ground motion modeling case because of some simplifying assumptions that are appropriate for the 10,000-year seismic ground motion case, arising from the low probability of many of the EBS damage mechanisms, but not for the 1,000,000 year simulation. This section summarizes the numerical accuracy and stability of the calculations and integrations over aleatory uncertainty for each modeling case, as described in more detail in *Total System Performance Assessment Model/Analysis for the License Application* (SNL 2008a, Section 7.3.2).

Seismic Ground Motion Modeling Case for 10,000 Years—Expected annual dose for the seismic ground motion modeling case is numerically evaluated in two steps (SNL 2008a, Section 7.3.2.6.1). First, the annual dose at time τ from a seismic event occurring at time t and resulting in damage fraction A, for each realization, $D_{SG}(\tau|[1, t, A], \mathbf{e})$, is calculated using the

GoldSim component of the TSPA model (Section 2.4.2.1.5.4), for each of a sequence of times for seismic events and a set of damage fractions. The term "damage fraction" is more precisely defined as the fraction of waste package surface area that consists of stress corrosion cracks. Second, the GoldSim results are used by the EXDOC_LA component of the TSPA model to calculate expected annual dose. The EXDOC_LA code calculates the expected dose over aleatory uncertainty (using various numerical integration methods) and estimates statistics on expected dose over epistemic uncertainty for the modeling cases considered in the TSPA calculations (DOE 2007a).

For the 10,000-year period, validation of the calculation of expected dose involved three separate steps:

1. Demonstration that expected dose calculations are numerically accurate

2. Justification of assumptions about linearity in damage fraction

3. Justification of simplifications (generally, omissions) related to various forms of EBS damage in the seismic consequences abstraction, such as drip shield damage, drift collapse, and rupture/puncture of the waste package.

To demonstrate that the expected dose calculations conducted by EXDOC_LA are numerically accurate, the number of times of seismic events is increased from $N = 6$ to 12, and the number of damage fractions is increased from $M = 5$ to 8. The former set of 6 event times (at 200, 1,000, 3,000, 6,000, 12,000, and 18,000 years) and 5 damage fractions (10^{-7}, 10^{-6}, 10^{-5}, 10^{-4}, 10^{-3}) is called the base case, and is the basis for the dose results in Section 2.4.2.2.1 (Figure 2.4-25). The latter set of 12 event times (at 100, 1,600, 3,200, 4,800, 6,400, 8,000, 9,600, 11,200, 12,800, 14,400, 16,000, and 19,200 years) and 8 damage fractions (10^{-9}, 10^{-8}, 10^{-7}, 10^{-6}, 10^{-5}, 10^{-4}, 10^{-3}, 5×10^{-3}) that is used to test numerical accuracy is called the expanded case.

EXDOC_LA computes the expected dose for the 10,000-year seismic ground motion modeling case by interpolating between single dose histories generated for event time and each damage fraction (SNL 2008a, Section 6.1.2.4.4), and performing numerical integration using the interpolated dose histories. Because the dose histories maintain similar shapes as the event time and damage fraction change (SNL 2008a, Figures 7.3.2-8 through 7.3.2-10), the interpolation scheme implemented in EXDOC_LA is justified.

Figure 2.4-55 compares the expected annual dose over 20,000 years for five different epistemic realizations calculated for the base case and for the expanded case, using the times of seismic events and damage fractions listed above (SNL 2008a, Section 7.3.2.6). Figure 2.4-55 shows that increasing the number of event times and the number of damage fractions does not change the expected dose calculation for any realization. Therefore, the discretization used to calculate expected dose is adequate and the calculation of expected dose is numerically accurate.

Additivity in Annual Dose from Multiple Seismic Events—One important assumption made for the numerical integration used to compute expected dose for the 10,000-year seismic ground motion modeling case is the assumption that the annual dose from two or more events causing cumulative damage to waste packages is reasonably approximated by the sum of the annual doses from the events modeled independently (SNL 2008a, Section 6.1.2.4.4). Calculations have shown that the change in dose is proportional to changes in damage fraction (open crack area), up to the damage fraction of about 10^{-5} (SNL 2008a, Figure 7.3.2-12). Beyond a damage fraction of 10^{-5}, dose increases less than linearly with increasing damage fraction. Thus, when two or more seismic events cause a cumulative damage fraction exceeding 10^{-5}, this additivity assumption results in an overestimate of the dose resulting from seismic events.

To estimate the degree of overestimation of dose due to this additivity assumption, the expected dose from one seismic event is compared to the expected dose from all seismic damaging events for codisposal packages. Comparing the expected dose from the first damaging event to the expected dose from all damaging events shows that the second and subsequent damaging events do not change the magnitude or range of uncertainty of expected dose to any great extent (SNL 2008a, Figures 7.3.2-13 and 7.3.2-14). Consequently, the additivity assumption for multiple events does not result in a significant overestimate of the expected dose.

Simplifications to the Seismic Consequence Abstraction for 10,000 Years—For 10,000 years, the distribution of expected annual dose for the seismic ground motion modeling is approximated by examining only the occurrence of stress corrosion cracking damage to codisposal waste packages with the drip shield intact and without significant rockfall, and without considering the effects of corrosion processes. This does not represent any changes to FEPs screening but, rather, a TSPA simplification based on TSPA consequence analyses that have shown that other damage mechanisms are insignificant in the first 10,000 years. In particular, corrosion processes do not appreciably thin the waste package outer barrier in 10,000 years (Figure 2.4-23); hence, these processes need not be explicitly represented in this modeling case. The contributions to expected annual dose from futures involving drip shield plate or framework failure within 10,000 years are low enough that these failures are omitted from the calculation. The expected volume of rockfall within 10,000 years is small enough that it is reasonable to omit the changes to temperature and seepage caused by rockfall. Rupture and puncture of codisposal waste packages are not included because the probability that these events occur within 10,000 years is low enough that the expected dose consequence from these events is also low. Finally, damage to TAD-bearing commercial SNF waste packages, either by cracking or rupture, is omitted because the low probability of seismic damage to commercial SNF waste packages results in low estimates of the expected dose consequence from commercial SNF waste packages. Each of these approximations is justified in *Total System Performance Assessment Model/Analysis for the License Application* (SNL 2008a, Section 7.3.2.6.1.3), through consequence calculations that show that the dose consequences from these processes are low compared to the process of crack damage to codisposal waste packages.

Seismic Ground Motion Modeling Case for 1,000,000 Years—Expected annual dose for the seismic ground motion modeling case for 1,000,000 years is calculated using a Monte Carlo technique for sampling aleatory uncertainty (SNL 2008a, Equation 6.1.2-23). First, a Latin hypercube sampling of size 300 is generated for uncertain epistemic parameters. Next, for each vector $\mathbf{e}_i$ in the epistemic Latin hypercube sampling, an aleatory sample is randomly generated, consisting of 30 independent sequences $\{\mathbf{a}_{ij}\}_{j=1,30}$ of seismic events and corrosion failures. Then, annual dose at time τ from the combination of corrosion processes and seismic ground motion events, $D_{N+SG}(\tau|\mathbf{e}_i, \mathbf{a}_{ij})$, is calculated. For each vector $\mathbf{e}_i$ in the epistemic Latin hypercube sampling, expected annual dose $\overline{D}_{N+SG}(\tau|\mathbf{e}_i)$ over aleatory uncertainty is computed as a numerical average over the 30 samples:

$$\overline{D}_{N+SG}(\tau|\mathbf{e}_i) = \frac{1}{30}\sum_{j=1}^{30} D_{N+SG}(\tau|\mathbf{e}_i, \mathbf{a}_{ij}) \qquad \text{(Eq. 2.4-36)}$$

Mean annual dose $\overline{\overline{D}}_{N+SG}(\tau)$ is computed as a numerical average over the 300 values of expected annual dose:

$$\overline{\overline{D}}_{N+SG}(\tau) \cong \frac{1}{300}\sum_{i=1}^{300}\left(\frac{1}{30}\sum_{j=1}^{30} D_{N+SG}(\tau|\mathbf{e}_i, \mathbf{a}_{ij})\right) \qquad \text{(Eq. 2.4-37)}$$

Because of the Monte Carlo technique used in the seismic ground motion modeling case for 1,000,000 years, the size (30) of the aleatory sample, and the wide variability in the effects of a seismic event (caused by the multiple damage abstractions to EBS components), it is not reasonable to presume that the expected dose would be as numerically stable for each individual epistemic vector $\mathbf{e}_i$ as it is for other modeling cases (SNL 2008a, Section 7.3.2.6.2).

Figure 2.4-56 compares expected dose for an aleatory sample size of 30 to expected dose for an aleatory sample size of 90, for epistemic Realizations 1 through 5. The similarity in each pair of expected dose results indicates that increasing the aleatory sample size does not produce a qualitatively different expected dose, although at any particular time the expected dose could vary significantly. However, as shown in Figure 2.4-48, the mean annual dose calculated by Equation 2.4-37 is statistically stable. The confidence bounds follow the overall mean quite closely, and the upper confidence bound is consistently about twice the magnitude of the overall mean, indicating that the overall mean dose is statistically stable.

Igneous Intrusion Modeling Case—Expected annual dose in the igneous intrusion modeling case, for each epistemic sample $\mathbf{e}_i$, is numerically evaluated in two steps (SNL 2008a, Section 7.3.2.4). First, for each of a sequence of times for igneous intrusions, annual dose at time τ from an intrusion occurring at time, t, $D_{II}(\tau|[1, t], \mathbf{e})$, is calculated using the GoldSim component of the TSPA model (Section 2.4.2.1.5.3). Second, the GoldSim results are used by the EXDOC_LA component of the TSPA model to calculate expected annual dose.

The accuracy of the numerical evaluation is examined by increasing the number of times of igneous intrusions for which GoldSim results are calculated from $N = 10$ to 50 (SNL 2008a, Table 7.3.2-1). For each single dose history $D_{II}(\tau|[1, t], \mathbf{e})$, its shape is similar for different times of intrusion within the same climate period, indicating that the interpolation techniques within the EXDOC_LA software are justified (SNL 2008a, Figure 7.3.2-3).

Figure 2.4-57 compares the expected annual dose over 20,000 years for 5 epistemic realizations calculated, using the 10 intrusion times for the base case, and again using the 50 intrusion times for the expanded case. The comparison shows that 10 intrusion times are sufficient to obtain a numerically accurate calculation of expected dose over 20,000 years. Figure 2.4-58 compares the expected annual dose over 1,000,000 years for five epistemic realizations calculated using the 10 intrusion times for the base case, and again using the 50 intrusion times for the expanded case. Figure 2.4-58 shows that 10 intrusion times are sufficient to obtain a numerically accurate calculation of expected dose over 1,000,000 years.

Volcanic Eruption Modeling Case—Expected annual dose for the volcanic eruption modeling case, for each epistemic sample $\mathbf{e}_i$, is numerically evaluated in two steps (SNL 2008a, Section 7.3.2.5). First, for each of a sequence of times for eruption events and a Latin hypercube sampling of uncertain aleatory parameters describing an eruption event, annual dose at time τ from an eruption event occurring at time t and described by parameters $\mathbf{u}_k$ and affecting one waste package, $D_{VE}(\tau|[1, t, 1, \mathbf{u}], \mathbf{e})$, is calculated using the GoldSim component of the TSPA model (Section 2.4.2.1.5.3). Second, the GoldSim results are used by the EXDOC_LA component of the TSPA model to calculate expected annual dose.

Validation of the calculation of expected dose involved two steps: (1) demonstration that the size of the Latin hypercube sampling of uncertain aleatory parameters is sufficient; and (2) demonstration that the integration over time of the eruption event is numerically accurate. Sufficiency of the size of the Latin hypercube sampling for aleatory parameters is demonstrated by increasing the Latin hypercube sampling size from 40 to 80 (SNL 2008a, Section 7.3.2.5). The numerical accuracy of the integration over time is demonstrated by increasing the number of specified times from the set (0, 10, 100, 600, 2,000, 4,000, 6,000, 10,000, 14,000, and 18,000 years) for the base case to the set (0, 10, 40, 100, 240, 400, 600, 800, 1,000, 2,000, 4,000, 6,000, 10,000, 14,000, and 18,000 years) for the expanded case (SNL 2008a, Table 7.3.2-2). The aleatory parameters included in the Latin hypercube sampling described by $[\mathbf{u}]$ are eruptive power, eruptive velocity, eruptive duration, wind speed, and wind direction.

Figure 2.4-59 shows the expected dose resulting from the two different Latin hypercube sampling sizes (40 vs. 80) for five realizations of epistemic parameters. The expected dose curves shown on Figure 2.4-59 use the eruption times for the base case. The expected dose is generally greater for the larger Latin hypercube sampling, but the difference is no more than 10%, and is relatively constant throughout the 1,000,000-year period. Consequently, the Latin hypercube sampling size of 40 used in the base case is adequate to estimate expected dose.

Because dose from volcanic eruption constitutes most of the total dose during the first 1,000 years, it is most important to verify the accuracy of the volcanic eruption dose during this time period. Additional event times were added primarily during the first 1,000 years, as listed above. Figure 2.4-60a shows the expected dose for 20,000 years calculated using the specified eruption times for the base case, and again using the additional times for the expanded case, for the first five epistemic realizations. Figure 2.4-60b focuses on the expected dose for the first 1,000 years. The expected dose curves shown in Figure 2.4-60 use the Latin hypercube sampling of size 40 for aleatory parameters describing eruptive power, eruptive velocity, eruptive duration, wind speed, and wind direction. The expected dose does not significantly change when more event times are used, either during the first 1,000 years or throughout the 20,000-year period. Consequently, the 10 specified eruption times for the base case provide a sufficiently accurate calculation of expected dose (SNL 2008a, Section 7.3.2.5). This same sort of stability with respect to the integration over event times also is evident in the expected dose calculation for 1,000,000 years because the eruption processes remain the same through time (SNL 2008a, Section 7.3.2.5).

Nominal Modeling Case—Because the uncertain aleatory variables in the nominal modeling case are not sampled separately from the epistemic variables, the expected annual dose is the same as the annual dose calculated directly by GoldSim for each epistemic sample $\mathbf{e}_i$. Discussion of the numerical accuracy of the mean dose for the nominal modeling case is provided in Section 2.4.2.2.2.2.

Waste Package Early Failure Modeling Case—Since expected annual dose for the waste package early failure modeling case involves only sums rather than numerical integration, the calculation of expected annual dose does not require an estimate of numerical accuracy (SNL 2008a, Section 7.3.2.2). The EXDOC_LA calculation of expected dose for the waste package early failure modeling case is verified by reproducing the EXDOC_LA results using Mathcad (SNL 2008a, Section 7.3.2.2).

Drip Shield Early Failure Modeling Case—Since expected annual dose for the drip shield early failure modeling case involves only sums rather than numerical integration, the calculation of expected annual dose does not require an estimate of numerical accuracy stability (SNL 2008a, Section 7.3.2.3). The EXDOC_LA calculation of expected dose for the drip shield early failure modeling case is verified by reproducing the EXDOC_LA results using Mathcad (SNL 2008a, Section 7.3.2.3).

Seismic Fault Displacement Modeling Case—Expected annual dose for the seismic fault displacement modeling case is numerically evaluated in two steps (SNL 2008a, Section 7.3.2.7). First, for each of a sequence of times for fault displacement events, each waste package type, and a set of damage areas, annual dose at time τ from a fault displacement event occurring at time t resulting in damage area A to 100 waste packages of type r, $D_{SFr}(\tau|[1, t, 100, A], \mathbf{e})$, is calculated using the GoldSim component of the TSPA model (Section 2.4.2.1.5.4). The 100 waste packages are placed proportionally into each percolation subregion based on the spatial area of the subregion, and within each subregion, proportionally into seeping and nonseeping locations. Second, the GoldSim results are used by the EXDOC_LA component of the TSPA model to calculate expected annual dose.

To determine if the expected dose calculations performed using EXDOC_LA are numerically accurate, the number of times for fault displacement events is increased from $N = 6$ to 12, and the number of damage areas is increased from $M = 3$ to 5. The former set of 6 event times (at 200, 800, 2,000, 4,000, 8,000, 18,000 years) and 3 damage fractions (1/3, 2/3, 1) is called the base case and is the basis for the dose results in Section 2.4.2.2.1 (Figure 2.4-27). The latter set of 12 event times (at 200, 1,600, 3,200, 4,800, 6,400, 8,000, 9,600, 11,200, 12,800, 14,400, 16,000, 19,200 years) and 5 damage fractions (1/12, 1/6, 1/3, 2/3, 1) that is used to test numerical accuracy is called the expanded case.

EXDOC_LA computes the expected dose for the seismic fault displacement modeling case by interpolating between single dose histories for the different event times and damage areas, and by performing numerical integration using the interpolated dose histories. Because the dose histories maintain similar shapes as the event time and damage fraction change, the interpolation scheme implemented in EXDOC_LA is justified (SNL 2008a, Section 7.3.2.7).

Figure 2.4-61 compares the expected annual dose over 20,000 years for five epistemic realizations calculated for the base case and the expanded case using the times of seismic events and damage fractions listed above (SNL 2008a, Section 7.3.2.7). Using the additional event times and damage areas in the expanded case increased the expected dose by up to about 30% in all five realizations. Because the individual dose histories have very little dependence on damaged area (SNL 2008a, Figure 7.3.2-25), the change in expected dose is due to the additional event times included in the numerical integration. However, further extension of the number of event times up to $N = 23$ did not result in additional increases in expected dose (SNL 2008a, Section 7.3.2.7[a]). Inclusion of additional event times in the baseline expected dose calculation would improve the accuracy of the baseline results. However, because the seismic fault displacement modeling case is not a significant contributor to total dose (Figure 2.4-18), the improvement in the accuracy of this modeling case does not justify the additional event times.

2.4.2.2.3 Consistency and Reasonableness of Repository Performance and the Performance of Individual Components or Subsystems

[NUREG-1804, Section 2.2.1.4.1.3: AC 2(3)]

There are a number of methods and analyses capable of demonstrating that "repository performance and the performance of individual components or subsystems are consistent and reasonable," in order to address NUREG-1804, Section 2.2.1.4.1.3, Acceptance Criterion 2(3). The analyses and explanations in Section 2.4.2.2.2 have already demonstrated this to a large degree, through an explanation of key aspects of the behavior of the total mean annual dose and the mean annual dose for the individual modeling cases, including the behavior of the individual radionuclides. Various dependencies of repository performance (i.e., dose) on subsystem parameters and behavior were pointed out, including dependencies on the failure rates and degradation characteristics of the drip shield and waste package, various transport characteristics, characteristics of the in-package environment, and characteristics of the occurrence rates of disruptive or early failure events. Additional detailed explanations of the dependency of dose on the most important uncertain parameters that characterize individual model components can be found in Section 2.4.2.3.3, which is the presentation of uncertainty propagation in the TSPA model. Thus, Section 2.4.2.3.3 also helps address Acceptance Criterion 2(3).

In this section, however, more in-depth descriptions are presented of how the dose behavior is consistent with the behavior of the subsystems, through the detailed explanation and analysis of selected single-realizations from the set of 300 epistemic realizations. These analyses are collectively designated as "single-realization deterministic analyses," and they have been formulated for five of the key modeling cases for the TSPA (SNL 2008a, Section 7.7.1[a]): (1) the nominal modeling case; (2) the waste package early-failure modeling case; (3) the drip shield early-failure modeling case; (4) the igneous intrusion modeling case; and (5) the seismic ground motion modeling case. Of these cases, two have been chosen for discussion here: (1) the nominal modeling case, which includes the majority of FEPs that form the basis of all of the groundwater modeling cases; and (2) the seismic ground motion modeling case, which represents the most probable set of long-term futures for the repository. These single-realization analyses also enhance confidence in the credibility of the TSPA model and are a key aspect of model validation as described in Sections 2.4.2.3.2 and 2.4.2.3.2.3.2.1.

The single-realization analyses provide a useful insight into the interaction of several submodels under varying thermal-mechanical-chemical-physical conditions in the repository. They help in understanding the coupling of the EBS, unsaturated zone, and saturated zone transport models and how their behavior influences the annual dose to the RMEI in a given realization. Within each barrier that reduces and delays radionuclide releases (i.e., the EBS and Lower Natural Barrier), the interaction of various submodels under a given set of physical-chemical conditions is described in detail, which provides confidence that the submodels are coupled as intended and their behavior can be explained in a logical manner leading to the dose result. Besides explaining the interaction of submodels, the transport behavior of major dose contributing radionuclides is also described and highlighted in the various single-realization analyses for the given modeling cases.

The methodology for calculating the expected annual dose (expectation of annual dose over aleatory uncertainty) for the various modeling cases is described in Section 2.4.2.1, which distinguishes epistemic uncertainty from aleatory uncertainty in the TSPA model. Although the treatment of aleatory uncertainty varies by modeling case, the general methodology for selecting a single realization for detailed analysis is similar in all modeling cases. First, an epistemic uncertainty vector, $\mathbf{e}_i$, is chosen from the set of 300 epistemic uncertainty realizations. The criteria for selecting $\mathbf{e}_i$ is such that the general behavior of the expected annual dose $\overline{D}_J(\tau|\mathbf{e}_i)$ for modeling case J is similar to the mean annual dose $\overline{\overline{D}}_J(\tau)$ (expectation over aleatory and epistemic uncertainty) and the magnitude of the expected annual dose is somewhat higher than the mean annual dose over the time periods of interest. This choice is intended to select epistemic realizations that highlight processes of interest in each modeling case (i.e., processes that contribute to the mean result).

Since the expected annual dose $\overline{D}_J(\tau|\mathbf{e}_i)$ itself represents an average over a number of realizations of aleatory uncertainty, it must be further broken down to select a realization representing an individual aleatory uncertainty vector $\mathbf{a}$. The aleatory vector is chosen by comparing each annual $D_J(\tau|\mathbf{a},\mathbf{e}_i)$ to the annual dose from other aleatory vectors in the set and selecting an aleatory realization which best describes the behavior of the expected annual dose. This process is not necessary for the nominal modeling case, which has no explicitly represented aleatory uncertainty, but is necessary for the other modeling cases. For the seismic ground motion modeling case, one GoldSim realization $D_J(\tau|\mathbf{a},\mathbf{e}_i)$, representing a unique combination of epistemic and aleatory uncertainty, is chosen for detailed analysis.

2.4.2.2.3.1 Single-Realization Deterministic Analysis for the Nominal Modeling Case

This section presents an analysis of a single realization from the 300 realization base-case run (random seed #1) for the nominal modeling case for the 1,000,000-year simulation duration (SNL 2008a, Section 7.7.1.5[a]). The nominal scenario class consists of a single modeling case that represents the set of possible repository futures with no disruptive events or early failures of drip shields and waste packages. Moreover, the nominal modeling case serves as a "reference system state" from which all other modeling cases are developed (SNL 2008a, Section 8.2.1). A single epistemic vector is selected for further analysis in such a manner that the expected annual dose is broadly representative of the modeling case and similar in behavior to the mean annual dose. Epistemic vector 286 ($\mathbf{e}_{286}$), which is equivalent to GoldSim Realization 286, is chosen for further analysis (Figure 2.4-62). The distribution of expected annual dose for 300 epistemic vectors shown in Figure 2.4-62 implicitly account for aleatory uncertainties in nominal degradation processes, such as time, location, and degree of damage to each waste package. Note that there is no net dose to the RMEI within the 10,000-year regulatory period in the nominal case because neither drip shields nor waste packages are calculated to fail in that period.

Two minor peaks in the mean annual dose are apparent early on, at around 40,000 and 80,000 years (Figure 2.4-62). These are the result of waste packages failing by stress corrosion cracking from two realizations (out of the total of 300 realizations). After about 100,000 years, the mean annual dose steadily increases as a result of gradual waste package failures. Step-wise increases in the mean annual dose noticeable around 200,000, 300,000, 500,000 and 700,000 years, are due to increases in the number of waste package failures following those time points and result from the coarse time discretization employed in the waste package degradation software code WAPDEG at late time-periods. WAPDEG calculates the corrosion rates at the timesteps provided in the waste package thermal history input files from the multiscale thermal-hydrologic model abstraction (SNL 2008a, Section 6.3.2.3). The thermal history files have coarse temporal resolution past 100,000 years (due to small changes at late time periods) leading to evaluation of temperature at 200,000; 300,000; 500,000, 700,000; and 1,000,000 years. The stress corrosion crack growth rate is given by a power law function of stress intensity factor and repassivation slope n (SNL 2008a, Equation 6.3.5-14). The stress intensity factor is evaluated at the beginning of each WAPDEG timestep and is a function of the crack depth that drives the crack propagation. The large timesteps taken past 100,000 years combined with the sensitivity of the crack growth rate to the stress intensity factor, which is raised to the power $4n$, where n has a mean value of 1.165 (SNL 2007e, Table 8-15), can cause dramatic changes in the crack growth rate at each timestep (SNL 2008a, Section 7.3.3.7[a]). As a result, the crack growth rate can change from a small value for the timestep in which the crack initiates to a much larger value at the beginning of the next timestep, resulting in almost immediate penetration of many cracks and failure of waste packages (SNL 2008a, Section 7.7.1.5[a]). An assessment of this temporal discretization for the nominal modeling case indicates that it has a negligible effect on the results (Section 2.4.2.3.2.2.2).

Figure 2.4-63 shows the major radionuclides that contribute to the expected annual dose for Realization 286 of the nominal modeling case. Of these, the relatively long-lived, highly soluble and mobile radionuclides ^{99}Tc and ^{129}I are the primary contributors with relatively minor contributions from the long-lived, sparingly soluble, and highly sorbing ^{135}Cs at very late times. Thus, the behavior of this single realization is similar to the mean behavior of the nominal modeling case, shown in Figure 2.4-22b, but with lower late-time contributions from ^{237}Np and ^{242}Pu. Between 250,000 and 300,000 years, the annual dose for Realization 286 exhibits small step increases that result from a single codisposal waste package failure in the non-seeping environment of percolation subregion 2 and two codisposal waste package failures in the seeping environment of percolation subregion 2. All three codisposal waste package failures are caused by stress corrosion cracking failure on the outer lids prior to the drip shield failure, which occurs at 304,000 years.

Figures 2.4-64a and 2.4-64b, illustrate the number and timing of waste package failures within each percolation subregion for the codisposal and commercial SNF waste packages. These waste package failures occur in both the non-seeping and seeping environments of each percolation subregion. By the end of the simulation at 1,000,000 years, a total of 7,716 commercial SNF waste packages have failed compared to a total of 3,227 failed codisposal waste packages (out of a total of 8,213 commercial SNF waste packages and 3,416 codisposal waste packages). However, the average failed area (per failed waste package) remains very small throughout the simulation, on the order of 1 cm^2, as illustrated in Figure 2.4-65. This breached area remains relatively small because the failures are generally only due to stress corrosion cracking in the lid welds. In particular, only percolation subregion 1 for commercial SNF waste package has a general corrosion patch failure within the simulated time frame, which occurs after 950,000 years, leading to a very small increase in area in percolation subregion 1. Thus, because only stress-corrosion-crack failures occur on most of the waste packages for the majority of the simulation, advective releases are not important and radionuclides are primarily transported by diffusion out of the waste package.

The rates at which ^{129}I, ^{135}Cs, and ^{242}Pu are released (integrated over all percolation subregions) from the EBS components, unsaturated zone, and saturated zone are shown on Figures 2.4-66, 2.4-67, and 2.4-68, respectively. For ^{129}I the curves that represent these release rates generally lie close to each other, which is indicative of each radionuclide being transported as a solute with little to no retardation through the engineered barrier and natural systems. The transport of ^{135}Cs (as solute and reversibly sorbed on the colloids) exhibits the same behavior through the EBS and the unsaturated zone but has significant retardation through the saturated zone. For ^{242}Pu (dissolved and reversibly sorbed on colloids), the mass released from the waste form is large relative to the mass released from the waste package, invert, unsaturated zone, and saturated zone. This behavior reflects retardation due to sorption onto corrosion products inside the waste package.

Figures 2.4-69 and 2.4-70 compare the advective and diffusive releases of ^{129}I and ^{242}Pu (dissolved and reversibly sorbed on colloids) from all failed waste packages in all percolation subregions. There is no advective release from codisposal waste packages since there are no general corrosion patch failures. However, because there is corrosion patch failure for commercial SNF waste packages in percolation subregion 1 past 950,000 years, there is some advective release, but it is still negligible compared to diffusive release. The advective release for ^{242}Pu (dissolved and reversibly sorbed on colloids) is not shown since it is below the lower bound on the y-axis. The step increase in diffusive releases coincides with the step increases in waste package failures but, except for these minor step changes, the diffusive releases remain steady for ^{129}I and show gradual increase for ^{242}Pu. This is attributed to the failure rate of the waste packages. In other words, despite the small diffusive release area, the high concentration of ^{129}I tends to cause rapid release (relative the million-year time scale) from each failed waste package. This causes the ^{129}I release curve (in either Figure 2.4-69 or Figure 2.4-66) to follow the waste package failure rate (the derivative of the cumulative failure curves in Figure 2.4-64). The release of ^{242}Pu (dissolved and reversibly sorbed on colloids), in addition to being similarly affected by the waste package failure rate, is also impacted by sorption on the corrosion products inside the waste package as well as a relatively low aqueous solubility, which reduces the concentration gradient. Combined with a small breach area per package (Figure 2.4-65), these factors cause ^{242}Pu to be released slowly from each failed waste package. As a result, as packages fail through time, the ^{242}Pu release rate from all failed packages increases. Thus, the ^{242}Pu release rate tends to mirror the cumulative waste package failure curve rather than the instantaneous failure rate curve, which was the case with ^{129}I. Releases from commercial SNF waste packages dominate that of codisposal waste packages because (a) comparatively more commercial SNF waste packages are failed, and (b) there is comparatively larger inventory for the radionuclides of interest on a per package basis in a commercial SNF waste package.

The mass fraction of ^{129}I passed to the unsaturated zone matrix and fracture continuum from the EBS at the repository level is shown in Figure 2.4-71. The fraction of mass going into fractures increases in proportion to the fraction of waste packages in the seeping environment versus non-seeping environment for a given percolation subregion. The fraction of waste packages assigned to a seeping environment is directly proportional to the seepage fraction for the given percolation subregion, which generally increases from percolation subregion 1 to 5 resulting in an increased proportion of mass being released to the unsaturated zone fractures. Since ^{129}I is neither sorbed nor limited by solubility, the diffusive mass release from the waste package remains largely a function of waste form degradation rate and concentration inside the waste package. The change in the waste package to invert concentration gradient between non-seeping environment and seeping environment due to flow through the invert has limited effect on the diffusive releases of ^{129}I per failed waste package. Thus the fraction of ^{129}I mass passed to an unsaturated zone fracture for a given percolation subregion is proportional to the number of failed waste packages in a seeping environment compared to the non-seeping environment and thus directly related to the seepage fraction, which increases from percolation subregion 1 to 5. Note that although no water is modeled to flow advectively through the waste packages (since waste package failures are only due to stress corrosion cracks), the seeping environments have in-drift seepage which flows around the waste packages (and drip shields) to the invert and, thus the diffusive releases out of the waste package are carried advectively from the invert into the fractures of the unsaturated zone with less mass release into the matrix. In the non-seeping environment the transport through the invert is primarily by diffusion into the matrix continuum due to large effective diffusive area of the matrix continuum (SNL 2008a, Section 6.3.8.3).

The mass fraction of ^{242}Pu (dissolved and reversibly sorbed on colloids) passed to the unsaturated zone matrix and fracture continuum from the EBS at the repository level is shown in Figure 2.4-72. In contrast to the fracture mass fraction of ^{129}I, a relatively larger fraction of ^{242}Pu is passed into the fractures, indicating a disproportionately larger contribution from waste packages located in the seeping environments compared to the non-seeping environment. This is because highly sorbed species such as ^{242}Pu have a lower concentration in the waste package than a nonsorbing species such as ^{129}I, and the diffusive flux is primarily controlled by the concentration gradient between the waste package and the invert. In the seeping environment the flow through the invert causes the concentration gradient to increase (due to reduction in distance to the effective zero concentration boundary from the waste package) leading to disproportionately larger diffusive mass flux from the seeping environment than the non-seeping environment per failed waste package. As a result, most of the ^{242}Pu mass released in a given percolation subregion is from the contribution of waste packages in the seeping environment that are released to the unsaturated zone fracture continuum.

Radionuclide transport through the saturated zone is governed by sampling four breakthrough curves for each radionuclide from a set of 200 Monte Carlo realizations representing epistemic uncertainty in saturated zone flow and transport properties. (The four breakthrough curves represent the four saturated zone release zones at the water table, as described in Section 2.3.9.3.4.) For TSPA Realization 286 in this single realization analysis, the saturated-zone Monte Carlo Realization 33 was sampled. Solute transport of ^{129}I and other nonsorbing species in the saturated zone is relatively rapid, as shown by release rates for the saturated zone when compared to the unsaturated zone in

Figure 2.4-66. In contrast, dissolved ^{242}Pu (with sampled K_d of about 84.2 mL/g for saturated-zone volcanic matrix rock and 87.1 mL/g for saturated-zone alluvium) and to a much greater extent dissolved ^{135}Cs (with sampled K_d of about 5,986 mL/g for saturated-zone volcanic matrix and 562 mL/g for saturated zone alluvium), undergo sorption while being transported through the saturated zone and hence are highly retarded, as indicated in Figures 2.4-67 and 2.4-68.

^{242}Pu is transported both as a dissolved species and sorbed onto colloids, both reversibly and irreversibly. The irreversible fraction is further partitioned into a fast traveling and a slow traveling fraction of colloids (Sections 2.4.2.3.2.1.8 and 2.4.2.3.2.1.10). Figure 2.4-73 shows the contribution to the mean annual dose of ^{242}Pu transported as dissolved and reversibly sorbed, as well as the dose associated with ^{242}Pu transported irreversibly on colloids (for both the slow and fast fractions). The figure indicates that while colloidal irreversibly sorbed ^{242}Pu exists and is transported in the Lower Natural Barrier, its contribution to the mean annual dose is small and the majority of the dose is from the dissolved plus reversibly sorbed ^{242}Pu (SNL 2008a, Section 7.7.1.5[a]).

The above descriptions of cause-and-effect relationships between degradation, release, and transport and their influence on dose for the nominal modeling case help demonstrate consistency between the repository performance and the performance of individual components of the TSPA model.

2.4.2.2.3.2 Single-Realization Deterministic Analyses for the Seismic Ground Motion Modeling Case

Seismic ground motion modeling cases for the 10,000-year and 1,000,000-year simulation duration are evaluated somewhat differently due to a separate computational methodology employed for calculating the expected dose. In the 10,000-year calculations, a dose response function is determined by specifying a combination of waste package damage time and waste package damage area for each GoldSim realization, which is then used to compute expected dose (SNL 2008a, Equation 6.1.2-22). For the 1,000,000-year calculation, a sequence of seismic events is generated randomly for each GoldSim realization and the damaged area of the waste package is determined from seismic damage abstractions implemented in TSPA based on the magnitude of the event and the state of the waste package, drip shield, and drift at the time of the event. For the 10,000-year calculation, the dose consequences are approximated by only examining the occurrence of stress corrosion cracking damage to codisposal waste packages under intact drip shields, since other effects make only a minor contribution to expected dose for the seismic ground motion modeling case (SNL 2008a, Section 7.3.2.6.1.3). Because of these differences in methodology, cause and effect relationships are simpler for the 10,000-year single realization analysis.

2.4.2.2.3.2.1 Seismic Ground Motion Modeling Case for the 10,000-Year Period

This section presents an analysis of a single realization from the 9,000-realization base-case run (random seed #1) for the seismic ground motion modeling case for the 10,000 year simulation duration (300 epistemic samples times 30 aleatory samples equals 9000 realizations) (SNL 2008a, Section 7.7.1.7[a]). The expected annual dose is presented on Figure 2.4-74, where each of the 300 realizations represent expected annual dose for one epistemic uncertainty vector.

The expected annual dose for a given epistemic uncertainty vector $\mathbf{e}$ is generated by taking an expectation over a sample of 30 aleatory uncertainty vectors. The dose response functions for 30 aleatory uncertainty vectors are calculated by specifying six discrete damage times (at 200, 1000, 3000, 6000, 12000, and 18000 years) over five fractional waste package damage areas (10^{-7}, 10^{-6}, 10^{-5}, 10^{-4}, and 10^{-3}). As mentioned above, for the 10,000 year simulation, the dose consequences are approximated by only examining the occurrence of stress corrosion cracking damage to codisposal waste packages under an intact drip shield, because of the low consequences of other processes, such as the effects of rockfall and drift degradation, waste package puncture and rupture, general corrosion of the waste package and drip shield, and seismic crack damage to commercial SNF waste packages. Because the drift-degradation is not considered, the thermal-hydrologic processes in the EBS remain the same as under nominal conditions. The expected annual dose for each epistemic uncertainty vector is described in Section 2.4.2.1.5.4 (also see Equation 2.4-26).

A single epistemic vector (out of sample size of 300 epistemic vectors) is selected for further analysis in such a manner that the expected annual dose is broadly representative of the modeling case and similar in behavior to the mean annual dose curve. Based on this, epistemic vector 155 ($\mathbf{e}_{155}$) was chosen for further evaluation (Figure 2.4-74). The thirty aleatory vectors corresponding to ($\mathbf{e}_{155}$) are represented by GoldSim Realizations 4,621 through 4,650 (Figure 2.4-75). The expected annual dose from epistemic vector 155 was developed from the aleatory vectors illustrated on Figure 2.4-75 using the integral over aleatory uncertainty indicated in Equation 2.4-26. Of the aleatory vectors shown in Figure 2.4-75, the eighth aleatory vector ($\mathbf{a}_8$), which is equivalent to GoldSim Realization 4,628, was selected for further analysis (dashed red curve). In this aleatory vector, the seismic damage time is specified at 1,000 years and the fractional damaged area of the codisposal waste package is specified at 10^{-5}. It should be noted that the “realization” examined here is not a representative repository future (unlike the single-realization examples for the nominal modeling case and the 1-million-year seismic ground motion modeling case, which represent a repository future). Rather it is stylized dose curve used in the numerical integration that produces the expected annual dose shown in Equation 2.4-26. (Note: Only 20 of the aleatory vectors corresponding to epistemic vector 155 are visible in Figure 2.4-75. The other 10 occur at times beyond 10,000 years but are used in the interpolation and quadrature methodology of EXDOC_LA.)

The conditional total annual dose from Realization 4,628 ($\mathbf{e}_{155}$, $\mathbf{a}_8$) is presented on Figure 2.4-76 along with the annual dose curves from the major dose-contributing radionuclides. The dominant radionuclides are ^{99}Tc, ^{129}I, ^{14}C, ^{36}Cl, and ^{79}Se, with negligible contributions from the remaining radionuclides. The annual dose increases rapidly following the waste package damaging event at 1,000 years, reaching a maximum around 2,000 years and then declining gradually with time as the radionuclide mass is depleted. The bump noticeable around 2,000 years is a result of climate change from monsoonal to glacial-transition climate that occurs at 2,000 years after emplacement. The dose behaviors for ^{99}Tc, ^{129}I, ^{14}C, and ^{36}Cl are nearly identical to each other because of their similar transport characteristics through the EBS, unsaturated zone, and saturated zone, since all of these radionuclides are mobilized without solubility controlling mineral phases and with no sorption in the EBS and Lower Natural Barriers. The relative differences in dose among them are primarily due to their different inventory masses, decay rates, and BDCFs. The transport of ^{79}Se is somewhat different from the rest because ^{79}Se is sorbed in the unsaturated zone and saturated zone, although it has no solubility controlling mineral phase. Hence for the purpose of describing the transport behavior of major dose contributing radionuclides, only ^{99}Tc (the highest dose contributor among radionuclides that have similar transport characteristics) and ^{79}Se are considered in the following discussion.

All codisposal waste packages in all five percolation subregions fail at 1,000 years in this realization. The number of failed packages in a given percolation subregion is proportional to the repository area occupied by that percolation subregion. As a result, 40% of the waste packages belong to percolation subregion 3, 25% each to percolation subregions 2 and 4, and 5% each to percolation subregions 1 and 5. In each percolation subregion, the number of waste packages are further distributed among seeping and non-seeping environments based on the seepage fraction for that percolation subregion. The number of failed waste packages for all percolation subregions distinguished by seeping and non-seeping environments is shown in Figure 2.4-77. Note that for a given percolation subregion most of the waste packages fall in the non-seeping environment due to the relatively small calculated seepage fraction in intact or moderately degraded drifts, which is the situation in the first 10,000 years. For example, the seepage fraction for percolation subregion 3 is about 0.33, so only 33% of the waste packages assigned to percolation subregion 3 belong to the seeping environment; the remaining 67% belong to the non-seeping environment. The seepage fraction for a given percolation subregion remains constant over the simulation duration and is based on the determination of the fraction of seeping locations at 10,000 years in the given percolation subregion.

Since the drip shields remain intact and stress corrosion cracking on the codisposal waste package surface due to vibratory ground motion is the only waste package damage mechanism, no advective transport of radionuclides can occur through the waste package. The only release mechanism out of the waste package is by diffusion along the diffusive pathways inside the waste package and through the cracks on the waste package outer barrier to the invert. Since the fractional damage area to the waste package outer barrier in this realization is specified to be 10^{-5}, it is equivalent to a diffusive area of 3.26×10^{-4} m^2 (note that the outer surface area of the codisposal waste package is given as 32.6 m^2), which is applied only over the waste package outer barrier thickness (computed to be 0.0301 m, the distance from the outside of the inner vessel to the outside of the outer barrier). Inside the waste package the diffusive areas and diffusive lengths for the discretized transport domains are larger (SNL 2008a, Section 6.3.8). Thus, the narrow cracks in the Alloy 22 outer barrier control the diffusive transport rate and act as a choke point for diffusive releases.

The diffusive releases of ^{99}Tc from the failed codisposal waste packages for various percolation subregions (combined over seeping and non-seeping environments) are shown in Figure 2.4-78. The diffusive release for percolation subregion 3 is the highest, as expected, due to greatest number of failed waste packages among various percolation subregions. Although the number of failed waste packages is the same among percolation subregions 2 and 4, and among percolation subregions 1 and 5, the relative peak releases are different because of higher seepage fractions for percolation subregion 4 (compared to 2) and 5 (compared to 1) leading to a greater proportion of waste packages being placed in a seeping environment. Diffusive release from a waste package placed in a seeping environment, compared to a non-seeping environment, tends to be higher due to different downstream boundary conditions. Drift seepage water flows through the invert in the seeping environment, which has the effect of moving the zero concentration boundary closer to the waste package, thereby increasing the concentration gradient from the waste package to the invert. The diffusive releases of ^{79}Se from failed codisposal waste packages for various percolation subregions are similarly affected, as shown in Figure 2.4-79. The magnitude of ^{79}Se release, however, is much smaller than ^{99}Tc, due primarily to lower inventory mass per failed codisposal waste package (about 12.5 g) compared to ^{99}Tc (about 960 g per failed codisposal waste package), thus leading to lower concentrations in the waste package and a lower diffusive gradient. Also, the free water diffusion coefficients of the two radionuclides are slightly different. ^{99}Tc has a free water diffusion coefficient of 1.95×10^{-9} m^2/s, while that for ^{79}Se is lower, at 1.04×10^{-9} m^2/s.

Within percolation subregion 3, the diffusive and advective mass fluxes of ^{99}Tc from the EBS are compared in Figure 2.4-80 for the seeping and non-seeping environments. Even though the releases from the waste package are only diffusive, because of liquid flow in the invert the advective flux from the EBS is greater in the seeping environment. For the non-seeping environment, the diffusive flux from EBS is greater than the advective flux (which is only due to imbibition flow in the invert). Since the total mass flux for the non-seeping environment is greater than that for the seeping environment for percolation subregion 3 (due to larger number of failed waste packages in the non-seeping environment), the results for the non-seeping environment are analyzed in more detail below.

The dissolved concentrations of ^{99}Tc out of the various transport domains in the EBS are shown in Figure 2.4-81. The concentrations in the HLW and DOE SNF waste form sub-domains and in the corrosion products domain are equal because of fast transport of ^{99}Tc inside the waste package arising from the large diffusive areas modeled. As shown in Figure 2.4-81, the HLW glass is nearly completely degraded by about 4,000 years. Despite that, the ^{99}Tc mass in the waste form and corrosion products domains is not fully depleted, and the concentration declines gradually. This is attributed to the low diffusive area of 3.26×10^{-4} m^2 in the transport cell representing the few stress corrosion cracks in the Alloy 22 outer barrier. This small diffusive area reduces the diffusive conductance across the outer barrier and thus exerts a strong influence on the concentration gradient and the resulting mass transport rate. As a result, the concentration in the outer barrier cell is considerably reduced compared to the upstream waste form cells. The diffusive mass fluxes of ^{99}Tc exiting the downstream boundaries of the various EBS domains are compared in Figure 2.4-82. A large reduction in diffusive flux across the outer barrier at early times is apparent, when compared to the waste form domains, thereby causing retention of appreciable mass in the waste package for thousands of years following the breach. Also, the diffusive release out of the upstream cell representing the corrosion products domain virtually overlaps that of the downstream outer barrier cell because the diffusive conductance between the two domains is controlled by the very small diffusive area in the Alloy 22 outer barrier.

The initial sharp increase in concentration noticeable in Figure 2.4-81 is due to the delayed onset of transport following the seismic event at 1,000 years, as the relative humidity remains below the threshold value of 95% (required to initiate transport) until 1,080 years. As a result, almost 80 years of HLW mass is accumulated from degradation prior to the onset of release. Similarly, since all of the DOE SNF mass is degraded instantaneously following the waste package breach it is also all available for release after 1,080 years. The characteristics of diffusive release and concentration gradients for ^{79}Se are similar to that for ^{99}Tc, and are not shown here.

The mass released from the EBS (for each percolation subregion summed over the seeping and non-seeping environments) is passed to the unsaturated zone by partitioning the mass into the fracture and matrix nodes of the unsaturated zone transport model at the repository horizon. The fraction of ^{99}Tc and ^{79}Se mass that is passed to the fractures is shown in Figures 2.4-83 and 2.4-84, respectively. In almost all percolation subregions (except for percolation subregion 1) the mass fraction going into the fracture continuum (compared to the matrix) is greater than 0.5 initially following the breach and then diminishes rapidly. This is because initially the mass flux from the seeping environment, which is predominantly passed into the unsaturated zone fracture continuum, is greater than the non-seeping environment (due to a higher initial concentration gradient between the waste package and invert, caused by flow through the invert). Eventually, the mass contribution from the non-seeping environment predominates (since more waste packages are failed in the non-seeping environment) and more mass diffuses into the unsaturated zone matrix continuum due to its larger effective diffusive area connection with the invert. After 4,000 years, steady state conditions pertain, once the HLW waste form is fully degraded and the release is controlled by the small diffusive area through the waste package outer barrier. Among the various percolation subregions, the fraction of mass released into the fracture is proportional to the seepage fraction. Thus percolation subregion 5 (seepage fraction of 0.44) has relatively greater mass going into the fractures than percolation subregion 1 (seepage fraction of 0.16). As a result, the sharp increase noticed around 2,000 years due to climate change is most pronounced in percolation subregion 5 and least in percolation subregion 1.

The cumulative release over all percolation subregions from various transport domains in the EBS and Lower Natural Barriers is shown in Figure 2.4-85 for ^{99}Tc and Figure 2.4-86 for ^{79}Se (SNL 2008a, Section 7.7.1.7[a]). For ^{99}Tc, considerable delay in release occurs out of the waste package compared to the release out of the waste form due to the small diffusive area in the outer barrier. A small delay is noticed for the invert early on (designated "EBS" in the figure) due to transient conditions as the concentrations build up in the invert leading to increased release rates. After few thousand years, the mass released from the EBS matches that released from the waste package indicating limited barrier capability of the invert for a non-sorbing radionuclide with no solubility control. The cumulative release curve for the unsaturated zone indicates some delay compared to the release from the EBS. This is attributed to the majority of the mass entering the unsaturated zone in the matrix nodes and undergoing slower transport. Due to fracture-matrix interaction, the mass that is released into the matrix continuum slowly diffuses into the fracture continuum, where it is then rapidly transported to the water table by advection. Thus, although the majority of the mass enters the unsaturated zone through matrix nodes, it generally reaches the water table via the fractures, due to matrix diffusion from the matrix back to the fractures. For this particular realization of the saturated zone breakthrough curves, only a small transport delay occurs in the saturated zone-as a result of longitudinal dispersion and fracture-matrix diffusive interaction. This is demonstrated in the breakthrough curves for ^{99}Tc in the saturated zone for all four regions, as shown in Figure 2.4-87. For this particular sampling of the saturated zone breakthrough curves (saturated-zone Realization 33), the median breakthrough time to the accessible environment is about 200 years. The long tail that extends for thousands of years indicates high degree of dispersion due to the fracture-matrix interaction as the mass that initially diffused into the saturated zone matrix moves back into the fracture and is eventually transported out.

The cumulative releases for ^{79}Se (Figure 2.4-86) show similar behavior to ^{99}Tc (Figure 2.4-85) for the release from the waste form, waste package, and EBS. However, in contrast to ^{99}Tc, the transport of ^{79}Se is significantly retarded in the unsaturated zone and saturated zone. This is because of reversible sorption of ^{79}Se in the unsaturated zone and in the saturated zone volcanic matrix and saturated zone alluvium. The sampled K_d for the unsaturated zone tuff matrix is about 9.3 mL/g (for zeolitic units), 7.4 mL/g (for devitrified units), and 4 mL/g (for vitric units). The sampled K_d for the saturated zone matrix in the volcanic units is about 16.4 mL/g and that for the saturated zone alluvium is about 13.4 mL/g. In the unsaturated zone matrix, even with small sampled K_d values, the retardation is significant since the concentration gradient from the matrix to the fracture is further reduced due to sorption in the matrix (SNL 2008a, Section 7.7.1.7[a]). By 10,000 years only about 41% of the total mass released from the EBS is released out of the unsaturated zone. In the saturated zone, the delay is even more pronounced as only about 20% of the mass that enters from unsaturated zone is released out of the saturated zone model boundary by 10,000 years. Figure 2.4-87 shows the breakthrough curves from the four saturated zone regions indicating significant retardation for ^{79}Se, with a median breakthrough time of around 20,000 years. Compared to the transport of an unretarded species such as ^{99}Tc, the effective retardation factor of ^{79}Se in the saturated zone, for this realization, is about 100 (based on the ratio of median travel times of ^{79}Se to ^{99}Tc).

The release rates out of the saturated zone model boundary (to the accessible environment) for ^{99}Tc and ^{79}Se are shown in Figure 2.4-88 for Realization 4,628. The yearly saturated-zone mass releases are mixed into 3,000 acre-ft of water (the annual water usage by the RMEI as defined by 10 CFR 63.312) to compute the mass concentrations, which are subsequently converted to activity concentrations (curies per liter of water), and then multiplied by the corresponding BDCFs to give annual dose to the RMEI. The end result is shown in Figure 2.4-76.

2.4.2.2.3.2.2 Seismic Ground Motion Modeling Case for the 1,000,000-Year Period

This section presents an analysis of a single realization (SNL 2008a, Section 7.7.1.4[a]) from the 9,000-realization base-case run (random seed #1) for the seismic ground motion modeling case for the 1,000,000 year simulation duration (300 epistemic samples times 30 aleatory samples equals 9,000 realizations). The expected annual dose is presented on Figure 2.4-89, where each of the 300 realizations represent expected annual dose for one epistemic uncertainty vector. The expected annual dose for each epistemic uncertainty vector is generated by taking an expectation over a sample of 30 aleatory uncertainty vectors, as described in Section 2.4.2.2.2.3 (also see Equation 2.4-36). A single epistemic vector is selected for further analysis in such a manner that the expected annual dose is broadly representative of the modeling case and similar in behavior to the mean annual dose curve. The epistemic uncertainty vector 155 is selected, as indicated on Figure 2.4-89. This is the same epistemic sample as the previously described single-realization simulation for the 10,000-year period.

Epistemic vector $\mathbf{e}_{155}$ corresponds to the 30 corresponding aleatory sampling sequences that are GoldSim Realizations 4,621 through 4,650 (Figure 2.4-90). Of these, GoldSim Realization 4,641 is selected for further analysis (solid red curve). Note that Realization 4,641 represents epistemic uncertainty vector 155 and aleatory uncertainty vector (i.e., seismic event sequence) 21 (i.e., $\mathbf{a}_{21,155}$). The total annual dose from Realization 4,641 is presented on Figure 2.4-91 along with the dose contribution from major radionuclides. In general, the annual dose profile shows four peaks, of which two occur before 100,000 years and the remaining two around 200,000 years. Before 300,000 years, the dominant radionuclides are ^{99}Tc, ^{129}I, ^{79}Se, ^{239}Pu, but afterwards the dose is predominantly from ^{242}Pu with minor contribution from ^{135}Cs and ^{237}Np. The dose increases gradually past 300,000 years and there is no dose prior to 24,500 years.

Seismic events are modeled as a Poisson process that are generated randomly with the specified rate of 4.287×10^{-4} per year (equal to the difference between maximum annual exceedance frequency of 4.287×10^{-4} per year and the minimum annual exceedance frequency of 10^{-8} per year) (SNL 2008a, Section 6.6.1.3.2). Over the course of any simulation, many seismic events will occur, with an average value of 429 events (computed by multiplying the specified rate of the Poisson process, 4.287×10^{-4} per year by the simulation time period of 1,000,000 years). For Realization 4,641, as shown on Figure 2.4-92, a total of 460 seismic events occur over the simulated duration. The horizontal component of the PGV corresponding to each seismic event is also shown, which is calculated from the mean bounded seismic hazard curve (SNL 2008a, Figure 6.6-6) by uniformly sampling the annual exceedance frequency between the minimum and maximum values for each event and choosing the corresponding PGV value.

The probability of damage from an event is calculated separately for the codisposal and commercial SNF packages, primarily due to the inclusion of the TAD canister in the commercial SNF packages, which increases its structural strength. Though the response surface for the probability of damage is different between codisposal and commercial SNF packages, they are both functions of the PGV and the residual stress threshold of Alloy 22. The PGV value varies by each seismic event (as shown on Figure 2.4-92), because it represents aleatory uncertainty, while the residual stress threshold of Alloy 22 is an epistemic uncertain parameter with a sampled value of 91.92% of the Alloy 22 yield strength for this particular realization, 4,641. The residual stress threshold can vary uniformly from 90% to 105% of the yield strength and thus the value of 91.92% indicates a sample from the lower end of the distribution. A lower residual stress threshold value results in a greater probability of damage to the waste package during a given seismic event; however, the actual damage depends on a number of other conditions, such as whether the waste package has intact internals or degraded internals, whether or not the drip shield framework and plate are intact, or whether or not the waste package is covered by rubble. These conditions are determined by various seismic consequence abstractions.

Based on the drip shield plate and framework fragility analysis (SNL 2008a, Section 6.6.1.3.5), which is a function of drip shield plate and framework thickness at the event time, the fraction of the drift filled by rubble (in lithophysal zones) at the event time, and the PGV of the event, it is calculated that the drip shield framework does not fail until about 90,000 years and the drip shield plates do not fail until 270,000 years (Figure 2.4-93). At the time of drip shield plate failure, the fraction of drift filled by rubble is still less than half (about 0.43). However, the time of drip shield plate failure (after which the drip shield no longer has any barrier capability) is still significantly earlier than the drip shield failure time would be from general corrosion processes alone, which is computed to occur around 307,000 years for this realization. (Note that drip shield failure due to rockfall in the nonlithophysal zone is a screened-out FEP, as indicated in Section 2.4.2.3.2.1.12.3.)

The first waste package damage time from a seismic event (SNL 2008a, Section 6.6.1.3.8) is determined separately for codisposal and commercial SNF waste packages, and is calculated as the earliest of (a) the first damage time to the intact waste package (with intact internals) moving freely beneath the intact drip shield (either by stress corrosion cracking or by rupture), (b) the first damage time to the waste package surrounded by rubble (using the degraded internals damage abstraction) after the drip shield (either framework or plate) has failed, or (c) the first damage time to the waste package by puncture after the drip shield plate has failed. For codisposal waste packages in Realization 4,641, the first waste package damage is caused by a seismic event at about 24,100 years, which is much earlier than the drip shield framework and plate failure times, and is calculated from the damage abstraction for the intact waste package moving freely beneath the intact drip shield. The horizontal PGV of this seismic event is about 0.7 m/s which, at the sampled residual stress threshold of 91.92%, gives the probability of codisposal waste package damage to be about 0.22 (SNL 2008a, Figure 6.6-11a). This value is compared to a random number generated by sampling a uniform distribution between 0 and 1 for each seismic event, such that if the probability of damage exceeds the random number then the waste package damage would occur. This random number simply represents the aleatory (i.e., irreducible) uncertainty in the consequences of seismic events (SNL 2007c, Table 6-91). For the seismic event at 24,100 years, the random number is sampled at 0.15 and thus codisposal waste package damage occurs. All codisposal waste packages fail at this time, since there is no spatial variability from seismic damage (except possibly from slightly varying average waste package thicknesses in the different percolation subregions). The number of codisposal waste packages failing in each percolation subregion for seeping and nonseeping environments is shown on Figure 2.4-94.

For commercial SNF waste packages with intact internals, the probability of sustaining damage from a seismic ground motion event is extremely small (SNL 2008a, Figure 6.6-10a), and does not occur in the simulation time period of 1,000,000 years. However, the waste package breach times from nominal stress corrosion cracking of the closure lid welds are much earlier than this. These nominal stress corrosion cracking breach times differ for each percolation subregion due to spatial variability in the thermal profiles of the waste package, which affects the rate of general corrosion thinning of the protective compressive-stress layer on the outside of the Alloy 22. (This layer must be corroded away before crack propagation can initiate.) The first stress corrosion cracking breach of commercial SNF waste packages in Percolation Subregion 1 occurs at around 188,000 years, at around 168,000 years in Percolation Subregion 2, and around 204,000 years in Percolation Subregions 3, 4, and 5. Failure of additional commercial SNF waste packages from nominal processes occurs based on the calculated waste package failure history for each percolation subregion. The resulting total number of commercial SNF packages that fail in each percolation subregion for seeping and nonseeping environment is shown in Figure 2.4-95. Noticeable jumps in the number of failed waste packages around 300,000 years and 500,000 years reflect coarse time discretization used by WAPDEG at late simulation time periods.

Since all codisposal waste packages simultaneously fail around 24,100 years from seismic damage, the damaged area of a waste package increases from zero to an initial small area due to the first appearance of cracks. It then increases discretely from subsequent seismic events that cause damage (using damage abstraction calculations for waste packages with degraded internals under intact drip shield) but remains relatively small, as shown for Percolation Subregion 3 (Figure 2.4-96). The initial damage area increases sharply past 49,000 years, followed by a few more increases from events that cause damage. After failure of the drip shield plate (around 270,000 years) the waste package damage abstraction is based on the waste package surrounded by rubble, and the probability of seismic crack damage becomes very small except at high PGV levels (SNL 2008a, Figure 6.6-15) (i.e., very rare earthquake events), leading to no failure from subsequent seismic events until the seismic event that occurs at about 850,000 years, which has a PGV of about 1.9 m/s (Figure 2.4-92). After 200,000 years there are small, gradual increases in the opening area due to continuing stress corrosion cracking from nominal processes. Beyond 500,000 years, patches from general corrosion processes start to appear and the total opening area increases rapidly. The breach area history for the commercial SNF waste packages is similar to that for codisposal waste packages, except for the start time which is much later, as shown for the Percolation Subregion 3 on Figure 2.4-97. Following the first stress corrosion cracking failure from nominal processes around

204,000 years, the waste package internals are assumed to be degraded. Thus, the waste package is more susceptible to damage from seismic events. The opening area from stress corrosion cracking then increases discretely as a result of subsequent seismic events, although there is some small gradual increase in the opening area due to continuing stress corrosion cracking from nominal processes. Nevertheless, the breach area remains relatively small until general corrosion patches appear after about 600,000 years.

Calculations of the seismically damaged area that use the degraded internals abstraction are based on the thickness of the waste package outer barrier (SNL 2008a, Figures 6.6-10 to 6.6-17), in addition to the sampled PGV and the residual stress threshold value. Two end member seismic damage abstractions are generally used in the TSPA model. One is based on an average 23 mm outer barrier thickness and is applied if the average outer barrier thickness is greater than or equal to 23 mm. The second abstraction is based on an average 17 mm outer barrier thickness applied if the average outer barrier thickness is less than or equal to 17 mm (this happens rarely and typically near the end of the simulated time period) (Figure 2.4-23). For average outer barrier thicknesses between 23 mm and 17 mm, the damage is based on the linear interpolation between the two end-member damage abstractions. Inside-out corrosion of the outer barrier begins once the waste package is breached, which accelerates thinning of the waste package outer barrier and makes it more susceptible to both seismic damage and general corrosion patches. Profiles of mean thicknesses of waste package outer barriers for both codisposal and commercial SNF waste packages in Percolation Subregion 3 are shown on Figure 2.4-98, along with waste package failure fractions. The initial thicknesses of both types of waste package are the same but diverge due to the initiation of inside-out corrosion of all codisposal waste packages following seismic damage around 24,100 years. On the other hand, the commercial SNF waste packages do not begin to fail until after 200,000 years, and they typically fail over an extended period. Because of this difference in failure time, failed commercial SNF waste packages are, on average, thicker than failed codisposal waste packages, making commercial SNF waste packages less susceptible to seismic damage and general-corrosion-induced patch failures compared to codisposal waste packages (SNL 2008a, Section 7.7.1.4[a]). This is the primary reason for the smaller opening area and longer time taken for patches to appear on commercial SNF waste packages (Figure 2.4-97) compared to codisposal waste packages (Figure 2.4-96).

Because general corrosion patches on the waste packages (either commercial SNF or codisposal) do not appear until 500,000 years or later, all mass released from failed waste packages until that time is by diffusion through stress corrosion cracks (advective water flow through stress corrosion cracks is screened out in excluded FEP 2.1.03.10.0A. Advection of liquids and solid through cracks in the waste package (Table 2.2-5)). ^{99}Tc is a major dose contributor, and its diffusive mass flux out of codisposal waste packages for various percolation subregions is shown on Figure 2.4-99(a). Note that the relative magnitude of release rates among percolation subregions is proportional to the number of failed waste packages in each percolation subregion (Figure 2.4-94). Releases start when waste packages are first damaged (around 24,100 years), then decrease over the next approximately 25,000 years as steady-state conditions are established. Release rates increase again around 49,500 years due to a sharp increase (about 30-fold) in the waste package damage area (Figure 2.4-96) related to the occurrence of another damaging seismic event (Figure 2.4-92). Even though most of the HLW glass waste form has degraded by 40,000 years, as well as the DOE SNF fuel, not until about 55,000 years does most of the ^{99}Tc mass gets released from the waste package. This delay reflects the role of small cracks in reducing the mass release, despite the lack of a solubility controlling solid for ^{99}Tc and consequent large concentration gradients out of the waste package.

In contrast, the diffusive mass flux of ^{242}Pu (a major dose contributor past 500,000 years) out of the failed codisposal waste packages remains relatively constant (Figure 2.4-99(b)). It follows the waste package outer barrier area opening curve, which is an indication that diffusive release of plutonium is proportional to the total waste package opening area (Figure 2.4-96). Slow relative release of ^{242}Pu is maintained throughout the simulation for a variety of reasons, including (a) the longer half-life of ^{242}Pu (~ 375,000 years) compared to that of ^{99}Tc (~ 213,000 years); (b) the dissolved concentration inside the waste form domain is limited by the solubility controlling mineral phase (SNL 2008a, Section 6.3.7.5) so that not all of the degraded mass is available for release; (c) sorption of ^{242}Pu in the corrosion products domain retards its transport and reduces the concentration gradient for diffusive flux; and (d) small diffusive areas associated with waste package outer barrier reduces the mass flux (SNL 2008a, Section 7.7.1.4[a]). Of these four factors, the most important is sorption onto the steel corrosion products inside the waste package. For example, in Percolation Subregion 3 for the seeping environment, 1,055 codisposal waste packages fail around 24,100 years. Total initial ^{242}Pu mass in the codisposal inventory (combined HLW and DOE SNF masses) is approximately 38.65 g/pkg (grams per codisposal package) (SNL 2008a, Section 7.7.1.4[a]), which includes an adjustment based on uncertainty in the inventory. By using the decay rate of 1.85×10^{-6} per year, the maximum mass of ^{242}Pu at the time of waste package breach would be about 36.97 g/pkg, and about 35.31 g/pkg at 49,000 years, when the breach area increases (Figure 2.4-96). Based on the results of the transport calculation, the mass of ^{242}Pu sorbed onto corrosion products at 49,000 years is about 35.30 g/pkg, which accounts for almost all of the available mass. The mass is slowly released by kinetically-limited desorption from corrosion products into the solution, thereby controlling both dissolved concentration (Figure 2.4-100) and diffusive flux. Note that a mechanistic competitive sorption model that considers kinetic sorption and desorption processes is implemented for plutonium in the corrosion products domain (Section 2.4.2.3.2.1.7). As a result, variations in ^{242}Pu concentration within the corrosion products domain are moderated, even though upstream concentrations (in the waste form domain) can vary over a larger range based on time-varying degradation rates and solubility limits.

The diffusive flux of ^{99}Tc and ^{242}Pu from all five percolation subregions for commercial SNF waste packages is shown on Figure 2.4-101. The release from percolation subregion 2 precedes releases from other percolation subregions as expected, because commercial SNF waste packages fail in percolation subregion 2 first (Figure 2.4-95). Figure 2.4-97 shows the evolution of the commercial SNF waste package outer barrier opening area for percolation subregion 3 in a seeping environment. The ^{99}Tc diffusive releases from commercial SNF waste packages are sustained for much longer times than are releases from codisposal waste packages (compare Figures 2.4-99a to 2.4-101a) due to the more gradual failure of commercial SNF waste packages as shown in Figure 2.4-95. However, once all commercial SNF waste packages in a given percolation subregion have failed by nominal stress corrosion cracking (typically by about 550,000 years) and almost all of the commercial SNF waste form has degraded, the ^{99}Tc mass is depleted relatively quickly out of the waste package, but still takes over ten thousand years to be fully released. Compared to ^{99}Tc release, diffusive release of ^{242}Pu is more gradual and follows the breach area curve rather than the commercial SNF waste package failure curve. The increase in diffusive releases after 800,000 years is caused by an increased number of general corrosion patch openings, which significantly increases the total waste package breach area (Figure 2.4-97). Continually available ^{242}Pu inventory in the commercial SNF waste packages is maintained by sorption-desorption reactions with corrosion products, in contrast to the quick release behavior of ^{99}Tc. Figure 2.4-102 shows that most of the ^{242}Pu mass released from the inventory is sorbed on the corrosion products and then is gradually released by desorption, thereby controlling the dissolved concentration and diffusive release out of the waste package. (Note that the curve showing the mass sorbed on corrosion products also includes the effects of radioactive decay.)

The time histories for pH and ionic strength in the corrosion products domain are shown on Figure 2.4-103. The first sharp decline in ionic strength occurs around 380,000 years when lithophysal rubble completely fills the drift (a consequence of multiple seismic events, as shown on Figure 2.4-93). At that time, the differential temperature and relative humidity time histories for high thermal conductivity rubble is imposed leading to a small increase in relative humidity from 0.9956 to 0.9984. Since this increase in relative humidity corresponds to an equivalent increase in activity of water, it causes an appreciable decrease in ionic strength, indicating its high degree of sensitivity to relative humidity under vapor influx conditions (SNL 2008a, Section 6.3.7.2.2). The second decline in ionic strength that occurs around 712,000 years is caused by water flowing through the waste package after general corrosion patches have formed and exceeding a flux threshold of 0.1 L/yr, which is the threshold for changing the in-package chemistry abstraction from the vapor influx abstraction to the liquid influx abstraction (Section 2.4.2.3.2.1.7). Despite the changes in ionic strength over the course of the simulation, pH in the corrosion products domain remains nearly constant as a result of buffering by surface complexation reactions (SNL 2008a, Section 7.7.1.4[a]).

Figure 2.4-104 compares the concentration of ^{242}Pu that is associated reversibly and irreversibly with colloids to the dissolved concentration in the waste package (corrosion products domain) for both codisposal and commercial SNF waste packages. The concentration of ^{242}Pu (i.e., the sum of dissolved mass per unit water volume and the mass per unit water volume reversibly associated with colloids; denoted as “aqueous”) overlays the dissolved concentration, indicating that the mass of ^{242}Pu reversibly associated with colloids is negligible. The concentrations of various colloid types over time for both codisposal and commercial SNF waste packages are shown in Figure 2.4-105. Different types of colloids become stable at different times, based on their stability relationships (SNL 2008a, Figure 6.3.7-11). Commercial SNF waste form colloids remain unstable throughout the simulation and therefore maintain a constant minimum concentration. The HLW glass waste form colloids become stable first, followed by uranium colloids, even while there is no advection through the waste package and ionic strength remains relatively high. Following the opening of general corrosion patches and the advent of advective flow, groundwater colloids and iron oxyhydroxide colloids become stable, primarily because of decrease in ionic strength (Figure 2.4-103) (SNL 2008a, Section 7.7.1.4[a]). Due to a combination of small colloid concentrations and relatively small sampled K_d for plutonium, the plutonium mass reversibly associated with colloids remains negligibly small compared to the mass in the dissolved state (Figure 2.4-104). However, the concentration of ^{242}Pu irreversibly associated with HLW glass waste form colloids and iron oxyhydroxide colloids becomes greater than the dissolved ^{242}Pu at various times, as shown in Figure 2.4-104.

Total EBS releases (i.e., summed over all percolation subregions) of ^{99}Tc and ^{242}Pu in dissolved state, dissolved and reversibly associated with colloids (denoted as “aqueous”), and irreversibly sorbed on colloids from both commercial SNF and codisposal waste packages are shown on

Figure 2.4-106. (The EBS release of ^{242}Pu mass irreversibly sorbed on commercial SNF waste form colloids, is not shown as it is negligible due to the instability of those colloids.) As expected, the amount of mass released from commercial SNF waste packages exceeds that released from codisposal waste packages due to the greater number of commercial SNF waste packages and larger inventory on a per package basis (SNL 2008a, Tables 6.3.7-1 and 6.3.7-5). Until the general corrosion patches appear and advection starts, at around 700,000 years, most of the ^{242}Pu mass released from the waste package is in the dissolved state and very little is irreversibly associated with colloids (Figure 2.4-106), even though the concentration of ^{242}Pu irreversibly associated with colloids is higher than the dissolved concentration in the waste package (as shown by the example in Figure 2.4-104). This is because prior to the opening of patches, only diffusive release can occur through the waste package and the colloid-facilitated transport is limited by the diffusion coefficient of colloid particles, which is computed to be about 700 times smaller than that for the dissolved plutonium based on the sampled colloid particle diameter (SNL 2008a, Section 7.7.1.4[a]). Once advection through the waste package starts, the transport of mass irreversibly associated with colloids becomes important.

The majority of the mass (from both commercial SNF and codisposal waste packages) passed from the EBS to the unsaturated zone at the repository horizon goes into fracture nodes in the unsaturated zone, rather than into the matrix nodes as shown on Figure 2.4-107 for ^{242}Pu. This is because the majority of the waste packages in a given percolation subregion (except for percolation subregion 1) are in the seeping environment where drift seepage that flows out through the invert carries the mass advectively through the fractures, even though most of the mass is diffusing out of the waste package. For percolation subregion 1, the fraction of mass going into the fractures is initially relatively small (about 0.4) but increases (to approximately 0.9) around 81,500 years. This behavior is due to the change in seepage flux, which remains relatively small (about 0.005 m^3/yr) until around 81,500 years and then increases to about 0.08 m^3/yr. This is because at this time, the nonlithophysal locations in all percolation subregions are considered to be significantly degraded from drift degradation based on the drift seepage model abstraction (i.e., rockfall volume exceeds 0.5 m^3 per meter), resulting in the seepage flux for such locations to change from the intact drift seepage abstraction to the percolation flux (SNL 2008a, Section 6.3.3.1.2). The relative effect of this change is greatest for percolation subregion 1 because, compared to other percolation subregions, it has (a) the smallest ambient seepage rates prior to the drift collapse and (b) the highest fraction of nonlithophysal locations (about 32%).

The cumulative mass releases from the EBS, unsaturated zone, and saturated zone are compared in Figure 2.4-108 for ^{99}Tc, ^{242}Pu (dissolved and reversibly sorbed on colloids; denoted as “aqueous”), and ^{242}Pu (irreversibly sorbed on all colloids) (SNL 2008a, Section 7.7.1.4[a]). The transport characteristics are quite different for ^{99}Tc and ^{242}Pu in the unsaturated zone and saturated zone domains, since ^{99}Tc is transported without retardation whereas ^{242}Pu (aqueous) experiences significant retardation due to sorption onto the tuff matrix and alluvium (SNL 2008e, Table 6-7; SNL 2008f, Section 6.5.3.1 and Table 4-3). Not much retardation is apparent in the unsaturated zone and saturated zone domains for ^{242}Pu irreversibly sorbed onto colloids because the diffusive interaction between fractures and matrix continua for mass irreversibly sorbed onto colloids is assumed to be negligible and, once the mass enters the fracture continuum (at the boundary of the unsaturated zone and the EBS), it tends to stay there (SNL 2008e, Section 6.4.5; SNL 2008f, Section 6.5.2.6). Although a small fraction (0.00168) of irreversible mass associated with colloids travels unretarded through the unsaturated zone and saturated zone (designated as the “fast fraction") (SNL 2008a, Section 6.3.8.3), almost all irreversible mass on colloids undergoes some retardation due to interaction between colloid particles and fracture surfaces. Despite this interaction, the mass irreversibly associated with colloids travels rapidly through the unsaturated zone and saturated zone. As shown on Figure 2.4-108, almost all the mass released from the EBS for both ^{99}Tc and ^{242}Pu (irreversibly sorbed onto colloids) is also released at the saturated zone model boundary within a relatively short period compared to the simulation time of 1,000,000 years. In contrast, the mass of ^{242}Pu (aqueous) released from the unsaturated zone and saturated zone model boundaries at the end of the simulation is reduced compared to that released from the EBS, indicating significant retardation (about 65% is released out of the unsaturated zone while only 31% is released out of the saturated zone). Although most of the ^{242}Pu (aqueous) radionuclide mass is passed to the fracture nodes of the unsaturated zone at the upstream boundary with the EBS, matrix diffusion from the fracture continuum into the matrix continuum in the unsaturated zone creates a retardation effect in the unsaturated zone (SNL 2008a, Section 7.7.1.4[a]). This effect is significant for ^{242}Pu but not for ^{99}Tc because of sorption of the ^{242}Pu in the unsaturated zone rock matrix (Figure 2.4-107).

The mass exiting the unsaturated zone is passed to one of the four corresponding saturated zone source regions (Section 2.4.2.3.2.1.10). For each of the four saturated zone source regions there are 200 pre-generated saturated zone breakthrough curves for a given species (SNL 2008a, Section 6.3.10.2), representing epistemic uncertainty in various transport parameters. Due to their different transport characteristics through volcanic units and alluvium, separate sets of breakthrough curves are used for ^{99}Tc, ^{242}Pu (aqueous), ^{242}Pu (fast traveling fraction irreversibly associated with colloids), and ^{242}Pu (slow traveling fraction irreversibly associated with colloids). The breakthrough curves are pre-generated as an impulse response function to a unit pulse and are convolved with the incoming unsaturated zone mass flux by using the convolution integral approach to produce the saturated zone mass flux at the location of the RMEI. In this particular single realization, saturated zone epistemic sample 122 was selected.

The breakthrough times of ^{99}Tc, ^{242}Pu (dissolved and reversibly sorbed on colloids; denoted as "aqueous"), and ^{242}Pu (slow traveling fraction irreversibly associated with colloids) are compared for all four zones on Figure 2.4-109. The breakthrough curves for ^{242}Pu (fast traveling fraction irreversible on colloids) are not presented because very little mass is transported by them. The median breakthrough time of ^{99}Tc (represented by the 0.5 point on the cumulative breakthrough curve) from all four saturated zone regions is significantly earlier than that for ^{242}Pu (aqueous) and for ^{242}Pu (slow traveling fraction irreversible on colloids). However, the long tail noticeable in the breakthrough curve for ^{99}Tc for the remaining half of its input mass results from longitudinal and transverse dispersion in the volcanic units and alluvium as well as matrix diffusion in the dual porosity volcanic domain. The ^{242}Pu (aqueous) breakthrough curve is similarly impacted by dispersion and diffusion mechanisms but further impacted by sorption processes in both the volcanic matrix and alluvium. For saturated zone breakthrough curve 122, the initially sampled plutonium K_d for the volcanic matrix units is approximately 120 mL/g, and about 107 mL/g for the alluvium (SNL 2008f, Table A-1[b]), which results in considerable retardation. Nearly all the plutonium (> 0.999 fraction) is transported in the dissolved phase, with a small fraction (< 0.001) being transported via reversible sorption on the groundwater colloids. This is because the sampled groundwater colloid concentration in the saturated zone is about 0.11 mg/L and the sampled K_d for plutonium on colloids is about 6,560 mL/g, which when multiplied together, provides the fraction of ^{242}Pu mass transported colloidally versus that transported in dissolved form. This fraction is usually designated as K_c and in this case is equal to 0.000722.

The release rates out of the saturated zone for ^{99}Tc, ^{242}Pu (dissolved and reversibly sorbed on colloids; denoted as "aqueous"), and ^{242}Pu (irreversibly associated with colloids for both fast and slow traveling fractions) are shown on Figure 2.4-110 for Realization 4,641, and all three reflect their release rates out of the EBS (Figure 2.4-106). The saturated zone releases are converted into annual dose to the RMEI by mixing the annual saturated zone releases in 3,000 acre-feet of water (annual water usage by the RMEI) to compute the mass concentrations, converting the mass concentration into concentration of radioactivity (in curies per liter of water), and then multiplying by the corresponding BDCFs. The end result is shown on Figure 2.4-91, which mirrors the behavior shown in Figure 2.4-110.

2.4.2.2.3.3 Summary of Single-Realization Analyses

The above single-realization analyses for the nominal and seismic ground motion modeling cases have examined important aspects that control the release and movement of radionuclides through the EBS and Lower Natural Barrier. They have shown that the behavior of the various submodels is reasonable when taken in the context of the sampled parameter values and the behavior of other submodels. The analyses show that the submodels are coupled properly and that the TSPA model as a whole functions in a reasonable fashion, demonstrating consistency among the various submodels and consistency between total repository performance (dose) and the individual model component behavior. In general, analysis of single realizations provides a unique insight into the interactions of various submodel processes within the TSPA model. A comprehensive explanation detailing how the transport of key radionuclides is affected by coupling between various components of the EBS, unsaturated zone, and saturated zone domains subsequent to waste package failure, under varying physical-chemical-thermal-mechanical conditions, provides confidence that the various submodel processes are working as expected, thus providing confidence in the TSPA model. The next section provides further confidence in the TSPA model and its results through a significant suite of additional validation and confidence-building activities.

2.4.2.3 Credibility of the TSPA Results

[NUREG-1804, Section 2.2.1.3.1.3: AC 1(2); Section 2.2.1.3.2.3: AC 1(3); Section 2.2.1.3.3.3: AC 1(2), (5), (7); Section 2.2.1.3.4.3: AC 1(2); Section 2.2.1.3.5.3: AC 1(3); Section 2.2.1.3.6.3: AC 1(3); Section 2.2.1.3.7.3: AC 1(3); Section 2.2.1.3.8.3: AC 1(3); Section 2.2.1.3.9.3: AC 1(3); Section 2.2.1.3.14.3: AC 1(3); Section 2.2.1.4.1.3: AC 3]

The last of the three acceptance criteria in NUREG-1804, Section 2.2.1.4.1.3, deals with the credibility of the TSPA results, which is interpreted to mean various activities associated with confidence-building, verification, and validation for the TSPA model. The four specific subcriteria are:

1. Assumptions made within the total system performance assessment code are consistent among different modules of the code. The use of assumptions and parameter values that differ among modules of the code is adequately documented;

2. The total system performance assessment code is properly verified so there is confidence that the code is modeling the physical processes in the repository system in the manner intended. The transfer of data between modules of the code is conducted properly;

3. The estimate of the uncertainty in the performance assessment results is consistent with the model and parameter uncertainty; and

4. The total system performance assessment sampling method ensures that sampled parameters have been sampled across their ranges of uncertainty.

Section 2.4.2.3 is organized along the lines of these subcriteria. This section also addresses proposed 10 CFR 63.114(a)(7), regarding the requirement to "Provide the technical basis for the models used to represent the 10,000 years after disposal…such as comparisons made with outputs of detailed process-level models…"

2.4.2.3.1 Consistency of Assumptions and Parameter Values within the Total System Performance Assessment Code

[NUREG-1804, Section 2.2.1.3.1.3: AC 1(2); Section 2.2.1.3.2.3: AC 1(3); Section 2.2.1.3.3.3: AC 1(2), (5), (7); Section 2.2.1.3.4.3: AC 1(2); Section 2.2.1.3.5.3: AC 1(3); Section 2.2.1.3.6.3: AC 1(3); Section 2.2.1.3.7.3: AC 1(3); Section 2.2.1.3.8.3: AC 1(3); Section 2.2.1.3.9.3: AC 1(3); Section 2.2.1.3.14.3: AC 1(3); Section 2.2.1.4.1.3: AC 3(1)]

This section addresses Acceptance Criterion 3(1) in Section 2.2.1.4.1.3 of NUREG-1804 by showing consistency of assumptions among various components of the TSPA model and by documenting any assumptions and parameter values that differ among "modules of the (TSPA) code" or, equivalently, among different submodels of the TSPA model. Modeling assumptions and parameter values used in the development of model abstractions have been presented in Section 2.3. Sections 5 and 6 of each model report that forms the basis of an abstraction described in Section 2.3 document the assumptions made in the development of that model. These assumptions have been presented in Section 2.3 during the course of the discussion of the abstractions. Because the TSPA model is composed of the model abstractions documented in Section 2.3, it also is based on the same set of assumptions. Consistency of assumptions among these model abstractions is mainly verified through assuring consistent interaction within the TSPA model. Because the development of the TSPA model and its underlying abstractions has been an iterative process (Section 2.4.2.3.2.3.4), consistency in assumptions among the various abstractions has constantly improved, such that for the TSPA any differences or inconsistencies among abstractions or "modules," as discussed in Sections 2.4.2.3.1.1 through 2.4.2.3.1.12, are conservative or of low risk significance. Also, over the course of the TSPA iterative process, many recommendations and comments from technical review teams regarding consistency and differences of assumptions between submodels have been resolved and incorporated in subsequent TSPA models (Section 2.4.2.3.2.3.4). Note that consistency between related model abstractions, including consistency of assumptions, is relevant to some acceptance criteria from NUREG-1804, Section 2.2.1.3 Model Abstractions (i.e., Section 2.2.1.3.1.3, Acceptance Criterion 1(2); Section 2.2.1.3.2.3, Acceptance Criterion 1(3); Section 2.2.1.3.3.3, Acceptance Criteria 1(2), 1(5), and 1(7); Section 2.2.1.3.4.3, Acceptance Criterion 1(2); Section 2.2.1.3.5.3, Acceptance Criterion 1(3); Section 2.2.1.3.6.3, Acceptance Criterion 1(3); Section 2.2.1.3.7.3, Acceptance Criterion 1(3); Section 2.2.1.3.8.3, Acceptance Criterion 1(3); Section 2.2.1.3.9.3, Acceptance Criterion 1(3); and Section 2.2.1.3.14.3, Acceptance Criterion 1(3)). As a result, the discussion in Section 2.4.2.3.1 helps to address these acceptance criteria in addition to addressing Acceptance Criterion 3(1) in NUREG-1804, Section 2.2.1.4.1.3.

Different levels of model complexity are used to analyze various parts of the repository system based on their importance to dose and to barrier performance. The different levels of complexity and different degrees of uncertainties in various model abstractions have resulted in some different assumptions being applied to the different modules in the TSPA code. Accordingly, it is important to document potential differences in assumptions and parameters among modules or submodels of the TSPA model and code (SNL 2008a, Sections 6.3 to 6.6). However, before documenting those differences and their potential effect on the TSPA, the following is a high-level summary of the consistent set of parameters and processes that are propagated in the TSPA model and code (Section 2.4.2.3.2.1):

- Consistent propagation of the effects of climate changes through the unsaturated zone flow, EBS thermal-hydrologic environment, EBS chemical environment, drift-scale seepage, EBS flow and transport, unsaturated zone transport, and saturated zone flow and transport submodels. (Note: Based on 10 CFR 63.305(b) and (d), only present-day BDCFs are used in the TSPA model, which, in addition to ensuring consistency with the regulation, also represents a reasonably conservative approach for the dose assessment and is appropriate for wetter climate conditions (Section 2.3.10.5.1.1).)

- Consistent propagation of unsaturated zone percolation fluxes through the unsaturated zone flow, EBS thermal-hydrologic environment, EBS chemical environment, drift-scale seepage, EBS flow and transport, and unsaturated zone transport submodels.

- Use of consistent rock properties (e.g., hydrologic, thermal, structural, chemical) in the unsaturated zone flow, EBS thermal-hydrologic environment, EBS chemical environment, drift-scale seepage, drift degradation, unsaturated zone transport, and seismic consequences submodels.

- Use of consistent transport processes, such as advection, diffusion, sorption, matrix diffusion, colloid-facilitated transport, and radioactive decay and ingrowth in the EBS transport, unsaturated zone transport, saturated zone transport, and biosphere submodels, while accounting for differences in materials and conditions.

- Consistent propagation of chemical conditions (e.g., P_{CO2}, water compositions) through the waste form degradation and mobilization, EBS chemical environment, waste package degradation, and EBS transport submodels.

- Consistent propagation of in-drift thermal-hydrologic conditions (e.g., temperatures, relative humidities) through the waste form degradation and mobilization, drift seepage, in-drift condensation, EBS chemical environment, waste package and drip shield degradation, EBS flow transport, seismic consequences, and igneous consequences submodels.

The above is only a partial list of consistent assumptions and parameters among different modules of the TSPA code. Other examples are provided in Section 2.4.2.3.2.1 which describes the flow of information among different modules of the TSPA code, including the outputs that are passed from one module to another. The conclusions section for each of the model abstractions in Section 2.3 also discusses consistencies between TSPA model abstractions and the underlying process models.

The following subsections discuss the limited assumption and parameter differences among the TSPA submodels and model components and how such differences are accounted for. In each case, assumption and/or parameter differences are conservative.

2.4.2.3.1.1 Submodel Differences Related to EBS Thermal-Hydrologic Environment

In-Drift Axial Fluid Flow—The multiscale thermal-hydrologic process model, which provides the basis for the in-drift temperature and relative humidity abstraction of the TSPA model, does not consider the longitudinal transport of water vapor along the length of the emplacement drifts. Thus, the influence of evaporation, transport, and condensation in the heated and unheated regions of the drifts, which result in a cold trap effect, is not fully accounted for. On the other hand, the influence of the longitudinal transport of water vapor and associated condensation on the drift walls is approximated in the in drift natural convection and condensation process model (SNL 2007f, Section 6.3). Therefore, there is a conceptual difference between the multiscale thermal-hydrologic process model and the in-drift natural convection and condensation process model.

Effect on the TSPA Model—If longitudinal vapor transport were included in the multiscale thermal-hydrologic model, condensation in the unheated regions of the repository would affect the longitudinal variation of predicted in-drift temperature and relative humidity, with the effects on relative humidity having the greater potential impact because vapor transport could result in drier conditions than those predicted by the multiscale thermal-hydrologic process model (SNL 2008d, Section 7.8[a]). The thermal effects associated with the evaporation and condensation tend to dampen longitudinal temperature and relative humidity variations because heat would more effectively move from the hotter regions in a drift where the water evaporates to the cooler regions of the drift where the water vapor condenses. Thus, the waste-package-to-waste-package variation in temperature and relative humidity could be reduced. However, *Multiscale Thermohydrologic Model* (SNL 2008d, Section 7.5.3) and *In-Drift Natural Convection and Condensation* (SNL 2007f, Section 6.3.7.2.4) indicate that these longitudinal mass/energy transfer processes have an insignificant effect on the primary multiscale thermal-hydrologic model predictions of temperature and relative humidity.

2.4.2.3.1.2 Submodel Differences Related to Drift-Scale Seepage and In-Drift Condensation

In-Drift Evaporation—In-drift evaporation of seepage flow is not included in the drift seepage submodel in any of the scenario classes at temperatures less than 100°C (Section 2.3.3.2.1.2), even though below boiling evaporation is a process that is modeled in the multiscale thermal-hydrologic process model (Section 2.3.5.4.1), drift wall condensation submodel (Section 2.3.5.4.2), and the EBS chemical environment submodel (Sections 2.3.5.3 and 2.3.5.5).

Effect on the TSPA Model—Not including evaporation of seepage flux leads to an overestimate in the TSPA model of: (1) the water present at any point in time; (2) the amount of water flux through the invert and/or waste package; and, therefore, (3) the radionuclide mass released (SNL 2008a, Section 6.3.3.3.1).

Repository Boiling Temperature—The thermal seepage model uses 100°C for the boiling temperature of water while the drift wall condensation model uses 96°C, which is the actual boiling temperature at the repository horizon.

Effect on the TSPA Model—The 100°C threshold for thermal seepage (Section 2.4.2.3.2.1.3) means that seepage starts sooner and water is available for transport sooner (SNL 2008a, Section 6.3.3.3.1). This approach is conservative and can lead to earlier doses to the RMEI. Justification of the approach is documented in *Abstraction of Drift Seepage* (SNL 2007g, Section 6.5.2.2): "…the remaining uncertainty related to the predictive effectiveness of the vaporization barrier needs to be accounted for in the abstraction. This is done by using a threshold temperature higher than the nominal boiling temperature to define the duration of the boiling period for abstraction."

Form Factor—The in-drift condensation process model incorporates a form factor to reduce the amount of Stage 3 condensation that falls onto the drip shield because some condensation does not occur above the waste package but drains down the drift wall into the edge of the invert. Thus the mean Stage 3 drift-wall condensation rate used in the TSPA model includes a form factor ($f = 0.178$) (SNL 2007f, Section 6.1.1[a] and Figure 6-5[a]), which represents the fraction of the exposed perimeter of the drift that is directly above the drip shield. Thus, some portion of the condensate is not considered in the TSPA calculations. The fraction that is not considered is 0.822. In contrast, the seepage model applies all seepage that occurs anywhere in the drift to the crown of the drift (which subsequently falls onto the drip shields above each waste package location (SNL 2008a, Section 6.3.6.4.2)) without the use of a form factor (SNL 2007f, Sections 8.3.1.1 and 6.1.1[a]).

Effect on the TSPA Model—Condensate on the drift wall will tend to imbibe into the host rock or run down the drift walls and flow into the edges of the invert. This condensate would not contribute to transport through the waste package and would contribute negligibly to transport through the invert (SNL 2007f, Section 8.3.1.1). Accordingly, not explicitly addressing this portion of the condensate has a negligible effect on the TSPA model.

Thermal-Hydrologic Differences between Condensation and Multiscale Thermal-Hydrologic Model Abstractions—The condensation model does not explicitly consider the thermal-hydrologic behavior of the rock mass. The inclusion of rock characteristics in the condensation model would be expected to affect the predicted condensation distributions. For example, the presence of the capillary behavior of the rock would tend to reduce the evaporation rate and increase the imbibition rate, both of which would decrease the net condensation rate (SNL 2008a, Section 6.3.3.3.1).

Effect on the TSPA Model—The different responses arising from these differing model assumptions tend to decrease with time as the repository cools and the condensation rate goes to and remains zero after only about 2,000 years following permanent closure (SNL 2008a, Section 6.3.3.2.2). Also, a decrease in condensation rate, if included, would reduce water flux through the invert and/or waste package and therefore would tend to reduce the radionuclide mass released by advective transport.

Water Balance—Various different assumptions, parameters, and underlying process models for the EBS thermal-hydrologic environment, drift-seepage, and drift-wall condensation submodels mean that there is no explicitly enforced water balance (liquid or vapor) among these abstractions in the TSPA model (SNL 2008a, Section 6.3.3).

Effect on the TSPA Model—It is assumed for each of these submodels that there is sufficient water to support the gas and liquid flow rates predicted by that model, possibly resulting in an overestimate of flow rates, as well as an overestimate of the number of waste packages that are in a seeping environment (SNL 2008a, Section 6.3.3). These overestimates would result in higher rates of radionuclide transport, leading to higher doses to the RMEI. Therefore, this approach is conservative.

2.4.2.3.1.3 Submodel Differences Related to EBS Chemical Environment

Seepage Water Compositions—The in-package chemistry abstraction does not use the predicted (crown seepage) water composition from the EBS chemical environment submodel as its starting waters (SNL 2008a, Section 6.3.7.2.1). Instead, the in-package chemistry abstraction uses a liquid influx model based on the composition of typical pore waters (SNL 2007h, Section 4.1.2).

Effect on the TSPA Model—The initial starting waters used in the in-package chemistry abstraction are intended to represent seepage compositions that would enter a breached waste package, especially over the long term. The starting water compositions used in the analysis capture the spread of the pore water compositions from Yucca Mountain. As these starting waters cover the spectrum of observed porewater compositions, the use of these compositions is appropriate. Furthermore, use of these data in the in-package chemistry model ensures feeds to the TSPA model will reflect the compositional variation of the initial water composition (SNL 2007h, Section 4.1.2). Perhaps the main point, however, is that the reactants inside the waste package, either the fuel or the steel corrosion products, buffer the water chemistry (e.g., the pH) and thereby cause differences in starting composition to have minimal effect in TSPA (SNL 2007h, Section 6.10.1.1[a]) (Section 2.3.7).

Partial Pressure of CO_2—The in-package chemistry submodel uses the in-drift EBS chemical environment submodel for P_{CO2} in the waste package rather than calculating the P_{CO2} inside the waste package.

Effect on the TSPA Model—Using a single P_{CO2} for the drift, invert, and waste package conditions is the best way to have a consistent gas phase composition throughout the drift and is actually a good approximation because gas transport in and out the waste package is relatively fast. In addition, while in-package pH does depend on P_{CO2}, in-package ionic strength does not depend on the value of P_{CO2} (SNL 2007h, Section 6.6.3[a]).

2.4.2.3.1.4 Submodel Differences Related to Waste Package and Drip Shield Degradation

Salt Separation on the Waste Package Surface—The TSPA model includes a relative humidity threshold to account for a potential salt separation process during seepage water evaporation (SNL 2008a, Section 6.3.5.2.2). In this process, water evaporation on the Alloy 22 waste package surface will first cause the precipitation of chloride-rich salts (e.g., halite or sylvite) and then the remaining nitrate-rich brine will flow away, leaving behind these solids rich in Cl^-. In this case, the EBS chemical environment lookup tables (see Section 2.3.5.5.4) no longer apply (SNL 2007i, Sections 6.12.3 and 6.15.1.3). For implementation purposes, the TSPA model assumes that localized corrosion always initiates upon rewetting of the salt film (i.e, when the relative humidity rises above the relative humidity threshold for salt separation). This implementation for the waste package localized corrosion initiation and propagation submodel represents potential differences between several submodels: drift seepage, EBS flow, EBS chemical environment, and the localized corrosion aspect of waste package degradation. The EBS chemical environment submodel assumes well-mixed equilibrium conditions for chemistry in the drift (SNL 2007i, Section 5.1.2). Applying the well-mixed assumption, the effects of salt separation are not considered when calculating the pH and ionic strength of the invert water. Therefore, salt separation is not included in that submodel. In addition, evaporation and flow on a small scale of the possible salt separation phenomenon is masked by uncertainties at the larger scale of the drift seepage submodel or the EBS flow submodel. Evaporation is integral, however, to the equilibrium chemistry response surfaces that are the output of the EBS chemical environment submodel. In order to handle this difference among the underlying process models, a conservative assumption is implemented in the TSPA model, using the salt-separation relative humidity as a threshold for initiation of localized corrosion on the surface of the waste package (Section 2.3.5.5.4.3).

Effect on the TSPA Model—Considerations of water volume show that such salt separation is not expected to occur, and if it were to occur, it would be limited in spatial extent. The approach taken in the TSPA is conservative by assuming that conditions conducive to localized corrosion will exist over the entire surface of the waste package, while in actual repository environments, the volume of brines formed from evaporation are expected to be much less than that required to cover the entire waste package. For example, developing a saturated chloride-rich brine requires the seepage water to concentrate by more than 10,000 times (SNL 2007j, Figure 6-7). That is, 1 L of seepage water will result in less than 0.1 mL of chloride-rich brine solution. The TSPA conservatively assumes there will be sufficient brine volume to cause a continuous water film over the waste package surface, which overestimates the potential for initiating localized corrosion where the brine volumes are insufficient to form such a film. In any case, because of the robustness of the drip shield, crown-seepage-induced localized corrosion has no effect on any modeling case except the drip shield early failure case, where it is assumed to cause failure of the waste package under the defective drip shield. (In the seismic fault displacement modeling case, the damage caused by localized corrosion is assumed to be subsumed in the damage caused by shearing of the waste package (Section 2.4.2.3.2.1.5).)

2.4.2.3.1.5 Submodel Differences Related to Waste Form Degradation and Mobilization

Waste Form Temperature versus Waste Package Surface Temperature—The TSPA model treats waste form temperature as if it were the same as the waste package temperature, derived from the multiscale thermal-hydrologic model abstraction (SNL 2008a, Section 6.3.7). It is expected that waste form temperatures would be higher than waste package surface temperatures, and the effect of hotter temperatures is not included in the waste form submodels.

Effect on the TSPA Model—The submodels of the TSPA model that directly depend on the waste form temperature are the in-package chemistry submodel for commercial SNF waste packages, the commercial SNF waste form degradation submodel, the HLW glass degradation submodel, and the EBS transport submodel. In the TSPA model, it is assumed that water will not accumulate in the waste package if the temperature is greater than 100°C. Because the waste form temperature would be greater than the waste package surface temperature, any transport calculations using the lower waste-package temperature would be conservative because water would be modeled as accumulating sooner in the waste form, allowing radionuclide transport at an earlier time. (Note: By the time the waste package surface temperature drops to 100°C, the difference between the waste-form temperature and waste-package surface temperature is estimated to be about 2°C or less (BSC 2008, Figures 4 to 13).)

In-Package Chemistry and the Instantaneous Degradation of Commercial SNF—*In-Package Chemistry Abstraction* (SNL 2007h) does not consider instantaneous degradation of commercial SNF in the range of conditions analyzed with the process model and in the development of the subsequent abstraction. Very fast degradation rates were considered but not instantaneous degradation of commercial SNF. However, within the TSPA model, instantaneous degradation of the commercial SNF occurs in the waste package early failure modeling case and in the seismic ground motion and seismic fault displacement modeling cases when the seismic event damages commercial SNF waste packages, and the commercial SNF is exposed to waste package temperatures exceeding 100°C. It also occurs in the igneous intrusion modeling case. In the TSPA, instantaneous degradation means the entire waste inventory is available for transport at the radionuclide solubility limits at the time of the degradation.

Effect on the TSPA Model—Within the TSPA model, when a damaged commercial SNF waste package is exposed to temperatures exceeding 100°C, the calculated commercial SNF degradation rate is replaced with a rate that instantaneously degrades the exposed waste form, as recommended by CSNF Radionuclide Release Model (SNL 2008a, Section 6.3.7.4.1.3). Because the in-package pH conditions are controlled by the buffering capacity of the commercial SNF degradation products (SNL 2007h, Section 6.3.4.1[a]), instantaneous degradation of commercial SNF means the maximum pH buffering capacity will be achieved almost immediately, at which time the pH conditions will be well constrained. Well-buffered chemical solutions are part of the in-package chemistry abstraction; therefore, the implemented pH abstraction is sufficient to encompass this instantaneous commercial SNF degradation condition.

The ionic strength abstraction for commercial SNF waste packages under vapor influx conditions is based on Pitzer model calculations for simple salt solutions (SNL 2007h, Section 6.10.2.2[a]). Since the Pitzer model calculations are independent of the commercial SNF degradation rate, assuming instantaneous commercial SNF degradation would not impact the ionic strength abstraction for commercial SNF waste packages under vapor influx conditions.

A sensitivity analysis has been conducted to evaluate the impact of degradation rates on ionic strength for commercial SNF waste packages under liquid influx conditions (SNL 2007h, Section 6.6.5[a]). It reveals that although the commercial SNF degradation rate does impact the calculated ionic strength in commercial SNF waste packages, the variation is generally less pronounced than that in codisposal waste packages. The variation calculated by the sensitivity analysis due to uncertainty in the degradation rates of commercial SNF waste form and other waste package materials has been incorporated in the ionic strength abstraction for commercial SNF waste packages under liquid influx conditions (SNL 2007h, Section 6.10.2.1[a]). Moreover, additional uncertainty has been introduced into the ionic strength abstraction by extrapolations (SNL 2007h, Section 8.2.2[a]).

Thus, the impact of instantaneous degradation of commercial SNF on the ionic strength for commercial SNF waste packages under liquid influx conditions is captured in the abstraction, and the ionic strength abstraction is sufficient to cover the condition following the instantaneous degradation of commercial SNF inside a failed waste package.

Representation of Codisposal Fuel—The most numerous codisposal waste package configuration in the repository design contains five DOE HLW glass logs and one DOE SNF canister, split between the CDSP-Long and CDSP-Short configurations. These configurations represent 3,197 codisposal waste packages or 93.6% of the total number of codisposal waste packages. However, the CDSP-MCO configuration (total of 219 waste packages or 6.4% of the total) accounts for 87% of the inventory for the DOE SNF waste (SNL 2008a, Tables 6.3.7-1, 7.5-1, and 7.5-3). That is why the in-package chemistry model simulates the CDSP-MCO waste package. However, for radionuclide transport calculations (e.g., for mass of degradation products), the TSPA model simulates the CDSP-Long waste package containing Three Mile Island SNF canisters (SNL 2007k, Section 6.3.4.6). The major differences between this CDSP-Long waste package and the CDSP-MCO waste package are that: (1) the HLW glass waste-form domain in the TSPA EBS transport submodel contains five HLW glass canisters instead of two, and (2) the DOE SNF waste-form domain contains UO_2 instead of uranium metal.

Effect on the TSPA Model—The parameters that could potentially be impacted by the difference between the EBS transport submodel and the in-package chemistry submodel are pH, ionic strength, and fluoride. The main difference in the conceptual models for the HLW glass waste-form domain would be the total volumes of materials and water, which are 2.5 times larger in the EBS transport submodel (five canisters instead of two). This is important only with respect to the turnover rate (i.e., the inverse of the residence time), which affects ionic strength. For a given liquid influx rate, the turnover rate would be 40% (2/5) of the turnover rate of the CDSP-MCO waste package. A lower turnover rate increases the effects of degradation rates, which in turn affect ionic strength. However, a reduction of 60% in the turnover rate is well within the order-of-magnitude uncertainty of the ionic strength abstraction (SNL 2007h, Section 6.10.8.2[a]). The fluoride abstraction, which is only a function of ionic strength (SNL 2007h, Section 6.10.3[a]), is therefore also negligibly affected. The pH abstraction is not affected at all because it is not a function of turnover rate.

In the DOE SNF waste-form type, the Three Mile Island fuel will quickly degrade to schoepite in the presence of water, similarly to the behavior of N Reactor fuel and commercial SNF. Schoepite will be the dominant alkalinity buffer in the DOE SNF waste form cell in the EBS transport submodel for either codisposal configuration, either CDSP-MCO or CDSP-Long (Section 2.3.7). Equilibrium dissolution of schoepite prevents pH from rising much above 7 at high carbon dioxide fugacity and much above 9 at low carbon dioxide fugacity (SNL 2007h, Sections 6.3.4[a] and 6.10.1[a], Figure 6-43[a]). On the acid side, degradation of the stainless-steel structural materials, which are present regardless of the SNF type, produce oxides that define the pH minimum. Thus, the pH abstractions for N Reactor fuel (CDSP-MCO) can be used for Three Mile Island fuel in the DOE SNF waste-form domain. Ionic strength and fluoride abstractions of the CDSP-Long waste package can also be approximated by the CDSP-MCO abstractions in the DOE SNF waste-form domain because the degradation products are similar and because other potential effects are small compared to the order of magnitude uncertainty of the ionic strength abstraction.

Other important DOE SNF fuel types are mixed-oxide, carbide, and aluminum-based fuels (SNL 2008a, Table 7.5-3). The justification for using the CDSP-MCO fuel chemistry (pH, ionic strength, and fluoride) to represent them is contained in *In-Package Chemistry Abstraction* (SNL 2007h, Section 6.6.6[a]).

2.4.2.3.1.6 Submodel Differences Related to EBS Transport

Water Balance in the TSPA Model Within the EBS—Differences related to the water balance in the EBS fall into two categories, one related to water flow and the other to water volumes.

There are two potential inconsistencies with respect to water flow through various EBS components in the TSPA model: (1) the reduction in water flow due to evaporation and consumption by chemical reactions is not explicitly addressed in most EBS submodels; and (2) the condensation flux calculations are performed separately from the multi-scale thermal-hydrologic model calculations that are used to define the temperature and relative humidity conditions in the EBS. These issues have already been addressed in Sections 2.4.2.3.1.1, 2.4.2.3.1.2, and 2.4.2.3.1.6.

With respect to inconsistencies or differences related to water volume in the EBS, these calculations in the TSPA are primarily based on phenomenological laws for fluid retention in porous media. For example, the saturation and water volume in the invert are calculated based on the soil-moisture retention relationships of crushed tuff, while the saturation of the corrosion products and waste form rind under no-flow conditions are computed as a function of relative humidity based on measured adsorption isotherms. Although most calculations for the saturations (and water volumes) are based on phenomenological laws, some assumptions must be made under certain conditions. These include the assumption of 100% saturation of corrosion products and waste form rind under water-flowing conditions (SNL 2008a, Section 6.3.8.4.1). In addition, some inconsistencies in water volumes exist among process-level models mainly due to the limitation of the models used in the calculations. For example, a minimum water volume is assumed for in-package chemistry calculations. Assuming a minimum water volume keeps the ionic strengths less than 4 molal, the effective limit of the thermodynamic databases and the B-dot activity coefficient equation used in the EQ3/6 computer code. This minimum water volume is independent of the relative humidity and temperature histories as predicted in the multiscale thermal-hydrologic model abstraction and is likely larger than what is expected at low relative humidity conditions.

Chemical processes in the EBS will both consume and produce water. Conversion of commercial SNF to schoepite ($UO_3{:}2H_2O$) and steel to goethite (FeOOH) and other hydrated corrosion products will likely remove large quantities of incoming water. Over time, hydrated phases will alter to less hydrated phases and release water in the process. While water uptake by waste form degradation is expected to be relatively fast, the release of water from dehydration reactions is expected to be slower. The overall uptake and release of water over time is a complex function of water availability, temperature, and time and is difficult to predict accurately. The assumption of no water uptake or release will tend to over-predict the water saturation in a breached waste package.

For diffusion-dominated modeling cases after breach of the outer Alloy 22 waste package barrier, the following assumptions are made in the TSPA model with respect to the water balance inside the waste package: (1) sufficient condensate water is available for waste form degradation and metal alloy (e.g., steel) degradation; and (2) sufficient water vapor is present to establish a continuous film of liquid water on fuel and corroded-metal surfaces under no-flow conditions when relative humidity is greater than 95%, which is thick enough to permit diffusive transport of radionuclides from the waste package either as dissolved species or bound to colloids.

Effect on the TSPA Model—Within the EBS, water balance issues have more of an effect in diffusion-dominated modeling cases, where the limited water availability controls the degree of liquid saturation inside the waste package and, therefore, the radionuclide transport rates through the waste package. In the advection-dominated modeling cases, the water balance related issues are not as important, because sufficient water flows through the waste package to result in a rapid turnover rate with respect to pore volume in the waste package and thus the assumption of complete saturation is reasonable. The overall effect of the previous assumptions regarding the complete saturation inside the waste package under flowing conditions is an overestimate of the rate of release of radionuclides.

With respect to diffusion-dominated cases, the assumption that there is a high-enough vapor flux to instantly saturate the waste-package internals to local equilibrium conditions (which is the assumption underlying the use of an adsorption isotherm) will overestimate the rate of radionuclide releases by ignoring kinetic constraints on waste-form degradation with respect to water availability for reactions and by assuming bulk chemical and bulk diffusion transport conditions (a continuous liquid pathway to the outside of the waste packages).

2.4.2.3.1.7 Submodel Differences Related to Unsaturated Zone Transport

Unsaturated Zone Transport Properties—There are several flow-related parameters used in the site-scale unsaturated zone flow model that are also used in the unsaturated zone transport submodel to describe the diffusion of dissolved radionuclides between the fractures and the rock matrix. Several of these parameters, used in a deterministic manner in the unsaturated zone flow model, are sampled from distributions in the unsaturated zone transport model to describe the uncertainties associated with the fracture/matrix diffusion process. Parameters handled stochastically to describe the fracture/matrix diffusion process but deterministically to generate the flow fields (Section 2.3.2.4.2.2) are fracture porosity, fracture frequency (the inverse of fracture spacing), and the active fracture model parameter γ.

Effect on the TSPA Model—The matrix-diffusion process implemented in the unsaturated zone transport submodel is sensitive to various physical parameters that are also used to define the unsaturated zone flow fields. Because the matrix-diffusion process may be very sensitive to these parameters, it is important to propagate the parameter uncertainties into the unsaturated zone transport submodel. However, as discussed below, the unsaturated zone flow model is not as sensitive to changes in these parameters. Therefore, differences between parameter values used to develop the flow fields and those used to describe the effect of matrix diffusion for a given TSPA realization will have little effect on the TSPA results.

A study presented in *UZ Flow Models and Submodels* (BSC 2004b, Section 6.8.1) indicates that the site-scale unsaturated zone flow model is relatively insensitive to changes in the active fracture model parameter γ. In the steady-state site-scale unsaturated zone flow model, the active fracture model γ influences the partitioning of water flow between the fractures and rock matrix. The conclusion of the study noted that changing the active fracture model γ in the flow model will have only a small effect on matrix liquid saturations, water potentials, and average percolation fluxes. This may also indicate that γ values, estimated based on flow calibrations, may not be well constrained and the application of a greater uncertainty for transport calculations is valid.

The aperture values used in the unsaturated zone transport submodel are generated from fracture porosity and fracture frequency (the inverse of fracture spacing) values. In general, the large permeability contrast between the fractures and rock matrix (SNL 2007b, Appendix B) will dictate that the rock matrix will not contribute much to the flow process (minimizing the influence of fracture spacing on flow), and matrix diffusion will be the dominant process controlling mass retardation in the rock matrix. In addition, fracture porosities are important in defining the transient matrix-diffusion process in the unsaturated zone transport submodel, but as storage terms in the site-scale unsaturated zone flow model, do not influence results of the steady-state model. It should also be noted that fracture permeabilities and the van Genuchten α parameter are related to fracture apertures. A sensitivity study on flow model parameters showed relatively small differences between base-case flow fields and flow fields generated by changing fracture permeabilities and the van Genuchten α parameter (BSC 2005a, Section 6.3). Studies presented in Sections 6.6.3 and 6.6.4 of *Particle Tracking Model and Abstraction of Transport Processes* (SNL 2008e) also showed that transport in the unsaturated zone is generally less sensitive to changes in flow parameters than to changes in the transport properties. The analyses showed that the transport results were insensitive to the van Genuchten α parameter. Transport results showed greater sensitivity to changes in fracture permeability compared to that of the van Genuchten α parameter, but as noted, the changes were relatively small.

It should also be pointed out that even though the values of parameters used to develop the unsaturated zone flow fields do not exactly match the values used to generate the matrix-diffusion parameters, the parameters used to describe both flow and transport are mainly derived from the same data sources (SNL 2008e, Sections 6.5.5.4 of Addendum 1, 6.5.7, and A.4 of Addendum 1; SNL 2007b, Section 6.1.5; SNL 2007l). An exception is the ranges of values of the active fracture model parameter γ as discussed in *Particle Tracking Model and Abstraction of Transport Processes* (SNL 2008e, Section 6.5.6 of Addendum 1).

Unsaturated Zone Mass Release to the Saturated Zone—The unsaturated zone transport submodel utilizes FEHM's multi-species particle tracking option to simulate the advective-dispersive transport of mass releases from the EBS through the unsaturated zone to the water table, which defines the top of the saturated zone. EBS radionuclide releases to the unsaturated zone are generated for five percolation subregions that are classified by specific ranges of percolation rates defined from low to high, so that the five percolation subregions (1, 2, 3, 4, and 5) contain 5%, 25%, 40%, 25% and 5% of the waste packages, respectively. In the unsaturated zone transport particle tracking analysis, radionuclides from the EBS are released at nodes corresponding to the percolation subregions. Each repository node is assigned to one of five corresponding percolation subregions. For each percolation subregion, the mass released from the EBS over each time step, is transported through the unsaturated zone until reaching exit nodes at the water table. The exit nodes are grouped into four collecting bins representing NE, NW, SE and SW zones that are spatially based on the saturated zone source regions defined in *Saturated Zone Flow and Transport Model Abstraction* (SNL 2008f, Section 6.5.2.13 and Figure 6-27). For each time step, all particles reaching the exit nodes in a given quadrant are summed to give the total unsaturated zone mass release rate for that quadrant. This creates four source terms that are applied to the four saturated zone source regions 1 (NW), 2 (NE), 3 (SW), and 4 (SE) (SNL 2008f, Figure 6-27). Saturated zone source regions 1, 3, and part of 2 are located directly below the repository. The other portion of source region 2 and source region 4 are located east of the repository to capture radionuclides that were diverted beyond the footprint of the repository by lateral transport. At each time step, the mass from the four source terms generated for the unsaturated zone collecting bins is applied at four release points in the saturated zone, one for each of the equivalent saturated zone source regions. The use of four release points provides a computationally efficient way to evaluate transport within the saturated zone while maintaining the effects of spatially variant features. To propagate uncertainty through the model, the release point locations for each of the four saturated zone source regions are randomly selected for each realization.

Effect on the TSPA Model—Release of mass from each unsaturated zone collecting bin to a randomly selected location in its equivalent saturated zone source region will focus the mass releases at four locations (one for each saturated zone source region). The use of a point source will overestimate the concentration of the radionuclides near the source (SNL 2008f, Section 6.5.2.13), yet is of little consequence 18 km downgradient because the breakthrough across the compliance boundary is unlikely to be significantly different for a slightly smeared source region beneath the repository compared to the point release used in the saturated zone abstraction model.

2.4.2.3.1.8 Submodel Differences Related to Saturated Zone Flow and Transport

Saturated Zone Release Location—The three-dimensional saturated zone flow and transport abstraction model, which is used to simulate the transport of all parent radionuclides and first-generation decay products, is based on three dimensional simulations that use a random release location beneath the repository within each of the four saturated zone source regions (Section 2.3.9.3.4.1). However, the one-dimensional saturated zone flow and transport abstraction, used for several radioactive decay products farther down in the decay chains (Section 2.4.2.3.2.1.10), is based on a central release location within each of the four source regions. This can result in different transport behavior for isotopes of the same chemical element in a given realization. For example, the saturated zone flow and transport of ^{234}U is simulated with the three dimensional model, whereas the saturated zone flow and transport of ^{233}U is simulated with the one dimensional model. Thus, for certain realizations, where the three dimensional random-release model produces a significantly different transport pathway than the one dimensional central location model, the transport times through the saturated zone for the two radionuclides can be different (Section 2.3.9.3.4.2.2 and SNL 2008a, Section 6.3.10.4.1).

Effect on the TSPA Model—The effect of this difference is minimal because the central release location used in the one-dimensional saturated zone flow and transport abstraction is representative of the average behavior taken over multiple realizations (SNL 2008a, Section 6.3.10.4.1). A comparison of the two saturated zone transport models is presented in *Saturated Zone Flow and Transport Model Abstraction* (SNL 2008f, Section 7.3.2[b]).

2.4.2.3.1.9 Submodel Differences Related to Biosphere Transport and Exposure

Volcanic Tephra Particle Size—The size of resuspended particles used to calculate the inhalation component of the dose to the RMEI is smaller than the particle size in the ASHPLUME code (Section 2.3.11.4.2.2) used to predict atmospheric transport (advection and diffusion) and surface deposition (gravitational settling) of the tephra from a volcanic eruption (SNL 2008a, Section 6.3.11). The inhalation dose is calculated in the biosphere process model by using inhalation dose coefficients for 1 µm particles, while the ASHPLUME model predictions concern particles greater than 15 to 30 µm. This is because of the ASHPLUME model's inability to accurately represent the transport of tephra particles of mean diameter less than approximately 15 µm (Jarzemba et al. 1997, Section 2.1; SNL 2007m, Section 1.3.1). Because the typical mean diameter of tephra particles after an eruption is generally much larger than 15 to 30 µm, the ASHPLUME model is appropriate for calculating the distribution of the majority of the mass of potential tephra and radionuclide releases from a possible future eruption at Yucca Mountain (SNL 2007m, Section 1.3.1). However, ASHPLUME does not accurately model the particles in the respirable (less than 4 µm) and thoracic (less than 10 µm) size range, which are more important for the evaluation of inhalation doses (BSC 2005b, Section 6.5.5.1).

Effect on the TSPA Model—This apparent difference in the particle size distribution of tephra deposited at the location of the RMEI and the particle size distribution used to calculate inhalation dose to the RMEI becomes less significant with time as tephra particles weather and radionuclides diffuse and attach to small soil particles. The processes that cause redistribution of the contaminated tephra after the volcanic eruption, as well as other natural processes and human activities at the location of the RMEI, could change the initial particle size distribution of deposited tephra. For the purpose of calculating the inhalation component of dose in the volcanic eruption modeling case, the size of resuspended particles is assumed to be 1 micron, an inhalable size. A study completed in *Characteristics of the Receptor for the Biosphere Model* (BSC 2005b, Section 6.5.5.2) regarding the effect of differences in particle size on predicted inhalation dose concluded that the application of dose coefficients for particles with activity median aerodynamic diameter of 1 µm will not underestimate the doses from inhalation of resuspended material and that these dose coefficients are adequate for use in the biosphere model.

2.4.2.3.1.10 Submodel Differences Related to Early Waste Package and Drip Shield Failures

No inconsistencies have been identified among model components or submodels in the early failure scenario class, because its effect on the TSPA model is limited to replacing the nominal scenario class conceptual models for drip shield and waste package degradation with the early failure conceptual models. These models are simpler, in the sense that failure mechanisms are not treated in detail and failure is assumed to occur at the beginning of the simulation.

2.4.2.3.1.11 Submodel Differences Related to Igneous Processes

In-Package Chemistry and the Instantaneous Degradation of Commercial SNF—The *In-Package Chemistry Abstraction* (SNL 2007h) does not consider instantaneous degradation of commercial SNF in the range of conditions analyzed with the process model and in the development of the subsequent abstraction. This difference and its effect on the TSPA have been discussed above in Section 2.4.2.3.1.7.

Volcanic Tephra Particle Size—The difference between the atmospheric transport and biosphere transport submodels is the same as mentioned in Section 2.4.2.3.1.9.

2.4.2.3.1.12 Submodel Differences Related to Seismic Processes

Degradation of the Internal Structures After Breach of Outer Corrosion Barrier—In the seismic ground motion modeling case calculations, once the Alloy 22 is breached due to nominal degradation processes or seismic damage, it is assumed that the internal structure of the waste package will instantly degrade as a structural element leading to significant loss of waste package structural strength by the time of the next seismic event (SNL 2008a, Section 6.6). As a result, the damage abstractions for the fully degraded internals are applied after the waste package is breached for the first time. This is a conservative assumption and is inconsistent with the slow degradation of steel internals modeled in the EBS transport model, where the stainless-steel is expected to last for tens of thousands of years on average, thus maintaining the integrity of the waste package for a much longer duration than the time to the next seismic event.

Effect on the TSPA Model—Using the waste package damage abstraction for the fully degraded internals for the first seismic event that occurs after first breach, whether from nominal degradation processes or seismic consequences, is conservative as it would lead to a larger damage area on the waste package due to the lower structural strength of the waste package, and will likely result in a greater diffusive release rate out of the waste package. The slower degradation of the internals used in the EBS transport model results in a slower formation of corrosion products, whose main effect is sorption of radionuclides. This is appropriate because the use of a very rapid steel degradation rate in the EBS transport model (similar to the instantaneous degradation in the seismic model) would be nonconservative, since it would produce a greater mass of sorbing corrosion products at earlier times. (Note that the steel degradation rate used in the EBS transport model is an epistemically uncertain parameter, based on a range of measured rate data.)

2.4.2.3.1.13 Summary

The preceding differences in model conceptualizations and assumptions are the most important examples of those differences between submodels in the TSPA model (SNL 2008a, Sections 6.3 to 6.6). These differences reflect modeling assumptions and simplifications made in different abstractions used as input to TSPA. These differences do not affect the appropriateness of the assumptions for use in TSPA to evaluate postclosure performance.

2.4.2.3.2 TSPA Model and Code Verification, Validation, and Confidence-Building *[NUREG-1804, Section 2.2.1.4.1.3: AC 3(2)]*

Verification and validation for a computer model of a complex physical system involves a series of activities designed to generate and enhance confidence in the model's conceptualization and results during and after model development. The modeling process starts with the modeler's understanding of the physical system. A conceptual model is then formulated based on available information, using some assumptions, simplifications, and idealizations. The conceptual model is translated into a mathematical model and then implemented into a numerical model. An appropriate computer code/software suite is selected or developed to implement the numerical model. The input to the computer code is prepared, and the code is executed to obtain the model output.

Preparation of a validated model for a complex system such as the Yucca Mountain repository is an iterative evolutionary process (Eisenberg et al. 1999) as the FEPs for the system are progressively better understood through testing, analyses, and refinement of the conceptual model, and improvements are made in the computer software needed to implement the numerical model. This TSPA model is a result of such an iterative evolutionary process. Earlier versions of the TSPA model were subjected to independent peer reviews; for example, the TSPA-VA peer review (Budnitz et al. 1999) and the TSPA-SR peer review (OECD and IAEA 2002). The TSPA-SR is the direct precursor to the TSPA-FEIS model (Williams 2001) from which the TSPA model for the license application (the present TSPA) is developed.

The aforementioned international peer review of the TSPA-SR model was jointly organized by the Nuclear Energy Agency of the Organization for Economic Cooperation and Development and the International Atomic Energy Agency of the United Nations. This International Review Team recommended a number of improvements and changes to result in more confidence in and robustness of the TSPA model. A summary of the International Review Team comments and the subsequent work conducted to improve the current TSPA model, as development progressed to the TSPA-FEIS and then to the TSPA model, can be found in *Total System Performance Assessment Model/Analysis for the License Application* (SNL 2008a, Appendix E, Table E-1).

Confidence-building and validation of the TSPA model consisted of a sequence of activities consistent with the requirements contained in *Quality Assurance Requirements and Description* (DOE 2007b, Supplement SIII.2.6). This is part of the overarching requirement in 10 CFR 63.142 describing quality assurance criteria applicable to “all activities that are important to waste isolation.” Two categories of procedural activities were used to develop the TSPA model and ensure that it is valid for its intended use: (1) those conducted during development of the model; and (2) those conducted after development of the model (SNL 2008a, Section 7).

During-Development Model Validation Activities—The major activities (SNL 2008a, Section 7) performed to build confidence in the adequacy of the technical approach used during the model development process include the following (Section 2.4.2.3.2.2):

- Verification of inputs and software (Section 2.4.2.3.2.2.1)
- Model stability testing (Section 2.4.2.3.2.2.2)
- Uncertainty characterization reviews (Section 2.4.2.3.2.2.3)
- Surrogate waste form analyses for DOE and naval SNF (Section 2.4.2.3.2.2.4).

Post-Development Model Validation Activities—The procedurally defined validation level for the TSPA model requires at least two of the post-development model validation activities described in the TSPA model report (SNL 2008a, Section 7). In addition, several additional postdevelopment model validation activities were conducted to enhance confidence in the TSPA model. The postdevelopment activities (Section 2.4.2.3.2.3) include the following:

- Corroboration of abstraction model results with the results of the validated mathematical model or process model from which the abstraction model is derived (Section 2.4.2.3.2.3.1).

- Corroboration of system model results with the results of the validated mathematical model(s) from which the system model is derived, including corroboration with results of auxiliary analyses used to provide additional confidence in the system model results (Section 2.4.2.3.2.3.2). These auxiliary analyses include comparison of the TSPA model results with (1) deterministic analyses of single realizations from various modeling cases (Section 2.4.2.3.2.3.2.1); (2) comparison of the TSPA model results with the Simplified TSPA analysis (Section 2.4.2.3.2.3.2.2); (3) comparison of the TSPA model results with the TSPA results produced by the Electric Power Research Institute (EPRI) using its independently developed model and software, IMARC (Section 2.4.2.3.2.3.2.3); and (4) the results of the PMA providing objective evidence for assessing performance margin and an estimate of the degree of conservatism in the TSPA model (Section 2.4.2.3.2.3.2.4).

- Comparison of the relevant portions of the TSPA model with appropriate analogue information. Such comparisons include: (1) quantitative comparisons of the TSPA model components with analogous volcanic eruptive conditions (Cerro Negro), and (2) a detailed qualitative description of the groundwater flow and transport of radionuclides from a natural system (Peña Blanca) analogous to Yucca Mountain (Section 2.4.2.3.2.3.3).

- Summary of past technical reviews of the TSPA model, including addressing and implementing the comments and recommendations of these review panels (Section 2.4.2.3.2.3.4).

Successful completion of all of the model verification and validation activities described in Section 7.0 of the TSPA model report (SNL 2008a) demonstrates that the “TSPA code provides a credible representation of repository performance” per Acceptance Criterion 3 of NUREG-1804, Section 2.2.1.4.1.3.

The analyses carried out for the verification and validation of the TSPA model are listed in Table 2.4-8 (SNL 2008a, Table 7.1-1[a]). Table 2.4-8 shows the category/subcategory of each model activity (analysis or set of analyses), the purpose of the activity, a brief description of the activity, and the section where the detailed discussion of the results is found. Summaries of the results of each of the analyses in Table 2.4-8 are given below in the subsections of Section 2.4.2.3.2.

NUREG-1804, Section 2.2.1.4.1.3, Acceptance Criterion 3(2) contains an expectation that "The transfer of data between modules of the code is conducted properly..." While this criterion is satisfied by the various validation activities outlined above, a description of how information is passed between submodels of the TSPA model, discussed in Section 2.4.2.3.2.1, provides additional support. Furthermore, in order to discuss the transfer of data and information among the various TSPA model components and submodels, it is also necessary to provide a description of the implementation of these submodels within the TSPA system model. Thus, Section 2.4.2.3.2.1 also provides this context. Following the extensive description of implementation and information flow in Section 2.4.2.3.2.1, Sections 2.4.2.3.2.2 and 2.4.2.3.2.3 summarize the analyses described above that satisfy the procedurally mandated during-development and post-development validation activities.

Finally, as explained in more detail at the end of Section 2.4.2.2.2.1, because of the iterative nature of the TSPA, many of the validation activities described in this section were conducted with an earlier version (v5.000) of the TSPA model than the version (v5.005) used to produce the final annual dose curves presented in Section 2.4.2.2.1 above. For example, the numerical stability analyses were based on v5.000 (Section 2.4.2.2.2.1), as were most of the verification analyses described in Section 2.4.2.3.2.2.1. Each validation activity for TSPA model v5.000 was reviewed to determine which activities were affected by changes made between TSPA model v5.000 and v5.005. Where validation activities could potentially be affected by model changes, these validation activities were repeated using v5.005 to verify that model changes did not adversely affect the overall validation of the TSPA model (SNL 2008a, Sections 7[a] and 7.3.1.5[a]). Based on the types of changes from v5.000 to v5.005, the combined validation activities for v5.000 and v5.005 are sufficient to show validation and confidence in v5.005, the version used to provide the annual dose curves in Section 2.4.2.2.1. The difference in the calculated dose between the two models is shown in Figure 2.4-111.

2.4.2.3.2.1 TSPA Model Integration and Transfer of Data Between Modules of the TSPA Code

This section provides an overview of how model components and submodels are connected within the TSPA model and how information flows between them. In order to assess compliance with the performance objectives of 10 CFR 63.113, the TSPA model integrates the individual FEPs that are included in the models and parameters presented in Section 2.3. The TSPA model structure then couples these models and parameters for the evaluation of repository performance (SNL 2008a, Section 6.1.4). The major model components in the TSPA model are listed in Table 2.4-1 and shown in Figures 2.4-1 to 2.4-7. The model components provide complete coverage of the relevant included FEPs shown in the FEP inclusion tables in Section 2.3 (e.g., Table 2.3.1-1). As noted in Section 2.2.1, the individual included FEPs can affect multiple components of the repository system and can be included in multiple models or parameters. This will become apparent in the discussion of information flow between submodels in this section.

The primary focus of this section is the description of the TSPA model for the nominal scenario class. The nominal scenario class reflects the initial starting conditions expected for the proposed repository system and therefore is a natural starting point for presenting the model structure and design. A summary of event-driven differences in the TSPA model structure and information flow for the early failure, igneous, and seismic scenario classes is presented in Section 2.4.2.3.2.1.12 following the nominal scenario class description. For all scenario classes, the separation of aleatory and epistemic uncertainty with respect to parameter values is maintained as described in Sections 2.4.1 and 2.4.2.1.1. The structure of the model components and submodels reflect this separation.

The TSPA model components and submodels for the following process areas are briefly discussed here and in much more detail in Section 2.3:

- Unsaturated zone flow
- EBS thermal-hydrologic environment
- Drift-scale seepage and in-drift condensation
- EBS chemical environment
- Waste package and drip shield degradation
- EBS flow
- Waste form degradation and mobilization
- EBS transport
- Unsaturated zone transport
- Saturated zone flow and transport
- Biosphere.

This list corresponds to model components and submodels previously presented on Figure 2.4-2 and in Table 2.4-1. This list is a combination of model components and submodels that represent the order in which these TSPA model components are discussed in the *Total System Performance Assessment Model/Analysis for the License Application* (SNL 2008a, Section 6.3). The intent is to list the models in the order that information flows within the TSPA model. Therefore, it is necessary to list the submodels of the EBS environment and EBS flow and transport model components separately. For example, as described below, the EBS flow submodel provides the waste form degradation and mobilization model component with the flow rate of water through a failed waste package as a function of time. This information is used by the waste form degradation and mobilization model component to calculate in-package chemical conditions and radionuclide concentrations in waste packages. This information in turn is used as input to the EBS radionuclide transport submodel that calculates radionuclide transport through the waste package and EBS. Thus, following the flow of information in the TSPA model requires an expansion of the eight principal model components compared to what is displayed on Figure 2.4-1. Table 2.4-1 maps the outline of Section 2.3 to the eight principal TSPA model components and associated submodels depicted on in Figure 2.4-2.

Figure 2.4-112 schematically depicts the flow of information between the TSPA model components and submodels for the nominal scenario class. TSPA model components implemented outside of the GoldSim model file are shown outside of the dashed border on Figure 2.4-112. The abstraction information provided by external models is input to the GoldSim model file. Information transferred via internally generated outputs used as downstream inputs between model components and submodels within the GoldSim model file is shown within the dashed border on Figure 2.4-112. The primary output from each submodel and abstraction is denoted by a numerical index (Outputs 1 to 20) and described in Sections 2.4.2.3.2.1.1 to 2.4.2.3.2.1.12. A more detailed representation of information flow within the TSPA model can be found in Appendix G of *Total System Performance Assessment Model/Analysis for the License Application* (SNL 2008a).

Although this section describes what type of information is passed from one submodel to another, it only summarizes how the passed information is used in the downstream submodel. More detailed descriptions regarding how the information is used in the submodels can be found in Section 6.3 of *Total System Performance Assessment Model/Analysis for the License Application* (SNL 2008a).

2.4.2.3.2.1.1 Unsaturated Zone Flow

The first process model providing key input to the TSPA model is the three-dimensional, dual-permeability, site-scale unsaturated zone flow model. Unsaturated zone flow in the TSPA model refers to the percolation of groundwater through the unsaturated rocks between the land surface and the groundwater table and includes the site-scale unsaturated zone flow, infiltration changes, and future climates states. The unsaturated zone flow model abstraction is comprised of 16 steady-state flow fields generated by the three-dimensional site-scale unsaturated zone flow model (SNL 2007b, Section 6.6). The sixteen flow fields consist of four flow fields representing uncertainty for each of three climates and for deep percolation flux specified by proposed 10 CFR 63.342(c)(2) for the post-10,000 year period. The climates used in the TSPA model are the present-day, monsoon, and glacial-transition. As described in Section 2.3.2.5.2, for the first 10,000-year period after closure (the present-day, monsoon, and glacial-transition climate states), 12 flow fields are generated using the three-dimensional, site-scale model with input parameters based on unsaturated zone calibrated properties. These flow fields are developed from spatially varying net infiltration maps generated for each of the three climate states (present-day, monsoon, and glacial-transition) described in Section 2.3.1.3.3.1.2. For the post-10,000-year period, proposed 10 CFR 63.342(c)(2) specifies that the average deep percolation rate through the repository is to be based on a log-uniform probability distribution from 13 to 64 mm/yr. The four flow fields representing uncertainty for the post-10,000-year period are developed to spatially distribute water flux while matching the specified average percolation rates. This is accomplished by using infiltration maps implemented for the pre-10,000-year period and scaling the infiltration rates such that the target values for the average infiltration rate averaged over the repository footprint matches the selected average percolation flux rates in the repository footprint taken from the log-uniform distribution.

Net infiltration rates at Yucca Mountain were estimated for the first 10,000 year period after closure through studies of present and future climates and through studies of processes and parameters that control and affect precipitation and infiltration over a range of uncertain conditions (Section 2.3.1) (SNL 2008g). Based on these studies, a total of 12 net infiltration maps were developed. They include four maps each for the present-day, monsoon, and glacial transition climate states. For each of the first three climate states, the four representative uncertainty cases used in the unsaturated zone flow model were selected from an initial set of 40 infiltration uncertainty maps. These maps were generated using the infiltration model MASSIF (SNL 2008g, Section 6.5) described in Section 2.3.1.3 (SNL 2008a, Section 6.3.1.2), in conjunction with Latin hypercube sampling (2 replicates of 20 realizations each) of climate data and values of parameters that control the processes of precipitation and infiltration. The four representative infiltration maps for each climate used in the development of the associated unsaturated zone flow model flow fields are the 10th, 30th, 50th, and 90th percentile realization outputs of the Latin hypercube sampling analysis. The percentile position is based on the spatially averaged mean annual net infiltration for each realization.

In the development of the infiltration maps, only climate, shallow soil layer, and near surface rock information were considered. Data from the deep unsaturated zone were used to indicate which infiltration scenario generates a flow field that best fits observed data not used in the calibration efforts, and by doing so help derive appropriate weighting factors for sampling the uncertain flow fields. Chloride and temperature data from the Yucca Mountain site unsaturated zone are especially amenable for this purpose (SNL 2007b, Section 6.8.3). The final probabilities associated with these flow fields have been determined by calibrating the flow fields to the subsurface chloride and temperature data as described in Section 2.3.2.4.1.2.4.5. The calibration yielded probabilities of approximately 0.6191, 0.1568, 0.1645, and 0.0596 for flow fields based on the 10th, 30th, 50th, and 90th percentile realizations of the infiltration model; thus the unsaturated zone flow fields are taken to be representative of the 31st (0.5 * 0.6191), 70th (0.6191 + 0.5 * 0.1568), 86th (0.6191 + 0.1568 + 0.5 * 0.1645), and 97th (0.619 + 0.157 + 0.165 + 0.5 * 0.0596) percentiles of the uncertainty in unsaturated zone flow, and are characterized by the infiltration maps used to define the upper boundary condition of the unsaturated zone flow model.

The unsaturated zone process model simulates three-dimensional, dual-permeability, steady-state flow conditions, and generates 12 three-dimensional flow fields representing the 10th percentile, 30th percentile, 50th percentile, and 90th percentile infiltration boundary-condition scenarios within three different climate states for the 10,000-year period after repository closure. Applying the maximum climate duration from the climate analysis (BSC 2004c, Table 6-1), the three climate states used in the TSPA model for the first 10,000 years after permanent repository closure are: (1) present-day climate for the first 600 years after waste emplacement; (2) monsoon climate for the 600 to 2,000 years after waste emplacement; and (3) glacial-transition climate for the period 2,000 years after waste emplacement to 10,000 years after closure (SNL 2008a, Section 6.3.1.2).

As specified in proposed 10 CFR 63.342(c)(2), prescribed deep percolation rates are used to represent flow fields for the timeframe from 10,000 years to 1,000,000 years after repository closure. These percolation rates are specified by NRC as constant spatially averaged values for the deep percolation rates at the repository horizon, sampled log-uniformly between 13 and 64 mm/yr. In order to correlate the pre-10,000-year infiltration uncertainty, represented by the four infiltration scenarios (10th, 30th, 50th, and 90th) with the NRC-specified uncertainty distribution for post-10,000-year calculations, four additional flow fields are generated for the period after 10,000 years. To define the four additional flow fields, four target values for average percolation fluxes through the repository footprint were chosen from the NRC prescribed distribution. For consistency with the uncertainty associated with the four flow fields representing each of the first three climate states, the target values were chosen based on the weighting functions, 0.6191, 0.1568, 0.1645, and 0.0596 (Section 2.3.2.4.1.2.4.5.5) derived for the first three climate states. The weighting functions were used to define four probability bins for the post 10,000 year flow fields. The 31st, 70th, 86th and 97th percentile values of the NRC defined log-uniform distribution of percolation fluxes (21.29, 39.52, 51.05, and 61.03 mm/yr), which are the midpoints of the probability bins, were then selected as the target values (SNL 2008a, Section 6.3.1.2). The 12 infiltration maps generated for the present-day, monsoon, and glacial transition climate states were used as the basis for developing infiltration maps for the post-10,000-year period. Starting with the 12 infiltration maps, the average infiltration through the repository footprint at the upper boundary of the unsaturated zone was calculated for each map. The four infiltration maps, with average infiltration rates through the repository footprint, that most closely matched chosen average target percolation rates were then used as a basis for defining the spatial variability of the infiltration maps used to generate the four additional flow-fields. As determined by the analysis, the infiltration rate maps that most closely matched the four target values of the deep percolation flux for the post-10,000-year period were the present-day 90th percentile, the 50th percentile glacial transition, the 90th percentile glacial transition, and the 90th percentile monsoon. The four infiltration maps were then scaled so that the average infiltration through the repository footprint would match the target values (Section 2.3.2.4.1.2.4.2). Note that the average percolation fluxes (within the repository footprint) at the repository are very close to the average infiltration rates (within the repository footprint) at the unsaturated zone upper boundary, which allows scaling the infiltration maps to be used to meet the NRC criterion specified in proposed 10 CFR 63.342(c)(2). The resulting water fluxes at the ground surface over the unsaturated zone model domain, as well as through the repository footprint for the post-10,000-year period, are shown in Table 2.3.2-15.

The 16 flow fields and unsaturated zone hydrologic properties generated by the site-scale unsaturated zone flow process model are used by the multiscale thermohydrologic process model (Section 2.3.5.4.1.2.1) (SNL 2008d, Sections 6 and 8) for the development of EBS environment thermal-hydrologic conditions and are accessed directly by the unsaturated zone transport submodel (SNL 2008e, Sections 6 and 8). Climate change is implemented within the TSPA model unsaturated zone calculations by assuming step changes in boundary conditions for unsaturated zone flow and utilizing the flow field corresponding to the selected infiltration scenario and climate state. This implementation is based on the assumption that changes in flow fields due to climate state apply instantaneously in the multiscale thermal-hydrologic model and unsaturated zone transport model component (SNL 2008a, Section 6.3.1.3). These unsaturated zone flow fields are used as a boundary condition to specify the percolation flux in the multiscale thermal-hydrologic model, consisting of liquid flux in fracture and matrix continua at the base of the PTn above the repository horizon.

The description for output #1, discussed below, pertains to arrow #1 on Figure 2.4-112. Note that output #1 feeds multiple submodels (i.e., both the multiscale thermal-hydrologic model and the unsaturated zone transport model).

Output 1 (Unsaturated Zone Flow—Multiscale Thermal-Hydrologic Model and EBS Thermal-Hydrologic Coupling)—For each infiltration scenario and climate state, the following are outputs from the site-scale unsaturated zone flow process model (SNL 2007b). These outputs are passed to the multiscale thermal-hydrologic model process models:

- The three-dimensional numerical grid
- The percolation flux at the base of PTn units above each subdomain location for each infiltration scenario and climate period
- Unsaturated zone hydrologic properties.

Output 1 (Unsaturated Zone Flow—Unsaturated Zone Transport Coupling)—The 16 flow fields generated by the site-scale unsaturated zone flow model are input to the TSPA database to be read by the unsaturated zone transport submodel. These files contain values for fracture and matrix liquid flux and liquid flux between fracture and matrix, along with liquid saturation, that are accessed by the unsaturated zone transport submodel during TSPA model simulations.

For each infiltration scenario and climate state, the following output is passed to the unsaturated zone transport model implemented within TSPA (Figure 2.4-112):

- The three-dimensional numerical grid representing the model domain
- Three three-dimensional steady-state flow fields including:
  - Fracture continuum liquid flux
  - Matrix continuum liquid flux
  - Water table levels
- Fracture continuum liquid saturation
- Matrix continuum liquid saturation
- Liquid flux between matrix and fracture continua.

The specification and use of the 16 flow fields, numerical grid, and percolation flux ensures that the physical phenomena, assumptions, and couplings between climate, infiltration, unsaturated zone flow, EBS thermal-hydrologic environment, and unsaturated zone transport are consistently implemented in the TSPA model.

2.4.2.3.2.1.2 Engineered Barrier System Thermal-Hydrologic Environment

The EBS thermal-hydrologic environment submodel implements the multiscale thermal-hydrologic model and abstraction (SNL 2008d, Section 6.2[a] and Appendix III[a]) in the TSPA model (SNL 2008a, Section 6.1.4.2), as shown on Figure 2.4-112. A summary of the development of the multiscale thermal-hydrologic model abstraction can be found in Section 2.3.5.4. The multiscale thermal-hydrologic model incorporates important design features, such as the thermal loading strategy, repository footprint, physical layout within the drift, and the EBS design, and materials. This model also includes integrated inputs from the climate and infiltration models described in Section 2.3.1 and the unsaturated zone flow model described in Section 2.3.2. The following paragraphs describe its application for the development of the EBS thermal-hydrologic abstraction and how this abstraction is used in the TSPA model.

The EBS thermal-hydrologic environment abstraction is based on two-dimensional, drift-scale, dual-permeability thermal-hydrologic models combined with one-, two-, and three-dimensional, thermal-conduction-only models at the drift- and mountain-scale. The multiscale thermal-hydrologic model combines these thermal-hydrologic and thermal-conduction-only models in a methodology that incorporates thermal interactions between waste packages, between waste packages and other EBS components, and between the EBS and the surrounding hydrogeologic environment at the repository scale, as described in Section 2.3.5.4.1. The multiscale thermal-hydrologic model abstraction results describe heat-related responses within and among the component parts of the emplacement drifts, including the effects of repository-scale heat transfer to the surrounding environment.

The multiscale thermal-hydrologic model simulates two categories of waste packages (Section 2.3.5.4): commercial SNF waste packages containing SNF from pressurized water reactors (PWRs) or boiling water reactors (BWRs), and codisposal waste packages that contain defense HLW and DOE SNF (SNL 2008d, Table 6.2-6[a]). Each waste fuel type has a different rate of heat generation over time. To develop the time histories of heat generated by the waste in the repository, the multiscale thermal-hydrologic model considers a nominal waste package sequence consisting of six commercial SNF waste packages and two codisposal waste packages producing results for eight distinct, local heating conditions for each repository subdomain.

The multiscale thermal-hydrologic process model accounts for the following natural and engineered system features:

- Repository-scale variability of percolation flux
- Temporal variability of percolation flux, as influenced by climate change
- Uncertainty in percolation flux addressed by the 10th, 30th, 50th, and 90th percentile infiltration scenarios
- Uncertainty in thermal properties of the repository host rock using mean, high, and low values of thermal conductivity
- Variation in thermal properties between stratigraphic units in and around the repository
- Repository-scale variability of overburden thickness
- Edge cooling effect relative to the repository footprint
- Repository design features including waste packages, drip shields, invert dimensions, invert material properties, drift spacing, waste package spacing, and duration of preclosure ventilation
- Waste package-to-waste package variability in heat generation rate
- Time- and distance-dependent heat removal efficiency of preclosure drift ventilation.

The effects of climate change and the resulting infiltration due to precipitation are included by changing the percolation flux boundary condition at the base of the PTn at prescribed times during the simulations. Including the preclosure ventilation period, the climate changes implemented in the multiscale thermal-hydrologic model are consistent with the climate changes discussed in Section 2.4.2.3.2.1.1. A 50-year preclosure period with drift ventilation is included at the beginning of the multiscale thermal-hydrologic model analyses and is accounted for in the input to the TSPA model (SNL 2008d, Sections 5.2.3 and 6.1.4, Table 4.1-1). However, because the TSPA model analyzes postclosure performance, the TSPA model uses the abstraction results starting at the time of closure at the end of the ventilation period in 2117 (SNL 2008a, Section 6.3.7.1.1 and Table 6.3.7-4a). The assumption is made that the entire waste package inventory of the repository is emplaced at the same time (in 2067, approximately 50 years after the start of waste emplacement). The 50-year preclosure ventilation period is the minimum time that any waste package location in the repository will experience ventilation (SNL 2008d, Section 5.2.3). Climate-induced changes to water table elevation are not included in the thermal-hydrologic submodels of the TSPA model because the elevation of the water table is not expected to have an impact on the computed in-drift environments (SNL 2008d, Section 5.1.5).

The multiscale thermal-hydrologic model accounts for the epistemic uncertainty in percolation flux and host-rock thermal conductivity on the thermal-hydrologic environment conditions, using simulations conducted for the 10th, 30th, 50th, and 90th infiltration scenarios in combination with the low, mean, and high values of the host-rock thermal conductivity, using the suite of 16 flow fields described above, which represent the four climate states for each of the four infiltration scenarios. (Note that the fourth “climate state,” which begins at 10,000 years after permanent closure, is represented by the percolation flux distribution specified in proposed 10 CFR 63.342(c)(2) for the post-10,000 year period.). As described in Section 2.3.5.4.1, only seven of the possible 12 combinations of percolation flux (at the base of the PTn) and host-rock thermal conductivity are actually simulated (SNL 2008a, Sections 6.1.4.2 and 6.3.2.2). Four of the seven cases involve the four percolation flux or infiltration scenarios combined with the mean host-rock thermal conductivity, while an additional three cases are used in conjunction with these four mean host-rock thermal conductivity cases to capture the impact of uncertainty in host-rock thermal conductivity: 10th percentile infiltration scenario with low- and high-thermal conductivity, and 90th percentile infiltration scenario with high-thermal conductivity. The thermal-hydrologic data sets associated with the remaining five of the 12 possible combinations of percolation flux and host-rock thermal conductivity are provided to the TSPA model by using one or more of the previously identified seven cases as surrogates. During TSPA model simulations, these five cases use their associated values of percolation flux, but refer to one of the other seven cases for their thermal-hydrologic data (SNL 2008d, Section 6.3.15[a]). The three analyzed thermal conductivities were assigned probability-weighting factors of 0.29, 0.37, and 0.34 for the low, mean, and high host-rock thermal conductivities, respectively (SNL 2008a, Section 6.3.2.2). Also, the infiltration submodel uses weightings of 0.6191, 0.1568, 0.1645, and 0.0596 for the 10th, 30th, 50th, and 90th percentile infiltration scenarios, respectively (SNL 2008a, Table 6.3.1-2). The combination of the four probability weightings for infiltration scenario uncertainty and the three probability weightings for host-rock thermal conductivity uncertainty are used to determine the aggregate probability weightings for the 12 multiscale thermal-hydrologic model data sets provided as input to the TSPA model (SNL 2008a, Table 6.3.2-3).

The multiscale thermal-hydrologic model subdivides the repository footprint into 3,264 equal area subdomains (SNL 2008d, Section 6.2.12[a]). Each of these subdomains is equally sized in area, 81-m wide by 20-m long, where the length component is along the waste emplacement drift axis (SNL 2008d, Section 6.2.12.1[a]). For each of the four infiltration/thermal conductivity scenarios, the multiscale thermal-hydrologic model calculates time-dependent thermal-hydrologic variables, temperature, and relative humidity for six representative commercial SNF waste packages, and two representative codisposal waste packages at each subdomain location. In addition, the multiscale thermal-hydrologic model calculates time-dependent values for average drift-wall temperature, duration of boiling at the drift wall, invert temperature, invert saturation, and invert liquid flux at each of the 3,264 subdomain locations.

Before any information is passed to downstream submodels, two sets of analyses are performed. In the first analysis, the 10th percentile, glacial-transition values of percolation flux at each of the subdomain locations are used to group each of the locations into one of five repository percolation subregions, based on percolation flux at the base of the PTn (SNL 2008a, Section 6.3.2.2.1). The second analysis involves determining a single representative commercial SNF waste package and a single representative codisposal waste package for each percolation subregion (SNL 2008a, Section 6.3.2.2.2). Representative waste packages are selected for each percolation subregion to represent the spatial variability in repository conditions that control radionuclide release from the repository (SNL 2008a, Section 6.3.2.2.1). The determination of the repository subregions and the selection of the representative waste packages are summarized as follows.

The values of percolation flux for each subdomain location were sorted in ascending order to form a cumulative distribution function and then grouped together based on the five percolation subregion quantile ranges of 0.0 to 0.05, 0.05 to 0.3, 0.3 to 0.7, 0.7 to 0.95, and 0.95 to 1.0 (SNL 2008a, Section 6.3.2.2.1). The multiscale thermal-hydrologic model subdomain locations and associated thermal-hydrologic information corresponding to the percolation values in each of these quantile groups are designated as belonging to repository percolation subregions 1 through 5, respectively. The five repository percolation subregions are shown on Figure 2.4-113. Analyses have shown that it is appropriate to use the subregion grouping based on the 10th-percentile infiltration scenario, glacial-transition climate percolation conditions for all infiltration conditions and climate states (SNL 2008a, Section 6.3.9.3).

As mentioned above, the multiscale thermal-hydrologic model abstraction produces two sets of outputs that are indexed by fuel type and percolation subregion. One set contains the comprehensive multiscale thermal-hydrologic model output (e.g., waste package temperature and relative humidity, drift-wall temperature, percolation flux, and fraction of lithophysal unit) for each of eight possible waste package/drip shield combinations at each subdomain location in each percolation subregion for each fuel type. The waste package and drip shield degradation model component and the drift seepage submodel each use this information. As described in Section 2.3.5.4.1.3.1, for the comprehensive set of multiscale thermal-hydrologic model outputs, the discrete-heat-source, drift-scale, thermal-conduction-radiation (DDT) submodel of the multiscale thermal-hydrologic model actually calculates thermal histories for six full waste packages and two half waste packages. The TSPA abstraction of this for waste package corrosion processes uses the temperature and relative humidity histories from the complete set of six full and two half packages at each subdomain location (SNL 2008a, Section 6.1.4.5).

The other set, or "representative" set, contains the waste package temperature and relative humidity; the drift-wall temperature; and the invert temperature, relative humidity, liquid flux, and saturation only for the "representative" commercial SNF waste package and codisposal waste package in each percolation subregion. These representative waste packages provide the thermal-hydrologic conditions for a representative group of waste packages in the TSPA model. For example, based on the aforementioned quantiles, Percolation Subregion 3 represents 40% of the emplaced waste packages, Percolation Subregions 1 and 5 represent 5% each of the emplaced waste packages, and

Percolation Subregions 2 and 4 represent 25% each of the emplaced waste packages. Thus, of the total of 8,213 commercial SNF packages in the TSPA model (SNL 2008a, Table 6.3.7-1), 3,285 would be in Percolation Subregion 3 and would be characterized by the associated representative thermal-hydrologic curves from the multiscale thermal-hydrologic model abstraction. Similarly, of the total of 3,416 codisposal packages in the TSPA model (SNL 2008a, Table 6.3.7-1), 1,366 would be in Percolation Subregion 3 and would be characterized by the associated representative thermal-hydrologic curves from the multiscale thermal-hydrologic model abstraction.

The representative commercial SNF waste packages and codisposal waste packages in each percolation subregion are selected by analyzing the peak waste package temperature and duration of boiling at the waste package for each waste package of a given type within a percolation subregion. Each representative waste package is the one whose simulated peak waste package temperature and drift-wall boiling period is closest to the calculated median value for peak waste package temperature and the median boiling period duration in the selected percolation subregion, as described in *Multiscale Thermohydrologic Model* (SNL 2008d, Appendix VIII[a]). After this process is completed, temperature and relative humidity for each representative waste package and associated drip shield, average drift-wall temperature, average invert temperature, average invert saturation, and average invert flux are stored in a file set that is directly accessible by the TSPA model. The data in this file set are accessed by the EBS thermal-hydrologic environment submodel to provide representative thermal-hydrologic responses for each subregion. These thermal-hydrologic responses serve as input to the drift wall condensation submodel, the EBS chemical environment submodel, the EBS flow submodel, the waste form degradation and mobilization model component, and the EBS transport submodel. For ease of presentation, the waste package and drip shield degradation model component and the waste form degradation and mobilization model component are shown in Figure 2.4-112 rather than the individual submodels that comprise these model components (Table 2.4-1).

As noted in Section 2.3.2.4, the ambient percolation flux distribution above the repository horizon is unaffected by mountain-scale repository thermal-hydrologic effects until it reaches the boiling condensation zones surrounding the emplacement drifts. Between the base of the PTn unsaturated zone layer and the repository horizon, ambient percolation flux is generally vertically downward with no lateral diversion caused by layering or heterogeneity in the hydrologic units. Therefore, the repository-scale percolation flux distribution at the repository horizon is assumed to be the same as the percolation flux distribution between the base of the PTn and the top of the Topopah Spring welded tuff (TSw) (SNL 2008d, Section 5.1.2).

As described in Sections 2.4.2.3.2.1.3 and 2.4.2.3.2.1.6, in addition to being discretized according to percolation subregion, representative waste package groups in the TSPA model are further subdivided into no-seeping and seeping environments. However, the thermal-hydrologic conditions for each representative waste package are identical for seeping and nonseeping environments (SNL 2008a, Section 6.3.2.3[a]). The 10 representative thermal hydrologic histories applied to the waste packages groups in the TSPA model closely matched the median history of a large group of waste packages that, as modeled, included the effects of percolation, dry out, and rewetting of the host rock above the repository. As such, the thermal hydrologic history is expected to be representative of a waste package whether it is exposed to seepage or not (SNL 2008d, Section 6.2.12.1[a]).

Following is the output from the multiscale thermal-hydrologic process model to the EBS thermal-hydrologic environment submodel:

Output 2 (Multiscale Thermal-Hydrologic Process Model—EBS Thermal-Hydrologic Submodel Coupling)—The following outputs are passed from the multiscale thermal-hydrologic model described in Section 2.3.5.4 through the multiscale thermal-hydrologic model abstraction to the EBS thermal-hydrologic environment submodel (Figure 2.4-112):

- Definition of the five repository percolation subregions
- Percolation flux at the base of the PTn
- In-drift thermal-hydrologic environment (e.g., waste package temperature and relative humidity, drift-wall temperature for each fuel type, commercial SNF, and codisposal waste package).

Following are the various outputs from the EBS thermal-hydrologic environment submodel to other TSPA submodels.

Output 3 (EBS Thermal-Hydrologic—Drift Seepage and Drift-Wall Condensation Coupling)—The following outputs are passed from the EBS thermal-hydrologic environment submodel to the drift seepage and drift wall condensation submodel for each of the five percolation subregions (Figure 2.4-113):

- The percolation flux at the base of the PTn for each infiltration scenario and climate state at each subdomain location (drift seepage submodel)
- The average percolation flux at the base of the PTn for each infiltration scenario and climate state, averaged over the percolation subregion (drift wall condensation submodel)
- The drift-wall temperature surrounding each of the eight waste packages (two codisposal waste packages and six commercial SNF waste packages) at each subdomain location in each percolation subregion (drift seepage submodel)
- Time-dependent temperature for the drift wall and the waste package for the representative codisposal waste package and the representative commercial SNF waste package, including the time that these temperatures drop to 96°C (drift wall condensation submodel)
- The fraction of lithophysal unit at each location.

Output 4 (EBS Thermal-Hydrologic—Waste Package and Drip Shield Degradation Coupling)—The following outputs are passed from the EBS thermal-hydrologic environment submodel to the waste package and drip shield degradation model component, which then calculates waste package and drip shield failures for each of the five percolation subregions. Drip shield temperatures and relative humidities produced by the multiscale model are not needed in the TSPA model because degradation of the drip shield is not dependent on temperature or relative humidity (Section 2.3.6):

- Time-dependent waste package surface temperature on each of the eight waste packages (two codisposal waste packages and six commercial SNF waste packages) at each subdomain location in each percolation subregion
- Time-dependent waste package surface relative humidity on each of the eight waste packages (two codisposal waste packages and six commercial SNF waste packages) at each subdomain location in each percolation subregion.

The following outputs are passed from the EBS thermal-hydrologic environment submodel to the localized corrosion initiation analysis, although this arrow is not specifically shown on Figure 2.4-112 (the model is discussed in Section 2.3.6.4 and results of the analysis are described below in Section 2.4.2.3.2.1.5):

- Time-dependent waste package surface temperature on each of the eight waste packages (two codisposal waste packages and six commercial SNF waste packages) at each subdomain location in each percolation subregion
- Time-dependent waste package surface relative humidity on each of the eight waste packages (two codisposal waste packages and six commercial SNF waste packages) at each subdomain location in each percolation subregion.

Thermal-hydrologic conditions on the waste package and drip shield surfaces are not provided to the EBS chemical environment submodel of the TSPA model because general corrosion, discussed in Section 2.3.6.3.2, and stress corrosion cracking processes, discussed in Section 2.3.6.5, are not chemistry dependent (SNL 2008a, Section 6.3.5.1.2). However, the thermal-hydrologic conditions on the waste package and drip shield surfaces are provided to the EBS chemical environment submodel of the TSPA localized corrosion initiation analysis. Furthermore, although the Alloy 22 localized corrosion abstraction described in Section 2.3.6.4 is part of the TSPA model, there are no modeling cases in which the detailed results of the localized corrosion abstraction result in a dose consequence (SNL 2008a, Section 6.3.5.2.3 and Appendix O). The only modeling case impacted by localized corrosion is the drip shield early failure modeling case, where it is assumed that the waste packages underneath the failed drip shields are failed by localized corrosion (Section 2.4.2.3.2.1.5). Because the occurrence rate is so low for early drip shield failures, this assumption is conservative but only slightly.

Output 5 (EBS Thermal-Hydrologic—EBS Chemical Environment Coupling)—The following outputs are passed from the EBS thermal-hydrologic environment submodel to the EBS chemical environment submodel for each of the five percolation subregions:

- Time-dependent temperature for the invert for the representative codisposal waste package and the representative commercial SNF waste package
- Time-dependent relative humidity for the invert for the representative codisposal waste package and the representative commercial SNF waste package

- Time-dependent temperature for the drift wall for the representative codisposal waste package and the representative commercial SNF waste package
- Averaged glacial-transition percolation rate for each infiltration scenario for each percolation subregion, used to determine the residence time allotted for water-rock interactions.

Output 6 (EBS Thermal-Hydrologic—EBS Flow Coupling)—The following outputs are passed from the EBS thermal-hydrologic environment submodel to the EBS flow submodel for each of the five percolation subregions:

- Time-dependent waste package surface temperature for the representative codisposal waste package and the representative commercial SNF waste package
- Time-dependent invert temperature for the representative codisposal waste package and the representative commercial SNF waste package
- Time-dependent liquid flux for the representative codisposal waste package and the representative commercial SNF waste package.

Output 7 (EBS Thermal-Hydrologic Environment—Waste Form Degradation and Mobilization Coupling)—The following outputs are passed from the EBS thermal-hydrologic environment submodel to the waste form degradation and mobilization model component for each of the five percolation subregions:

- Time-dependent waste package surface temperature for the representative codisposal waste package and the representative commercial SNF waste package
- Time-dependent waste package surface relative humidity for the representative codisposal waste package and the representative commercial SNF waste package.

Output 8 (EBS Thermal-Hydrologic—EBS Transport Coupling)—The following outputs are passed from the EBS thermal-hydrologic environment submodel to the EBS transport submodel for each of the five percolation subregions:

- Time-dependent waste package surface temperature for the representative codisposal waste package and the representative commercial SNF waste package
- Time-dependent waste package surface relative humidity for the representative codisposal waste package and the representative commercial SNF waste package
- Time-dependent temperature in the invert for the representative codisposal waste package and the representative commercial SNF waste package
- Time-dependent saturation in the invert for the representative codisposal waste package and the representative commercial SNF waste package.

The specification and use of the time-dependent output of the EBS thermal-hydrologic submodel, described in the preceding section, ensures that the important heat-driven physical phenomena (e.g., temperature, relative humidity, and saturation) and thermal couplings between drift seepage and condensation, waste package and drip shield degradation, the EBS chemical environment, EBS flow, waste form degradation and mobilization, and EBS transport are consistently implemented in the TSPA model.

2.4.2.3.2.1.3 Drift Seepage and Drift-Wall Condensation

This section describes the information transfer from the drift seepage and drift wall condensation submodels. Drift seepage model development is described in Section 2.3.3 and incorporates relevant information from the climate and infiltration described in Section 2.3.1 and unsaturated zone flow described in Section 2.3.2. Drift wall condensation model development is described in Section 2.3.5.4.2.

Water contacting drip shields and waste packages is expected to originate from two sources: (1) seepage of groundwater from the unsaturated zone above the repository into the emplacement drifts (SNL 2007g, Section 1); and (2) water-vapor condensate dripping from the walls of the drifts (SNL 2007f, Sections 6.3, 8.3, 6[a], and 8[a]). Percolation flux at the base of the PTn is used as the source of water for drift seepage and drift-wall condensation. The TSPA model calculates drift seepage and drift-wall condensation flow rates using the drift seepage submodel and the drift wall condensation submodel, respectively. These two flow rates are combined in the EBS flow submodel (Section 2.4.2.3.2.1.6) to yield a total dripping rate.

Drift Seepage—Drift seepage refers to the flow of liquid water from the unsaturated zone above the repository into waste emplacement drifts. The drift seepage submodel calculates two quantities: (1) the fraction of waste package locations that experience seepage; and (2) the average seepage flow rate for waste package locations that have seepage. The calculations are performed for each fuel type in each percolation flux subregion.

As indicated in Figure 2.4-112, water seepage into emplacement drifts on the scale of a waste package is a process that is modeled outside of the TSPA model, and the results are then abstracted (SNL 2007g) for use in the TSPA model simulations (Sections 2.3.3.2.4, 2.3.3.3.4, and 2.3.3.4). The abstracted results are based on drift-seepage simulations conducted for ambient (BSC 2004d) and thermal periods (BSC 2005c).

The drift seepage abstraction calculations differ for significantly degraded drifts in nonlithophysal units and collapsed drifts in lithophysal units versus intact or moderately degraded drifts in nonlithophysal or lithophysal units (Sections 2.3.3.2.3.4.2, 2.3.3.2.4.2.2, and 2.3.3.3.4). Note that seepage flux is impacted in nonlithophysal zones when a significant level of degradation is attained. This level is defined by a rockfall volume of 0.5 m^3 per meter of waste package length, well below the level of rockfall used to define partial (between 5 and 60 m^3 per meter) or full drift collapse (60 m^3 per meter or greater) in a lithophysal zone. In the nominal scenario class (and in any modeling case prior to drift collapse), moderate drift degradation is assumed, rather than drift collapse, in both lithophysal and nonlithophysal units. This degradation effect is included by increasing the predicted seepage rates for intact drifts by 20% (SNL 2007g, Section 6.7.1.2). However, in the seismic scenario class (Section 2.4.2.3.2.1.12.3), drift collapse eventually occurs in lithophysal units and degradation significant enough to affect the seepage process also occurs in nonlithophysal units. For the seismic ground motion modeling case (Section 2.3.4), partial collapse is considered in the lithophysal units, by comparing the cumulative rubble volume generated by seismic events to a lower and an upper threshold (5 and 60 m^3 per meter, respectively) to determine whether to (1) use the intact drift seepage abstraction, (2) interpolate between intact drift seepage abstraction and collapsed drift seepage abstraction, or (3) use the collapsed drift seepage abstraction (Section 2.3.3) (SNL 2007g, Section 6.2.2[a]). In the nonlithophysal units, once a significant degree of drift degradation has occurred, the intact drift seepage abstraction is no longer appropriate. The cumulative rubble volume generated by seismic events is compared to a threshold rubble volume (0.5 m^3 per meter of waste package length) to determine whether (1) the intact drift seepage abstraction is used or (2) the local percolation flux is used (SNL 2007g, Sections 6.2.3[a]). For the seismic fault displacement modeling case, drift collapse is assumed to occur at the time of the event (SNL 2008a, Section 6.6.1.3.9). Drift collapse is not considered for the igneous scenario class, since the drifts are filled with basalt by the intrusive event (Section 2.3.3.2.1.2).

Analyses performed with the thermal-hydrologic seepage process model for intact drifts have shown that thermal seepage (seepage that is influenced by heat generated by the waste package (Sections 2.3.3.3.1 and 2.3.3.3.4)) will always be less than ambient seepage and that thermal seepage never occurs when water boils in the rock close to the emplacement drifts (BSC 2005c, Section 6.2.4). The intact drift seepage abstraction sets the thermal seepage equal to zero during the period of above-boiling temperatures at the drift wall. The threshold temperature that defines when seepage can occur is set to 100°C (SNL 2007g, Sections 6.5.2.2 and 6.7.1.2). After the temperature falls below 100°C, thermal seepage is set equal to the estimated ambient seepage. For collapsed or significantly degraded drifts, the thermal seepage abstraction sets the seepage equal to the estimated ambient seepage at all times in the postclosure period (Section 2.3.3.3.4). This is based on the results of analyses that found that with the expanded drift opening, the rock temperature at the crown is almost always below 100°C (SNL 2007g, Section 6.4.3.4). Thus there is no vaporization barrier in the intact rock to prevent water flow into a rubble-filled drift (SNL 2007g, Section 6.5.3). Waste-package and drift-wall temperature histories, as well as times when boiling ceases at the drift wall, are discussed in Section 2.3.5.4.1.3.2.

For the igneous intrusion modeling case (Section 2.4.2.3.2.1.12.2), flow diversion associated with capillary effects is not considered (Section 2.3.3.2.4.2), and the abstraction sets the seepage rate equal to the local percolation rate at the base of the PTn multiplied by the footprint area of the considered drift segment (waste package length of 5.1 m times the 5.5-m width of an intact drift (SNL 2008a, Section 6.5.1.1)). This abstraction is applied from the time at which the igneous event occurs.

The drift seepage submodel implements the drift seepage abstraction (SNL 2007g, Section 6.7.1) to determine the fraction of waste packages that are expected to experience seepage and the average seepage rate (m^3/yr per waste package) onto those waste packages that experience seepage (SNL 2008a, Section 6.3.3.1). The results of the drift seepage submodel seepage rate calculations (seepage rate versus time) are passed within the TSPA model in the form of 10 one-dimensional tables, one table for each waste package type (i.e., commercial SNF and codisposal) in each percolation subregion (SNL 2008a, Section 6.3.3.1.3). As indicated below, the EBS flow submodel uses the results for determining seepage rate and the fraction of waste packages that experiences seepage. The drift seepage submodel also calculates the fraction of each percolation subregion that is in nonlithophysal rock. The drift wall condensation submodel uses these results since drift collapse occurs at a different rate in lithophysal and nonlithophysal rock and condensation is assumed not to occur in collapsed drift regions.

The simulated drift-seepage flux is calculated within the TSPA model for the ambient and thermal periods for a range of representative percolation flux rates, and for ranges of fracture permeability log(k) and fracture capillary-strength parameter ($1/\alpha$) values for intact and collapsed drifts (SNL 2008a, Section 6.3.3.1.2). The drift-seepage analysis performed external to the TSPA model provides two response surfaces: (1) mean seepage flux into the drift as a function of long-term percolation flux, k, and $1/\alpha$; and (2) the standard deviation of seepage flux into the drift as a function of long-term percolation flux, log(k), and $1/\alpha$.

The drift seepage submodel and associated software implements spatial variability distributions for k and $1/\alpha$ and the flow focusing factor (f_{ff}) for the percolation flux, as well as epistemic uncertainty distributions for the seepage uncertainty factors, Δlog(k) and $\Delta 1/\alpha$ as described in the drift seepage abstraction (SNL 2007g, Section 6.7.1.1). The following steps are completed at each of the 3,264 multiscale thermal-hydrologic model subdomain locations for each of the six representative commercial SNF waste packages and models two representative codisposal waste packages (Figure 2.3.3-43). The spatial variability distributions are evaluated for log(k), $1/\alpha$, and f_{ff} at each location. The log(k) and $1/\alpha$ values are adjusted by adding to them the uncertainty factors, Δlog(k) and $\Delta 1/\alpha$, sampled from the uncertainty distributions for each realization. For each location, the percolation flux at the base of the PTn, adjusted for climate changes and the sampled infiltration scenario, is provided by the EBS thermal-hydrologic environment submodel. These percolation flux values are then multiplied by the f_{ff} to yield values of the adjusted percolation flux. The adjusted log(k) and $1/\alpha$ values, along with the adjusted percolation flux at each location, are used to evaluate the response functions for ambient mean seepage and the standard deviation of ambient seepage. These two quantities are used to form a uniform distribution for ambient seepage that ranges between mean seepage −1.7321 standard deviations and mean seepage +1.7321 standard deviations (SNL 2007g, Section 6.5.1.3). This distribution is sampled to yield the ambient seepage for each waste package at each location (Sections 2.3.3.2.3.6.4 and 2.3.3.2.4.3).

As noted above, the thermal seepage condition at each waste package location is used to modify the calculated ambient seepage (e.g., for an intact or moderately degraded drift there is no seepage when the drift-wall temperature is greater than 100°C, otherwise there is ambient seepage). This process is completed for each of the 3,264 multiscale thermal-hydrologic model subdomain locations. This results in a calculated drift-seepage flux for every waste package at every subdomain location for the given infiltration scenario and climate state. Then, for each fuel type in each percolation subregion, the average seepage flow rate for waste package locations with seepage is calculated, along with the fraction of waste package locations that have seepage. The coupling between the EBS thermal-hydrologic environment and the drift seepage model in this manner ensures that important design features such as the thermal loading strategy are incorporated into the TSPA implementation of drift seepage.

Drift-Wall Condensation—As described in Section 2.3.5.5.4.2, there is a potential for water vapor in the emplacement drift atmosphere to condense on cooler portions of the drift walls. The rate of condensation at a location on the drift wall depends on the availability of water at that location. The rate at which water is available generally increases with an increase in percolation flux, increasing water transport through the invert, and decreasing axial dispersion within the drifts (SNL 2007f, Section 8.3.1.1). The TSPA drift wall condensation submodel calculates the fraction of waste package locations dripped on by drift-wall condensate and the average rate of condensation in each percolation subregion for each waste package type. These quantities are determined from two correlations: (1) a correlation for average condensation rate versus average percolation flux; and (2) a correlation for the fraction of waste package locations dripped on by drift-wall condensate versus average percolation flux. The average percolation flux for each repository percolation subregion is calculated by averaging the percolation fluxes at the base of the PTn at each subdomain location in that subregion using the comprehensive multiscale thermal-hydrologic model abstraction data (Section 2.3.5.4.1). The impact on drift-wall condensation of epistemic uncertainty in drip shield ventilation and axial dispersion is accounted for by selecting between four cases with an equal probability: (1) ventilated drip shield-low axial dispersion; (2) ventilated drip shield-high axial dispersion; (3) unventilated drip shield-low axial dispersion; and (4) unventilated drip shield-high axial dispersion (Section 2.3.5.4.2.3.1) (SNL 2007f, Section 6.1.2[a]). Drip shield ventilation permits gas exchange through the joints in the drip shield and the equilibration of water vapor partial pressure on both sides of the drip shield. Axial dispersion may occur whether evaporation occurs at the invert surface or at the bottom of the invert. For each TSPA model realization, one of these four drift-wall condensation cases is sampled as an epistemic uncertainty, and the average rate of condensation and fraction of waste package locations that are dripped on by drift-wall condensate is calculated for each percolation subregion and waste package type (SNL 2008a, Section 6.1.4.3). The average rate of condensation dripping from drift walls is combined with drift seepage to increase the dripping flow rate through the EBS in each percolation subregion for each fuel type in the seeping environments (see below), based on the seepage fraction and the condensation fraction. For waste packages in a nonseeping environment, drift wall condensation does contribute to the dripping flow rate through the EBS (SNL 2008a, Section 6.3.6.3).

Three stages are defined for drift-wall condensation. Stage 1 occurs when the temperature of all the emplacement drifts is above the boiling point of water and no condensation occurs. Stage 2 begins when the temperature of the first emplacement drift drops below boiling. During Stage 2, all drifts in which codisposal waste packages are located exhibit condensation, but because SNF waste packages are hotter than codisposal waste packages, no condensation will exist in drifts in which SNF waste packages are located. Stage 3 begins when the temperature of the last waste package in a percolation subregion drops below boiling. During Stage 3, up to about 2,000 years after closure, the regression fits of condensation rate and condensation probability in an emplacement drift versus average percolation rate in the drift (SNL 2008a, Section 6.3.3.2.2) are used to calculate drift-wall condensation. The regression response surface for probability of condensation in a drift is equated to the fraction of waste package locations that have condensation in a percolation subregion by using average percolation rate in a subregion as input to the condensation response surface. The drift wall condensation model predicts no significant rate of condensation after 2,000 years (SNL 2008a, Section 6.3.3.2.2; SNL 2007f, Section 8.1[a]).

As described for FEP 2.1.08.14.0A, Condensation on underside of drip shield (Table 2.2-1) (SNL 2008c, Section 6), has been excluded, based on low consequence.

As described in Section 2.4.2.3.2.1.6, the EBS flow submodel treats waste packages with seepage separately from waste packages with no seepage. For each percolation subregion and each fuel type (commercial SNF or codisposal), the TSPA model includes two dripping environments, which are based on the above inputs from the drift seepage and drift-wall condensation submodels: (1) the seeping environment, which includes dripping above the waste package from drift seepage and could also include drift-wall condensation; and (2) the nonseeping environment, which includes the waste packages that are not exposed to drift seepage, but are possibly exposed to drift-wall condensation. This has the effect that during Stage 2 every codisposal waste package receives the full condensation flux, regardless of whether it is in a seeping or nonseeping environment (SNL 2008a, Section 6.3.3.2.2). As mentioned, inputs to the EBS flow submodel include the drift-seepage rate and the drift-wall condensation rate, as well as the fraction of waste package locations exposed to drift-seepage and the fraction of waste package locations exposed to drift-wall condensation.

Output 9 (Drift Seepage and Drift Wall Condensation—EBS Flow Coupling)—The following outputs are passed from the drift seepage and the drift wall condensation submodels to the EBS flow submodel, for each percolation subregion (Section 2.1.2.1.6):

- Time-dependent drift-seepage rate for the representative codisposal and commercial SNF waste package locations
- The fraction of codisposal and commercial SNF waste package locations in seeping environments
- The average time-dependent condensation rate for the representative codisposal and representative commercial SNF waste package locations
- The fraction of codisposal and commercial SNF waste package locations in condensate environments.

Figure 2.1-5 illustrates the repository average seepage rates calculated by the drift seepage submodel (Section 2.1.2.1.6). The fraction of waste packages in a seeping environment in the TSPA model is fixed for the simulation time and is a function of whether or not each waste package location experienced seepage at any time during the modeled duration (SNL 2008a, Section 6.3.3.1.3). Thus, there will be a different fraction of waste packages in the seeping environments in the GoldSim model file for the 10,000-year simulations compared to the 1,000,000-year simulations.

2.4.2.3.2.1.4 Engineered Barrier System Chemical Environment

As described in Section 2.3.5, the in-drift chemical environment is a function of the initial pore-water chemistry of the host rock, the thermal chemistry evolution in the rock (described in Section 2.3.5.3), thermal-hydrologic evolution in the rock and emplacement drift (described in Section 2.3.5.4), and the thermal chemistry evolution in the emplacement drift (described in Section 2.3.5.5). It also includes integration of the results of seepage and condensation in the emplacement drifts described in Sections 2.3.3 and 2.3.5.4, respectively.

The time-dependent evolution of the chemical-environment variables, pH and ionic strength, in the emplacement drift invert is determined by the time-dependent composition of water and gas entering the emplacement drift and how these water and gas compositions evolve as the water evaporates under the prevailing thermal-hydrologic conditions within the invert. Time histories of seepage water and gas compositions are computed in the TSPA model in each percolation subregion based on the EBS physical and chemical environment abstraction response surfaces (SNL 2007i), as described in Sections 2.3.5.3.4 and 2.3.5.5.4, using temperature and percolation flux inputs from the EBS thermal-hydrologic environmental submodel. To model the effects of the time-varying EBS chemical environment on radionuclide releases in the TSPA model, the representative commercial SNF and codisposal waste packages are used, as introduced in Section 2.4.2.3.2.1.2.

The near field chemistry model and seepage dilution/evaporation abstractions (Sections 2.3.5.3 and 2.3.5.5) described in the EBS physical and chemical environment abstraction (SNL 2007i) are implemented by the EBS chemical environment submodel. The EBS chemical environment submodel quantifies P_{CO2} in the drift and invert; pH and ionic strength in the invert water; and pH, $[Cl^-]$, and $[NO_3^-]$ in the crown seepage water. Various physical and chemical processes in the waste packages and geochemical processes in the invert depend on the output from the EBS chemical environment submodel. The P_{CO2} inside the waste packages influences the degradation of the waste forms and the solubility of the radionuclides inside failed waste packages. The P_{CO2} in the invert influences the solubility of the radionuclides in the invert. Brines that form by evaporative concentration from seepage, which enters the invert by dripping or by imbibition, can influence radionuclide mobility (i.e., radionuclide solubility and colloid stability) in the invert. The ionic strength of water in the invert will control the stability of colloidal suspensions transporting sorbed radionuclides and could also influence the solubility of radionuclides in the invert. The pH, $[Cl^-]$, and $[NO_3^-]$ of the crown seepage water dripping onto a waste package are parameters used to assess the initiation of localized corrosion of the waste-package outer shell (Section 2.4.2.3.2.1.5).

The EBS chemical environment submodel, as implemented in the TSPA model and the localized corrosion initiation analysis, simulates the aforementioned temporal changes of P_{CO2}, pH, ionic strength, $[Cl^-]$, and $[NO_3^-]$ by using response surfaces in the form of chemical composition lookup tables (SNL 2007i, Section 6.15). P_{CO2} is used as an input to the dissolved concentration limits submodel and the in-package chemistry submodel, as applied to the interior of a failed waste package. P_{CO2}, pH, and ionic strength are used as inputs to the dissolved concentration limits submodel and the EBS colloids submodel, as applied in the invert. The pH, $[Cl^-]$, and $[NO_3^-]$ are used as inputs to the localized corrosion initiation analysis to assess the potential to initiate localized corrosion on the waste package outer shell (Section 2.4.2.3.2.1.5). The algorithm for P_{CO2} calculates the P_{CO2} as a function of time and incoming seepage water composition. The response surfaces for pH, ionic strength, $[Cl^-]$, and $[NO_3^-]$ are functions of incoming seepage water composition, temperature, relative humidity, and P_{CO2}. The EBS thermal-hydrologic environment submodel provides the comprehensive time histories of waste package temperature and relative humidity to the EBS chemical environment submodel crown seepage chemistry calculations, and provides the representative waste package time histories to the EBS chemical environment submodel invert chemistry calculations. Although the EBS chemical environment submodel provides P_{CO2} in the drift to the in-package chemistry submodel, it does not provide aqueous composition variables because it has been shown (SNL 2007h, Section 6.6.2[a]) that the chemistry inside a failed waste package is insensitive to incoming water composition.

The analyses of the evolution of the chemical environment in the EBS (SNL 2007i) included evaluations of likely changes to the compositions of gas, water, and solids within the emplacement drifts under repository conditions. The following influences were evaluated for their potential to cause compositional changes in water in the EBS:

- The compositions of water and gas that enter the drifts from the host rock
- Changing thermal conditions in the drifts
- The interactions of seepage water and gas with introduced engineered materials
- The compositions of evaporating or condensing waters within the drifts.

The overall conceptual model follows a packet of host-rock water as it migrates toward the emplacement drifts. As infiltrating water moves downward toward the repository, it moves through a thermal gradient. The thermal gradient extends from the land surface to the repository level, and changes through time as the repository drifts cool. The thermal gradient is calculated by summing contributions from the natural geothermal gradient and the heat generated by radioactive decay in the drifts (SNL 2007i, Section 6.3.2.4.3). The water interacts with minerals in the rock, maintaining equilibrium with calcite and amorphous silica, present in excess, and dissolving alkali feldspar, while precipitating out one or more secondary phases. The rate of feldspar dissolution is a function of the temperature at any location along the percolation path, and is calculated using a temperature-dependent dissolution rate. The dissolution rate is estimated for ambient conditions from the degree of alteration that the tuff has undergone since it erupted 12.8 million years ago, and is adjusted for temperature using literature data for the activation energy for feldspar dissolution (SNL 2007i, Section 6.3.2.1).

As seepage waters enter drifts, either by dripping from the drift crown or by imbibition into the invert, their chemical compositions will change in response to changes in the relative humidity in the drifts (SNL 2008a, Section 6.3.4.1). Throughout the thermal period of the repository (depending on the relative humidity in the drifts), evaporative concentration and associated mineral precipitation can occur in the drifts. After the thermal period, when relative humidities are high, dilution by adsorption of water vapor can occur (SNL 2007i, Section 6.3.3). Evaporation increases aqueous species concentrations, mineral precipitation, and the concentration of the most soluble components in brines. In accordance with the geochemical divide principle, the composition of the seepage water changes according to the sequence of minerals that precipitate from that solution as a function of initial water composition, thermal conditions, relative humidity, and gas composition where the evaporation occurs (SNL 2007i, Section 6.3.3.1).

The following major processes are represented by the EBS chemical environment submodel in the TSPA (SNL 2008a, Section 6.3.4.2):

- Temporal evolution of incoming seepage water composition, where seepage includes dripping from the drift crown and imbibition from the host-rock matrix into the invert

- Changing P_{CO2} in the drifts and the invert

- Evaporative evolution/dilution of seepage water that contacts the drip shield and waste package and percolates through the invert.

Evolution of Incoming Seepage Composition—The EBS physical and chemical environment abstraction defines a range of four possible starting waters as representative of the potential range of the Topopah Spring Tuff pore water compositions (SNL 2007i, Sections 4.1.1 and 6.6). The four input waters (Groups 1 through 4) were chosen statistically to represent the variability in 34 measured TSw water compositions upon evaporation and, as such, span the natural variability of pore-water compositions in repository units. The uncertainty in the starting water composition is represented by randomly selecting one of the four water types for each realization, with equal probability weighting for each starting water type (SNL 2008a, Section 6.3.4.2). As the ambient or "starting" water percolates from the surface, it interacts with the rock. Interactions with the host rock modify the water composition. These compositional changes due to water-rock interactions are strongly affected by the waste-induced thermal field that develops in the TSw above the repository. Ultimately, this compositionally altered water is what enters the drift and affects the chemical conditions in the drift. The degree of alteration is determined by the amount of water-rock interaction, quantified by the parameter called the water-rock interaction parameter. The water-rock interaction parameter is affected by the percolation rate through the rock and the temperature field through which the water passes. Ambient conditions are characterized as having zero water-rock interaction, relative to the starting water composition. The model follows a packet of water from the surface as it passes through the time-dependent thermal field to the repository, taking into account the climate changes that change percolation flux and the velocity of the water.

The EBS physical and chemical environment abstraction defines the water-rock interaction parameter as a time-dependent function of the glacial transition percolation flux and the thermal measure (Section 2.3.5.3.4). The thermal measure is defined as the sum of peak waste package temperature (in °C) and the duration of boiling (in years). This is a heuristic parameter because it is expressed in mixed dimensional units. However, the summed value captures the effects of variations in the thermal history of a given waste package due to location in the repository, assumed rock properties (e.g., thermal conductivity), and waste package specific heat generation rates. Therefore, it provides a useful metric for discriminating between thermal histories at different repository locations. The percolation rate also can influence the thermal measure of the waste package because high percolation tends to cool the repository more quickly. The glacial transition flux is used as an indicator of how fast the water moves through the thermal field, because the glacial transition climate period represents the majority of the first 10,000 years after repository closure and because the maximum dose during the first 10,000 years occurs during the glacial transition climate. The thermal measure and glacial transition percolation flux has been extracted from the multiscale thermal-hydrologic model results for the representative waste packages used in TSPA. Once the thermal measure and glacial transition flux is specified, the time-dependent value of the water-rock interaction parameter, which has been parametrically evaluated for different thermal measures and different percolation fluxes, can be found from the water-rock interaction parameter lookup table (Section 2.3.5.3.4).

P_{CO2} as a Function of Time—The time history of P_{CO2} in the drift is the result of competing processes such as degassing, precipitation, and diffusion and advection of gas in the fractures (SNL 2008a, Section 6.3.4.2). The minimum potential P_{CO2} time history is calculated from the bounding case of high gas flow through fractures. The maximum potential P_{CO2} time history could occur if the drift were a completely closed system and the water moved down through the temperature field without degassing. These two bounding cases provide the range of P_{CO2}. TSPA uses a uniform stochastic variable to interpolate between the upper and lower bound P_{CO2} time histories in each realization (SNL 2007i, Section 6.15.1). The actual P_{CO2} in the drift is calculated by scaling between ambient (0.001 bars) and the minimum or maximum, using the sampled value from the uniform distribution.

Evaporative Evolution of Seepage at the Drift Crown and in the Invert—Equilibrium compositions of aqueous solutions and mineral precipitates that could form from seepage water within the emplacement drifts are calculated by the in-drift precipitates/salts process model (SNL 2007j). Calculations of water compositions at chemical equilibrium were performed using the geochemical equilibrium code, EQ3/6 Version 8.0, and a Pitzer thermodynamic database developed specifically for that purpose. The in-drift precipitates/salts process model simulates the evolution of water in the drifts as it evaporates from its initial composition into concentrated brine. The abstractions developed for the EBS physical and chemical environment apply the in-drift precipitates/salts process model to potential seepage water compositions, representing the four starting waters, modified by differing degrees of water-rock interaction. As discussed in Section 2.3.5.5.4.2.1, the abstraction for evaporative evolution of seepage water consists of lookup tables generated with the precipitates/salts model that provide tabulated values of pH, ionic strength, [Cl^-], and [NO_3^-] for each of the four starting waters at discrete in-drift values of the water-rock interaction parameter, relative humidity, in-drift P_{CO2}, and temperature (SNL 2008a, Section 6.3.4.2).

Within the TSPA model, the EBS chemical environment submodel evaluates the EBS physical and chemical environment abstraction to determine the chemistry of seepage water at two different locations in a drift. One location of water is seepage water dripping from the drift crown and potentially contacting the waste package, and the second location of water is the invert water that originated as water dripping from the drift crown or imbibing from the host rock. Seepage water dripping from the drift crown could flow onto the drip shields and, in the event of a failed drip shield, subsequently contact waste package surfaces. Water dripping from the drift crown can reach the invert either directly, or by first contacting the drip shields and/or waste packages before it reaches the invert. The actual water chemistry on the waste package surface, inside the waste package, and in the invert is determined by the scenario class, the seeping or nonseeping environment, whether or not the waste package and/or drip shield is intact, and whether or not drift wall condensation occurs (SNL 2007i, Table 6.15-1; SNL 2008a, Table 6.3.4-4).

Model Uncertainties—There are four major types of uncertainty in the TSPA submodel associated with the EBS chemical environment: (1) uncertainty in the initial host-rock water composition (i.e., the four possible initial water compositions mentioned above); (2) uncertainty in the water-rock interaction parameter, which is associated with uncertainties in the feldspar dissolution rate; (3) uncertainty in the time evolution of carbon-dioxide partial pressure in the drift; and (4) uncertainties in the aqueous composition variables that control solubility and corrosion potential within the drift (i.e., pH, ionic strength, chloride concentration, and nitrate concentration). Multiple sources of uncertainty underlay some of these, such as the water-rock interaction parameter, which is dependent on mineral abundances, water-rock ratio, dissolution rates, and flow velocity (SNL 2007i, Section 6.12).

Chemistry of the Invert Water—The first step in determining values of pH and ionic strength in the invert water is determining the in-drift P_{CO2} (Section 2.3.5.3.4). The P_{CO2} is a function of the temperature, the amount of water-rock interaction, and the starting water composition. Once the P_{CO2} is determined, the chemical compositions (i.e., pH and ionic strength) are found in the lookup tables as a function of water-rock interaction, P_{CO2}, temperature, and relative humidity. In each realization, one of the four water types of incoming water composition is randomly sampled, and this water type is implemented for each representative waste package in each repository percolation subregion.

Consider a codisposal waste package in a nonseeping environment in a repository percolation subregion. For each realization, the TSPA model determines the pH and ionic strength in the invert water for that waste package at any point in time during the postclosure period, as follows. First, the average invert temperature volume-averaged over the invert at time, *t*, is determined from the multiscale thermal-hydrologic model time histories of temperature that correspond to that representative waste package. Then, the relative humidity of the invert is calculated using the material and the two-phase hydrologic properties of the invert, the properties of water, and relative humidity caps as described in the multi-scale process model (SNL 2008d, Appendix XV). The appropriate P_{CO2} at time, *t*, is calculated as a function of the water-rock interaction and the waste package temperature. To determine pH and ionic strength in the invert water at time, *t*, the set of chemical composition lookup tables corresponding to the starting water and the degree of water-rock interaction are accessed, and the values of temperature, relative humidity, and P_{CO2} are used to interpolate between tabulated values to determine the corresponding pH and ionic strength. The pH and ionic strength are adjusted for epistemic uncertainty and variability by sampling uncertainty distributions for each parameter once per realization (SNL 2008a, Section 6.1.4.4). This procedure is performed for each percolation subregion (although the epistemic uncertainties are common to all percolation subregions).

Chemistry of the Seepage Water—The EBS chemical environment submodel also uses the same chemical composition lookup tables to determine abstracted values of time-dependent pH, chloride and nitrate concentrations, and chloride-to-nitrate ratios for seepage water entering the drift and contacting the drip shield and waste package. These abstracted variables are used to assess the potential for localized corrosion initiation on the waste package outer surface. This application of the EBS chemical environment submodel is implemented in the ancillary localized corrosion initiation analysis for the TSPA, as summarized in the next section, rather than directly in the main TSPA model (SNL 2008a, Appendix O). However, the output files from the localized corrosion initiation analysis, which are time histories of the waste-package failure fraction due to localized corrosion calculated using the chemistry of the seepage water, are read directly by the TSPA model (SNL 2008a, Section 6.3.5.2).

Output 10 (EBS Chemical Environment—Waste Form Degradation and Mobilization Coupling)—The following outputs are passed from the EBS chemical environment submodel to the waste form degradation and mobilization model component for each percolation subregion and each representative waste package (commercial SNF and codisposal) in seeping and nonseeping environments:

- The time-dependent pH in the invert radionuclide solubility calculated using the dissolved concentration limits submodel are applied in the invert by the EBS transport submodel

- The time-dependent ionic strength in the invert radionuclide solubility calculated using the dissolved concentration limits submodel are applied in the invert by the EBS transport submodel
- The time-dependent P_{CO2} in the drift (provided to the waste form degradation and mobilization model component; radionuclide solubility calculated using the dissolved concentration limits submodel are applied in the invert by the EBS transport submodel).

2.4.2.3.2.1.5 Waste Package and Drip Shield Degradation

The abstraction models associated with the performance of waste packages and drip shields are discussed in Section 2.3.6. The two primary design functions of the drip shields are to prevent seepage and condensate water from dripping directly on the waste packages and to provide protection from rockfall damage to the waste packages. The two primary design functions of the waste packages are to isolate the waste from the repository environment and, after waste package failure, to limit and delay the release of radionuclides to the EBS. Excluding the consequences of disruptive events, the TSPA submodel for waste package degradation includes five degradation modes: general corrosion, microbially influenced corrosion, stress corrosion cracking, localized corrosion, and early failure (Section 2.3.6). However, the TSPA only includes general corrosion and early failure of the drip shield, since other drip shield degradation modes have been determined to be insignificant to the performance of the repository (Section 2.2). Early failure of the waste package and drip shield is discussed in Section 2.4.2.3.2.1.12.1.

The relationships between the waste package and drip shield degradation model component and other TSPA model components and submodels are illustrated on Figure 2.4-112. The primary submodel supplying input to the waste package and drip shield degradation model component is the EBS thermal-hydrologic environment submodel (Section 2.4.2.3.2.1.2), which provides exposure conditions (i.e., temperature and relative humidity) on waste package outer surfaces. Output from the waste package and drip shield degradation model component is provided to the waste form degradation and mobilization model component and the EBS flow and EBS transport submodels in the form of time-dependent tabulations of the fraction of waste packages and drip shields failed and the average breached area per failed waste package and drip shield.

TSPA model implementation of localized corrosion is accomplished by exercising several interfaced TSPA model components and submodels in combination with the localized corrosion initiation abstraction in a probabilistic framework external to the TSPA model. A stand-alone analysis is used to compute time-dependent brine chemical composition and corrosion potential on waste package outer surfaces. Outputs of the stand-alone localized corrosion initiation uncertainty analysis are the fraction of locations in the repository that have the potential for localized corrosion initiation on the waste package (SNL 2008a, Figure O-2). These results are used to justify not incorporating the localized corrosion initiation analysis directly in the TSPA dose calculations (SNL 2008a, Section 6.3.5.2), as discussed below.

Titanium alloy drip shields will be installed over the waste packages just prior to repository closure (Section 1.3.4.7.2). As long as they remain substantially intact, the drip shields will divert water that seeps into the drift away from the waste packages and preclude damage to waste packages resulting from rockfall. Because titanium alloys are highly corrosion resistant, drip shield failure will not occur under nominal conditions until approximately 230,000 years postclosure (SNL 2008a, Section 6.3.5.1.3). However, when subject to seismic ground motion and the resulting rockfall, drip shields can fail as early as about 25,000 years (Figure 2.1-11a).

Waste packages will prevent contact between water and waste as long as they are not breached, and will limit water flow and radionuclide migration even after the waste packages are breached (SNL 2008a, Section 6.3.5.1). The waste packages have a dual-metal design consisting of an inner vessel and a waste package outer barrier. The inner vessel is composed of a 50-mm-thick layer of stainless-steel type 316. The waste package outer barrier is a 25-mm-thick layer of Alloy 22, a corrosion-resistant nickel-based alloy (SNL 2007n, Table 4-1; Table 1.5.2-7). Both of these values used in the TSPA, 50 mm for the inner vessel and 25 mm for the outer barrier, are slightly smaller than the design values shown in Figures 1.5.2-2 through 1.5.2-8.

The drip shields and waste packages are expected to be subject to many potential degradation mechanisms after repository closure. Several of these degradation mechanisms have been determined inconsequential under repository-relevant exposure conditions. Nominal and early-failure processes that may result in degradation of the waste packages and drip shields, and thereby impact their barrier functionality, are discussed in detail in Section 2.3.6. Seismically induced drip shield and waste package degradation mechanisms (SNL 2007c), and their interactions with nominal degradation mechanisms, are described in Section 2.3.4. Igneous-induced drip shield and waste package degradation is presented in Section 2.3.11. The TSPA implementation of nominal degradation processes is discussed below. The TSPA implementation of event-driven waste package and drip shield degradation processes (i.e., early failure, seismic, and igneous events) is discussed in Section 2.4.2.3.2.1.12.

The nominal scenario class is represented by a single modeling case. This modeling case considers waste packages that fail as a result of degradation processes not associated with early failure or disruptive events. The TSPA model implementation of the waste package degradation modes for the nominal scenario class modeling case is described in the following.

Waste Package General Corrosion, Stress Corrosion Cracking, and Microbially Influenced Corrosion—General corrosion rates of the waste package outer surface are temperature-dependent and include epistemic uncertainty and spatial variability. The variation in general corrosion rates at a temperature of 60°C, as determined by long-term, weight-loss measurements across the waste package surface (SNL 2007o, Section 6.4.3) is represented by a cumulative distribution function, as discussed in Section 2.3.6.3.2.1 and shown in Figure 2.3.6-9. This cumulative distribution function is sampled for every general corrosion "patch" on every waste package simulated in a percolation subregion. (As discussed in Section 2.3.6.3.4.1, general corrosion is modeled by dividing the waste package surface into subareas, referred to as patches—each patch having a surface area of ~230 cm^2—used to simulate the spatial variability of general corrosion across the waste package surface.) Considering that sampling occurs over the entire waste package surface of about 1400 patches (SNL 2008a, Section 6.3.5.1.2), the extremes of the sampled distribution of corrosion rates (equivalent to the 99.9th percentile value) will be sampled for at least one patch on each waste package. It is these maximum or near maximum values of corrosion rates, when combined with the thermal dependency of the corrosion rate, the microbially influenced corrosion enhancement factor, and the thermal history that waste packages experience, that determine the time of general corrosion first patch penetration through the outer corrosion barrier, as presented in Figure 2.1-10b. As shown in Figure 2.3.6-9, the cumulative distribution function for the general corrosion rate at 60°C is considered to have epistemic uncertainty associated with it. Also, the temperature dependency of the Alloy 22 general corrosion rate is treated as an epistemic uncertainty and is represented by a truncated normal distribution. The development of the temperature-dependent general corrosion rate cumulative distribution function is described in Sections 2.3.6.3.2.2 and 2.3.6.3.3, and presented in Figures 2.3.6-9 to 2.3.6-14. The uncertain temperature dependency and the 60°C general corrosion rate cumulative distribution function, are used to calculate the temperature-dependent general corrosion rate (as a function of time for each realization) for every patch on every simulated waste package in a percolation subregion.

As noted in Section 2.3.6.3.2.3, microbially influenced corrosion is represented by an enhancement factor applied to the general corrosion rate of the waste package outer surface (i.e., general corrosion rate times the enhancement factor). The enhancement factor is applied to the entire waste package outer barrier general corrosion rate only when the relative humidity at the waste package outer corrosion barrier surface is above a threshold value of 75% to 90% (sampled uniformly) (SNL 2007o, Section 6.4.5). The microbially influenced corrosion enhancement factor is uniformly distributed between the values 1 and 2, and the entire variance of this distribution is due to patch-to-patch variability (SNL 2007o, Section 8.2).

Another potential failure mode considered for waste packages is stress corrosion cracking in the closure lid. Stress corrosion cracking can be initiated on a smooth surface (incipient cracks) or at an existing weld flaw (due to manufacturing defects). Flaws in the closure-lid welds are likely sites for stress corrosion cracking. The details and bases of the waste package stress corrosion cracking abstraction are described in Section 2.3.6.5. Incipient crack parameters (size and density) are not treated as uncertain. Two characteristics of weld flaws are treated as epistemic uncertainties: flaw-size distribution and flaw-count distribution. These flaw characteristics are both represented by gamma distributions, and each is sampled once per realization with the same values used for each lid weld. Stress corrosion cracking is determined by stress and stress intensity factor profiles in the closure-lid weld regions and subsequent crack growth from the flaw sites. The epistemic uncertainty in stress and stress intensity profiles is represented by a scaling factor that is sampled from a truncated normal distribution (SNL 2007e, Section 8.4.2.2). The epistemic uncertainty in the threshold stress for initiating incipient crack growth is sampled from a uniform distribution representing a fraction of the yield strength of Alloy 22 (SNL 2007e, Section 8.4.2.3 and Table 8-15). The crack growth rate is a function of the stress intensity factor and the repassivation slope, n. Epistemic uncertainty in the repassivation slope is represented by a truncated normal distribution (SNL 2007e, Section 8.4.2.3 and Table 8-15).

The effects of general corrosion, microbially influenced corrosion, and stress corrosion cracking on the Alloy 22 waste package are compiled by the WAPDEG DLL, which is called by the TSPA model software, GoldSim. The WAPDEG software simulates the spatial variability in waste package degradation. The main inputs to WAPDEG include an input array of real numbers that specify degradation models and degradation model parameters, text files of waste package thermal-hydrologic histories, and text files of additional distributions and tables. The software structure accommodates models, treated as events, which affect specific degradation processes. In the TSPA model, WAPDEG simulates corrosion degradation of waste packages by two penetration modes: patch penetration (due to general corrosion), and crack penetration (due to crack tip growth or stress corrosion cracking). As discussed in Section 2.3.6, general corrosion of Alloy 22 is implemented in WAPDEG using the general linear functional form and the stress corrosion cracking model is implemented in WAPDEG using the slip dissolution and film rupture model for crack initiation and propagation. General corrosion that is enhanced by microbially influenced corrosion is implemented in WAPDEG using a microbially influenced corrosion event. The slip dissolution and film rupture model is implemented in WAPDEG using a slip dissolution event.

In the TSPA model nominal modeling case, 10 WAPDEG DLL simulations are run per realization, one for each representative waste package type (commercial SNF and codisposal) in each of the five repository percolation subregions. This process is described as follows. The EBS thermal-hydrologic environment submodel provides temperature and relative humidity histories for eight waste packages (six commercial SNF waste packages and two codisposal waste packages) at each of the 3,264 subdomain locations. The process begins by randomly sampling a maximum of 500 thermal-hydrologic histories for a given fuel type in a percolation subregion. If the percolation subregion contains fewer than 500 histories, then all histories in the percolation subregion are used. The WAPDEG DLL is part of the TSPA model, and is run at the start of each EBS calculation. The WAPDEG DLL reads in the temperature and relative humidity histories and calculates time-dependent degradation for each waste package. This information is used by the WAPDEG DLL to calculate the following output: (1) the cumulative number of waste package failures as a function of time; (2) the average number of patches per failed waste package as a function of time; and (3) the average number of cracks per failed waste package as a function of time (SNL 2008a, Section 6.3.5.1.3), as illustrated in Section 2.1.2.2.6.

Drip Shield General Corrosion—In the TSPA model nominal modeling case, general corrosion is the only drip shield degradation mechanism modeled in the waste package and drip shield degradation submodel (SNL 2008a, Section 6.1.4.5). This process is modeled as being independent of temperature and relative humidity, and is initiated at the time of repository closure. The uncertainties in the general corrosion rates for the inner and outer surfaces of the drip shields are calculated separately because the environments above and below the drip shields are not expected to be similar (SNL 2007p, Section 6.5.2, 8.1[a]). These distributions represent epistemic uncertainty in drip shield general corrosion rates. The major difference between the inner and outer surfaces of the drip shields is that the outer surfaces will be exposed to a more complex chemical environment because of dust and/or seepage on or in contact with the outer surfaces of the drip shields and will experience an aggressive corrosion rate. The inner surfaces are not expected to be exposed to seepage water and will experience a benign corrosion rate. The drip shield general corrosion model abstraction includes a constant general corrosion rate with time, as described in Section 2.3.6.8.1.1. The variation in the general corrosion rate of the drip shield is considered to be due only to uncertainty (spatial variability in the general corrosion rate is not modeled). For these reasons, unlike the waste packages, each drip shield is modeled as a single entity (inner and outer surface distributions) independent of repository environment. This treatment is appropriate because the primary failure mode for drip shields is structural failure, as described in Section 2.3.4, after accounting for drip shield thinning due to general corrosion. For each realization, a single general corrosion rate is sampled from each general corrosion rate distribution (one for the outer surface and one for the inner surface) and applied to all drip shields (SNL 2008a, Section 6.1.4.5). Using this conceptual model for drip shield general corrosion, all drip shields in the repository fail by general corrosion at the same time for any given realization (SNL 2008a, Section 6.3.5).

In the nominal scenario class, the drip shields are failed as a barrier to flow when the corroded thickness of the drip shield plates equals or exceeds the initial thickness of the drip shield plates. The earliest possible drip shield failure time is calculated by combining the most severe degradation rates from the aggressive and benign distributions (top side and bottom side distributions). Using these distributions values at the 0.9999 probability level gives an aggressive rate of 5.75×10^{-5} mm/yr and a benign rate of 0.824×10^{-5} mm/yr. Combining these gives a rate of 6.57×10^{-5} mm/yr, corresponding to an earliest possible failure time for all drip shields of about 230,000 years (SNL 2008a, Section 6.3.5.1.3).

The general corrosion of the Titanium Grade 29 framework is required in the implementation of the drip shield damage abstraction in the seismic ground motion modeling case. The general corrosion abstraction for Titanium Grade 29 in repository environments was developed in terms of the comparative behavior of Titanium Grade 29 versus Titanium Grade 7 (SNL 2007p, Section 6.2[a]). A cumulative distribution function for the general corrosion rate ratio of Titanium Grade 29 to Titanium Grade 7 was developed. This cumulative distribution function is to be sampled independently for every realization of the TSPA model.

Localized Corrosion—Localized corrosion on waste packages occurs when a waste package is contacted by deleterious brine (SNL 2007o, Section 8.1, Figure 8-1). Because localized corrosion due to dust deliquescence and condensation has been screened from TSPA (Section 2.2) (SNL 2007q, Section 7.1.5), localized corrosion is only possible in those cases where the drip shield fails to perform its function. Thus, in the TSPA model, only crown seepage water chemistry has the potential to fail waste packages due to localized corrosion and only waste packages that have drip shield plate failures coincident with crown seepage contacting the waste package are susceptible to localized corrosion failures (SNL 2008a, Section 6.3.5.2).

The consequence of localized corrosion on the waste package is treated differently for each of the seven modeling cases, but it is never significant enough to have a meaningful effect on the total annual dose curve. The localized corrosion initiation analysis (SNL 2008a, Appendix O) revealed that the period of favorable conditions for localized corrosion initiation in the absence of a drip shield is due to chemical alteration of seepage water due to thermal conditions in the repository during the first 12,000 years after closure. Beyond this time, the chemistry of the seepage water is benign and localized corrosion no longer initiates.

For the nominal modeling case, the first drip shield failure by general corrosion does not occur until about 230,000 years (SNL 2008a, Section 6.3.5.1.3), so localized corrosion of the Alloy 22 waste package does not impact this modeling case. In the seismic ground motion modeling case, there is a low probability (SNL 2008a, Section 7.3.2.6.1.3.2 and Figure 7.3.2-16) of drip shield plate failure occurring before 12,000 years. Because of this low probability, the actual dose consequence of drip shield plate failure is estimated to be low enough that it need not be explicitly calculated for the 10,000-year seismic ground motion modeling case (SNL 2008a, Section 7.3.2.6.1.3.2). The same justifications apply to the 1,000,000-year seismic ground motion modeling case, when considering localized corrosion, because only the first 12,000 years after closure are relevant.

Localized corrosion does not impact the seismic fault displacement modeling case even though there could be failed drip shields during the 12,000 years after closure that seepage water could initiate localized corrosion (SNL 2008a, Section 6.3.5.2.3 and Appendix O). The argument for this assertion is based on the observation that, when the drip shield is failed and the waste package damage area is larger than one third of the waste package cross sectional area, the releases cease to change significantly as more damage is applied (SNL 2008a, Section 7.3.2.7 and Figure 7.3.2-25). Because the releases from the waste package are insensitive to the damage area when more than one third of the lid area is damaged, it is not expected that additional localized corrosion damage will affect the dose result.

For the early failure drip shield modeling case, the drip shield is failed at time zero and localized corrosion on the waste package beneath the early failed drip shield is assumed to occur. For the early failure waste package modeling case, the waste package is fully failed at time zero and localized corrosion would result in no additional damage to the early-failed waste package.

In the igneous intrusion modeling case there are no localized corrosion failures prior to the igneous event because the drip shields remain intact until about 230,000 years (i.e., localized corrosion is treated the same as in the nominal modeling case prior to the igneous event). After the event, all of the waste packages and drip shields are fully damaged and localized corrosion would result in no additional damage to the waste packages. For the volcanic eruption case, it is assumed that the impacted waste packages are unaffected by any other processes or events (SNL 2008a, Section 6.1.1.5).

Localized corrosion of the titanium alloys in the drip shields does not occur for relevant repository conditions and thus is excluded from the TSPA (FEP 2.1.03.03.0B, Localized corrosion of drip shields, Table 2.2-1) (SNL 2008c, Section 6).

In the following outputs from the waste package and drip shield degradation submodel to other submodels, a "failed" waste package is defined to be a waste package that has either through-wall stress corrosion cracks or through-wall general corrosion patches or both.

Output 11 (Waste Package—EBS Flow Coupling)—The following outputs are passed from the waste package and drip shield degradation model component to the EBS flow submodel (Figure 2.4-112) for each percolation subregion and each waste package type (commercial SNF and codisposal waste packages):

- The time that all drip shields fail (Figure 2.1-8)
- The time-dependent average number of patch penetrations per failed waste package (Figures 2.1-16b and 2.1-17b).

Output 12 (Waste Package—Waste Form Coupling)—The following outputs are passed from the waste package and drip shield degradation model component to the waste form degradation and mobilization model component (Figure 2.4-112) for each percolation subregion and each waste package type (commercial SNF and codisposal waste packages):

- The time-dependent fraction of waste packages failed (Figure 2.1-9).

Output 13 (Waste Package—EBS Transport Coupling)—The following outputs are passed from the waste package and drip shield degradation model component to the EBS transport submodel (Figure 2.4-112) for each percolation subregion and each waste package type (commercial SNF and codisposal waste packages):

- The time-dependent fraction of waste packages failed (Figure 2.1-9)
- The time-dependent average waste package surface area failed by cracks per failed waste package (Figures 2.1-13b and 2.1-15b)
- The time-dependent average waste package surface area failed by general corrosion (patches) per failed waste package (Figures 2.1-16b and 2.1-17b).

2.4.2.3.2.1.6 Engineered Barrier System Flow

As described in Section 2.3.7.12, the EBS flow submodel defines the pathways for water flow in the EBS and specifies how the volumetric flow rate is computed for each pathway (SNL 2007k, Section 6). Pathway flow rates are primarily used as inputs to the TSPA EBS transport submodel. The two main sources for advective flow of water in the EBS are drift-seepage (SNL 2007g, Section 8.2[a]) and drift-wall condensation (SNL 2007f, Sections 8.1[a] and 8.2[a]). The flow rates associated with these two sources of advective flow are combined in the EBS flow submodel to yield a total dripping flow rate. An additional (but small) source of advective inflow to the EBS is imbibition into the invert crushed tuff from the surrounding unsaturated zone rock matrix (SNL 2007k, Section 6.3.1.1). The EBS thermal-hydrologic environment submodel provides this input and calls it the liquid flow in the invert. The EBS flow submodel also determines the fraction of waste packages that are dripped upon, by drift seepage and/or drift-wall condensation, in each percolation subregion. Information flow between the EBS flow submodel and other TSPA model components and submodels is shown on Figure 2.4-112.

Eight primary flow pathways are modeled in the EBS flow submodel (SNL 2007k, Sections 6.3.2 and 6.3.3):

1. **Seepage and Drift-Wall Condensation**—This is the dripping water flow from the crowns (roofs) of the drifts. The term “dripping” includes drift seepage and any condensation that occurs on the walls of the drifts on the sections above the drip shields. As noted in Section 2.4.2.3.1.2, approximately 64% of the condensate flows down the drift walls into the edges of the invert and not onto the drip shield. This condensate is not accounted for in the TSPA model.

2. **Flow through the Drip Shields**—The flow rate through the drip shields is dependent on whether the drip shield is present and performing its barrier function. Drip shield failure occurs due to general corrosion (SNL 2007p), which is modeled as occurring uniformly on inner and outer drip shield surfaces.

3. **Diversion around the Drip Shields**—Liquid water flow from either seepage or drift-wall condensation that bypasses a waste package due to a functioning drip shield, and subsequently flows through the invert.

4. **Flow through the Waste Packages**—Two general types of openings can exist in the waste packages. These are: (1) stress corrosion cracks resulting from residual stress or seismic ground motion; (2) patch breaches resulting from general corrosion, localized corrosion, or seismic damage (rupture, puncture, or fault displacement damage). Advective flow through a waste package requires the presence of openings due to patch breaches. Advection of liquid water through stress corrosion cracks in the waste packages is excluded from the TSPA model (FEP 2.1.03.10.0A, Advection of liquids and solids through cracks in the waste package, Table 2.2-1) (SNL 2008c, Section 6). Advective flow into the waste packages, through the waste form, and out of the waste packages is modeled as being independent of the location of patches on the surface of the waste packages (i.e., a “flow-through” configuration is used rather than a “bathtub” configuration (SNL 2007k, Section 6.4.1)).

5. **Diversion around the Waste Packages**—The portion of the dripping water that does not flow into the waste packages and therefore bypasses the waste forms and flows directly to the invert.

6. **Flow into the Invert**—All advective water flow (condensate and/or seepage) exiting the waste packages is modeled as flowing into the invert, independent of breach location on the waste packages. In addition, as mentioned in #3 and #5, the seepage and condensate water that is diverted around the waste packages and drip shields flows into the invert. The presence of the emplacement pallets is ignored in the abstraction of EBS flow, and the waste packages are modeled as being in direct contact with the invert (SNL 2007k, Section 6.3.1.1).

7. **Imbibition Flow to the Invert**—Water can be imbibed from the host-rock matrix into the side of the invert. The EBS thermal-hydrologic environment submodel provides the rate of water imbibition into the invert from the host rock.

8. **Flow from the Invert to the Unsaturated Zone**—The flow from the invert to the unsaturated zone is split so that a portion goes into the unsaturated zone fractures and a portion goes into the unsaturated zone matrix. The portion of the advective flow from the invert equal to the total dripping flux (i.e., seepage flux plus drift-wall condensation flux) flows directly into the unsaturated zone fractures. The portion of the advective flow from the invert that is equal to the imbibition flux flows into the unsaturated zone matrix.

The above pathways are time-dependent in the sense that total dripping flow, drip shield failures, and waste package breaches will vary with time and percolation subregions. Advective water flux in the EBS (derived from drift seepage and condensation) transports radionuclide mass to the unsaturated zone; however, once the mass crosses the EBS-unsaturated zone boundary, it is transported advectively according to the fracture and matrix liquid fluxes in the unsaturated zone submodel, which are based on the unsaturated zone flow fields.

For each percolation subregion, the TSPA model includes two dripping environments: (1) the seeping environment, which includes dripping above the waste packages from drift seepage and possibly drift-wall condensation; and (2) the nonseeping environment, which includes the waste packages that are not exposed to drift seepage, but could be exposed to drift-wall condensation (Section 2.4.2.3.2.1.3, which describes how drift-wall condensation is not likely after about 2,000 years). Inputs to the EBS flow submodel for each waste package type and repository percolation subregion include:

- The flow rate on a representative waste package due to seepage
- The flow rate on a representative waste package due to drift-wall condensation
- The fraction of waste package locations with seepage
- The fraction of waste package locations with drift-wall condensation
- The average number of patch penetrations per failed commercial SNF drip shield and codisposal drip shield (either 0 or the entire drip shield surface area, since spatial variability is conceptualized to be insignificant)
- The average number of patch penetrations per failed commercial SNF waste package and codisposal waste package.

The seepage rate and the condensation rate on each representative waste package in each percolation subregion and for each fuel type are combined in the TSPA model to yield a total dripping rate for each representative waste package.

The seepage fraction and seepage rate from the drift seepage submodel is passed to the EBS flow model. The seepage fraction determines the number of waste packages placed in seeping (seepage + condensate) and nonseeping (condensate only or nondripping) environments in each percolation subregion. The seepage rate and the condensation rate on each representative waste package are added in the TSPA model to yield a total dripping rate onto the drip shield and into the invert for waste packages in a seeping environment (for each representative waste package in each percolation subregion and for each fuel type). In the seeping environment, the invert flux also includes the imbibition flux predicted by the multiscale thermal-hydrologic model (flow pathway 7, described above). For a nonseeping environment, only the drift-wall condensation rate is used above the waste package, but invert flow includes both drift wall condensation and imbibition from the host rock into the side of the invert.

Any of the 3,264 multiscale thermal-hydrologic model subdomain locations that have seepage at any time during the simulation will be included in the fraction of waste package locations in the seeping environment. This seepage fraction is fixed for the simulation time and is primarily a function of the percolation rates at the ending time of the simulation (SNL 2008a, Section 8.3.3.1.1[a]), since percolation rates generally increase through time (SNL 2008a, Section 6.3.3.1.3). Because of the different percolation flux maps at 10,000 versus 1,000,000 years (i.e., glacial-transition percolation rates versus the post-10,000-year percolation rates derived from the distribution specified in the proposed 10 CFR 63.342(c)(2)), different fractions of waste packages are modeled in the seeping environments in the GoldSim model file for the 10,000-year simulations compared to the 1,000,000-year simulations (Tables 2.1-6, 2.1-7, 2.1-9, and 2.1-8).

The advective rate of water flow through each breached waste package is proportional to the total dripping rate and the average number of patch penetrations on each waste package (SNL 2007k, Section 6.5.1.1). This flux-splitting model, which allows a portion of the flow to go through the patches and a portion to bypass the patch openings, introduces two uncertain (epistemic) flux-splitting parameters to characterize the fraction of flow that enters patch penetrations on the waste packages. These two parameters are sampled once per realization and are applied to all representative waste packages that have advection through patches (or any other breaches, with the exception of stress corrosion cracks).

The number of corrosion patches on a failed waste package, N_{pWP}, is the time-dependent parameter that controls the fraction of impinging flow that can enter and flow through the waste packages. It can potentially vary from zero to the maximum number of patches (1,430 for a commercial SNF package (SNL 2008a, Section 6.3.5.1.2)) depending on the modeling case. N_{pWP} increases with time due to general corrosion in the seismic ground motion and nominal modeling cases. It is set to the maximum value in the igneous intrusion, waste package early failure, and drip shield early failure modeling cases, allowing all impinging flow to enter a waste package (SNL 2008a, Section 6.3.6.2). In the seismic fault displacement modeling case, it is based on the number of patches equivalent to the waste package damaged area caused by faulting. N_{pWP} is set to a value corresponding to a single drill hole area in the human intrusion case.

Because the flow splitting model is based on the fractional opening length along the crown of the waste package, rather than the fractional opening area over the entire waste package, the flow splitting fraction reaches a value of 1 (i.e., all the impinging flow can enter a waste package) well before N_{pWP} reaches its maximum. For the mean value of 1.2 for the waste package flux-splitting uncertainty distribution, only about 62 general corrosion patches (out of a total of 1,430) are required on a commercial SNF waste package to allow 100% of the impinging flow to enter a waste package (SNL 2008a, Section 6.3.6.2). This is only 4% of the area of the waste package (excluding the lids). Because the drip shield general corrosion model does not include spatial variation between drip shields or between patches on individual drip shields, all the drip shield patches fail when drip shield failure occurs. Thus, the flow splitting model for drip shields, and its associated epistemic uncertainty, has no effect in the TSPA model.

Outputs from the EBS flow submodel are used by: (1) the waste form degradation and mobilization model component, which uses the flow rate through a failed waste package to calculate pH and ionic strength in the waste package; and (2) the EBS transport submodel, which uses the flow rate through a failed waste package and volumetric flow rate through the invert to calculate advective transport of radionuclides through a failed waste package and through the invert to the unsaturated zone below the repository.

Output 14 (EBS Flow—Waste Form Degradation Coupling)—The following output is passed from the EBS flow submodel to the waste form degradation and mobilization model component (Figure 2.4-112) for each representative waste package group in each percolation subregion, and for the seeping and nonseeping environments, as appropriate:

- The volumetric flow rate of water through the waste package as a function of time.

Output 15 (EBS Flow—EBS Transport Coupling)—The following outputs are passed from the EBS flow submodel to the EBS transport submodel for each representative waste package group in each percolation subregion, and for the seeping and nonseeping environments, as appropriate:

- The flux through the invert pore space as a function of time
- The volumetric flow rate of water through the waste package as a function of time
- The fraction of waste packages in a seeping environment
- The fraction of waste packages in a nonseeping environment.

2.4.2.3.2.1.7 Waste Form Degradation and Mobilization

The waste form degradation and mobilization model component, shown on Figure 2.4-112, consists of five submodels: (1) initial radionuclide inventory submodel, which defines the radionuclide inventory and radionuclides of importance for the TSPA; (2) in-package chemistry submodel, which evaluates in-package chemical conditions; (3) waste form degradation rate submodel, which calculates the degradation rates of commercial SNF, DOE SNF, and HLW glass waste forms; (4) solubility (or dissolved concentration limits) submodel, which calculates solubilities (i.e., dissolved concentration limits) of radioactive elements in a failed waste package and in the invert; and (5) EBS colloids submodel, which calculates colloidal concentrations of radionuclides in a failed waste package and in the invert. Solubilities and colloidal concentration of radionuclides serve as inputs to the EBS transport submodel, which calculates radionuclide transport within the waste packages from the waste form to the EBS and through the EBS to the unsaturated zone below the repository.

In the TSPA model the three categories of waste form (commercial SNF, DOE SNF, and HLW glass) are contained and disposed in two types of waste packages: commercial SNF and codisposal. The codisposal waste packages will contain DOE SNF and HLW glass. As was done in *Total System Performance Assessment for the Site Recommendation* (CRWMS M&O 2000a), waste packages containing naval SNF waste forms are represented as commercial SNF waste packages. An evaluation of this conservatism is presented in Section 2.4.2.3.2.2.4.

Key inputs to the submodels for the waste form degradation and mobilization model component include: (1) a set of initial materials within the waste package and the materials, major elemental compositions and physical and chemical properties; (2) time-dependent water flux into a failed waste package provided by the EBS flow submodel; (3) temperature and relative humidity in the waste package provided by the EBS thermal-hydrologic environment submodel; and (4) partial pressure of CO_2 in the gas phase (P_{CO2}) provided by the EBS chemical environment submodel.

The abstractions that support the submodels in the waste form degradation and mobilization model component are implemented to describe single representative commercial SNF and codisposal waste packages, as described in Section 2.4.2.3.2.1.2. The pertinent properties for a single representative waste package are scaled to the total number of waste packages that have failed in each percolation subregion. These properties include the mass of available inventory, pore water volumes, mass of solid materials, advective flow rates, and diffusion areas (GoldSim Technology Group 2007a, Chapter 5).

The five submodels discussed in this section deal with processes that govern the mobility of radionuclides inside a failed waste package. In general, the radionuclide inventory of each waste package are either immediately available for transport upon waste package failure, or bound in a matrix that must first degrade before the inventory is available for transport inside the waste package. As the waste form degrades, waste form alteration products are formed. The available inventory from the degraded waste form, and that which was immediately available upon waste package failure, is released into the pore water of the alteration product. The available inventory is dissolved in this pore water solution up to the solubility limits of its constituents. As the waste form degrades, waste form colloids are also formed that could facilitate the release of the radionuclides from the breached waste packages to the environment. Although these processes are closely coupled to the release and transport of radionuclides from a failed waste package into the environment, the transport of available radionuclides by diffusion and advection is part of another submodel; the EBS transport submodel described in the next section.

Although a cladding degradation submodel is shown in Figure 2.4-2, in the TSPA model no performance credit is taken for Zircaloy or stainless-steel cladding as a mechanism to prevent radionuclide release or inhibit commercial SNF waste form degradation (SNL 2007r, Section 6.2[a]). The justification for this assumption is explained in Section 2.3.7.6.

Radionuclide Screening—Radionuclides contained in the waste packages include fission products from reactor operations, actinides from neutron capture in uranium and plutonium, and activation products from neutron irradiation of structural materials and trace elements. Altogether, these fission products, actinides, and activation products constitute more than 100 radionuclides that could be collectively present in the waste packages at the time of repository closure. Many of the radionuclides have short half-lives, low solubilities and/or strongly sorbing characteristics, or are present in small quantities. Therefore, such radionuclides cannot be significant contributors to estimated dose. As a result, only a subset of radionuclides needs to be considered in the evaluation of repository postclosure performance. The process of eliminating the low dose contributors is called radionuclide screening (SNL 2007s).

Radionuclides were screened by calculating a radionuclide-screening product for each radionuclide. The radionuclide-screening product, which is roughly proportional to dose, is obtained by multiplying the screening factor for each radionuclide by the curie content of that radionuclide in the inventory. To evaluate the relative importance of each radionuclide for dose contribution calculations, the calculation of radionuclide screening factors considered consumption of locally produced vegetables, fish, meat, and milk; water consumption; inadvertent ingestion of soil; inhalation; and exposure to contaminated ground (SNL 2007s, Appendix A). The screening products were ranked from largest to smallest and then summed, starting with the largest, the screening products of each contributing radionuclide were included in the sum. For each waste type, time frame, solubility group, and transport affinity group, the radionuclides determined to contribute the first 95% of the summed radionuclide-screening products were considered potentially important and retained for analysis. The 95% threshold does not directly correlate with calculated dose at the site boundary over the regulatory time period, but rather is based on a set of conservative hypothetical scenarios (SNL 2007s, Section 6.2.1). The results of the screening process are shown in Table 2.3.7-2, which represent the radionuclides that are simulated in the TSPA model.

Radionuclide Inventory—The waste form degradation and mobilization models require the radionuclide inventory in each representative commercial SNF waste package and each representative codisposal waste package (SNL 2007t). The results of the inventory calculations are described in Section 2.3.7.4 and are summarized in Tables 2.3.7-3, 2.3.7-4, and 2.3.7-5. Epistemic uncertainty in the initial emplaced inventory is shown in Table 2.3.7-6. The three waste-form categories (commercial SNF, DOE SNF, and HLW glass) are contained and disposed in two types of waste packages: commercial SNF waste packages and codisposal waste packages. The codisposal waste packages will contain DOE SNF and HLW glass. The inclusion of mixed-oxide SNF and lanthanide borosilicate glass HLW in the TSPA model is accomplished by adding radionuclide-specific inventories to the GoldSim source term (SNL 2007t, Sections 5.7[a] and 6.4.1[a]). More specifically, the lanthanide borosilicate glass inventory amounts are added to the HLW portion of the initial radionuclide inventory and the mixed-oxide SNF is added to the commercial SNF portion of the initial radionuclide inventory. Waste packages containing naval SNF are represented as commercial SNF waste packages containing commercial SNF inventory (Section 2.4.2.3.2.2.4).

The commercial SNF radionuclide quantities in Table 2.3.7-3 are for commercial SNF that is, on average, 23 years out of reactor on arrival at the repository, based on disposal rights (SNL 2007t, Section 7.1.1[a] and Table 7-1[a]; CRWMS M&O 2000b, Table 5). For a later repository opening date than in previous TSPAs, use of the same waste stream at a later date, rather than an older waste stream due to decay, is conservative with respect to radionuclide inventory and heat. Waste is emplaced for a period of up to 50 years, depending on the amount of onsite aboveground aging required for the hottest waste packages. Ventilation will continue until the closure time used in the TSPA calculation, 2117, which is, approximately 100 years after the start of waste emplacement. The radionuclide quantities shown in Tables 2.3.7-3 and 2.3.7-4 are at times specific to the type of waste. The times of the waste form inventories are 2067 for commercial SNF (approximately 50 years after the start of emplacement), 2030 for HLW and DOE SNF, 2035 for MOX, and 2003 for lanthanide borosilicate glass. For the TSPA thermal calculation, it is assumed that the waste is emplaced simultaneously in 2067, and has an average age of 23 years at emplacement (Section 2.3.7.4.1.2) (SNL 2008a, Section 6.3.6.2). Waste that is 23 years old has more radionuclide content than older waste, and hence is conservative with respect to radionuclide inventory and heat. HLW and DOE SNF radionuclide quantities in the above tables are those calculated at 2030 (SNL 2007t, Sections 6.4.1 and 7.1.1[a]). TSPA modeling of all three waste sources will account for decay occurring from the time of emplacement (or inventory calculation) to repository closure, which is assumed to occur in 2117.

Radionuclide releases are calculated by taking into account the number of breached waste packages in each specific type of environment. Accounting for seep versus no seep conditions, commercial SNF versus codisposal fuel, and the possibility of localized corrosion, created six major groupings of waste packages in the TSPA model for each of the five percolation subregions. These representative waste package groups include:

- Codisposal waste package in a nonseeping environment
- Codisposal waste package in a seeping environment that will not have localized corrosion damage

- Codisposal waste package in a seeping environment that could have localized corrosion damage

- Commercial SNF waste package in a nonseeping environment

- Commercial SNF waste package in a seeping environment that will not have localized corrosion damage

- Commercial SNF waste package in a seeping environment that could have localized corrosion damage.

In-Package Chemistry—The in-package chemistry submodel is used to determine the pH, ionic strength, and total carbonate concentration in the water in contact with the waste form (including the basket or canister and other waste form support) and/or waste form degradation products. Within the waste package, the chemistry of the water in contact with waste package corrosion products is determined by the EBS radionuclide transport submodel. The in-package chemistry submodel is implemented using response surfaces and parameter distributions for six different abstraction conditions: one waste form domain within the commercial SNF waste packages and two waste form domains in the codisposal waste packages for both dripping (liquid influx) and non-dripping (vapor influx) conditions. pH in the in-package chemistry submodel is implemented by sampling uncertainty distributions that are dependent on ionic strength and P_{CO2}. Ionic strength is determined by sampling uncertainty distributions whose range is a function of the relative humidity within the breached waste package for nondripping conditions and by sampling uncertainty distributions whose range is a function of the seepage rate through a breached waste package and the duration that the waste packages have been failed for dripping conditions. The total carbonate concentration is calculated using a temperature, P_{CO2}, and pH-dependent equation. This calculated value of total carbonate concentration includes no additional uncertainty. Inputs to the in-package chemistry submodel include volumetric flow rates of seepage into a failed waste package as provided by the EBS flow submodel, the P_{CO2} provided by the EBS chemical environment submodel, and the temperature and relative humidity provided by the EBS thermal-hydrologic environment submodel.

The in-package chemistry abstractions are derived from the output of the in-package chemistry process models (SNL 2007h) and provide either parameter distributions or response surfaces for the TSPA model. The vapor influx model and the liquid influx model have separate process and abstraction models, which allow the TSPA model to implement nonseeping and seeping conditions. There are a total of 12 abstractions (six for ionic strength and another 6 for pH) for the three waste form domains (commercial SNF, HLW, and DOE SNF) under two different water influx conditions. The $\sum CO_3$ abstraction is represented as a single equation for liquid influx and vapor influx conditions for commercial SNF only because HLW glass and DOE SNF degradation rate calculations do not require this parameter.

The abstractions of in-package chemistry for bulk water in a waste package are applicable for oxidizing conditions ($10^{-0.7}$ bars), a P_{CO2} range of 10^{-4} to $10^{-1.5}$ bars, a temperature range from 25°C to 100°C, a relative humidity for vapor influx equal or higher than 95%, and a water volumetric flux (hereafter referred to as “flux”) for liquid influx equal or higher than 0.1 L/yr (SNL 2007h, Section 8.1[a], Table 8-1[a]).

The abstraction for the in-package chemistry submodel (Section 2.3.7.5) consists of five parts for each of the three waste-form domain (i.e., for commercial SNF, HLW, and DOE SNF): (1) determination of whether or not bulk water is present in the waste form domains; (2) determination of which abstraction is to be used (liquid influx or vapor influx); (3) calculation of ionic strength; (4) calculation of pH; and (5) calculation of the total concentration of aqueous carbonate (for commercial SNF only).

1. **Applicability of Bulk Water Chemistry**—Under nondripping conditions, radionuclide transport from the waste form domain to the corrosion product domain requires a continuous film. A continuous film is not expected in the waste form domain when the relative humidity is below 95% (SNL 2007h, Section 6.10.9.1[a]). Thus in the TSPA model, bulk water chemistry is not determined when the relative humidity is below 95% and vapor influx conditions prevail. Whenever the water inflow rate is less than 0.1 L/yr and relative humidity is lower than 95%, the chemistry abstractions for bulk water conditions do not result in a meaningful pH and ionic strength from the vapor influx model (SNL 2007h, Section 6.10.9.1[a]). Given the ultimately small volume of water film being considered at these relative humidity conditions (relative humidity < 95%), virtually all of the waste form materials degraded under these conditions will be precipitated in place and not be available for transport. In the absence of bulk water, the in-package chemistry submodel determines the pH to be applied in the pH-dependent waste form degradation rate models, applying fixed values or sampled values from uncertainty distributions sampled once per realization. This pH is not used for other pH-dependent models within the waste form domain. The solubilities for all radionuclides, including colloidal species, are set to zero so that no transport is allowed (SNL 2008a, Section 6.3.7.2.2).

2. **Liquid Influx versus Vapor Influx**—Whenever the relative humidity is greater than 95% or the water inflow rate is greater than or equal to 0.1 L/yr, the in-package chemistry submodel for bulk water is applicable, and a decision is made to select one of the two abstractions (the vapor influx versus the liquid influx) to generate outputs for ionic strength and pH. The choice depends on the relative humidity, the water flux rate, and the abstraction that predicts lower ionic strength. Ionic strength and pH are calculated using the vapor influx abstraction whenever the liquid influx rate is less than 0.1 L/yr (and the relative humidity is equal or greater than 95%). At or above 0.1 L/yr, ionic strength and pH are calculated using the liquid influx abstraction. An exception is made when the vapor influx abstraction predicts an ionic strength that is lower than the ionic strength from the liquid influx abstraction. The lower of the two values is applied to determine the pH (SNL 2007h, Section 6.10.9.1[a]).

3. **Ionic Strength**—Ionic strength abstractions for the vapor influx case are given as functions of relative humidity with uncertainty added. The mean value is a piecewise linear function of relative humidity. The uncertainty range is between the mean value times the lower uncertainty factor and the mean value times the upper uncertainty factor. Ionic strength abstractions for the liquid influx case are functions of water inflow rate through the breached waste packages and time since the representative waste package breached (SNL 2008a, Section 6.3.7.2.2). Uncertainties are also included in the

logarithm of ionic strength abstractions for the liquid influx case and are presented as a deviation from the mean value.

4. **pH**—When the water influx rate is greater than or equal to 0.1 L/yr, the liquid influx pH abstraction will be used to determine in-package pH ranges. The maximum and minimum pH values are functions of $p\mathrm{CO}_2$ (the negative logarithm of P_{CO2}) and log ionic strength. When the water influx rate is less than 0.1 L/yr, the vapor influx pH abstraction will be used to determine in-package pH ranges. The maximum and minimum pH values are functions of $p\mathrm{CO}_2$ and log ionic strength. For a given $p\mathrm{CO}_2$, the pH values have a uniform distribution between the minimum and maximum pH values (SNL 2007h, Sections 6.10.9.1[a] and 6.10.9.3[a]).

5. **Total Carbonate Concentration**—The total carbonate concentration is used in the degradation rate law for the commercial SNF waste form. An expression for total carbonate concentration (mol/kg) as a function of temperature, pH, and P_{CO2} is based on equilibrium mass action expressions (SNL 2007h, Section 6.10.5).

Outputs from the in-package chemistry submodel are provided for each representative waste package and each representative early failed waste package, if available, in seeping and nonseeping environments in each percolation subregion and consist of:

- pH as a function of time
- Ionic strength as a function of time
- Total carbonate concentration as a function of time.

These outputs are used internally in the TSPA model by the waste form degradation and mobilization model component as inputs to the rate equations for the waste form degradation submodels, the dissolved concentration limits submodel, and EBS colloids submodel.

Cladding—Most of the commercial SNF is encased in Zircaloy cladding, with only 1% of commercial SNF encased in stainless-steel cladding. Zircaloy cladding and stainless-steel cladding are modeled as being failed upon emplacement of the waste packages in the repository. Thus, in the TSPA model, no credit is taken for any type of barrier capability of the commercial SNF (and DOE SNF) cladding (SNL 2007r, Section 6.2[a]). (Note: Naval SNF waste packages are represented in the TSPA as commercial SNF waste packages (Section 2.4.2.3.2.2.4).)

Waste Form Degradation—Waste form degradation is modeled within the TSPA model using empirical formulas for the degradation rate developed for the three different waste form types: commercial SNF, DOE SNF, and HLW.

Commercial SNF is isolated from repository environmental conditions until a waste package is breached. After the waste package is breached, the commercial SNF will be exposed to humid air or dripping water. Upon exposure to moisture, radionuclides can be released by two mechanisms: (1) instantaneous release of the gap fraction and grain boundary inventory; and (2) matrix dissolution under alkaline or acidic conditions (BSC 2004e, Section 8.1). Four radioelements are in the instantaneous release inventory: cesium, iodine, technetium, and strontium (BSC 2004e, Section 6.3). The fraction of the inventory emplaced in the repository that makes up the initial release inventory for each of these four radionuclides is determined by sampling four distributions representing epistemic uncertainty. These distributions are sampled once per realization. Similarly, the ^{14}C hardware inventory is treated as instantaneous release inventory. It originates from neutron activation of stainless-steel hardware outside the fuel rods and is specified to be 18% of the ^{14}C inventory in a commercial SNF waste package (SNL 2007t, Section 6.7 and Table 7-1[a]).

Degradation of the commercial SNF fuel matrix by oxidative dissolution is modeled using two rate formulas, one for $pH < 6.8$ and one for $pH \geq 6.8$ (BSC 2004e, Section 8.1). Commercial SNF degradation rate formulas are a function of specific surface area of exposed fuel, temperature, total carbonate concentration, $P\mathrm{o}_2$, and in-package pH. A triangular distribution is used to represent epistemic uncertainty in a specific surface area of exposed fuel. The commercial SNF degradation rate is calculated using input provided by two submodels: the EBS thermal-hydrologic environment submodel provides the time-dependent temperature of the commercial SNF, and the in-package chemistry submodel provides time-dependent pH and total carbonate concentration inside the failed waste package. The EBS transport submodel calculates the mass and saturated volume for the degraded commercial SNF rind. These parameters are used to determine radionuclide concentrations in the fuel rind and to model transport from the commercial SNF rind into the waste package.

The DOE SNF in a failed codisposal waste package is modeled as being immediately available for dissolution and mobilization. Because of this simplification, no rate equation or rate parameters are necessary to implement the DOE SNF waste form degradation abstraction for DOE SNF in the TSPA model (BSC 2004f, Sections 6.2 and 8.1). Each time a codisposal waste package fails, the DOE SNF inventory associated with the failed waste package, after accounting for decay and ingrowth, is made immediately available for transport (subject to solubility constraints) in the volume of water associated with the degraded DOE SNF (SNL 2008a, Section 6.3.8.2). Once released, radionuclides are available for transport through the waste packages to the EBS.

Degradation of HLW glass is initiated if the waste package is breached and the relative humidity is greater than or equal to 44% or when a liquid flux through the waste package prevails (BSC 2004g, Sections 6.7 and 8.1). The rate of degradation is determined by a rate expression that applies to the amount of glass exposed to humid air, dripping water, or immersion. The coefficients in the rate equation are dependent on whether or not acidic or alkaline conditions prevail. Below 100°C, the rate equation is a function of an effective rate constant, temperature, pH, and the surface area of the HLW glass. Above 100°C, up to 125°C, the pH from in-package chemistry submodel is not applied, instead the pH-dependence is replaced with a fixed value. The result for the rate calculations is equivalent to setting the pH to 10 (BSC 2004g, Section 8.1). The effective rate constant is treated as an epistemic uncertainty, and is represented by distributions for acidic and alkaline conditions. The greater of the two calculated rates is used as the degradation rate (BSC 2004g, Section 8.1). The surface area of the glass is calculated as the product of the specific surface area of the glass and the glass exposure factor. The exposure factor is treated as an epistemic uncertainty and is used for alkaline and acidic conditions (SNL 2008a, Table 6.3.7-32). The EBS transport submodel calculates the mass and saturated volume for the degraded HLW rind. These parameters, along with dissolved concentration limits, are used to determine radionuclide concentrations in the HLW rind.

Outputs from the waste form degradation submodel for HLW glass, commercial SNF, and DOE SNF degradation are provided for each representative waste package as applicable in seeping and nonseeping environments, and in each percolation subregion, as follows:

- The degradation rate of HLW glass
- The degradation rate of commercial SNF fuel
- The instantaneous degradation of DOE SNF fuel.

These outputs, along with the dissolved concentration limits, are used in the waste form degradation and mobilization model components in conjunction with the EBS radionuclide transport submodel to determine the concentration of radionuclides in water in the associated degraded fuel rind.

Dissolved Radionuclide Concentration Limits—Within the TSPA model, the dissolved concentrations limits submodel implements the dissolved concentrations limits abstraction (SNL 2007u) to calculate solubilities for 8 elements; plutonium (Pu), neptunium (Np), uranium (U), thorium (Th), americium (Am), protactinium (Pa), tin (Sn), and radium (Ra). For technetium (Tc), carbon (C), iodine (I), cesium (Cs), strontium (Sr), selenium (Se), and chlorine (Cl), no solubility-controlling solids are expected to form under repository conditions; therefore, their solubilities are not evaluated or defined and their dissolution is constrained by the waste inventory and the degradation rates of the waste form (SNL 2008a, Table 6.3.7-33). The output of the dissolved concentration limits submodel is used in the TSPA model to constrain the dissolved concentrations of radioactive elements in the waste packages and the invert.

Four types of uncertainties—(1) in the K_{sp} values of solubility controlling solids and aqueous species, (2) of activity coefficients, (3) in water chemistry, and (4) in temperature—have been evaluated in the dissolved concentration limits abstraction (SNL 2007u, Section 6.3.3). The first two types of uncertainties are combined together by the mean-square-root approach and are collectively called “thermodynamic uncertainties.” The third type of uncertainty is presented as the uncertainty associated with fluoride concentrations. The last type of uncertainty (i.e., uncertainty in temperature) is treated using a bounding approach. In other words, the solubility calculations are conducted at a temperature of 25°C and are applied for all temperatures greater than 25°C (up to 100°C). The use of solubility values calculated at 25°C for higher temperatures is bounding because the solubility of actinides in carbonate systems, such as will prevail in the EBS, decreases with increased temperature, which is called retrograde solubility (SNL 2007u, Section 6.3.3.3).

Outputs from the dissolved concentration limits abstraction can be divided into three groups: (1) elements whose solubility is a function of pH and $\log f_{CO_2}$; (2) radium solubility that is a function of pH only; and (3) elements for which no solubility limits are defined (SNL 2007u, Section 8.1). The first group consists of the actinide elements plus tin: americium, neptunium, plutonium, protactinium, thorium, uranium, and tin. The abstracted solubility models for these elements are in the form of lookup tables with pH and $\log f_{CO_2}$ as the independent variables. Two uncertainty terms accounting for uncertainties associated with thermodynamic properties and variations in water chemistry are also included for this group of elements. The exception to this treatment is protactinium, where the thermodynamic uncertainty is replaced by uncertainty in the choice of an analogue element. For tin, the uncertainty term associated with variations in fluoride concentrations is not given because the calculated tin solubility is not sensitive to fluoride concentrations (SNL

2007u, Section 6.19). For radium, solubility values are given as a step function of pH, and uncertainties were not included.

Two different solubility models have been developed for neptunium (SNL 2007u, Section 6.6). These two models are based on different solubility-controlling solid phases: Np_2O_5 and NpO_2. The NpO_2 solubility model is used within waste packages when reductants (commercial SNF fuels or stainless steels) remain. After reductants within waste packages are consumed, Np_2O_5 is assumed to be the solubility-controlling mineral phase. For the invert, the Np_2O_5 solubility model is always applied.

There are two methods used to calculate uranium solubility based on different chemistries of in-package fluids (SNL 2007u, Section 6.7). In the first method, the amounts of silica and alkaline elements in the fluid are far less than the amount of available uranium, which precludes the ubiquitous formation of uranyl silicates (e.g., Na-boltwoodite) and their use as solubility controlling phases. In the second method, the amount of silica and alkaline species are comparable to the amount of available uranium, so uranyl silicates can readily precipitate. These two methods apply as follows:

- Method 1. Commercial SNF waste packages breached in the nominal or seismic scenario classes
- Method 2. Codisposal waste packages breached under all scenario classes, commercial SNF waste packages breached in the course of the igneous intrusion, and for all evaluations in the invert.

Using the first method, uranium solubility is controlled by schoepite under all pH and f_{CO2} conditions. This method is used because the source of the degrading water in a commercial SNF waste package in the nominal, early failure, or seismic scenario classes is water vapor entering the waste packages, which has low or no initial dissolved sodium or silica (SNL 2007u, Section 6.7.3).

Using the second method, uranium solubility is controlled by schoepite, Na-Boltwoodite, or $Na_4UO_2(CO_3)_3$, depending on the pH and f_{CO2}. In this environment, silica is available to the degrading waste from the codisposal glass, surrounding igneous material, and invert construction material, so two additional base solubility lookup tables are defined. The solubility limits for schoepite solubility extend over lower pH values, but at higher pH values, the solubilities of either Na-boltwoodite or $Na_4UO_2(CO_3)_3$ are applicable (SNL 2007u, Section 6.7.4). Uncertainties in $\log K_{sp}$ and fluoride concentrations are added to the base solubilities, which are functions of pH, f_{CO2}, and ionic strength.

Under repository environmental conditions, no solubility-controlling solids are expected to form for carbon, cesium, chlorine, iodine, selenium, and technetium (SNL 2007u, Section 8.1); therefore, no solubilities are defined for these elements. Although strontium could precipitate in carbonates and sulfates under repository conditions, for the purpose of simplicity (and because its very short half-life means that there is very little risk), its solubility is also assumed to be undefined. An "undefined" solubility in the TSPA model means that the release of these elements is controlled by the waste inventory and degradation rates associated with the waste forms.

Solubilities are evaluated as a function of time to account for the evolution of pH and f_{CO2} during the postclosure period. One or more epistemic uncertainty terms are evaluated by sampling their respective distributions once per realization and are added to each time-dependent solubility value. The in-package chemistry submodel and the EBS chemical environment submodel provide the pH, ionic strength, and f_{CO2} inputs to the dissolved concentration limits submodel when the solubilities are evaluated in the waste package environment and in the invert, respectively.

Outputs from the dissolved concentration limits submodel are provided for each representative waste package as applicable in seeping and nonseeping environments, and for each percolation subregion, as follows:

- The time-dependent solubilities for americium, neptunium, plutonium, protactinium, thorium, uranium, and tin

- The time-dependent value of radium solubility, which can be one of two values depending on pH.

These outputs are used by the EBS transport submodel to constrain radionuclide concentrations for the pore waters associated with the commercial SNF rind, the DOE SNF rind, and the HLW glass rind, as well as the in-package corrosion products and the invert.

Colloid Concentration and Stability—The TSPA model EBS colloids submodel calculates the types and concentrations of colloids potentially generated after waste package failure. Three types of colloids are considered: (1) waste-form-degradation colloids, which are generated from degradation of the glass waste form and SNF waste forms; (2) corrosion-product (iron oxyhydroxide) colloids produced from the degradation of the steel components in the waste packages; and (3) (iron oxyhydroxide) colloids present in natural seepage water entering the EBS. Nine radionuclides can potentially sorb on the colloids: plutonium, americium, cesium, protactinium, thorium, tin, radium, uranium, and neptunium. Inputs to the EBS colloids submodel include pH and ionic strength in the waste package provided by the in-package chemistry submodel, dissolved radionuclide concentrations in the waste package and invert from the EBS transport submodel, and pH and ionic strength in the invert provided by the EBS chemical environment submodel.

Colloid Type—As previously mentioned, three types of colloids are considered in the waste form and in-drift colloid concentration abstraction (SNL 2007v, Section 6.5) and are accounted for in the EBS colloids submodel implemented in the TSPA model.

1. **Waste Form Degradation Colloids**—(a) Glass Waste Form Colloids—Experimental work has shown that quantities of colloids containing plutonium are generated from glass waste during the degradation process. These colloids are a mixture of clays, zeolites, and oxides, but are predominantly clays (SNL 2007v, Section 6.3.3). (b) Residue Commercial SNF Waste Form Colloids—A layer of plutonium and zirconium-rich oxides forms, and is possibly suspended, at the reaction front of degrading commercial SNF waste forms (SNL 2007v, Section 6.3.4). (c) Uranium Mineral SNF Waste Form Colloids—Colloidal-sized particles of uranium minerals such as uranophane have been observed in solutions in contact with degrading commercial

SNF. Degrading uranium metal DOE SNF has been shown to release colloid-sized particles of UO_2 (SNL 2007v, Sections 6.3.5 and 6.3.6).

2. **Corrosion Product Colloids**—Iron oxyhydroxides derived from the corrosion of steel components in the repository will occur in three forms: (1) large-sized corrosion products consisting of immobile materials; (2) large particles that settle out; and (3) colloid-sized particles that could potentially transport sorbed radionuclides (SNL 2007v, Section 6.3.8).

3. **Seepage Water Colloids**—Colloid concentrations in saturated zone groundwater were used in the waste form and in-drift colloid concentration abstraction to estimate the colloid concentrations in seepage water that could enter a failed waste package. There is a wide range in natural groundwater colloid concentrations in the Yucca Mountain vicinity over a relatively narrow range of groundwater ionic strength.

Colloid Stability—The stability of a colloidal suspension is controlled by electrostatic and chemical processes at colloid surfaces and by the attractive and repulsive forces between colloids. Higher ionic strength and higher temperature cause colloidal suspensions to become unstable and the colloids to coagulate. Another factor in colloid stability is pH. Colloids become unstable and flocculate near a pH value (zero point of charge) that is characteristic for a particular colloid mineralogy because of reduced repulsive forces between the colloids. These competing forces and processes are abstracted as an ionic strength threshold (that is dependent on pH), above which the colloid suspensions are unstable (SNL 2007v, Section 6.3).

Radionuclide Attachment—Radionuclides could be attached to colloids in many ways. In some cases the attachment and detachment is relatively fast compared to the residence time and can be described as an equilibrium sorption process via a K_d sorption model. In other cases, attachment is fast, but detachment very slow, as in coprecipitation where the radionuclide becomes embedded in the host colloid. This type of attachment is more complex to model and is referred to here as irreversible or kinetic attachment. Attachment to the types of colloids is approximated as follows (SNL 2008a, Section 6.3.7.6.1):

1. Waste form degradation colloids

    a. Glass degradation colloids – reversible and irreversible
    b. Commercial SNF degradation rind colloids – irreversible
    c. SNF uranium mineral colloids – reversible

2. Iron oxyhydroxide colloids – reversible and irreversible

3. Groundwater colloids – reversible.

Nine elements are modeled for reversible sorption to waste form and groundwater colloids: plutonium, americium, cesium, protactinium, thorium, tin, radium, uranium, and neptunium. This list represents the radionuclides most likely to exhibit dose-significant colloidal transport. Two of these elements, plutonium and americium, are modeled as being irreversibly attached to iron oxyhydroxide colloids, glass degradation colloids, and commercial SNF degradation colloids.

Reversible sorption on waste form and groundwater colloids is modeled by adjusting the sampled K_d value such that the sorption capacity of the colloids is not exceeded (SNL 2007v, Sections 6.3.12.1, 6.3.12.2, and 6.3.12.3).

Modeling sorption of dominant actinides in the inventory (uranium, neptunium, plutonium, americium, and thorium) to iron oxyhydroxide surfaces (both stationary corrosion products and iron oxyhydroxide colloids) is performed using a surface complexation-based competitive sorption model. The surface-complexation model is a mechanistic model based on a single-site diffuse-layer model that couples the pH in the corrosion products domain with the type of surface complexes formed under varying chemical conditions and sorption site densities. The model is applicable to a wide range of concentrations and accounts for competition among various actinides for the finite number of sorption sites. The stationary corrosion products and iron oxyhydroxide colloids are considered to be a mixture of goethite and ferrihydrite, the proportion of which is treated as uncertain (SNL 2007k, Section 6.5.2.4). Sorption of uranium, neptunium, and thorium is modeled as an equilibrium sorption process by computing an effective K_d (based on abstraction of surface complexation modeling results) while the sorption of plutonium and americium is modeled as a kinetic process. However, the kinetic sorption model is applied differently to stationary corrosion products and iron oxyhydroxide colloids, such that only irreversible sorption is considered on iron oxyhydroxide colloids (i.e., there is no desorption of plutonium and americium) while both kinetic sorption and desorption reactions are considered for stationary corrosion products (SNL 2007k, Section 6.5.2.4.6). The surface complexation model results are also used to determine a pH response surface in the corrosion products domain for each representative waste package group in the TSPA model.

At each time step in the TSPA model calculations, the EBS colloids submodel uses in-package ionic strength, and pH, to evaluate the stability of colloid suspensions inside the waste package. It then uses the dissolved radionuclide concentrations to calculate the reversible sorption of each of the nine modeled radionuclides onto the smectite (waste form and groundwater colloids), uranium mineral colloids, and iron oxyhydroxide colloids. The EBS colloids submodel also calculates the irreversible sorption of plutonium and americium onto glass, commercial SNF, and steel corrosion products colloids (SNL 2008a, Section 6.3.8.3).

The colloid and radionuclide concentration values in the waste packages, along with the ionic strength and pH of the solution and dissolved radionuclide concentrations in the solution, serve as source terms for the invert. The EBS chemical environment submodel (Section 2.4.2.3.2.1.4) calculates the ionic strength and pH of the invert water. Based on the values of ionic strength and pH in the invert, the EBS colloids submodel determines colloid suspension stabilities and concentrations for the invert conditions and redistributes available radionuclide mass based on the distribution coefficients and the total mass of each type of colloid. These colloids and associated radionuclides are then subject to transport through the invert and into the unsaturated zone.

Several epistemic uncertainties related to colloid suspension stability and colloid-associated radionuclide concentrations are represented by distributions that are sampled once per TSPA model realization. These uncertain parameters include the equilibrium sorption distribution coefficients, the specific surface area of iron oxyhydroxide colloids, the groundwater colloid concentration, and the forward rate constant for irreversible (kinetic) sorption (SNL 2008a, Section 6.1.4.7).

Output 16 (Waste Form Degradation and Mobilization—EBS Transport Coupling)—The following outputs are passed from the waste form degradation and mobilization model components to the EBS transport submodel for each representative waste package group in seeping and nonseeping environments, and for each percolation subregion (Figure 2.4-112):

- The mass of radionuclides available for transport through the EBS
- The concentrations limits of radionuclides inside a failed waste package and in the invert
- The concentrations of radionuclides (plutonium and americium) irreversibly attached (embedded) in waste-form colloids
- The concentrations of radionuclides (americium and plutonium) that are irreversibly attached to iron oxyhydroxide colloids
- The concentrations of radionuclides (americium, plutonium, protactinium, cesium, thorium, tin, radium, uranium, and neptunium) that are reversibly attached to colloids.

2.4.2.3.2.1.8 Engineered Barrier System Transport

The EBS transport submodel (SNL 2007k, Section 6) is described in Section 2.3.7.12. The EBS transport submodel calculates the time-dependent mass flux of radionuclides from failed waste packages through the EBS to the unsaturated zone transport submodel once the waste form starts degrading and transport becomes possible. The transport calculations are based on various time-dependent inputs (provided by various submodels described earlier), such as:

- Water flow through failed waste packages and the underlying invert
- Temperature, relative humidity, saturation in the invert, and imbibition flux from the host rock exiting the invert under gravity-driven flow
- The waste form dissolution rates for the various waste forms
- Solubility limits
- Colloidal concentrations and sorption coefficients required to define the mobilized concentration of colloid associated radionuclides.

The EBS consists of the emplacement drift, the drip shield, the waste package on an emplacement pallet, and an invert constructed with steel supports and filled with crushed tuff between the steel framework. The conceptual model of radionuclide transport through the EBS discretizes the system into three primary domains: (1) the waste form domain; (2) the waste package corrosion products domain; and (3) the invert domain composed of crushed tuff. An additional domain, the EBS-unsaturated zone interface, is included beneath the invert domain to establish a boundary condition for calculating the diffusive flux from the invert to the unsaturated zone and to compute the mass flux fraction going into the unsaturated zone fracture and matrix continua. The waste form and corrosion products domains are more specifically described below by the waste package type (commercial SNF or codisposal) (SNL 2007k, Section 6.5.2.5):

- Commercial SNF waste package
  - Commercial SNF Waste Form Domain—Waste form (Commercial SNF rods), basket tubes (Stainless Steel Type 316), absorber plates (Stainless Steel Type 304B4)
  - Corrosion Products Domain—TAD canister (Stainless Steel Type 316), guide assembly (Stainless Steel Type 316), inner vessel (Stainless Steel Type 316)
- Codisposal waste package
  - HLW glass waste form subdomain—HLW glass, HLW glass canisters (Stainless Steel Type 316)
  - DOE SNF waste form subdomain—DOE SNF (SNF and Stainless Steel Type 304), DOE SNF canister (Carbon Steel Type A 516, Stainless Steel Type 304, and Stainless Steel Type 316)
  - Corrosion products domain—Divider plate (Carbon Steel Type A 516), inner brackets (Carbon Steel Type A 516), outer brackets (Carbon Steel Type A 516), support tube (Carbon Steel Type A 516), inner vessel (Stainless Steel Type 316).

Radionuclide transport through each domain occurs by advection and diffusion (SNL 2008a, Figure 6.3.8-4). After the waste package fails (breached by either corrosion, seismic damage, igneous intrusion, or early failure mechanisms), a portion of the water that may flow through the drip shield could enter the waste package, mobilizing radionuclides from the degraded waste form, and transporting these radionuclides into the unsaturated zone. Diffusion is the primary transport mechanism when the water flux into the waste package is negligibly small or zero. Advective transport becomes important when there is appreciable flow through the waste package. Advective transport can only occur after the drip shield failure and after general corrosion patch failures have occurred on waste packages or when the waste package is damaged by igneous intrusion and ruptured or punctured by a seismic event. In the EBS transport submodel, diffusive transport along the surface of the emplacement pallet is conservatively ignored and the waste packages are modeled as being in direct contact with the invert (SNL 2007k, Sections 6.3.1.1).

Conceptually, the waste form domain represents that portion of the fuel that has degraded to rind (alteration product), along with corrosion products from degradation of the steel basket structure that surrounds the fuel assemblies or canisters that surround the glass waste. The waste form degradation processes include dissolution of commercial SNF and HLW glass, rapid degradation of DOE SNF, and formation of waste form colloids from the alteration of HLW glass and SNF (Section 2.4.2.3.2.1.7). Radionuclides may be reversibly sorbed or embedded irreversibly in the waste form colloids. The amount of each radionuclide mobilized from a waste form is limited by the solubility of the radionuclide in water and the amount of the radionuclide associated with suspended colloids. Colloids can be important to the total system performance because they can increase the mass release of radionuclides from the waste package. Both dissolved and colloid associated radionuclide mass are transported by advection and/or diffusion to the waste package corrosion products domain.

The codisposal waste package has two waste types (HLW and DOE SNF) and thus the codisposal waste form domain is divided into two subdomains, one for the HLW and the other for the DOE SNF. This is required because the representative codisposal waste package for EBS transport calculations consists of five cylindrical canisters containing HLW glass logs surrounding a central canister of DOE SNF (SNL 2007k, Section 6.3.3.1). After the waste package is breached, the HLW glass degrades at a specified rate to a clay like alteration product. However, the DOE SNF degrades almost instantaneously to oxides and hydrated oxides of uranium. In addition to the ongoing fuel degradation, the steel support framework inside the inner vessel of the waste package will corrode gradually, allowing the HLW glass logs to collapse slowly within the inner vessel, such that the general cylindrical shape of the glass logs is retained. On the other hand, because DOE SNF degrades almost instantaneously, and with no credit taken for the canister, it is conceptualized that DOE SNF would not retain its cylindrical geometry, and may settle near the bottom of the interior of the inner vessel. The transport characteristics are expected to be different in each waste form subdomain. Because the EBS transport submodel is a one-dimensional model, the two waste form subdomains are modeled sequentially, such that the HLW domain is upstream of the DOE SNF domain. The mass released from the degradation of HLW glass moves to the DOE SNF domain by advection and/or diffusion and then is transported to the corrosion products domain. Because of the one dimensional assumption, each waste form subdomain and the corrosion products domain have the same seepage and/or condensation flux (SNL 2007k, Section 6.5.2.1.2).

Conceptually, the corrosion products domain is composed of corroded internal components of the waste package, predominantly from the inner vessel and TAD canister. The internal components of a breached waste package will degrade slowly over thousands of years, forming corrosion products (assumed to be iron oxyhydroxides) that can sorb and delay the release of radionuclides from the waste package (SNL 2007k, Sections 6.4.2, 6.3.4.2, and 6.5.2.2.1). Degradation of the internal waste package components results in two types of materials: (1) stationary iron oxyhydroxide corrosion products that are assumed to remain in the waste package; and (2) iron oxyhydroxide colloids that are mobile and can move out of the waste package. A mechanistic surface complexation-based competitive sorption model is developed in the corrosion products domain for modeling sorption of dominant actinides in the inventory (uranium, neptunium, plutonium, americium, and thorium) to both the stationary corrosion products and iron oxyhydroxide colloids over the range of pH and P_{co_2} expected in the repository over the simulation timescales. The mass of corrosion products in a breached waste package varies over time, from zero when the waste package is first breached to a maximum amount (SNL 2007k, Table 6.3-8) when all of the steel in the domain is corroded. The mass, at any given time, is computed by linearly interpolating over the lifetime of each of the two major types of steel comprising the internal components of a waste package-carbon steel and stainless steel (SNL 2007k, Section 6.5.2.2.1). Only the mass of corrosion products contributed by goethite and ferrihydrite is used in competitive sorption calculations of radionuclides, while for water vapor adsorption calculations the entire mass of corrosion products is used, including nickel oxides and chromium oxides (SNL 2007k, Section 6.3.4.2.1). Reversible sorption of radionuclides onto groundwater (seepage-water) colloids and waste form colloids that are passing through the corrosion products domain is also modeled (SNL 2007k, Section 6.3.4.2).

In the invert domain of the EBS transport submodel (SNL 2008a, Section 6.3.8.2.4), radionuclide transport occurs by both advection and diffusion and the mass flux of radionuclides (in both the dissolved state and associated with colloids) is passed to the unsaturated zone. Reversible sorption of radionuclides on the crushed tuff is also considered. The EBS-unsaturated zone interface domain is conceptualized to apply an effective semi-infinite zero-concentration boundary condition for computing the diffusive flux from the invert to the unsaturated zone. It is also used to calculate the mass fraction going into the unsaturated zone fracture and matrix continua (SNL 2007k, Section 6.6.3.3).

For each transport domain, the following one-dimensional mass balance equations are considered (SNL 2007k, Section 6.5.1.2):

- Transport of dissolved radionuclide species and radionuclide species that are reversibly sorbed onto three types of colloids: iron oxyhydroxide, waste form, and groundwater

- Transport of kinetically (and irreversibly) sorbed radionuclide species on iron oxyhydroxide colloids

- Kinetic sorption of radionuclide species onto stationary corrosion products in the waste package

- Transport of embedded (irreversibly sorbed) radionuclide species in waste form colloids

- Decay and ingrowth for a given radionuclide.

The EBS transport model is implemented using the cell pathway capability in the GoldSim software (GoldSim Technology Group 2007a). Each domain is modeled by one or more cells and an array of cells is used to model part of the near field unsaturated zone below the invert. As mentioned above, modeling the near field unsaturated zone serves to establish an effective far-field zero concentration boundary for computing the diffusive flux from the invert to the unsaturated zone (SNL 2007k, Section 6.5.2.6). A dual continuum approach for modeling the near field unsaturated zone is implemented by creating an overlapping continuum of unsaturated zone matrix and fracture cells (SNL 2008a, Figure 6.3.8-9).

The number of cell pathways in the finite difference network and the discretization of the cells are chosen in such a way as to capture the physical and chemical properties of the EBS components with respect to radionuclide transport. The cell pathway acts as an equilibrium batch reactor, where radionuclide mass is modeled as instantaneously and completely mixed and partitioned among all media, fluid or solid, within the cell (SNL 2007k, Section 6.5.2.7.1). Both advective and diffusive transport mechanisms can be explicitly represented using the cell pathways. When multiple cells are linked together via advective and diffusive connections, the performance of the cell network is mathematically described using a coupled system of differential equations, and is mathematically equivalent to a finite difference network. The GoldSim software numerically solves the coupled system of equations to compute the radionuclide mass present in each cell and the mass fluxes between cells as a function of time. Both initial and boundary conditions for a cell are defined explicitly, and systems of varying geometry can be modeled.

The EBS transport calculations in various domains of the cell network are performed for a representative commercial SNF and codisposal waste package located in each percolation subregion for the seep and nonseep environments. The mass fluxes computed for the representative waste package are scaled by the number of failed waste packages (GoldSim Technology Group 2007a, Chapter 5) for the given seep and nonseep environment to determine the total mass released to the unsaturated zone transport model. Radionuclide transport is assumed not to occur when the temperatures are greater than 100°C due to a lack of bulk water and the lack of a continuous water film on the degradation products. In addition, transport inside the waste package is not allowed when waste package relative humidity is less than 95% and there is no flow through the waste package or when the flow rate is less than 0.1 L/yr (Section 2.4.2.3.2.1.7). For all other thermal conditions, a continuous thin film of water is assumed inside the waste package, which behaves as bulk liquid in order to allow radionuclides to dissolve and diffuse, including the colloids (SNL 2007k, Section 5.5; SNL 2007h, Section 6.10.9.1[a]). Species-dependent free-water diffusion coefficients are applied that are corrected for tortuosity and temperature for each domain. The diffusion coefficient for the colloids is separately computed based on the sampled size of the colloids (SNL 2007k, Section 6.3.4.4).

Several epistemic uncertainties related to transport through the waste packages and the invert are represented by distributions sampled once per realization (SNL 2008a, Section 6.1.4.8). In the waste packages, these include: (1) the water adsorption isotherm parameters (used to determine the water content in the pore volume of the degraded waste forms and corrosion products); (2) surface properties such as specific surface area and sorption site density of the stationary corrosion products; (3) corrosion rate of in-package stainless-steel and carbon-steel components; (4) diffusive path length from the waste package to the invert; and (5) uncertainty in pH from surface-complexation calculations that determine the pH in the stationary corrosion products domain, which in turn determines radionuclide solubilities and colloid stability. In the invert, these include radionuclide sorption coefficients (empirically based) and an invert diffusion coefficient for radionuclide diffusion.

The diffusive transport across the boundary between the single-continuum invert domain and the dual continuum unsaturated-zone domain is derived by enforcing radionuclide mass flux continuity between the invert and the host rock with harmonic averaging of the effective diffusivity, which determines the proportion of invert diffusive releases transported into the host-rock matrix continuum versus that transported into the host-rock fracture continuum. This partitioning of the advective mass flux is imposed as follows: the total advective mass flux leaving the invert is based on the combined fluid flux in the invert (a combination of seepage, condensation, and imbibition flux) but when the advective mass flux is passed to the unsaturated zone, it is partitioned so that the advective fraction carried by the imbibition flux is sent to the unsaturated zone matrix, while the remainder (seepage plus drift-wall condensation) is sent to the unsaturated zone fractures. This partitioning is based on the results of the multiscale thermal-hydrologic model modeling for imbibition flux, which is described in Section 2.4.2.3.2.1.2. The calculated radionuclide mass flux crossing the boundary between the single-continuum invert domain and the dual continuum EBS unsaturated zone domain is passed directly to the coupled, three-dimensional, dual-permeability model, FEHM used for unsaturated zone transport as a function of time for each representative waste package (SNL 2008a, Section 6.3.8.3).

Three different types of radionuclide mass fluxes are passed to the unsaturated zone transport submodel. The first type of mass flux is applicable for all radionuclides transported in the TSPA model. This flux includes all of the radionuclide mass that exists in the dissolved state or is reversibly sorbed onto the three different colloid types: groundwater, waste form, and iron oxyhydroxide. After it is input to the unsaturated zone transport submodel, this mass is repartitioned onto the groundwater colloids in the unsaturated zone based on the sampled colloid concentration and sorption coefficients defined for the unsaturated zone transport submodel. Plutonium and americium irreversibly sorbed onto waste-form and iron oxyhydroxide colloids form the basis for the next two mass flux types. These masses are defined in the EBS transport submodel as distinct species. After exiting the EBS, and before being passed to the unsaturated zone transport submodel, these two types of irreversibly sorbed radionuclide mass are added together for each irreversibly sorbed radionuclide. The total irreversibly sorbed mass for either plutonium or americium species is then repartitioned onto a fast and a slow colloid fraction for transport through the unsaturated zone and saturated zone. The fraction of irreversible colloids that travel unretarded through the unsaturated zone and saturated zone is called the fast fraction, while the remaining colloids that undergo some degree of retardation are called the slow fraction. A value of 0.00168 is used in the TSPA to represent the fast fraction of colloids. The remaining fraction of 0.99832 is transported as the slow fraction (SNL 2008a, Section 6.3.8.3).

The radionuclide mass flux, calculated by the EBS transport submodel and released from the five repository percolation subregions, enters the unsaturated zone repository release nodes (FEHM grid nodes) that reside within the subregions. The number of unsaturated zone repository release nodes receiving radionuclide mass depends on the number of waste packages that have failed at each time step in a given percolation subregion. To simulate waste packages failing at different locations and releasing mass in a given percolation subregion, the repository release nodes in the unsaturated zone corresponding to that percolation subregion are randomly selected without replacement (SNL 2008a, Section 6.3.9.3). If the number of failed waste packages in a group exceeds the number of unsaturated zone repository release nodes in a percolation subregion, releases are allocated evenly to all unsaturated zone repository release nodes in the percolation subregion. In order to model releases from EBS for the early-failure cases, the mass release is uniformly distributed over unsaturated zone repository release nodes associated with the specific percolation subregion (SNL 2008a, Section 6.1.2.4.2[a]). In particular, in both the waste package and drip shield early failure modeling cases, aleatory uncertainty in the location of the early failed waste package within its assigned percolation bin is implicitly considered by assigning the mass released from the waste package uniformly across the bin. The uniform mass release is implemented by distributing the mass released by the waste package equally to all the unsaturated zone particle tracking model's repository release nodes (Section 2.4.2.3.2.1.9) associated with the specific percolation subregion.

The following time-dependent outputs are calculated for each waste package group in each percolation subregion.

Output 17 (EBS Transport–Unsaturated Zone Transport Coupling)—The following outputs are passed from the EBS transport submodel to the unsaturated zone transport submodel for each for each percolation subregion (releases are first summed over seeping environments and fuel type):

- For each distinct radionuclide species, the radionuclide mass release rate to the unsaturated zone matrix and fracture continua for each of two states: (1) dissolved plus reversibly sorbed onto colloids; and (2) irreversibly sorbed onto colloids
- For each distinct radionuclide species, the fraction of radionuclide mass released into the fracture continuum versus the matrix continuum of the unsaturated zone release nodes.

2.4.2.3.2.1.9 Unsaturated Zone Transport

Unsaturated zone transport is modeled within the TSPA model by the unsaturated zone transport submodel. The technical bases and model abstractions that support the unsaturated zone transport submodel are described in Section 2.3.8. Consistent with the unsaturated zone flow submodel, the unsaturated zone transport submodel is a dual-continuum model. The unsaturated zone transport submodel implements a particle-tracking transport algorithm (SNL 2008e, Sections 6 and 8) that is part of the three-dimensional, dual-permeability, finite-element software code, FEHM. In the unsaturated zone transport submodel, fracture and matrix transport are coupled and calculated using the FEHM residence-time transfer-function particle-tracking technique (SNL 2008e, Section 6.4). This technique is a cell-based approach (Section 2.3.8.5.1) in which particles move from cell to cell in the FEHM numerical grid. Particle movement from cell to cell is computed probabilistically based on flow balance, dispersivity, and matrix diffusion. The fracture matrix interactions are evaluated using transfer functions when diffusive transport between fracture and matrix is simulated. The transfer functions used in the TSPA model are defined using dual-permeability numerical solutions of the transport equations for parallel flow in a fracture and adjacent rock matrix and diffusion normal to the flow direction (SNL 2008e, Appendix C).

The 16 steady-state unsaturated zone flow fields (Section 2.4.2.3.2.1.1) representing each combination of infiltration scenario and climate change plus the post-10,000-year percolation scenario, are accessed directly by the TSPA model. The FEHM particle tracking code transports particles with the same dual-permeability spatial grid as used in the unsaturated zone flow model component, including the same infiltration and liquid saturation values. When climate changes, the TSPA model uses the unsaturated zone flow fields associated with the new climate for the given infiltration scenario.

The FEHM particle tracking code receives inputs at run time directly from the TSPA software code, GoldSim, and from a set of external files. At run time, GoldSim passes direct inputs to FEHM, such as the flow-field index (used to select the desired unsaturated zone flow field abstraction based on climate state and infiltration scenario), the number of radionuclides, and the number of repository zones (i.e., percolation subregions) (SNL 2008a Section 6.3.9.3). GoldSim also passes inputs from the EBS, such as the combined EBS releases for both waste package types (from each of the five percolation subregions), the ratio of the EBS release applied to fractures to the total EBS release (which is used to apportion the released radionuclides between fracture and matrix nodes), and the total number of failed commercial SNF waste packages and codisposal waste packages in each repository subregion (SNL 2008a, Section 6.3.9.3). The FEHM DLL receives new inputs from GoldSim at every time step in each realization. FEHM must also read in a set of external files that provides many inputs including control parameters, deterministic transport parameters, and values for all the stochastic transport parameters. As noted in Section 2.4.2.3.2.1.8, the mass release rate of dissolved radionuclides and reversibly sorbed radionuclide mass on colloids from the EBS are combined and released to the unsaturated zone where this mass is reequilibrated within the unsaturated zone between the aqueous phase and the groundwater colloids modeled in the unsaturated zone. Americium and plutonium isotopes that are irreversibly sorbed onto colloids are transported separately as fast and slow fractions.

The following unsaturated zone transport processes are simulated:

- Advective-dispersive transport of dissolved radionuclides in the fracture and matrix continua and between continua
- Fracture-matrix interaction and matrix diffusion
- Sorption of dissolved radionuclides in the matrix continuum
- Advective-dispersive transport of colloids with radionuclides attached (transport of colloids is explicitly simulated when radionuclides are considered to be irreversibly attached and implicitly simulated in conjunction with the transport storage term when radionuclides are considered to be reversibly sorbed)
- In the fracture continuum retardation of colloids, on which radionuclides are reversibly and irreversibly sorbed
- Colloid size exclusion at fracture-matrix continua interfaces
- Radioactive decay and ingrowth
- Climate change and its effect on fluid flow rates in the unsaturated zone
- Rise in water table elevation and its effect on radionuclide release to the saturated zone.

For each realization, a set of uncertain material properties for unsaturated zone transport is sampled and the values or parameters generated from the sampled values are used in the unsaturated zone particle tracking code. These epistemic uncertainty distributions (SNL 2008a, Section 6.3.9) include matrix adsorption coefficients, matrix diffusion coefficients (as generated from sampled values of tortuosities and species-dependent values of free-water diffusion coefficients), fracture apertures (as generated from sampled values of fracture porosity and fracture frequency), active fracture model gamma parameters, colloid equilibrium sorption parameters (as generated from sampled values of sorption coefficients onto colloids and colloid concentrations), and colloid retardation factors for unsaturated zone transport.

.

Some of the uncertainty in unsaturated zone transport results from uncertainties passed to the unsaturated zone transport submodel from other submodels. For example, there is uncertainty in infiltration and unsaturated zone flow from the site-scale unsaturated zone flow process model; uncertainty in the number of failed waste packages from the waste package and drip shield degradation model component; and uncertainty in numerous EBS parameters and processes used to define the radionuclide source term received from the EBS transport submodel. These uncertainties from upstream submodels are passed to the unsaturated zone transport submodel either implicitly through the passing of the radionuclide fluxes and ratios of fluxes applied to the unsaturated zone fractures versus total fluxes (fractures and rock matrix) from GoldSim to FEHM, or explicitly through the passing of data, such as the number of waste packages failed in each percolation subregion or indices denoting which infiltration scenario to apply (10th percentile, 30th percentile, 50th percentile, or 90th percentile scenario). For each sampled infiltration scenario, a set of four steady-state flow fields corresponding to present day, monsoonal, glacial-transition, and post-10,000-year flow fields is read in by the FEHM particle tracking software for that realization. As described in Section 2.4.2.3.1.7, because unsaturated zone transport processes tend to be more sensitive to rock property uncertainties, some unsaturated zone rock properties are treated as uncertain for the unsaturated zone transport submodel, but not for the site-scale unsaturated zone flow process model (e.g., active fracture gamma—Section 2.3.8.5.2.4). Also, some of the uncertain parameters derived for the unsaturated zone transport submodel, such as matrix sorption and matrix diffusion coefficients, are used in the EBS transport submodel for sections of cell networks representing the unsaturated zone directly below the repository (SNL 2008a, Section 6.3.8.2.4).

In the unsaturated zone transport submodel, radionuclide sorption on the rock matrix is approximated using a linear, equilibrium sorption model characterized by a single parameter, the sorption coefficient or K_d for each radioelement. A set of three probability distributions for the K_ds have been developed for each radioelement (Section 2.3.8.3.1). Each set of K_ds describes the radioelement sorptive behavior in each of three major rock types (vitric, devitrified, and zeolitic tuffs) in the unsaturated zone (SNL 2007w, Section 6.1.2.3). These effective sorption coefficients are a function of many factors, including mineralogy, groundwater aqueous chemistry, and heterogeneity at scales smaller than those considered in the numerical model.

In the TSPA model, unsaturated matrix diffusion coefficients (Section 2.3.8.5.2.4) are generated as the product of the matrix tortuosities for specified rock groups and the free-water diffusion coefficients for the elements considered (SNL 2008e, Section 6.5.5 of Addendum 1). The tortuosities are based on a correlation between matrix diffusion, porosity, and saturated permeability developed from diffusion data in saturated samples by Reimus et al. (2007). To adapt the relationship for the unsaturated zone, porosity is replaced by water content, and saturated permeability is replaced by effective permeability.

Part of the conceptual model upon which the unsaturated zone transport submodel is based is the active fracture model of Liu et al. (1998). The active fracture model (Section 2.3.8.4.1) takes into consideration the fact that due to the nonlinearities associated with unsaturated flow, only a portion of fractures in the unsaturated zone fracture network are subject to water flow, while the others are bypassed. The active fracture model assumes that, because only a portion of the fractures in a network have water flowing through them, there is an impact on the effective fracture spacing, the fracture/matrix interface area, and the number of active fractures in a grid block. In the TSPA model, the spacing between flowing fractures is calculated as a function of the geometric fracture spacing, fracture saturation, fracture residual saturation, and the active fracture model parameter, γ. In the TSPA model, a constant fracture residual saturation of 0.01 is used for all layers (SNL 2008e, Section 6.5.6).

In addition to adjusting the spacing between flowing fractures, the active fracture conceptualization calls for an adjustment to the interface area across which matrix diffusion occurs. The interface adjustment accounts for the reduction of the wetted area within an individual fracture and for the reduction in area caused by the smaller number of active fractures. This adjustment to the interface area is a reduction by a factor of the effective saturation (SNL 2008e, Appendix C). The area reduction associated with the active fracture model is a conservative representation for situations in which radionuclide mass is introduced into the fracture continuum, which occurs for all waste packages in seeping zones (SNL 2008a, Section 6.3.9.2).

In the TSPA model, except in fault zones, where the medium is treated as a fracture continuum with low effective porosity and sorption on the rock surfaces, fracture retardation factors are set to 1.0. In the TSPA model this causes there to be no sorption on fracture surfaces of radionuclides with respect to transport time through the unsaturated zone fractures (SNL 2008e, Section 6.5.8).

As described previously, reversible and irreversible sorption of radionuclides onto colloids is accounted for in the unsaturated zone transport submodel. When the sorption process is irreversible, a very large number (10^{20}) is assigned to the colloid equilibrium sorption coefficient, K_c (SNL 2008e, Sections 6.4.5 and 6.5.12), which represents the ratio of radionuclide mass transported colloidally versus the mass transported as dissolved species. For reversible radionuclide sorption on the colloids, the K_c values are calculated by multiplying a radionuclide sorption coefficient for a species onto a colloid by the colloid concentrations in the water.

A colloid retardation factor, R_{coll}, is used in the TSPA model to simulate the impact of reversible filtration of the reversible and irreversible colloids in fractures (SNL 2008a, Section 6.3.9.2). Colloid transport data obtained under saturated conditions from the C-Wells and other field and lab tests provide a conservative measure of unsaturated zone colloidal transport (SNL 2007x, Sections 6.3 and Appendix D). The characterization of colloid transport is believed to be conservative because colloidal transport under saturated conditions would be greater than colloidal transport under unsaturated conditions (Section 2.3.8.3.4). Thus, the cumulative distribution function for colloid retardation factors in the unsaturated zone is consistent with the cumulative distribution function for the colloidal retardation factor in volcanic units for the saturated zone. This cumulative distribution function is applied to the "slow" fraction of colloids described in Section 2.4.2.3.2.1.8. There is also a "fast" fraction of colloids escaping retardation due to physical and chemical processes. In the TSPA model, this fraction is equal to 0.00168 and is based on a reasonably conservative estimate of the residence time of colloid particles in the natural system (SNL 2008e, Section 6.5.13; SNL 2008a, Section 6.3.8.3). Fast-fraction colloids do not sorb on fracture surfaces ($R_{coll} = 1$) and do not participate in matrix diffusion processes.

In the unsaturated zone transport submodel, the longitudinal fracture dispersivity is set to 10 m, which represents a value chosen from the lower end of the field studies (SNL 2008e, Section 6.5.2). Compared to the effects of matrix diffusion and the large-scale heterogeneities in the unsaturated zone, dispersivity effects are expected to have a small influence on the breakthrough curves.

Outputs from the unsaturated zone transport submodel at each time step are radionuclide mass release rates from the fracture and matrix continua at the base of the unsaturated zone model domain (i.e., at the water table or unsaturated zone/saturated zone interface). These radionuclide mass releases for each species are grouped or integrated spatially into four zones, called unsaturated zone collecting bins, to be transferred by four sets of saturated zone breakthrough curves in the saturated zone transport submodel (SNL 2008a, Section 6.3.9.3). When the climate changes, the elevation of the water table is instantaneously set to the elevation associated with the new flow field, where the water table has been set to a minimum of 850 m above mean sea level (Section 2.3.8.5.3), representing an up to 120-m water table rise for any climate past the present-day climate (i.e., at any time 600 years after waste emplacement). Any radionuclides in the unsaturated zone below the new and higher water table elevation when the climate changes are immediately removed from the unsaturated zone and provided as inputs to the saturated zone flow and transport submodel (SNL 2008a, Section 6.3.9.3).

As mentioned above, radionuclide releases from the unsaturated zone to the saturated zone are grouped into four unsaturated zone collecting bins. The total radionuclide mass release rate from the base of the unsaturated zone grid for matrix and fracture continua in each of these four collecting bins is released to a single location in the equivalent saturated zone source region. The location of the random release point for each realization in each saturated zone source region is selected during the generation of the saturated zone convolute abstraction breakthrough curves using a three-dimensional saturated zone convolution integral transport method, performed by the software code SZ_Convolute. The location of the unsaturated zone release point used in each realization is, therefore, implicit to the sampled breakthrough curve used in the saturated zone convolution integral approach (Section 2.4.2.3.2.1.10). The sum of the fracture and matrix radionuclide mass release rates is released from the four unsaturated zone collecting bins to four corresponding saturated zone capture zones and then fed to the three-dimensional saturated zone convolution integral transport model, performed by the software code SZ_Convolute, and to the one-dimensional saturated zone pipe transport model at each TSPA model time step (Sections 2.3.9.3.4.1 and 2.3.9.3.4.2).

Output 18 (Unsaturated Zone Transport–Saturated Zone Transport Coupling)—The following outputs are passed from the unsaturated zone transport model component to the saturated zone flow and transport submodel (Figure 2.4-112; SNL 2008a, Section 6.1.4.9):

- For each distinct radionuclide species and unsaturated zone outflow region, the summed release rate from the unsaturated zone matrix and fracture continua for the radionuclide mass dissolved plus reversibly sorbed onto colloids

- For certain radionuclide species, as appropriate, and for each unsaturated zone outflow region, the summed mass release rate from the unsaturated zone matrix and fracture continua, for each of two states: (1) radionuclide mass irreversibly sorbed onto the slow fraction of colloids and (2) radionuclide mass irreversibly sorbed onto the fast fraction of colloids.

2.4.2.3.2.1.10 Saturated Zone Flow and Transport

The saturated zone flow and transport submodel for the TSPA model is described in Section 2.3.9. The saturated zone flow and transport submodel evaluates the transport of radionuclides from their introduction at the water table below the repository to the accessible environment located at the southern boundary of the controlled area at 36° 40′ 13.6661″ North latitude (10 CFR 63.302), approximately 18 km from the repository footprint in the predominant direction of groundwater flow. The groundwater used annually by the hypothetical farming community is assumed to contain all radionuclide mass in the saturated zone that annually crosses the regulatory boundary (i.e., the captured radionuclide mass is mixed in the 3,000 acre-ft of annual groundwater usage) (10 CFR 63.312(c)). For the saturated zone flow and transport abstraction used in the TSPA model (SNL 2008f, Section 6.3.1), groundwater flow between the repository and the accessible environment is modeled using three-dimensional, steady-state flow conditions. A dual-porosity representation is used for the fracture network in the volcanic rocks beneath the repository, while the alluvium and valley-fill deposits are modeled as single-porosity media.

Several processes are involved in the transport of radionuclides through the saturated zone and are explicitly included in the TSPA model simulations, as described in Section 2.3.9. These are advection, dispersion, matrix diffusion in fractured media, sorption of radionuclides, colloid-facilitated transport, radioactive decay, and radioactive ingrowth.

- Advective transport is the primary process for the transport of radionuclides from the saturated zone to the accessible environment. In the volcanic hydrogeologic units in the first part of the saturated zone pathway, advection only occurs in the fracture continuum (i.e., in the fracture continuum portion of the dual-porosity model) due to the very high contrast in permeability between the fractures and the rock matrix. The alluvium at the end of the saturated zone pathway is modeled with advective transport through a homogeneous single-porosity medium.

- Dispersion of radionuclide mass, which includes hydrodynamic dispersion and molecular diffusion, occurs in the fractured volcanic units and in the alluvium, with longitudinal dispersion typically much greater than transverse dispersion.

- Matrix diffusion in fractured volcanic units causes transfer of dissolved radionuclide mass from the flowing groundwater within fractures to the relatively stagnant groundwater contained in the pores of the rock matrix. The mass transfer, which could be in either direction, is a function of the concentration of the radionuclide in the fractures and matrix. The process of matrix diffusion of colloids is considered to be small and thus is not included in the TSPA model (SNL 2008a, Section 6.3.10.1).

- Radionuclide sorption in the fractured volcanic zones occurs in the rock matrix only. In the alluvium, sorption occurs in the effective porosity of the alluvium.

- Colloid-facilitated transport can occur by two modes: (1) when radionuclides are reversibly sorbed onto colloids and (2) when radionuclides are irreversibly attached onto colloids. The "slow" fraction of the colloids with irreversibly attached radionuclides (Section 2.4.2.3.2.1.9) undergoes filtration during transport, which is represented by a retardation factor in the saturated zone flow and transport model component. The fast fraction of colloids (Section 2.4.2.3.2.1.9) is assumed to have no filtration or other such retardation mechanisms.

- Radioactive decay and ingrowth occurs for all radionuclides. The two different treatments of decay and ingrowth for various radionuclides (i.e., the use of the three-dimensional versus one-dimensional transport models) are described below.

In addition to the radionuclide mass flux from the unsaturated zone (Section 2.4.2.3.2.1.9), the saturated zone flow and transport submodel receives additional inputs from several other sources (Section 2.3.9.3.4.1.1). The climate analysis (BSC 2004c) provides the duration of climate states, while estimates of the scaling factors for groundwater flow rates in the saturated zone under future climatic conditions are based on several sources, including simulations of net infiltration in the area near Yucca Mountain (SNL 2008g), weighting factors for alternative infiltration maps derived from calibration of the site-scale unsaturated zone flow model (SNL 2007b), and corroborative information from simulations using the Death Valley regional groundwater flow model (D'Agnese et al. 1999). In particular, based on the ratio of infiltration fluxes in different climate states and other considerations, when climate change occurs, the saturated zone flow and transport submodel accounts for the change in saturated-zone specific discharge through a set of climate-state-specific, groundwater-flow scaling factors (SNL 2008f, Section 6.5[a]). The multipliers on the constant specific discharge are 1.9 for the monsoon climate and 3.9 for the glacial transition climate. The glacial transition multiplier is also used for the post-10,000-year period climate. The climate state groundwater flow scaling factors are based on mean case conditions and do not include uncertainty in groundwater flux estimates within a given climate state because this uncertainty is captured by uncertainty in the distribution of the groundwater specific discharge multiplier. The uncertainty in this multiplier is applied to all of the climate states.

The TSPA saturated zone flow and transport submodel uses two abstractions to describe saturated zone flow and transport: (1) a three-dimensional saturated zone flow and transport abstraction; and (2) one-dimensional saturated zone flow and transport abstraction. The range of applicability of these two abstractions is related to ingrowth, as explained below. The three-dimensional abstraction is preferred because of its more robust methodology for representing physical-chemical processes and flow paths; however, the one-dimensional abstraction must be used for many of the radioactive decay products produced by ingrowth during transit through the saturated zone, as discussed below.

Twenty-seven of the 31 screened-in radionuclides are tracked and transported by the saturated zone transport submodel. The four radionuclides not tracked and transported are ^{245}Cm, ^{241}Pu, ^{227}Ac, and ^{228}Ra—secular equilibrium with the parent radionuclide is assumed for ^{227}Ac and ^{228}Ra; the half-life of ^{241}Pu is too short for it to reach the accessible environment, and ^{245}Cm has a small initial inventory (but its decay to ^{241}Am is accounted for in the source term) (SNL 2008a, Table 6.3.7-6). The radionuclides tracked by the saturated zone flow and transport model component are divided into 12 groups based on their transport characteristics. These 12 groups and their modes of transport are summarized in Table 2.3.9-16. The 12 groups of radionuclides are divided among three modes of radionuclide transport: (1) solute transport, (2) colloid-facilitated transport of radionuclides reversibly attached onto colloids, and (3) colloid-facilitated transport of radionuclides irreversibly attached onto colloids. For example, the nonsorbing radionuclides of carbon, technetium, iodine, and chlorine are grouped together because their migration is identical. Similarly, the radionuclides of americium, thorium, and protactinium reversibly attached onto colloids are grouped together because of their similar sorption characteristics. The radionuclides of plutonium and americium are transported as either reversibly and irreversibly attached onto colloids (SNL 2008f, Section 6.5.3[a]).

Using the 12 representative radionuclide groups, the three-dimensional saturated zone flow and transport process model (SNL 2008f) is run outside the TSPA model. It is used to perform a series of probabilistic transport simulations for an instantaneously applied unit mass to obtain cumulative mass breakthrough curves at the 18-km regulatory boundary for each of the 12 representative radionuclide groups. For each realization, parameters containing epistemic uncertainty are sampled and used in the three-dimensional and one-dimensional saturated zone flow and transport models (SNL 2008f, Table A-1[b]). Two hundred realizations of the three-dimensional saturated zone flow and transport process model for the four source regions provide 9,600 breakthrough curves at the regulatory boundary (i.e., 12 × 200 × 4). The uncertain parameters include: (1) effective porosity in the alluvium; (2) values of the distribution coefficient, K_d, in the tuff and alluvium; (3) parameters used for irreversible and reversible sorption onto colloids; (4) longitudinal dispersivity; (5) transverse dispersivity; (6) point source location within one of the four source regions; (7) horizontal permeability anisotropy; (8) fraction of the groundwater flow path within the alluvium; and (9) parameters related to matrix diffusion in the tuff (SNL 2008f, Table A-1[b]).

The unit mass breakthrough curves generated by the three-dimensional saturated zone flow and transport process model, in combination with a convolution integral method, are used by the three-dimensional saturated zone flow and transport abstraction in the TSPA model to calculate transport in the saturated zone to the accessible environment. The convolution technique, performed by the SZ_Convolute DLL, inherently assumes the system being simulated exhibits a linear response to the input function and a steady-state flow condition in the saturated zone. The convolution integral method takes a time-dependent, point-source radionuclide mass from the unsaturated zone transport submodel, which represents the total mass release rate over one of the four unsaturated zone collector regions, and integrates it with the appropriate unit mass breakthrough curve for that radionuclide to determine the mass flux of radionuclides across the 18-km boundary. The areal placement of the unit mass point source in each of the four saturated zone source regions varies randomly from realization to realization, reflecting uncertainty in the location of radionuclide release from waste packages and transport pathways in the unsaturated zone. Changes in recharge and groundwater flux in the saturated zone associated with climate variations are approximated as step changes from one steady-state flow condition to the next. There are separate convolution integral calculations for each radionuclide and each of the four source regions.

One limitation of the convolution integral method in the three-dimensional saturated zone flow and transport abstraction is that, while it accounts for radioactive decay, it cannot account for ingrowth. Thus, it is only strictly applicable for some of the radionuclides (i.e., the top parents in the various decay chains). However, its applicability is extended to some radioactive decay products by using an "inventory boosting" technique. For example, consider ^{237}Np. Its parent, ^{241}Am, will decay in the saturated zone transport pathway to produce some ^{237}Np. Thus, the ^{237}Np that enters the accessible environment will be partly from ^{237}Np that crosses the unsaturated zone/saturated zone interface below the repository and partly from ^{241}Am decay within the saturated zone. However, since the three-dimensional saturated zone transport model includes a more rigorous conceptualization of the spatially variable flow paths, it is preferable to apply it to ^{237}Np, even though it does not account for ingrowth from the decay of ^{241}Am. To assure that it is applied conservatively, at each time step any mass of ^{241}Am entering the saturated zone from the unsaturated zone is decayed for the remaining length of the simulation time and added to the ^{237}Np mass entering the saturated zone from the unsaturated zone. Because the mass of the parent species is not reduced while boosting the inventory of its decay product, this "inventory boosting" method results in a conservative overestimation of the mass of radionuclides transported in the saturated zone (SNL 2008a, Section 6.3.10.4.2). However, it is only applied to radionuclides that travel at approximately the same effective velocity (i.e., considering sorption) or more slowly than their decay products. This is the case for ^{241}Am/^{237}Np. It is also the case for ^{238}U/^{234}U, ^{238}Pu/^{234}U, ^{243}Am/^{239}Pu, and ^{240}Pu/^{236}U, and ^{242}Pu/^{238}U (SNL 2008a, Section 6.3.10). A one-dimensional saturated zone flow and transport abstraction that includes full chain decay is used for the rest of the species (^{235}U, ^{231}Pa, ^{233}U, ^{229}Th, ^{232}Th, ^{230}Th, and ^{226}Ra). Also for the end members of four decay chains (^{231}Pa, ^{229}Th, ^{232}Th, and ^{226}Ra) (Figure 2.4-21), transport of the mass of that species released from the unsaturated zone is simulated using the three-dimensional saturated zone flow and transport abstraction. The transport of the mass generated by ingrowth of these radionuclides from radionuclides ahead of it in the decay chain is evaluated using the one-dimensional saturated zone flow and transport abstraction. The mass releases from the one-dimensional and three-dimensional abstractions are then summed before being used by the biosphere submodel (SNL 2008f, Section 6.5.3[b]).

The one-dimensional saturated zone flow and transport abstraction is incorporated directly in the TSPA model as three one-dimensional pipe segments using GoldSim pipe pathway elements (Section 2.3.9.3.4.2). All radionuclides are transported with the one-dimensional abstraction; however, only a subset of these is passed from the one-dimensional abstraction to the biosphere submodel. The others (i.e, the top level radionuclides in the four decay chains, plus the decay products mentioned above, plus the fission-product radionuclides) are passed to the biosphere submodel from the three-dimensional abstraction, namely, ^{14}C, ^{135}Cs, ^{137}Cs, ^{129}I, ^{90}Sr, ^{99}Tc, ^{243}Am, ^{239}Pu, ^{241}Am, ^{240}Pu, ^{242}Pu, ^{238}Pu, ^{36}Cl, ^{79}Se, ^{126}Sn, ^{237}Np, ^{234}U, ^{232}U, ^{236}U, and ^{238}U (SNL 2008a, Table 6.3.7-6). The rates of groundwater flow within individual pipe segments of the one-dimensional abstraction are adjusted to match the flow rates in the three-dimensional saturated zone flow and transport abstraction. The flow path length of the first segment is constant. The flow path length of each of the last two segments is a function of two uncertain parameters: the first represents uncertainty in the horizontal permeability anisotropy, and the second represents uncertainty in the northwestern boundary of the alluvium. These two parameters are sampled once per saturated zone realization. Values of transport parameters in the one-dimensional saturated zone pipe segments correspond to the values used in the three-dimensional saturated zone flow and transport abstraction in each TSPA realization. The TSPA model coordinates the consistent, random selection of radionuclide breakthrough curves for the three-dimensional transport abstraction and the material properties for the one-dimensional transport abstraction for each realization.

Output 19 (Saturated Zone Transport—Biosphere Coupling)—The following output is passed from the saturated zone flow and transport submodel to the biosphere submodel:

- For each distinct radionuclide species transported in the three-dimensional saturated zone model, the summed release rate at the 18-km accessible environment boundary from the four saturated zone source regions for the mass dissolved plus reversibly sorbed onto colloids

- For certain radionuclide species transported in the three-dimensional saturated zone model, the summed release rate at the 18-km accessible environment boundary from the four saturated zone source regions for each of two states: (1) irreversibly sorbed onto the slow fraction of colloids, and (2) irreversibly sorbed onto the fast fraction of colloids
- For each distinct radionuclide species transported in the one-dimensional saturated zone model (whose dose will be computed based on the results of the one-dimensional model), the summed release rate at the 18-km accessible environment boundary from the four saturated zone source regions for the mass dissolved plus reversibly sorbed onto colloids.

2.4.2.3.2.1.11 Biosphere

The biosphere model component of the TSPA model estimates the annual radiation dose to the RMEI expected if radionuclides are released to the accessible environment from the repository after closure. The annual dose to the RMEI is calculated using BDCFs within the biosphere submodel that convert radionuclide releases to dose. The BDCFs are developed using the Environmental Radiation Model for Yucca Mountain Nevada (ERMYN) (SNL 2007y) as described in Section 2.3.10 and implemented using the GoldSim software. The BDCFs include dose contributions from all potential exposure pathways (ingestion, inhalation, external radiation) at the location of the RMEI in order to calculate the predicted annual total dose required to evaluate compliance with the individual protection standards in proposed 10 CFR 63.311 and proposed 10 CFR 63.321.

For the set of scenario classes considered in the TSPA model, there are two possible radionuclide release pathways from the repository to the accessible environment: one through groundwater and one through the atmosphere via volcanic eruptions. These two radionuclide release pathways result in the two exposure scenarios and two corresponding sets of BDCFs (SNL 2007y). To eliminate possible confusion with the TSPA scenario classes, these two exposure scenarios are called the exposure cases in the TSPA model. The TSPA model combines the appropriate BDCFs with the estimates of radionuclide concentrations in groundwater derived from the saturated zone transport abstraction models (Section 2.3.10.5.1) or in surface soil mixed with volcanic tephra derived from the volcanic tephra redistribution model (Section 2.3.10.5.2).

For the groundwater exposure case, radionuclides enter the accessible environment from one or more wells that extract contaminated groundwater from the saturated zone aquifer. As specified in 10 CFR 63.312(c), the well water used by the RMEI has average concentrations of radionuclides based on an annual water demand of 3,000 acre-ft. Thus, the mass flux rate of radionuclides from the saturated zone flow and transport submodel is diluted or mixed in an annual water demand of 3,000 acre-ft. Human exposure arises from using the contaminated water for domestic and agricultural purposes. Groundwater BDCFs apply to the nominal scenario class modeling case, the drip shield early failure modeling case, the waste package early failure modeling case, the seismic ground motion modeling case, the seismic fault displacement modeling case, the igneous intrusion modeling case, and the human intrusion scenario. In the volcanic ash exposure case, radionuclides are released as contamination in volcanic tephra that is dispersed into the atmosphere and deposited on the ground, with possible redistribution by hillslope and fluvial processes leaving contaminated tephra mixed with surface soil. Human exposure occurs in the accessible environment with the transport of radionuclides from surface soil to other environmental media such as foodstuffs, inhalable contaminated atmospheric particulate matter, and groundshine. Volcanic ash BDCFs apply to the volcanic eruption modeling case.

To facilitate modeling for dose calculations, a reference biosphere is developed, as described in Section 2.3.10.2.1. The reference biosphere represents the environment inhabited by the RMEI along with associated human exposure pathways and parameters (10 CFR 63.102(i)). Required characteristics of the reference biosphere are specified in 10 CFR 63.305(a), (b), (d), and proposed (c), and the RMEI is a hypothetical person who meets the criteria of 10 CFR 63.312. To meet the requirement of 10 CFR 63.312(b), the dietary and living style characteristics of the RMEI were determined based on surveys of people living in the Amargosa Valley combined with the 2000 census data (Bureau of the Census 2002), as well as regional and national information on behavioral patterns and food intake (USDA 2000; EPA 1997; ICRP 1994; BSC 2005b).

As indicated in Section 2.3.10.2.2, the biosphere submodel in the TSPA uses dose coefficients from Federal Guidance Report 13 (EPA 2002) to convert radionuclide intake or external exposure to dose. Dose coefficients for external exposure are equal to the effective dose per unit time per unit radionuclide concentration in the soil and are developed using tissue weighting factors consistent with International Commission on Radiological Protection Publication 60 (ICRP 1991). The dose coefficients for inhalation and ingestion are equal to the committed effective dose per unit radionuclide intake by inhalation or ingestion and are also developed using tissue weighting factors and the dosimetric methods based on International Commission on Radiological Protection Publication 60 (ICRP 1991). This approach is in compliance with proposed 40 CFR Part 197, Appendix A, as required by proposed 10 CFR 63.2.

Groundwater Exposure Case—In the groundwater exposure case, radionuclides are introduced into the accessible environment with groundwater pumped from wells for agricultural and domestic purposes. Once in the accessible environment, the radionuclides migrate through various environmental components. During this migration, some of the radionuclides give rise to a dose to the RMEI through one of three exposure pathways: inhalation, ingestion, or external exposure (Section 2.3.10.2.3). Each of the exposure pathways is modeled using the diet, living style, and other characteristics of the RMEI (Section 2.3.10.2.2). The biosphere process model for the groundwater exposure case considered a series of eight submodels, representing five environmental media: soil, air, plant, animal, and fish (Section 2.3.10.2.5). The radionuclides in each of these components can result in exposure to the RMEI.

The following environmental transport processes are explicitly included in the biosphere process process model for the groundwater exposure case (SNL 2007y, Section 6.3.1.3):

- Radionuclide accumulation in surface soil layers as a result of long-term cultivation using contaminated water
- Resuspension of contaminated soil
- Radionuclide deposition on crop surfaces by dry processes (resuspension of contaminated soil and subsequent adhesion of soil particles onto vegetation surfaces)
- Radionuclide deposition on crop surfaces by interception of contaminated irrigation water

- Removal of surface contamination by weathering processes
- Translocation and retention of contaminants from the deposition site to the edible tissues of vegetation
- Radionuclide uptake from soil by plants through the roots
- Release of radionuclides in gaseous phases, ^{222}Rn and $^{14}CO_2$, from the soil into the air with subsequent inhalation
- Photosynthesis by crops of $^{14}CO_2$ from the atmosphere
- Radionuclide intake by animals through consumption of contaminated feed, water, and soil, followed by transfer to animal products
- Radionuclide transfer from water to air through use of evaporative coolers
- Radionuclide transfer from water to fish.

The TSPA only considers the release and transport of the primary radionuclides. To avoid underestimating annual dose to the RMEI, the biosphere process model accounts for the decay products of the primary radionuclides after they are introduced into the accessible environment. The short-lived decay products with half-lives of less than 180 days are considered to be in secular equilibrium with the parent radionuclide, and their radiation dose contributions are included in the BDCF for the primary radionuclide or a long-lived decay product of the primary radionuclide (SNL 2007y, Sections 6.3.1.4 and 6.3.5). The biosphere process model also accounts for the buildup of the primary radionuclides in soil, as well as the decay and ingrowth of long-lived decay products in the soil as a result of long-term irrigation (from 25 years up to 1,000 years) (SNL 2007y, Sections 6.4.1.1 and 6.4.1.2). In this case, the BDCF contributions of the long-lived decay products created in the soil are added to that of the parent primary radionuclides. The output of the biosphere process model provides the groundwater case BDCFs for all primary radionuclides and the following combination of radionuclides where the effect of longer-term decay products are included with the BDCF of the initial primary radionuclide: ^{226}Ra and ^{210}Pb, shown on TSPA model dose plots as ^{226}Ra.

Volcanic Ash Exposure Case—The biosphere conceptual model for the volcanic ash exposure case uses a similar reference biosphere and human receptor as the groundwater exposure case. The major difference between the exposure cases is that in this case, the radionuclide source consists of contaminated tephra deposited on the ground surface and mixed with soil, rather than the multiple uses of contaminated groundwater (SNL 2007y, Section 6.3.2). The following environmental transport processes are explicitly included in the biosphere process model for the volcanic ash exposure case (SNL 2007y, Sections 6.5.2, 6.5.3, and 6.5.4):

- Resuspension of contaminated soil and tephra from undisturbed soils and activities that disturb the soil surface

- Dry deposition of radionuclides on crop surfaces, including resuspension of contaminated soil and subsequent adhesion of soil particles on crop surfaces
- Removal of surface contamination by weathering processes
- Translocation and retention of contaminants from the site of deposition to the edible portions of crops
- Radionuclide uptake by crops through the roots
- Radionuclide intake by animals through consuming contaminated feed and soil, and subsequent transfer to animal products
- Release of radon (^{222}Rn) from the soil.

Because the groundwater is contaminant-free in the volcanic ash exposure case (to demonstrate compliance with the individual protection standard, the dose from this case is added to the doses from the modeling cases that involve groundwater contamination), fewer exposure pathways are considered than for the groundwater exposure case. In particular, as described in Section 2.3.10.2.6, the volcanic ash exposure case does not include a contribution to annual dose from ingestion of drinking water, ingestion of locally produced fish, or inhalation of indoor aerosols generated by evaporative coolers. In addition, the dose contribution from ^{14}C in solid or gaseous forms is not considered because ^{14}C is a negligible contributor to dose in the volcanic ash exposure case (SNL 2007s, Tables 6-7 and 6-8). The consideration of short-lived nonprimary radionuclide decay products in the volcanic ash exposure case is the same as discussed above for the groundwater exposure case (i.e., their contributions to dose are included in the BDCFs of the parent radionuclide).

Climate Change—Based on various considerations summarized in Section 2.3.10.1, present-day climate BDCFs were determined to (1) represent a suitable balance between the requirements of 10 CFR 63.305(b) and proposed 10 CFR 63.305(c); (2) meet the requirements of 10 CFR 63.305(a) and (b); and (3) be appropriate for the assessment of doses to the RMEI for the entire 10,000 year period following repository closure, and for the period beyond 10,000 years within the period of geologic stability, as prescribed by proposed 10 CFR 63.302.

Uncertainty Methodology—BDCFs for the groundwater and the volcanic ash exposure cases were calculated using probabilistic analysis in a series of simulations for each of the screened-in radionuclides tracked in the TSPA model (SNL 2007y). To incorporate uncertainty into the TSPA model input, BDCFs are calculated in a manner to propagate the uncertainties of the biosphere process model input parameters. For groundwater BDCFs, this is accomplished by conducting a series of 1,000 stochastic model realizations using the ERMYN code (Section 2.3.10.1) for each radionuclide. The resulting set of BDCFs incorporates the uncertainty from those input parameters. The sampling is structured so that for a given iteration, the sampled value for each nonradionuclide-specific parameter is the same for every radionuclide. This approach ensures that the correlation between BDCFs arising from the commonality of receptor and environmental characteristics is retained. Similarly, the BDCFs for the volcanic eruption modeling case are generated stochastically using 1,000 realizations of the ERMYN code. In the TSPA model, for either the groundwater exposure case or the volcanic ash exposure case, a discrete distribution whose output is an integer from 1 to 1,000, inclusive, is used to randomly select a particular set of values from the BDCF tables (SNL 2008a, Section 6.3.11.3). The selected BDCFs for each radionuclide are then multiplied by the appropriate radionuclide concentrations (in the groundwater or soil) to compute annual dose to the RMEI.

As described in Section 2.3.10.2.5, for the groundwater exposure case, radionuclide concentrations in groundwater are calculated from the annual radionuclide mass flux provided by the saturated zone flow and transport model component uniformly mixed in the annual water demand of 3,000 acre-ft (10 CFR 63.312(c)). The annual dose to the RMEI was then calculated by assuming a linear relationship between radionuclide concentrations in groundwater and the resulting doses (i.e., BDCFs are not a function of concentration). As stated in Section 2.3.10.2.5, to calculate BDCFs that are independent of time (or, equivalently, independent of concentration), radionuclide concentrations in groundwater are considered constant over time (SNL 2007y, Section 6.3.1.4) in the development of the BDCFs. This assumption allows separate and independent calculations of time-dependent radionuclide concentrations in the TSPA model and time-independent BDCFs in the biosphere process model. Based on this assumption, BDCFs are calculated in the biosphere process model as the annual dose per unit concentrations of radionuclides in groundwater (i.e., Sv/yr per Bq/m^3), and the annual dose is calculated in the TSPA model as the product of the BDCFs and radionuclide concentrations in groundwater.

For the volcanic eruption modeling case, the BDCFs are multiplied by the appropriate concentrations; one concentration is in the resuspendible soil layer and the other is the concentration averaged over the tillage depth (SNL 2008a, Section 6.3.11.2). As described in Section 2.3.10.5.2, for the volcanic ash exposure case, the biosphere process model produces three BDCF component for each radionuclide. The first component accounts for exposure to sources external to the body, ingestion, and inhalation of radon decay products. The second and third BDCF components accounts for inhaling airborne particulates. The short-term inhalation component represents inhalation exposure during the first year following a volcanic eruption. This term is used together with the time function, as described in Section 2.3.10.3.2.2, to calculate short-term increase in inhalation exposure, due to elevated levels of airborne particulate matter, after a volcanic eruption, relative to the conditions existing before and long after an eruption. With time, mass loading will return to the preeruption level. These conditions are described by the long-term inhalation component, which represents exposure from inhalation of resuspended particulates under nominal conditions (i.e., when the mass loading is not elevated as the result of volcanic eruption) (Section 2.3.10.2.6). None of these three components of the volcanic ash exposure case BDCFs are applicable during the time of active eruption of a volcano (Section 2.4.2.3.2.1.12.2). They are only applicable after tephra deposition and redistribution at the RMEI location. The potential dose that occurs immediately during an active eruption, while ash is actively falling, has been shown to be of low consequence (SNL 2008a, Section 6.5.2.4), and is therefore not included in the computation of total dose.

In addition to the annual dose calculation, the biosphere model component also includes the calculations of activity concentration in groundwater and beta-photon doses for evaluating compliance with the groundwater protection limits (SNL 2008a, Section 6.3.11.2). As specified at 10 CFR 63.331 (Table 1), three limits are evaluated for compliance, including the gross alpha concentration in groundwater, the radium concentration in groundwater, and the annual dose from beta- and photon-emitting radionuclides ingested by daily consumption of two liters of groundwater. These calculations are based on the activity concentration of each primary radionuclide in groundwater, as calculated from radionuclide concentrations that are provided by the saturated zone flow and transport model component. Natural background activity concentrations are added to calculated values for comparison with the limit for combined ^{226}Ra and ^{228}Ra activity concentration in groundwater (5 pCi/liter), and with the limit for gross alpha activity concentration (15 pCi/liter). Beta-photon doses to the whole body and individual organs are calculated using dose coefficients from Federal Guidance Report 13 (EPA 2002; SNL 2007y, Section 6.15.1.2).

The biosphere model component is the last component in the chain of TSPA model components and, thus, has no output coupling; rather, the biosphere model component outputs are the time evolution of stochastic dose histories and other parameters (alpha activity and organ/whole body doses) required by 10 CFR 63.331 (Table 1) to evaluate repository system performance.

Output 20 (Biosphere Output)—The following outputs are passed from the biosphere model component at each time step:

- The annual dose incurred by the RMEI for every radionuclide under consideration in the groundwater and volcanic ash exposure cases
- The gross alpha concentration in groundwater (including ^{226}Ra but excluding radon and uranium)
- The combined ^{226}Ra and ^{228}Ra concentration in groundwater
- The annual whole body and individual organ doses from beta- and photon-emitting radionuclides by daily consumption of two liters of groundwater.

2.4.2.3.2.1.12 Events

In addition to the analysis of the nominal scenario class described in the preceding sections, the TSPA model is used to analyze early failure events and disruptive events. The early-failure scenario class considers early failure of waste packages and drip shields captured in two separate modeling cases: (1) the waste package early-failure modeling case, and (2) the drip shield early-failure modeling case. Disruptive events modeled in TSPA are induced by either igneous activity or seismic activity. The igneous scenario class includes two modeling cases: (1) the igneous intrusion modeling case and (2) the volcanic eruption modeling case. The seismic scenario class includes two modeling cases: (1) the seismic ground motion modeling case, and (2) the seismic fault displacement modeling case.

2.4.2.3.2.1.12.1 Early Failure Scenario Class

Manufacturing and handling defects could result in the early failure of waste packages (Section 2.3.6.6) or drip shields (Section 2.3.6.8.4). The manufacturing and handling processes that affect waste packages are based on the waste package fabrication and handling processes described in Sections 1.5.2 and 1.2.4, respectively. The manufacturing and handling processes that affect drip shields are based upon drip shield fabrication and handling processes described in Section 1.3.4. The purpose of early failure analysis is (1) to evaluate the types of defects or imperfections that could occur in a waste package or drip shield and potentially lead to its early failure, and (2) to estimate a probability of occurrence for each. Only the outer (Alloy 22) barrier for the waste package is investigated. No corrosion performance credit is taken for the structural (stainless steel) inner vessel of the waste package; therefore, it is not analyzed.

Early Waste Package Failures—The waste package early failure modeling case in the early failure scenario class considers all waste packages that fail early due to manufacturing or material defects, including improper preemplacement operations. The implementation of early waste package failures in the TSPA model consists of specifying the number of waste packages that fail early in a realization and how these waste packages are distributed among the different waste package types. In the TSPA model early failure waste package analysis, both types of waste packages are considered: (1) codisposal waste packages, and (2) commercial SNF waste packages.

As described in Section 2.3.6.6, 13 potential mechanisms that could result in early failed waste packages have been identified (SNL 2007a, Section 6.1.6). Of these 13 flaws or processes, seven were identified as potentially significant for the waste package outer corrosion barrier. The seven processes retained for further analyses were (SNL 2007a, Section 6.3):

- Weld flaws
- Improper heat treatment of outer corrosion barrier
- Improper heat treatment of outer corrosion barrier lid
- Improper stress relief of outer corrosion barrier lid (low plasticity burnishing)
- Waste package mishandling damage
- Improper base metal selection
- Improper weld filler material.

These processes were assessed for probability of occurrence and consequences for postclosure performance of the waste packages. A more detailed analysis was done for waste package weld flaws (SNL 2007a, Section 6.3.1) than for the other six processes. This analysis resulted in distributions for the size and number of undetected weld flaws. The implementation of the weld flaw analysis is not part of the early failure analysis but is part of the waste package degradation analysis (Section 2.3.6.5). The occurrence of an undetected defect is assumed to result in early failure of the waste package; hence, the probability distribution for the rate of occurrence of undetected defects is equivalent to a probability distribution for the rate of waste package early failures. The occurrence of undetected defects is assumed to be independent between waste packages; hence, waste package early failure is also independent between waste packages (Section 2.3.6.6.3.2.7) (SNL 2008a, Section 6.4.2.1). Thus, no distinction is made between the different types of waste package (e.g., commercial SNF, DOE SNF-Short, DOE SNF-Long, and others). Among these defects, improper heat treatment is by far the dominant process in terms of probability (SNL 2007a, Section 6.5). The consequence common to these types of defects is an increased susceptibility to stress corrosion cracking. However, as discussed below, the analysis assumes that the entire waste package fails at the time of repository closure.

Both major types of uncertainty, aleatory and epistemic, are represented in the failure distributions for early waste package failures and early drip shield failures. Consider early waste package failure first. Because waste package early failure is independent between waste packages, the number of waste package early failures can be represented by a Poisson distribution for any particular value of the failure rate, λ_{EW}, of waste package early failures. The epistemic uncertainty in the failure rate is sampled from a lognormal distribution with a median of 4.14×10^{-5} and an error factor of 8.17 (SNL 2008a, Table 6.4-2). Based on this distribution, the probability of at least one waste package early failure is 0.442 in any given repository future for the mean value of the failure rate, λ_{EW}. The expected number of early-failed waste packages is 1.09 and the conditional expected number, given that one or more waste package early failure occurs, is 2.46 (SNL 2008a, Section 8.2.2). In a particular TSPA realization, the number of early failed waste packages, the type of waste package affected and the location of each early failure are treated as aleatory uncertainties.

Analyses predict rates for the introduction of defects into waste package fabrication but do not predict the impact on the waste package performance (SNL 2007a, Table 7-1). Waste package failure will only occur after degradation processes take place. However, a realistic estimate of the time at which components with defects will fail is difficult to develop. Therefore, for implementation in the TSPA model, complete failure of the waste package with respect to radionuclide containment is assumed at the time of repository closure (SNL 2007a, Section 6.5.2).

For waste package early failure implementation, the waste packages are divided into the two major fuel-type groups: commercial SNF early failed waste packages and codisposal early failed waste packages. The GoldSim component of the TSPA model computes the dose resulting from early failure of a single waste package of each type occurring in each of the five percolation subregions, with and without seepage in each percolation subregion, for a total of 20 dose histories for each epistemic realization. The GoldSim results are then combined in the EXDOC_LA software with the sampled rate of waste package early failure, the distribution of the numbers of waste packages of each type, and the seepage fraction for each percolation bin to calculate the expected dose for each epistemic realization. The mean or median dose is then estimated from the ensemble of expected dose results at each point in time. General corrosion of the drip shields is included in the waste package early failure modeling case, which shows that at around 300,000 years, the approximate mean time of drip shield failure (SNL 2008a, Section 8.3[a]), the onset of advection will cause an increase in the release of solubility-limited radionuclides from the few early-failed waste packages. Other than the differences in the waste package and drip shield degradation model components, the waste package early failure modeling case invokes the same model components and submodels used in the nominal scenario class (Figure 2.4-114).

Early Drip Shield Failures—The distribution for the number of early failure drip shields is developed in an analogous manner to the development for early failure waste packages (Sections 2.3.6.8.4 and 2.3.6.6). The drip shield early failure modeling case considers all drip shields that fail early from manufacturing or material defects, including improper preemplacement operations. The implementation of early drip shield failures in the TSPA model consists of sampling the number of drip shields that fail early in a realization and how these drip shields are distributed among the different waste package types. In the TSPA models, early failure drip shield analysis, both types of waste packages are included: (1) codisposal waste packages, and (2) commercial SNF waste packages.

As described in Section 2.3.6.8.4, the same possible defect mechanisms identified for the waste packages are also considered for the drip shields. Of these mechanisms, four have been identified as potentially significant mechanisms leading to possible early drip shield failure:

- Improper heat treatment
- Base metal selection flaws
- Improper weld filler material
- Emplacement errors.

For these possible drip shield defects, the probability of occurrence and consequences for postclosure performance is assessed (Section 2.3.6.8.4). The four processes are analyzed using an event tree/fault tree approach (SNL 2007a, Section 6.4). The probabilities of occurrence for the four drip shield early failure mechanisms are combined to yield a probability distribution for the rate of occurrence of undetected defects in drip shields. The occurrence of an undetected defect is assumed to result in complete failure of the drip shield as a barrier to seepage at the time of repository closure (SNL 2007a, Section 6.5.2); hence, the probability distribution for the rate of occurrence of undetected defects is equivalent to a probability distribution for the rate of drip shield early failures. The occurrence of undetected defects is assumed to be independent between drip shields; hence, drip shield early failure is also independent between drip shields.

Similarly to the modeling of early failure waste package failures described above, both major types of uncertainty, aleatory and epistemic, are represented in the failure distributions for early drip shield failures. Because drip shield early failure is independent between drip shields, the number of drip shield early failures can be represented by a Poisson distribution for any particular value of the failure rate, λ_{ED}, of drip shield early failures. This rate of drip shield early failure is considered uncertain and is sampled from a lognormal distribution with a median of 4.30×10^{-7} and an error factor of 14 (SNL 2007a, Table 7-1). Based on this distribution, the probability of at least one drip shield early failure is 0.0166 in any given repository future, for the mean value of the failure rate, λ_{ED}. The expected number of early failed drip shields is 0.0181 and the conditional expected number, given that one or more drip shield early failure occurs, is 1.09 (SNL 2008a, Section 8.2.2). In a particular TSPA realization, the number of early failed drip shields, the type of waste package affected and the location of each early failure are treated as aleatory uncertainties.

As with the waste package, analyses predict rates for the introduction of defects into drip shield fabrication, but did not predict the impact on repository performance (SNL 2007a, Table 7-1). Failure of the drip shield due to corrosion will only occur after degradation processes take place, hundreds or even thousands of years after emplacement. However, a realistic estimate of the time at which components with defects will fail is difficult to develop. Therefore, for implementation in the TSPA model, complete failure of the drip shield with respect to its seepage diversion function is assumed at the time of repository closure (SNL 2007a, Section 6.5.2).

The TSPA models a drip shield early failure by removing the drip shield as a barrier to seepage at the time of repository closure and allowing the full volume of seepage to contact the waste package (SNL 2008a, Section 6.4.1.3). The TSPA model assumes that a waste package in a seeping location that is underneath an early failed drip shield experiences localized corrosion once seepage contacts the waste package. Localized corrosion completely compromises the outer barrier of the waste package, allowing the advective and diffusive transport of radionuclides. Analysis of the localized corrosion initiation abstraction shows that localized corrosion initiation conditions can be present in the repository for up to 12,000 years after repository closure at a few locations in the repository in a small number of epistemic realizations (SNL 2008a, Appendix O). However, rather than incurring significant computational expense to account for the epistemic uncertainty and the temporal and spatial variation in the initiation of localized corrosion, a simplifying assumption of initiating localized corrosion once seepage contacts the waste package is made, because it has a negligible effect on the total dose summed over all modeling cases, given the very small value (0.0181) for the expected number of early drip shield failures.

Drip shield early failures occurring in locations that do not experience seepage contribute negligibly to the total expected dose because, in a location without seepage, localized corrosion does not occur, since the waste package surface is not wetted. Since localized corrosion does not occur, and the drip shield early failure modeling case does not address other events (i.e., seismic events) that could compromise the waste package integrity, there are no mechanisms in the drip shield early failure modeling case that would lead to releases from a waste package in a location without seepage (SNL 2008a, Section 6.4.1.3). Therefore, the assumption of negligible dose impact in a location without seepage is justified.

The GoldSim component of the TSPA model computes the dose resulting from a single drip shield early failure occurring in each of the five percolation subregions in a seeping environment, and affecting each type of waste package (commercial SNF or codisposal) for a total of 10 dose histories for each epistemic realization. The GoldSim results are then combined in the EXDOC_LA software with the sampled rate of drip shield early failure, the distribution of the numbers of waste packages of each type, and the seepage fraction for each percolation subregion, to calculate the expected dose for each epistemic realization. In this calculation, the expected dose includes the probability that the early failed drip shield may occur in a non-seeping location. The mean or median dose is estimated from the ensemble of expected dose results at each point in time. Other than the differences in the waste package and drip shield degradation model component, the drip shield early-failure modeling case invokes the same modeling components and submodels used in the nominal scenario class.

Figure 2.4-114 schematically depicts the flow of information between the principal TSPA model components and submodels for the two early failure modeling cases. The flow of information between submodels in these two modeling cases is similar to the nominal scenario class modeling case depicted in Figure 2.4-112, with the following exceptions. The waste package and drip shield degradation model component, which combines the localized corrosion and general corrosion processes in the nominal scenario class, is replaced with early failure degradation modes for the waste packages and/or drip shields. Based on the assumptions above about the extent of waste package degradation for either early waste package failure or early drip shield failure, localized corrosion and general corrosion of waste packages can result in no additional damage to the early failed waste package; therefore, the waste package damage and failure areas calculated by the waste package and drip shield degradation model component are not applicable in the waste package early failure modeling case. Drip shield degradation by general corrosion is still applicable in the waste package early failure modeling case. As discussed above, general corrosion of drip shields provides no additional damage to early failed drip shields, and therefore the drip shield damage and failure areas calculated by the waste package and drip shield degradation model component are not applicable in the drip shield early failure modeling case. Waste package degradation by localized corrosion is assumed to occur instantly once a waste package beneath an early failed drip shield is contacted by seepage water. Early failure of a drip shield covering an early failed waste package is not considered in TSPA calculations because the probability of their colocation is so low (SNL 2007a, Table 6-11).

Outputs 11, 12, and 13—As shown in Figure 2.4-114, these outputs to the EBS flow, waste form, and EBS transport submodels described in Section 2.4.2.3.2.1.5 will change somewhat compared to their values in the nominal scenario class, based on the description above.

2.4.2.3.2.1.12.2 Igneous Scenario Class

As described in Section 2.3.11, FEPs associated with possible future igneous activity at the repository site are incorporated in the TSPA model because the mean annual probability of repository intersection by an igneous intrusion is slightly greater than the probability threshold value for exclusion (proposed 10 CFR 63.342(b)). Separate probabilities have been estimated for repository intersection by a basalt dike (intrusion modeling case) (Section 2.3.11.2.2) and for eruption through an emplacement drift (volcanic eruption modeling case) (Section 2.3.11.4.2.1). These two modeling cases encompass all the screened-in FEPs (Table 2.3.11-1) and related consequences associated with disruption of the repository by an unlikely future igneous event. Information transfer among modules of the TSPA code related to the two igneous scenario class modeling cases is discussed below.

Igneous Intrusion—As described in Section 2.3.11.3, the igneous intrusion modeling case represents a potential basaltic dike intersecting the repository without surface eruption within the repository boundary, including the post-intrusion effects from heat, potential impacts on EBS features, and changes in water chemistry following reaction with cooled basalt. The flow characteristics of the intruding magma are assumed to be such that it fills every drift within the repository. Hence, all waste packages and drip shields are assumed to be so damaged that they no longer have water diversion or waste isolation capability. The waste-package inner vessels and outer barriers, and the waste forms (commercial SNF, HLW, and DOE SNF (including naval SNF)) are considered fully degraded at the time of the event. Magma intrusion is assumed not to damage the invert, so it is modeled in TSPA in a similar fashion to other modeling cases. Because an intruded drift will fill with magma within 15 to 25 minutes (depending on the width of the dike) (SNL 2007z, Sections 6.3.3.5.6), the igneous event is treated as instantaneous in the TSPA model. The magma then cools and solidifies in the emplacement drifts. Radionuclides dissolved in water moving through the basalt will be transported by the groundwater downward through the invert and the unsaturated zone to the water table, and then to the accessible environment by flow and transport processes in the saturated zone in the same manner as the nominal scenario class modeling case. Because the drift opening is filled with magma, water contacting the waste is no longer modeled as seepage, but as the local percolation flux traveling through the host rock (SNL 2008a, Section 6.5.1.1).

For the igneous intrusion modeling case (Figure 2.4-115), the TSPA model selects input parameter values from the appropriate distributions of each model components and submodels for each realization of the igneous intrusion modeling case. Using these inputs, the fate of the radionuclides mobilized by the igneous intrusion is evaluated using the nominal scenario class TSPA model components and submodels for flow and transport of the released radionuclides in the invert of the

EBS, unsaturated zone, and saturated zone. Modifications to the nominal scenario class are as follows (SNL 2008a, Section 6.5.1.1):

- The annual frequency of a dike intersecting the repository footprint ranges from approximately 7.4×10^{-10} to 5.5×10^{-8} for the 5th and 95th percentiles, respectively, with a mean annual frequency of 1.7×10^{-8} (Section 2.3.11.2.2.3). This mean annual frequency, which is independent of the event consequences (i.e., size, duration, power) is applied to the igneous intrusion and volcanic eruption modeling cases.

- Because nominal degradation processes do not progress sufficiently in 10,000 years to release any radionuclides (Figures 2.1-10 and 2.1-9), the igneous intrusion modeling case for 10,000 years does not evaluate any pre-intrusion degradation of the waste packages, drip shields, waste forms, or emplacement drifts. However, for the one-million-year timeframe in the igneous intrusion modeling case, the nominal processes of degradation of the waste packages, drip shields, and waste forms do occur until the time of the igneous intrusion, potentially allowing for decreases in waste package inventory (SNL 2008a, Section 6.5.1.1). The inclusion of nominal processes before the igneous intrusion prevents overcounting any radionuclides released to the accessible environment by nominal processes prior to the igneous intrusion (Section 2.4.2.1.5.3).

- The intruded drifts have a seepage flux equal to the local percolation flux (SNL 2007g, Section 6.7.1.1), i.e., capillary effects at the drift wall are not explicitly addressed (Section 2.3.11.3.2.9). The volumetric seepage rate is, therefore, obtained by applying the percolation flux at the base of the Paintbrush nonwelded hydrologic unit (PTn), provided by the EBS thermal-hydrologic environment submodel for the appropriate percolation flux subregion, to the projected area of the emplacement drift. In particular, the volumetric seepage rate for a single waste package is set equal to that obtained by applying the flux at the base of the PTn to the 5.1-m-long by 5.5-m-wide drift segment representing the drift footprint for one waste package. Prior to the igneous intrusion, the seepage response surfaces provide the seepage flow rates and seepage fractions applicable for nominal conditions.

- The drip shields and waste packages provide no hindrance to flow because they are assumed to be fully damaged at the time of the igneous intrusion (SNL 2007z, Section 8.1.2). All waste forms are assumed to be instantly degraded (Section 2.3.11.3.2.4).

- In the igneous intrusion modeling case, all EBS and in-package chemistry-related submodels and parameters are the same as in the nominal scenario class modeling case, with the exception of the uranium solubility submodel. As indicated in Section 2.4.2.3.2.1.7, method 2 for uranium solubility is used for the igneous intrusion modeling case. Method 2 is based on the presence of silica in the aqueous environment. In particular, the presence of basalt in the drifts implies that Na-boltwoodite needs to be included as a uranium solubility-controlling phase (SNL 2007u, Section 6.7.3). More specifically, two additional base solubility lookup tables are defined for this case, which include schoepite, Na-boltwoodite, and $Na_4UO_2(CO_3)_3$, depending on the pH and $f\mathrm{co}_2$.

- Drift-wall condensation is assumed to be zero after the event because basalt fills the drifts due to the igneous intrusion (SNL 2008a, Table P-6).

- The EBS thermal-hydrologic environment submodel for the igneous intrusion modeling case differs from that used for the nominal scenario class modeling case, in that it accounts for the temperature increase within and around the drift due to the intrusion of magma that fills the drift. Temperatures of the waste packages, drip shields, and the invert spike to a maximum temperature (1,150°C) at the time of the intrusion and then cool back to ambient conditions (i.e., preigneous intrusion) over a 100-year time period (SNL 2007z, Section 6.4.6 and Table 6-13). The in-drift relative humidity, invert liquid saturation, and invert liquid flux are also affected. For temperatures above 100°C, no releases are allowed from the waste packages, under the assumption that continuous water films are not present inside the waste package. The condition of no radionuclide transport is accomplished by assigning radionuclide solubilities a value of 0 mg/L (this is the same for all other modeling cases when the temperature rises above 100°C) (SNL 2008a, Section 6.5.1.1.2).

Figure 2.4-115 schematically depicts the flow of information between the principal TSPA model components and submodels for the igneous intrusion modeling case. The flow of information between submodels in this modeling case is similar to the nominal scenario class modeling case depicted on Figure 2.4-112, but with the exceptions noted above (SNL 2008a, Section 6.5).

Volcanic Eruption—The volcanic eruption modeling case in the TSPA model considers the possibility of one or more volcanic eruptive conduits along a magmatic dike(s) that intersects repository waste packages, eruption of contaminated magma products to the ground surface, dispersal of the contaminated tephra by wind and deposition downwind, and redistribution of contaminated tephra by surface sedimentary processes (Section 2.3.11.4). The volcanic eruption modeling case also estimates the number of waste packages intersected by eruptive conduits. The component representing airborne transport and deposition is the ASHPLUME model and code, which is called by the GoldSim code and predicts the distribution of contaminated tephra on the ground at the location of the RMEI on the Fortymile Wash alluvial fan and in the associated upstream watershed. A final component of the model considers redistribution of contaminated tephra by surface sedimentary processes after deposition. This component is the Fortymile Wash tephra redistribution model (FAR software), which is also called by the GoldSim code, and estimates waste concentration in surface soils at the RMEI location by considering the amount of contaminated tephra that could be eroded from hillslopes, transported down Fortymile Wash, and deposited at the RMEI location as a result of surface sedimentary processes.

The volcanic eruption modeling case in the TSPA model evaluates only the posteruption consequences due to waste deposited at the location of the RMEI directly or redistributed from upstream in the Fortymile Wash watershed. It does not evaluate annual dose received during the active volcanic eruption phase, when the waste is transported and dispersed in the atmosphere. The active eruption phase is evaluated separately (SNL 2008a, Section 6.5.2.4) to show that the mean annual dose during the active eruption phase is small compared to the mean annual dose during the posteruption time period.

Implementing the volcanic eruption modeling case for the TSPA model includes determining the probability of the eruption and its consequences. The approach employs a Monte Carlo technique to account for parameter uncertainties, including the future time at which an eruption could occur and the possibility that more than one igneous event could occur in the future evolution of the repository. The probability of the eruption is represented as a conditional probability that one or more eruptive conduits would intersect an emplacement drift given the intersection of the repository by a basaltic dike. The annual frequency of an eruption actually carrying waste to the ground surface is estimated by multiplying the sampled frequency of intrusion (mean equal to approximately 1.7×10^{-8} years) (BSC 2004a, Table 7-1) by two factors. One factor is the fraction of eruptive conduits that intersect the repository footprint, which is 0.28 (SNL 2007aa, Section 7.2) (Section 2.3.11.4.2.1). The second factor is the probability that a conduit intersects a drift given an intersection with the repository footprint. This factor is 0.297 because the small conduit diameters relative to drift spacing means there is an approximately 70.3% probability that a conduit will form between drifts and not impact any waste packages (SNL 2008a, Table 6.5-3).

As shown in Figure 2.4-116, four submodels are considered in the volcanic eruption modeling case. Volcanic interaction with the repository submodel describes the number of waste packages that are expected to be destroyed by, and entrained in, a volcanic eruption, and the amount of waste available for atmospheric transport. The atmospheric transport submodel describes the atmospheric transport of this erupted tephra/waste mixture and eventual deposition on the land surface. The tephra redistribution submodel describes the redistribution of the contaminated tephra to the location of the RMEI and the diffusion of tephra into the soil column at that location. The volcanic ash exposure submodel uses the volcanic ash BDCFs to estimate mean annual dose to the RMEI, which was previously presented in the biosphere model component (Section 2.4.2.3.2.1.11).

Volcanic Interaction with the Repository Submodel—The quantity of waste erupted into the atmosphere in any one event is conceptualized in the volcanic eruption modeling case as depending on the distribution of waste packages in the emplacement drifts, the number and size of eruptive conduits intersecting the drifts, the degree of damage to those waste packages, the amount of waste from the waste packages entrained into the erupting material, and the fraction of magma erupted into the tephra cloud (Section 2.3.11.4.2). Only waste packages located partially or entirely within a magmatic conduit are assumed to be affected by the eruption, making all the waste in these waste packages available for entrainment in the erupting magma. The mass of waste incorporated in the tephra plume from an eruptive event depends on the waste inventory, the number of waste packages intersected, and the fraction of waste-containing magma erupted as a tephra plume instead of lava flows or as a scoria cone. The fraction of each waste package type, commercial SNF or codisposal, and hence the mass and inventory content of waste erupted is proportional to the fraction of commercial SNF versus codisposal waste packages emplaced in the repository (SNL 2008a, Section 6.5.2.1.1).

The waste packages hit analysis (SNL 2007aa, Section 7.2) indicates there is approximately a 28% probability that a conduit will form within the repository footprint given an igneous intrusion event. The small conduit diameters relative to drift spacing mean that approximately 70.3% of the conduits intersecting the repository footprint would intersect between drifts and therefore not impact any waste packages. In the 8.3% (28% times 29.7%) of cases in which one or more packages are hit, the most likely number hit is four and the maximum number hit is seven (Figure 2.3.11-12b). The mass of waste hit is multiplied by the magma partitioning factor to account for the partitioning of magma into surface lava flows, scoria cone, and tephra plume (SNL 2007m, Section 6.5.2.22). The magma partitioning factor is specified as a uniform distribution from 0.1 to 0.5 and represents the fraction of magma erupted into the tephra plume to be considered in the volcanic eruption modeling case (Section 2.3.11.4.2.2.2). Based on analogues for an eruption at Yucca Mountain, the scoria cone and lava flows deposits typically cover a few square kilometers (Section 2.3.11.2.1.2). Therefore, waste potentially deposited with surface lava flows and scoria cone is excluded from the TSPA analysis on the basis of low consequence at the RMEI location (SNL 2008a, Section 6.5.2.1.1).

Atmospheric Transport Submodel—The conceptual model for the atmospheric transport submodel is a vertical column of heated tephra and waste particles, resulting in a buoyant plume that reaches neutral buoyancy at some level in the atmosphere (Section 2.3.11.4.2.2). The plume is then transported downwind and, because of dispersive processes, spreads out laterally as it is transported. Solids fall from the plume as it travels depending on the wind speed, particle density, and settling velocity. The pyroclastic material ejected into the atmosphere from a volcanic eruption eventually falls to the ground surface and forms a contaminated tephra sheet of varying thickness extending and thinning, generally, downwind from the volcanic vent (SNL 2007m, Section 6.3). Atmospheric transport and deposition of erupted waste is evaluated using the ASHPLUME code (SNL 2007m, Section 6.5) implemented directly in the TSPA volcanic eruption model as a DLL.

The ASHPLUME code simulates a violent Strombolian eruption with entrainment of radioactive waste in the erupted plume as waste particles attached to the pyroclastic fragments in the plume. In the TSPA implementation, the maximum waste particle size is equal to the tephra particle size. The wind speed and direction that result in atmospheric transport of the erupted material are represented in the ASHPLUME code in terms of cumulative distribution functions specified for 1-km height increments between 0 and 13 km above the mountain. Once selected, the wind speed and direction are assumed to be constant throughout the eruption duration in the ASHPLUME model (SNL 2007m, Section 7.6). The atmospheric transport submodel predicts the ground-level concentrations (areal density, g/cm^2) of tephra and waste directly deposited at the location of the RMEI and the spatial distribution of tephra and waste in the Fortymile Wash watershed for a simulated volcanic event. The tephra concentration in the Fortymile Wash watershed is converted into volcanic tephra thickness by the tephra redistribution submodel and potentially redistributed to the RMEI location along with incorporated waste.

Tephra Redistribution Submodel—Waste-contaminated tephra deposited on the ground surface in Fortymile Wash by the atmospheric transport submodel could potentially be redistributed to the RMEI location due to hillslope and fluvial processes (SNL 2007ab, Section 6.2). Therefore, the waste concentration used in the biosphere submodel to determine dose consists of contributions from waste-contaminated tephra at the RMEI location deposited directly when atmospheric conditions move the eruptive plume toward that location, and any waste-contaminated tephra redistributed from upstream after being deposited in the Fortymile Wash watershed. Three major processes are considered in the tephra redistribution conceptual model: (1) mobilization from hillslopes, (2) mixing and dilution with uncontaminated sediments during channel transport, and (3) diffusion into the soil column at the RMEI location.

The location of the RMEI is specified in the same area for the igneous eruption case as all other modeling cases so that dose estimates are calculated at a consistent location for the nominal, intrusion, and eruption modeling cases. This means that model realizations with wind blowing away from this location and the Fortymile Wash do not contribute to dose calculations (SNL 2008a, Section 6.5.2.1.3).

The tephra redistribution model uses a spatially distributed analysis of hillslopes and channels in the drainage basin upstream of the Fortymile Wash alluvial fan apex to estimate the mass of tephra and waste that could be transported from the upper drainage basin to the RMEI location by hillslope and fluvial processes. The model mobilizes and transports tephra and waste deposited on the landscape toward the RMEI location if it falls on steep slopes or on active channels. Before the mobilized tephra and waste are deposited at the RMEI location, they are transported through the alluvial channel system, where mixing with uncontaminated channel sediments leads to dilution. Mixing occurs during flood events as sediment and tephra are entrained from the bed, mixed by turbulent flow, and redeposited on the bed.

The tephra and waste transported from the upper drainage basin, and primary tephra and waste deposited at the RMEI location, provide the initial conditions for redistribution of radionuclides into the soil column at the RMEI location. The tephra redistribution submodel considers the migration of radionuclides within the soil as a diffusion process due to suspension and redeposition of fine particles by infiltration, and physical mixing of soil particles by freeze-thaw cycles and bioturbation (Section 2.3.11.4.2.3.1) (SNL 2008a, Section 6.5.2.1.3). The time-dependent concentration resulting from the diffusion process is used by the volcanic ash exposure submodel to calculate dose to the RMEI.

The results of the tephra redistribution submodel calculations are passed to the volcanic ash exposure submodel for dose calculations. The results consist of four time series of waste mass concentration: (1) concentration on interchannel divides averaged over the tillage depth, (2) concentration on interchannel divides averaged over the resuspendable surface layer, (3) concentration in distributary channels averaged over the tillage depth, and (4) concentration in distributary channels averaged over the resuspendable surface layer. The concentrations on interchannel divides and distributary channels are combined using the weighting factor, F, for the fraction of the alluvial fan composed of channels (and $1-F$ for the fraction of the alluvial fan composed of divides) to determine the two soil source terms used in the calculation of doses: the areal radionuclide concentration in surface soil and the mass radionuclide concentration in the resuspendable soil layer. Both source terms are then converted into activity concentrations of the individual radionuclide species based on total repository inventory (SNL 2008a, Section 6.5.2.2). These radionuclide activity concentrations are then combined with the appropriate BDCFs to determine dose (SNL 2008a, Sections 6.5.2.1.3 and 6.5.2.1.4). As mentioned in Section 2.4.2.3.2.1.11, this dose is a result of short-term and long-term inhalation of suspended ash and soil, as well as, external exposure, ingestion, and inhalation of radon decay products (SNL 2008a, Section 6.5.2.2).

The tephra redistribution submodel is implemented in the TSPA volcanic eruption model using the computer code FAR V 1.2. The FAR V 1.2 code is implemented as a DLL that is called by GoldSim. The ASHPLUME code calculates the direct waste and tephra deposition results (g/cm^2) at the RMEI location, followed by an additional calculation (using the same input parameters) at the many grid points covering the Fortymile Wash watershed. Both calculations serve as input to the FAR code, which then calculates the redistribution of the contaminant load upstream of the RMEI location due to fluvial processes.

Figure 2.4-116 schematically depicts the flow of information between the principal TSPA model components and submodels for the volcanic eruption modeling case. The flow of information between submodels in this modeling case is quite different than the other modeling cases, such as the nominal scenario class modeling case depicted on Figure 2.4-112, because this eruptive case is for atmospheric transport of contaminants rather than groundwater transport of contaminants.

2.4.2.3.2.1.12.3 Seismic Scenario Class

Mechanical processes that occur during a significant seismic event (i.e., an event with the capacity to degrade or rupture waste packages and/or drip shields) have the potential to compromise the functionality of the waste packages and drip shields as barriers to radionuclide release. For significant vibratory ground motions, impacts can occur between adjacent waste packages and between a waste package and its emplacement pallet, the surrounding drip shield, and the invert. Impacts can also occur between drip shields and emplacement pallets, the invert, and the drift wall. Dynamic loads induced by vibratory ground motions can result in impacts on drip shields in the postclosure period. Lithophysal and nonlithophysal rubble induced by vibratory ground motion can result in static loads on drip shields.

The seismic ground motion modeling case has a relatively large contribution to total dose to the RMEI (Section 2.4.2.2), and a detailed discussion is presented here regarding its implementation in the TSPA model (SNL 2008a, Section 6.6) and the associated information flow. The seismic scenario class evaluates the effects of seismic hazards (Section 2.3.4) (vibratory ground motion and fault displacement) on releases of radionuclides through groundwater. These seismic hazards could result in mechanical disruption of EBS features (Section 2.1.2.2) in response to vibratory ground motion and to the lithophysal rubble induced by vibratory ground motion. The FEPs and associated models related to seismic damage in the EBS are applicable to both the 10,000-year analyses and the post-10,000-year analyses.

The seismic scenario class is composed of two modeling cases: the seismic ground motion modeling case and the seismic fault displacement modeling case. Seismic hazards associated with vibratory ground motion and fault displacement could result in the following effects:

- Ground motion-induced lithophysal rubble on drip shields and on waste packages if a drip shield were to fail
- Direct ground motion-induced shaking of drip shields, waste packages, and pallets
- Fault displacement acting on drip shields and waste packages
- Changes in the seepage, temperature, and humidity environment for EBS features within the emplacement drift, caused by the accumulation of lithophysal rubble.

FEP analyses (Section 2.2) indicate that these seismic hazards will not significantly alter the long-term flow of water through the mountain. Thus, groundwater transport away from the damaged packages is calculated using the nominal scenario class models, and doses to humans from contaminated groundwater are determined using BDCFs for the groundwater exposure case. Following a seismic event and the breaching of waste packages, radionuclides are mobilized and transported from the EBS into the repository host rock. The mobilized radionuclides can then be transported by water percolating through the unsaturated zone to the water table, and then to the accessible environment by flow and transport processes in the saturated zone.

The seismic scenario class considers seismic events in the mean annual exceedance frequency range of 4.287×10^{-4} to 10^{-8} per year. The upper bound on the mean annual exceedance frequency is based on the minimum PGV threshold for the onset of seismically induced damage (SNL 2007c), Section 6.4.3) and the lower bound is prescribed by regulation (proposed 10 CFR 63.342(a)). The relationship between annual exceedance frequency (i.e., probability) and the PGV (i.e., consequence) is based on a PSHA performed to assess the seismic hazards of vibratory ground motion and fault displacement at Yucca Mountain (CRWMS M&O 1998). The seismic scenario class modeling cases use the mean hazard curves for ground motion and fault displacement developed as a result of the PSHA, rescaled to give an upper bound on horizontal PGV at the repository horizon equal to 4.07 m/sec (Section 2.3.4.3.3). The use of the mean hazard curve is conservative relative to the median hazard curve, because it typically lies above the 80th percentile of the distribution of hazard curves (Section 2.3.4.3.2.2), so the mean is dominated by the larger values of the distribution (SNL 2008a, Section 6.6.1.2).

The model components and submodels of the TSPA model for the seismic scenario class are shown on Figure 2.4-117. Many of the TSPA model components and submodels utilized in the seismic scenario class are the same as those described for the nominal scenario class. For example, the model components and submodels for flow and transport in the unsaturated zone and saturated zone are the same as those for the nominal scenario class. However, some of the model components and submodels differ, including (Figure 2.4-117):

- Waste package and drip shield degradation model component
- Drift seepage submodel and drift wall condensation submodel of the unsaturated zone flow model component
- EBS thermal-hydrologic environment submodel of the EBS environment model component.

EBS Degradation History—The mechanical response of EBS components to a seismic event will be highly dependent on the in-drift configuration of EBS components and on the structural integrity of the EBS components at the time of the seismic event. The mechanical response of a drip shield shortly after repository closure could be quite different than its mechanical response in a collapsed drift—where a drip shield is covered by rubble and fails under the combined static load from rubble and dynamic load from vibratory ground motion. The future configuration of the EBS components has been represented by three idealized configurations, as shown in Figure 2.3.4-52. The initial configuration is the as-emplaced EBS configuration, with an intact drip shield and minimal rubble in the drifts. In this configuration, waste packages can move freely beneath drip shields. The next configuration represents an intermediate state of the system where the legs of a drip shield have buckled under combined rubble/ground motion load (i.e., the drip shield framework has failed), but the drip shield plates remain intact. In this configuration, a drip shield loaded by rubble collapses onto a waste package, transmitting the rubble load to the waste package and inhibiting free movement of the waste package and emplacement pallet during a seismic event. The final state of the system is when rubble surrounds waste packages after failure of the drip shield plates. The transition between these configurations is determined by fragility curves for the drip shield framework and plates, based on the intensity of the seismic event and on the thickness of drip shield components and accumulated rubble load at the time of the seismic event.

The structural integrity of the EBS components is determined by process-level structural response calculations (SNL 2007ac). The various states of drip shield failure (due to framework failure or plate failure) lead to three distinct damage mechanisms for waste packages. The first mechanism, referred to as kinematic damage, exists when waste packages are free to move beneath drip shields (Figure 2.3.4-51a). The second and third damage mechanisms occur when the motion of waste packages is restricted and are shown on Figures 2.3.4-51b and 2.3.4-51c. These mechanisms are referred to as damage for a waste package beneath (loaded by) a buckled drip shield (i.e., the drip shield framework has failed) and damage for a waste package surrounded by rubble, respectively.

The future state of the internal structures within waste packages is also important to the type and degree of damage to the outer Alloy 22 barrier. The internal structure includes a 5-cm-thick inner vessel of stainless steel, a TAD canister (for commercial SNF), and the basket structure that supports the fuel rod assemblies within the waste packages. These steel internal structures could degrade much faster than Alloy 22, depending on the in-package chemical environment, the residual stress near welds in the inner vessel, and the potential for galvanic contact between the Alloy 22 outer corrosion barrier and the stainless-steel inner vessel. Given the uncertainties related to these long-term degradation processes, the future state of the internals is represented as either intact or degraded in the process-level structural calculations. The internals remain intact structurally until the first breach of the outer corrosion barrier, after which time they are treated as a degraded material with minimal strength and minimal cohesion (Section 2.3.4.5.2.1.2.5). Breach refers to any penetration of the outer corrosion barrier. The first breach will usually occur from nominal stress corrosion cracking in the lid welds or in response to seismic events (SNL 2007c, Section 6.1.3). Since the upper bound of the exceedance frequency of seismic events that could result in damage to the EBS is 4.287×10^{-4}/yr (SNL 2007c, Section 6.4.3), the typical time interval between seismic events is about 2,300 years. This is the shortest expected interval between potentially damaging seismic events. However, based on the actual seismic consequence abstractions, a more typical mean interval to the time of the first event that damages codisposal waste packages with intact internals is about 134,000 years, when averaged over all epistemic and aleatory uncertainty in the seismic consequence models, such as the residual stress threshold (based on a recurrence frequency of 7.484×10^{-6}/yr). This is comparable to the expected lifetime of the 50-mm-thick stainless steel inner vessel (assuming double-sided corrosion and a mean corrosion rate of 0.267×10^{-6} m/yr) (SNL 2007k, Table 8.2-4), which is about 94,000 years, if in-package chemical conditions remain similar to a fresh water environment, which is the expected condition until after drip shield failure (SNL 2007c, Section 6.1.3). Thus, the internal structure of the codisposal waste packages would be expected to be degraded before the time of the next seismic event that could damage a waste package with structurally sound internals—and even more so for commercial SNF packages because the recurrence interval between damaging events is much greater than for codisposal packages, based on a recurrence frequency of 5.249×10^{-9}/yr, due to the presence of the TAD. (Note that in the TSPA model the seismic degraded internals abstraction is applied after the first damaging event and the recurrence interval between damaging seismic events for codisposal waste packages with degraded internals is much smaller than the recurrence interval for the intact internals abstraction because of the lack of internal structural strength after the internals are degraded. The recurrence interval for damage to codisposal waste packages with degraded internals is equal to about 34,000 years, based on a recurrence frequency of 2.956×10^{-5}/yr. Thus, the application of the degraded internals abstraction is a conservative approximation, since the lifetime of the internals is significantly larger than this 34,000-year recurrence interval.)

Methodology for Seismic Consequence Abstractions for Drip Shield and Waste Package Damage—Three primary sets of process-level calculations form the basis of the drip shield and waste package degradation abstraction. These are: (1) a three-dimensional kinematic calculation for waste package and drip shield damage due to vibratory ground motion appropriate for the early postclosure period during which relatively little EBS degradation occurs, (2) a calculation for deformation and damage of a drip shield under static and dynamic conditions appropriate for the postclosure period associated with intermediate levels of EBS degradation, and (3) a calculation for a waste package surrounded by rubble used to estimate damage at late times during the postclosure period after extensive degradation of the EBS (SNL 2007ac, Section 7.2.1).

As discussed in Section 2.3.4.5, three-dimensional kinematic calculations are used to examine the motion and impact of multiple waste packages, pallets, and drip shields in an emplacement drift (SNL 2008a, Section 6.6.1.2.2). The objective of these analyses is to define the history of impact parameters (impact velocity, impact force, angle of impact, location of impact) for collisions of the waste packages, pallets, and drip shields as a function of the applied ground motion time histories, and to determine the associated probability of rupture and damaged areas on a waste package. Seventeen separate ground motion time histories are used, and each is used at four different PGV levels, spanning the magnitude of possible damaging ground motions at the repository. Separate kinematic calculations are performed for each PGV level of each ground motion time history.

The kinematic calculations are appropriate when the drip shield is intact and the waste package can move freely beneath the drip shield. At late times, when the degraded drip shield plates fail, the waste packages will be surrounded by rubble, which essentially precludes further kinematic damage. The waste package failure mechanisms are now stress corrosion cracking from the static rubble load and puncture of the waste package by the internals in response to low probability but high amplitude vibratory ground motions. Rubble in the lithophysal zone is most relevant here because the small particle size of the lithophysal rubble means it can more easily slip or fall through gaps or tears in the plates of the drip shield, and because the lithophysal zones encompass approximately 85% of the emplacement drifts in the repository. Thus, in TSPA, all waste packages are assumed to be in lithophysal zones for the purposes of seismic damage consequence calculations (SNL 2007c, Section 6.9). The damage induced by the rubble surrounding the waste package is based on the two-dimensional coupled rubble/structural response of the Alloy 22 outer barrier during vibratory ground motion. The internals of the waste package are assumed to be in a degraded state for this configuration. The input data for the calculations of a single waste package surrounded by rubble include 17 ground motion time histories at four PGV levels, elastic and plastic properties of the outer barrier, and the bulk properties of degraded waste package internals (SNL 2007ac, Section 6.5.1.1).

The consequences to the EBS of seismic activity are propagated into the TSPA model. However, the potential for spatial variability of ground motions to produce spatially varying seismic damage to the waste packages and drip shields has not been explicitly represented in the degradation behavior of waste packages and drip shields in the TSPA model. Although this type of spatial variability is not explicitly represented within the TSPA, it has been included at the drift scale in the kinematic calculations, through the variability of friction factors on a package-by-package basis and in the abstraction of damaged areas for the two or three central waste packages in the kinematic calculations (SNL 2007c, Section 8.1). At larger scales (e.g., drift-to-drift), seismic ground motion waves are assumed to have similar effects throughout the repository. However, limited spatial variability is incorporated in the TSPA through seismic coupling with nominal degradation processes. In particular, variable thermal-hydrologic environment (i.e., temperature history) among the five TSPA percolation subregions results in spatially variable seismic damage to waste packages, due to the variable thickness of the waste packages among the subregions. Within a percolation subregion all waste packages receive the same seismic damage. Drip shields are modeled to have no spatial variability with respect to seismic damage or with respect to nominal corrosion damage.

Seismic consequence analyses for the various EBS components are further characterized and subdivided in the following set of models for the TSPA:

Rockfall from Ground Motion—Rockfall induced by vibratory ground motion has the potential to fill the emplacement drifts during the period of geologic stability for dose assessment (proposed 10 CFR 63.302). Rockfall in the nonlithophysal zones refers to the large rock blocks that may be ejected from the nonlithophysal units of the repository during vibratory ground motion. Rockfall in the lithophysal zones refers to the fractured and rubblized material surrounding the drip shield and filling the drifts during partial or complete collapse of drifts. In the lithophysal zones, the rock mass has very low compressive strength and is permeated with void spaces of varying size (SNL 2007c, Section 6.7.1). The rock volume from multiple seismic events is defined as the sum of the volumes from the individual seismic events. Examination of the mean curves shows that the mean volume in the lithophysal rock is a factor of 32 to 188 greater than the mean volume in the nonlithophysal rock for the 1.05 and 2.44 m/s PGV levels, respectively (SNL 2007c, Section 6.7.2.1).

Partial or complete drift collapse can also impact the temperature and relative humidity of the outer surface of a waste package in lithophysal regions of the repository because rubble fills the collapsed drift, essentially forming a thermal blanket covering these waste packages. Furthermore, drift collapse impacts seepage flux and drift-wall condensation in the emplacement drifts in the lithophysal zones. Seepage flux is also impacted in nonlithophysal zones when a significant level of degradation is attained. This level of strong degradation is defined by a rock volume of 0.5 m^3 per meter of waste package length, well below the level used to define partial or full drift collapse in a lithophysal zone (between 5 and 60 m^3 per meter). However, these effects of drift collapse (lithophysal) or strong degradation (nonlithophysal) on seepage and temperature are only important after 10,000 years because of the relatively long time required to fill the drifts with rubble (SNL 2008a, Figure 7.3.2-19). Therefore, for all 10,000-year dose calculations the effect of drift collapse or strong degradation on seepage and seismic consequences is negligible and therefore not included in the dose calculations, based on TSPA analyses (SNL 2008a, Section 7.3.2.6.1.3.4). Not explicitly accounting for the effects of drift collapse or strong degradation means that the seepage abstraction for intact or moderately degraded drifts is applied and the thermal inputs from the multiscale thermal-hydrologic abstraction are those for an intact drift. Section 2.3.3.4.1.1 gives more details of the implementation of the seepage submodel for the seismic scenario class.

Drip Shield Failure from Ground Motion—The mechanical response of drip shields to vibratory ground motion, which could adversely affect the ability of a drip shield to prevent flow from reaching a waste package, is characterized by three mechanisms (SNL 2007c, Sections 6.8 and 6.10) described below. However, only the first of the three is included in the TSPA model because the latter two are of low consequence.

- The static load from rubble combined with the dynamic load during a seismic event could buckle a drip shield framework or rupture drip shield plates. Buckling or rupture compromises the capacity of a drip shield to deflect seepage and rubble away from a waste package. The effects of this mechanism are included in the TSPA model.

- The static load from rubble combined with the dynamic load during a seismic event could deform the plates on the crown of a drip shield. High levels of residual tensile stress could lead to accelerated degradation processes like stress corrosion cracking. However, because advective flow through stress corrosion cracks in drip shields has been screened out based on low consequence (FEP 2.1.03.10.0B, Advection of liquids and solids through cracks in the drip shield, Table 2.2-1) (SNL 2008c, Section 6), the abstraction for drip shield damage due to rubble loading in the lithophysal units has been excluded from the TSPA model.

- Impacts by large rock blocks in unfilled or partly filled drifts in nonlithophysal units could deform drip shields or fail plates and axial stiffeners on the crown of a drip shield. Failed drip shield plates provide a potential pathway for seepage to contact the waste packages. The abstraction for drip shield damage due to rock block impacts in the nonlithophysal units has not been included in the TSPA model based on an analysis that shows that the impact of this damage mechanism is small. This screening analysis is documented in excluded FEP 1.2.03.02.0B, Seismic-induced rockfall damages EBS components (Table 2.2-1) (SNL 2008c, Section 6).

The mechanical response or fragility analysis for drip shields (Section 2.3.4.5.3) defines the probability of failure as a function of the thickness and plastic load capacity of drip shield components, the static rubble load on drip shields, and the vertical component of peak ground acceleration for the seismic event (SNL 2007c, Section 6.8). Fragility curves are developed for two modes of failure: (1) buckling or collapse of the drip shield framework caused by buckling of the sidewalls of the drip shield and (2) rupture or tearing of drip shield plates. A third failure mode, from lateral waste package impacts to the drip shield or from longitudinal impacts of the waste package on the bulkhead support beams, was considered but not incorporated into the TSPA model. This third failure mode is not represented in TSPA for two reasons. First, lateral impact of the waste package on the drip shield does not cause catastrophic failure of the drip shield. Second, high velocity longitudinal impacts of the waste package on the bulkhead support beams exposed on the underside of the crown of the drip shield occur infrequently, even at the 4.07 m/s PGV level (SNL 2007c, Section 6.8.5 and Table 6-41), which is the maximum ground motion considered in the TSPA.

Regarding drip shield framework failure by sidewall buckling, calculations to represent degraded states of the system were performed for PGV levels of 0.2, 0.4, 1.05, 2.44, and 4.07 m/s; for thickness reductions of 0, 5, 10, and 13 mm for the plates and structural elements of the framework; and for drifts 10%, 50%, and 100% filled with lithophysal rubble (Section 2.3.4.5.3.4). Compared to the analysis for plate failure, discussed below, results indicate that the probability of framework failure is always higher than the probability of plate failure for a given rubble load and PGV. The framework is expected to always collapse before the plates rupture (SNL 2007c, Section 6.12.2, Step 8). If the drip shield framework fails for a seismic event, the drip shields will continue to prevent seepage from contacting the waste packages. Plate failure must subsequently occur for seepage to pass through the drip shield. There is no spatial variability for drip shield collapse (i.e., all drip shields collapse at the time of the damaging event).

Regarding drip shield plate failure, finite-element calculations were performed to define the plastic (nonlinear) load-bearing capacity of the curved plates on the crown of a drip shield (SNL 2007c, Section 6.8.2.1). These calculations defined the magnitude of the uniform load that causes an element of the plate to exceed the failure criteria for Titanium Grade 7, which are based on accumulated plastic strain and maximum stress (SNL 2007ac, Section 6.4.3.1.3). The plates were initially 15 mm thick. For these calculations, the ultimate plastic load capacity of a drip shield is determined as a function of plate thickness, the static load from rubble in the drift, and the vertical peak ground acceleration. Calculations to represent degraded states of the system are performed for 15-mm-, 10-mm-, and 5-mm-thick plates; for PGV levels of 0.2, 0.4, 1.05, 2.44, and 4.07 m/s; and for drifts 0%, 10%, 50%, and 100% filled with rubble. If drip shield plates fail for a seismic event, then all drip shields fail to prevent seepage from contacting the waste packages (no spatial variability) (SNL 2007c, Section 1.2). After drip shield plate failure, the mechanical response of waste packages to seismic events is determined by the abstraction, discussed below, for a waste package surrounded by rubble.

Waste Package Failure from Ground Motion—The potential failure mechanisms for the response of waste packages to vibratory ground motion (Section 2.3.4.5) are described as follows (SNL 2007c, Sections 6.5, 6.6, and 6.9):

- **Stress Corrosion Cracks**—Dynamic loads that dent waste packages could cause permanent structural deformation with residual stress. The damaged or deformed area that exceeds a residual stress threshold is conceptualized to result in a tightly spaced network of stress corrosion cracks. The network of stress corrosion cracks is considered to immediately form once the residual tensile stress threshold is exceeded, providing potential pathways for radionuclide transport and release (SNL 2007e, Section 6.7).

- **Rupture**—Dynamic loads on waste packages free to move during a seismic event have the potential to result in a rupture (tear) of a waste package if the local strain exceeds the ultimate tensile strain. The extreme deformation from a major seismic event could produce tensile strains in the Alloy 22 and weaken the outer corrosion barrier, potentially resulting in a ruptured outer corrosion barrier from a subsequent extreme seismic event (SNL 2007c, Section 6.1.2). The rupture is conceptualized to be along a crease that lies in a plane normal to the central axis of the waste package. The failed area can be represented as a circumferential band around the waste package for transport calculations in TSPA (SNL 2007c, Section 6.6.2.1). Ruptured waste packages provide potential pathways for seepage and for radionuclide transport and release. Waste package rupture occurs only for waste packages free to move under intact drip shields.

- **Puncture**—The probability of rupture for waste packages with degraded internals (i.e., a degraded stainless steel inner vessel) surrounded by rubble is zero because the strain on the outer corrosion barrier is always below the ultimate tensile strain for Alloy 22 (SNL 2007ac, Section 6.5.1). However, sharp edges of fractured or partly degraded internal components could puncture a severely deformed outer corrosion barrier. The waste package internals are assumed to degrade as structural elements after the outer corrosion barrier is first breached. Extreme deformation of the cylindrical outer corrosion barrier can eliminate the free volume within the outer corrosion barrier, allowing the sharp corners or sharp edges from degraded internal elements to puncture the outer corrosion barrier when it is surrounded by lithophysal rubble (SNL 2007c, Section 6.1.2). The punctured area is conceptualized to be a small patch on the surface of the outer corrosion barrier (SNL 2007c, Section 6.9.1). Punctured waste packages provide potential pathways for seepage and for radionuclide transport and release. Waste package puncture occurs only for waste packages with degraded internals, surrounded by lithophysal rubble.

Kinematic and structural response calculations were performed to develop stress corrosion cracking damage estimates for the failed waste package surface area for commercial SNF and codisposal waste packages under intact drip shields (SNL 2007c, Sections 6.5.1 through 6.5.4 and 6.6.1 through 6.6.4). The results from the structural response calculations were evaluated for three values of the residual stress threshold for Alloy 22: 90%, 100%, and 105% of the yield strength of Alloy 22. Kinematic damage abstractions were developed for three future states of commercial SNF and codisposal waste packages (Section 2.3.4.5):

- 23-mm-thick outer corrosion barrier with intact internals
- 23-mm-thick outer corrosion barrier with degraded internals
- 17-mm-thick outer corrosion barrier with degraded internals.

For either intact or degraded internals, there is no waste package-to-waste package spatial variability for the conditional damaged area within each percolation subregion (SNL 2007c, Section 1.2). For a single package, the damaged area is randomly located on the cylindrical surface of the outer corrosion barrier. The total damaged area increases with each seismic event that causes damage to the waste package outer corrosion barrier. For the commercial SNF waste package with intact internals, damage occurs only at the highest (4.07 m/s) PGV level (SNL 2007c, Section 6.5.1.2).

Structural response calculations were also performed to develop stress corrosion cracking damage estimates for the failed waste package surface area of a commercial SNF waste package surrounded by rubble (SNL 2007c, Sections 6.9.1 through 6.9.9). Two damage abstractions were developed for a waste package with degraded internals that is surrounded by lithophysal rubble (Section 2.3.4.5.4.2.1):

- 23-mm-thick outer corrosion barrier with degraded internals
- 17-mm-thick outer corrosion barrier with degraded internals.

Damage for waste packages with intact internals is not calculated for waste packages surrounded by rubble. A waste package becomes surrounded by rubble after the drip shield framework and drip shield plates have failed (Section 2.3.4.5.1) during a seismic event and the drifts have partially or completely collapsed. This is expected to occur at late times after repository closure (Figure 2.1-11). For codisposal waste packages the outer corrosion barrier is expected to have been breached at these times by stress corrosion cracking induced by seismic events, resulting in degraded internals (Figure 2.1-12d). In contrast, the probability of seismic-induced stress corrosion cracking damage to commercial SNF waste packages with intact internals under intact drip shields (SNL 2008a, Figure 6.6-10) is much lower than that of codisposal waste packages (zero at PGV less than 2.44 m/sec), so it is not very probable that they will be breached by seismicity at the time the "surrounded by rubble" abstraction applies. Therefore, commercial SNF waste packages are not expected to have degraded internals at the time of drip shield failure (SNL 2008a, Section 6.6.1.2.2.2) except for the small fraction of commercial SNF waste packages that have developed nominal stress corrosion cracks in the closure lid welds, as discussed below (Figure 2.1-10a). However, regardless of the time scale, the damage abstractions for degraded internals will be conservative relative to the response with intact internals, so this approach is conservative (SNL 2007c, Section 6.9). Separate abstractions are not developed for commercial SNF and codisposal waste packages surrounded by rubble because the results for the commercial SNF waste packages provide a reasonable estimate of damage to the codisposal waste packages (SNL 2007c, Section 6.9.10 and Table 6-48).

Lithophysal rubble is selected for the dynamic load on waste packages. The analysis acknowledges that large rock blocks would tend to have point loading contacts in localized areas on a waste package, but the cumulative loading from the lithophysal rubble is expected to be significantly greater because the volume of lithophysal rubble is much greater than the volume of nonlithophysal rockfall (SNL 2007c, Section 6.7.2.1, Table 6-32, and Figure 6-58).

In the seismic scenario class ground motion modeling case, waste package damage is accumulated for successive events and added to the damage caused by nominal corrosion processes (SNL 2008a, Section 6.6.1.3.1). Within a percolation subregion there is no spatial variability in the waste package thickness used to determine the consequences of each seismic event; therefore, if a seismic event damages an intact waste package in a percolation subregion, it damages all intact waste packages assigned to the same percolation subregion. The exception to this is when nominal corrosion failures precede seismic damage. In this case, damage abstractions for damaged waste packages (i.e., waste packages with degraded internals) are applied to the failed waste packages and the damage abstractions for intact waste packages are applied to the intact waste packages. As a simplification, if the consequences of an event result in damage to the intact waste packages, all packages are damaged and the accumulated damage on the previously failed packages is conservatively added to the damage applied to the newly failed waste packages. For waste packages subject to stress corrosion cracking damage, the effective transport area for a damaged waste package is much smaller than the damaged area (defined as the area with residual tensile stress) because transport occurs through a network of stress corrosion cracks, rather than through the total damaged area that exceeds the residual stress threshold. The effective area for flow and transport is based on the crack density model and associated scaling factor for Alloy 22 (SNL 2007e, Section 6.7). The distribution representing the scaling factor has a mean value of 0.00819 (SNL 2008a, Section 6.6.1.1.2).

Commercial SNF or codisposal waste packages that can move freely beneath a drip shield can rupture from the accumulation of severe deformation due to multiple impacts, which can accumulate in either one seismic event or multiple seismic events. The probability of rupture for the 23-mm-thick outer corrosion barrier with intact internals is determined to be zero (SNL 2007c, Sections 6.5.1.1 and 6.6.1.1). However, for commercial SNF or codisposal waste packages with degraded internals, the effect of multiple waste package-to-pallet impacts is assessed by evaluating the severity of accumulated deformation. The degree of deformation is used to define the probability of rupture. When a waste package is ruptured, the failed area is determined by sampling a uniform distribution for failed area, with a lower bound of zero and an upper bound equal to the cross-sectional area of the waste package outer corrosion barrier (SNL 2008a, Section 6.6.1.2.2.2). This failed area allows advective flow through and advective and diffusive transport out of ruptured commercial SNF or codisposal waste packages.

For a waste package surrounded by rubble, loss of waste package integrity is conceptualized to occur from puncture by sharp internal fragments, rather than rupture of the outer corrosion barrier due to impact with other EBS components. Analyses show that punctures will occur more often than ruptures, particularly for 17-mm outer corrosion barriers and at lower PGVs (SNL 2008a, Sections 7.3.2.6.1.3.5 and 7.3.2.6.1.3.6). When waste packages are punctured, the failed area is determined by sampling a uniform distribution with a lower bound of zero and an upper bound of 0.10 m^2 (SNL 2007c, Table 6-90). This failed area allows advective flow through punctured waste packages and advective and diffusive transport out of the punctured waste packages.

Fault Displacement—The expected number of waste package failures that occur due to fault displacement is a small fraction of the total number of waste packages in the repository. The number of failed waste packages is estimated based on an understanding of the displacements that could occur on these faults and geometrical considerations (SNL 2007c, Section 6.11). A fault displacement that occurs in an emplacement drift could cause a sudden discontinuity in the profile of the drift. This could result in one portion of the drift being displaced vertically or horizontally relative to the adjacent section. Such a discontinuity in the drift could cause shearing of the waste package and drip shield located over the fault if the fault displacement exceeds the available clearance in the EBS.

Given the complexity of the response of EBS components and the invert to a fault displacement, a simplified failure criterion is applied to determine shear failure in a collapsed drift. If the fault displacement exceeds one-quarter of the outer diameter of the outer corrosion barrier (about 0.4 m to 0.5 m), the waste package fails from shear (SNL 2007c, Section 6.11.1.2). This simple failure criterion is appropriate because waste package failures from fault displacement events only occurs from extremely low-frequency, high-amplitude fault displacements, corresponding to an annual exceedance frequency of less than or equal to 2.5×10^{-7} per year (SNL 2007c, Table 6-67). At frequencies greater than this value, no effects of fault displacement are considered in the TSPA. Fault damage to waste packages is assumed to allow flow into waste packages (if seepage is present) and allow advective and diffusive transport out of waste packages. When a waste package fails from fault displacement, the associated drip shield is also presumed to fail, causing damage to the total surface area of the drip shield.

Uncertainty—Uncertainty in the seismic scenario class is directly represented in the TSPA model by defining uncertain parameters that are sampled either once per realization (epistemic parameters) or multiple times per realization (i.e., at the occurrence of each seismic event (aleatory parameters)). The uncertainty in the input parameters for the underlying process models, and its propagation in the TSPA model, is summarized as follows (SNL 2007c):

- The structural response calculations for the responses of waste packages that are affected by vibratory ground motion include three principal sources of uncertainty: (1) the ground motion time histories (aleatory uncertainty), (2) the metal-to-metal friction coefficient (epistemic uncertainty), and (3) the metal-to-rock friction coefficient (epistemic uncertainty) (SNL 2008a, Section 6.6.1.2.4). The variations of these uncertain input parameters are simultaneously included in the 17 structural response calculations at each seismic hazard level, using a Latin hypercube sampling.

- All analyses of rock rubble include 15 ground motion time histories as the primary source of aleatory uncertainty (SNL 2008a, Section 6.6.1.2.4). In the lithophysal units, the rock compressive strength is an epistemically uncertain input parameter that is represented as five discrete levels of rock strength. In the nonlithophysal units, the synthetic fracture pattern is an epistemically uncertain input parameter (SNL 2008a, Section 6.6.1.2.4).

- The abstractions of damaged areas on waste packages and drip shields that are used by TSPA contain both forms of uncertainty, aleatory (e.g., due to intrinsic variability in the seismic ground motion time histories and spatial variability in waste package thicknesses used to characterize the damage abstractions), and epistemic (e.g., due to uncertainty in the residual stress threshold for stress corrosion cracking in Alloy 22 and uncertainty in general corrosion rates).

Figure 2.4-117 schematically depicts the flow of information between principal TSPA submodels for the seismic scenario class. The flow of information between submodels in the seismic scenario class is very similar to the nominal scenario class, as depicted on Figure 2.4-112. As mentioned earlier, the submodels for the seismic scenario class are the same as those implemented for the nominal scenario class, with two main exceptions:

- Ground motion and fault displacement damage to drip shields and waste packages is calculated as a function of the seismic events, in conjunction with the nominal damage determined by calculations with the WAPDEG DLL for expected degradation and corrosion processes (SNL 2007c), although some simplifying assumptions are used for the 10,000-year calculations because of the low consequences of some of the damage mechanisms (Section 2.4.2.1.5.4).

- Drift seepage in the lithophysal and nonlithophysal units is calculated based on the degradation state of the drift. Drift-wall condensation in the lithophysal regions ceases once the drift is fully collapsed. Because drift degradation in the nonlithophysal regions is conceptually different than drift collapse in the lithophysal regions, drift wall condensation in the nonlithophysal regions is not affected by drift degradation. Furthermore, there can be a thermal perturbation to the in-drift thermal-hydrologic environment for a collapsed drift. Because the thermal perturbations are applied to the representative waste package, which is in the lithophysal region, all waste packages, including those in the nonlithophysal region, experience a thermal perturbation from drift collapse. Again, some simplifying assumptions are appropriate for the 10,000-year calculations (Section 2.4.2.1.5.4)

2.4.2.3.2.2 During-Development Model Validation Activities for the TSPA Code

As described above in Section 2.4.2.3.2, Section 7.0 of the TSPA model report (SNL 2008a) explains that confidence in the results of the TSPA model depends on two categories of model validation activities: (1) those conducted during development of the model, and (2) those conducted after development of the model. This section summarizes the various during-development activities that are outlined in Table 2.4-8. The major categories of during-development activities are verification of inputs/software, stability testing, uncertainty characterization reviews, and surrogate waste-form analyses for DOE and naval SNF.

2.4.2.3.2.2.1 Computer Code and Input Verification

This section discusses the verification of the TSPA model software, verification of DLLs as implemented in the TSPA model, verification of model inputs entered into the TSPA input database, and verification of the implementation of the submodel abstractions within the TSPA model. Also, coupling between submodels within the TSPA model is examined by verifying that the information generated by one submodel is fed correctly to successive submodels and that the information does not exceed the applicable range of the successive submodel.

A full understanding of the verification activities described below is enhanced by an understanding of the architecture of the TSPA GoldSim input model file and of the functionality of the GoldSim software itself. Additional details of the TSPA GoldSim input model file architecture are given in *Total System Performance Assessment Model/Analysis for the License Application* (SNL 2008a, Section 6.1.5). As previously mentioned in Section 2.4.2.2.2.1, most of the analyses referred to in this section were done with an earlier version (v4.042) of the TSPA model. TSPA Model v4.042 is a version of the model that is just prior to the creation of v5.000. The differences between v4.042 and v5.000 were evaluated and determined not impact the analyses discussed in this section. The analysis using v4.042 of the TSPA model is archived in DTN: MO0708TSPAPOST.000.

Selection and Verification of the Integrated System Software—GoldSim simulation software V 9.60.100 and V 9.60.300 serves as the integrating shell that links various submodels and codes that make up the TSPA model. GoldSim is a stochastic sampling program that integrates all the submodels, codes, and response surfaces together into a coherent structure that allows for consistent sampling of parameter values among the submodels. The GoldSim program is used to conduct multi-realization simulations of the entire repository system, using values for both aleatory and epistemic parameters sampled for each realization from uncertainty distributions. Thus, each realization of the total system has a unique set of the values of the input parameters. In addition, each realization is considered to be equally likely, unless importance sampling is used to emphasize some realizations (usually to increase the likelihood of sampling an unlikely event or parameter value). Multiple realizations of the TSPA model yield a distribution of radionuclide concentrations and annual dose to the RMEI that shows uncertainty in annual dose based on uncertainty in all of the submodels.

Much of the computational work for the TSPA model is done using separate software codes whose results are integrated within the GoldSim software as response surfaces, dynamic linked libraries, lookup tables, and inputs. For example, the unsaturated zone flow fields are computed using the software code Transport of Unsaturated Groundwater and Heat V1.6 (TOUGH2 V 1.6). Results of these detailed process-level calculations are abstracted for use in the TSPA model as multidimensional tables that are read into GoldSim at run time. Examples of these multidimensional tables include: (1) liquid flux and velocity fields for the unsaturated zone as a function of time and spatial location; and (2) temperature and relative humidity as a function of time and location within the repository.

Once the GoldSim runs are completed and the modeling case dose results are exported to text files, additional software is used to calculate the expected dose for most modeling cases. The GoldSim runs provide the inputs for these additional dose calculations, which are performed by the software code EXDOC_LA V 2.0 to calculate the expected dose. The EXDOC_LA V 2.0 code separates aleatory and epistemic uncertainty and integrates over the aleatory uncertainty for fixed values of the epistemic parameters to calculate an expected value, conditional on one epistemic element (one set of fixed and sampled variable epistemic parameters). This operation is repeated for each sample element, to obtain a group of expected results. Statistics (i.e., mean and percentiles) are calculated for these results. The treatment of aleatory uncertainty can be thought of as an inner loop in the calculation and the treatment of epistemic uncertainty as an outer loop (Section 2.4.1). For computational efficiency, the TSPA GoldSim modeling for most modeling cases is performed with specified aleatory quantities and EXDOC_LA V 2.0 is used to calculate the expected dose from these GoldSim runs. As an example, the GoldSim calculations for the igneous intrusion modeling case are performed for 10 specified event times and EXDOC_LA V 2.0 is used to determine the expected dose accounting for event times interpolated between these specified values and accounting for the probability of occurrence of each event.

Submodels are coupled into GoldSim by the following:

- External function calls to detailed process software codes, such as the unsaturated zone transport software, FEHM V 2.24, or the waste package degradation software, WAPDEG V 4.07

- Cell or pipe pathway elements in GoldSim—basically equilibrium batch reactors—which, when linked in series, provide a description of transport through selected parts of the repository system, such as in EBS transport

- Response surfaces, which take the form of multidimensional tables, representing the results of modeling with detailed process models that are run before running the TSPA model (e.g., inputs to the EBS thermal-hydrologic environment, such as temperature and relative humidity in the invert)

- Functional or stochastic representations of a submodel directly built into the GoldSim code, such as seismic ground motion damage or BDCFs.

GoldSim is selected as the TSPA integration code based on its capabilities and use in similar applications. GoldSim (V 9.60.100 and V 9.60.300) has the following general capabilities:

- Addresses the inherent variability and uncertainty that is present in complex systems by using Monte Carlo simulation
- Superimposes the occurrence and consequences of discrete events onto continuously varying systems
- Builds top-down models using hierarchical containers that facilitate the simulation of large, complex systems while keeping them easy to understand and navigate
- Dynamically links external programs or spreadsheets directly to the GoldSim software
- Directly exchanges information between any open connectivity compliant database and the software
- Provides a contaminant transport module to simulate the release, transport, and ultimate fate of mass within the system.

GoldSim was originally developed for the evaluation of radioactive waste disposal facilities. In the past decade, GoldSim has been used in the following applications (GoldSim Technology Group 2007b, pp. 8 and 9):

- Evaluation of the safety of the proposed HLW repository at Yucca Mountain, including the Site Recommendation
- Evaluation of potential host rocks as part of a program to select a disposal site for the Spanish Radioactive Waste Disposal Research efforts
- Evaluation of waste disposal sites in Los Alamos, New Mexico to aid in risk characterization and to help identify monitoring requirements for low-level radioactive waste disposal areas
- Evaluation of alternative remediation and closure options for abandoned uranium mill tailings facilities and mine workings in Germany and Canada
- Evaluation of waste disposal concepts in Japan, including integrated assessments for the disposal of high-level waste and spent fuel
- Evaluation of different conceptual models of the groundwater flow system on estimates of radionuclide migration at the Nevada Test Site
- Evaluation of clay and granite high-and intermediate-level waste disposal concepts in France by ANDRA (Agence Nationale Pour la Gestion des Dechets Radioactifs).

Each version of the GoldSim software is verified to meet all applicable performance requirements. Verification is performed in accordance with a verification plan by the vendor, GoldSim Technology Group (*Design Document for: GoldSim V 9.60* (DOE 2007c)). This verification program exercises the graphical user interface, internal functions, stochastic processes, contaminant transport code, and result displays to demonstrate that the software performs its numerical, logical, and input/output operations correctly. The verification used by the vendor consists of over 250 tests that cover the program capabilities, including the user interface, user defined expressions, internal functions, and distributed processing capabilities. These include:

- 93 basic functional tests
- 23 time and Monte Carlo tests
- 130 contaminant transport tests
- 17 reliability module tests.

Following applicable quality assurance requirements, specific vendor supplied tests from the vendor verification plan are executed to assess the adequacy of software functionality. These tests have demonstrated the satisfactory implementation of the TSPA functional requirements listed in *Requirements Document for: GoldSim v9.60* (DOE 2007d). For added confidence, key functions and capabilities of the simulation software are combined into four TSPA-developed tests and the results are compared to independently generated results. The independent tests are described in *Design Document for: GoldSim v9.60* (DOE 2007c, Section 7.2.1) and the results are shown in *Software Validation Report for: GoldSim v9.60 on Windows 2000* (DOE 2007e, Sections 4.2.34 to 4.2.37).

EXDOC_LA V2.0, which computes expected annual dose and summary metrics of expected annual dose (e.g., mean or median) from the realizations of annual dose provided by GoldSim, is verified through a series of 17 test cases described in the *Design Document for: EXDOC_LA Version 2* (DOE 2007a). These test cases are primarily designed to verify the software's capability of computing expected dose for each of the seven modeling cases. Results of the test cases are reported in Section 4.2 of *Software Validation Report for: EXDOC_LA Version 2.0* (DOE 2007f). These tests have demonstrated the satisfactory implementation of the EXDOC_LA functional requirements listed in *Requirements Document for: EXDOC_LA Version 2.0* (DOE 2007g).

Verification of Dynamically Linked Libraries—DLLs are integrated into the TSPA and perform two kinds of tasks: (1) data and file manipulations necessary to pass information back and forth between model components and to support the coupling of different model components within the TSPA code, and (2) implementation of model abstractions or portions of model abstractions within the TSPA code. All DLLs, regardless of the kind of task they perform, are first tested in accordance with the requirements of the software qualification procedure mentioned above to ensure they are functioning properly (SNL 2008a, Section 3). DLLs that perform the first kind of task, data or file manipulation, are evaluated by internal model checking and are also part of the model component and coupling confirmation processes described below. DLLs that perform the second kind of task, implementing a model abstraction or portion of a model abstraction, are confirmed by verification analyses, described below. A description of the verification analyses is provided in Table 2.4-9, along with a brief description of the analysis.

The general approach to verifying a DLL as a single module within an integrated model is as follows (SNL 2008a, Section 7.2). A validation test example reported in a model report or a validation test report with known results is first run on the stand-alone implementation of a DLL to verify that the correct answer appearing in the report or validation test report can be reproduced. In some instances, there could be small differences between the results reported in the analysis model report and those calculated by the stand-alone implementation. These small differences are accounted for and typically arise from differences in calculation schemes between the two model implementations (e.g., discretization, time stepping, and numerical solutions, as compared to analytical solutions). The next step is to run a single realization of a version of the TSPA model by providing the same set of inputs to the DLL as those run for the stand-alone model. The results from the TSPA model can be obtained either from an output file created by the DLL or from GoldSim model file elements that capture the outputs from the DLL. The results calculated from the single realization of the TSPA model are verified if they are exactly equal to those calculated by the stand-alone model (implementation of the DLL).

An example of the DLL verification methodology is the comparison of the TSPA model implementation of saturated zone transport to the test example given in the underlying process-level report (SNL 2008a, Section 7.2.4.1.8). The result from a transport base-case simulation developed in *Site-Scale Saturated Zone Transport* (SNL 2008h) is compared to the TSPA model (v4.042) results. The saturated zone source term in the TSPA model is defined by assigning a unit mass flux (1.0 g/yr) for a sorbing radionuclide (^{237}Np) that includes radioactive decay. This source term is assigned to the unsaturated zone transport submodel output element that feeds mass out of the unsaturated zone and into the saturated zone at source region 1. The mass input into this region is then input into the SZ_Convolute DLL in the TSPA model. The ^{237}Np mass flux output from the SZ_Convolute DLL is passed into the model elements, which sums all mass flux out of the three-dimensional saturated zone transport submodel. The results of the TSPA model simulation are then compared to the single-realization transport median case breakthrough curve provided by the site-scale saturated zone process model. The mass flux from the two simulations are plotted on Figure 2.4-118 and indicate good overall agreement. There is a slight deviation at early times due to an increase in the time step size for the TSPA model.

Verification of coupling among TSPA model components and DLLs is also important, particularly at major submodel and model component interfaces (SNL 2008a, Section 7.2.5). This coupling includes flow and transport through the EBS, coupling at the EBS-unsaturated zone interface (between GoldSim and the FEHM DLL), and coupling at the unsaturated zone-saturated zone interface (between GoldSim and the SZ_Convolute DLL) (SNL 2008a, Section 7.2.5). This verification process is also shown in Table 2.4-9 and discussed in more detail later in this section. Confirmation of the appropriate integration of DLLs within the TSPA model is also realized by a variety of auxiliary analyses, such as single-realization deterministic analyses (Section 2.4.2.2.3).

Verification of Inputs in the TSPA Database—Parameters used in the analyses for the TSPA model are documented in the TSPA input database (SNL 2008a, Section 4.7). The TSPA input database categorizes, stores, and retrieves fixed and uncertain values of the TSPA model parameters and allows qualified/authorized analysts to view and update values in the database. Each TSPA model simulation accesses the database in order to obtain values for the model parameters. Parameter values are obtained from various sources (SNL 2008a, Table 4-1), as described below, and manually entered into the database. Parameter values are entered into the database using a number of forms to ensure traceability. These forms include a parameter identification form that serves as the primary means to enter parameters into the TSPA input database.

Before using parameter values in the TSPA model for the performance assessment analysis, each parameter undergoes a check of the parameter identification form to ensure that the information has been entered correctly. The parameter verification is documented on the parameter verification form. Only users with access to the TSPA model controlled access input database can verify parameter values. The verification process includes recording the checker's name along with the date and time to identify the last user who changed any one of the parameter categories. Thus, the integrity of the parameter values used in the TSPA model is ensured. Strict control of access, along with detailed documentation trail, ensures the security, integrity, and traceability of information entered into, or downloaded from, the TSPA input database (SNL 2008a, Section 4.7).

The input database captures values for fixed and uncertain parameters, coefficients in response surface equations, lookup tables, time series data, stochastic distributions, and external files used by TSPA software. To ensure direct inputs to the TSPA model file are documented, they are also captured on parameter entry forms, described below. Inputs captured by the TSPA input database and parameter entry forms consist of three general types and are documented in output DTNs. The three types of inputs are:

1. Direct inputs from controlled sources used directly in the TSPA model
2. Inputs from controlled sources, but adapted for use in the TSPA model
3. Inputs generated and used by TSPA analysts in the TSPA model.

Inputs of the first type are acquired by TSPA analysts from the Technical Data Management System or from the reports that provide input to the TSPA model. These inputs are used directly in the TSPA model without modification. These parameter values are entered in the TSPA input database and documented on a parameter entry form. Inputs of the second type are also acquired by TSPA analysts from the Technical Data Management System or from the reports that provide input to the TSPA model. These inputs are used directly in the TSPA model with minor formatting, such as rounding to a specified number of significant digits, removing duplicate input values in defined lookup tables, sorting input values numerically, or converting inputs to units required by the appropriate TSPA submodel or analysis. Inputs of the third type are acquired by TSPA analysts from the Technical Data Management System or from the reports that provide input to the TSPA model and are processed by TSPA analysts before being captured in the TSPA input database and on a parameter entry form. Inputs of the third type include formatting direct inputs through the use of TSPA-generated software, manipulating inputs from controlled sources to be consistent with TSPA conceptual models, and correlating and sampling of the values of the uncertain parameters used internally by the TSPA model GoldSim files, and externally by TSPA model DLLs. All TSPA software used for reformatting data (SNL 2008a, Table 3-1) is subject to quality assurance procedures, such as software configuration management.

All parameter names, parameter values, and parameter references used in support of the TSPA model are documented in parameter entry forms. Parameter entry forms document both parameters that were downloaded from the TSPA input database and parameters entered directly into the TSPA model. Parameter entry forms provide the following information:

1. List of parameters, parameter descriptions, parameter values, and references
2. Directions or roadmaps to the location(s) of the information in the references
3. Explanations of any transformations, files, or parameters created by a TSPA analyst
4. Signatures documenting that inputs were appropriately selected from analysis and/or model reports and used in the TSPA model.

Verification of Single Model Components—The TSPA model is composed of submodels derived from abstraction models documented in various reports. Similar to the approach taken for DLL testing, GoldSim model file results are compared with results of stand-alone implementations documented in reports or validation test reports. The approach used to verify the submodels implemented in the TSPA model is based on the source of information provided in the supporting report namely:

- Lookup tables
- Abstraction equations with ranges of input values
- A qualified stand-alone GoldSim model containing the abstraction or DLL.

When inputs or results are in the form of a lookup table or abstraction equation, a verification subroutine is implemented in the GoldSim model file (SNL 2008a, Section 7.2.4). The verification subroutine calculates results for a range of input values under which the lookup table or abstraction equation is valid. Results from the GoldSim model file calculations are compared with values estimated from the lookup tables and/or equations presented in the underlying report. A good match between the expected values and GoldSim model file-calculated values indicates that the abstracted model has been verified.

Where TSPA submodels or components receive inputs from qualified DLLs or retrieve information from qualified external databases, the verification process involves checking to ensure that the GoldSim model is correctly linked to the TSPA input database and the correct values are returned. In addition, checking also verifies that equations were implemented correctly.

Finally, as described earlier in this section, where an external DLL represents a single model component or when a simple GoldSim model is available in an analysis/model report, the verification process involves conducting test runs presented in the report or in DLL software qualification documents. Verification runs in the TSPA model are set to simulate the runs presented in the validation documentation (i.e., the TSPA model is run with the same set of inputs as those presented in the DLL validation). Outputs of the GoldSim model are compared to results presented in the DLL validation.

As an example of the type of verification testing conducted for single model components, consider the verification of the EBS transport submodel (SNL 2008a, Section 7.2.4.1.6), which is verified by comparing the results of dissolved radionuclide transport and colloid facilitated radionuclide transport within the EBS from the TSPA model and a finite-difference approximation of the governing mass balance equations implemented in a Microsoft Excel spreadsheet (*Transport_Calc_Appendix_B.xls* in output DTN: SN0703PAEBSRTA.001). The mass balance equations tested describe the transport of radionuclides (^{239}Pu) and associated colloids with irreversible sorption onto iron oxyhydroxide colloids and the stationary corrosion products, as well as reversible sorption onto both waste form and groundwater colloids within the waste package.

Two verification cases were conducted. The first includes both advective and diffusive transport and the second includes only diffusive transport. The input parameter values for both the TSPA model and the Excel spreadsheet implementation were set to the same values, including a specified constant flow rate. Figure 2.4-119 is a comparison of the results for the case that includes both advection and diffusion. This case shows good agreement (i.e., less than 5% difference) between the TSPA model (v4.042) results and those based on the finite difference approximation of the sample calculation, except for the initial time steps where the difference is approximately 10%. The comparison for the case with only diffusive transport is shown on Figure 2.4-120. This case shows good agreement for the dissolved ^{239}Pu and ^{239}Pu reversibly sorbed onto groundwater and waste form colloids, as well as for the ^{239}Pu irreversibly sorbed onto the stationary corrosion products (i.e., less than 5% difference except for the initial time steps where the difference is approximately 10%). The agreement is less perfect for ^{239}Pu irreversibly sorbed to the FeOH colloids (labeled as "Concentration_in_Water [^{239}Pu^{If}]"). In this case, the differences at the initial time steps between the TSPA model (v4.042) results and those based on the finite-difference approximation range from 50% to 100%. The differences decrease rapidly with time, and, by the time the system reaches a steady state, there is only a 2% difference in value. Given the different solution methods used in the TSPA model and in the Excel spreadsheet calculations, the agreement is considered sufficient for the intended use of the submodel.

Verification of Coupling among Submodels and Model Components—During-development verification of the coupling of submodels and TSPA model components within GoldSim consisted of checking the model implementation during development of the TSPA model, including verification of the DLLs and the single model components described above. After development, the verification of coupling among TSPA model components is confirmed through auxiliary analyses, discussed above in Section 2.4.2.2.3, which demonstrates that the TSPA model yielded the expected results.

As indicated at the end of Table 2.4-9, the two cases of submodel coupling involve the two primary barrier/feature interfaces related to the transport of radionuclides: EBS to unsaturated zone and unsaturated zone to saturated zone. The following discussion describes the verification testing of the EBS–unsaturated zone coupling as an example of this verification method.

The EBS–unsaturated zone interface domain in the GoldSim input model file is included beneath the invert domain for modeling EBS radionuclide transport in the TSPA model. The primary purpose of the EBS–unsaturated zone interface domain is to establish an effective zero-concentration boundary condition at some distance away from the base of the invert to compute the diffusive flux from the invert to the unsaturated zone and the fraction of total mass flux that goes into the unsaturated zone fracture and matrix continua. For this purpose, the EBS–unsaturated zone interface domain is discretized into four layers and the zero concentration boundary is applied at the base of the fourth layer, approximately 18 m below the invert (SNL

2008a, Sections 6.3.8.3 and 7.2.5.1). The dual continuum of overlapping matrix and fracture continua is represented by cell pathways using GoldSim. Grid sizes (cell pathway dimensions) are more refined near the base of the invert to accurately capture the higher concentration gradient in the region. A collector cell is placed beneath the fourth layer and is given a very large water volume to simulate an effective zero concentration boundary. This collector cell acts as a sink for all the mass flux from the unsaturated zone cells.

An analysis is performed to evaluate the appropriateness of the location of the effective zero concentration boundary for the diffusive flux calculation from the invert. In this study, the effective zero concentration boundary is applied at the base of the invert and then moved down one layer at a time. The effect of the placement of this boundary is evaluated in terms of the diffusive flux from the invert. It is expected that, as the distance to the zero concentration boundary increased, the diffusive flux from the invert would decrease and converge to a true value. Because analytical solutions do not exist for a dual continuum representation, the convergence of the invert diffusive flux with increasing distance to the zero concentration boundary is deemed adequate for evaluating the appropriateness of the location of the effective zero concentration boundary.

The study is performed for a nonsorbing radionuclide such as ^{99}Tc. The radionuclide mass is injected in the invert cell at 100 years, and the concentration is held constant in the invert at 100 mg/L. The study was only performed for a nonseeping environment for Percolation Subregion 3 for commercial SNF waste packages, where the release from the invert was primarily diffusive (a small advective component was also present due to imbibition flux from the host rock into the invert). A total of 300 realizations are run to sample the epistemic uncertainty in the hydrologic properties of the invert and the unsaturated zone. The results of the study are shown on Figure 2.4-121 to compare the total mean diffusive mass flux of ^{99}Tc from the invert for varying placement of the zero concentration boundary. Almost all of the diffusive mass flux from the invert goes into the matrix continuum, as the effective diffusive area for the matrix continuum is much greater than that for the fracture continuum. As expected, the diffusive flux decreases as the zero concentration boundary is moved farther down from the invert. The diffusive flux at 10,000 years for the case where the zero concentration is applied at the base of the invert is about 7.4 g/yr, but reduces to about 0.62 g/yr when the boundary is placed at the base of the first layer (a distance of about 0.66 m from the base of invert). The diffusive flux reduces further to about 0.55 g/yr when the zero concentration boundary is placed at the base of the second layer (a total distance of about 1.97 m from the base of invert) and then to about 0.54 g/yr when the zero concentration boundary is applied to the base of the third and fourth layers (at total respective distances of 6.97 m and 16.97 m).

This analysis indicates that it is important to properly locate the zero concentration boundary when the dominant radionuclide mass flux from the invert is diffusive, and that the discretization chosen for the EBS-unsaturated zone interface domain is adequate for coupling the EBS and unsaturated zone.

Verification of Range of Applicability of Submodels and Model Components—The range of applicability of submodels and model components is verified to ensure that under all conditions (realizations) of the TSPA model, one submodel does not pass information to another submodel that drives the downstream submodel beyond its range of validity (SNL 2008a, Section 7.2.6 and Appendix P).

The type of verification performed to ensure that the range of applicability is properly defined within the TSPA model depends on the nature of the implementation. In some cases, logic is built into the TSPA model to verify that the inputs are within the appropriate range. If an input is outside its valid range, a flag is set. In other cases, logic is built into the TSPA model so that if a parameter value is selected outside the valid range, the value is reset to the bounding value depending on whether the value is greater than or less than that of the range (SNL 2008a, Section 7.2.6).

In the 1,000,000-year performance runs of the TSPA model, waste packages attain ambient temperatures. The ambient temperature from the EBS thermal-hydrologic submodel (SNL 2008a, Section 6.3.2) can be as low as 17°C. The lower temperature limit for the in-package chemistry abstraction (SNL 2007h, Section 1[a]), and the dissolved concentration limits abstraction (SNL 2007u, Section 6.3.3.3) is 25°C. The lower temperature limit for the HLW glass waste form degradation abstraction is 20°C (BSC 2004g, Section 1.2). As discussed below, the application of these three submodels below the stated range of applicability is not expected to have a significant effect on the EBS release calculations; therefore, the TSPA model applies the provided abstractions below the lower temperature limits without further modifications.

In the in-package chemistry abstraction the pH and ionic strength abstractions were developed for conditions at 25°C, but there is no explicit temperature dependence in the abstractions for pH and ionic strength within the waste form domain. Through the use of sensitivity studies and conservative modeling choices, the effects of temperature were determined to be negligible and the range of applicability was extended up to temperatures of 100°C (SNL 2007h, Section 6.6[a] and 8.1[a]). Because of the pH buffering capacity in the waste form cells results in a high degree of confidence in the minimum and maximum pH at 25°C (SNL 2007h, Section 6.10.8.1[a]) and because sensitivity studies reveal that temperature has a negligible effect on ionic strength (SNL 2007h, Section 6.6.6 and 6.6[a]), the application of pH and ionic strength abstractions developed at 25°C to temperatures as low as 17°C is not anticipated to produce results that are outside the range of uncertainty captured in the abstractions for pH and ionic strength (SNL 2008a, Table P-6).

The dissolved concentration limits abstraction reports that actinides in carbonate systems, such as those that will prevail in the EBS, have retrograde solubility. Abstractions for the solubility of actinides were developed for conditions at 25°C and include additional uncertainty to expand the temperatures range of applicability up to 100°C, but there is no explicit temperature dependence in the abstractions for actinide solubility in the EBS (SNL 2007u, Section 6.3.3.3). The TSPA model applies the dissolved concentration limits abstraction at temperatures below 25°C. Because actinides have retrograde solubility, it is possible that dissolved concentration limits below 25°C could be higher than those implemented in the TSPA model. But because the dissolved concentration limits abstraction includes treatment of the major uncertainties (SNL 2007u, Section 6.3.3), it is expected that dissolved concentration limits at lower temperatures would be within the range of uncertainty captured in the dissolved concentration limits abstraction (SNL 2008a, Section 7.2.6[a]). Radium solubility is higher at higher temperatures and the abstraction developed at 100°C is conservatively applied to all temperatures below 100°C.

The HLW glass waste form degradation abstraction has explicit temperature dependence in the rate expression and below 20°C the TSPA model applies the applicable temperature in the rate expression. The lower temperature limit of the HLW glass waste form degradation abstraction was determined by the ranges considered in the experimental results used to validate the rate model

(BSC 2004g, Section 7.3), which showed that the Arrhenius relationship for glass degradation rate is maintained between 20°C and 90°C. This relationship is not expected to change between 17°C and 20°C. Therefore applying the rate model at 17°C to HLW glass that is still intact within the waste form domain when the waste package temperatures drop below 20°C, is not expected to have any effect on mass transport calculations (BSC 2004g, Section 6.5.2.1).

For the 10,000-year simulations, the temperatures remain within the range of validity (SNL 2008a, Section 7.2.6[a]).

2.4.2.3.2.2.2 Model Stability Testing

Model stability testing includes three types of stability tests: statistical stability, temporal stability, and spatial stability. Statistical stability testing involves a number of activities to demonstrate that a sufficient number of realizations have been run to achieve a numerically stable mean dose, as required by NUREG-1804, Section 2.2.1.4.1.3: Acceptance Criterion 2(1). Statistical stability with respect to the sample size for both epistemic uncertainty and aleatory uncertainty has previously been discussed in Section 2.4.2.2.2. The remaining three types of model stability testing occurring as part of the TSPA model during-development validation activities address discretization of the temporal and spatial domains of the model. The three primary activities to address this discretization are summarized here: time stepping, spatial variability, and number of particles in the unsaturated zone transport submodel.

Temporal stability tests (i.e., tests for the appropriate time step size necessary to achieve a stable solution) have been conducted for four modeling cases: waste package early failure, igneous intrusion, seismic ground motion, and nominal. Spatial variability/discretization in the TSPA model involves studying the scale at which the repository must be modeled. In particular, because of computational constraints, the TSPA model does not simulate the individual performance of each of the 11,629 waste packages (Section 2.3.7.4.2) modeled as emplaced in the repository, but groups the waste packages into representative waste package groups. Spatial stability examines the effect of these waste package groupings for the early failure drip shield modeling case. Finally, the particle-tracking algorithm used by FEHM, the software program that numerically solves for radionuclide transport in the unsaturated zone, discretizes the mass balance equations into finite-sized particles, each carrying a finite amount of the mass flux through the unsaturated zone. The smoothness and accuracy of the numerical solution is a function of this “number discretization” and several tests, summarized below, validate the stability of this discretization using the drip shield early failure, igneous intrusion, and seismic ground motion modeling cases.

Verification of Temporal Discretization—An important issue related to the stability of the TSPA model results is temporal discretization of the model. In order to estimate the movement of radionuclides, the TSPA model calculates the movement of radionuclides by numerically solving partial differential equations in various model components and submodels (e.g., unsaturated zone transport which employs the FEHM particle-tracking software to discretize the solution, or EBS flow and transport, which uses the GoldSim cell-pathway algorithm to discretize the solution). The temporal discretization (i.e., the size of time steps) could affect the accuracy of the solution to the differential equations, and thus affect the outputs of the TSPA model. Several different TSPA model runs are performed to evaluate the potential for variability in model output due to time step size. The analysis demonstrates that the output of the TSPA model is not significantly affected by reducing the size of time steps (SNL 2008a, Section 7.3.3).

The waste package early failure, seismic ground motion, igneous intrusion, and nominal modeling cases were selected for the temporal stability analysis. These modeling cases encompass the range of events and processes that result in radionuclide transport. Each modeling case describes repository performance subsequent to failure of parts of the EBS, although the time and nature of the failures varies between modeling cases. When a waste package fails, the initial mobilization of radionuclides out of the failed waste package generates an impulse of mass into the models for transport, the resolution of which will depend on the time steps used in the TSPA GoldSim model file.

The waste package early failure modeling case models the diffusive release of radionuclides from an initial waste package failure under an intact drip shield. The time step analysis for this modeling case examines releases from both types of waste package (codisposal and commercial SNF) in one of the 10 possible environments (i.e., 5 percolation subregions and two dripping conditions). The seismic ground motion modeling case during the first 10,000 years simulates the diffusive releases that result from seismic events that affect all codisposal waste packages in all environments. As mentioned earlier, analyses have shown that the chance of failure of a commercial SNF package due to seismic events is too small to result in significant consequences for the first 10,000 years. The igneous intrusion case simulates the release of radionuclides primarily by advection, and includes all waste packages in all environments. For the time period of 1,000,000 years, the igneous intrusion modeling case is analyzed for temporal stability, because this modeling case represents the extreme transient effect of an event that completely compromises the engineered barrier at a single time. In contrast, the seismic ground motion modeling case describes much smaller degrees of degradation and failure of the components of the EBS through time as a result of corrosion processes and seismic events. The seismic ground motion modeling case essentially models a series of less extreme events. If the time step scheme for 1,000,000 years is adequate for the igneous intrusion modeling case, it is reasonable to expect that this same time step scheme would be adequate for the seismic ground motion modeling case (SNL 2008a, Section 7.3.3.1).

The nominal modeling case is also examined for temporal stability for the 1,000,000-year time period. However, the time steps that are varied in the nominal modeling case are those used in the WAPDEG software that determines the time and number of waste packages that failed due to nominal corrosion. The time steps used in the GoldSim component to solve transport equations for the nominal modeling case are the same as used in the igneous intrusion modeling case. Thus, the temporal stability analysis for the igneous intrusion modeling case determines temporal stability of the GoldSim component for the nominal modeling case as well. The drip shield early failure and seismic fault displacement modeling cases use the same time step scheme as is used in the waste package early failure, seismic ground motion and igneous intrusion modeling cases. The submodels included in the drip shield early failure, and seismic fault displacement modeling cases differ from the waste package early failure seismic ground motion, and igneous intrusion modeling cases primarily in characterizing the failure of parts of the EBS. Radionuclide mobilization and transport are computed with a similar set of submodels in all of these modeling cases. Therefore, if the time step scheme is shown to be adequate for the waste package early failure, seismic ground motion, and igneous intrusion modeling cases, the temporal stability analysis need not be conducted for the remaining modeling cases.

The volcanic eruption modeling case uses a different time step scheme than the other modeling cases because of the highly-transient nature of the eruptive processes. This time step scheme employs one-year time steps after an eruption. Because the quantity computed by the modeling case is the annual dose (i.e., dose averaged over a year), reducing the time step below one year is not warranted. Thus, no temporal stability analysis is necessary for the volcanic eruption modeling case (SNL 2008a, Section 7.3.3.1).

Separate calculations are performed for each of two time periods: 20,000 years, and 1,000,000 years following repository closure. A time period of 20,000 years is used instead of 10,000 years in order to examine the failure of commercial SNF packages, whose in-package relative humidity does not rise above 95% (the threshold for release) until around 10,000 years (Section 2.4.2.3.3.5.2). For each time period, one base time-step scheme is used for all modeling cases. The base time step scheme uses shorter time steps during the period of time immediately following repository closure, when environmental variables such as temperature and relative humidity are changing more rapidly. As repository environmental conditions become stable, longer time steps are employed.

The temporal stability of the selected modeling cases is examined by introducing additional, shorter time steps immediately following the events that fail components of the engineered barrier. For each modeling case, two additional simulations are constructed and run, varying the time-step scheme from the baseline TSPA model (SNL 2008a, Table 7.3.3-1). Each simulation calculates repository performance for the first five of 300 epistemic realizations of the baseline TSPA model. The time step analysis is conducted for five epistemic realizations, rather than the full set of 300, which is sufficient to expose any systematic effect on model results of varying the time steps. TSPA model runs with different time step sizes were compared graphically to determine the effect of refining the time steps. A number of different temporal stability tests were conducted (SNL 2008a, Section 7.3.3), examples of which are discussed below.

Waste Package Early Failure Modeling Case—The TSPA models waste package early failures as occurring at repository closure. Because the drip shield above the waste package remains functional in this modeling case, seepage does not contact the early failed waste packages and, as a result, radionuclides transport out of the waste package is by diffusion only. Diffusion does not begin until sufficient water is present inside the waste package. Because the rate of water accumulation depends on temperature and relative humidity within the drift, diffusive transport begins at different times for different waste packages and realizations.

The waste package early failure modeling case considers a total of 20 possible combinations of aleatory variables: five different percolation subregions, two waste package types, and either dripping or nondripping conditions (Section 2.4.2.1.5.2). The ensemble of 20 annual dose histories is used to compute expected annual dose. Figure 2.4-122 shows the expected annual dose for each of five epistemic realizations for the two alternative time step schemes. The similarity in expected dose for the two-time step schemes gives confidence that the waste package early failure modeling case is stable with respect to temporal discretization.

Igneous Intrusion Modeling Case—In the igneous intrusion modeling case, annual dose is computed by the GoldSim component of the TSPA model at each of a set of specified intrusion times (SNL 2008a, Table 7.3.2-1). For each epistemic realization, the ensemble of aleatory dose histories (one for each intrusion time) is used to compute expected dose. At the time of an intrusion, the drip shield and waste package cease to isolate the waste from seepage waters. Immediately after an intrusion, relatively large quantities of radionuclides can enter the natural system over a few time steps. Temporal stability is tested for the 1,000,000-year and 20,000-year calculations by considering alternative time step schemes (SNL 2008a, Table 7.3.3-1). As mentioned above, the alternative time step schemes add additional, shorter time steps immediately after the modeled intrusions to provide better resolution of the effects of each intrusion.

Expected annual dose is computed for each of five epistemic realizations using an increased time step scheme (SNL 2008a, Section 7.3.3.4). One dose history is computed for each epistemic realization and for the 10 specified igneous event times. Figure 2.4-123 shows the expected dose results for the five epistemic realizations. Although small variations can be observed for the two time-step schemes, each expected dose history's shape and magnitude are similar. Thus, the time step scheme used in the igneous intrusion modeling case is adequate. The similarity in expected dose occurs because expected dose at time τ involves taking the expectation of the dose at time τ from all possible events that could occur prior to time τ. Because the dose that follows an event appears as a pulse, both the magnitude and duration of each pulse influence the expected dose. When the alternative scheme with shorter time steps is used, the pulse of dose that immediately follows an event is larger in magnitude, but shorter in duration. Consequently, with the alternative time steps, the expected dose at time τ is determined by fewer, larger pulses of dose prior to τ. However, similar values of expected dose result in the base-case time-step scheme, which produces dose pulses of lower magnitude and longer duration. The similarity in expected dose shows that the time-step scheme provides sufficient resolution of the annual dose to obtain a stable value for the integral defining expected dose.

Seismic Ground Motion Modeling Case—In the seismic ground motion modeling case for the first 10,000 years, annual dose is computed by the GoldSim component of the TSPA model at each combination of a specified event time and specified damage fraction (SNL 2008a, Table 7.3.2-3). For each epistemic realization, the ensemble of dose histories (one for each combination of event time and damage fraction) is used to compute expected dose. At the time of a seismic event, damage to the waste package allows water to build inside the waste package, and when sufficient water is present, radionuclides begin to diffuse out of the waste package and into the natural system. It is possible that relatively large quantities of radionuclides would enter the natural system over a few time steps following a seismic event. Temporal stability is tested by reducing the time step size. The alternative time-step schemes add additional, shorter time steps immediately after the modeled seismic event to provide better resolution of the events effects (SNL 2008a, Table 7.3.3-1).

The event time is fixed at 1,000 years and the damage fraction at 10^{-6}. The base-case time steps are applied up to the time of the event. After the event, the first alternative time-step scheme uses 10-year time steps until 10,000 years and then reverts to the base-case time step for the remainder of the calculation. The second scheme uses one-year time steps until 2,000 years, followed by the base-case time steps until 20,000 years. The base-case time steps are 40-year time steps from the time of the event at 1,000 years until 10,000 years. Figure 2.4-124 shows the annual dose for each of five epistemic realizations and the three time-step schemes. The overall shape of the dose history for each epistemic realization is similar for all time-step schemes. The dose following the seismic event generally occurs sooner after the event when using the alternative time step schemes. However, unlike the igneous intrusion modeling case, the dose does not exhibit a large peak followed by rapid decline, but rather reaches and maintains a steady state. In the igneous intrusion modeling case, the engineered barrier does not restrict radionuclide transport after the intrusion, whereas in the seismic ground motion modeling case, only a small fraction of waste package surface is damaged, which in turn constrains the rate of radionuclide transport. The expected dose for the seismic ground motion modeling case will be determined by the magnitude of the steady-state dose after the seismic event. Because the magnitude of the steady-state dose is similar for the base case and the alternative time-step schemes, the minor differences in annual dose shown on Figure 2.4-124 will have no significant effect on expected dose.

Nominal Modeling Case—In the nominal modeling case, annual dose is computed by the GoldSim component of the TSPA model based on a time history of waste package failures due to nominal corrosion processes (i.e., general corrosion, microbial influenced corrosion, stress corrosion cracking), which is calculated by the WAPDEG software. The WAPDEG software employs a separate temporal discretization for the thermal histories of emplaced waste packages than the time steps used in the GoldSim component to determine transport of radionuclides. Temporal stability of the time steps used by WAPDEG is tested by reducing the sizes of these time steps, and propagating the revised histories of waste package failure through the GoldSim component.

In the TSPA, a relatively coarse time-step discretization is used in the general corrosion calculations beyond 200,000 years, when repository temperature and relative humidity have reached ambient conditions. In the temporal stability study (SNL 2008a, Section 7.3.3.7[a]), the time-step discretization used by the general corrosion calculations is refined by adding time steps; the number of time steps is increased from 68 in the TSPA to 279 in the temporal stability run. The new time-step discretization was selected so that the maximum timestep size used in the general corrosion calculations was 10,000 years, rather than up to 300,000 years in the TSPA.

Results of the stability analysis (SNL 2008a, Section 7.3.3.7[a]) indicate that the alternative time-step scheme produces smoother results for the nominal modeling case. In particular, the sharp increases in expected annual dose at 200,000; 300,000; 500,000 and 700,000 years (Figure 2.4-22) are smoothed by the use of shorter time steps. Comparison of the distribution of expected annual dose (SNL 2008a, Figure 7.3.3-12[a]) between the temporal discretization cases shows that both the magnitude of expected annual dose and the range of uncertainty in expected annual dose are similar. This similarity in statistics for expected annual dose for the two timestep schemes indicates that the nominal modeling case is sufficiently stable with respect to the temporal discretization used in computing general corrosion.

Verification of Spatial Discretization—Different scales exist within the TSPA model relative to how spatially dependent information is used in various submodels. The key areas within the TSPA model where spatial variability is finely discretized are site-scale unsaturated zone flow, EBS thermal-hydrologic conditions, unsaturated zone transport, and saturated zone flow and transport. Saturated zone flow and transport does not share the same domain as the other three spatially-variable submodels, and is implemented using a three-dimensional model (although a few radionuclides are simulated with a one-dimensional model—see Section 2.4.2.3.2.1.10). The unsaturated zone flow and unsaturated zone transport submodels use the same dual-permeability spatial grid and, therefore, have the same spatial variability. The EBS thermal-hydrologic submodel shares the domain of the two unsaturated zone submodels, but uses a different, finer, spatial grid.

Spatially discrete information used at one scale (e.g., unsaturated zone flow submodel) could be combined or averaged in order to be used at a different scale (e.g., drift seepage submodel and drift wall condensation submodel). The TSPA model "inherits" these different spatial scales from the process models that feed it, namely the unsaturated zone flow, EBS thermal-hydrologic environment, unsaturated zone transport, and saturated zone flow and transport abstractions. The appropriateness of the spatial discretization and scales of these abstractions are investigated and validated for their intended use in the TSPA within each process model's respective report, as indicated in Section 2.3. However, the TSPA model effectively adds its own spatial discretization by subdividing the repository into five percolation subregions at the EBS submodel level (SNL 2008a, Section 6.3.2), i.e., upscaling from the finer discretization in the underlying abstractions. The main purpose of this section is to describe the use of representative thermal-hydrologic histories (Section 2.4.2.3.2.1) within the percolation subregions at the EBS-submodel level in lieu of using the comprehensive thermal-hydrologic dataset and discuss what impact, if any, this spatial discretization has on the results of the EBS releases that feed the unsaturated zone.

The EBS thermal-hydrologic environment submodel implements the thermal-hydrologic environment in and around an emplacement drift from the multiscale thermal-hydrologic model abstraction. The multiscale thermal-hydrologic model abstraction results include the spatial discretization of thermal-hydrologic conditions of the EBS and its components, as well as the variability of these results due to uncertainties with the percolation flux and the host-rock thermal conductivity inherited from the site-scale unsaturated zone flow process model. These spatially discretized inputs to the TSPA are provided by the multiscale thermal-hydrologic model abstraction at two scales: a fine-scale or comprehensive data set which is appropriate for determining waste package failure histories due to general or localized corrosion, and a coarse-scale or representative data set, which is presumed to be sufficient for capturing waste-form mobilization and transport processes (as demonstrated in this section). The representative thermal-hydrologic data set involves the discretization of the repository domain into a specified number of subregions (five) based upon percolation flux. Each subregion's thermal-hydrologic conditions are characterized by one representative element of the comprehensive thermal-hydrologic dataset, which is meant to be representative of the thermal-hydrologic conditions everywhere within that specific percolation subregion.

As described in Section 2.4.2.3.2.1.2, to characterize the variability in repository thermal-hydrologic conditions, the multiscale thermal-hydrologic model subdivides the drifts in the repository footprint into 3,264 equal area subdomains corresponding to 20-m repository drift segments (SNL 2008d, Section 6.2.12[a]). For each of the 12 percolation flux/host-rock thermal conductivity cases (SNL 2008a, Table 6.3.2-3), the multiscale thermal-hydrologic model abstraction includes the time-dependent thermal-hydrologic variables, temperature, and relative humidity for six different possible commercial SNF waste packages and two different possible codisposal waste packages at each of the 3,264 repository subdomains (SNL 2008d, Tables 5.4-1 and 6.3-13, and Section 6.2.17[a]). This comprehensive data set is used for the waste package degradation and seepage submodels of the TSPA. For other submodels in the GoldSim model file, related to waste-form mobilization and transport, the use of this comprehensive data set is not necessary for computing expected dose, as demonstrated below. Therefore, the multiscale thermal-hydrologic model also provides an abstraction of the comprehensive thermal-hydrologic data set by first grouping 3,264 repository subdomains into one of the five repository percolation subregions (Figure 2.4-3), as described in Section 2.4.2.3.2.1.2 (SNL 2008a, Section 7.3.4.2.2). Next, the multiscale thermal-hydrologic model determines a representative thermal-hydrologic history associated with a single commercial SNF waste package and a single codisposal waste package for each percolation subregion. This representative thermal-hydrologic data is then used as input to the EBS submodel and propagated throughout the rest of the of the TSPA model. The thermal-hydrologic variability analysis summarized below demonstrates the appropriateness and validity of using the representative thermal-hydrologic histories as inputs to the EBS submodels of the TSPA, as opposed to using the comprehensive data set.

As mentioned in Section 2.4.2.3.2.1.2, the 10th percentile infiltration scenario for the glacial transition climate is used to define the five percolation subregions for all simulations. Of the 3,264 multiscale thermal-hydrologic model subdomains in the comprehensive data set, there are 163, 817, 1,300, 820, and 164 subdomains in Percolation Subregions 1, 2, 3, 4, and 5, respectively (5%, 25%, 40%, 25%, and 5%), with the following characteristics:

- The subregions are not completely contiguous in space, but are located throughout the repository
- Each subregion includes both edge and interior repository subdomain locations
- The five selected subregions have a fixed set of repository subdomain locations for all realizations of the TSPA model, regardless of infiltration and host-rock thermal conductivity scenario or climate state. However, the percolation flux values calculated for each percolation subregion will be different depending on the percolation flux/host-rock thermal conductivity scenario and/or climate state being considered.

To conduct the spatial stability analysis (SNL 2008a, Section 7.3.4), the TSPA model is exercised over a range of percolation flux percentiles, host-rock thermal conductivities, and percolation subregions that represent the range of thermal-hydrologic conditions from the driest and hottest to the wettest and coolest, with appropriate conditions in between. Radionuclide releases from the EBS for a 1,000,000-year compliance period were used as the benchmark for comparison between the two types of thermal-hydrologic histories (i.e., representative versus comprehensive) (SNL 2008a, Section 7.3.4.3). Since there is both a diffusive and an advective component to the release of radionuclides from the EBS, comparisons were made for both the drip shield early failure (advection-dominated transport) and the waste package early failure (diffusion-dominated transport) modeling cases. For illustration, only the results of the drip shield early failure modeling case are shown here.

For the runs using a representative thermal-hydrologic data set, the TSPA model is run for a specified number of "realizations" corresponding to the number of subdomains for a specific percolation subregion, but with the epistemic and aleatory variables (including infiltration and host-rock thermal conductivity) fixed to be the same for each realization. However, the same representative thermal-hydrologic history is used for all realizations. For the drip shield early failure modeling case, only a single drip shield over a commercial SNF waste package and a single drip shield over a codisposal waste package are allowed to fail during each realization. For the runs using the comprehensive thermal-hydrologic data set, the epistemic and aleatory variables are again fixed, but the model is looped over the set of thermal-hydrologic histories corresponding to the number of subdomains in the given percolation subregion (i.e., each realization had a different thermal-hydrologic history). To reduce the computational time of these runs to a more manageable quantity, only one of the six thermal-hydrologic histories associated with the six commercial SNF waste packages at each subdomain (or loop) is used, and only one of the two thermal-hydrologic histories associated with the two codisposal waste packages at each subdomain (or same loop) is used. These are chosen randomly.

Note that the curves marked "comprehensive" in Figure 2.4-125 represent the radionuclide release histories using the full set of thermal-hydrologic curves from all multiscale thermal-hydrologic model subdomains (i.e., assuming each package in a percolation subregion has a unique thermal-hydrologic history) (derived from the comprehensive set of thermal-hydrologic histories), whereas the curves marked "representative" assume that every package in a given subregion has the same thermal-hydrologic conditions corresponding to the single representative thermal-hydrologic history for that percolation subregion (but different for commercial SNF versus codisposal). For each set of thermal-hydrologic variability runs, a comparison of the means of the radionuclide cumulative releases of ^{99}Tc, ^{129}I, and ^{239}Pu from the EBS is the benchmark to gauge the appropriateness of using a representative thermal-hydrologic history versus a comprehensive thermal-hydrologic history with respect to spatial discretization. Figure 2.4-125 shows the EBS releases for the representative thermal-hydrologic data set compared to the case using the comprehensive thermal-hydrologic data for the drip shield early failure modeling case, 10th percentile infiltration scenario, low host-rock thermal conductivity, and Percolation Subregion 3. After about 1,000 years, the EBS cumulative releases of these radionuclides are very similar for both the representative and comprehensive thermal-hydrologic data sets. This is typical of other percolation flux percentile, host-rock thermal conductivity, and percolation subregion cases (SNL 2008a, Section 7.3.4.3.2).

The EBS releases that used the thermal-hydrologic histories from the comprehensive data set generally begin earlier than the cases that used a representative thermal-hydrologic history. Figure 2.4-126 compares the commercial SNF waste package temperature histories below 100°C for the representative and comprehensive thermal-hydrologic data sets. The commercial SNF waste package temperature histories for the representative thermal-hydrologic data sets are similar to the means of the commercial SNF waste package temperature histories associated with the comprehensive thermal-hydrologic data set for each respective percolation flux percentile, host-rock thermal conductivity, and percolation subregion case. This illustrates that the representative thermal-hydrologic data set can be used as a surrogate for the comprehensive thermal-hydrologic data sets with respect to spatial discretization. The upper and lower bound waste package temperatures from the comprehensive thermal-hydrologic data sets are shown on the figure. Since the TSPA model requires the waste package temperature to drop below 100°C before transport from the EBS can be initiated, and since there is some spread between the lower bound and the mean commercial SNF waste package temperatures from the comprehensive thermal-hydrologic data set, the EBS releases from these cases start earlier than those that used the representative thermal-hydrologic data.

FEHM Particle Tracking Stability—In the TSPA model, radionuclide transport through the unsaturated zone is simulated using the FEHM (Zyvoloski et al. 1997) residence time transfer function particle tracking technique, as described in *Particle Tracking Model and Abstraction of Transport Processes* (SNL 2008e, Section 6.4 and Appendix C). To have confidence in the results generated by the particle tracking model, it is important to examine the stability of the TSPA model results relative to the number of particles being used. For particle tracking models, the accuracy of the model is a function of the number of particles used to represent the source releases; the greater the number of particles, the greater the degree of accuracy. As the number of particles increases, a level will be reached where results stabilize and there will be little change in results associated with increasing the number of particles. In the TSPA model, the input for the maximum number of particles allowed in the TSPA model is 900,000 per species. To test the stability of the results in reference to the number of particles used in the TSPA model, two supplemental simulations were performed with 500,000 and 750,000 particles being the maximum allowed. The input to FEHM is the maximum number of particles allowed. The number of particles actually used by a specific species during a simulation is limited because FEHM is designed to hold back particles for any species that has mass introduced to the system from ingrowth in addition to the mass released from the unsaturated zone.

To evaluate the particle tracking model's stability, with reference to the number of particles used in the TSPA model, stability testing was performed using Version 5.000 of the TSPA model (SNL 2008a, Section 7.3.5). This study considered the 10,000-year drip shield early failure, the 1,000,000-year igneous intrusion, and the 10,000-year seismic ground motion modeling cases. The drip shield early failure modeling case results used a single aleatory realization comprised of percolation subregion 3 waste packages and commercial SNF fuel type. The igneous simulations used a single aleatory realization with an event time of 250 years. The seismic ground motion modeling case simulations used a single aleatory realization comprised of a 10^{-6} damage fraction and an event time of 200 years. For each chosen case, the results for five epistemic realizations were examined closely to evaluate the effect of reducing the number of particles used in the simulations. Single realizations were examined because the averaging process used to compute mean dose would likely hide the differences. As described below, analytical results using 500,000 and 750,000 for the maximum number of particles were graphically compared to the TSPA model (900,000 particles) results to assess the sensitivity of the model to the maximum number of particles.

All parameters, except for the maximum number of particles allowed (900,000; 750,000; or 500,000) and, where applicable, the FEHM input parameter defining the number of particles assigned per mole, were the same for each set of simulations. In general, for the unsaturated zone submodel particle tracking analysis, particles are assigned on a per time step basis. An exception has been made for the igneous and early failure scenarios where ^{99}Tc and ^{129}I particles are assigned on a particle per mole basis. This allows for a more accurate depiction of the spike-like portion of their EBS releases to the unsaturated zone. This technique more accurately simulates the portions of the release that are large contributors to dose. The major radionuclides considered in this analysis were ^{99}Tc, ^{233}U, ^{234}U, ^{237}Np, and total ^{239}Pu (combined reversible and slow and fast irreversible colloids). The above species cover a range of transport behavior and are large contributors to dose.

Figures showing results of the particle tracking stability test can be found in (SNL 2008a, Section 7.3.5). This stability test indicates that the use of 900,000 particles in the TSPA model analyses provides a stable result with respect to the number of particles used in all three of the modeling cases (drip shield early failure modeling case, igneous intrusion modeling case, and seismic ground motion modeling case). Reducing the maximum number of particles to 750,000 or

500,000 is shown to have little effect on the total mean annual dose results. Likewise, maximum dose results showed that the reductions in the maximum number of particles used to represent the EBS releases had little influence on the TSPA model results. A more detailed comparison of annual doses for representative radionuclide species and unsaturated zone mass flux releases showed that slight differences in particle tracking results associated with the reductions to the number of particles representing source releases (and ingrowth contributions) represent differences in the refinement of source terms to the saturated zone. This difference in the source terms is dampened by the time mass has been transported 18 km.

2.4.2.3.2.2.3 Uncertainty Characterization Reviews

An NRC requirement for repository performance assessment is to include an appropriate treatment of parameter uncertainty and variability (proposed 10 CFR 63.114(a)(2)). Specific details on how the NRC determines conformance with this requirement are given in NUREG-1804, Section 2.2.1.3. To address this requirement, a systematic review of uncertainty and variability characterizations of key TSPA parameters was conducted (SNL 2008a, Section 7.4). Particular emphasis was placed on consistency, defensibility, and traceability of the uncertainty representations, and these were modified as necessary.

Reviews were performed to scrutinize the uncertainty characterizations of key TSPA input parameters and their associated abstractions. Probability distributions for several key parameters were subsequently modified or independently derived to improve their treatment of uncertainty and variability. The technical reviews focused on: (1) confirming that the parameter representations reflect the major sources of uncertainty and/or variability, (2) verifying that the probability distributions were derived using sound statistical methods and interpretations, and (3) ensuring model parameter representations (i.e., probability distributions) are reasonable and defensible, as opposed to depicting extreme variations (10 CFR 63.304(4)) that could potentially introduce risk dilution.

The multidisciplinary review team of scientists and engineers included expertise in probability and statistics, uncertainty analysis, TSPA modeling, and knowledge of the regulatory guidance regarding consistent treatment of uncertainty and variability. In addition, selected YMP subject matter experts provided support on as needed basis and facilitated the reviews of data, parameters, and model abstractions. The general work scope of the parameter uncertainty review team included:

- Familiarizing YMP subject matter experts with methodologies for analyzing data uncertainties and variabilities, as well as use of statistical techniques to derive probability distributions (i.e., probability density functions and cumulative density functions)

- Performing independent statistical analyses and interpretations of laboratory and field data

- Checking the appropriateness of probability distributions chosen to fit data and ensuring consistency with respect to the quantity of available data

- Deriving probability distributions using advanced statistical techniques, including subjective methods such as Bayesian updating
- Ensuring parameter values are representative of component model scale (i.e., upscaling data from small-scale samples and tests to the physical scale of the model)
- Examining subjective probability distributions to ensure that informal professional judgments were reasonable and consistent

The uncertainty characterization reviews examined in detail the uncertainty and variability characterizations for key TSPA input parameters (SNL 2008a, Tables 7.4-1 through 7.4-3). While the reviews primarily focused on scrutinizing the technical basis, they also included consistency aspects of the NRC review method for data uncertainty described in NUREG-1804, Section 2.2.1.3 for the 14 abstraction topics. In addition, the supporting documentation was reviewed and critiqued with respect to clarity and transparency. Specific review findings and actions for specific TSPA parameters are documented in *Total System Performance Assessment Model/Analysis for the License Application* (SNL 2008a, Section 7.4.5). The results of the reviews, and resulting actions, are incorporated in the model abstractions described in Section 2.3.

2.4.2.3.2.2.4 Surrogate Waste-Form Analyses

During the last four decades, the United Sates government (including the DOE and its predecessor agencies, as well as the U.S. Navy) has generated several hundred varieties of spent fuel from weapons production, nuclear propulsion, and research missions. See Sections 1.5.1.3 and 1.5.1.4 for additional detail on the various DOE SNF types. A method described by Fillmore (1998, Section 2) allows the grouping of these varieties of DOE SNF. The DOE SNF types are grouped into 11 categories based on fuel matrix parameters (DOE 2000, Section 8). The number of DOE SNF categories helps streamline repository analyses of the spent fuels. Table 2.4-10 lists the DOE SNF categories and a representative fuel in the category that best fits the characteristics of the category (DOE 2000).

As discussed below, the TSPA replaces the 11 categories of DOE SNF with two surrogate waste forms, one for naval SNF and one for the other 10 categories (SNL 2008a, Section 7.5). The purpose of the surrogate waste-form analyses described here is to show the appropriateness of (1) the surrogate representation of a waste package of naval SNF (Category 1 DOE SNF) by a waste package of commercial SNF and (2) the surrogate representation of DOE SNF (whose inventory in the TSPA model is a weighted average of Categories 2 through 11) in the TSPA model.

Naval SNF Analysis—For naval SNF, analyses were performed to validate the use of commercial SNF as a surrogate for naval SNF in the TSPA model (SNL 2008a, Table 7.5-5). Probabilistic analyses were conducted for the drip shield early failure and igneous intrusion modeling cases. The results of failure for a single waste package of commercial SNF were compared with the failure of a single waste package of naval SNF. Quantitative comparison of naval SNF and commercial SNF inventories for the major radionuclide contributors to dose were made for the other modeling cases (volcanic eruption, human intrusion, and seismic ground motion).

Naval SNF is placed in its own category because: (1) the design of naval SNF is significantly different from the other DOE SNF designs (Categories 2 through 11); (2) the structure of naval SNF will remain virtually intact well beyond 10,000 years, for the nominal and early failure scenario classes, impacting repository performance much later than DOE SNF designs; and (3) the design of naval SNF is classified. To justify using a surrogate for naval SNF in the TSPA, naval SNF is analyzed using source terms (i.e., rates of release of the various radionuclides) provided by the Naval Nuclear Propulsion Program Technical Support Document, Section 2.3.7, in special cases of the TSPA analyses developed for the drip shield early failure and igneous intrusion modeling cases.

For these analyses, the naval SNF source term provided by the Naval Nuclear Propulsion Program is modeled in a failed commercial SNF waste package, and these radionuclide releases are then subject to all of the transport processes that are applied to degraded commercial SNF (e.g., solubility, sorption, and chemistry along the transport pathway from the EBS to the RMEI) in the TSPA model.

For the drip shield early failure modeling case, a single drip shield is failed at emplacement, and the waste package underneath this drip shield is also modeled to be failed at emplacement (a conservative representation of possibly favorable conditions for localized corrosion of Alloy 22). Two simulations were run: one for a single commercial SNF waste package, and one for a single waste package, where the naval source term replaced the commercial SNF source term. The simulations were run for 10,000 years and used a unified sampling of epistemic and aleatory uncertainty over 300 model realizations. Unified sampling means that the waste package is located randomly in any percolation subregion and any seeping environment for any of the 300 realizations. The results, in terms of a mean annual dose over the unified sampling of epistemic and aleatory uncertainty, are shown on Figure 2.4-127. The results show that over a 10,000-year period, the dose associated with the naval source term is less than that of the commercial SNF source term. At 10,000 years, the mean annual dose from a failed waste package with a naval source term is about two orders of magnitude lower than the mean annual dose for a failed commercial SNF waste package, justifying the use of a commercial SNF waste package as a surrogate for a naval waste package.

A similar analysis to validate the use of a commercial SNF waste package as a surrogate for naval waste package was conducted using the igneous intrusion modeling case (SNL 2008a, Section 7.5.3.3). For the commercial SNF and naval source term stylized analysis, the time of the igneous intrusion was forced to occur at a specified time step, and a single waste package was failed. The simulations were run for 10,000 years and used a sampling of epistemic uncertainty over 300 model realizations. The results, in terms of a mean annual dose, are shown on Figure 2.4-128. As with the drip shield early failure modeling case, the results for the igneous intrusion modeling case show that over a 10,000-year period, the dose associated with the naval source term is less than that of the commercial SNF source term, again justifying the use of a commercial SNF waste package as a surrogate for a naval waste package.

The analyses reflect: (1) the structure of naval SNF (Naval Nuclear Propulsion Program Technical Support Document, Section 2.3.7); (2) slower dissolution of naval SNF (Naval Nuclear Propulsion Program Technical Support Document, Section 2.3.7); and (3) smaller radionuclide inventories of naval SNF as compared to commercial SNF on a per waste package basis (SNL 2008a, Section 7.5.3.1). The analyses confirm that the dose resulting from a waste package of naval SNF is lower than the dose resulting from a waste package of Zircaloy-clad commercial SNF for the early failure and igneous intrusion modeling cases (SNL 2008a, Sections 7.5.3.2 and 7.5.3.3).

The disposition of commercial SNF as a surrogate for naval SNF for other TSPA modeling cases is done by demonstrating that the naval SNF inventory of the radionuclides that are the major contributors to the mean annual dose is less than the commercial SNF inventory on a per package basis. These analyses include:

- The radionuclides that contribute most to dose in the seismic scenario class, seismic vibratory ground motion modeling case (SNL 2008a, Section 7.5.3.7)
- The radionuclides that contribute most to dose in the igneous scenario class, volcanic eruption modeling case (SNL 2008a, Section 7.5.3.4)
- The radionuclides that contribute most to dose in the human intrusion modeling case (SNL 2008a, Section 7.5.3.5)

The justification for the nominal modeling case is based on the absence of waste package failures for the first 10,000 years (SNL 2008a, Section 7.5.3.6). Also, the disposition of commercial SNF as a surrogate for naval SNF has been analyzed for the radionuclides that contribute most to dose for one million years after repository closure (SNL 2008a, Section 7.5.3.1), and this analysis shows lower activities for the naval SNF inventory on a per package basis for the key radionuclides.

Based on the above analyses, the 417 naval waste packages in the modeled repository are conservatively represented as 417 commercial SNF waste packages in the total 8,213 waste packages of commercial SNF (SNL 2007t, Table 7-3[a]).

The above analyses are also applicable to the groundwater protection standards at 10 CFR 63.331, which consider the 10,000-year maximum mean activity concentrations for radium (^{226}Ra and ^{228}Ra) and the alpha emitters (including ^{226}Ra but excluding radon and uranium isotopes), and the 10,000-year maximum mean annual dose for the beta and photon emitters. In particular, the activity released on a per package basis as a function of time for ^{226}Ra and ^{228}Ra is lower for the nominal/early failure naval SNF inventory (Naval Nuclear Propulsion Program Technical Support Document, Section 2.3.7) compared to the commercial SNF inventory, as are the activities of their parent actinide isotopes (namely, ^{234}U and ^{230}Th for ^{226}Ra, and ^{236}U and ^{232}Th for ^{228}Ra). The activity released as a function of time for the alpha, beta, and photon emitters associated with the nominal/early failure naval SNF inventory are also lower when compared to the commercial SNF inventory. Since the activity curves of the radionuclides considered in the groundwater protection standard for the nominal/early failure naval SNF inventory are bounded by the commercial SNF inventory, and taking into account the structure and slower dissolution of the naval SNF, commercial SNF is an appropriate surrogate for naval SNF with respect to the groundwater protection standards.

DOE SNF Analysis for Categories 2 through 11—The TSPA model represents Categories 2 through 11 of the DOE SNF using a surrogate fuel dissolution model (BSC 2004f, Sections 6.1.12 and 8.1). In particular, the abstraction represents each of the DOE SNF categories with an instantaneous degradation and dissolution model, based on uranium metal dissolution (i.e., N Reactor or Category 7 DOE SNF). Therefore, in the analysis of DOE SNF in the TSPA, all of the radionuclides are available for release immediately after waste package failure. The TSPA model uses the surrogate inventory for the DOE SNF that is documented in *Initial Radionuclide Inventories* (SNL 2007t, Table 7-1[a]) and *Waste Stream Composition and Thermal Decay Histories for LA*.

The validation analyses summarized here confirm that using uranium metal fuel with instantaneous dissolution (SNL 2008a, Section 7.5) is an appropriate surrogate to represent Categories 2 through 11 of DOE SNF. The analyses were conducted by using the TSPA model to simulate the performance of each of the individual DOE SNF categories, using a less conservative dissolution model (SNL 2008a, Table 7.5-4) for each, and then comparing the results to the performance of the surrogate fuel. The data used to model each of the individual fuel categories are from *Additional DOE Spent Nuclear Fuel Information in Support of TSPA Analysis* (Loo et al. 2004, Sections 6 and 7).

To investigate the relative performance of the other 10 categories of DOE SNF versus the surrogate, the drip shield early failure modeling case was chosen. This case failed one waste package and drip shield at time zero and thus removed the variability of the engineered barrier. This analysis tested whether the surrogate waste form gives dose curves comparable to the sum of the doses from the individual DOE SNF types weighted by the fraction of waste packages of each type. A degradation rate for each fuel category was developed and applied to the TSPA model to compare the results of individual categories of DOE SNF to the DOE SNF surrogate spent fuel (Loo et al. 2004, Section 6). The degradation rate is the product of a dissolution rate times a fuel surface area.

The TSPA model file, v5.000_GS_9.60.100.gsm, was modified to have no commercial SNF or high-level waste glass inventory, so that differences in dose due to DOE SNF were not masked by the commercial SNF and HLW releases. To simplify the calculation and to focus on the variability due to DOE SNF dissolution, only the largest percolation subregion, Subregion 3, was modeled. The seeping case was chosen because the doses from packages with dripping are higher. The epistemic uncertainty was unmodified and the resulting analysis used 300 realizations for 1,000,000 years.

A series of TSPA analyses were then conducted, based on the expected performance of each of the DOE SNF categories, to provide confidence that the surrogate fuel used in the TSPA model is a reasonable representation of all of the DOE SNF that will be emplaced in the repository (SNL 2008a, Section 7.5). The analyses included (1) the comparison of the dose from the surrogate fuel with the weighted sum of the doses from the DOE SNF categories (which is the only one presented here, since it is the most important one from a risk perspective—Figure 2.4-129), (2) the comparison of the surrogate fuel with each DOE SNF fuel category, and (3) the evaluation of impacts from uncertain parameters (e.g., degradation mechanisms, surface areas, number of waste packages, radionuclide inventory, free inventory, and bounding radionuclide inventory). The results in Figure 2.4-129, which are discussed in more detail below, are mean dose for both the 10,000-year time period and the post-10,000-year time period. Since the median is lower in magnitude than the mean, this comparison of the means is suitable for both time periods.

The dose from each category is expected to differ from the surrogate because of differences in the (1) degradation rate of the matrix, (2) fraction of bound inventory, and (3) inventory of key radionuclides per package. Some categories will yield lower doses and some will yield higher doses, but the weighted sum of the dose from all categories will be similar to the dose from the surrogate. It was the purpose of this analysis to confirm that the dose from the surrogate adequately represents the weighted sum of the dose from all categories.

The degradation rate of the matrix for the surrogate was set to instantaneous, so early dose from the surrogate that is controlled by degradation rate will bound or be equal to the dose from the various categories. The effect of degradation rate is only expected to be seen for the categories with slow degradation rates. Figure 2.4-130 shows the degradation rates of the categories, and only Categories 4 and 6 have rates slow enough to impact releases from the waste package at early times (i.e., these two categories are expected to have lower doses during early times before all the fuel has degraded).

Figure 2.4-129 shows a comparison of a single waste package of DOE SNF surrogate with the weighted sum of the annual dose from DOE SNF Categories 2 through 11. The weighted-sum annual dose lines up well with the surrogate curve and has about the same maximum dose. (The weighting of the annual dose in each category is based on the number of waste packages in the category (SNL 2008a, Table 7.5-3).) The analyses of the individual Categories 2 through 11 (SNL 2008a, Section 7.5.4) show that the DOE SNF surrogate is a reasonable representation of all categories except Category 2 (plutonium/uranium alloy), Category 6 (uranium/thorium oxide), and Category 7 (uranium metal) where significant differences occur due to higher-per-package inventories of key dose contributors (^{14}C, ^{99}Tc, and ^{234}U for Category 2, ^{233}U for Category 6, ^{237}Np, ^{226}Ra, and ^{230}Th for Category 7). However, Category 2 DOE SNF only accounts for about 0.5% of the total waste packages of DOE SNF, Category 6 DOE SNF fills only 1.6% of the waste packages, and Category 7 DOE SNF fills 6.6% of the waste packages. When the weighted sum (based on the number of waste packages) is taken of all the individual DOE SNF categories, the resulting weighted-sum dose curve compares well with the DOE SNF surrogate. The weighted-sum dose curve is dominated by the contribution from the Category 7 fuel at early and late times, and by the contribution from the Category 6 fuel from about 2,500 to 268,000 years. The mean dose of the surrogate bounds that of the weighted sum from about 40,000 years to about 400,000 years. The maximum mean dose from the surrogate has the same magnitude as the weighted sum, but occurs later in the simulation.

The DOE SNF surrogate radionuclide inventory is based on *Source Term Estimates for DOE Spent Nuclear Fuels* (DOE 2003). These inventories were updated in Revision 1 of *Source Term Estimates for DOE Spent Nuclear Fuels* (DOE 2004). The DOE SNF surrogate based on updated Revision 1 inventories is also plotted on Figure 2.4-129 for comparison.

2.4.2.3.2.3 Post-Development Model Validation Activities for the TSPA Code

As described in Section 2.4.2.3.2, confidence in the results of the TSPA model is in part based on satisfying the two categories of model validation activities: (1) those conducted during development of the model; and (2) those conducted after development of the model. This section summarizes the post-development activities, which are listed in Table 2.4-8. The major categories of post-development activities are corroboration of abstraction results with the underlying validated process models, corroboration of the TSPA model results with auxiliary analyses, corroboration of the TSPA model results with relevant man-made and natural analogues, and incorporation of the comments and recommendations from independent technical reviews.

2.4.2.3.2.3.1 Corroboration of Abstraction Results with the Underlying Validated Process Models

One of the post-development validation criteria described in Section 7.0 of the TSPA model report (SNL 2008a) is “corroboration of abstraction model results to the results of the validated mathematical model or process model from which the abstraction model was derived” (SNL 2008i). For the TSPA model, there is no single abstraction model and no single process level model. Rather, the TSPA model is an integration and coupling of a set of abstraction models, and in some cases, process models themselves. Thus, using this criterion to help validate the TSPA model consists of examining its use in the underlying reports that provide abstractions to the TSPA model. In particular, the abstractions and their underlying process models are validated during their individual development and post-development validation phases. These validation activities and their results are documented in the corresponding reports for each model. As a means of validating the abstractions, their results were corroborated with their underlying process models.

Section 2.3 summarizes the evidence for validation of the model abstractions against the underlying process models. In addition, many of these validation activities are summarized in *Total System Performance Assessment Model/Analysis for the License Application* (SNL 2008a, Section 7.6 and Table 7.6-1).

2.4.2.3.2.3.2 Auxiliary Analyses

Another of the post-development validation criteria described in Section 7.0 of the TSPA model report (SNL 2008a) is “corroboration with results of auxiliary analyses used to provide additional confidence in the system model results” (SNL 2008i). This is one of a more extensive set of post-development confidence-building activities undertaken for the TSPA model and consists of four major types of analyses (SNL 2008a, Section 7.7), which are: single-realization deterministic analyses; comparison of the TSPA model results with a Simplified TSPA analysis produced using an independently developed code to represent repository performance; comparison of the TSPA model results with the performance assessment independently performed by EPRI using its Integrated Multiple Assumptions and Release (IMARC) code; and a PMA, in which some of the key conservative assumptions in submodels comprising the TSPA model are relaxed to demonstrate that the overall effect of using a set of conservative assumptions is an overestimate of mean total dose. *Management and Technical Support Peak Dose Sensitivity Analysis* (DOE 2005) presents a precedent for the Simplified TSPA analysis in a non-qualified peak-dose sensitivity analysis using a simplified performance assessment model analogous to but not as rigorous as earlier versions of the TSPA model.

2.4.2.3.2.3.2.1 Single-Realization Deterministic Analyses

Analyses of single realizations provide an insight into the coupling of various submodel processes within the TSPA model by investigating the interactions and cause-effect relationships between various model components, which in turn provide an enhanced understanding of the performance of the system as a “sum of its parts” (SNL 2008a, Section 7.7.1). A comprehensive explanation detailing how the transport of key radionuclides is effected by the coupling of various components of the EBS, unsaturated zone, and saturated zone domains, under varying thermal-chemical-hydrologic-mechanical conditions, provides confidence that the various submodel processes are working as expected. Another important benefit of single-realization analyses is model verification and error-checking in the sense that any implementation errors are usually brought to light by their unexpected effects on release or dose histories, or on any other type of model metric, such as radionuclide concentrations.

Six different single-realization analyses were chosen for single realization analyses (SNL 2008a, Section 7.7.1[a]) to cover the range of waste package failure mechanisms considered in the TSPA and to highlight the various processes affecting and controlling the radionuclide releases under various thermal and chemical conditions. The six cases are (1) the waste package early failure modeling case, (2) the drip shield early failure modeling case, (3) the igneous intrusion modeling case, (4) the seismic ground motion modeling case for the 1,000,000-year period, (5) the nominal modeling case, and (6) the seismic ground motion modeling case for the 10,000-year period. Example results of three individual analyses (the nominal modeling case, the seismic ground motion modeling case for the 10,000-year period, and the seismic ground motion modeling case for the 1,000,000-year period) have already been presented in detail in Section 2.4.2.2.3 to satisfy the NUREG-1804, Section 2.2.1.4.1.3, Acceptance Criterion 2(3), related to demonstrating consistency and reasonableness of "repository performance and the performance of individual components or subsystems."

As summarized in Section 2.4.2.2.3, within each transport model domain, the interaction of various submodels (and their abstractions) under a given set of physical-chemical conditions is described in detail, providing confidence that the submodels are coupled as intended and their behavior can be explained in a logical manner leading to the resulting annual dose curve. Besides explaining the interaction of submodels, the transport behavior of major dose contributing radionuclides is also described and highlighted in the various modeling cases. For example, the waste package early failure and drip shield early failure modeling cases highlight the controls on transport at early times when the repository is hot, and show the effect of climate changes while the drip shields are still intact. In contrast, the igneous intrusion modeling case and seismic ground motion modeling case for 1,000,000-year period show the effects of various processes occurring late in time and when the drip shields are breached. In all cases, early releases following waste package failure are dominated by nonsorbing- and nonsolubility-limited radionuclides such as ^{99}Tc and ^{129}I, while the late time releases are dominated by longer-lived, solubility-limited radionuclides that undergo sorption processes, such as ^{242}Pu, ^{237}Np, and ^{239}Pu.

2.4.2.3.2.3.2.2 Comparison with the Simplified TSPA Analysis

An analysis has been developed to evaluate repository performance utilizing simplified representations of the mathematical equations that describe many of the degradation, release, and transport processes occurring in the natural and engineered barriers. This analysis, called the Simplified TSPA analysis, is being used as one of the auxiliary analyses to build confidence and corroborate the TSPA model (SNL 2008a, Section 7.7.2). The Simplified TSPA analysis was developed as a stand-alone computer program written in FORTRAN 90 and compiled/linked using Compaq Visual Fortran$^{\text{TM}}$.

The Simplified TSPA analysis is a higher-level abstraction than the TSPA model. In general, it includes the same FEPs that are considered in the TSPA, but the manner in which they are modeled is simpler. This simplification primarily involves removing a considerable amount of detail included in the TSPA related to spatial and temporal variability and treating the repository system with a more "average" representation. In addition, process-level modeling results are further abstracted for inclusion in the Simplified TSPA analysis and some processes are omitted, such as colloid-facilitated transport of radionuclides. The Simplified TSPA analysis is a reasonable simplified representation of the repository system because it is based on the same process- and abstraction-level modeling captured in the analyses and model reports that support the TSPA model. Thus, its technical bases are identical to those of the TSPA model. However, the Simplified TSPA analysis is different than the TSPA model both in its structure and computational method. Details of the simplified conceptual models and their implementation are provided in *Total System Performance Assessment Model/Analysis for the License Application* (SNL 2008a, Appendix L). A summary of the key differences between the TSPA model and the Simplified TSPA analysis is given in *Total System Performance Assessment Model/Analysis for the License Application* (SNL 2008a, Table 7.7.2-1).

The greatest degree of simplification is in the modeling of radionuclide transport within the unsaturated zone and saturated zone. A one-dimensional semi-analytic model of groundwater transport with radionuclide decay was developed using average properties for each hydrologic unit in the unsaturated zone and saturated zone. The unsaturated zone is represented by two regions and three layers. The layers represent geologic units below the repository and the regions represent the area of the repository that is and is not underlain by zeolitic rock. Average hydrologic properties are determined from the calibrated property sets contained in *Calibrated Unsaturated Zone Properties* (SNL 2007l). The saturated zone is divided into three segments: (1) fractured-volcanic rock from underneath the repository to 5 km down gradient; (2) fractured-volcanic rock from 5 km to 13 km down gradient to the alluvium contact; and (3) alluvium to the 18 km compliance location (Section 2.3.9.2.4.1). Radionuclides exiting the unsaturated zone enter the first segment. This simplified approach provides a reasonable representation of the general behavior of the breakthrough curve, rather than the detailed behavior of groundwater flow and radionuclide transport within the unsaturated zone and saturated zone.

A more complex, but still simplified, analysis was developed to model radionuclide transport within the EBS. The relative complexity of this portion of the Simplified TSPA analysis, compared to the unsaturated zone and saturated zone models, is necessary to calculate a reasonable estimate of the rate that radionuclides are released from the EBS. This portion of the analysis includes submodels that calculate the rate and manner that the waste packages degrade, the rate that the waste forms degrade, and rate that radionuclides are transported through the engineered barriers. Both general corrosion and stress corrosion cracking processes are considered in the waste package degradation submodel. General corrosion is represented in the Simplified TSPA analysis as being dependent on both temperature and relative humidity for each of 1000 locations on a waste package surface and in each of 100 regions over the repository area. Stress corrosion cracking is considered for the waste package outer barrier closure lid weld regions. A waste form degradation rate function is applied after waste package failure to provide the source to the EBS transport submodel. The EBS transport submodel in the Simplified TSPA analysis is discretized into three regions representing waste form, corrosion products, and invert. The analysis also considers seeping and non-seeping environments.

The Simplified TSPA analysis is used to simulate four of the modeling cases analyzed using the TSPA model: (1) waste package early failure, (2) nominal, (3) seismic ground motion, and (4) igneous intrusion. Example results from the first two of these are presented here.

Waste Package Early-Failure Modeling Case—Figure 2.4-131a presents the total mean annual dose history for the waste package early failure modeling case using the Simplified TSPA analysis. This total mean annual dose history for the Simplified TSPA analysis takes into account the number of early waste package failures modeled by a Poisson distribution (SNL 2008a, Section L2.8.2). Figure 2.4-131a also shows the estimate of mean annual dose associated with the radionuclides that contribute most strongly to the total mean annual dose for the waste package early failure modeling case using the Simplified TSPA analysis. Figure 2.4-131b provides a comparison at various times between the total mean annual dose for the Simplified TSPA and the total mean annual dose for the TSPA.

The results shown on Figure 2.4-131 indicate that the total mean annual dose and the individual radionuclide mean annual dose are within about an order of magnitude of those obtained for the waste package early failure modeling case simulated over a 1,000,000-year period with the TSPA model shown on Figure 2.4-36. In addition, the most significant radionuclides are also similar with the mobile radionuclides ^{99}Tc and ^{129}I dominating for the first 2,000 years after repository closure, followed by ^{237}Np until approximately 15,000 years after repository closure, ^{239}Pu until approximately 200,000 years after repository closure, then ^{242}Pu and ^{229}Th. The TSPA results (Figure 2.4-36) also show that the mobile and soluble radionuclides (^{99}Tc, ^{129}I, and ^{14}C) dominate first, while the solubility-limited and less-mobile radionuclides (^{239}Pu, ^{242}Pu, ^{237}Np, and ^{226}Ra) become important later.

The overall trends of the TSPA results and the Simplified TSPA analysis results are very similar except for ^{229}Th being a key radionuclide at later times in the Simplified TSPA analysis while ^{226}Ra is shown to be a key radionuclide at later times in the TSPA model. Two factors contribute to the increased importance of ^{229}Th in the Simplified TSPA analysis relative to the TSPA model (SNL 2008a, Section 7.7.2.1): (1) the Simplified TSPA analysis uses a rough approximation to handle radioactive chain decay in the unsaturated zone and saturated zone, which increases ^{229}Th relative to ^{230}Th artificially increasing its importance as compared to the TSPA model, and (2) in the Simplified TSPA analysis, ^{229}Th is assumed to transport through each component of the natural system with the properties of uranium until it exits that component. However, thorium would travel more slowly through the natural barriers than uranium because it has a higher sorption coefficient. Thus, the modeling approach for the natural barrier system in this Simplified TSPA analysis leads to artificially high transport rates for thorium and results in higher annual doses, as is seen for ^{229}Th in this modeling case. (The TSPA model transports thorium with its own high sorption coefficient.)

Comparing Figures 2.4-36 and 2.4-131 shows that the Simplified TSPA analysis yields higher mean annual total and individual doses, particularly over the first 10,000 years, than the TSPA model. This is because the Simplified TSPA analysis assumes that both the degraded waste forms and corrosion products within the waste package are fully saturated, whereas the TSPA model calculates the saturation as a function of relative humidity. This results in lower diffusive transport rates in the EBS, especially for the commercial SNF waste packages, in the TSPA model, until waste-package temperatures decrease.

Nominal Modeling Case—The nominal modeling case accounts for the waste packages that fail under nominally expected conditions because of general corrosion and stress corrosion cracking and for drip shield failure under nominally expected conditions because of general corrosion. Figure 2.4-132 presents the total annual dose histories for the nominal modeling case using the Simplified TSPA analysis. Figure 2.4-132 also shows the estimate of mean annual dose associated with the radionuclides that contribute most strongly to the total mean annual dose for the nominal modeling case using the Simplified TSPA analysis. The results shown on Figure 2.4-132 indicate that the total mean annual dose and the individual radionuclide mean annual dose are within about an order of magnitude at late times, when the mean curve reaches a maximum, compared to those obtained for the nominal modeling case simulated over a 1,000,000-year period with the TSPA model, as shown on Figure 2.4-22b. In addition, the most significant radionuclides are also similar with the soluble and mobile radionuclides ^{129}I and ^{99}Tc dominating, and the less mobile radionuclide ^{135}Cs to a lesser extent. The mean annual dose of solubility-limited radionuclides (i.e., ^{237}Np and ^{242}Pu) is shown to steadily increase to 1,000,000 years in both models. These trends are consistent with those of the TSPA model shown in Figure 2.4-22b.

The difference in the time that stress corrosion cracking begins between the Simplified TSPA analysis and the TSPA model results in the major difference in the annual dose histories for the nominal modeling case. In a sense, the annual dose histories from the Simplified TSPA analysis are translated outward in time by a few hundred thousand years. However, the general trend in the annual dose between the two models is quite similar and the maximum mean annual dose calculated using the Simplified TSPA analysis is within about a factor of three of that calculated by the TSPA.

Although not shown here, the Simplified TSPA analysis and the TSPA model results match more closely for the seismic ground motion modeling case and the igneous intrusion case than for the two cases shown above (SNL 2008a, Figures 7.7.2-9[a] and 7.7.2-12[a]), being within a factor of 6 at all times for the former case and a factor of about 3 at all times for the latter case.

2.4.2.3.2.3.2.3 Comparison with EPRI Model

The EPRI has been conducting iterative assessments of the total system performance of the candidate radioactive waste repository at Yucca Mountain, Nevada for many years. The objective of EPRI's performance assessment is to provide an independent third-party assessment of key technical and scientific issues associated with the proposed geologic repository at Yucca Mountain. The EPRI performance assessment was developed by an independent organization based on independently developed methodology and its own total system performance code: the Integrated Multiple Assumptions and Release Code (IMARC).

This section summarizes the comparison between the EPRI performance assessment analysis and the TSPA model results. As with the Simplified TSPA analysis, the purpose of the comparison is to corroborate the TSPA model results with results of auxiliary analyses used to provide additional confidence in the system model results. Apparent differences between the two models can be traced to the fact that the EPRI performance assessment does not incorporate the most recent updates included in the TSPA model (SNL 2008a, Section M2.4). Most of the input to the EPRI performance assessment analysis corresponds to an earlier version of the TSPA model. As a result, an exact comparison between the results from the EPRI performance assessment analysis and from the TSPA model is not possible. However, the overall features of the dose history curves can be compared and, combined with an evaluation of the apparent differences, this provides a means for enhancing confidence of the general methodology and strategy used in the TSPA model.

The EPRI performance assessment and the DOE TSPA approaches lie at two ends of a spectrum of TSPA analysis methods. The EPRI approach relies on a logic-tree or probability-tree approach that assigns specific probabilities to each potential outcome or branch of the tree based on the probabilities of precursor branches. The end result is a specific probability being assigned to each consequence realization or outcome. The DOE TSPA approach is a Monte Carlo sampling-based approach, which assigns equal probabilities to each outcome and, in general, simulates many more future states or future outcomes of repository performance. Given these differences, confidence is enhanced when the two approaches yield similar results, or if the differences in the results are based on the different assumptions and models underlying the two TSPAs. The differences between IMARC and the TSPA model are in the details of the implementation and the specifics of the assumptions, models, parameters, and couplings used.

The most recent comprehensive description of the IMARC is Version 8 (Kozak and Kessler 2005). More recent updates and implementations in the IMARC were reported in November 2005 (Apted and Ross 2005). The latest documentation includes various analyses related to Yucca Mountain, such as *Effects of Seismicity and Rockfall on Long-Term Performance of the Yucca Mountain Repository* (Apted and Kessler 2005), a final report in November 2006 on the effects of multiple seismic events (Apted 2006), and a December 2006 progress report (Apted and Ross 2006). However, these analyses predate the most recent updates of abstractions incorporated in the TSPA model.

EPRI Model Methodology and Uncertainty Treatment—In general, the EPRI performance assessment analysis represents a more simplified implementation of the various process models and associated uncertainty compared to the TSPA model. Logic tree analysis is used for uncertainty propagation of parameters, which are described using a limited number of probable states (e.g., high, medium, and low values), and their likelihoods (Kozak and Kessler 2005, Figure 2-3). Logic trees (also known as probability trees) combine individual scenarios resulting from uncertain discrete events and/or parameter states. As such, they are a special case of decision trees containing only chance nodes but no decision nodes. The logic tree is ordered so that independent effects are placed to the upstream (left) side, and dependent effects are organized to the downstream (right) side. Each branch is assigned a probability, conditional on the values of the previous branches leading to that node. All possibilities must be considered in building the logic tree, so that probabilities for branches originating from each node sum to one.

The TSPA model accounts for the epistemic uncertainty of parameters, model components, and/or assumptions by sampling uncertainty distributions of large numbers of parameters or model inputs using Monte Carlo simulations. Furthermore, the TSPA model accounts for aleatory uncertainty associated with the timing of igneous and seismic events, as well as spatial variability associated with infiltration and seepage. On the other hand, the EPRI performance assessment does not consider aleatory uncertainty. The EPRI performance assessment assumes fixed times for the occurrence of igneous and seismic events and does not account for spatial variability of infiltration, but assumes spatially uniform infiltration. The EPRI performance assessment does account for epistemic uncertainty in infiltration rates in the logic-tree analyses using high, median, and low infiltration rates, each with a different probability.

Similar to TSPA model, the EPRI performance assessment considers different scenarios, which include nominal, igneous, a seismic scenario, and a human intrusion scenario, although the human intrusion scenario has only been studied in a preliminary fashion. The focus of the comparison described here between the EPRI performance assessment and TSPA model is on the nominal scenario class. The following section summarizes the implementation of the different model components in the EPRI performance assessment for comparison to the TSPA model.

EPRI Model Structure—The IMARC code solves for transport of radionuclides in groundwater for an abstracted concept of the Yucca Mountain repository behavior. The different model components are incorporated into the EPRI performance assessment model as lookup tables, failure distribution curves, and numerical submodels. IMARC includes three major numerical submodels describing: (1) near-field radionuclide release and transport, (2) unsaturated zone flow and transport beneath the repository, and (3) saturated zone flow and transport.

The unsaturated zone above the repository is represented by lookup tables providing the fraction of the repository with active groundwater flow, where the groundwater flux is controlled by net infiltration rates into the upper unsaturated zone which, in turn, depends on the climate state. EPRI considers three climate states corresponding to step changes in infiltration rates (EPRI 2002):

- Greenhouse period (0 to 1,000 years)
- Interglacial period (1,000 to 2,000 years) similar to present-day climate
- Full glacial period (2,000 to one-million years).

Uncertainties in the amount of net infiltration that depend on rainfall and temperature for the different climate states are included in a lookup table of low, moderate, and high net infiltration.

Degradation of waste packages and drip shields is represented by failure distribution curves, which were generated by Monte Carlo simulations of models describing various failure mechanisms implemented in the EPSPA code (EPRI 2002) and in its successor EBSCOM code (Apted and Kessler 2005). Input to these Monte Carlo simulations included uncertainty distributions of model parameters describing different degradation mechanisms for drip shields, waste packages, and cladding. The different corrosion processes include the following.

For the drip shield:

- Initial failure due to undetected manufacturing defect or emplacement error
- General corrosion (main failure mechanism)
- Hydrogen-induced cracking (low probability).

For the waste package in the nominal scenario:

- Initial failure due to undetected manufacturing defect
- General corrosion and microbiologically influenced corrosion (main failure mechanism)
- Localized corrosion (low probability)
- Stress-corrosion cracking (for the outer and middle waste package closure lids).

The TSPA model considers five degradation processes that include general corrosion, microbially-induced corrosion, stress corrosion cracking, early failure, and localized corrosion, which correspond largely to those listed above for the EPRI model.

In the EPRI performance assessment, a near-field model comprises all the components inside the drift, including the drip shield, waste package, cladding, waste form, pedestal, and invert. The release of radionuclides from the near field is computed using the COMPASS (Compartment Model for Partially Saturated Repository Source Terms) code (Kozak and Kessler 2005). Releases from the repository are only assumed to occur after the thermal pulse has significantly dissipated. The COMPASS near-field model consists of different components and solves mass transfer across these compartments, including waste, corrosion product, a pallet or basalt layer, invert, near-field rock matrix and fracture, and far-field rock (Kozak and Kessler 2005, Figure 5-1). In addition, the COMPASS model considers diversion of seepage water entering the drift and flowing into the invert, thereby bypassing the waste. The waste that contains the radionuclide inventory degrades after water contact following waste package and cladding failure. For specific radionuclides bound in the waste form, the release of radionuclides in water is constrained by solubility limits. Overall, the median solubility limits used in the EPRI model fall within the range of those used in the TSPA model, except neptunium, which is slightly below the range given in TSPA (SNL 2008a, Table M-4).

In the COMPASS model, radionuclides released from the waste form are transported by diffusion and advection through the corrosion product, a pallet or basalt layer, invert, and near-field rock fractures and rock matrix (diffusion only) to the far-field rock (Kozak and Kessler 2005, Figure 5-1). The compartments (or modeling domains) are assumed to be partially saturated, forming a continuous water pathway, and water flows through the near-field fractures only in wet conditions. The hydrologic behavior of the near field is represented by two zones representing dripping and nondripping conditions, for which different cumulative probability curves of failure versus time are computed for drip shield, waste packages, and cladding. The COMPASS model did not consider colloid-facilitated transport of radionuclides.

The unsaturated zone is represented by the second numerical submodel embedded within the IMARC "UZ-code," which is represented by several one-dimensional vertical columns approximating spatial variations of repository releases and different lengths corresponding to spatial and temporal variations in the water table. The vertical discretization distinguishes the main unsaturated zone layers, which are each discretized in greater detail. The model accounts for variations in saturations associated with variations in permeability, capillary pressure, porosity, and fracture spacing for both fractures and matrix in each geologic layer. Transport of radionuclides accounts for dispersion, decay, diffusion, and sorption. At the base of the unsaturated zone, the flux of radionuclides exiting the unsaturated zone is used as a time series input to the saturated-zone code.

The saturated zone is represented by the third numerical submodel embedded within the IMARC. The saturated zone submodel in the EPRI model (saturated-zone code) consists of two segments, representing the fractured tuff (15-km downgradient) and the other subsequent alluvial segment (5 km), which extends 2 km beyond the location of the RMEI. For transport simulation in the tuff, the model considers steady-state groundwater flow in the fracture only. Boundary conditions for the transport simulation include prescribed mass fluxes from the unsaturated zone model along the footprint of the repository, and infiltration along the entire water table. Similar to the unsaturated zone model, transport is affected by fracture flow and sorption in the tuff and in the alluvium. This submodel simulates flow and transport through the natural barriers of the saturated zone.

The resulting fluxes of radionuclides in the groundwater at 18 km are assumed to enter the biosphere via groundwater used by the RMEI. These radionuclide fluxes in the groundwater are adjusted to concentrations based on the annual water demand of 3,000 acre-ft (3.7×10^6 m^3/yr) (10 CFR 63.312(c)). These concentrations are then multiplied by the radionuclide-specific BDCF to produce the dose to the RMEI for individual radionuclides at a given time of output concentration. These individual radionuclide doses are then summed to produce the total dose to the RMEI as a function of time.

Main Differences between EPRI Model and TSPA Model—Overall, the EPRI model accounts for the same model components and considers the same FEPs as the TSPA model (SNL 2008a, Appendix M2.4). The EPRI model implementation is a more simplified abstraction of the relevant processes and uncertainty in model parameters. The EPRI model uses a logic tree approach and cumulative distributions of failure curves of different EBS components. Even though these distributions were derived from Monte Carlo simulations, uncertainty parameters were not sampled in the EPRI model, but mean parameter values were used as input in IMARC. Main differences in model components include:

- The EPRI model considers a single infiltration domain distinguishing wet and dry conditions, compared to five percolation subregions with different percolation rates and unsaturated zone properties in the TSPA model.

- A comparison of the EPRI seepage rates and seepage fractions (Kozak and Kessler 2005) with those given in *Abstraction of Drift Seepage* (SNL 2007g) indicates that the seepage rates used in the EPRI performance assessment analysis are higher than those in the TSPA model, while the seepage fractions are lower (SNL 2008a, Figure 7.7.3-1).

- The computed waste package failure distribution curves for the nominal scenario in the EPRI performance assessment are shown on Figure 2.4-133a (Apted and Ross 2005, Figure 5-7, “Updated WP OK, DS OK”), indicating onset of waste package failures at about 500,000 years. The EPRI performance assessment only considers 8,160 commercial SNF waste packages, of which about 10% or approximately 816 are failed at 1,000,000 years. In the TSPA nominal modeling case, the probabilistic projections of waste package breaches exhibit a low probability of a stress corrosion crack penetration prior to 200,000 years (Figure 2.1-10a); however, as indicated in Figures 2.4-133b and 2.1-9, by 500,000 years approximately 15% of the waste packages have some type of breach, with about 54% or approximately 6,280 failed waste packages on average by 1,000,000 years. This is a higher failure rate than in the EPRI performance assessment.

- The EPRI model only considers the inventory of SNF in commercial SNF packages compared to the TSPA model, which includes DOE SNF and HLW in DOE SNF waste packages.

- The EPRI model accounts for gradual cladding failure following waste-package failure, whereas the TSPA model takes no commercial SNF cladding credit.

- The radionuclide inventory used in the EPRI model is based on that given in *Initial Radionuclide Inventories* (SNL 2007t, Table 7-1), which has subsequently been revised to include MOX and LaBS glass waste inventories (SNL 2007t, Table 7-1[a]). The TSPA is based on the latter. Also, the EPRI model only considers 12 radionuclides, whereas the TSPA model considers 32 radionuclides, including ^{135}Cs and ^{79}Se, which contribute to total dose at late time (SNL 2008a, Section 6.3.7.1).

- Overall, the EPRI BDCFs are higher than those used in TSPA model, which would result in higher doses in the EPRI model for the same concentration.

Total Dose Comparison for the Nominal Case—Figure 2.4-134 compares the computed mean radionuclide doses for the EPRI nominal scenario (Apted and Ross 2005, Figure 5-10) with the computed mean doses from the TSPA model for the combined nominal modeling case and the waste package early failure modeling case (SNL 2008a, Figure 7.7.3-3). The results indicate a similar pattern for the nominal scenario characterized by a significant increase in dose after several hundred thousand years. The early failure dose is represented by the dose increase after about 500 years in the TSPA model, which does not appear in the EPRI performance assessment until about 5,000 years. The maximum total annual dose in the EPRI nominal scenario is about 2.0×10^{-2} mrem at 1,000,000 years, compared to about 5.5×10^{-1} mrem at about 740,000 years for the combined nominal and early-failure modeling cases in the TSPA model. The main contributor to total dose at late time is ^{129}I in both cases. The differences between the EPRI performance assessment and the TSPA model results can be accounted for by differences in seepage fraction and seepage rates through the repository; early-failure representation and EBS failure curves; inventory, both in terms of waste type and individual radionuclides; solubility limits and sorption characteristics in the unsaturated zone and saturated zone; groundwater specific discharge in the saturated zone; and number of corrosion-failed waste packages.

Even though the seepage rates used in the EPRI performance assessment are significantly higher than the corresponding rates in the TSPA model (SNL 2008a, Figure 7.7.3-1), the seepage fraction values are significantly smaller. The fewer number of packages that are subjected to seepage conditions causes a reduction in radionuclide release from the EBS, and contributes to the lower mean dose observed in the EPRI performance assessment as compared to the TSPA model.

The EPRI performance assessment only accounts for commercial SNF waste and considers the failure of cladding, whereas the TSPA model accounts for commercial SNF, DOE SNF, and HLW waste, but does not take credit for cladding in commercial SNF waste packages. Consequently, the overall dose release in the EPRI performance assessment is delayed both for the early failure case and for the nominal case. Also, the lower rate of waste package failures by stress corrosion cracking and general corrosion in the EPRI performance assessment further contributes to later onset and lower values of dose. In addition, the EPRI performance assessment uses a value of 0.37 m/yr for the groundwater specific discharge (Apted and Ross 2005, Section 5.5.2.4.2), whereas the TSPA model uses a distribution of values ranging between 0.3 and 7.5 m/yr (SNL 2008f, Table 6-6). The larger values of groundwater specific discharge used in the TSPA model contribute to earlier arrival of radionuclides in the groundwater, and hence to earlier observance of dose to the RMEI.

The EPRI performance assessment only considers 12 radionuclides compared to 32 radionuclides in the TSPA model (SNL 2008a, Table M-5). During early failure, ^{14}C is shown to contribute significantly to total dose in the TSPA model, which is not considered in the EPRI performance assessment. At late time, the dominant radionuclides contributing to total dose include ^{129}I, ^{99}Tc, ^{135}Cs, ^{79}Se, ^{242}Pu, and ^{237}Np in the TSPA model. The dominant radionuclides in the EPRI performance assessment include ^{129}I followed by ^{237}Np, ^{233}U, and ^{229}Th. However, the EPRI performance assessment does not consider ^{135}Cs and ^{79}Se.

Solubility limits used in the EPRI performance assessment indicate significantly lower values for neptunium, plutonium, and thorium compared to the range given in the TSPA model. On the other hand, sorption characteristics used in the EPRI performance assessment for the unsaturated zone are significantly lower for uranium and plutonium compared to those in the TSPA model. However, this does not affect ^{129}I, ^{99}Tc, and ^{135}Cs, which represent the main contributor to total dose in the TSPA model.

In general, the main features of the EPRI annual dose curves for the nominal scenario compare reasonably well with the TSPA model, and the differences between the two can be explained. The differences can be attributed mostly to differences in seepage and in different implementation of the inventory and EBS failure characteristics. This is partly due to the fact that the EPRI performance assessment uses results from earlier versions of the DOE analysis/model reports.

2.4.2.3.2.3.2.4 Performance Margin Analysis and the Evaluation of Conservatisms

As described in Section 2.4.2.3.2, the required validation level for the TSPA model requires use of at least two post-development model validation activities. However, the TSPA model validation efforts exceed procedural requirements (SNL 2008a, Section 7) because in addition to the post-development validation activities discussed above, the validation efforts included several additional post-development activities to enhance confidence in the TSPA model. One of these additional post-development validation activities is the corroboration of system model results with the results obtained using the PMA. The PMA provides additional confidence in the TSPA model results by examining the effect of conservatisms on the model results.

Conservative assumptions were introduced in the formulation of the TSPA submodels and in selected submodel parameters so as to not underestimate the radiological risk associated with imprecise knowledge (i.e., epistemic uncertainties) in repository processes and parameters. Individual conservatisms introduced at the submodel level (Section 2.3), however, can be manifested to differing degrees at the system level (e.g., with respect to mean annual dose) depending on the sensitivity of the system-level performance metric to the underlying submodel. Consequently, a set of selected conservatisms has been evaluated to:

1. Confirm that, when propagated individually through the TSPA model, they are conservative with respect to the total system performance measures (e.g., total mean or median annual dose)

2. Quantify the extent to which the conservatisms, individually and collectively, overestimate the projected annual dose presented in Section 2.4.2.2.1

3. Assess that evaluated conservatisms did not introduce any risk dilution in the TSPA results (e.g., reduce the total mean or median annual doses).

To perform these evaluations, a separate set of TSPA calculations was conducted and is referred to as the PMA (SNL 2008a, Section 7.7.4). The PMA calculations parallel those of the TSPA (Section 2.4.2.2), but focus on evaluating the impact of the more risk-important conservatisms embedded in TSPA model components and submodels.

Because the TSPA is thought to provide a reasonable expectation that dose is not underestimated, the PMA evaluation considers the impact of the removal of some key conservatisms. In particular, based on prior review comments and recommendations (Section 2.4.2.3.2.3.4) from various TSPA review teams, possible conservatisms and nonconservatisms were identified and then examined in light of the TSPA submodels to determine which were risk significant. Potentially risk-significant nonconservatisms were addressed through analyses and modifications of the TSPA submodels. Some risk-significant conservatisms were also addressed through modifications of the TSPA submodels, as appropriate. Other conservatisms are examined here using the PMA. The PMA gauges the collective impact of the conservatisms on the total annual dose.

The introduction of conservative models and assumptions during submodel development and/or derivation of parameter uncertainty characterizations is consistent with the position in NUREG-1804 (Section 2.2.1): "Conservative estimates for the dose to the reasonably maximally exposed individual may be used to demonstrate that the proposed repository meets NRC regulations and provides adequate protection of public health and safety…." For the most part, the conservatisms in the TSPA are introduced so as to not underestimate the effects of processes that promote radionuclide release and transport. Other conservatisms are also implicitly introduced as a result of not taking credit for processes or conditions that could potentially enhance containment and isolation (e.g., the assumption of no commercial SNF cladding credit). In these cases, the PMA examines the effect of including a potentially beneficial FEP that was excluded from TSPA.

A discussion of the various conservatisms in the TSPA (SNL 2008a, Sections 6.3 to 6.6) and their technical bases is provided in the conclusions of the major subsections of Section 2.3 (e.g., Section 2.3.6.9 discusses conservatisms related to waste package and drip shield corrosion). A subset of these judged to be most important from a risk perspective with respect to overall performance of the repository is chosen for further evaluation in the PMA. The PMA assesses the effect of replacing these TSPA model assumptions and conceptualizations with less conservative formulations of the corresponding submodel. The alternative formulations are plausible; however, because the technical bases and associated data for the alternative formulations are not as rigorous and complete as the formulation used in the TSPA model, the alternatives were not used in the TSPA (SNL 2008a, Appendix C). The changes to the TSPA inputs for the PMA primarily focus on the following:

- Including additional coupling among different physical and chemical processes;

- Narrowing parameter uncertainty distributions in cases where conservative bounding values were assumed; and

- Including less conservative alternative conceptual models.

PMA Methodology—In the PMA, the postclosure performance is analyzed over a set of modeling cases with the removal of selected conservatisms (SNL 2008a, Table C5-1). As discussed in Section 2.4.2.1, the TSPA demonstration of performance for the individual protection standard is based on summing the expected annual doses over six out of the seven modeling cases that represent the four primary scenario classes. These seven modeling cases are (1) nominal, (2) waste package early failure, (3) drip shield early failure, (4) igneous intrusion, (5) volcanic eruption, (6) seismic ground motion, and (7) seismic fault displacement. The PMA is conducted over the 10,000-year and post-10,000-year postclosure periods for comparison with the TSPA. It is not necessary to evaluate the nominal modeling case beyond 10,000 years because it, separately, does not contribute to the calculation of total annual dose for the post-10,000-year period (Sections 2.4.2.1 and 2.4.2.2). Rather, the seismic ground motion modeling case includes the effects of the nominal processes over the post-10,000-year period. Also, there is no significant dose contribution from the nominal modeling case in the first 10,000 years. The volcanic eruption modeling case is also not evaluated because none of the changes included in the PMA impact this case.

To demonstrate the performance margin inherent in the TSPA dose projections, the mean of the projected total (i.e., summed over the modeling cases) annual dose to the RMEI is used to evaluate the performance margin for both the period within 10,000 years after disposal and the period after 10,000 years through the period of geologic stability. The total mean annual dose for the PMA is recalculated by replacing the selected set of TSPA modeling cases with the results of the PMA modeling cases.

PMA Models and Parameters—The PMA is initiated by incorporating the changes into the TSPA submodels used for the nominal modeling case. A detailed description of each of these changes and how they were implemented in terms of modifications to TSPA submodels is presented in *Total System Performance Assessment Model/Analysis for the License Application* (SNL 2008a, Section C6). A summary of the specific changes to each TSPA model component is as follows:

Drift-Scale Unsaturated Zone Flow (SNL 2008a, Section C6.2):

- **Reduced seepage flux to the waste package based on a less conservative hydrologic cross-section for the representation of collapsed drift geometry (drift seepage submodel)**—In the TSPA model, the seepage abstraction (Section 2.3.3.2.4.2) accounts for the possible collapse of drifts in lithophysal units using a specific seepage lookup table (SNL 2007g, Section 6.4.2.4). This collapsed-drift lookup table is generated from seepage simulations conducted with the seepage model for performance assessment (BSC 2004d) assuming a rubble-filled circular opening with 11 m diameter as the final state after collapse. In the TSPA model seepage component, the total flow of liquid water from the fractured lithophysal formation into a rubble-filled opening is considered seepage, independent of the actual seepage location, and downstream TSPA model components, such as those for radionuclide mobilization and transport, use this total seepage rate. Use of an 11 m-diameter results in a conservative treatment that overestimates the seepage flux over the 5.5 m drift, because the mostly gravity-driven flow in the rubble-filled opening would effectively prohibit contact of water with the waste packages or waste forms for off-center seepage locations. Such a treatment is chosen in the TSPA model to account for possible uncertainties in the seepage modeling approach for collapsed drifts. A less conservative TSPA treatment would assume that only water that enters the drift in the 5.5-m-wide center section (the original intact drift diameter) be considered seepage (i.e., only then would it be considered in downstream TSPA components with impact on radionuclide mobilization and transport). Water that seeps outside of this center section would not be addressed, because it would bypass the waste package or waste form in the drift center. To evaluate the importance of the above conservatism, an alternative seepage lookup table for collapsed drifts, developed from a revised seepage model for performance assessment simulations, is included in the PMA. The alternative (or PMA) lookup table gives seepage only when the seepage location is in the 5.5-m-wide center section of the rubble-filled opening (SNL 2008a, Figure C6-2).

Waste Package and Drip Shield Degradation (SNL 2008a, Section C6.3):

- **Drip shield general corrosion rates computed based on fluoride-ion concentration threshold instead of fixed and pervasive condition of aggressive corrosion**—For simplicity, the TSPA model applies a conservative "aggressive-condition" drip shield general corrosion rate (Section 2.3.6.8.1.1 and Figure 2.3.6-46) to the topside surface of drip shields when they are exposed to seepage dripping, regardless of the changes in water chemistry due to the thermal evolution of the repository. In the PMA, the chemical environment for drip shield general corrosion is determined explicitly from the incoming seepage water compositions calculated by the EBS chemical environment submodel (Section 2.3.5). For drip shields whose topside surface is exposed to dripping seepage water, the general corrosion environment (i.e., aggressive or benign) is determined as a function of the seepage water chemistry. When the fluoride concentration exceeds 9.5 mg/L (0.5 mM), an aggressive environment is assumed to be present on the topside of the drip shield. As seepage water compositions return to near ambient conditions, the fluoride concentration drops below 9.5 mg/L and the environment is switched to benign conditions. (Fluoride concentrations in the ambient pore waters are all significantly lower than the critical value of 9.5 mg/L for aggressive corrosion (SNL 2007i, Table 4.1-3).)

- **Implementation of stress corrosion cracking of Alloy 22 in the seismic scenario class using a less conservative representative yield stress threshold**—In the TSPA model, the presence of high residual tensile stress induced by seismic vibratory ground motion is assumed to result in stress corrosion cracking of the Alloy 22. The degree of damage is primarily a function of both the average thickness of the Alloy 22 outer barrier (resulting from general corrosion) and the uncertain residual stress threshold above which stress corrosion cracks are assumed to propagate through the entire remaining thickness of the Alloy 22. The structural response calculations for the waste package exposed to seismic induced vibratory ground motions were evaluated for three values of the residual stress threshold for Alloy 22: 90%, 100%, and 105% of the yield strength of Alloy 22 (SNL 2007c, Section 6.1.4 and Tables 6-11 and 6-26). For the PMA, a less conservative range from 100% to 105% of the yield strength of Alloy 22 is used to evaluate damage to the waste package outer barrier during a seismic event. Application of the less conservative range for residual stress threshold in the PMA will decrease the number of waste packages damaged during a seismic event.

- **Inclusion of an alternative distribution of breached area as a result of localized corrosion on the waste package outer barrier**—In the TSPA model, it is conservatively assumed the waste package surface area affected by localized corrosion (SNL 2008a, Section 6.3.5.2.2) is the entire surface area of the waste package, which is subsequently removed as a barrier to water inflow and transport of radionuclides. In the PMA, the results of an alternative conceptual model (SNL 2007o, Sections 6.4.4.8.3) are used to establish a minimum waste package area subject to crevice corrosion processes from localized corrosion. The alternative conceptual model considers a minimum waste package creviced surface area based on the waste package-to-emplacement pallet contact area. The calculated minimum waste package-pallet contact area is 1.924×10^4 mm^2. Therefore, the minimum creviced area is about 0.05% of the total waste package surface area of 36.074 m^2 for the commercial SNF waste-package configuration. The maximum available area for localized corrosion is the area of the waste package wetted by seepage. In the absence of specific information regarding local environments on the waste package, the PMA samples the area of the waste package failed by localized corrosion between the range of the entire waste package surface area exposed to seepage (assumed to be 100%) and the calculated minimum of 0.05% of the waste package surface area used in the alternative conceptual model. Because the conditions for waste package localized corrosion require that drip shields be failed during the thermal period (within approximately 12,000 years after closure), this alternative impacts the drip shield early failure modeling case.

Engineered Barrier System (EBS) Flow (SNL 2008a, Section C6.4):

- **Inclusion of a detailed in-package water balance to account for the mass fluxes of water through the waste packages**—The objective of this PMA submodel is to obtain a less conservative estimate of the quantity of water available inside a breached waste package for waste degradation and radionuclide transport. This analysis involves a higher degree of coupling of the thermal evolution, waste degradation, and water transport. The amount of water is modeled as a function of relative humidity in the EBS, dripping rate, distribution of failed openings on the waste package outer barrier, and extent of waste degradation. The following processes (SNL 2008a, Figure C6-5) are included in the model:

  - Water diffusion and advection through failed openings in the waste package
  - Water consumption by chemical reactions
  - Capillary and osmotic effects on water saturation in alteration products
  - Dripping water run-off from the waste package surface.

  The PMA water balance analysis: (1) accounts for water consumption by reactions, and (2) fully couples hydrologic effects (e.g., the sheet flow on the waste package surface and capillarity effect of porous corrosion products) and chemical processes (e.g., water consumption and salt release by reactions; the depression of water activity with increasing dissolved salt concentration).

Waste Form Degradation and Mobilization (SNL 2008a, Section C6.5):

- **Inclusion of a higher resolution in-package chemistry model that accounts for pore-water chemistry and spatial scale**—The purpose of this PMA submodel is to generate abstractions to predict pH in the pore water of waste-form degradation products exposed to liquid or vapor influx. The predicted pH is used to calculate concentrations of radionuclides and colloids. Unlike the TSPA model, the ionic strength inside a waste package is no longer calculated in the PMA; it is calculated in the water balance model (SNL 2008a, Section C6.4). The scope of the PMA in-package chemistry calculations is similar to that of the TSPA model. The same three in-package chemistry waste-form cells are considered (SNL 2007h, Section 1). The ranges of independent parameters, such as the partial pressure of CO_2 (g) (10^{-4} to $10^{-1.5}$ bars), temperature (25°C), and flow rate (0 to >100 L/yr), are also similar. The primary difference between the two models is that in the PMA in-package chemistry abstraction, liquid water is assumed to be restricted to the pores of the available degradation products. The minimum ratio of the volume of degradation products, V_s, to the volume of liquid water, V_w, is set at V_s/V_p, where V_p is the volume of pore space. In these simulations, V_s/V_p is 1.5, corresponding to a porosity of 0.4. Thus, V_s/V_w is 1.5 when the pores are fully saturated with water. The high range of V_s/V_w ($\geq$1.5) in the PMA abstraction is accomplished by decreasing the amount of water in the simulations, compared to the abstraction used in the TSPA. The PMA calculations for in-package chemistry consist of two parts. The first part is used to construct the functional dependence of pH on waste degradation kinetics for cases where vapor diffusion is a dominant mechanism for water transport through a breached waste package. The second part is to establish the relationship between the water chemistry and the flux of liquid water that percolates the waste package.

- **Included long-term degradation rate models for commercial SNF and high-level (radioactive) waste (HLW) glass waste forms**—In the TSPA model, the commercial SNF waste-form degradation rate is calculated as a function of temperature, oxygen fugacity, total carbonate concentration, and pH (BSC 2004e), based on a set of conservative assumptions that overestimate the rate and extent of waste degradation. The objective of the PMA is to remove some of these conservatisms. In the PMA, the functional dependence on water chemistry remains the same as in the TSPA model. However, the distribution range of the effective surface area of commercial SNF is modified based on fractional release rate measurements from fuel rod segment tests (BSC 2004e). Two additional scaling factors are also included to capture the effect of long-term dissolution and the decrease in radiolysis. Key parameters used in the TSPA model for the HLW glass degradation rate are based on short-term experimental dissolution rate data for a variety of HLW glasses. Because laboratory dissolution rates tend to be many times faster than long-term field rates reported for natural glasses, the TSPA model for glass degradation is conservative, especially at long times (e.g., greater than several hundred years) following breach of a waste package. The glass degradation model in the PMA introduces time dependence to the reaction affinity (based on the growing thickness of the reaction rind). In particular, the parameter k_E in the TSPA model has been separated into its constituent factors [$k_E = k_0(1-Q/K)$], where k_0 is the intrinsic rate constant and $(1-Q/K)$ is the reaction affinity term. The value for k_0 recommended is essentially equal to the value of k_E used for the acid-leg rate equation in the TSPA model (BSC 2004g, Table 8-1) and because k_0 is considered an intrinsic property independent of pH and temperature, k_0 is the same for both pH legs in the model. The most probable value for the final reaction affinity, $(1-Q/K)_{\text{Final}}$, which represents the dissolution rate at long times as the system approaches equilibrium, is chosen so that the long-term rate is approximately equal to long-term reaction rates reported for basaltic glass in nature (Gordon and Brady 2002). Another term in the PMA HLW glass degradation rate is the critical reaction-rind thickness, T_{RC}. This is the thickness of the reaction rind for which mass transport through the reaction rind begins to dominate the exchange of glass constituents between the bulk glass and solution and, therefore, begins to dominate the reaction affinity, $(1-Q/K)$. The value of T_{RC} used in the model is based on observations of reaction rinds from a variety of glass dissolution experiments. The PMA degradation rates computed from this model based on the less conservative reaction affinity still remain well above dissolution rates estimated for natural basaltic glasses, and the time for the model rates to reach a rate comparable to the estimated long-term rates of natural basalts is about 1,000 times longer than achieved in nature, so even the PMA abstraction remains conservative (SNL 2008a, Section C6.5.1).

- **Included credit for initial clad failure fractions in place of conservatively assuming all cladding is failed at time of emplacement**—In the TSPA model, no credit is taken for commercial SNF cladding as a barrier in all scenario classes, primarily to mitigate risks associated with on-site inspection of cladding prior to encapsulation in the waste package (SNL 2007r, Section 6.2.1.2[a]). In the PMA, the "as received" (i.e., mostly intact) cladding condition is applied to commercial SNF for the nominal and early failure scenario classes during the first 10,000 years postclosure.

- **Reduced uncertainty ranges for solubilities of neptunium, uranium, and plutonium**—The TSPA dissolved concentration limits submodel captures the extent of various uncertainties in thermodynamic data by combining them additively (in log-space) to generate an uncertainty envelope. However, because these uncertainties are not simply additive, this method tends to overestimate the actual uncertainty in any single result. The PMA abstraction uses a simpler method to bound uncertainties based on comparisons with solubility data or methods advanced by a sanctioning body such as the Organisation for Economic Co-operation and Development/Nuclear Energy Agency in its thermodynamic data compilations when solubility data is lacking. The uncertainty in the PMA abstraction is to a large extent similar to the approach used to develop the uncertainty range for the ε_1 parameter in the TSPA model (SNL 2007u). The PMA approach is to provide uncertainties on selected actinide solid solubilities that are based on available experimental solubility and thermodynamic data reported in the scientific literature or in specialized data compilations. The recommended uncertainties and associated distributions for the relevant actinide solids in log solubility (given in molality units) were in essence based on comparisons of EQ3/6 code predictions with measured solubilities. In cases where solubility data were either not available or very limited, the uncertainties were then based on evaluations of thermodynamic data described in the Organisation for Economic Co-operation and Development/Nuclear Energy Agency compilations for the actinide solid of interest. The assigned uncertainty bounds are to be implemented in a continuous form as a function of pH and f_{CO2}. There is no attempt to propagate explicit uncertainties in the values of pH and ionic strength because: (1) solubility and related uncertainty data for the solids of interest are not abundant, (2) it would require a more involved analysis in the characterization of uncertainty propagation as a result of changes in aqueous speciation, and (3) it is noted that moderate changes in ionic strength (e.g., 0.5 to 1 molal) do not result in significant changes in the predicted solubilities.

Unsaturated Zone Flow and Transport Submodel (SNL 2008a, Section C6.6):

- **Use of a colloid diversity model, which treats variability in colloidal particle transport as stochastic (aleatory) uncertainty, rather than as an epistemic uncertainty that applies to all colloid particles**—The TSPA submodel for colloid-facilitated transport of radionuclides in the unsaturated zone is considered conservative because it does not account, except in a coarse way, for the inherent variability of transport properties of individual colloids in a colloid population. In the PMA, an alternate representation of colloid-facilitated contaminant transport is introduced that treats the variability of mobility of individual colloids as a process inherent to the colloid population, rather than as observations that lead to epistemic uncertainty in the transport properties characterized by a single uncertain parameter. The process of retardation via attachment and detachment of colloids on immobile surfaces is often modeled with time and space invariant parameters; here it is modeled assuming a diverse population of transport properties that account for the inherent variability of colloid size, surface charge and chemical properties, mineralogy, and the concomitant impact on colloid mobility. The critical concept is the assumption that the transport properties of colloids in nature are heterogeneous. The colloid diversity treatment is formulated to account for these heterogeneities.

- **Matrix diffusion effects on radionuclide transport**—Changes for the PMA include the addition of a diffusion-scaling factor, and the use of the discrete fracture model as an alternative conceptual model for fracture/matrix interaction. In the TSPA (SNL 2008a, Section 6.3.9.2), the diffusion coefficient for each radioelement is computed as the product of the diffusive tortuosity, τ_D, and the free-water diffusion coefficient, D_{free}. For the PMA, the effect of a presumed increase in the effective diffusion coefficient due to scale effects is modeled by applying a multiplication factor to the effective diffusion coefficient, so that the scaled effective diffusion coefficient, D_{eff}, is given by:

$$D_{eff} = f_d \tau_D D_{free} \qquad \text{(Eq. 2.4-38)}$$

  where f_d is the scale factor for matrix diffusion. To assign a parameter uncertainty distribution for f_d, the modeling efforts to reconcile the results of unsaturated zone transport field tests have been examined. To obtain a good match to the tracer tests in Alcove 8–Niche 3, the interface area had to be scaled upward by a factor of 45 above that of the original data (SNL 2007b, Section 7.8.3.2 and Figure 7.8-9). Based on this and other test data, and considerations about uncertainties already included in other unsaturated zone transport parameters (such as the active fracture model parameter), a uniform distribution of the scale factor from 1 to 45 is used in the PMA. Since the analyses leading to the value of 45 are obtained using models with fine discretization near the flowing fracture(s), this parameter uncertainty distribution is only compatible with a discrete fracture submodel. A discrete fracture submodel is used for the PMA to eliminate the conservatism that the TSPA dual-permeability model represents (greater breakthrough at short travel times) and because the discrete fracture submodel is compatible with the scale factor uncertainty distribution just described. A series of simulations with the

FEHM particle tracking model (using the discrete fracture submodel) show favorable comparisons, especially at late travel times, to a matrix-fracture system-multiple interactive continua transport model and to a particle tracking model that employed a completely different numerical algorithm (SNL 2008e, Section 7.2.2).

- **Addition of uncertainty to the degree of climatically-induced water table rise**—In the TSPA model, future climate conditions are simulated assuming that the system instantaneously changes from one steady-state flow field to another at the time the climate changes. Future climates in the first 10,000 years after closure, termed the monsoonal and glacial-transition climate states, are represented by higher infiltration rates and higher associated unsaturated zone flow velocities compared to the present-day conditions. In addition, the water table in the unsaturated zone transport model under future climate states is assumed to rise to an elevation of 850 m for all realizations, a nominal rise of 120 m from the present-day value. In the TSPA model, this rise of 120 m is adopted without uncertainty—an approach considered conservative with respect to the unsaturated zone transport times, because 850 m is considered an upper bound elevation, and the higher water table shortens the travel distance and travel times through the unsaturated zone. In the PMA, the water table elevation is considered an uncertain parameter with a distribution whose range has an upper bound of 850 m. A workshop was previously conducted to quantify uncertainty in past water table rise at Yucca Mountain. This was accomplished by convening a group of technical experts in the areas of hydrology, geochemistry, mineralogy, and statistics/uncertainty to represent and consider the multiple lines of evidence regarding this process. The workshop consisted of a series of presentations on previous studies and new geochemical information relevant to past water table rise at Yucca Mountain, followed by a quantitative assessment of uncertainty in water table rise by the entire group. The resulting uncertainty distribution ranged from 750 to 850 m elevation, with a median of about 780 m (SNL 2008a, Figure C6-29). This distribution is treated as epistemic uncertainty in the PMA and applied to future climates in a manner similar to the step-change water table rise associated with the future climate treatment in the TSPA model (i.e., at the onset of the monsoon climate at 600 years).

Saturated Zone Transport Submodel (SNL 2008a, Section C6.7):

- **Introduction of a dual-porosity interface model between the unsaturated zone and saturated zone**—While the unsaturated zone transport submodel uses a dual-continuum model (i.e., transport of radionuclides in the direction of flow in both the fracture and matrix continua), the saturated zone flow and transport submodel uses a dual porosity model in the fractured volcanic tuff beneath the repository (i.e., transport in the direction of flow only in the fracture continuum). Thus, the radionuclide mass reaching the water table from both the unsaturated zone fractures and matrix is combined at the unsaturated zone-saturated zone interface and transferred directly to the dual-porosity saturated zone three-dimensional and one-dimensional transport models. This is equivalent to assuming that the radionuclide mass instantly diffuses out of the unsaturated zone matrix and into the saturated zone fractures at the interface between the unsaturated zone and saturated zone. This approximation is conservative. The PMA abstraction described in this section modifies the TSPA model by introducing matrix transport at the interface between the unsaturated zone and saturated zone. In particular, the radionuclide mass releases from the unsaturated zone matrix cells are separated from the releases through fracture cells. The releases from the matrix cells at the water table are then routed through a submodel that simulates diffusion from the unsaturated zone matrix into the saturated zone fractures, based on a dual porosity conceptual model implemented with a GoldSim cell network.

- **Addition of colloid diversity model and retardation of irreversibly sorbed radionuclides**—The TSPA saturated zone abstraction for colloid transport of irreversibly sorbed radionuclides applies to plutonium and americium (SNL 2008f, Section 6.5.2.11). A large fraction of these colloids, designated the "slow fraction," are retarded by attachment/detachment processes while a small fraction, known as the "fast-fraction," are transported unretarded (Sections 2.4.2.3.2.1.9 and 2.4.2.3.2.1.10). In the TSPA model (SNL 2008f, Section 6.5.2.11), transport of irreversible colloids for the slow fraction in both the volcanic units and the alluvium is calculated using single retardation factors per realization (one for the volcanic units and another for the alluvium). However, some experimental observations suggest that there may be significant variability (diversity) in the attachment/detachment rate constants resulting from differences in water chemistry, colloid size, colloid mineralogy, colloid surface charge, and characteristics of sorption sites on the aquifer media. For the PMA, the colloid diversity model assigns a wide range of retardation factors to individual colloid particles within a given TSPA realization based on their diverse sizes, shapes, compositions, and surface properties (Robinson et al. 2007). In addition, the development of the colloid retardation factor distributions has been modified to better address the uncertainty in the colloid transport experimental data and, particularly, in the extrapolation of these data to the TSPA time and distance scales. The retardation factor distributions, as well as the fast fraction value, are travel-time dependent. This colloid diversity approach is implemented in both the saturated zone three-dimensional and one-dimensional transport models.

- **Addition of enhanced radionuclide sorption in potential reducing (anoxic) regions of the saturated zone**—Potential variations in redox conditions in the saturated zone could have impacts on the migration of redox-sensitive radionuclide species released from the repository at Yucca Mountain (BSC 2006). Under reducing geochemical conditions, the solubility limit can be lower and the sorption coefficient can be higher for radioelements such as technetium and neptunium. Potential precipitation from lower solubility limits and retardation from enhanced sorption would lead to longer transport times in the saturated zone if groundwater flow paths from beneath the repository encountered reducing conditions before reaching the boundary of the accessible environment. The base-case conceptual model of saturated zone transport in the TSPA implicitly assumes oxidizing conditions in the saturated zone (SNL 2008h, Table 5-1). As a result of the oxidizing conditions, technetium is modeled with no sorption (i.e., no retardation) in both the volcanic units and the alluvium (SNL 2008h, Table C-14[a]). The objective of this component of the saturated zone PMA is to simulate the transport of technetium and neptunium with enhanced sorption in zones of potentially reducing geochemical conditions. The conceptual model used in the saturated zone PMA is that the resulting enhanced sorption for these redox-sensitive radioelements would occur in the volcanic tuff matrix of the fractured volcanic units in reducing zones within the saturated zone. For the purposes of the saturated zone PMA and associated enhanced sorption of technetium and neptunium, reducing conditions are defined as geochemical conditions in which the Eh is less than approximately 100 mV. For the PMA, the model zone of uncertain dimensions is defined in the three-dimensional saturated zone flow and transport abstraction model to represent the location of reducing conditions. A separate value for the sorption coefficients in the volcanic matrix is assigned within this zone, relative to the values assigned to the volcanic units and alluvium under oxidizing conditions. The saturated zone one-dimensional transport model is also modified by subdividing the GoldSim pipe elements so that separate pipe segments exist for oxidizing and reducing conditions. The dimensions of the reducing zone, which begins beneath the repository, include an uncertain length (downgradient towards the RMEI) sampled between 4 km and 10.8 km and an uncertain width (perpendicular to the flow direction) sampled between 0 km and 2.8 km. The uncertainty distributions for the sorption coefficients of technetium and neptunium are identical normal distributions, with a mean of 1,000 mL/g and standard deviation of 150 mL/g (SNL 2008a, Table C6-9).

- **Less conservative distribution for saturated-zone flowing interval porosity**—The flowing interval porosity is defined as the volume of the pore space through which significant groundwater flow occurs relative to the total volume. It characterizes the flowing intervals rather than all fractures. Estimates of this parameter are based on theoretical models, pumping tests, and tracer data. For the TSPA model, a cumulative distribution in the range 10^{-5} to 10^{-1} is used (SNL 2008f, Section 6.5.2.5 and Table 6-8). To define the lower bound value, estimates of fracture porosity of intact cores of volcanic rock are used. It has been noted that this lower bound might be low for a bulk-average parameter (i.e., average value over the volcanic zone) being applied at the kilometer scale (i.e., the saturated zone model domain) (SNL 2008f, Section 6.5.2.3; SNL 2008a, Section C6.7.1). Thus, it has been suggested that an alternate lower bound be considered. Therefore, for the PMA, the lower bound has been raised from 10^{-5} to 10^{-4} based on Exploratory Studies Facility (ESF) and field tests (SNL 2008f, Section 6.5.2.5), as well as tracer tests in low-permeability fractured rocks (Guimera and Carrera 2000).

- **Account for correlation between flowing interval porosity and groundwater specific discharge in the saturated zone**—In the TSPA model, the groundwater specific discharge (which is the function of permeability) and flowing interval porosity are uncorrelated variables (SNL 2008f, Section 6.5.2). In a fractured flow aquifer, there are theoretical and geometric arguments that suggest the two parameters are at least partially correlated. As fracture density and apertures increase, one would expect both flowing interval porosity and permeability to also increase. A correlation factor applicable to Yucca Mountain conditions would provide a less conservative simulation of flow and transport in the saturated zone. Yucca Mountain experimental data are not currently available for the development of a permeability-porosity correlation for the saturated zone volcanic and alluvial units; therefore, a literature review was conducted to find experimental data that are applicable to the Yucca Mountain setting. Rank correlation was used on the data, with a resulting correlation value of 0.64.

Seismic Scenario Class (SNL 2008a, Section C6.8):

- **Less conservative crack area density model for seismically induced damage on Alloy 22**—After the seismic event, the surface area of the Alloy 22 that exceeds the residual tensile stress threshold is considered damaged and is conceptualized to result in a tightly spaced network of stress corrosion cracks (SNL 2007c, Sections 6.1.4). Application of a residual tensile stress threshold for seismic failures is nonmechanistic in the sense that detailed calculations for potential crack initiation and potential crack propagation are not used to determine the actual failure time after a seismic event. Rather, a network of stress corrosion cracks is considered to immediately form once the residual tensile stress threshold is exceeded, providing potential pathways for radionuclide transport and release (SNL 2007c, Sections 6.1.4). To assess the potential for radionuclide release through these cracks, it is necessary to assess the possible number of cracks in the damaged area and the opening areas of these cracks. The TSPA model samples a uniform distribution from 3.27×10^{-3} to 1.31×10^{-2} for the crack area density (i.e., total crack opening area per unit damage area) for waste package seismic damage. This distribution includes several conservatisms related to crack geometry and the methodology for calculating crack density (SNL 2007e, Section 6.7.3.3). An alternative model for the crack area density yields a value at room temperature of 7.22×10^{-3} (SNL 2007e, Section 6.7.4). For the PMA, the crack area density is changed to a constant value equal to the lower bound used in the TSPA model, 3.27×10^{-3}. This lower bound represents a less conservative value and more closely resembles the results of the alternative model.

- **Evaluation of the seismic consequence abstraction using a less conservative range of residual stress threshold for seismic ground motion damage**–This PMA change has already been described under the waste package submodel changes.

PMA Results—The PMA total mean annual dose is calculated replacing the selected set of five TSPA modeling cases (identified at the beginning of this section) with PMA results. The TSPA results for the volcanic eruption modeling case are combined with the PMA results to calculate the PMA total mean annual dose (since the volcanic eruption case remained unchanged for PMA). A comparison of the total mean annual dose history for the PMA and the TSPA is shown on Figure 2.4-135, for the 10,000-year and the post-10,000-year periods. However, because the PMA is based on a prior version of the TSPA model (v5.000), three curves are shown in Figure 2.4-135: (1) the TSPA annual dose curve based on Version v5.000 of the TSPA model (SNL 2008a, Appendix P), (2) the PMA annual dose curve based on Version v5.000 of the TSPA model, and (3) the TSPA annual dose curve based on Version v5.005 of the TSPA model. The latter is the dose shown in Section 2.4.2.2.1 to demonstrate compliance with the individual protection standard (Section 2.4.2.2.2 discusses the two versions of the TSPA model).

A few conclusions can be drawn from Figure 2.4-135:

1. The PMA results confirm that the analyzed set of submodel conservatisms described above, when propagated through the TSPA model, do not underestimate total mean annual dose.

2. Relative to the TSPA model results, the maximum of the PMA total mean annual dose is lower by more than an order of magnitude for the 10,000-year time period and lower by a factor of two for the post-10,000-year time period.

3. The evaluated conservatisms did not introduce any risk dilution in the TSPA results, as demonstrated by the absence of higher maximum doses in the PMA results for either the probabilistic projections of the total annual dose (SNL 2008a, Figures 7.7.4-1 and 7.7.4-4) or the projected total mean annual dose shown in Figure 2.4-135 (SNL 2008a, Section 7.7.4.2[a]).

2.4.2.3.2.3.3 Natural Analogues

Analogues to repository conditions and materials, both natural and anthropogenic, provide a means to compare repository conditions and materials to observed conditions and materials for time periods relevant to the lifetime of the repository (proposed 10 CFR 63.114(a)(7)). The National Research Council has endorsed the use of natural analogues as “natural test cases, geological settings in which naturally occurring radioactive materials have been subjected to environmental forces for millions of years” (National Research Council 1990, p. 27). Analogues can provide quantitative and/or qualitative evidence to assess expected repository performance covering geologic time scales. Analogues, although not the same as controlled laboratory or field experiments, can provide insights and build confidence in the conceptual and numerical models that are used to represent processes and events that could affect repository performance.

The results of natural analogue analyses relevant to the long-term geologic storage of nuclear waste serve as corroborative input to several of the analysis and model reports that support the model components and submodels of the TSPA model. Natural analogues relevant to the assessment of the long-term performance of the Yucca Mountain repository are discussed in *Natural Analogue Synthesis Report* (BSC 2004h). Some of the analogues to the process models and submodels of the TSPA model are briefly summarized below (SNL 2008a, Section 7.8). Following these summaries is a description of two investigations of natural analogues describing geologic processes that could affect the Yucca Mountain repository performance. These analogues, which provide corroborative evidence for the TSPA model, are the 1995 volcanic eruption at Cerro Negro, Nicaragua (SNL 2008a, Section 7.8.1), and radionuclide transport at the Nopal I uranium deposit in the Sierra Peña Blanca in Chihuahua, northern Mexico (SNL 2008a, Section 7.8.2).

2.4.2.3.2.3.3.1 Process Model Analogues

Drift Stability—Neolithic flint mines (approximately 4,000 to 3,000 B.C.), and Roman mines and aqueducts demonstrate that man-made underground openings can remain open and stable for thousands of years and natural caves near Carlsbad, New Mexico have remained open for several million years (BSC 2004h, Section 15.7.1).

Waste Form Degradation—The reaction path for the alteration of SNF at Yucca Mountain is expected to be similar to that of geologically young, lead-free uraninite, with schoepite and becquerelite forming as intermediate products, followed by uranyl silicates. Natural uraninite and its alteration products, found at the Nopal I uranium deposit at Peña Blanca, have these characteristics, making this deposit a good analogue to the alteration of uranium oxide spent fuel (BSC 2004h, Section 15.7.2).

The concentrations of fission products can be used as tracers in minerals precipitated in the rock matrix and in dissolved radionuclides in groundwater surrounding naturally occurring uraninite deposits. Geochemical analysis of these minerals and groundwater chemistries provides a means of estimating natural dissolution rates at some natural analogue sites. When this approach was used at the uranium ore deposits at Cigar Lake, Canada, and Koongarra, Australia, where ore deposits are found under reducing and oxidizing conditions, respectively, the dissolution rate was found to be more rapid under the oxidizing conditions at Koongarra.

Other lines of evidence from geochemical investigations concerning dissolution at the natural analogue uraninite ore deposit at Oklo, Gabon, indicate that dissolution of ore minerals has been slight over the past two billion years. Under radiolysis conditions occurring at the time of criticality at Oklo, the estimated mobilization of the original uranium for transport was only several percent (BSC 2004h, Sections 4.3.2 and 15.7.2). Uranium, plutonium, neptunium, and americium were retained in the reactor zone for almost two billion years in the reduced environment of the Oklo reactor. There has been limited migration of technetium, ruthenium, rhodium, and palladium, and considerable migration of cesium, rubidium, strontium, and barium. Although conditions at Oklo's reactor zones are not like those expected at Yucca Mountain, study of the migration patterns for specific radionuclides gives useful insights regarding the behaviors of these species in various environments. For example, although evidence of intense radiolysis was observed at Oklo, only several percent of the available uranium was mobilized (BSC 2004h, Section 4.5).

With respect to degradation of the borosilicate HLW glass waste forms in the repository, although natural glasses are somewhat different in composition than borosilicate HLW glass, studies of natural glass alteration in comparable geological settings suggest that HLW glass will be stable in the Yucca Mountain repository environment (BSC 2004h, Section 15.7.2). This, in turn, suggests that degradation and dissolution rates for glass waste forms in Yucca Mountain are likely conservative (SNL 2008a, Section C6.5).

Waste Package Degradation—The analogues to common metals serve mainly to demonstrate that under ambient to slightly elevated temperatures, these metals can be stable for thousands of years, even under oxidizing conditions. The survival of metal archaeological artifacts over prolonged periods of time is related to the corrosion-resistant properties of metals and metal alloys, the development of protective passive film coatings with the onset of corrosion, and the location of artifacts in arid to semiarid environments. Such features were used in the selection of materials and a design configuration to enhance the durability of waste packages designed for the Yucca Mountain repository (BSC 2004h, Section 15.7.3).

Metal alloys similar to those being considered for the waste packages to be used at Yucca Mountain have few analogues found in nature. Josephinite, a complex rock found in remnants of the earth's mantle in Josephine County, Oregon, contains several nickel-iron alloys. The survival of the naturally occurring ordered nickel-iron alloy in josephinite for millions of years, with only relatively minor amounts of surface oxidation, indicates that this material is highly resistant to oxidation and other forms of corrosion that occur in its geologic environment. Although the composition of the nickel-iron alloy in josephinite differs from Alloy 22 in that it does not contain chromium, molybdenum, or tungsten, it does provide evidence that a similar alloy can remain passive over prolonged periods of time under oxygen-rich conditions similar to those expected at the Yucca Mountain repository (BSC 2004h, Section 15.7.3).

The slow degradation rates of chromium-bearing materials under ambient conditions are illustrated by the observed natural release of chromium from chromite contained in ultramafic rocks in the Sierra de Guanajuato, in Guanajuato State, central Mexico. Corrosion is observed to be concentrated along exsolution rims, which are analogues to structural defects on metal surfaces. However, although the chromite has undergone some alteration, it has survived for more than 140 million years (BSC 2004h, Section 15.7.3).

EBS Components—Although the invert crushed devitrified welded tuff does not have high concentrations of zeolite and clay minerals, the high surface area of crushed tuff is expected to provide sorption sites that will retard radionuclide transport. Adsorption of actinides in a gravel bed at Los Alamos, New Mexico provides qualitative evidence of radionuclide retardation at the contact between an invert-like material and underlying bedrock (BSC 2004h, Section 15.7.4).

The Pocos de Caldas, Brazil analogue illustrates that iron-bearing colloids have the potential to retard the transport of uranium and other spent fuel components by forming colloids that are then filtered from suspension at short distances. Degradation of steel structural elements in the EBS could contribute to this process (BSC 2004h, Section 15.7.4).

Drift Seepage—Analogues of the unsaturated zone support the analysis that most of the infiltrating water in the unsaturated zone is diverted around underground openings, and does not become seepage into these openings. The analogues show that this is true even for areas with much greater precipitation rates than those at Yucca Mountain. For analogues that show some seepage, at least some of the seepage that enters underground openings does not drip, but rather flows down the walls, as seen at dwellings excavated in tuffs at Goreme, Cappadocia, Turkey, and in efflorescent salts found in the leaking vaulted construction in Building 810 at the Denver Federal Center, Colorado (BSC 2004h, Section 8.3). In the few instances where dripping has been noted in settings analogous to Yucca Mountain, the drips can be attributed to asperities in the surface of the roof and ceiling of the openings, such as those seen at Carlsbad Caverns, New Mexico (BSC 2004h, Section 8.3). Thus, although most water would likely flow around emplacement drifts at Yucca Mountain, the analogue information indicates that the expected small amount of seepage that could occur would primarily flow down the walls of the drifts, and only a very small fraction will drip from drift-ceiling asperities. Drift seepage investigations at the Nopal I mine at the Peña Blanca natural analogue site showed wide variability in the location, timing, and amount of seepage, suggesting fast-flow fracture pathways (Dobson et al. 2008). More information on these investigations is presented below in the description of the Peña Blanca natural analogue.

Unsaturated Zone Flow and Transport—The Peña Blanca natural analogue site (SNL 2008a, Section 7.8.2), has conditions similar to those at Yucca Mountain. The Nopal I mine at Peña Blanca has groundwater chemistry analogous to the groundwater chemistry in the Yucca Mountain hydrogeologic system. Chemical analyses of groundwater sampled from beneath the ore deposit indicate that radionuclides leached from the deposit are mostly sorbed or reprecipitated in the rocks surrounding the ore deposit, and that there is little unsaturated zone transport. Nopal I also displays discrete alteration zones in fractured rocks intersected by likely groundwater flow paths (BSC 2004h, Section 15.7.11). The application of information describing the Peña Blanca natural analogue is described in more detail below.

Coupled Processes—Geochemical modeling of fluid compositions has been used to successfully predict observed alteration mineral assemblages at Yellowstone, Wyoming. Geothermal systems such as Yellowstone illustrate a variety of thermal-hydrologic-chemical processes relevant to the fractured, unsaturated flow system present at Yucca Mountain. Yellowstone and other geothermal systems in welded ash flow tuffs or other low permeability rocks indicate that the fluid flow is controlled by interconnected fractures. Alteration in low permeability rocks is typically focused along fracture-flow pathways. Only a small portion of the fracture volume needs sealing by precipitated minerals to effectively retard fluid flow. The principal minerals predicted to precipitate in the near field of the Yucca Mountain repository are amorphous silica and calcite, which are also commonly found as sealing minerals in geothermal systems (BSC 2004h, Section 15.7.7). Sealing in geothermal fields can occur over a geologically short time frame on the order of a few days to several years. The unsaturated conditions, lower temperatures, and much lower fluid-flow rates predicted for the Yucca Mountain system, in comparison to the conditions in geothermal systems, will result in less extensive water-rock interaction than observed in geothermal systems. For example, coupled processes are expected to have a much smaller effect on hydrogeologic properties at Yucca Mountain than are observed at Yellowstone. Thermal-hydrologic-chemical simulations conducted to date for the Yucca Mountain repository suggest that only 4% to 7% reduction in fracture porosity and less than one order of magnitude reduction in permeability are expected to occur in the near field as a result of amorphous silica and calcite precipitation.

The Marysvale hydrothermal uranium-molybdenum ore deposit in Utah, tuffaceous rocks in hydrothermal systems at the Long Valley Caldera, California, and the Valles Caldera, New Mexico suggest that uranium was concentrated and liberated from siliceous rocks in response to hydrothermal circulation and then concentrated in ferruginous and carbonaceous zones. The Valles and Long Valley studies indicate localized mobility of uranium and decay products in tuff and underlying sedimentary rocks at temperatures comparable to those expected during the first few thousand years in a nuclear waste repository environment (BSC 2004h, Section 11.5). However, this hydrothermal process will be of limited duration at Yucca Mountain because the decay of the waste heat causes the pore water to drop below boiling in the host rock surrounding the drifts one to two thousand years after waste emplacement.

Saturated Zone Transport—Some of the Uranium Mill Tailings Remedial Action Program sites are useful for evaluating radionuclide transport in the alluvial portion of the Yucca Mountain flow system. The conclusions derived from an analysis of the Gunnison, Colorado site are: (1) a fraction of the uranium originating at the site is transported in the alluvial aquifer at a rate similar to that at which a conservative constituent is transported, and (2) there is little evidence for lateral dispersion of contaminants in the downgradient direction. For the New Rifle, Colorado site, the main conclusions are: (1) dilution occurs in the downgradient direction, and (2) a small portion of the uranium is transported at almost the same rate as conservative constituents of natural groundwater, although the larger portion travels at a slower rate. The conclusions regarding uranium transport distances relative to conservative constituents must be tempered by uncertainties regarding the presence of complexing agents (BSC 2004h, Section 15.7.8).

In most studies of natural systems, a proportion of the total uranium, thorium, and rare earth elements in groundwater have been associated with colloids. Colloids can serve as sorbers of radionuclides and could be agents either of retardation or fast transport. Evidence from natural systems indicates that colloidal transport over kilometer-scale distances is limited. Observations from Los Alamos, New Mexico and the Nevada Test Site lend support to the concept that radionuclide transport in the saturated zone can be facilitated by colloids, but no natural analogue studies have been able to quantify the importance of this process (BSC 2004h, Section 15.7.8).

Biosphere—A literature survey regarding the behavior of radionuclides in soils in the Chernobyl, Ukraine area suggests that soil type influences the ecological half-life of radionuclides in the biosphere, both in regard to soil bioaccumulation factors and to advective and diffusive transport properties that limit radionuclide transfer to plant roots. Agricultural methods, including irrigation, tillage, and the types of crops that play an important role in radionuclide resuspension could have an effect on rural populations. Radionuclide resuspension is likely to increase the contamination of plant surfaces and would increase the inhalation dose for agricultural workers, especially for plutonium (BSC 2004h, Section 15.7.9). Radionuclide resuspension is included in the biosphere model (Section 2.3.10).

Volcanism and Seismic Effects on Drifts—Natural analogue investigations are part of the effort to understand volcanism in the Yucca Mountain area. Analogues have been used to assess the probability of dike eruption, plausible eruption styles, eruption parameters, and magma compositions, factors that have been used to increase confidence in the ability of the ASHPLUME model to simulate atmospheric dispersal following a theoretical eruption at Yucca Mountain (SNL 2007m, Section 7.3).

For seismic events, examples from observations of underground openings demonstrate that such openings are able to withstand ground shaking for peak ground acceleration as high as 0.4 g. The ability of underground openings to withstand ground shaking is increased by the thickness of overburden, competence of the rock surrounding the opening(s), decreased earthquake magnitude, and increased distance of the opening(s) from the earthquake epicenter. The bulk of evidence from analogue examples of seismic impacts to underground openings (particularly in settings similar to Yucca Mountain, such as responses to the Little Skull Mountain earthquake), demonstrates that damage to repository drifts from ground shaking during the postclosure period would be minimal (BSC 2004h, Section 15.7.10). However, for very distant future times, drift stability and degradation are modeled using an accumulation of minor damage in terms of loss of strength and rockfalls as described in Section 2.3.4.1.

2.4.2.3.2.3.3.2 Investigations Providing Corroborative Evidence

Performance Assessment Comparison with Ash Fall at Cerro Negro—The Cerro Negro volcano is one of a number of active basaltic volcanoes in a volcanic mountain range in Nicaragua. Cerro Negro is located on the Caribbean tectonic plate, and the volcanic activity expressed within this long volcanic mountain range, which extends from southern Mexico to Costa Rica, is directly related to subduction of the Pacific tectonic plate under the Caribbean tectonic plate. Volcanism at Cerro Negro has a 150 year history, with at least 22 documented eruptions. The eruption in 1995 produced a tephra volume of 0.004 km^3 (Hill et al. 1998), a volume similar to, but less than, the volume from the Lathrop Wells cone, which was approximately 0.07 km^3 (SNL 2007ad, Appendix C, Section C.7). The 1995 Cerro Negro eruption is analogous to the type of eruption that could occur at the Yucca Mountain repository. However, Cerro Negro's long history, shape, and magma production rate suggest that it represents a young composite volcano, rather than a simple, long-lived cinder cone (McKnight and Williams 1997). Because of the uncertainties associated with the atmospheric and eruption conditions of the Cerro Negro event, comparison of ash fall thicknesses between the observed distribution and the ASHPLUME result is qualitative. This comparison provides confidence that the ASHPLUME software code can give a reasonable representation of ash deposition for the type of eruption that could occur at Yucca Mountain.

The two-dimensional advection-dispersion model of Suzuki (1983) is implemented by the ASHPLUME code. The following two versions of the code were used to simulate the Cerro Negro ash thickness measurements:

- Version 1.4LV uses the volume and density of the ash to determine ash column height and mass (SNL 2007m, Section 1.2.1)

- Version 2.0 uses eruption power and event duration to determine column height and mass of ejecta (SNL 2007m, Section 1.2.1).

To evaluate the differences in the two ASHPLUME models and demonstrate that they can reasonably predict the ash fall distribution from the eruption of a basaltic cinder cone volcano, these two versions of ASHPLUME were used to simulate a Cerro Negro eruption, and the results were compared to Cerro Negro ash thickness measurements. A slightly different version, ASHPLUME_DLL_LA Version 2.1, was used for the TSPA model to calculate ash fall for the volcanic eruption modeling case. ASHPLUME_DLL_LA Versions 2.1 and ASHPLUME Version 2.0 are identical computationally. ASHPLUME_DLL_LA Version 2.1 only differs in its ability to interface with the Fortymile Wash Ash Redistribution code for TSPA calculations.

As shown on Figure 2.4-136, the ASHPLUME calculations compare well with the observed thicknesses at distances from the volcanic vent greater than 10 km. For distances less than 10 km, the ASHPLUME results give ash thickness values greater than the observed thicknesses. The lobe on the northern side of the map of measured ash thickness is interpreted to be a result of variations in wind direction or speed or both that occurred during the eruption. This variation accounts for some of the discrepancy, because ASHPLUME assumes a constant wind speed and direction for a given simulation. Figure 2.4-136 compares ASHPLUME V1.4LV and ASHPLUME V2.0 to show the overall consistency between the two versions.

The results generally show that the ASHPLUME model can reasonably predict the ash-fall distribution and ash-fall thickness from the eruption of a basaltic cinder cone volcano similar to Cerro Negro. Thus, the Cerro Negro ash fall calculation method can be used to simulate eruptive releases of ash either near the Yucca Mountain repository or through the repository involving waste package destruction and aerial distribution of radionuclides.

ASHPLUME is used in two additional natural analogue studies performed for the Lathrop Wells Cone in Nevada and Cinder Cone in California, as documented in *Atmospheric Dispersal and Deposition of Tephra from a Potential Volcanic Eruption at Yucca Mountain, Nevada* (SNL 2007m, Sections 7.3.3 and 7.3.4). Comparing prehistoric ash thickness distribution with simulations using ASHPLUME V 2.0 provides confidence that the ASHPLUME code can estimate ash thickness for simulated possible future volcanic eruptions involving the Yucca Mountain repository.

Nopal I Uranium Mine at Peña Blanca, Chihuahua, Mexico—The Peña Blanca natural analogue is a naturally occurring uranium ore deposit analogous to the Yucca Mountain repository. The Nopal I mine site provides an analogue for the evolution fate of SNF when it is placed in a geologic repository. Hydrogeologic investigations accompanied by the installation of observation wells have provided opportunities to test the strength of the analogy between Nopal I and the repository, and provide confidence in the performance of the Yucca Mountain repository with respect to the transport of radionuclides that could be released from the repository.

The Peña Blanca natural analogue Nopal I uranium mine is located in the Sierra Peña Blanca range, approximately 50 km north of Chihuahua City, Chihuahua, Mexico (Murphy 1995). The Peña Blanca Nopal I uranium deposit is geologically, climatically, geochemically, and hydrologically analogous to Yucca Mountain, and it has approximately three million years of exposure to oxidation (Murphy et al. 1991; BSC 2004h, Section 10.4). The Nopal I uranium deposit (Murphy and Codell, 1999) originally consisted of uraninite, a mineral directly analogous to SNF, which is largely composed of uranium oxide. The essence of the analogue of Nopal I to Yucca Mountain as described by Pearcy et al. (1993) is as follows:

- Climate—Nopal I and Yucca Mountain are located in arid to semi-arid regions. Annual rainfall at Nopal I is approximately 240 mm/yr (Murphy et al. 1990, p. 271) and mean annual precipitation at Yucca Mountain is estimated to be in the range of 170 to 250 mm/yr (SNL 2008g, Section F2.1[a] and Table F-6[a]).

- Geology—The Peña Blanca district containing the Nopal I mine and Yucca Mountain are fault blocks in the Basin and Range structural geological province. The Nopal I mine and Yucca Mountain contain Tertiary volcanic rocks consisting of welded and nonwelded ash-flow tuffs, and both overlie older carbonate rocks.

- Hydrogeology—The Nopal I mine and Yucca Mountain are located in the unsaturated zone under oxidizing conditions more than 100 m above the saturated zone.

- Geochemistry—The uraninite ore at the Nopal I mine has been altered to secondary uranium minerals, such as oxyhydroxides (e.g., schoepite) and uranyl silicates (e.g., boltwoodite and uranophane). The SNF at Yucca Mountain will be primarily uranium oxide, which is essentially uraninite, and the fuel is also expected to be altered to schoepite and uranyl silicates (BSC 2004h, Sections 4.2.2 and 4.4.2).

Previous studies of the Nopal I deposit have focused on the geochemical aspects of the oxidation, transport, and reprecipitation of uranium mineral phases in the matrix and bedrock (Pearcy et al. 1993; Pickett and Murphy 1997; Pearcy 1994; Goldstein et al. 2003). These studies show that uranium, protactinium, and thorium have low groundwater concentrations. The analysis of rock samples collected from fractures on the exposed 0.0 and +10 benches show that actinides released from the ore deposit precipitated in fracture filling minerals within a few tens of meters from the deposit (Goldstein et al. 2003).

A water collection system, with 240 collection points, installed in the adits of the Nopal I mine, collected data on the pattern and intensity of seepage into the mine (Dobson et al. 2008). The results of this investigation showed wide variability in the location, timing, and amount of seepage. Highly heterogeneous seepage volumes and arrival times coinciding with fractures were observed in the adits. A few fast flow paths had high amounts of seepage occurring shortly after rain events. Other parts of the mine experienced slow steady seepage, indicating relatively slow flow paths and associated longer residence times, consistent with higher uranium concentrations in the water and uranium-isotope disequilibrium. The delayed seepage indicates that the host rock can exert a dampening effect on infiltration. These seepage investigations support the heterogeneous seepage distribution in the TSPA seepage submodel.

Summary of Peña Blanca Natural Analogue—Radionuclide transport by groundwater is the most likely transport mechanism that could affect the performance of the Yucca Mountain repository. Despite some uncertainty in the estimated direction and gradient of groundwater flow, the Peña Blanca natural analogue site offers a unique opportunity to examine the groundwater flow and transport of uranium and its decay products in a climatic and geologic setting very similar to that of Yucca Mountain. Both sites are set in volcanic tuff in an oxidizing unsaturated zone, and are in similar semiarid environments. The Peña Blanca natural analogue at the Nopal I uranium deposit displays the following contrasts and similarities with respect to the Yucca Mountain repository:

- A fully loaded Yucca Mountain repository will likely contain 154 times more uranium than the Nopal I mine (Murphy and Codell 1999).

- The time scale at Nopal I is on the order of three million years. The performance period for the Yucca Mountain repository is 1,000,000 years for compliance with the proposed 10 CFR 63.302.

- The hydrogeologic configuration of the Nopal I mine is relatively simple. The ore body is exposed at land surface with an approximately 200-m-thick unsaturated zone above the saturated zone. The saturated zone at Yucca Mountain is at a comparable distance below the repository, mainly in volcanic rocks underlain by Paleozoic carbonate rocks, whereas at Nopal I, the saturated zone is primarily in the Cretaceous limestone found in and beneath the Sierra Peña Blanca. Seepage investigations indicate heterogeneity in seepage into the Nopal I mine with higher seepage rates coincident with fractures (Dobson et al. 2008).

- There are no naturally occurring radioactive ore deposits in the host rocks for the Yucca Mountain repository (BSC 2004i, Section 3.6.2), although there are occurrences of radioactive elements in minerals in the host rocks and fracture fillings. Thus, radionuclide transport calculations through the tuffs below the repository horizon are, of necessity, approximations of what would occur in the event that waste is emplaced at the repository. At Nopal I, the natural uranium from the ore body not only dissolves and migrates, but also produces and transports its decay products.

- The regional, surface-water-discharge location for the Nopal I ore deposit is approximately 10 km from the deposit, versus an approximate 60 km to 80 km travel distance to the nearest surface-water discharge for the Yucca Mountain flow system at the Franklin Lake Playa (DOE 2002, Section 5.3 and Appendix I, Sections I.1 and I.4.5).

Observations at the Nopal I uranium-ore deposit at the Sierra Peña Blanca provide insight with which to estimate the migration and or sequestration of uranium and other radionuclides from the Yucca Mountain repository. The paragenesis of uraninite at the Nopal I site parallels the paragenetic degradation sequence observed for uranium-oxide spent fuel in laboratory experiments simulating a moist, unsaturated repository.

Studies regarding both large ore-bearing boulders and other uraniferous material removed from the Nopal I mine indicate that uranium and other radionuclides are mobile and can be transported in the soil and shallow bedrock, or subject to plant uptake. The observations show that uranium leached from the ore deposit is apparently exchanging with uranium minerals that precipitate in fractures around the ore deposit. The analysis of water samples from observation wells at the Nopal I site show that despite the precipitation of radionuclides, there is sufficient uranium for it and some of its decay products to be transported through the Cretaceous limestone below the Sierra Peña Blanca. However, the observed groundwater concentrations are very low, probably due to reprecipitation and/or sorption of uranium and other radionuclides in the unsaturated zone and saturated zone.

The Nopal I mine was originally composed of uraninite, which is essentially the same material as SNF. Hydrogeologic and geochemical investigations at the Nopal I natural analogue indicate that there has been relatively little transport of the radionuclides from the ore deposit, and that few radionuclides have traveled very far from their sources. There are observed concentrations of uranium in the groundwater beneath the Nopal I ore body, but the concentrations are generally less than 1 ppm, except during a brief period just after drilling the observation wells. In addition, the original ore body composed of uranium oxide has been altered to relatively stable uranyl silicates that do not provide large amounts of radionuclides for transport. Geologic investigations of core samples indicate that oxidative leaching of uraninite in the ore body was followed by a later lower-temperature precipitation of uraninite in the unsaturated zone above the saturated zone. The analysis of water samples collected from wells completed in the saturated zone beneath and downgradient from the ore deposit show that although there are radionuclides present in the groundwater, their concentrations are generally in the ppb range. In addition, the heterogeneous nature of the unsaturated zone provides opportunities for leached radionuclides to be naturally sequestered in mineralized fractures or the bedrock matrix. Analyses of soil and vegetation in the vicinity of high-grade uranium ore stockpiles indicate that the leached radionuclides and radionuclides taken up in vegetation are temporarily sequestered and kept from transport.

The Peña Blanca natural analogue provides an example of the dissolution, fate, and transport radionuclides released from the Nopal I mine through an unsaturated zone and saturated zone that are analogous to the Yucca Mountain repository site. The degradation and leaching of the Nopal I ore deposit is analogous to that expected for nuclear material to be emplaced at the Yucca Mountain repository. The Nopal I site indicates that material with a composition very similar to SNF has been subject to dissolution, but the leached material has been largely sequestered by paragenesis, mineral precipitation, or sorption onto clays or other minerals in the near vicinity of the ore body. Considering the analogous nature of the Nopal I site with respect to the Yucca Mountain repository, and that the Nopal I site is at land surface, the apparent immobilization and sequestering of uranium and other radionuclides leached from the ore deposit indicate that radionuclides released from the uranium deposit do not migrate far from their sources, except for a very small fraction that migrates at the very low rates suggested by the very low concentrations in the water samples taken downgradient. Thus, the performance observed at the Nopal I Peña Blanca provides insight and confidence in the long-term performance of the Yucca Mountain repository.

2.4.2.3.2.3.4 Iteration and Independent Technical Review

The development of the TSPA model has involved substantial independent review of the successive iterations of the TSPA model and the performance assessments conducted with the different versions of the model. These critical reviews conducted during the development of the different iterations of the TSPA model, including the current TSPA model, have resulted in numerous recommendations and comments that were addressed by Yucca Mountain Project staff associated with the model development process. The recommendations and the agreed-upon comment responses contributed to the incremental changes made in successive iterations of the TSPA, culminating in the present TSPA. Implementation of the results of the critical reviews has contributed to continuous improvement to the TSPA models, and adds to the confidence that the TSPA model meets the performance goals of proposed 10 CFR 63.311, proposed 10 CFR 63.321, and 10 CFR 63.331. In addition to the various post-development model validation activities described in preceding sections, the TSPA technical work plan (SNL 2008i) requires documenting recommendations from prior technical reviews of the preceding versions of the TSPA model.

The TSPA methodology and associated technical review cycles are iterative (Section 2.4.2.3.2). The general TSPA process adopted by the DOE follows the methodology described by the NRC (NUREG-1636; Eisenberg et al. 1999). In addition, DOE utilized the methods developed by Cranwell et al. (1990, Sections 2 and 3), to arrive at a representative set of scenarios used to evaluate the Yucca Mountain repository. The TSPA model uses these well-established iterative methodologies to analyze the ability of the Yucca Mountain repository's natural and engineered barriers to isolate nuclear waste following repository closure. Performance assessments and related supplemental analyses of the Yucca Mountain repository were initiated following the publication of the Nuclear Waste Policy Amendments Act of 1987, Public Law No. 100-203. The performance assessments of the Yucca Mountain repository are periodically updated, each building on and extending the scope and results of the previous TSPA. The iterative assessments incorporate both an improved understanding of the processes affecting repository performance and, through additional field observations and laboratory analyses, better identification and quantification of the parameter values used in the TSPA. The iterative process involves continuing activities, including technical reviews, to enhance confidence that the model meets and exceeds the goal for its intended use, which is to: (1) demonstrate a reasonable expectation that the individual protection standard after permanent closure of proposed 10 CFR 63.311 is met; (2) the individual protection standard for human intrusion in proposed 10 CFR 63.321 is met; and (3) the separate standards for protection of groundwater in 10 CFR 63.331 are met.

Early probabilistic TSPAs for the Yucca Mountain repository include TSPA 91 (Barnard et al. 1992), TSPA 93 (Wilson et al. 1994), TSPA 95 (CRWMS M&O 1995), and TSPA-VA (DOE 1998, Volume 3). The more recent TSPA iterations include TSPA-SR (CRWMS M&O 2000a) and TSPA-FEIS (Williams 2001).

TSPA iterations, such as those mentioned above, are evaluated and independently reviewed by technical staff and various external organizations. Reviewers generally make recommendations for improvements to consider in future TSPA iterations. During the last decade, three technical reviews were conducted on the previous versions of the TSPA. Two peer reviews that contributed to the development of the TSPA model are: (1) the TSPA peer review conducted in 1999 (Budnitz et al. 1999), which evaluated the TSPA model used for the Viability Assessment (DOE 1998, Volume 3); and (2) an evaluation by an international review team summarized in *An International Peer Review of the Yucca Mountain Project TSPA-SR* (OECD and IAEA 2002; SNL 2008a, Appendix E), which evaluated the TSPA model used for the Site Recommendation (CRWMS M&O 2000a). More recently, during 2004 and 2005, an independent validation review team, composed of individuals independent from those who developed the TSPA model, performed a critical review, completed in 2006, of the initial drafts of the TSPA model used to support the license application (SNL 2008a, Sections 7.9.1, 7.9.2, and 7.9.3).

In addition to the three formal technical reviews mentioned above, the Nuclear Waste Technical Review Board performs routine reviews on key areas of the YMP, as mandated by Congress. The Nuclear Waste Technical Review Board focuses its review effort on three broad technical areas of the project: preclosure operations, postclosure repository performance, and system integration. The Nuclear Waste Technical Review Board reviews of the TSPA effort are captured in its review focus on postclosure repository performance. The Nuclear Waste Technical Review Board comments on the TSPAs and the DOE responses to the Board's comments are captured in the Nuclear Waste Technical Review Board reports and correspondences presented on its websites. These comments and recommendations contributed to the improvements made in previous iterations of the DOE performance assessment, leading to the current TSPA.

DOE documented its responses to recommendations of prior review teams, as required by the TSPA technical work plan. The International Review Team made 27 specific recommendations in its final report (OECD and IAEA 2002, Section 5.3) for future improvements in the preparation and submission of the license application. *Total System Performance Assessment Model/Analysis for the License Application* (SNL 2008a, Table E-1) tabulates the International Review Team recommendations and describes DOE work performed by the project to implement these 27 recommendations.

A set of seven recommendations from the Independent Validation Review Team has similarly been implemented. The seven recommendations are addressed in *Total System Performance Assessment Model/Analysis for the License Application* (SNL 2008a, Section 7.9.3.3). A large set of associated comments was addressed and documented in *Total System Performance Assessment Model/Analysis for the License Application* (SNL 2008a, Table 7.9-1).

2.4.2.3.3 Consistency of Uncertainty in the Performance Assessment Results with Model and Parameter Uncertainty

[NUREG-1804, Section 2.2.1.4.1.3: AC 3(3)]

This section addresses NUREG-1804, Section 2.2.1.4.1.3, Acceptance Criterion 3(3), which states the expectation that "The estimate of the uncertainty in the performance assessment results is consistent with the model and parameter uncertainty," by presenting uncertainty and sensitivity analyses that demonstrate the consistent propagation of uncertainty from inputs (models and parameters) to outputs (expected annual dose). This section also addresses NUREG-1804, Section 2.2.1.4.1.3, Acceptance Criterion 2(3), which states the expectation that: "Repository performance and the performance of individual components or subsystems are consistent and reasonable…"

To provide the background on how uncertainty in inputs is propagated through the TSPA model to uncertainty in outputs (such as dose and releases) and how this is used to analyze and understand the TSPA model results, three sections are presented that briefly summarize (1) the overall TSPA analysis structure and its basis in the separation of aleatory and epistemic uncertainties (Section 2.4.2.3.3.1), (2) the limitations of uncertainty and sensitivity analysis techniques (Section 2.4.2.3.3.2), and (3) the type of uncertainty and sensitivity methods and metrics used to analyze the propagation of uncertainty in the TSPA model (Section 2.4.2.3.3.3). Representative results from the uncertainty and sensitivity analyses (SNL 2008a, Appendix K) are then presented for the following modeling cases: nominal modeling case (Section 2.4.2.3.3.4), drip shield early failure modeling case (Section 2.4.2.3.3.5), waste package early failure modeling case (Section 2.4.2.3.3.5), and seismic ground motion modeling case (Section 2.4.2.3.3.6). In addition, results are presented for total expected annual dose to the RMEI from all modeling cases (Section 2.4.2.3.3.7).

2.4.2.3.3.1 Treatment of Parameter and Model Uncertainty in the TSPA Model

Sources of Uncertainty—Uncertainties are inherent in projections of the geologic and environmental conditions surrounding the Yucca Mountain repository into the future. As stated in 10 CFR 63.304(1): "…absolute proof is impossible to attain for disposal due to the uncertainty of projecting long-term performance…" Assessment of long-term performance must necessarily take these uncertainties into account, and the discussion and analysis of the quantitative estimates of this performance (e.g., estimates of mean annual dose) will necessarily present the impacts of uncertainties on those estimates, as already shown in the expected annual dose plots of Section 2.4.2.2.1.

The TSPA model accounts for uncertainty in two categories: aleatory uncertainty and epistemic uncertainty. Aleatory uncertainty arises from inherent uncertainty about the occurrence of future events that could affect the repository and the random effect of these events on repository performance. Because aleatory uncertainty cannot be reduced by the acquisition of additional data or knowledge, this kind of uncertainty is also referred to as irreducible uncertainty. Examples of aleatory uncertainty considered in the TSPA model include the number and location of early failed waste packages, time and amplitude of seismic ground motion events, and timing of igneous events. The major types of aleatory uncertainties included in the TSPA model are listed in Table 2.4-5.

The second category is epistemic uncertainty, which is the specific type analyzed in the uncertainty and sensitivity analyses of this section. Epistemic uncertainty stems from a lack of knowledge about a quantity believed to have a fixed (or deterministic) value. Sources of epistemic uncertainties include incomplete data, measurement errors, and estimates based upon expert judgment. Unlike aleatory uncertainty, epistemic uncertainty is potentially reducible with additional data and knowledge. In the TSPA model, epistemic quantities are generally inputs to specific submodels developed to use single values for these quantities. A particular epistemic quantity can be a parameter that characterizes a probability distribution (e.g., the mean value of the fracture permeability distribution used to calculate drift seepage), a field of values selected from alternative sets (e.g., the flow field in the unsaturated zone), or a parameter that characterizes a physical-chemical process (e.g., the temperature dependency of general corrosion of Alloy 22 or the unsaturated-zone fracture frequency). The major categories of epistemic uncertainties included in the TSPA model are indicated in Table 2.4-6.

Probabilistic Framework for Implementing the TSPA Model—Aleatory and epistemic uncertainties are quantified using probability distributions. However, in the TSPA model, the numerical treatment of the two categories of uncertainty is different, as has been described in Sections 2.4.2.1 and 2.4.2.2.2.1. Because the aleatory uncertainties vary between modeling cases, treatment of aleatory uncertainties also varies among modeling cases; however, as first described in Section 2.4.1, an expectation over aleatory uncertainty is taken for each modeling case and for each epistemic sample ($i = 1, \ldots, 300$) in order to derive the (epistemic) uncertainty distribution for the annual dose curve, i.e., the set of 300 expected annual dose curves in the various figures in Section 2.4.2.2.1. The compliance metrics (either mean or median) are based on this epistemic uncertainty distribution, and this set of expected dose curves is analyzed by sensitivity analysis techniques to ascertain how model results are affected by epistemic input uncertainties. These regression-based sensitivity analyses are discussed in this section.

Regression-based sensitivity analyses are not applied to determine the importance of aleatory uncertainties because of the relatively small number of aleatory uncertain parameters. However, uncertainty analyses have been conducted to show the effect on model results of varying aleatory parameters, such as timing of igneous intrusion events (SNL 2008a, Figures J7.2-1 and J7.2-11), spatial variability related to the type and location of early failures (SNL 2008a, Figures J6.2-2 and J6.3-2), and time of occurrence and amount of seismic damage (SNL 2008a, Figures J8.3-1, J8.3-2, and J8.4-1). An example of the range of aleatory uncertainty considered in the TSPA model is shown in Figure 2.4-90, for the 1,000,000-year seismic ground motion modeling case. This figure illustrates the effects associated with the timing and magnitude of seismic events. Specifically, this figure illustrates a set of 30 different event sequences with earthquakes of varying magnitude occurring randomly in time. The expectation over this aleatory uncertainty in event timing and magnitude is shown as the heavy dashed curve in this figure, which represents the expected annual dose for a given sampling of epistemic parameters that is applied to each of the 30 aleatory event sequences. Each of the 300 expected annual dose curves in Figure 2.4-25 is derived from a similar set of 30 random event sequences. Thus, the mean and median annual dose curves for the seismic ground motion case shown in Figure 2.4-25 are derived from, and consistent with, the aleatory uncertainty in the timing and magnitude of the seismic events. A discussion of the propagation of aleatory uncertainty for the other modeling cases is found in Appendix J of *Total System Performance Assessment Model/Analysis for the License Application* (SNL 2008a).

As described in Section 2.4.2.3.4, epistemic uncertainties are addressed using a Monte Carlo technique employing a Latin hypercube sampling of the epistemically uncertain quantities. The same Latin hypercube sample is used in each of the modeling cases. This method allows a mapping of the uncertainty in model inputs (parameters) to the corresponding uncertainty in model output (estimates of performance, such as dose) and also allows results from each modeling case to be combined into estimates of total expected annual dose. Uncertainty in the model outcome is quantified via multiple model realizations using Latin hypercube sampling to select values for uncertain input parameters. This probabilistic modeling method permits (1) obtaining a representative range of possible outcomes (and the likelihood of each outcome) to quantify uncertainty (e.g., to produce quantitative metrics representing the range of uncertainty like 5th and 95th percentiles), and (2) analyzing the relationship between the uncertain inputs and uncertain outputs to provide insight into the effect of the uncertain inputs (SNL 2008a, Section 6.1.3).

Propagation of Uncertainty—The Monte Carlo analysis in the TSPA model involves the following four steps:

1. **Select Imprecisely Known Input Parameters to be Sampled**—The TSPA model includes several thousand parameters, several hundred of which are treated as uncertain. These parameters are developed in the individual process models and abstractions, as documented in their respective model reports.

2. **Construct Probability Distribution Functions for Each Parameter**—These distributions are specified in terms of either empirical distribution functions or coefficients of parametric distributions. The magnitude of uncertainty and type of probability distribution used to characterize the uncertainty are documented in the underlying process model reports.

3. **Generate a Sample Set by Selecting a Parameter Value from Each Distribution**—The TSPA model samples the aforementioned parameter distributions to calculate estimates of repository performance for the range of repository futures and parameters. The TSPA model uses Latin hypercube sampling (Section 2.4.2.3.4) for epistemic uncertainty, where the range of each parameter is divided into intervals of equal probability, and a value is selected at random within each interval. Latin hypercube sampling provides a more complete coverage of the range of values of an uncertain parameter than unstratified sampling. Where the expectation of aleatory uncertainty is computed by numerical quadrature, values for aleatory parameters are determined by the quadrature's discretization; where Monte Carlo methods are used, aleatory parameter values are determined either by random or Latin hypercube sampling, depending on the modeling case (Section 2.4.2.1.5).

4. **Calculate Outcomes for the Sample Set and Aggregate Results for All Samples**—The TSPA model evaluates repository performance for each of the randomly generated parameter sets in the scenario class of interest. This is an operation consisting of multiple model realizations where the outcome (i.e., annual dose as a function of time) is computed for each sampled parameter set. The aggregation of all results produces distributions of system performance measures (e.g., expected dose) for the modeling case. After all the required model realizations have been completed, the overall uncertainty in the model outcome can be characterized by probability distributions of the system performance measures (e.g., Figure 2.4-10 in Section 2.4.2.2.1).

2.4.2.3.3.2 Limitations and Applicability of Uncertainty and Sensitivity Analyses

For an input parameter to be ranked as important with respect to its influence on uncertainty of the output (e.g., uncertainty in mean or median annual dose), two conditions must be fulfilled: (1) the input parameter must be characterized by an uncertainty range with a probability distribution; and

(2) it must significantly influence the key physical processes, such as radionuclide release and transport, that produce the dose to the RMEI. Both of these aspects are considered in this section (i.e., the uncertainty of the input as modeled in TSPA, and the physics of the processes impacted by the parameter and how these processes might influence the mean annual dose). Parameters that might intuitively be thought of as important, such as the thickness of the waste package outer container, are not identified as important in this context if they were treated as known quantities (i.e., they have no variance). Similarly, the relative importance of uncertainties bounded with fixed values (e.g., through conservative assumptions) also cannot be quantified through the statistical approaches in this section. However, these limitations do not detract from the usefulness of evaluating the significance of uncertainty as it affects the predicted distribution of dose. Another important example of the apparent insignificance of a particular parameter or model uncertainty relates to the comparative importance of different radionuclide species and whether the radionuclide is transported as a dissolved species or attached to colloid particles. For example, uncertainties in neptunium, plutonium, and uranium solubilities could be determined insignificant contributors to the uncertainty in calculated total mean annual dose received by the RMEI if that dose is dominated by much more soluble and less retarded species, such as technetium, carbon, and iodine, as in the seismic ground motion modeling case and the waste package early failure modeling case in the first 10,000 years (Figures 2.4-26 and 2.4-36).

2.4.2.3.3.3 Uncertainty and Sensitivity Analysis Procedures

The propagation of epistemic uncertainty in the TSPA model can be represented by (SNL 2008a, Section K2):

$$\mathbf{y} = \mathbf{f}(\mathbf{e}), \qquad \text{(Eq. 2.4-39)}$$

where $\mathbf{e} = [e_1, e_2, \ldots, e_{N_E}]$ is the vector of epistemically uncertain inputs ($N_E = 392$) to the TSPA model, $\mathbf{y} = [y_1, y_2, \ldots, y_{N_Y}]$ is a vector of epistemically uncertain TSPA results or outputs (e.g., EBS release rate, unsaturated zone cumulative release, expected annual dose, etc.), and the function $\mathbf{f}$ corresponds to the suite of models that constitute the TSPA modeling system. So, although this representation is simple, the actual function $\mathbf{f}$ is complex. A high-level summary of the elements of $\mathbf{e}$ and their associated distributions is given in Table 2.4-11.

The TSPA employs uncertainty and sensitivity analysis procedures based on a mapping between analysis inputs and analysis results generated through the use of Latin hypercube sampling. A Latin hypercube sample:

$$\mathbf{e}_i = [e_{1i}, e_{2i}, \ldots, e_{N_{Ei}}], i = 1, \ldots, N_{LHS} \qquad \text{(Eq. 2.4-40)}$$

is generated from the epistemically uncertain inputs consistent with the probability space used to characterize epistemic uncertainty (Section 2.4.2.1). The TSPA analysis uses a Latin hypercube sampling sample of size $N_{LHS} = 300$ from the probability distributions that characterize the elements of e_j of $\mathbf{e}$. Table 2.4-11 indicates correlations between inputs that were honored in the Latin hypercube sample. Helton and Davis (2003) provide additional information on Latin hypercube sampling—as does Section 2.4.2.3.4.

Evaluating TSPA results for each member $\mathbf{e}_i$ of the Latin hypercube sample in Equation 2.4-40 generates a mapping:

$$\mathbf{y}_i = \mathbf{f}(\mathbf{e}_i), i = 1, 2, \ldots, N_{LHS} \qquad \text{(Eq. 2.4-41)}$$

from epistemically uncertain TSPA inputs contained in $\mathbf{e}_i$ to epistemically uncertain TSPA results contained in $\mathbf{y}_i$. Once generated, this mapping forms the basis for both uncertainty analysis and sensitivity analysis. Specifically, the weights or probabilities associated with the individual Latin hypercube sampling elements (i.e., $1/N_{LHS}$) permit the construction of distributions for elements of $\mathbf{y}$ that characterize epistemic uncertainty, and the mapping itself can be explored with a variety of sensitivity analysis procedures to determine the effects of individual elements of $\mathbf{e}$ on elements of $\mathbf{y}$ (e.g., what is the effect of residual stress threshold for stress corrosion cracking on expected annual dose?). The structure and implementation of analyses of this type are extensively discussed in the review by Helton et al. (2006). The only element of $\mathbf{y}$ summarized in this section is expected annual dose (except for the illustrative example in Figure 2.4-137). However, many other analyses of other result elements of $\mathbf{y}$ have been analyzed, such as seepage rate; number of failed waste packages; average breached area of failed waste packages; temperature and relative humidity of the waste packages; EBS release rate and cumulative EBS release of major radionuclides; unsaturated zone release rate and cumulative release of major radionuclides; and saturated zone release rate and cumulative release of major radionuclides (SNL 2008a, Table K3-4).

The primary sensitivity analysis procedures used for the TSPA results involve the determination and presentation of partial rank correlation coefficients (PRCCs), stepwise rank regression analyses, and scatterplots.

PRCCs—PRCCs provide a measure of the strength of the monotonic relationships between an independent variable e_j (i.e., an element e_j of $\mathbf{e}$, such as the temperature-dependent slope for Alloy 22 general corrosion) and a dependent variable y_k (i.e., an element y_k of $\mathbf{y}$, such as expected annual dose) after a correction has been made to remove the monotonic effects of the other independent variables in the analysis (i.e., the elements of $\mathbf{e}$ other than e_j). Most of the elements of $\mathbf{y}$ under consideration are functions of time. For such variables, the presentation of PRCCs as functions of time provides an informative display of sensitivity analysis results (i.e., the dependency of uncertainty in output on uncertainty in input).

As indicated by the name, PRCCs involve the analysis of rank-transformed data. With this approach, the values for variables are replaced with their ranks and then the PRCCs are calculated with these ranks rather than with the original values for the variables. Specifically, the smallest value of a variable is given a rank of 1; the next largest value is given a rank of 2; equal observations are assigned the average of what their ranks would have been if they had not been equal; and so on up to the largest value, which is given a rank equal to the number of sample elements in use (i.e., $N_{LHS} = 300$ in the TSPA). Although no variable transformation is universally successful in improving the resolution of a sensitivity analysis in the presence of nonlinear relationships, the rank transformation is a broadly effective and useful means of enhancing the insights in sensitivity analyses based on partial correlation and also in sensitivity analyses based on stepwise regression.

In the example in Figure 2.4-137, the N_{LHS} (= 300) time-dependent results for the variable under consideration (i.e., *NCSFL*, number of failed commercial SNF waste packages in Percolation Subregion 3 under nominal conditions) are presented in the top-left plot (i.e., Figure 2.4-137a) and the corresponding PRCCs are presented in the top-right plot (i.e., Figure 2.4-137b). To compute PRCCs as a function of time, at each time τ there are N_{LHS} (= 300) values of y_k and e_j used to compute the PRCC (where y_k is equal to *NCSFL* in this case and e_j is any epistemically uncertain parameter, such as the temperature-dependency of Alloy 22 general corrosion or the infiltration scenario). A PRCC for y_k is calculated with respect to each uncertain input parameter (i.e., all elements e_j of $\mathbf{e}$). Then, the PRCCs are plotted versus the time at which they were calculated to show the effect of e_j on the dependent variable y_k as a function of time. To limit the number of time-dependent PRCC curves in a given plot frame, the PRCC plots only show PRCC curves for the six variables (i.e., the six elements e_j of $\mathbf{e}$) with the largest PRCCs in absolute value over the time interval under consideration. Further, plots are only shown for variables whose PRCCs exceed 0.3 in absolute value at some point in time.

Values of PRCCs fall in the interval [−1, 1], with: (1) positive PRCCs indicating that two variables tend to increase and decrease together (i.e., the independent variable has a positive effect on the dependent variable), (2) negative PRCCs indicating that two variables tend to move in opposite directions (i.e., the independent variable has a negative effect on the dependent variable), and (3) the absolute value of a PRCC indicating the strength of the relationship between two variables (i.e., a PRCC close to 1 in absolute value indicates a strong monotonic relationship between two variables after the removal of the monotonic effects associated with the other independent variables under consideration; a PRCC close to 0 in absolute value indicates no monotonic relationship after the removal of the monotonic effects associated with the other variables under consideration; and the strength of the effect increases as the absolute value of a PRCC increases from 0 to 1). Thus, in the example in Figure 2.4-137b, *WDGCA22* has a negative effect on *NCSFL,* with this effect increasing with time; *WDZOLID* has a positive effect on *NCSFL*, with this effect increasing with time; and *INFIL*, *WDNSCC*, *THERMCON*, and *SCCTHR* having small negative effects on *NCSFL*, with these effects also increasing with time.

Stepwise Rank Regression—An alternative to the use of PRCCs is to carry out stepwise rank regressions to determine the effects of uncertain analysis inputs on analysis results of interest, such as expected annual dose. In analyses of this type, the regressions are carried with rank-transformed variable values as previously discussed rather than with the original variables. Similar to PRCCs, the effect of the rank transformation is to transform monotonic relationships into linear relationships. Further, the rank transformation tends to reduce the skewing effects of outliers.

In a stepwise rank regression, the single independent variable that makes the largest contribution to uncertainty in the dependent variable is selected in the first step. Then at the second step, the single independent variable that, in conjunction with the first variable, makes the largest contribution to the uncertainty in the dependent variable is selected. This process then continues until no additional variables are found that make identifiable contributions to the uncertainty in the dependent variable. At this point, the stepwise selection process terminates. In the context of stepwise regression analysis, variable importance is indicated by: (1) order of selection in the stepwise selection process, (2) incremental changes in R^2 values with successive entry of individual variables into the regression model, and (3) the sign and size of the standardized rank regression coefficients in the final regression model.

As an example, stepwise rank regressions for *NCSFL* at 600,000, 800,000, and 1,000,000 years are shown in Figure 2.4-137c. For the analysis at each time, the first column lists the independent variables in the order of selection in the stepwise process; the second column lists the cumulative R^2 value with the entry of each variable into the regression model; and the third column lists the standardized rank regression coefficients for the variables in the final regression model.

The R^2 value corresponds to the fraction of uncertainty in the dependent variable accounted for by a regression model. Thus, R^2 values monotonically increase as additional variables are added to the regression model and, for a very successful regression analysis, approach one as additional variables are added to the model. The standardized rank regression coefficients provide a measure of the fractional contribution of individual independent variables to the uncertainty in the dependent variable under consideration. Further, like PRCCs, a positive standardized rank regression coefficient indicates that the independent and dependent variable tends to increase and decrease together, and a negative standardized rank regression coefficient indicates that the independent and dependent variable tend to move in opposite directions.

Related, but not identical, information is provided by PRCCs and standardized rank regression coefficients. Specifically, PRCCs measure the strength of the monotonic relationship between an independent variable and a dependent variable after correcting for the effects of other independent variables, and standardized rank regression coefficients measure the fractional contribution of an individual independent variable to the uncertainty in the dependent variable under consideration. However, when there are no correlations between the independent variables (i.e., the variables in the Latin hypercube sampling) at a fixed time, an ordering of variable importance based on the absolute value of PRCCs is the same as an ordering of variable importance based on the absolute value of standardized rank regression coefficients.

Scatterplots and Boxplots—In addition to PRCCs and stepwise rank regression analyses, the uncertainty and sensitivity analyses for the TSPA model make use of scatterplots and boxplots to present and explain the relationships between independent and dependent variables. A scatterplot is simply a plot of the points (e_{ji}, y_{ki}), i = 1, 2, …, N_{LHS}, where e_{ji} are the sampled values for an independent variable and the y_{ki} are the corresponding sampled values for a dependent variable. If e_j has a significant effect on y_k, this will be apparent in the scatterplot; if e_j does not have a significant effect on y_k, the points in the scatterplot will have a random distribution conditional on the marginal distributions for e_j and y_k. For example, scatterplots involving the pair (e_{ji}, y_{ki}) = ($WDGCA22_i$, $NCSFL_i$), $i = 1, 2, \ldots, N_{LHS} = 300$, for results obtained at 600,000 and 800,000 years are presented in Figure 2.4-137d and e. As shown, a strong and complex relationship exists between *WDGA22* and *NCSFL*. In some instances, scatterplots can reveal relationships that may be too complex to be adequately captured by the simple numerical relationships provided by PRCCs and stepwise rank regression analyses.

One other type of uncertainty display used in this section is a boxplot (e.g., Section 2.4.2.3.3.5.1). The boxplots, as used here, better illustrate relationships for some parameters, by showing the trend of some quantiles of the distribution. For example, as shown in Section 2.4.2.3.3.5.1, the parameter *INFIL* only has four values, so a scatterplot with *INFIL* on the *x*-axis would only display four vertical lines of data points. This is much less useful than what can be shown with a boxplot. The upper end of the box is the 75th percentile of the distribution, the lower end of the box is the 25th percentile, the line in the middle of the box is the 50th percentile, the bar on the end of the whisker that extends from the upper end of the box is the 90th percentile, and the bar on the end of the whisker that extends from the lower end of the box is the 10th percentile. By plotting the data in this way, the trend is clearer. For example, the generally increasing trend of dose with INFIL can be observed by examining the trend in the 50th and 75th percentiles.

More detailed information on the sensitivity analysis techniques used here is available in several reviews (Helton et al. 2006; Helton and Davis 2000).

2.4.2.3.3.4 Uncertainty and Sensitivity Analyses for the Nominal Scenario Class

The nominal scenario class consists of the set of futures in which no disruptions of any kind (i.e., early drip shield or waste package failures, igneous events, and seismic events) occur (Section 2.4.2.1). This section presents uncertainty and sensitivity analysis results for annual doses associated with the nominal modeling case of the nominal scenario class.

The uncertainty and sensitivity analyses for total dose to the RMEI (*DOSTOT*, mrem/yr) for the nominal modeling case are summarized in Figures 2.4-138 and 2.4-139. (Dose units of mrem/yr are shown on the plots in this section rather than annual dose units of mrem.) Nonzero values for *DOSTOT* begin at about 20,000 years as a result of waste package failure and then show a general tendency to increase (Figure 2.4-138a, b) (SNL 2008a, Section K4.5[a]). However, some dose curves, and especially some of the curves with the largest values for *DOSTOT*, change from increasing to decreasing at some point in time. This change results from inventory depletion, and hence decreasing releases for highly mobile species such as ^{99}Tc and ^{129}I. The difference between Figure 2.4-138a and Figure 2.4-138b is simply in the number of realizations displayed. All 300 epistemic realizations are displayed in Figure 2.4-138a; however, because they appear so dense on the plot, it tends to obscure some behaviors of the individual realizations. By displaying only the first 50 out of 300 realizations, some behaviors of the individual realizations can be more easily discerned. These two types of plots will be shown for all of the modeling cases described in this section.

The PRCCs in Figure 2.4-138c indicate that the uncertainty in *DOSTOT* is dominated by *WDGCA22* (temperature-dependency slope coefficient associated with the general corrosion rate for Alloy 22, 1/°C), with *DOSTOT* tending to decrease as *WDGCA22* increases. This effect results because the general corrosion rate for Alloy 22 decreases at late times and cooler temperatures as the slope-term *WDGCA22* increases (it increases at very early times and hot temperatures; however, low temperatures dominate most of the 1,000,000-year postclosure period). Smaller effects are indicated for *SCCTHR* (stress corrosion cracking threshold, MPa), *WDZOLID* (scale factor used to incorporate uncertainty into the stress intensity factor for the closure-lid weld), *THERMCON* (host-rock thermal conductivity), *WDNSCC* (stress corrosion cracking growth rate exponent), and *CPUCOLWF* (concentration of irreversibly attached plutonium on glass colloids when colloids are stable (mol/L)). The variables *SCCTHR*, *WDZOLID*, *THERMCON*, and *WDNSCC* affect *DOSTOT* through their effects on waste package failure. Specifically, increasing *SCCTHR* increases the residual stress level at which stress corrosion cracking initiates and thus reduces failures at the closure-lid weld; increasing *WDZOLID* increases the tensile stress at the closure lid and thus increases failures at the closure-lid weld; increasing *THERMCON* tends to lower waste package temperatures and thus reduce the rate of corrosion at very early times; and increasing *WDNSCC* tends to increase the threshold stress intensity factor, which determines the threshold stress at which stress corrosion cracks propogate, and thus reduces failures at the closure-lid weld. The variable *CPUCOLWF* has small effects throughout the simulation time related to the colloidal-facilitated release and transport of plutonium from the HLW glass inventory.

More detailed sensitivity analysis results for *DOSTOT* are provided by the regression results in Figure 2.4-139a. Specifically, *WDGCA22* is the dominant variable with R^2 values of 0.78, 0.85, and 0.63 at 400,000 years, 600,000 years, and 800,000 years, respectively. Actually, the indicated R^2 values tend to underrepresent the effect of *WDGCA22* because of the nonlinear relationship between *WDGCA22* and *DOSTOT* shown in the scatterplots of Figure 2.4-139b, c, and d). Specifically, as mentioned above, large values of the slope-term *WDGCA22* result in small values for *DOSTOT* at late times because of a lower general corrosion rate at the late-time cool temperatures, and hence limit radionuclide releases because of fewer general corrosion patch failures. Small values of *WDGCA22* result in larger values for *DOSTOT* at late times because of the higher corrosion rates at late-time cool temperatures and the attendant higher releases due to more general corrosion patch failures. (Lower values of the slope-term *WDGCA22* mean that general corrosion has less dependence on temperature and is closer to the base 60°C general corrosion rate throughout time, whereas higher values of *WDGCA22* mean that the temperature-dependent general corrosion rate is higher at early times (high temperatures), but low at late times (cool or ambient drift temperature).)

In addition to *WDGCA22*, the regressions in Figure 2.4-139a indicate small effects of the following variables that affect waste package failure: *WDZOLID*, *THERMCON*, *INFIL* (infiltration scenario), *SCCTHR*, *WDNSCC*, and *WDGCUA22* (pointer variable used to select the distribution of base corrosion rates for Alloy 22 at 60°C over the patches on the waste packages). The effects of *WDZOLID*, *THERMCON*, *SCCTHR*, and *WDNSCC* have already been discussed in conjunction with Figure 2.4-138c. Like *THERMCON*, the negative effect associated with *INFIL* probably results because increased values for *INFIL* result in lower waste package temperatures, and thus lower rates of corrosion at early times. The variable *WDGCUA22* has a small positive effect on the uncertainty in *DOSTOT*. Specifically, *WDGCUA22* is a pointer variable used to select three uncertain distributions that derive from both the uncertainty in a base corrosion rate for Alloy 22 at 60°C and the uncertainty that exists in the prediction of small-scale variability in chemical and physical conditions across patches used in the modeling of waste package degradation. Increasing *WDGCUA22* results in higher overall corrosion rates and thus higher values for *DOSTOT*.

The regressions in Figure 2.4-139a also indicate very small effects of several variables related to physical processes (Table 2.4-11). However, the effects of these variables are minor given the much larger effects of variables related to waste package failure. That the waste package failure uncertainty variables are dominant is to be expected, as they directly determine available inventory for release.

2.4.2.3.3.5 Uncertainty and Sensitivity Analyses for the Early Failure Scenario Class

The early failure scenario class is defined on the basis of futures that involve one or more early failure events. This section presents uncertainty and sensitivity analysis results for the drip shield early failure modeling case and waste package early failure modeling case of the early failure scenario class.

2.4.2.3.3.5.1 Uncertainty and Sensitivity Analyses for the Drip Shield Early Failure Modeling Case

Expected Annual Dose to the RMEI over [0, 20,000 yr]—The uncertainty and sensitivity analyses for expected dose to the RMEI (*EXPDOSE*, mrem/yr) over the time interval [0, 20,000 yr] resulting from early drip shield failure are summarized in Figures 2.4-140 and 2.4-141. The expected dose to the RMEI, *EXPDOS*, tends to show a sharp early peak prior to 1,000 years and then monotonically decreases over time, with the peak prior to 1,000 years resulting from the release of ^{99}Tc. At the time of this peak, maximum values for *EXPDOSE* are in the vicinity of 0.01 mrem/yr, although the values for most sample elements are considerably smaller (Figure 2.4-140a, b). After the early peak, *EXPDOSE* has an approximate range of from 10^{-7} to 10^{-3} mrem/yr.

The PRCCs in Figure 2.4-140c indicate that the uncertainty in *EXPDOSE* is dominated by *PROBDSEF* (probability that a randomly selected drip shield will experience an early failure), with the value for *EXPDOSE* increasing as *PROBDSEF* increases. This effect results because increasing *PROBDSEF* increases the expected number of drip shields that experience early failure, and hence increase *EXPDOSE*.

In addition to *PROBDSEF*, smaller effects are indicated for *SZFIPOVO* (flowing interval porosity in the volcanic units of the saturated zone), *SZGWSPDM* (groundwater-specific discharge multiplier in the saturated zone; as sampled, *SZGWSPDM* is actually the logarithm of the indicated multiplier), *SEEPUNC* (pointer variable used to determine uncertainty in local seepage rates), *THERMCON* (host-rock thermal conductivity), and *INFIL* (infiltration scenario) (Figure 2.4-140c. A negative effect is indicated for *SZFIPOVO* at early times (i.e., prior to 3,000 years), with this effect then going to zero. This effect results because increasing *SZFIPOVO* increases the time required for the initial releases of mobile species such as ^{99}Tc to reach the location of the RMEI (i.e., results in a lower Darcy velocity in the fractured volcanics). The positive effect associated with saturated zone *GWSPDM* results from increasing the Darcy velocity in the saturated zone, which in turn moves radioactive species more rapidly to the location of the RMEI. This effect is especially pronounced at early times (i.e., prior to 2,000 years) because increasing *SZGWSPDM* decreases the travel time of the highly mobile, highly soluble radioactive species, such as ^{99}Tc, to the location of the RMEI.

Both *THERMCON* and *INFIL* have small positive effects on *EXPDOSE* at early times (i.e., prior to 3,000 years). These effects are related to the influence of these variables on waste package thermal conditions. Specifically, increasing *THERMCON* or *INFIL* tends to reduce EBS temperatures and thus reduce the time at which releases from the waste packages can begin (i.e., the time when the drift-wall temperature and the waste-form temperature drop below boiling). After 3,000 years, *THERMCON* has essentially no effect on *EXPDOSE* (although the slightly negative correlation between 3,000 and 9,000 years can be explained as an effect related to waste-form degradation as discussed in the next section for the waste package early failure case). However, *INFIL* continues to have a small effect resulting from increased water flow (seepage) through the EBS that occurs as *INFIL* increases in value. In particular, for this drip shield early failure case, which has no drip shield or waste package barrier, increased seepage and concomitant increased advection through the waste form results in a linear increase for releases of solubility-limited radionuclides, such as ^{239}Pu and ^{240}Pu, which are important contributors to the expected annual dose after about 6,000 years (Figure 2.4-34).

More detailed sensitivity analyses for *EXPDOSE* are provided by the regression analyses in Figure 2.4-141a. The dominant effect of *PROBDSEF* on the uncertainty in *EXPDOSE* is indicated by R^2 values of 0.70, 0.71, and 0.63 for the regressions containing only *PROBDSEF* at 3,000, 5,000, and 10,000 years. After *PROBDSEF*, the most important variable is *SEEPUNC*. However, the incremental effect associated with *SEEPUNC* is small as the R^2 values for the regression models containing both *PROBDSEF* and *SEEPUNC* are 0.77 and 0.78 at 3,000 and 5,000 years, respectively (SNL 2008a, Appendix K5.7.1[a]).

After *PROBDSEF* and *SEEPUNC*, smaller effects are indicated for a number of variables in the stepwise regression analysis. For example, the following additional variables are indicated as affecting *EXPDOSE* at 10,000 years: *INFIL*, *SEEPPRM* (mean fracture permeability in lithophysal rock units, m^2; as sampled, *SEEPPRM* is actually the logarithm of the indicated permeability), *ALPHAL* (capillary strength parameter in lithophysal rock units used in the seepage abstraction), *MICTC99* (biosphere dose conversion factor for ^{99}Tc), *MICPU239* (biosphere dose conversion factor for ^{239}Pu), *PHCSS* (pointer variable used to determine pH in commercial SNF waste-form cell 1 under liquid influx conditions), *CPUCOLWF* (concentration of irreversibly attached plutonium on stable glass colloids, mol/L), *SZCOLRAL* (colloid retardation factor in alluvial unit of the saturated zone, dimensionless; as sampled, *SZCOLRAL* is actually the logarithm of the indicated retardation factor), *RHMU0* (scale factor used to represent uncertainty in chloride concentration in drift waters for relative humidities in the range [0, 0.2]; as sampled, *RHMU0* is actually the logarithm of the indicated scale factor), and *DSFLUX* (flux splitting factor for drip shield). Specifically, the positive effect associated with *INFIL* results from increasing water flux through the EBS; the negative effects associated with *SEEPPRM* and *ALPHAL* result from increasing water diversion around the EBS; the positive effects associated with *MICTC99* and *MICPU239* result from increasing the received dose for a given exposure level; and the remaining variables have very small real or spurious effects. The appearance of *DSFLUX* is an example of a spurious effect in the linear regression model, as the drip shields are assumed to be completely destroyed in the drip shield early failure modeling case. A chloride concentration has an impact only on the localized corrosion submodel, the effect of *RHMU0* is also spurious.

The dominant effect of *PROBDSEF* is readily apparent in the scatterplot in Figure 2.4-141b. Further, the smaller effects of *SEEPUNC* and *INFIL* can be seen in the scatterplots in Figure 2.4-141b, c.

Several of the variables identified in the analysis with PRCCs (i.e., *SZFIPOVO*, *SZGWSPDM*, *THERMCON*) in Figure 2.4-140c do not appear in the regressions in Figure 2.4-141a. However, the times at which these variables have identifiable effects on *EXPDOSE* in Figure 2.4-140c are not the times at which the regressions in Figure 2.4-141a are performed.

Expected Annual Dose to the RMEI over [0, 1,000,000 yr]—The uncertainty and sensitivity analyses for expected dose to the RMEI (*EXPDOSE*, mrem/yr) over the time interval [0, 1,000,000 yr] resulting from early drip shield failure are summarized in Figures 2.4-142 and 2.4-143. The time-dependent results for *EXPDOSE* tend to decrease until about 200,000 years and then level off (Figure 2.4-142a, b). This decrease is due to the decay of ^{239}Pu, which has a half-life of 24,100 years (Figure 2.4-34). The values for *EXPDOSE* are bounded above by 0.01 mrem and, after 200,000 years, by 0.001 mrem.

The sensitivity analyses for the time interval [0, 1,000,000 year] are similar to those for the time interval [0, 20,000 yr]. Specifically, the sensitivity analysis with PRCCs for [0, 1,000,000 yr] in Figure 2.4-142c identifies the following variables as influencing the uncertainty in *EXPDOSE*: *PROBDSEF, INFIL, SEEPPRM, SZFIPOVO, SEEPUNC*, and *SZGWSPDM*. For both time periods, *PROBDSEF* is the dominant contributor to the uncertainty in *EXPDOSE*, with the other variables making much smaller contributions to the uncertainty in *EXPDOSE*. The PRCC plots are constrained to contain a maximum of six variables. As a result, the slight differences in the variables shown in Figures 2.4-140c and 2.4-142c result from slight variations in the importance of individual variables over the time intervals under consideration. For example, *THERMCON* would not have any effect on long-term doses, as it is only related to repository heating at early times.

More detailed sensitivity analyses for the time interval [0, 1,000,000 year] are provided by the regressions in Figure 2.4-143a. Similar to the regressions in Figure 2.4-141a, the dominant variable is *PROBDSEF*. Specifically, the dominant effect of *PROBDSEF* on the uncertainty in *EXPDOSE* is indicated by R^2 values of 0.47, 0.55, and 0.52 for the regressions containing only *PROBDSEF* at 50,000, 200,000, and 500,000 years. These values are lower than the corresponding R^2 values of 0.70, 0.71, and 0.63 obtained in the analyses in Figure 2.4-141a at 3,000, 5,000, and 10,000 years, which suggests that more variables are having small effects on the uncertainty in *EXPDOSE* at later times than is the case for the first 10,000 years. This is, in fact, borne out by the large number of variables indicated as having small effects on *EXPDOSE* in the regression analyses (Figure 2.4-143a). After *PROBDSEF*, the next most important variable in all three regressions is *INFIL*, with *EXPDOSE* tending to increase as *INFIL* increases from increased water flow through the EBS. Together, *PROBDSEF* and *INFIL* result in regressions with R^2 values of 0.55, 0.63, and 0.63 at 50,000, 200,000, and 500,000 years (SNL 2008a, Appendix K5.7.1[a]).

After *PROBDSEF* and *INFIL*, all three regressions select *SZGWSPDM*, *SEEPUNC*, and *SEEPPRM* as the next three variables to add to the regression models, although not necessarily in the same order (Figure 2.4-143a). Adding these three variables brings the R^2 values up to 0.73, 0.77, and 0.75 at 50,000, 200,000, and 500,000 years. As previously discussed, *SZGWSPDM* has a positive effect on *EXPDOSE* as a result of speeding up flow in the saturated zone; *SEEPUNC* has a positive effect on *EXPDOSE* as a result of increasing water flow through the EBS; and *SEEPPRM* has a negative effect on *EXPDOSE* as a result of increasing water flow around the EBS and thus reducing water flow through the EBS.

After *PROBDSEF, INFIL, SZGWSPDM, SEEPUNC,* and *SEEPPRM*, the regressions at 50,000, 200,000, and 500,000 years add 8, 11, and 11 additional variables, respectively, and produce models with R^2 values of 0.82, 0.86, and 0.87 (Figure 2.4-143a). Thus, as noted earlier, a large number of variables have small effects on the uncertainty in *EXPDOSE* at later times.

The dominant effect of *PROBDSEF* on the uncertainty in *EXPDOSE* is shown in the scatterplot in Figure 2.4-143b. In contrast, the much smaller effects of *INFIL* and *SZGWSPDM* on the uncertainty in *EXPDOSE* can been in Figure 2.4-143c and d.

2.4.2.3.3.5.2 Uncertainty and Sensitivity Analyses for the Waste Package Early Failure Modeling Case

Expected Annual Dose to the RMEI over [0, 20,000 Years]—The uncertainty and sensitivity analyses for expected dose to the RMEI (*EXPDOSE*, mrem/yr) over the time interval [0, 20,000 yr] resulting from early waste package failure are summarized in Figures 2.4-144 and 2.4-145. There is sharp peak in *EXPDOSE* between 1,000 and 2,000 years resulting from the release of ^{99}Tc from the failure of codisposal waste packages (Figures 2.4-36 and 2.4-144a). At the time of this peak, maximum values for *EXPDOSE* are around 0.1 mrem/yr, although the values for most sample elements are considerably smaller. After this initial early peak, *EXPDOSE* has values in a range from approximately 10^{-5} to 10^{-2} mrem/yr until a time of about 10,000 years.

At 10,000 years, there is a sharp jump in the values for *EXPDOSE* (Figure 2.4-144a and b). This jump results from the arrival of radionuclide at the RMEI location due to the releases from commercial SNF waste packages after their relative humidity exceeds 95%. The commercial SNF waste packages are hotter than the codisposal waste packages, resulting in releases from commercial SNF waste packages that are delayed until the waste package relative humidity increases to 95%, at which time a continuous water film is considered to have formed, resultant bulk chemical conditions can be calculated, and diffusive transport begins. The jump in *EXPDOSE* between approximately 9,000 and 14,000 years results from the arrival of ^{99}Tc from commercial SNF packages at the location of the RMEI. After this jump, the values for *EXPDOSE* again decrease as the pulse of ^{99}Tc passes.

This particular type of bimodal behavior of *EXPDOS*, with different peaks for the two waste types occurring nearly 10,000 years apart, does not occur for early drip shield failure (compare Figure 2.4-140a and b and Figure 2.4-141a and b). In particular, early drip shield failure is assumed to result in waste package failure and subsequent radionuclide releases only if the failed drip shield is experiencing seeping conditions (with the potential for localized corrosion of the Alloy 22). Thus, all releases for the drip shield early failure modeling case occur in seeping zones. Under these seeping conditions, the 95% threshold switch for in-package chemistry is not necessary (i.e., a continuous water film is assumed to be present in the waste form and corrosion products under seeping conditions). The 95% threshold is only applicable under nonseeping conditions, when adsorption of water vapor onto the waste-form surfaces is required to create bulk aqueous chemical conditions. Thus, in the drip shield early failure modeling case, there is no possibility of having this temporal disparity in the time of releases between the two fuel types.

The PRCCs in Figure 2.4-144c indicate that the uncertainty in *EXPDOSE* is dominated by *PROBWPEF* (probability that a randomly selected waste package will experience an early failure), with the value for *EXPDOSE* increasing as *PROBWPEF* increases. This effect results because increasing *PROBWPEF* increases the expected number of waste packages that experience early failure, and hence increases *EXPDOSE*. The PRCCs for *PROBWPEF* decrease in value from approximately 9,000 to 14,000 years as a result of the noise introduced into the analysis from the dispersal in pulse arrival times of the failed commercial SNF waste packages.

In addition to *PROBWPEF*, smaller effects are indicated for *INFIL* (infiltration scenario), *THERMCON* (host-rock thermal conductivity), *SZFIPOVO* (flowing interval porosity in the volcanic units of the saturated zone), *SZGWSPDM* groundwater-specific discharge multiplier (groundwater-specific discharge multiplier in the saturated zone; as sampled, *SZGWSPDM* is actually the logarithm of the indicated multiplier), and *DSNFMASS* (scale factor used to characterize uncertainty in the radionuclide inventory content of the DOE SNF fuel contained in codisposal waste packages) (Figure 2.4-144c). The effects of *SZFIPOVO* and *SZGWSPDM*, as well as the effect of *INFIL* at early times, are the same as previously discussed in conjunction with Figure 2.4-142c. The negative correlation with *INFIL* after about 2,500 years is discussed below in connection with the scatterplots. The effect of *THERMCON* is similar, although more pronounced. Increasing *THERMCON* leads to lower drift temperatures and earlier times at which the waste package temperatures drop below boiling (at which time radionuclide transport can initiate). This effect is evident in the positive correlation between *THERMCON* and *EXPDOSE* between 0 and 1,500 years. Between 2,500 years and 9,500 years, the correlation between *THERMCON* and *EXPDOSE* becomes negative. This change in correlation results from the effect of temperature on waste form degradation. Increasing temperature increases the dissolution rate of the HLW in codisposal waste packages (SNL 2008a, Section 6.3.7.4.3.2). Consequently, as *THERMCON* increases, temperatures decrease and HLW degradation slows, resulting in less radionuclide mass being available for mobilization and transport, and in turn reducing *EXPDOSE*. This pattern repeats for the commercial SNF waste, which starts diffusive transport at about 9,500 years. The positive effect associated with *DSNFMASS* results from increasing the amount of ^{99}Tc in codisposal waste packages and hence the dose from ^{99}Tc following the failure of these waste packages.

More detailed sensitivity analyses for *EXPDOSE* are provided by the regression analyses in Figure 2.4-145a. The dominant effect of *PROBWPEF* on the uncertainty in *EXPDOSE* is indicated by R^2 values of 0.62, 0.77, and 0.47 for the regressions containing only *PROBWPEF* at 3,000, 5,000, and 10,000 years. Similarly to the PRCCs for *PROBWPEF*, the R^2 value for the regression at 10,000 years decreases in value as a result of the noise introduced into the analysis by the dispersal of pulse releases arriving from the failed commercial SNF waste packages over approximately 9,000 to 14,000 years. Because of this noise, the final regression model at 10,000 years contains only 5 variables and has an R^2 value of 0.71. However, a clearer view of what is driving the uncertainty in *EXPDOSE* at 10,000 years is provided by the scatterplots in Figure 2.4-145b, c, and d. Specifically, the uncertainty in *EXPDOSE* is still dominated by *PROBWPEF* (Figure 2.4-145b), with smaller contributions to this uncertainty from *INFIL* (Figure 2.4-145c) and *THERMCON* (Figure 2.4-145d). The scatterplot for *PROBWPEF* (Figure 2.4-145b) shows an interesting pattern in that it contains two separate populations of points that each increase monotonically with *PROBWPEF*. The upper population of points consists of realizations in which the commercial SNF waste packages in one or more percolation subregions have begun diffusive transport (relative humidity interior to the waste package exceeds 95%) by 10,000 years. Because infiltration rates and temperatures vary between percolation subregions, the time at which diffusive transport begins also varies, with most commercial SNF waste packages beginning diffusive transport between 9,000 and 14,000 years, whereas codisposal waste packages begin diffusive transport between 500 and 3,000 years (SNL 2008a, Appendix K5.7[a]).

Figure 2.4-145c indicates that the expected dose at 10,000 years decreases as *INFIL* (infiltration scenario) increases. As *INFIL* increases, percolation rates increase, leading to an increase of the liquid saturation of the host rock and subsequent increase in the thermal conductivity of the host rock. Increased infiltration then leads to lower temperatures and higher temperature deltas. Because of these temperature effects, the difference in relative humidity on waste packages of different temperatures becomes more pronounced. Therefore, increasing infiltration results in the counter-intuitive effect that the warmer waste packages (commercial SNF waste packages) have lower relative humidity at higher values of infiltration. These lower values of relative humidity are less likely to permit diffusive transport, which in turn yields a negative relationship between *INFIL* and expected dose at 10,000 years. The relationship between infiltration, temperature, and relative humidity is described and documented in *Multiscale Thermohydrologic Model* (SNL 2008d, Section 6.3.20[b]).

Figure 2.4-145d indicates that expected dose at 10,000 years increases as *THERMCON* (host-rock thermal conductivity) increases. This correlation is valid at 10,000 years because at this time commercial SNF waste packages are just beginning diffusive transport, so the correlation indicates the positive relationship between *THERMCON* and *EXPDOSE*. If the correlation were performed after transport has begun, the relationship between *THERMCON* and *EXPDOSE* would be reversed, because at these times *THERMCON* affects waste degradation rates, as described above.

In contrast, more informative results are given by the regression analyses at 3,000 and 5,000 years (Figure 2.4-145a) without the added need to examine scatterplots. Specifically, both the indicated regressions select the following four variables after *PROBWPEF*: *MICTC99* (biosphere dose conversion factor for ^{99}Tc for modern interglacial climate), *MICC14* (biosphere dose conversion factor for ^{14}C for modern interglacial climate), *DSNFMASS*, and *UZFAG8* (fracture aperture for the tsw34, tsw35, tsw36, tsw37, and tsw38 rock units in the unsaturated zone). Increasing *MICTC99* and *MICC14* has a positive effect on *EXPDOSE* by increasing the dose from ^{99}Tc and ^{14}C, respectively; increasing *DSNFMASS* has a positive effect on *EXPDOSE* by increasing the amount of ^{99}Tc in codisposal waste packages and hence the dose from ^{99}Tc that results from the failure of these waste packages; and increasing *UZFAG8* has a negative effect on *EXPDOSE* by decreasing the proportion of radionuclides moving through fractures in the unsaturated zone. Specifically, increasing *UZFAG8* (fracture aperture for matrix diffusion in the unsaturated zone) is equivalent to decreasing the fracture-matrix interface area in the unsaturated zone beneath the drifts, which decreases the fracture-matrix diffusion rate. In seepage regions, this decreased exchange rate has a negligible impact on unsaturated zone transport and subsequent doses because nearly all of the EBS radionuclide releases go directly into the unsaturated zone fractures, which transport quite rapidly. However, in the portion of the repository residing in nonseeping zones, the radionuclide releases from the EBS go mostly into the unsaturated zone matrix continuum, which transports much more slowly and can only effect dose at the RMEI through back-diffusion into the unsaturated zone fracture continuum. Thus, for these realizations of an early-failed codisposal waste package residing in a non-seep zone (only codisposal waste packages contribute to dose for these regressions at 3,000 and 5,000 years), a decrease in fracture-matrix exchange caused by an increase in *UZFAG8* will result in a decreased dose. Collectively, the inclusion of *MICTC99, MICC14, DSNFMASS*, and *UZFAG8* increases the R^2 values for the two regressions to 0.74 and 0.86. After *MICTC99, MICC14, DSNFMASS*, and *UZFAG8*, the regressions add an additional six variables with small effects and result in final models that have R^2 values of 0.80 and 0.89. The regression models at 3,000 years tend to have smaller R^2 values than the regression models at 5,000 years because of the noise introduced by the arrival of the ^{99}Tc releases (i.e., compare the smoothness of the time-dependent releases at 3,000 and 5,000 years in Figure 2.4-144a and b).

Expected Annual Dose to the RMEI over [0, 1,000,000 yr]—The uncertainty and sensitivity analyses for expected dose to the RMEI (*EXPDOSE*, mrem/yr) over the time interval [0, 1,000,000 yr] resulting from early waste package failure are summarized in Figures 2.4-146 and 2.4-147.

Except for very early times, the values for *EXPDOSE* fall between 10^{-6} and 0.1 mrem/yr for the 0 to 1,000,000-year time interval (Figure 2.4-146a). For most Latin hypercube sample elements, the values for *EXPDOSE* monotonically decrease until about 300,000 years, at which time they show a sharp increase in value resulting from the failure of the drip shields from general corrosion. This failure allows seeping water to directly contact the failed waste packages, and as a consequence, produces larger radionuclide releases from the failed waste packages.

The single most important variable with respect to the uncertainty in *EXPDOSE* is *PROBWPEF* (probability that a randomly selected waste package will experience an early failure), with the value for *EXPDOSE* increasing as *PROBWPEF* increases. This effect results because increasing *PROBWPEF* increases the expected number of waste packages that experience early failure, and hence increases *EXPDOSE* (Figures 2.4-146c and 2.4-147a). The positive effect of *PROBWPEF* can be seen in Figure 2.4-147b.

Prior to 300,000 years, *ISCSNS* (pointer variable used to determine ionic strength in commercial SNF waste form cell under nonseeping conditions) and *SZGWSPDM* (groundwater-specific discharge multiplier in the saturated zone; as sampled, *SZGWSPDM* is actually the logarithm of the indicated multiplier) also have significant positive effects on the uncertainty in *EXPDOSE* (Figures 2.4-146c, and 2.4-147a). These effects result because increasing *ISCSNS* increases plutonium solubility, and increasing *SZGWSPDM* increases water flow in the saturated zone. After 300,000 years, *INFIL* (infiltration scenario) and *SZGWSPDM* are indicated as having positive effects on *EXPDOSE* (Figures 2.4-146c and 2.4-147a). This is because increasing *INFIL* increases water flow in the EBS and unsaturated zone, and increasing *SZGWSPDM* increases water flow in the saturated zone. After *PROBWPEF, ISCSNS, SZGWSPDM*, and *INFIL*, the analyses identify a number of additional variables with small effects on *EXPDOSE*.

2.4.2.3.3.6 Uncertainty and Sensitivity Analyses for the Seismic Scenario Class

The seismic scenario class is defined on the basis of futures involving one or more seismic events. This section presents uncertainty and sensitivity analysis results for the expected dose, *EXPDOSE*, associated with the seismic ground motion modeling case.

Expected Annual Dose to the RMEI over [0, 20,000 yr]—The uncertainty and sensitivity analyses for expected dose to the RMEI (*EXPDOSE*, mrem/yr) over the time interval [0, 20,000 yr] resulting from seismic ground motion events are summarized in Figures 2.4-148 and 2.4-149. For this seismic ground motion modeling case within the scenario class, *EXPDOSE* (mrem/yr) tends to monotonically increase over the time interval [0, 20,000 yr], and the range of possible values for *EXPDOSE* at 10,000 years is approximately [10^{-4}, 1 mrem/year] (Figure 2.4-148).

The PRCCs in Figure 2.4-148c indicate that the uncertainty in *EXPDOSE* is dominated by the residual stress threshold for stress corrosion cracking *SCCTHRP* expressed as a percent of the base value of Alloy 22 yield strength (specifically, *SCCTHRP* and the stress corrosion cracking threshold, *SCCTHR*, which is an important regression variable in the nominal modeling case, are related by *SCCTHR* = (*SCCTHRP*/100) (351 MPa), where 351 MPa is the yield strength of Alloy 22). The value for *EXPDOSE* decreases as *SCCTHRP* increases. This occurs because increasing *SCCTHRP* increases the stress required for initiating stress corrosion cracking, and thus decreases the probability that a given seismic ground motion event will cause waste package damage.

In addition to *SCCTHRP*, smaller effects are indicated for *SZGWSPDM* (groundwater-specific discharge multiplier in the saturated zone; as sampled, *SZGWSPDM* is actually the logarithm of the indicated multiplier), *SZFIPOVO* (flowing interval porosity in the volcanic units of the saturated zone), *INFIL* (infiltration scenario), *DSNFMASS* (scale factor used to characterize uncertainty in the radionuclide inventory content of DOE SNF contained in codisposal waste packages), and MICC14 (biosphere dose conversion factor for ^{14}C for modern interglacial climate) (Figure 2.4-148c). The variables *SZGWSPDM, DSNFMASS*, and MICC14 have positive effects on *EXPDOSE*, with these effects resulting because increasing *SZGWSPDM* increases water flow in the saturated zone, increasing *DSNFMASS* increases the amount of radionuclides in codisposal waste packages, and hence the dose from the failure of these waste packages, and increasing MICC14 increases the received dose from ^{14}C for a given exposure level. The variables *SZFIPOVO* and *INFIL* have effects at early times, but limited effects at later times. The negative effect for *SZFIPOVO* is from a reduced Darcy flux in the saturated zone and thus a delay in the arrival of radionuclides at the location of the RMEI. In contrast, the positive effect for *INFIL* is from accelerating the initial arrival of radionuclides at the location of the RMEI; specifically, increased values for *INFIL* result: (1) in cooler conditions in the EBS, which contributes to earlier radionuclide releases; and (2) in increased water flux in the EBS and unsaturated zone, which contributes to more rapid radionuclide movement (SNL 2008a, Appendix K7.7.1[a]).

More detailed sensitivity analyses for *EXPDOSE* are provided by the regression analyses in Figure 2.4-149a. The dominant effect of *SCCTHRP* on the uncertainty in *EXPDOSE* is indicated by R^2 values of 0.81, 0.86, and 0.88 for the regressions containing only *SCCTHRP* at 3,000, 5,000, and 10,000 years. After *SCCTHRP*, the regressions select a large number of variables with small effects on *EXPDOSE*. For example, the regression at 3,000 years then selects *SZGWSPDM, INFIL*, and *MICTC99* (biosphere dose conversion factor for ^{99}Tc for modern interglacial climate) and produces a model with an R^2 value of 0.87; the regression at 5,000 years selects MICTC99, DSNFMASS, and *MICC14* biosphere and produces a model with an R^2 value of 0.90; and the regression at 10,000 years selects *MICTC99, DSNFMASS*, and *HLWDRACD* (rate term for dissolution of HLW glass in codisposal waste packages under low pH conditions, g/m^2/day) and produces a model with an R^2 value of 0.91. After the first four variables, the regressions at 3,000, 5,000, and 10,000 years select an additional 12, 11, and 12 variables, respectively, and produce final models with R^2 values of 0.92, 0.94, and 0.95. Thus, the uncertainty in *EXPDOSE* is dominated by *SCCTHRP*, with small contributions to this uncertainty by many additional variables (SNL 2008a, Appendix K7.7.1[a]).

The doses that are integrated to obtain *EXPDOSE* arise primarily from ^{99}Tc. The importance of ^{99}Tc can be seen in the regression results at 10,000 years (Figure 2.4-149a). Specifically, the three variables selected immediately after *SCCTHRP* (i.e., *MICTC99, DSNFMASS*, and *HLWDRACD*) all affect the dose received from ^{99}Tc. For the 10,000-year dose calculations, only codisposal waste packages contribute to the dose because TAD-bearing commercial SNF packages have a very low probability of failure due to their greater structural strength (SNL 2008a, Section 7.3.2.6.1.3). Thus, although there is about seven times the ^{99}Tc inventory in commercial SNF waste packages compared to codisposal packages (SNL 2008a, Table 6.3.7-4a), the commercial SNF ^{99}Tc inventory does not make a significant contribution to these regression analyses.

The dominant effect of *SCCTHRP* on the uncertainty in *EXPDOSE* can be seen in Figure 2.4-149b. The much smaller effects associated with *MICTC99* and *DSNFMASS* can be seen in Figure 2.4-149c and d.

Expected Annual Dose to the RMEI over [0, 1,000,000 yr]—The uncertainty and sensitivity analyses for expected dose to the RMEI (*EXPDOSE*, mrem/yr) over the time interval [0, 1,000,000 yr] resulting from seismic ground motion are summarized in Figures 2.4-150 and 2.4-151.

The time-dependent values of *EXPDOSE* for the 1,000,000-year period in Figure 2.4-150a and b are much choppier than the values for the 20,000-year time period in Figure 2.4-148a and b. This difference is from the numerical procedures used over 20,000 years and 1,000,000 years, respectively, to evaluate the integrals that define *EXPDOSE* as well as the time-step discretization used for nominal corrosion processes (Section 2.4.2.3.2.2.2). Because the effects of the seismic ground motion events are relatively stable for the 20,000-year time period, it is possible to use a quadrature procedure to evaluate *EXPDOSE* for the 20,000-year time period (SNL 2008a, Eq. 6.1.2-22). This creates the relatively smooth time-dependent values for *EXPDOSE* in Figure 2.4-148a and b. In contrast, the effects of seismic ground motion events are much more complex for the 1,000,000-year time period. As a result of this complexity, it is not possible to use a quadrature procedure to evaluate the defining integral for *EXPDOSE* over this longer time period. Instead, it is necessary to use a sampling-based (i.e., Monte Carlo) integration procedure to evaluate the defining integral for *EXPDOSE*. As described in Section 2.4.2.2.2.3, 30 1,000,000-year futures involving seismic ground motion events were randomly sampled for each Latin hypercube sampling element, and then the 30 time-dependent dose results associated with these futures were vertically averaged at each point in time to produce the estimated time-dependent value for *EXPDOSE* for each sample element. Because individual seismic ground motion events are discrete occurrences that initiate radionuclide releases, dose curves associated with individual seismic futures (i.e., individual Latin hypercube sampling elements) tend to be choppy. This, in turn, leads to oscillations in the vertically averaged expected dose. In addition, the temporal discretization in the models for nominal corrosion processes introduces additional step changes in expected dose at 200,000, 300,000, 500,000, and 700,000 years (Section 2.4.2.3.2.2.2). The individual curves in Figure 2.4-150a and b will eventually trend to smooth mean curves if a sufficiently large number of futures is sampled for each Latin hypercube sampling element; however, this is not necessary to determine an accurate estimate of the mean or median (Section 2.4.2.2.2.3).

Most values for *EXPDOSE* Figure 2.4-150a and b are less than 10 mrem/yr, with a few values between 10 and 100 mrem/yr. The largest values for *EXPDOSE* in Figure 2.4-150a and b are associated with spikes that derive from single seismic ground motion events. These spikes would disappear if a larger aleatory sample were used (Section 2.4.2.2.2.3). Figure 2.4-150b is more informative than Figure 2.4-150a because the time-dependent values of *EXPDOSE* for individual Latin hypercube sampling elements are more distinct. Figure 2.4-150b indicates that there is a tendency for the individual realizations of *EXPDOSE* to decrease up to about 300,000 years due to the depletion of soluble radionucildes (i.e., ^{99}Tc and ^{129}I) in waste packages with seismic damage (Figure 2.4-26). In this time period, the values of *EXPDOSE* derive from the occurrence of seismic ground motion events and their effect on codisposal waste packages, since the failure of waste packages from nominal processes, due to stress corrosion cracking of the lid welds arising from general corrosion of the outer annealed Alloy 22 weld material, does not begin until about 150,000 years (Figure 2.1-9a). (It requires nominal stress corrosion cracking of the lid welds to fail the commercial SNF waste package internals, which causes the TAD-bearing commercial SNF packages to become susceptible to seismic damage from smaller, more frequent earthquakes.) The dominance of seismic ground motion events is indicated by the importance of the residual stress threshold *SCCTHRP*; specifically, the PRCCs in Figure 2.4-150c indicate that *SCCTHRP* dominates the uncertainty in *EXPDOSE* for approximately 200,000 years. This result is also indicated by the regression for *EXPDOSE* at 50,000 years in Figure 2.4-151a, where *SCCTHRP* is the first variable selected in the analysis with an R^2 value of 0.71.

Between 200,000 and 300,000 years the drip shields fail and waste packages start to fail from nominal processes. Consistent with this, the PRCCs in Figure 2.4-150c indicate that the uncertainty in *EXPDOSE* is now dominated by *WDGCA22* (temperature dependence coefficient associated with the general corrosion rate for Alloy 22, 1/°C). Specifically, *WDGCA22* is the temperature-dependent slope term of the Alloy 22 general corrosion rate, with the Alloy 22 corrosion rate decreasing (at late times and cooler temperatures) as *WDGCA22* increases. As indicated in Figure 2.4-138c, *WDGCA22* is the dominant variable with respect to the uncertainty associated with the failure of waste packages from nominal processes (see previous explanation in Section 2.4.2.3.3.4). After 400,000 years, the values for *EXPDOSE* tend to increase and are somewhat smoother than at earlier times (Figure 2.4-150a, b). This smoothness results from an increasing dominance of *EXPDOSE* by waste package failures deriving from nominal processes. In addition to *SCCTHRP* and *WDGCA22*, the PRCCs in Figure 2.4-150c indicate effects for several additional variables. However, the effects are small, and several are probably spurious. For example, *GP3NO3* (ratio of Cl^- to NO_3^- in Group 3 pore waters) could not have a real effect, as it only influences the localized corrosion model.

More detailed sensitivity analyses for *EXPDOSE* are provided by the regression analyses in Figure 2.4-151a. Specifically, *SCCTHRP* is the dominant contributor to the uncertainty in *EXPDOSE* at 50,000 years; *SCCTHRP* is the dominant contributor to the uncertainty in *EXPDOSE* at 200,000 years with contributions from *WDDSGC29 and WDGCA22*; and *WDGCA22* is the dominant contributor to the uncertainty in *EXPDOSE* at 500,000 years with a contribution from *SCCTHRP*. The individual regressions then add several additional variables with small effects on *EXPDOSE*. The final regression models at 50,000, 200,000, and 500,000 years have R^2 values of 0.77, 0.62, and 0.76 (Figure 2.4-151a), which are not particularly high, due in part to the choppiness of the values for *EXPDOSE* (Figure 2.4-150a and b) and the large number of processes that affect *EXPDOSE* for the 1,000,000-year seismic ground motion calculation.

For perspective, the scatterplots in Figure 2.4-151b, c, and d show the effects of *WDGCA22, SCCTHRP*, and *WDNSCC* (stress corrosion cracking growth rate exponent) at 500,000 years. The negative effects of *WDGCA22* and *SCCTHRP* can be easily seen in Figure 2.4-151b and c. The negative effect for *WDNSCC* is more subtle, but still discernable, in Figure 2.4-151d.

2.4.2.3.3.7 Uncertainty and Sensitivity Analyses for the Total Dose from All Scenario Classes

This section describes the uncertainty and sensitivity analyses for total expected dose (i.e., the dose summed over the six modeling cases) (Equations 2.4-19 and 2.4-21).

Total Expected Annual Dose to the RMEI over [0, 20,000 yr]—The uncertainty and sensitivity analyses for total expected dose to the RMEI (*EXPDOSE*, mrem/yr) over the time interval [0, 20,000 yr] resulting from all scenario classes are summarized in Figures 2.4-152 and 2.4-153.

The PRCCs in Figure 2.4-152c indicate that the three most important variables with respect to the uncertainty in *EXPDOSE* are *SCCTHRP* (residual stress threshold for stress corrosion cracking), *IGRATE* (rate of occurrence of igneous intrusive events, Year 1), and *SZGWSPDM* (groundwater-specific discharge multiplier in the saturated zone; as sampled, *SZGWSPDM* is actually the logarithm of the indicated multiplier). The negative effect associated with *SCCTHRP* results because increasing *SCCTHRP* occurs in waste packages being more resistant to seismic ground motion damage; the positive effect associated with *IGRATE* occurs because increasing *IGRATE* increases the probability of occurrence for igneous events; and the positive effect associated with *SZGWSPDM* occurs because increasing *SZGWSPDM* increases water flow in the saturated zone.

After *SCCTHRP, IGRATE*, and *SZGWSPDM*, smaller effects are indicated for *SZFIPOVO* (flowing interval porosity in the volcanic unit of the saturated zone) and *INFIL* (infiltration scenario) (Figure 2.4-152c). The negative effect associated with *SZFIPOVO* at early times is from initially slowing the movement of radioactive species in the saturated zone. The positive effect associated with *INFIL* is from its role in both speeding the cooling of the repository and increasing water flow in the EBS and unsaturated zone.

More detailed sensitivity analyses for *EXPDOSE* are provided by the regression analyses and associated scatterplots in Figure 2.4-153. Overall, the dominant variable with respect to uncertainty in *EXPDOSE* is *SCCTHRP*. Specifically, the regressions containing only *SCCTHRP* have R^2 values of 0.55, 0.66, and 0.69 at 3,000, 5,000, and 10,000 years, respectively (Figure 2.4-153a). After *SCCTHRP*, the next variable selected in all regressions is *IGRATE*; the inclusion of *IGRATE* raises the cumulative R^2 values to 0.62, 0.71, and 0.73. Thus, the effect of *IGRATE* on *EXPDOSE* is not as great as the effect of *SCCTHRP*. Consistent with the analysis of the PRCCs, *SZGWSPDM* is then the third or fourth variable selected in the three regressions analyses. The negative effect associated with *SCCTHRP* and the positive effects associated with *IGRATE* and *SZGWSPDM* are shown in Figure 2.4-153b, c, and d. After *SCCTHRP, IGRATE*, and *SZGWSPDM*, the regressions select a number of additional variables with small effects on *EXPDOSE*. The final regression models have R^2 values of 0.81, 0.85, and 0.82, which indicate that they are reasonably successful in accounting for the uncertainty in *EXPDOSE*. Some of the variables selected near the ends of individual regression analyses, which have very small effects on cumulative R^2 values, could be spurious. Nevertheless, some variables, such as *MICTC99* (biosphere dose conversion factor for ^{99}Tc for modern interglacial climate), which is in the top five regression parameters, would have a real effect. In particular, because the top radionuclide contributing to total mean annual dose in 10,000 years is ^{99}Tc, as shown in Figure 2.4-20, its appearance in the regression model makes sense.

Total Expected Annual Dose to the RMEI over [0, 1,000,000 yr]—The uncertainty and sensitivity analyses for total expected dose to the RMEI (*EXPDOSE*, mrem/yr) over the time interval [0, 1,000,000 yr] resulting from all scenario classes are summarized in Figures 2.4-154 and 2.4-155.

The time-dependent values for *EXPDOSE* are quite choppy as a result of the sampling-based calculation of the combined doses resulting from nominal processes and seismic ground motion events. Overall, most sample elements result in values for *EXPDOSE* in a range from 10^{-2} to 30 mrem/yr.

The PRCCs in Figure 2.4-154c indicate that the four most important variables with respect to the uncertainty in *EXPDOSE* are *SCCTHRP* (residual stress threshold; as sampled, *SCCTHRP* is a percent of a base value of 351 MPa and is related to the stress corrosion cracking threshold, *SCCTHR*, by $SCCTHRP = (SCCTHR \times 100)/(351\text{ MPa})$), *IGRATE* (rate of occurrence of igneous intrusive events, Year 1), *SZGWSPDM* (groundwater-specific discharge multiplier in the saturated zone; as sampled, *SZGWSPDM* is actually the logarithm of the indicated multiplier), and *WDGCA22* (temperature dependence coefficient associated with the general corrosion rate for Alloy 22, 1/°C). The negative effect associated with *SCCTHRP* results because increasing *SCCTHRP* increases the resistance of waste packages to seismic ground motion damage; the positive effect associated with *IGRATE* results because increasing *IGRATE* increases the probability of occurrence for seismic events; the positive effect associated with *SZGWSPDM* results because increasing *SZGWSPDM* increases water flow in the saturated zone; and the negative effect associated with *WDGCA22* results from its role in slowing the rate of general corrosion of Alloy 22 at late times and cooler temperatures, which in turn delays and reduces waste package failures due to both seismic ground motion events and general corrosion (as explained in Section 2.4.2.3.3.4).

Smaller effects are indicated for *SZFIPOVO* (flowing interval porosity in the volcanic unit of the saturated zone), and *EP1LOWPU* (scale factor used to incorporate uncertainty into plutonium solubility under low ionic strength conditions; as sampled, *EP1LOWPU* is actually the logarithm of the indicated scale factor).

More detailed sensitivity analyses for *EXPDOSE* are provided by the regression analyses and associated scatterplots in Figure 2.4-155. These results confirm the results in the PRCC plots in Figure 2.4-154c. In other words, *IGRATE*, *SZGWSPDM*, and *WDGCA22* generally appear as the top variables. However, for the regressions at 50,000 years and 200,000 years, *SCCTHRP* is also important, as that time period is dominated by seismic ground motion failures of codisposal waste packages. After 200,000 years, nominal corrosion processes become more important for the contribution to total dose from the seismic ground motion modeling case, so *SCCTHRP* drops lower in the regression for 500,000 years and *WDGCA22* enters the regression sooner. The final regression models at 50,000, 200,000, and 500,000 years have R^2 values of 0.67, 0.74, and 0.70, which are not particularly high. These values are probably due in part to the choppiness of the values for *EXPDOSE* (Figure 2.4-154a and b) and the large number of processes that affect *EXPDOSE* for the 1,000,000-year calculation. For perspective, the scatterplots in Figure 2.4-155b, c, and d show the effects of *IGRATE*, *WDGCA22*, and *SZGWSPDM* at 500,000 years, and the trends on these plots confirm the previous conclusions.

2.4.2.3.3.8 Summary of Uncertainty and Sensitivity Analyses

In summary, the various uncertainty and sensitivity analyses discussed in this section show that the uncertainty in the TSPA results (expected annual dose) can be explained by the uncertainty in the underlying parameters and models. In particular, the physical processes characterized by these uncertain parameters propagate through the couplings of various submodels in a logical fashion to produce a reasonable behavior of the expected dose distribution. A summary of the sensitivity analyses of the expected dose for the various modeling cases is presented in Table 2.4-12, which lists the most important uncertain input parameters and cross-references them to where they are discussed in Section 2.3.

2.4.2.3.4 Parameters Sampled across Their Ranges of Uncertainty in TSPA

[NUREG-1804, Section 2.2.1.4.1.3: AC 3(4)]

This section addresses NUREG-1804, Section 2.2.1.4.1.3, Acceptance Criterion 3(4), which requires that "the total system performance assessment sampling method ensures that sampled parameters have been sampled across their ranges of uncertainty." This acceptance criterion was shown to be satisfied in Section 2.4.2.1, which outlines how the full range of aleatory uncertainty is addressed in calculating performance assessment results, and in Section 2.4.2.2.2, which demonstrates statistical and numerical stability across both the aleatory uncertainty and the epistemic uncertainty in the underlying parameter distributions. The demonstration of statistical stability in Section 2.4.2.2.2 shows that the sample size for epistemic parameters is sufficient for computing the mean (or other statistic, such as median) or, equivalently, that the confidence interval about the mean is reasonably narrow. This indicates that the sampled parameters have been adequately sampled across their range of uncertainty. The demonstration of numerical stability in Section 2.4.2.2.2 involved showing adequate convergence of the quadrature and/or Monte Carlo techniques employed to compute expectations over aleatory uncertainty, which indicates that uncertainty in aleatory parameters has been adequately addressed. However, some additional background on the sampling methods, particularly Latin hypercube sampling, is useful.

Calculations of expected values for aleatory uncertainty are usually conducted with numerical integration based on quadrature techniques (SNL 2008a, Section 6.1.2), while calculations of expected values for epistemic uncertainty are conducted with a numerical integration based on Latin hypercube sampling because of its efficient stratification properties (Helton and Davis 2002; Iman 1992; McKay et al. 1979). In particular, Latin hypercube sampling shows less sampling variability than simple random sampling (McKay et al. 1979; Owen 1992; Stein 1987), and has been observed to produce stable results in several large analyses, even for relatively small sample sizes (Iman and Helton 1988; Iman and Helton 1991; Helton et al. 1995). Two modeling cases use sampling methods when evaluating expected values for aleatory uncertainty, the volcanic eruption modeling case and the 1,000,000-year seismic ground motion modeling case. Some of the aleatory parameters in the volcanic eruption modeling case (i.e., eruptive power, eruptive velocity, eruptive duration, wind speed, and wind direction), are sampled with the Latin hypercube sampling method to ensure sufficient sampling of the distribution extremes when the sample size is small (either 40 or 80 samples in the case of aleatory uncertainty for the eruption modeling case). The other aleatory parameters in the volcanic eruption modeling case (e.g., time of event and number of waste packages intersected) are addressed through a quadrature technique. The aleatory uncertainty in the 1,000,000-year seismic ground motion modeling case (Section 2.4.2.2.2.3) is addressed using random Monte Carlo sampling (sample size = 30). However, the statistical stability of this case is less robust due to the use of the random sampling and smaller sample size, as indicated in Figure 2.4-56.

Latin hypercube sampling operates in the following manner to generate a sample of size N_{LHS} from N_E variables (SNL 2008a, Section J3.5). The range of each variable (e.g., the range of each epistemic variable, e_{ji}) is divided into N_{LHS} intervals of equal probability, and one value is selected at random from each interval. The N_{LHS} values thus obtained for e_{1i} are paired at random and without replacement with the N_{LHS} values obtained for e_{2i}. These N_{LHS} pairs are paired at random and without replacement with the N_{LHS} values of e_{3i} to form N_{LHS} triples. This process is continued until a set of vectors in length N_E is formed. These N_E-tuples are of the form

$$\mathbf{e}_i = [e_{1i}, e_{2i}, \ldots, e_{N_E i}], \quad i = 1, \ldots, N_{LHS} \qquad \text{(Eq. 2.4-42)}$$

and constitute the Latin hypercube sample. As illustrated in Figure 2.4-156, for a Latin hypercube sampling of two variables (SNL 2008a, Figure J3.5-2), Latin hypercube sampling results in a dense stratification across the range of each variable (i.e., there is one value from each equal probability interval). Once the Latin hypercube sampling is generated, TSPA results are calculated for each sample element. For Latin hypercube sampling over epistemic uncertainty, the primary TSPA result is an expected dose history curve for each sampling of the epistemic parameters (300 realizations in total), where the expected dose is the expectation over the aleatory uncertainty, as shown in Figure 2.4-8.

To summarize, the use of Latin hypercube sampling over epistemic uncertainty—combined with methods for demonstrating statistical stability, such as replicated sampling—indicate that the Latin hypercube sampling method effectively samples epistemically uncertain parameters across their full ranges. The combined use of Latin hypercube sampling and random sampling, along with methods for demonstrating stability, indicate that the aleatory parameters have been effectively sampled across their full ranges (Section 2.4.2.2.2).

2.4.3 Demonstration of Compliance with the Individual Protection Standard for Human Intrusion

[NUREG-1804, Section 2.2.1.4.2.3: AC 1, AC 2, AC 3]

This section addresses requirements that must be met to demonstrate compliance with the individual protection standard for human intrusion (proposed 10 CFR 63.321). This section also addresses acceptance criteria in NUREG-1804, Section 2.2.1.4.2.3 and requirements of 10 CFR 63.113(d).

10 CFR 63.113(d) requires that the following performance objective for the geologic repository after permanent closure is met:

> The ability of the geologic repository to limit radiological exposures to the reasonably maximally exposed individual, in the event of human intrusion into the engineered barrier system, must be demonstrated through an analysis that meets the requirements at §§ 63.321 and 63.322 of subpart L of this part.

> Estimating radiological exposures to the reasonably maximally exposed individual requires a performance assessment that meets the requirements specified at § 63.114 of this subpart, and §§ 63.303, 63.305, 63.312 and 63.342 of subpart L of this part.

Proposed 10 CFR 63.321, *Individual Protection Standard for Human Intrusion*, specifies the following requirements under which human intrusion must be evaluated:

> (a) DOE must determine the earliest time after disposal that the waste package would degrade sufficiently that a human intrusion (see § 63.322) could occur without recognition by the drillers.
>
> (b) DOE must demonstrate that there is a reasonable expectation that the reasonably maximally exposed individual receives, as a result of human intrusion, no more than the following [mean (1) or median (2)] annual dose:
>
> > (1) 0.15 mSv (15 mrem) for 10,000 years following disposal; and
> >
> > (2) 3.5 mSv (350 mrem) after 10,000 years, but within the period of geologic stability.
>
> (c) DOE's analysis must include all potential environmental pathways of radionuclide transport and exposure, subject to the requirements at § 63.322.

NUREG-1804, Section 2.2.1.4.2.3, Acceptance Criterion 2(1) and Acceptance Criterion 2(2) state that the "total system performance assessment for human intrusion is performed separately from the overall total system performance assessment, and meets the requirements for performance assessments, specified in 10 CFR 63.114," and "the total system performance assessment for human intrusion is identical to the total system performance assessment for individual protection, except that it assumes the occurrence of a postulated human intrusion event with characteristics, as defined in 10 CFR 63.322 and excludes the consideration of unlikely natural features, events, and processes…" This section provides the results of the separately conducted human intrusion TSPA, which nevertheless shares many of the same submodels with the overall TSPA. Thus, where appropriate (i.e., except for the barriers, transport pathways, and FEPs specified to behave differently per 10 CFR 63.322), it is identical to the overall TSPA.

Section 2.4.3.1 summarizes the performance assessment model components and submodels for the human intrusion scenario. The earliest time a human intrusion could occur without recognition by the driller is presented in Section 2.4.3.2, including an evaluation of unlikely FEPs. The evaluation of the mean annual dose to the RMEI from a human intrusion event is discussed in Section 2.4.3.3, along with the stability and uncertainty of the results. Since the event is estimated to occur after 10,000 years, only the post-10,000-year performance is evaluated. Section 2.4.3.4 discusses the credibility for the TSPA representation of the human intrusion event and results.

The final dose results from the TSPA analyses for the individual protection standard in the event of a human intrusion are shown in Table 2.4-3.

2.4.3.1 TSPA Representation of the Human Intrusion Event
[NUREG-1804, Section 2.2.1.4.2.3: AC 3]

The effect of a human intrusion event is analyzed in the TSPA as a separate human intrusion modeling case. This modeling case estimates repository performance in the event that a stylized drilling intrusion intersects the repository, as required by 10 CFR 63.113(d). It is unlike the other modeling cases (described in Section 2.4.2), in the sense that the human intrusion modeling case is not a component of the calculation of annual dose to the RMEI evaluated against the individual protection standard of proposed 10 CFR 63.311. Rather, the results of the human intrusion modeling case are evaluated separately and compared to the individual protection standard for human intrusion specified in proposed 10 CFR 63.321. However, as stated in NUREG-1804, Section 2.2.1.4.2.3, Acceptance Criterion 2(2): "The total system performance assessment for human intrusion is identical to the total system performance assessment for individual protection, except that it assumes the occurrence of a postulated human intrusion event with characteristics, as defined in 10 CFR 63.322 and excludes the consideration of unlikely natural features, events, and processes." Thus, calculating a mean or median annual dose for the human intrusion modeling case resembles the calculation in the other modeling cases. Most of the epistemic uncertainty is the same, except for those models that are replaced with the borehole pathway (SNL 2008a, Section 6.1.4.12 and Appendix J11). The aleatory uncertainty in this modeling case is the type of waste package intersected and the location of the drilling intrusion (SNL 2008a, Section 6.7.3). The time of the intrusion is fixed in the TSPA analyses at 200,000 years, as described below, and the human intrusion scenario considers a single drilling intrusion into the repository.

10 CFR 63.322 specifies the assumptions DOE must make in constructing the performance assessment representation of human intrusion. Specifically, the NRC requires that "For the purposes of the analysis of human intrusion, DOE must make the following assumptions:

> (a) There is a single human intrusion as a result of exploratory drilling for ground water;
>
> (b) The intruders drill a borehole directly through a degraded waste package into the uppermost aquifer underlying the Yucca Mountain repository;
>
> (c) The drillers use the common techniques and practices that are currently employed in exploratory drilling for ground water in the region surrounding Yucca Mountain;
>
> (d) Careful sealing of the borehole does not occur; instead, natural degradation processes gradually modify the borehole;
>
> (e) No particulate waste material falls into the borehole;
>
> (f) The exposure scenario includes only those radionuclides transported to the saturated zone by water (e.g., water enters the waste package, releases

> radionuclides, and transports radionuclides by way of the borehole to the saturated zone); and
>
> (g) No releases are included which are caused by unlikely natural processes and events."

The human intrusion modeling case assumes that exploratory drilling activities intersect the repository and destroy a single drip shield and waste package without recognition by the drillers (SNL 2008a, Section 6.7.1). After penetrating a thinned (degraded by corrosion) drip shield and waste package, the drillers continue to bore a conduit to the saturated zone. The drillers penetrate a drip shield and waste package with an opening equal to the size of the drill bit. As a result, water enters the waste package, mobilizing radionuclides. The released radionuclides are transported out of the repository moving down the borehole to the saturated zone, and then through the saturated zone to the accessible environment.

The TSPA model components and submodels needed to calculate total system performance for the human intrusion modeling case include the following, given that a certain waste package is destroyed by the intrusion:

- Unsaturated zone flow
- EBS environment
- Waste form degradation and mobilization
- EBS flow and transport
- Unsaturated zone flow and transport
- Unsaturated zone flow down borehole
- Saturated zone flow and transport
- Biosphere.

These model components and submodels of the TSPA model for the human intrusion scenario are shown in Figure 2.4-157. The TSPA model framework for the human intrusion scenario is similar to that of the nominal scenario class (Figure 2.4-112); however, some of the submodels differ from those described in Section 2.4.2. These include the following, as indicated in Figure 2.4-157:

- Mechanical damage to waste packages and drip shields
- EBS flow and transport
- Unsaturated zone transport
- Saturated zone transport (slightly different).

The TSPA submodels for the human intrusion modeling case that are different from the submodels used in the nominal scenario class are discussed in more detail below (SNL 2008a, Section 6.7), including the information transferred between the submodels (Figure 2.4-158). A summary of the calculation methodology for the mean and median annual dose is also presented. The waste package and drip shield damage models, as related to drill bit penetration, are described in Section 2.4.3.2 in conjunction with the determination of the earliest time of occurrence of the human intrusion event.

2.4.3.1.1 EBS Flow and Transport for Human Intrusion

Conceptual Model—The human intrusion borehole is assumed to be drilled from the ground surface (at a random location within the footprint of the repository), through the drip shield and a single waste package (top and bottom), to the water table. As mentioned in Section 2.4.2.3.2.1.7, cladding is assumed to have no barrier function in the human intrusion performance assessment, as well as in the overall performance assessment. The waste package type is randomly selected, either a codisposal waste package or commercial SNF waste package, based on the proportion of these waste packages emplaced in the repository. The location of the intrusion is also unknown, and is therefore randomly placed in one of the five repository percolation subregions. After penetration of the waste package via a drilling event, water will flow into the waste package and waste form degradation and mobilization will occur. Nominal scenario class submodels for waste-form degradation and mobilization and EBS thermal-hydrologic environment (Section 2.4.2.3.2.1) were applied in the human intrusion scenario. Radionuclide mass is released from the intruded waste package to the EBS transport submodel (Section 2.4.2.3.2.1.8). Nominal scenario class submodels for transport of mass through the unsaturated zone to the saturated zone (Section 2.4.2.3.2.1.8) were modified for the human intrusion scenario calculation to simulate mass transport through a borehole pathway.

Implementation—For a human intrusion event, the waste package type (commercial SNF or codisposal), percolation rate (average percolation rate in one of the five percolation subregions for the given waste package type), and waste package location (i.e., saturated zone source region) need to be characterized. These three properties are treated as aleatory uncertainties and randomly selected based on their proportions in the repository (SNL 2008a, Section 6.7.3.1), as described in Section 2.4.3.1.4. Once the waste package type and percolation subregion are selected, the representative temperature and relative humidity time histories are applied to calculate the waste-form degradation rate, in-package chemistry, and transport properties in the EBS. The volumetric flow rate through the intruded waste package is calculated from the percolation flux at the base of the PTn lithologic unit for the selected percolation subregion by multiplying this percolation (Darcy) flux by a borehole cross-sectional area (0.0324 m^2) with dimensions based on current drilling practices for a typical water well (SNL 2008a, Section 6.7.3.1). This volumetric flow rate is the basis of the advective component of the EBS transport calculation, with no diversion of the water by the drip shield or waste package considered. For the diffusive component of the EBS transport calculation, the diffusive area is set equal to the cross-sectional area of the borehole, and the downstream concentration boundary condition is set to maximize diffusion out of the waste package.

2.4.3.1.2 Unsaturated Zone Transport for Human Intrusion

Conceptual Model—The advective and diffusive radionuclide mass flux (both dissolved and colloidal) from the waste package and the EBS transport model is assumed to be transported down the human intrusion borehole to the water table. The unsaturated zone borehole transport pathway is conceptualized to be an uncased borehole that undergoes degradation as a result of wall rock collapse shortly after it is drilled. To model transport through this degraded borehole, the matrix and fracture properties of the unsaturated zone rock types comprising the repository horizon are utilized. The borehole pathway is modeled as a single vertical fracture that extends from the surface, through the waste package, and down to the water table (as discussed in more detail below). The rubble fill in the borehole is considered to have properties similar to the undisturbed repository host rock matrix, while the fracture pathway within the rubble fill is given the fracture properties of the host rock. As a result, the collapsed matrix blocks are expected to occupy about 99% of the borehole volume while about 1% of the borehole volume is occupied by the fracture (consistent with the fracture porosity of the undisturbed rock). Although preferential pathways in the degraded borehole are expected to be tortuous and not consistently continuous throughout the length of the borehole and over the simulated time periods, the continuous vertical fracture pathway over the entire length of the borehole is assumed to simplify the modeling.

In contrast to the nominal scenario class, the unsaturated zone radionuclide transport abstraction model (using the FEHM code, Section 2.3.8.5) is not utilized in the unsaturated zone radionuclide transport calculation for the human intrusion scenario. Instead, the human intrusion modeling case uses a one-dimensional GoldSim pipe element to implement the borehole transport pathway below the repository. The mass released from the intruded waste package is passed to the one-dimensional pipe that simulates the borehole effects in the unsaturated zone beneath the waste package. The properties that define the borehole fill are chosen to be consistent with the near-drift rock properties used in the unsaturated zone transport submodel (SNL 2008a, Section 6.3.9), and the transport path length through the borehole is determined to be the vertical path length between the repository and the future water table. Because the repository host rock and water table elevations change over the unsaturated zone and saturated zone transport domains, the shortest possible transport path length based on the glacial transition water table is chosen. The volumetric water flux passed through the waste package for computing advective transport in the unsaturated zone is maintained throughout the borehole—there are no additional sources or sinks for water in the borehole.

Implementation—The borehole is conceptualized to be filled with the rubble of collapsed matrix blocks with a preferential fracture pathway with properties similar to the fractures in the undisturbed host rock near the drift. The volume fraction occupied by the preferential pathway is assumed to be the same as the fracture porosity of the undisturbed host rock. Other fracture properties, such as fracture aperture, porosity, and frequency (SNL 2008a, Table 6.7-5), are also assumed to be the same as that for the undisturbed rock type in the vicinity of the repository horizon (such as the TSw hydrogeologic unit). In particular, to be consistent with the unsaturated zone transport submodel, the property sets grouped for rock units tsw34, tsw35, tsw36, tsw37, and tsw38 are used to define the borehole properties (SNL 2008a, Table 6.7-6). For model simplification, although the borehole intersects other lithologic units, these values do not vary with depth.

The number of vertical fractures within the borehole was determined by considering the fracture frequency (calculated to be about four fractures per meter) and comparing it to the diameter of the borehole (approximately 0.2 m). This results in less than one fracture per borehole diameter, which is rounded up to one fracture for the borehole. Assuming vertical orientation of the fracture is consistent with the conceptualization of fractures in the unsaturated zone transport submodel (SNL 2008a, Section 6.7.3.2). The vertical fracture geometry is assumed to be parallel-plate geometry with no fracture infill material throughout the length of the borehole. The rubble filling the borehole surrounds the single fracture. The fracture aperture and fracture porosity (fraction of the borehole volume occupied by the fracture) are considered fixed at 0.00264 m and 0.0105, respectively, which are average values for the rock units tsw34, tsw35, tsw36, tsw37, and tsw38 of the unsaturated zone transport submodel.

Both advective and diffusive transport of radionuclides in the borehole are modeled using the pipe pathway in GoldSim. A dual-porosity approach is adopted, consistent with a discrete fracture surrounded by rock matrix. The cross-sectional area of the pipe pathway is defined to be equal to the plan area of the fracture ($\cong 0.0004\ m^2$; SNL 2008a, Table 6.7-6), while the matrix diffusion zones in the pipe pathway are used to define the rubble material that fills up the borehole around the fracture. The radionuclide mass flux from the waste package is passed into the fracture, where it advects vertically downwards and diffuses into the surrounding matrix normal to the flow. The maximum diffusive distance into the matrix is set equal to half the distance between two fractures (about 0.125 m), and the entire surface of the fracture wall within the borehole is assumed to be wetted for diffusive transfer to the matrix. No retardation of the radionuclides (dissolved or colloidal) is modeled on the fracture surface. A fracture longitudinal dispersivity value of 10 m is assumed in the fracture that is consistent with the values used in the unsaturated zone transport submodel (SNL 2008e, Section 4.1.6).

The saturation values for the fracture and matrix along with the matrix density and porosity are taken from the EBS-unsaturated zone interface model (SNL 2008a, Section 6.3.8.3), while the matrix tortuosity for diffusion calculations are those for Rock Group 3, which includes values for the TSw hydrogeologic unit. Within the matrix media, the radionuclides are assigned the sampled K_d values for devitrified units used in the unsaturated zone transport submodel for the entire pathway. For the mass transported irreversibly on colloids an assumption is made that there is no matrix diffusion. Also, for all radionuclides, including colloidally transported radionuclides, there is no sorption (i.e., no retardation) on fracture surfaces.

A flat-lying water table beneath the repository is estimated to be located at an elevation of about 850 m, based on the water table rise estimated to occur during the glacial-transition climate period (SNL 2008e, Section 6.4.8). For the repository elevation, a value of 1,040 m is assumed, which is consistent with the subsurface design where all repository drifts are at elevations of 1,039 m or higher (SNL 2007ae, Parameter 01-02). Thus, the path length of the borehole from the repository to the saturated zone is set at 190 m.

2.4.3.1.3 Saturated Zone Transport for Human Intrusion

Conceptual Model—Radionuclide mass from the unsaturated zone borehole is passed directly to the one-dimensional and three-dimensional saturated zone transport submodels and the transport of radionuclides through the saturated zone in the human intrusion scenario is identical to the nominal scenario modeling case, with one exception related to the distribution of mass at the unsaturated zone-saturated zone interface. From the borehole, the radionuclides are passed to one of the four saturated zone source regions. At this interface, radionuclide mass irreversibly associated with colloids is partitioned to fast and slow fractions (rather than at the EBS-unsaturated zone interface, as is done in the overall TSPA model, Section 2.4.2.3.2.1.8). The saturated zone source region is selected so that it corresponds spatially to the EBS percolation subregion intersected during the human intrusion event (SNL 2008a, Section 6.7.3.3). As discussed in the next section, the random saturated zone source region that the borehole intersects is an important aleatory uncertainty in the human intrusion modeling case.

Implementation—In order to apply spatial correlation between the EBS percolation subregions (where the radionuclides enter the borehole) and saturated zone source regions (where the radionuclides exit the borehole), the five EBS percolation subregions are mapped to the four saturated zone source regions. The relative areal fraction of the five EBS percolation subregions within the four saturated zone source regions is determined and used to represent the probability of each saturated zone source region to receive the radionuclide mass flux from the borehole. The saturated zone source region probability was determined by sorting the 560 unsaturated zone nodes into the five percolation subregions. Using the UTM coordinates for each of the 560 nodes, the nodes, labeled by percolation subregion, were then assigned to one of the four saturated zone quadrants (SNL 2008a, Section 6.7.3.3).

2.4.3.1.4 Calculation of Annual Dose for the Human Intrusion Scenario

Expected Annual Dose—The human intrusion scenario uses a Monte Carlo technique (Latin hypercube sampling) to calculate expected dose, which is the dose averaged over the aleatory uncertainties (Section 2.4.2.1) (SNL 2008a, Appendix J11). For each realization $\mathbf{e}_i$ of epistemically uncertain parameters, the expected annual dose $\bar{D}_{HI}(\tau|\mathbf{e}_i)$ at time τ is calculated by

$$\bar{D}_{HI}(\tau|\mathbf{e}_i) = \sum_{j=1}^{nA} D_{HI}(\tau|[1, r_j, q_j, SR_j], \mathbf{e}_i)/nA \qquad \text{(Eq. 2.4-43)}$$

where

nA = the number of aleatory realizations

r_j = the type of waste package (codisposal or commercial SNF) intersected in the jth aleatory realization

q_j = the percolation rate in the percolation subregion selected in the jth aleatory realization

SR_j = the saturated zone source region selected in the jth aleatory realization

$D_{HI}(\tau|[1, r_j, q_j, SR_j], \mathbf{e}_i)$ = the annual dose resulting at time τ from a human intrusion that intersects one waste package of type r_j that experiences percolation rate q_j and intersects the saturated zone in source region SR_j.

The quantity $D_{HI}(\tau|[1, r_j, q_j, SR_j], \mathbf{e}_i)$ is calculated directly by the GoldSim component of the TSPA model.

Mean or Median Annual Dose—As described in Section 2.4.2.1, the mean annual dose as a function of time is calculated by taking the expectation or average of $\bar{D}_{HI}(\tau|\mathbf{e}_i)$ at each time τ (i.e., it is an expectation of the annual dose $D_{HI}(\tau|[1, r_j, q_j, SR_j], \mathbf{e}_i)$ over both aleatory and epistemic uncertainty—see Equations 2.4-1 and 2.4-2). The median annual dose curve is the 50th percentile value of $\overline{D}_{HI}(\tau|\mathbf{e}_i)$ at each time τ.

Numerically, the TSPA model calculates the mean or median annual dose for the human intrusion scenario using the same two-step process. First, the TSPA model generates a set of 9,000 realizations (i.e., 9,000 annual dose histories) by using a Latin hypercube sample of 30 over the three aleatory parameters described earlier and a Latin hypercube sample of 300 over the epistemically uncertain parameters in all the submodels. The 300 epistemic samples match the 300 epistemic samples used for the overall performance assessment described in Section 2.4.2 (i.e., for all epistemic parameters that are common to the human intrusion TSPA and the overall TSPA, the 300 sample values are the same). The resulting 9,000 annual dose histories, $D_{HI}(\tau|[1, r_j, q_j, SR_j], \mathbf{e}_i)$, are then averaged in groups of 30, corresponding to the 30 aleatory samples for each $\mathbf{e}_i$, which produces 300 expected dose histories, $\overline{D}_{HI}(\tau|\mathbf{e}_i)$. These 300 expected dose histories are then averaged at each τ to produce the overall mean annual dose history, $\overline{\overline{D}}_{HI}(\tau)$, or their 50th percentile value is computed at each time τ to produce the median annual dose history. Since the human intrusion dose will not initiate until after 10,000 years (because the intrusion event is assumed to be at 200,000 years (Section 2.4.3.2.4)), the maximum of the median annual dose history is then compared to the dose metric of 350 mrem in proposed 10 CFR 63.311(a)(2) and proposed 10 CFR 63.321(b)(2).

2.4.3.2 Evaluation of the Earliest Occurrence Time of a Human Intrusion Event

[NUREG-1804, Section 2.2.1.4.2.3: AC 1]

This section documents the technical basis and associated analysis for evaluating the time of occurrence of a human intrusion event, as required by proposed 10 CFR 63.321(a). Consistent with the required assumptions for the analysis of human intrusion in 10 CFR 63.322(c), it is assumed that a driller would use the common techniques and practices currently employed in exploratory drilling for groundwater in the region surrounding Yucca Mountain. The time of the human intrusion event is taken to be the earliest time a driller would not recognize penetration into a waste package. Recognition of waste package penetration is based on drill performance characteristics observable at the surface. Such characteristics could be qualitative (i.e., smoothness of operation, excessive vibration or chatter, or drill bit wear or breakage) or quantitative (i.e., drill penetration rates, rotation speed, readily observable or measurable change in drilling fluid circulation, or changes in machinery hydraulic pressures required to maintain an existing drilling condition). The primary premise in the following discussion is that the earliest penetration time of a drip shield will be used as a conservative surrogate for the earliest penetration time for a waste package. Therefore, much of the analysis focuses on drip shield degradation modes and rates.

The human intrusion scenario considers the effects of a single well drilled from the land surface above the repository, that penetrates the repository and passes through a single drip shield and waste package into the underlying saturated zone, as described in Section 2.4.3.1. The earliest time at which a waste package could be breached without recognition by the drillers is determined by examining the degradation mechanisms of the drip shields and waste packages. Because degradation of waste packages and drip shields occurs gradually with time, the probability that a human intrusion could occur without recognition by the drillers increases with time.

Section 2.4.3.2.1 discusses the process of general corrosion of the waste package and drip shield. Section 2.4.3.2.2 discusses the occurrence of unlikely events, including drip shield and waste package early failures, as well as igneous and seismic events within 10,000 years of disposal. Section 2.4.3.2.3 discusses the potential for waste package penetration by common techniques used in exploratory drilling for groundwater in the Yucca Mountain region. A key part of the rock drilling discussion is the drill performance characteristics by which a driller would recognize that a metal object had been contacted, leading to courses of action by the driller to bypass that object. Finally, Section 2.4.3.2.4 summarizes the earliest possible penetration time of a waste package based on conservatively estimating the earliest failure of a drip shield by general corrosion.

2.4.3.2.1 General Corrosion of the Waste Package and Drip Shield

General corrosion of drip shields and waste packages occurs gradually over time, and the underlying metal retains its integrity and resistance to drilling until a significant amount of material is corroded, at which time the remaining thickness of the drip shield or waste package becomes insufficient to prevent penetration by a drill bit. Because the drip shield must be penetrated by the driller before the waste package can be penetrated, the penetration time for the drip shield is first examined in the analysis to determine the earliest time at which a human intrusion event could occur.

As described in Section 1.5.2.1, the waste package consists of two concentric cylinders: an inner vessel of Stainless Steel Type 316 (UNS S31600), designed for structural support, and a corrosion-resistant outer shell made of Alloy 22, a nickel-chromium-molybdenum alloy (Section 2.3.6.1). The drip shield, which is placed over the waste package, is an additional feature of the EBS. As described in Section 1.3.4.7, the drip shield plates are fabricated from Titanium Grade 7 (UNS R52400), a commercially available, nearly pure titanium alloy containing a small addition of palladium to provide a higher degree of corrosion resistance. The structural components of the drip shield (i.e., the drip shield framework) will be constructed using the higher-strength titanium alloy Titanium Grade 29 (UNS R56404), which has alloying elements aluminum and vanadium to provide the required strength and ruthenium for corrosion resistance. This titanium alloy is also highly corrosion resistant in a wide variety of chemical environments.

As long as they remain substantially intact, the drip shields will divert an inadvertent drilling event away from the waste package and preclude damage to a waste package (SNL 2008a, Section 6.7.2.3.3). The only drip shield corrosion mechanism modeled in the TSPA model is general corrosion (SNL 2008a, Section 6.3.5). This process is modeled as independent of temperature and relative humidity and is initiated at the time of repository closure. Because of the low corrosion rate of titanium alloy used for the drip shields, there is only a 0.0001 chance of drip shield failure under nominal conditions before approximately 230,000 years after permanent closure (SNL 2008a, Section 6.3.5.1.3), and only a 5% chance of drip shield failure before 280,000 years (Figure 2.1-8).

The TSPA model for waste package degradation includes four degradation modes: general corrosion, microbially influenced corrosion, stress corrosion cracking, and localized corrosion (SNL 2008a, Section 6.3.5). Because the waste package outer shell is highly corrosion resistant, waste packages will not be breached by nominal corrosion processes during the 10,000-year modeling period in the absence of localized corrosion (SNL 2007o, Section 8.1). In fact, waste package degradation models under nominal conditions indicate there is only a 5% chance of initial breaching of any waste package prior to about 170,000 years postclosure (Figure 2.1-9). However, this breaching is by nominal stress corrosion cracks in the closure lid-welds (Figure 2.1-10a) and would have no influence on the driller recognizing the waste package. The more important corrosion process in this regard is general corrosion, which can open patches on the cylindrical surface of the Alloy 22 outer barrier. As shown in Figure 2.1-10b, there is only a 5% chance of a general corrosion patch in any of the packages prior to approximately 600,000 years. Thus, the waste packages last substantially longer than the drip shields.

The potential effects of localized corrosion on the waste packages are conditional on a drip shield failure (SNL 2008a, Section 6.3.5.2.3). Until a breach of the drip shield occurs, the waste package itself is not susceptible to localized corrosion because it requires the presence of seepage water on the Alloy 22 surface. Under nominal conditions, localized corrosion of waste packages will not occur because drip shield failures are not expected until well after the chemical environment necessary for localized corrosion initiation has subsided (SNL 2008a, Section 6.3.5.2). Therefore, as stated above, in the earliest occurrence of a human intrusion event, localized corrosion is not a factor under nominal conditions (i.e., for conditions in the absence of likely disruptive events or likely early-failure events). Also, as discussed below, likely seismic events will not rupture of the drip shield (i.e., will not affect its seepage diversion capability), and early failure drip shield events are unlikely.

Given the slower general corrosion rates of the waste packages compared to the drip shields, until there is a drip shield failure, the waste package retains its structural integrity in the absence of disruptive or early failure events, which are discussed below.

2.4.3.2.2 Occurrence of Unlikely Events

Proposed 10 CFR 63.342(b) specifies that performance assessments conducted to show compliance with the human intrusion standard "…shall exclude the unlikely features, events, and processes, or sequences of events and processes, i.e., those that are estimated to have less than one chance in 10 and at least one chance in 10,000 of occurring within 10,000 years…" (i.e., an annual probability in the range of 10^{-5} to 10^{-8} per year). Therefore, FEPs with at least one chance in 10 of occurring within 10,000 years (i.e., an annual probability of greater than or equal to 10^{-5} per year) must be considered for the human intrusion calculations. The following events are discussed below with respect to this probability limit for unlikely FEPs: early failure of waste packages and drip shields, igneous events, and seismic events.

Early Failures—The probability of drip shield early failure (i.e., having an undetected defect that could cause an early failure) is determined from a lognormal distribution with a median value of 4.30×10^{-7} and an error factor of 14 (SNL 2007a, Table 7-1). Considering that 10 CFR 63.322 requires that a single waste package is penetrated during a human intrusion event, the probability that this waste package has an early failed drip shield is determined by the probability that any one drip shield sampled at random has an early failure. The mean value of this probability is 1.56×10^{-6} (SNL 2008a, Section 8.2), and is independent of time. Therefore, it can be excluded from consideration as an unlikely event because it is an event with less than one chance in 10 in 10,000 years, as defined by proposed 10 CFR 63.342(b).

The probability of a drilling intrusion intersecting an early failed waste package is not a consideration until after the drip shield has failed. At that time, the mean probability that a random waste package intersected by the driller will be an early failed waste package is determined from a lognormal distribution with a median of 4.14×10^{-5} and an error factor of 8.17 (SNL 2007a, Table 7-1). The mean value of this probability, calculated from the lognormal distribution, is 9.36×10^{-5} (SNL 2008a, Section 8.2). This would need to be accounted for in the calculation of the earliest occurrence time for a human intrusion event, except that, as described below (Section 2.4.3.2.4), it is assumed once the drip shield is penetrated, no additional credit is taken for corrosion time of the waste package (i.e., the time of the event is based on drip shield failure time). Thus, early failure waste packages, in combination with a human intrusion stylized analysis, can be excluded from consideration as an unlikely event.

Igneous Disruptive Events—Igneous disruptive events are unlikely (i.e., igneous intrusion of the repository footprint has an annual probability of less than 10^{-5} but greater than 10^{-8} with a mean annual occurrence frequency of 1.7×10^{-8} per year) (BSC 2004a, Table 7-1). Therefore, further consideration of an igneous event in conjunction with a human intrusion stylized analysis is excluded as an unlikely event (FEP 1.4.02.03.0A, Igneous event precedes human intrusion, Table 2.2-1) (SNL 2008c, Section 6). The exclusion is consistent with NRC requirements in proposed 10 CFR 63.342(b).

Seismic Disruptive Events—Seismic damage to drip shields and waste packages occurs from the mechanical response to seismically induced ground motion or fault displacement at the repository horizon (SNL 2007c). For seismic events to be considered when calculating the earliest time of a drilling intrusion, significant damage to the drip shield and waste package must occur with an annual probability greater than 10^{-5}. Since the drip shield must fail prior to waste package penetration, this analysis is concentrated on the probability of drip shield failure. Fault displacement hazards are considered first; then ground motion hazards.

The effect of fault displacement on the EBS is evaluated in terms of mean fault displacement hazard curves developed for faulting conditions mapped within the immediate vicinity of Yucca Mountain (SNL 2007c, Section 6.11 and Table 6-61). The expected number of waste packages and drip shields that fail from fault displacement is small because the number of waste packages potentially emplaced on known and generic faults is estimated to be 214, a small fraction of the approximately 11,000 waste packages in the repository (SNL 2007c, Section 6.12.2, p. 6-255). Seismic events capable of causing significant damage from fault displacement are unlikely because waste package failure due to shear displacement along faults intersecting the repository footprint has an annual probability of exceedance less than 2.2×10^{-7} per year for commercial SNF waste packages and less than 2.5×10^{-7} per year for codisposal waste packages (SNL 2007c, Table 6-65). Therefore, a seismic fault displacement event combined with a human intrusion stylized analysis can be excluded from consideration.

The effect of strong seismic ground motion is evaluated in terms of the mean bounded ground motion hazard curves developed for Yucca Mountain (SNL 2007c, Section 6.4.3 and Table 6-3). For the seismic ground motion, the threshold for considering the potential for damage to drip shields is reached if the residual stress from mechanical damage exceeds the residual stress threshold for titanium. The presence of residual stress induced by seismic events and/or related rockfall causes local barrier degradation from accelerated stress corrosion cracking or rupture of the drip shields (SNL 2007c, Sections 6.1.3 and 6.1.4). However, stress corrosion cracking does not necessarily cause changes to effective material properties that would preclude recognizing a change in conditions while drilling (FEP 1.4.02.04.0A, Seismic event precedes human intrusion, Table 2.2-1) (SNL 2008c, Section 6.2). In particular, a rotating drill bit that encounters a metallic object will behave significantly different than when encountering naturally occurring geologic materials (Section 2.4.3.2.3), even with an imposed residual stress and minor amounts of corrosion and cracking. In contrast, drip shield rupture caused by static or dynamic rockfall loading or impact (SNL 2008a, Section 6.6.1.2) needs to be evaluated with respect to the earliest time a waste package could be penetrated without recognition by the drillers (SNL 2008a, Section 6.7.2.2).

The drip shield rupture (or plate fragility) abstraction due to static and dynamic rock loading is a function of PGV, the thickness of the drip shield plate, and the static load on the plates from rockfall (SNL 2007c, Section 6.8 and Table 6-36). To determine whether drip shield plate rupture can be considered a likely event or not, the probability of drip shield rupture within 10,000 years is estimated by simulating 100,000 sequences of seismic events. The analysis concluded that this probability of plate failure is less than 3.4×10^{-4} in 10,000 years (SNL 2008a, Section 7.3.2.6.1.3.2), which is equivalent to 3.4×10^{-8}/yr and is significantly less than the unlikely/likely event probability threshold. This estimate is an upper bound on the probability of drip shield failure because the estimate assumed drip shield corrosion rates above the 99.99th percentile of the joint distribution for corrosion rate and the minimal value for the volume of intact lithophysal rock that must collapse to fill the drift (30 m^3 per meter).

The drip shield framework can also buckle and thereby cause the plates to settle onto the waste package, which might contribute to an earlier drilling penetration. However, this probability is also sufficiently low that it can be classified as an unlikely event (SNL 2008a, Section 7.3.2.6.1.3.3). In particular, assuming drip shield corrosion rates above the 99.99th percentile of the joint distribution for corrosion rate and the minimal value for the volume of intact lithophysal rock that must collapse to fill the drift (30 m^3 per meter), a simulation of 100,000 sequences of seismic events estimated the upper bound for the probability of drip shield framework failure before 10,000 years at approximately 3×10^{-3}, which is below the likely/unlikely event probability threshold of 0.1 in 10,000 years.

The other mechanism for rupture of a drip shield is from large rock block impacts in the nonlithophysal zones (FEP 1.2.03.02.0B, Stress corrosion cracking (SCC) of drip shields). These probabilities are given in *Seismic Consequence Abstraction* (SNL 2007c, Table 6-54). Given that the drip shield thickness is expected to be no less than 14.3 mm after 10,000 years, the probability of drip shield plate failure is no greater than about 0.06 for a PGV of 1.05 m/s (using linear interpolation between the 15 and 10 mm table entries for "damaged area with 1 drip shield failure"). Thus, similar to the above calculation for plate failure due to static and dynamic loading in the lithophysal zones, the probability of plate failure due to large rock block impacts is less than 0.06 in 10,000 years (since the probability of plate failure is zero for 0.4 m/s events (i.e., events with an annual exceedance frequency of 10^{-4} per year)). This again is less than the likely event threshold of 0.1 in 10,000 years. FEP 1.2.03.02.0B, Stress corrosion cracking (SCC) of drip shields (Table 2.2-1) (SNL 2008c, Section 6.2), is excluded in the overall TSPA based on a low consequence justification; however, the screening justification presented here is with respect to its potential impact on the time of earliest drilling intrusion penetration without recognition.

Based on the above justifications, all drip shield degradation processes associated with seismic ground motion events can be screened out of the human intrusion analysis, and are therefore not used to determine the earliest time of penetration of the drip shield or waste package without recognition.

Even in the unlikely event that a drip shield were damaged by a seismic event in 10,000 years, the chance of a waste package being damaged by seismicity in the same time period, in a way that it would not be recognized by the driller, is very low and below the likely/unlikely event probability threshold (i.e., less than one chance in 10 in 10,000 years). In particular, stress corrosion cracks due to seismically-induced residual stresses in the Alloy 22 would not compromise the structural integrity of the waste package (FEP 1.4.02.04.0A, Seismic event precedes human intrusion, Table 2.2-1) (SNL 2008c, Section 6.2); however, rupture or puncture of a waste package could compromise its structural integrity. However, as demonstrated in *Total System Performance Assessment Model/Analysis for the License Application* (SNL 2008a, Sections 7.3.2.6.1.3.5 and 7.3.2.6.1.3.6), both of these probabilities are less than 0.1 in 10,000 years. They can thus be excluded from the human intrusion scenario. In addition, as indicated in Figure 2.1-10b, open patch breaches due to general corrosion of a waste package occur long after 10,000 years.

2.4.3.2.3 Potential for Waste Package Penetration by Drilling

The following discussion presents several lines of evidence relevant to estimating the time when a human intrusion could occur based upon the earliest time that current technology and practices used for groundwater exploration could lead to waste package penetration without recognition by a driller. There are a number of operational parameters that would alert a driller that a change in downhole conditions would merit additional investigation, including a bit run (the removal of the bit from the hole for review and grading). These downhole conditions include loss of circulation, decreased penetration rate, increased drill string and bit instability, and increased drill string torque caused by differing material properties.

2.4.3.2.3.1 Initial Bit Selection and Drilling Principles

The following discussions regarding the human intrusion analysis are focused on typical practices used in exploratory drilling for water in the southwestern United States, as required by 10 CFR 63.322(c). Generally, the drilling method would be rotary drilling, with the drill string assembly consisting of the drill bit, a drill collar, the drill pipe, and, in some instances, the use of stabilizers. Roller bits are typically used in drilling water wells due to their low cost and wide range of operational flexibility (SNL 2008a, Section 6.7.2.3.1). The initial selection of bit type is usually based on what is known about the formation characteristics. The International Association of Drilling Contractors has developed a classification chart for selecting roller bits. Roller bits with characteristics of 7-1 or 7-2 (hard semiabrasive and abrasive formations) would be selected for drilling through the welded geologic units at Yucca Mountain based on geomechanical properties. Roller bits are designed to take advantage of brittle failure of the rock matrix to crush, break, and remove the rock in an efficient manner. The crushed and broken material is removed from the boring using circulated drilling fluids (air, water, or admixtures thereof) that also cool and clean the drill bit (SNL 2008a, Section 6.7.2.3.1).

In contrast, the failure mechanism that allows milling of ductile materials, such as the milling planned for drip shield and waste package construction, is significantly different from the failure mechanisms that allow drilling through brittle rock, and drill bits designed to induce metal failure mechanisms are not commonly used in exploratory drilling for water in the southwestern United States. Consequently, the type of bits typically used for water well drilling would either be severely damaged or unable to penetrate an intact or partially degraded drip shield and waste package.

2.4.3.2.3.2 Bit Operating Conditions and Change in Conditions

Bit operating conditions (i.e., drilling fluid properties and circulation rates, drill string stability, bit weight, and rotary speed) affect the rate of penetration and vibrations felt on the drill rig. These factors would be affected by the drilling assembly entry into the emplacement drift, and the bit operating conditions would be significantly affected by the rounded geometry of the emplacement drift, drip shield, and waste package.

The loss of drilling fluid circulation and sudden drop in weight on the bit when the drill bit breaks through the top of the emplacement drift would provide initial indications of significantly changed conditions. The loss of circulation would occur because of the flow of drilling fluids from the borehole and into the emplacement drift, which, at 5.5 m diameter and on the scale of a km in length, represents an essentially instantaneous increase in volume compared to the borehole volume. At that point, the driller would either try to continue drilling without compensating for the fluid loss in the hope of passing through the loss zone, try various additives in the drilling fluid to try to seal the formation, or pull the drill assembly and either change drilling methods or install a temporary or permanent casing to seal off the cavity (SNL 2008a, Section 6.7.2.3.2).

In the event of continued drilling, encountering an intact or partially degraded drip shield or waste package would prevent progress, and the lack of cooling from circulated fluids would eventually destroy the drilling bit and result in the drilling assembly being pulled from the hole (or otherwise cause the driller to consider alternative courses of action). Given the volume difference between the borehole and emplacement drift, it is implausible that any amount of additive would resolve the lost circulation problem, again leading the driller to some alternative course of action. Alternative courses of action, such as spot cementing through the loss zone or setting casing through the cavity, would involve pulling the drilling assembly from the borehole. In either scenario, the driller would then encounter continued volumetric problems or problems in trying to set casing due to the presence of the drip shield or waste package within the emplacement drift.

In addition to loss of circulation, the space between the crown or sides of the emplacement drift and the drip shield would cause the operating conditions to become unstable and evidence themselves by a sudden increase in rotation speed as the weight on the drill bit was unloaded, followed by a sudden drop in the drill assembly (i.e., essentially free fall until the drip shield or invert of the drift was encountered), and/or a significant increase in the amount of vibration at the surface. Any of these conditions would cause the destabilization of the drill bit (i.e., allow the bit to change direction from the original concentric alignment) and would trigger a response by the driller to address the change in conditions. This is particularly true as drilling conditions would noticeably change (due to the difference in rock and alloy material properties) if the drilling assembly came in contact with the drip shield material (Sections 2.4.3.2.3.3 and 2.4.3.2.3.4).

The conditions described above are based on the assumption that the drift has not collapsed. Rubble material in a collapsed drift could reduce the degree of these effects on drilling, but would not likely eliminate them. The analysis of drift degradation indicates that during the first 10,000 years, the ground support will completely lose its integrity, and drift degradation will occur due to strength decay of the rock mass within the lithophysal zone (BSC 2004j, Section 6.4.2.4). However, the collapse results in the bulking of, or increase in, the volume of the rock as the rock mass disintegrates into a number of pieces, resulting in increased porosity and overall volume. The resulting bulk properties of the fill are different from that of the intact rock mass. Loss of drilling fluid circulation would still occur, but perhaps could be accommodated by the driller. Additionally, the rubble pile of rocks would tend to move or shift under small loads, and the uneven loading on the drill bit would increase the lateral deviation forces (Bourgoyne et al. 1986, Chapter 5). As such, even if the drifts collapsed, the character of the rubble would be insufficient to stabilize the drill string. Severe wobbling bit action would result as the bit rotates if the drill collars or stabilizers above the bit are not held in a concentric position in the borehole.

2.4.3.2.3.3 Penetration of the Drip Shield and Waste Package

To have any possibility of penetrating an intact or partially degraded drip shield or waste package, the drilling assembly would have to contact the surfaces in an essentially perpendicular orientation. In general, deviation in alignment is caused by the character of the subsurface material. This is because lateral deviation forces increase with relatively small changes in the contact angle between the bit and drilled material (Bourgoyne et al. 1986, Chapter 5). Borehole deviations are also caused if there is too much or too little weight on the drill bit and differences in the pull-down force applied to the drill pipe during rotary drilling. Additionally, the varying hardness of different materials being penetrated deflects the bit from a consistent alignment.

Given that the top of the drip shield is curved and that most groundwater exploration holes are drilled in a near-vertical orientation (i.e., angle and directional drilling are possible, but are not typically used for groundwater exploration purposes due to increased difficulty and cost), the drill bit would have to make contact at the relatively small areas that make up the apex of the drip shield or waste package, where the surfaces are essentially perpendicular to the drill bit orientation. Only the apex of the drip shield or waste package provides a perpendicular surface for which drip shield and waste package geometry would not increase the lateral deviation forces (SNL 2008a, Section 6.7.2.3.3).

If the drilling assembly contacts any location other than the relatively small areas that make up the apex of the drip shield or waste package, then the relatively small drill bit diameter and high rotational speeds, and the increased strength of material used for the drip shield and waste package compared to the geologic materials (Section 2.4.3.2.3.4), would cause large lateral deviation forces and uneven loading on the bit. In turn, this would lead to drilling assembly instability, and the bit would essentially bounce and slide on the top or side of the engineered barriers and potentially cause the drill bit to slip off the drip shield or waste package apex. Consequently, no penetration of the waste package would occur. Furthermore, any non-slip contact with the drip shield or waste package would be accompanied by a noticeable increase in drill string torque and reduced rate of penetration as the bit teeth contacted the metallic alloy. At the surface, the driller would recognize these conditions as a lack of drill bit penetration and excessive vibration. High levels of vibration and correspondingly low rates of penetration, such as those observed with poorly designed bits when crossing hard and abrasive formations, would prompt the driller to adjust the rotary speed and weight-on-bit to reduce shock. In some cases, this could include removing the drilling assembly from the borehole to inspect the bit condition (Putot et al. 2000, p. 118), which would increase the chance for recognition of excessive bit wear and possible recognition that a metallic object had been encountered.

The ability of the drill string to penetrate a waste package as a result of a sudden drop, when the drill bit breaks through the top of the emplacement drift and the weight of the drill string free-falls and potentially impacts the apex of the engineered barriers, has also been considered. First, the drip shield itself would prevent penetration of the bit and drill string through the waste package. The location with the greatest likelihood of drill string penetration is at the drip shield crown (i.e., this would be a higher impact force than a glancing blow on the side of the drip shield). But the drip shield plate is actually strongest at the crown. A more probable impact scenario is that the drill string would hit away from the crown and bend the drip shield plate into contact with the waste package, which would create a more distributed load to the waste package, further reducing the impact velocity on the waste package itself. If the drill string could penetrate the drip shield, much of the impact energy to the waste package would be reduced by the penetration (or crushing) of the drip shield. However, even if the drill string could penetrate the drip shield, structural calculations carried out for the seismic mechanical damage assessment indicate that the drill string could not penetrate the waste package based on the force and energy of a sudden drop (SNL 2008a, Section 6.7.2.3.3).

2.4.3.2.3.4 Comparative Material Strength

Assuming that the drill bit does not slide off the apex of the drip shield, a significant change in downhole conditions would be recognized when the drill string contacts the drip shield because the failure mechanisms of brittle rock (such as that present at the repository host horizon) and ductile alloys (such as the materials used for drip shields and waste packages) differ significantly. These changes in failure mechanisms are so significant that specialized downhole techniques and tools are used to drill through metal. Milling (a technique used for drilling through metal) produces a different failure mechanism than the brittle failure that roller and hammer bits typically produce. Bits designed for drilling rock would not be efficient for drilling through metal and would likely be seriously damaged, and the milling techniques needed to bore metals are not used in rock drilling unless required for specialized applications (SNL 2008a, Section 6.7.2.3.4).

The mechanical properties of brittle and ductile materials, including their failure modes, are different (SNL 2008a, Section 6.7.2.3.4). Therefore, if the differences between milling and rotary drilling tools are ignored and rotary bits could be used to penetrate the engineered barriers, a measure for comparing strength properties between brittle (rock) and ductile (drip shield or waste package) materials is needed to differentiate the effect of the drilling tool on these two types of materials. Various properties could be used, including (1) the modulus of elasticity, (2) a comparison of the tensile strength of brittle materials to the yield strength of ductile materials, (3) a comparison of the compressive strength of rock materials and tensile strength and/or yield strength of metal alloys, and (4) a comparison of the shear moduli (if available) or a value of twice to three times the shear modulus to the modulus of elasticity (SNL 2008a, Section 6.7.2.3.4).

Studies conducted to correlate operational parameters to the rate of drill bit penetration indicate that the rate of penetration ranges from inversely proportional to the square of the strength of the material being drilled to inversely proportional to the strength of the material, all other factors being equal (SNL 2008a, Section 6.7.2.3.4). Assuming that a change in the penetration rate by a factor of

1.5 or greater (increase) or 0.66 or less (decrease) (i.e., some condition occurring before performance collapse) is sufficient to be noticed by a driller, a change in compressive strength of materials by a factor of 1.5 (or possibly less if one assumes the inverse square relationship) would cause a significant change in drilling conditions that would be recognized by the driller.

The mean compressive strength of the rock material ranges from 19.3 to 188.8 MPa (SNL 2008a, Table 6.7-3). At room temperature, the tensile strength (i.e., the peak stress on the stress-strain curve) of the drip shield materials ranges from 345 to 895 MPa (SNL 2008a, Table 6.7-4). Thus, the ratio of strengths ranges from about 1.8 (345/188.8) to as great as 46 (895/19.3). For the waste package material, the tensile strength at room temperature ranges from 550 MPa to 802 MPa (SNL 2008a, Table 6.7-4). This represents ratios of 2.9 (550/188.8) to as great as 42 (802/19.3). If one instead uses the yield strength (stress at which the material begins to deform plastically, which is less than the ultimate tensile strength) of the engineered barrier materials to compare to the rock compressive strength, the ratios decrease. For the drip shield material at room temperature, the factor ranges from 1.5 (275/188.8) to 23 (450/19.3), while for the waste package material at room temperature, the factors range from 1.3 (240/188.8) to as great as 21 (403/19.3) (based on values in *Total System Performance Assessment Model/Analysis for the License Application* (SNL 2008a, Table 6.7-4)). Given that all waste packages include Alloy 22 material in the outer barrier, the lower end of the range is bounded at a factor of 1.9 (358/188.8). Therefore, at room temperature there is a minimum factor of 1.9 for the waste packages and 1.5 for the drip shields. If one assumes an inverse proportionality of rock strength to rate of penetration, the penetration rates would decrease to less than 67% of the rock penetration rate when intersecting a drip shield and to less than 53% of the rock penetration rate when intersecting a waste package and therefore be recognizable, as previously discussed.

At elevated temperatures, such as those during the thermal period (i.e., 200°C), the strength properties of the drip shield material are reduced for Titanium Grades 7 and 16 (SNL 2008a, Section 6.7.2.3.4). The ratio reduces in range from 1.1 (207/188.8) to as great as 12 (228/19.3) based on tensile (drip shield material) and compressive (rock material) strength. However, the properties of the Alloy 22 outer barrier are not as significantly reduced, with a ratio of strengths for the elevated temperature ranges from 3.5 (662/188.8) to 36 (701/19.3). The minimum factor of 1.1 for the drip shield and rock strength comparison at elevated temperature would not by itself sufficiently change the penetration rate to be noticed by a driller. However, further penetration to a waste package, with a larger compressive strength change, would produce a sufficiently reduced penetration rate.

Comparisons based on the compressive strength of the rock and the tensile or yield strength of the engineered materials give large ratios, even at elevated temperatures, that would be recognized by the driller. Comparing the moduli of elasticity shows a minimum ratio of 3.2. These differences in compressive and tensile strengths and modulus of elasticity between the brittle rock and ductile engineered barrier materials would further contribute to lack of drill bit penetration and excessive vibration (SNL 2008a, Section 6.7.2.3.4).

Finally, the recognizable differences in penetration rate or vibrations are only applicable in the improbable situation of a rock drill bit hitting sufficiently near the engineered barrier apex to avoid bouncing or sliding (such as by impacting a metal crack) to initiate penetration into the engineered barrier. It is more likely that rotary bits for rock, which are not designed for drilling in metal, would simply bounce and slip off either the drip shield or waste package.

The factors described above are applicable even if the waste package internals are degraded to the point where waste package structural strength is lost or, in the case of the drip shield, the interlock mechanism is bent and penetrated by the drilling assembly.

2.4.3.2.3.5 Summary of Waste Package Penetration by Drilling

Selection of a bit for drilling involves knowledge of the characteristics of the rock. There are significant differences between the tensile strengths and other material properties of the geologic units at Yucca Mountain and the materials used for the drip shield and waste package. Because the materials used in the drip shields and waste packages have high tensile and yield strengths, and increased modulus of elasticity compared to the host rock properties, the teeth of a roller bit cannot penetrate deeply enough to cause sufficient strain for chipping to occur. Rather, if contact with the drip shield occurs, the rotation of the bit would result in a tearing or shearing action with associated and recognizable high torque values. Consequently, the ductility of the metals makes them nearly impenetrable by techniques used in drilling rock. Boring in metals typically requires using a milling technique. The downhole milling tools needed to penetrate an intact or partially degraded drip shield and waste package are not typically used in groundwater exploration, and the use of such tools would clearly indicate the recognition of penetration of some type of metallic, anthropogenic structure.

2.4.3.2.4 Earliest Time of Waste Package Penetration by Human Intrusion—Analysis Summary and Findings

Conclusions based on information presented above suggest that penetration of the drip shield and/or waste package would be recognized by the drillers if it were to occur before the waste packages and drip shields had sufficiently degraded. In particular, general corrosion of the drip shield is not expected to fail the drip shield plates before 230,000 years (Section 2.4.3.2.1). Prior to that time, neither general corrosion thinning nor stress corrosion cracking induced by seismic ground motion are expected to affect the integrity of the drip shield or waste package in such a way that a rotating drill bit and drill string could penetrate either feature without the recognition of a man-made barrier because the failure mode and drill bit interaction are significantly different for rock and metals, as discussed in Section 2.4.3.2.3. In general, until a rupture of the drip shield occurs, the structural integrity of the waste package is also maintained, providing an additional barrier to drill-bit penetration.

The analysis provided in this section demonstrates that an unrecognized intrusion will not occur prior to 10,000 years following closure of the repository, and that several possible modes of drip shield and waste package damage that might contribute to drilling penetration of the drip shield or waste package can be screened out as unlikely (per proposed 10 CFR 63.342(b)), including early failure and all damage modes related to seismicity. Considering the robustness of the waste package to general corrosion patch failure, as discussed in Section 2.4.3.2.1, an intrusion event unrecognized by the drillers would occur much later than 10,000 years. For example, there is only a 5% chance of having a general corrosion patch opening on a waste package prior to about 600,000 years (Figure 2.1-10b).

Thus, for the TSPA human intrusion scenario, the human intrusion event time based on drip shield general corrosion and observable effects on the drilling system is considered to occur no earlier than

200,000 years. This is a conservative assumption, as there is only a 0.0001 chance of drip shield general corrosion failure prior to 230,000 years and because waste package degradation (formation of open breaches) takes significantly longer than this. Thus, until some time after 230,000 years, there is a double barrier to drilling penetration of the waste forms. For the stylized human intrusion scenario, 200,000 years is conservatively assumed to be the earliest time a driller could penetrate a waste package without recognition. The dose results described below use this conservative intrusion time, without uncertainty.

2.4.3.3 Evaluation of Human Intrusion Dose to RMEI

[NUREG-1804, Section 2.2.1.4.2.3: AC 2, AC 3(4)]

As required by 10 CFR 63.113(d), a performance assessment was developed for the human intrusion standard that meets the requirements of 10 CFR 63.322. The probabilistic projections provide an estimate of the annual dose to the RMEI resulting from a stylized human intrusion drilling scenario, which is compared to the individual protection standard for human intrusion in proposed 10 CFR 63.321(b), paraphrased here as follows:

Based upon the time of intrusion, DOE must demonstrate that there is a reasonable expectation that the RMEI would receive no more than the following annual dose as a result of the human intrusion:

- A mean of 0.15 mSv (15 mrem) for 10,000 years following disposal

- A median of 3.5 mSv (350 mrem) after 10,000 years, but within the period of geologic stability.

This section discusses the results of the performance assessment that was conducted to evaluate compliance with these limits.

2.4.3.3.1 Annual Dose to the RMEI for the Human Intrusion Standard

To address the second requirement of the human intrusion standard (proposed 10 CFR 63.321(b)), a probabilistic TSPA, analogous to that used to demonstrate performance with the individual protection and groundwater protection standards (proposed 10 CFR 63.311 and 10 CFR 63.331), was conducted to make projections of the annual dose to the RMEI following a human intrusion event. The calculations of annual dose account for only the radionuclides released into groundwater pathway as a consequence of the intrusion, as specified in 10 CFR 63.322(f) and (g). Based on the analysis described in Section 2.4.3.2, the earliest time after disposal for the drilling intrusion is considered to be 200,000 years.

The type of waste package (i.e., commercial SNF or codisposal) penetrated is sampled in the TSPA so that the expected annual dose reflects the variability in the various waste forms (Section 2.4.3.1.4). Based on the proportion of emplaced waste package types, the probability of sampling a commercial SNF waste package is about 0.7, whereas the probability of selecting a codisposal waste package is about 0.3. The location of the penetration in the repository footprint is also sampled to reflect the range of percolation fluxes that induce waste-form dissolution and releases, as well as the entry point of the borehole and radionuclide releases into the saturated zone.

The incorporation of the aforementioned aleatory uncertainties into the calculation of both expected annual dose and total mean annual dose is described in Section 2.4.3.1.4, Equation 2.4-43.

As described in Sections 2.4.1 and 2.4.2.2.1.1.1, each of the total annual dose curves in the distribution of dose curves is an expectation over aleatory (irreducible or stochastic) uncertainty, which effectively averages out the uncertainty attributable to random occurrences, such as the type and location of the intersected waste package. Because each total annual dose curve (300 in the TSPA) is an expectation over aleatory uncertainty, each curve is called an "expected annual dose curve." The total mean or median annual dose curve is then computed by either applying the expectation (mean) operation or the median (50th percentile) operation at each point in time to this distribution of expected annual dose curves, as illustrated in Figure 2.4-8.

The expected annual dose histories (summed over all radionuclides) computed according to Equation 2.4-43 are shown in Figure 2.4-11 for the post 10,000-year period (i.e., these results will be compared to the individual protection standard for human intrusion at proposed 10 CFR 63.321(b)(2) for performance after 10,000 years but within the period of geologic stability). The mean, median, and 5th and 95th percentile curves are superimposed on each plot. The mean annual dose history, which is plotted as the red curve, is computed by taking the arithmetic average of the 300 expected annual dose values at each time τ along the curves. Similarly, the median dose history, plotted as the blue curve, is constructed by sorting the 300 expected values from lowest to highest at each time τ, and then averaging the two middle values. Curves for the 5th and 95th percentiles are also plotted to illustrate the uncertainty in the expected annual dose histories; 90% (or 270 of the 300 epistemic realizations) of the projected dose histories fall between these two percentile curves. The maximum median annual dose to the RMEI occurs at about 2,500 years after the intrusion event and is estimated to be less than 0.011 mrem, which is well below the regulatory limit of 350 mrem (10 CFR 63.321). The spread of values about the median annual dose is reflected in the 5th and 95th percentiles, which are approximately 0.0012 mrem and 0.029 mrem, respectively, at the time when the median achieves its maximum value.

The contributions of individual radionuclides for the human intrusion scenario to the total mean annual dose for the 1,000,000-year period after repository closure are shown in Figure 2.4-159. All dose curves on this figure are mean annual dose curves (as defined in Section 2.4.2.1.2). After the intrusion there is an initial pulse of highly soluble, non-sorbing radionuclides, such as ^{99}Tc (half-life 2.13×10^5 yrs) and ^{129}I (half-life 1.57×10^7 yrs), which dominate the maximum of the mean annual dose, and account for about 99% of the maximum median annual dose. After the pulse of ^{99}Tc and ^{129}I, the long-term dose to the RMEI occurs primarily from ^{242}Pu (half-life 3.75×10^5 yrs), with secondary contributions from ^{135}Cs (half-life 2.3×10^6 yrs) and ^{237}Np (half-life 2.14×10^6 yrs). As in a number of other modeling cases, such as the early-failure cases, ^{242}Pu is the most important dose contributor to expected annual dose at later times, after the highly soluble, nonsorbing radionuclides, such as ^{99}Tc and ^{129}I, have passed through the system. A comparison of the dose contributors for the human intrusion modeling case with those in the waste package early failure modeling case is given in Section 2.4.3.3.5.2.

As outlined in Section 2.4.3.4.3, the uncertain inputs that have the greatest influence on the uncertainty in expected annual dose following the human intrusion event are those identified for the transport of ^{99}Tc. These are the uncertainty in radionuclide content of commercial SNF (*CSNFMASS*), the logarithm of the scale factor that characterizes uncertainty in groundwater specific discharge (*SZGWSPDM*), and the infiltration scenario (*INFIL*). These variables determine the amount of ^{99}Tc and ^{129}I in the intruded waste package and the rate at which these radionuclides move through the Lower Natural Barrier (SNL 2008a, Section 8.1.3.2 [a]). After the initial pulse of ^{99}Tc and ^{129}I, sensitivity analyses identify several variables with influence on the uncertainty in the long-term expected annual dose that are primarily related to the mobilization of plutonium from the waste and to the rate of plutonium transport through the Lower Natural Barrier.

Thus, dose projections for the human intrusion performance assessment support a finding that there is a reasonable expectation the median annual doses to the RMEI would be well below the individual protection standard for human intrusion (SNL 2008a, Section 8.1.3.2[a]), specified at proposed 10 CFR 63.321.

2.4.3.3.2 Treatment of Likely Waste Package Degradation Processes

Section 2.4.3.2.2 described the screening of unlikely drip-shield degradation FEPs from the analysis of the earliest time after disposal that drilling penetration could occur without recognition. As noted, this earliest time is based on drip shield degradation, rather than actual waste package penetration. It also indicated that seismic rupture or puncture damage of a waste package, even in the unlikely event of a drip shield failure, are in themselves unlikely. However, all likely FEPs are to be included in the human intrusion performance assessment, consistent with proposed 10 CFR 63.342(b). For drip shield degradation, only the general corrosion process is considered a likely FEP, while for waste package degradation both nominal corrosion processes and seismic degradation of codisposal waste packages are likely FEPs. However, the effects of these likely waste package degradation FEPs are treated conservatively in this human intrusion analysis by effectively screening out their effects. In particular, as implied by 10 CFR 63.322, the main focus of the human intrusion scenario is on the incremental dose possible due to drilling penetration. Dose to the RMEI arising from nominal corrosion processes or likely seismic degradation FEPs is already part of the overall TSPA. Therefore, the only reason for including these FEPs in the human intrusion TSPA is if they could increase the dose due to a drilling penetration of a single waste package (SNL 2008a, Section 6.7.2.5). However, the opposite is true, as explained below.

It is probable, based on the results of the seismic ground motion modeling case (Section 2.4.2.2.1 and Figure 2.1-12), that codisposal packages will fail by seismically induced stress corrosion cracks before the postulated human intrusion event at 200,000 years, even for smaller ground motions that occur at annual frequencies greater than 10^{-5} per year (the likely/unlikely event probability threshold) (SNL 2008a, Section 6.7.2.5). For example, as described in *Total System Performance Assessment Model/Analysis for the License Application* (SNL 2008a, Section 7.3.2.6.1.3.7), the maximum frequency of events that causes stress corrosion cracking damage to a codisposal waste package is estimated to be 2.181×10^{-5} per year. For a Poisson process at this occurrence frequency, this is a 98.7% chance of one or more damaging seismic events within 200,000 years [$= 1 - \exp\{(-2.181 \times 10^{-5}/\text{yr})\,(2 \times 10^{5}\ \text{yrs})\}$]. Ignoring diffusive radionuclide releases through these cracks prior to the time of the drilling intrusion is conservative, however, because accounting for these diffusive releases would reduce the radionuclide content of the waste package, and consequently lower the ^{99}Tc and ^{129}I peaks that occur just after the time of intrusion at 200,000 years (Figure 2.4-159). Releases through these cracks would have smaller, but also conservative, effects on the actinide releases. The same logic applies to possible waste package damage prior to 200,000 years due to nominal stress corrosion cracking processes. The mean probability, i.e., the expectation over epistemic uncertainty, of seismic crack damage to codisposal waste packages under intact drip shields prior to 200,000 years is 0.54, which can be compared to the maximum probability of 0.987 quoted above. This is the average over the entire PGV range of the seismic hazard curve and over the entire range of epistemic uncertainty (e.g., uncertainty in the Alloy 22 residual stress threshold).

Regarding likely seismic crack damage and nominal corrosion damage (either cracks or patches) subsequent to the drilling intrusion penetration, these releases and subsequent dose are already included in the overall TSPA. Inclusion of these releases could only serve to lower the dose attributable to release down the borehole pathway, since the cracks and patches provide an avenue of escape into the unsaturated zone at spatial locations different than the borehole location (i.e., the occurrence of seismic crack damage and nominal corrosion patches and cracks would generally occur on a part of the waste package surface not in contact with the borehole pathway). Thus, these seismic or nominal waste package breaches would not contribute in any way to increasing the possible concentration of radionuclides in the water flowing down the borehole. In fact, if included, the releases associated with these patches and cracks would lower the concentration of radionuclides flowing down the borehole for nuclides that are not solubility-limited, such as ^{99}Tc and ^{129}I.

In summary, general corrosion and likely seismic degradation of the waste package can be conservatively omitted from the human intrusion TSPA, and are not part of the annual dose results shown in Section 2.4.3.3.

2.4.3.3.3 Statistical Stability of the Mean Annual Dose

This section addresses the NUREG-1804, Section 2.2.1.4.2.3, Acceptance Criterion 2(3) relating to statistical stability of the mean annual dose curve for human intrusion: “A sufficient number of realizations has been run using the total system performance assessment code, to ensure that the results of the calculations are statistically stable.” As mentioned in Section 2.4.2.2.2, stability relates to how much variability is observed in the outcome of interest, as model results are repeatedly calculated with different samples. The methodology used to compute statistical stability of the human intrusion TSPA is the same used for the overall TSPA, described in Section 2.4.2.2.2.

As described in Section 2.4.2.2.2.2, stability with respect to epistemic uncertainty is based on a replicated sampling procedure that uses three statistical replicates (three different random seeds) each of size 300 to generate TSPA model results. The mean annual dose and the distribution of uncertainty in the expected annual dose are compared for the three replicates. The three sample means are used to compute an overall mean and a 95% confidence interval about the overall mean. The confidence interval is displayed as an upper and lower bound. At each point in time, the overall mean annual dose is less than the upper bound of the confidence interval with probability 0.975.

Figure 2.4-160a shows the mean annual dose for each of the three replicates of the human intrusion modeling case, along with the median and the 5th and 95th percentiles of the distribution of uncertainty in the expected annual dose. Figure 2.4-160b displays the confidence interval for this modeling case. The high degree of similarity among the statistical metrics for the replicates and the very narrow confidence interval indicates that the mean annual dose for this modeling case is estimated quite accurately, and the epistemic sample size of 300 is more than adequate (SNL 2008a, Section 7.3.1).

2.4.3.3.4 Stability of the Expected Annual Dose

Numerical stability of the expected annual dose for the human intrusion scenario is demonstrated similarly to the way it is demonstrated for the overall TSPA, as described in Section 2.4.2.2.2.3. The TSPA model calculates expected annual dose $\overline{D}_{HI}(\tau|\mathbf{e}_i)$ for the human intrusion modeling case for each epistemic realization $\mathbf{e}_i$ (i.e., the expectation of dose over aleatory uncertainty, but conditional on epistemic uncertainty) as described by Equation 2.4-43 in Section 2.4.3.1.4. Equation 2.4-43 is numerically evaluated using a Monte Carlo technique (specifically, with a Latin hypercube sample). One drilling intrusion is modeled, and the time of intrusion is fixed at 200,000 years. For each of the 300 epistemic realizations $\mathbf{e}_i$, a Latin hypercube sample of 30 aleatory realizations $\{r_j, q_j, SR_j\}$ is generated, describing the type of waste package r_j, the percolation rate q_j, and the saturated zone source region SR_j at the location of the intrusion. For each combination of epistemic and aleatory realization, annual dose at time τ from an intrusion, $D_{HI}(\tau|[1, r_j, q_j, SR_j], \mathbf{e}_i)$, is calculated using the GoldSim component of the TSPA model, and is used in Equation 2.4-43 to compute expected annual dose (SNL 2008a, Section 7.3.2.8).

To demonstrate that the expected annual dose calculations are numerically stable, the size of the aleatory sample is increased from 30 to 90, and expected annual dose is calculated for the first five epistemic realizations. Figure 2.4-161 compares expected dose for the two aleatory sample sizes. Increasing aleatory sample size has no significant effect on the expected dose. Hence, an aleatory sample size of 30 is adequate to obtain a numerically stable estimate of expected annual dose.

2.4.3.3.5 Reasonableness and Consistency of Human Intrusion Repository Performance

Similarly to the discussion in Section 2.4.2.2.3, with respect to the overall performance assessment (in the absence of human intrusion), there are a number of methods and analyses that help to demonstrate that the human intrusion repository performance assessment is consistent with overall repository performance assessment and with the characteristics of the postulated human intrusion event, as described by NUREG-1804, Section 2.2.1.4.2.3, Acceptance Criterion 2(4). For example, detailed explanations of the dependency of dose on the most important uncertain parameters that characterize individual model components can be found in Section 2.4.3.4.3, which is the presentation of uncertainty propagation in the human intrusion modeling case. Thus, Section 2.4.3.4.3 helps address Acceptance Criterion 2(4). In the present section, however, in-depth descriptions are presented of how the dose behavior is consistent with the behavior of the subsystems, through the detailed explanation and analysis of a selected single realization from the set of 300 epistemic realizations. As described in Section 2.4.2.2.3, single-realization deterministic analyses provide a useful insight into the interaction of TSPA submodels. They help in understanding the coupling of the EBS, unsaturated zone, and saturated zone transport models and how their behavior influences the annual dose to the RMEI in a given realization, which provides confidence that the submodels are coupled as intended and their behavior can be explained in a logical manner leading to the dose result. The methodology for selecting a single realization for analysis has already been described in Section 2.4.2.2.3.

The single-realization analysis described below helps demonstrate that the human intrusion repository performance is consistent with the component models and the characteristics of the human intrusion event (e.g., the characteristics of the borehole pathway and the timing and nature of the degradation of the EBS components). Another part of this acceptance criterion is to demonstrate consistency of human intrusion performance with overall repository performance. This is also demonstrated by the single-realization analysis. However, another method of showing this is to compare the human intrusion repository modeling case with one of the modeling cases for repository performance in the absence of human intrusion. This is also described in Section 2.4.3.3.5.2.

2.4.3.3.5.1 Single-Realization Deterministic Analysis for the Human Intrusion Modeling Case

This section presents an analysis of a single realization from the 9,000 realization base-case run performed for calculating the expected dose for the Human Intrusion Modeling Case for the 1,000,000 year simulation duration. The expected annual dose is presented in Figure 2.4-162, where each of the 300 annual dose curves represents expected annual dose for one epistemic uncertainty vector. The expected annual dose for each epistemic uncertainty vector is generated by taking an expectation over a sample of 30 aleatory uncertainty vectors (Section 2.4.3.1.4). A single epistemic vector is selected for further analysis such that its expected annual dose is broadly representative of the modeling case and similar in behavior to the mean annual dose curve (Figure 2.4-162). The epistemic uncertainty vector 277 ($\mathbf{e}_{277}$) is selected for further analysis.

The thirty aleatory sampling vectors corresponding to $\mathbf{e}_{277}$ are GoldSim Realizations 8,281 through 8,310 (Figure 2.4-163). The thirty aleatory vectors fall into two annual dose groups: (1) the group with higher dose represents those realizations in which a commercial SNF waste package is selected, and (2) the group with lower dose represents those realizations in which a codisposal waste package is selected. The specific realization selected for further analysis is GoldSim Realization 8,309 (Figure 2.4-163), which is chosen from the first group (representing releases from a commercial SNF waste package). Realization 8,309 represents aleatory uncertainty vector 29 ($\mathbf{a}_{29}$), in which the commercial SNF waste package breached from a human intrusion event is located in percolation subregion 4 of the EBS and where the mass from the unsaturated zone borehole is passed to saturated zone source region 1.

In the stylized human intrusion modeling case, a borehole pathway is modeled as being drilled directly through a single drip shield and waste package vertically down to the water table. The time of this intrusion, which is assumed to result from exploratory drilling for groundwater, is fixed at 200,000 years (Section 2.4.3.2.4). Once the waste package is breached, the waste form is mobilized by nominal degradation processes to the vertical unsaturated zone borehole pathway. The vertical borehole pathway is modeled as being 190 meters in length and conceptualized as a dual-porosity medium consisting of a discrete vertical fracture surrounded by matrix consisting of rubble from partial collapse of the borehole. The fracture is assumed to be open so that the water that flows in the borehole moves through the fracture pathway. Also, the radionuclide mass released from the waste package (by diffusion and advection) is passed to the fracture pathway where it undergoes vertical advection within the fracture and lateral diffusion into the surrounding matrix due to fracture-matrix interaction. The single vertical fracture extends from the penetrated waste package to the water table. No retardation of colloids or solute is modeled on the fracture surface although species-dependent sorption coefficients are applied in the matrix (SNL 2008a, Section 6.7). Once in the saturated zone, radionuclides are transported to the accessible environment according to the one-dimensional and three-dimensional saturated zone transport models used for all other groundwater modeling cases (SNL 2008a, Section 6.1.4).

The major radionuclides contributing to annual dose for Realization 8,309 ($\mathbf{e}_{277}$, $\mathbf{a}_{29}$) are shown on Figure 2.4-164, along with the total annual dose for this modeling case. ^{99}Tc and ^{129}I are the major early dose contributors (before 300,000 years) following the waste package breach at 200,000 years, whereas ^{242}Pu becomes the dominant dose contributing radionuclide later on (with lesser contributions from ^{237}Np, ^{135}Cs, ^{79}Se, and ^{233}U). The early contribution to dose from ^{99}Tc and ^{129}I occurs because they travel unretarded through the waste package, the unsaturated zone borehole pathway, and the saturated zone. By contrast, ^{242}Pu, ^{237}Np, ^{135}Cs, ^{79}Se, and ^{233}U are retarded in these transport pathways to varying degrees and therefore contribute to dose much later. Because ^{99}Tc and ^{242}Pu are the dominant radionuclides with very different transport properties, they were chosen for further analysis.

The cumulative mass release of ^{99}Tc and ^{242}Pu from the waste form inventory following the failure of one commercial SNF waste package is shown on Figure 2.4-165. The waste form starts degrading following the breach at 200,000 years and, due to the relatively slow commercial SNF degradation rate (about 6.9×10^{-5} per year), it requires about 70,000 years to degrade 99% of the waste form. The rate at which ^{99}Tc is released from the degraded waste form and from the corrosion products in the waste package is shown on Figure 2.4-166. Because the dissolved concentration of ^{99}Tc is not limited by a solubility controlling solid, the mass of ^{99}Tc released from the degrading waste form is quickly transported out of the waste package by advection and diffusion. In this realization, the volumetric water flux through the waste package (and going to the unsaturated zone borehole) is calculated to be about 8.7×10^{-4} m^3/yr (which is equal to the calculated percolation rate of about 26.9 mm/yr times the borehole cross-sectional area of 0.0324 m^2 (SNL 2008a, Table 6.7-5)). However, this is a relatively low advective flux, which results in higher diffusive releases than advective releases through the waste package (in both waste form and corrosion products domains). Nevertheless, the mass release rate from the intruded waste package is still very high because of the implementation of a zero concentration boundary just outside the waste package to maximize the concentration gradient. Almost all of the ^{99}Tc mass is released by about 300,000 years, as indicated by the negligibly small release rates past this time period (Figure 2.4-166). The commercial SNF waste form degradation rate is the primary control on the release of ^{99}Tc out of the waste package. After the ^{99}Tc mass is made available for transport (i.e., mobilized by waste form degradation), it is transported out of the waste package with no appreciable delay.

The ^{242}Pu mass release from the waste form domain and the corrosion products domain of the waste package are shown on Figure 2.4-167. ^{242}Pu is modeled as being transported both as dissolved and reversibly sorbed on colloids (denoted as aqueous) and as irreversibly sorbed onto iron oxyhydroxide colloids and waste form colloids. Note that commercial SNF waste form colloids remain unstable throughout the simulation, so they contribute negligibly to the total mass released, whereas iron oxyhydroxide colloids remain unstable only until about 220,000 years, and thereafter contribute to the mass released. The diffusive release of ^{242}Pu (dissolved and reversibly sorbed on colloids) exceeds advective releases because most of the ^{242}Pu mass remains dissolved, with very little being reversibly sorbed onto groundwater and uranium mineral colloids. However, the mass that is irreversibly sorbed on the iron oxyhydroxide colloids is predominantly transported by advection (Figure 2.4-167) through the corrosion products, due to the small diffusion coefficient of colloids.

The concentrations of ^{242}Pu that is dissolved, and that which is irreversibly sorbed onto iron oxyhydroxide colloids, are both shown on Figure 2.4-168 for the waste form domain and the corrosion products domain. The dissolved concentration in the waste form domain is limited by the solubility of plutonium dioxide (PuO_2) in the waste form domain for several hundred thousand years following the breach. Because the solubility of PuO_2 is low, most ^{242}Pu mass from the degraded waste form is precipitated in the waste form domain. Plutonium is gradually depleted from the waste form domain by diffusion and advection, and not until 748,000 years is enough mass depleted so as to cause the plutonium concentration inside the waste form domain to drop below the solubility limit. The dissolved concentration of ^{242}Pu in the corrosion products domain remains small initially, as ^{242}Pu is sorbed onto corrosion products whose mass increases over time from degradation of steel. By 320,000 years, all of the steel in the corrosion products domain is degraded, and the maximum sorption capacity for corrosion products domain is reached. As ^{242}Pu continues to be transported from the waste form domain to the corrosion products domain, the dissolved concentration of ^{242}Pu in the corrosion products domain starts to build up after 320,000 years, reaching the solubility limit in that domain, which is maintained until all ^{242}Pu mass has been depleted in the waste form domain and the concentration of ^{242}Pu drops at 748,000 years (Figure 2.4-168). The concentration of ^{242}Pu in the corrosion products domain after this time is maintained by kinetically limited desorption of ^{242}Pu mass from the corrosion products. The concentration of ^{242}Pu that is irreversibly sorbed onto iron oxyhydroxide colloids also keeps increasing until about 748,000 years and then declines slowly as iron oxyhydroxide colloids are transported out, predominantly by advection (Figure 2.4-167). Because the concentration of ^{242}Pu irreversibly sorbed onto iron oxyhydroxide colloids is not limited by solubility, it exceeds the dissolved concentration within a short period. Nevertheless, because the diffusion coefficient of colloids is calculated to be much smaller than the diffusion coefficient of dissolved plutonium (by a factor of about 700), the diffusive mass flux of ^{242}Pu (aqueous), which is mostly dissolved mass, exceeds the advective mass flux of ^{242}Pu irreversibly sorbed onto iron oxyhydroxide colloids (Figure 2.4-167).

The mass released from the waste package is passed into the unsaturated zone borehole that consists of dual porosity fracture and matrix media. The borehole is modeled using the GoldSim pipe element pathway, where only one-dimensional vertical transport is considered. All of the mass released from the waste package is placed in the single vertical fracture, where it advects downward by gravity-driven unsaturated flow and diffuses laterally into the surrounding matrix medium. The volumetric flux of water applied to the fracture pathway is the same as that applied to the waste package (about 8.7×10^{-4} m^3/yr), which results in an average linear velocity of about 82 m/yr through the fracture medium, based on the fracture plan area of 4.2×10^{-4} m^2, fracture saturation of 0.025, and no infill material in the fracture. Thus, for a radionuclide species where fracture-matrix interaction is ignored, the travel time through the borehole length of 190 m should be less than three years.

The mass release of ^{99}Tc from the unsaturated-zone borehole virtually overlaps the mass release from the waste package (Figure 2.4-169), indicating negligible delay. This is expected because no retardation is modeled for ^{99}Tc. The release rate from the saturated zone is comparable with that of the waste package and unsaturated-zone borehole, indicating rapid transport through the saturated zone. The release rates for the dissolved and reversibly sorbed ^{242}Pu (denoted as aqueous) from the waste package, unsaturated zone borehole, and saturated zone are shown in Figure 2.4-170. The release rates out of the borehole are considerably smaller than the incoming release rates from the waste package. This is attributed to retardation in the matrix once the mass diffuses into the matrix from the fractures. The K_d for plutonium in the matrix is sampled to be about 115 mL/g (0.115 m^3/kg), which results in an effective retardation of about 1550 (using the matrix bulk density of 1980 kg/m^3 and matrix water content of 0.15). Because of the sorption, the concentration of ^{242}Pu in the matrix medium is reduced, thereby increasing the diffusive gradient (and diffusive flux) from the fracture to matrix thus limiting the mass available for advective transport through the fracture. The release rates out of the saturated zone are lower than that for the unsaturated zone borehole due to further retardation in the saturated zone volcanic and alluvium units.

The cumulative mass releases from the waste package, unsaturated zone borehole, and saturated zone for the ^{99}Tc, ^{242}Pu (aqueous) and ^{242}Pu (irreversibly sorbed on colloids) are shown in Figure 2.4-171. The cumulative releases of ^{99}Tc out of the waste package, unsaturated zone, and saturated zone virtually overlap indicating negligible retardation. Similarly, negligible retardation is indicated for ^{242}Pu (irreversibly sorbed on colloids) as the cumulative releases out of the waste package, unsaturated zone, and saturated zone virtually overlap. The fracture-matrix diffusive interaction for the mass irreversibly sorbed on colloids is not modeled in the unsaturated zone borehole and the saturated zone pathway due to the small diffusion coefficient of colloids. Thus the mass of ^{242}Pu irreversibly sorbed on colloids that is introduced into the unsaturated zone borehole fracture stays in the fracture and is advected out quickly. In the saturated zone some retardation of the colloids due to interaction with the fracture surfaces is modeled but the effects are small. In contrast, the cumulative mass released from the unsaturated zone borehole for ^{242}Pu (aqueous) indicates that at the end of the simulation (1,000,000 years) only a negligibly small fraction (< 0.004) of the mass released from the waste package is released out of the unsaturated zone borehole, and, of the mass released from the unsaturated zone borehole, only about half is released out of the saturated zone. Finally, even though the ^{242}Pu (aqueous) release is higher out of the waste package compared to the release of irreversibly sorbed ^{242}Pu mass on colloids, because of retardation of ^{242}Pu (aqueous) in the unsaturated zone borehole, the release of ^{242}Pu irreversibly sorbed on colloids becomes relatively larger out of the unsaturated zone borehole.

The ^{242}Pu mass irreversibly sorbed on colloids coming out of the unsaturated zone borehole is partitioned into a fast traveling fraction and a slow traveling fraction before being passed to the saturated zone. Almost all of the ^{242}Pu mass irreversibly sorbed (99.8%) travels as a slow fraction in the saturated zone with some retardation of the colloid particles in the volcanic units and alluvium while the remainder travels unretarded as a fast fraction. All of the mass from the unsaturated zone borehole is passed into the saturated zone source region 1, which is the source region chosen as part of the aleatory uncertainty in this realization. The mass release out of the saturated zone for ^{99}Tc, ^{242}Pu (dissolved and reversibly sorbed on colloids, denoted as aqueous), ^{242}Pu (irreversible on colloids traveling slowly), and ^{242}Pu (irreversible on colloids traveling fast) is shown in Figure 2.4-172. The long tail in the ^{99}Tc release past 300,000 years, after most of the mass has been released, results from fracture-matrix interaction in the saturated zone where the mass is released back into the fractures from the matrix.

The saturated zone releases are converted into annual dose by taking the annual releases out of the saturated zone for each radionuclide, dissolving them in the 3,000 acre-ft of water (annual usage at RMEI as defined by the regulation) to compute the mass concentrations, converting the mass concentration into concentration of radioactivity (in curies per liter of water), and then multiplying with the corresponding BDCFs. The end result of this is Figure 2.4-164, where dose for total ^{242}Pu (combined mass in dissolved state, reversibly associated with colloids, and irreversibly associated with colloids) is shown.

2.4.3.3.5.2 Comparison of the Human Intrusion Modeling Case with the Waste Package Early Failure Modeling Case

Human intrusion repository performance can be compared for consistency with overall repository performance as suggested by Acceptance Criterion 2(4) of NUREG-1804, Section 2.2.1.4.2.3; however, as outlined in the previous section, there are a number of important differences related to radionuclide mobilization and transport, as well as simply the timing of initial releases, which make it difficult to draw exact analogies. The most straightforward comparison is merely to realize that the submodels used in the human intrusion performance assessment are the same as those used in the overall performance assessment, except as noted in Sections 2.4.3.1 and 2.4.3.2. Nevertheless, although a number of important differences are present, such as the unsaturated-zone borehole pathway, an analogy between the human intrusion modeling case and the waste package early failure modeling case can be made. For example, both the waste package early failure modeling case and the human intrusion modeling case have an expected number of failed waste packages equal to approximately one (Section 2.4.2.2.1.2.4), and the expected annual dose curves represent an average of both commercial SNF and codisposal waste package behavior over all percolation subregions. Because the high solubility, nonsorbing radionuclides are the least affected by differences in the radionuclide mobilization and transport models, the similarities between the two cases is greatest for these two radionuclides, as borne out by a comparison of Figure 2.4-36b with Figure 2.4-164. In both cases, ^{99}Tc and ^{129}I are released as a sharp pulse at the time of failure and their peak doses are similar, being about 0.01 mrem shortly after waste package failure for both the waste package early failure modeling case and the human intrusion modeling case. Another radionuclide that has similar behavior between the two modeling cases is ^{135}Cs, which again has high solubility and is little affected by the mobilization behavior in the waste package, such as differences in in-package chemistry (SNL 2008a, Section 8.1.3.2[a]). It has a broad peak in both cases of about 2×10^{-5} mrem. Furthermore, EBS diffusive transport dominates EBS releases of fission products for both the human intrusion modeling case (Section 2.4.3.3.5.1) and the waste package early failure modeling case (because of the presence of the drip shield). This similarity of diffusive transport is most apparent for radionuclides with no colloidal or sorption processes inside the waste package, such as ^{99}Tc, ^{129}I, and ^{135}Cs, which is borne out by the similarities in behavior of these three radionuclides shown on Figures 2.4-36b and 2.4-164.

Low solubility, strongly sorbing actinides such as ^{242}Pu contribute strongly to late time dose in both cases but there are important differences in mobilization and transport behavior that make a straightforward comparison infeasible. For example, as indicated in Section 2.4.3.3.5.1, ^{242}Pu releases from the unsaturated and saturated zones in the human intrusion case are dominated by ^{242}Pu sorbed irreversibly on colloids, whereas dissolved ^{242}Pu dominates the waste package early failure modeling case because the colloids remain unstable inside the waste package up to the time of drip shield failure because of high ionic strength, resulting from the lack of advection. In contrast, the advective flux down the borehole pathway in the human intrusion case mobilizes irreversible ^{242}Pu. Finally, ^{239}Pu is important at early times in the waste package early failure case but not in the human intrusion case because of the relatively short half life of ^{239}Pu, which has experienced significant decay by the time of the human intrusion event at 200,000 years.

2.4.3.4 Credibility of the Human Intrusion Results

[NUREG-1804, Section 2.2.1.4.2.3: AC 2(4), AC 3]

The last of the three acceptance criteria in NUREG-1804, Section 2.2.1.4.2.3 deals with the credibility of the TSPA for the human intrusion event. The four specific subcriteria are similar to the comparable acceptance criteria in NUREG-1804, Section 2.2.1.4.1.3 for the overall TSPA code. The subcriteria in NUREG-1804, Section 2.2.1.4.2.3, Acceptance Criterion 3 are as follows:

1. Assumptions made on the method of transport from a breached waste package within the TSPA for evaluating the postulated intrusion event are consistent among different modules of the code. The use of assumptions and parameter values that differ among modules of the code is adequately documented

2. The TSPA code for evaluating human intrusion is properly verified, so that there is confidence that the code is modeling the physical processes in the repository system in a manner consistent with the characteristics of the postulated intrusion event. The transfer of data between modules of the code is conducted properly

3. The estimate of the uncertainty in the performance assessment results is consistent with the uncertainties considered in the characteristics of the postulated intrusion event and with model and parameter uncertainty; and

4. The sampling method used in the TSPA ensures that sampled parameters of the postulated intrusion event have been sampled across their ranges of uncertainty.

Section 2.4.3.4 is organized along the lines of these subcriteria. However, much of the material needed to satisfy these subcriteria has already been presented in Section 2.4.2, in conjunction with the overall TSPA for individual protection. In particular, since (as stated in NUREG-1804, Section 2.2.1.4.2.3, Acceptance Criterion 2(2)), the human intrusion TSPA is identical to the overall TSPA for individual protection, except for the occurrence of the human intrusion event and the exclusion of unlikely FEPs, much of the material relating to the credibility of the human intrusion TSPA will be described by reference to corresponding sections in Section 2.4.2. First is a brief discussion on the consistency of assumptions related to the human intrusion event (Section 2.4.3.4.1). Next is a brief section on verification, validation, and confidence-building activities that mainly refers to comparable activities related to the overall TSPA model and code, but includes some activities specifically related to the human intrusion analysis (Section 2.4.3.4.2). Third is a discussion of an uncertainty and sensitivity analysis conducted specifically for the human-intrusion TSPA (Section 2.4.3.4.3). Last is a brief section that references the sampling method used for the overall TSPA, since it is the same as that used in the human intrusion TSPA (Section 2.4.3.4.4).

2.4.3.4.1 Consistency of Assumptions and Parameter Values for the Human Intrusion

[NUREG-1804, Section 2.2.1.4.2.3: AC 3(1)]

This section addresses NUREG-1804, Section 2.2.1.4.2.3 Acceptance Criterion 3(1), relating to consistency of assumptions regarding “the method of transport from a breached waste package,” as well as differences regarding assumptions and parameter values among modules of the TSPA model. As discussed in Section 2.4.3.1, the method of transport in the saturated zone is the same in the human intrusion TSPA as the overall TSPA, even though the unsaturated-zone/saturated-zone interface is treated a little differently. However, the transport models assumed for both EBS transport and unsaturated zone transport are different from the overall TSPA, although the EBS transport model is quite similar. The details of EBS and unsaturated zone transport for the human intrusion TSPA have been discussed in Section 2.4.3.1. As previously explained, there is a consistent set of assumptions dealing with advective and diffusive transport of radionuclides among these two modules.

Furthermore, the discussion regarding consistency and/or differences of assumptions within the overall TSPA model, as described in Section 2.4.2.3.1, also applies to the human intrusion TSPA, except perhaps for those four areas mentioned in Section 2.4.3.1 where the overall TSPA model has been changed to accommodate the human intrusion event:

- Mechanical damage to waste packages and drip shields
- EBS flow and transport
- Unsaturated zone transport
- Saturated zone transport.

Of these four areas where changes to the overall TSPA model were made for the human intrusion modeling case, there are no real differences or inconsistencies in assumptions, except perhaps related to waste package degradation. In particular, as discussed in Section 2.4.3.3.2, in contrast to the overall TSPA, nominal waste package degradation processes and likely seismic waste package degradation processes are omitted from the human intrusion analysis. However, for the reasons presented there, this assumption is both appropriate and conservative.

2.4.3.4.2 TSPA Code Verification, Validation, and Confidence-Building for the Human Intrusion

[NUREG-1804, Section 2.2.1.4.2.3: AC 3(2)]

This section regarding TSPA code verification and confidence-building is similar to Section 2.4.2.3.2, which addresses the same subjects in the context of the overall TSPA model. As the two TSPAs are identical except for the occurrence and characteristics of the human intrusion event and the exclusion of unlikely FEPs, most of the during-development and post-development model validation activities described in Section 2.4.2.3.2 are also applicable to the human intrusion modeling case. However, some supplemental confidence-building activities are included to specifically build additional confidence in the human intrusion TSPA model:

1. A single-realization deterministic analysis for the human intrusion modeling case, which was already documented in Section 2.4.3.3.5, to help demonstrate consistency of the overall TSPA results with the characteristics of the human intrusion.

2. A stepwise rank regression uncertainty analysis on expected annual dose, which was documented below in Section 2.4.3.4.3 to show consistent propagation of uncertainty through the human intrusion TSPA. However, a secondary purpose of the uncertainty analysis is to enhance confidence in the human intrusion TSPA by explaining the cause-effect relationships of the uncertainty analysis on the basis of the underlying

physics of the submodels. As contemplated by NUREG-1804, Section 2.2.1.4.2.3, Acceptance Criterion 3(2), this builds confidence "that the code is modeling the physical processes in the repository system in the manner that is consistent with the characteristics of the postulated intrusion event." This uncertainty analysis, as well as the single-realization analysis, also helps to demonstrate proper transfer of data among modules of the code (Figure 2.4-158). Furthermore, transfer of data among modules of the code is described in Section 2.4.3.1 in conjunction with a description of the EBS, unsaturated zone, and saturated zone transport submodels.

3. Various input and submodel verification tests specific to the human intrusion TSPA, including verification of inputs in the TSPA database, the submodels such as the borehole pipe model, and coupling among the submodels. These analyses are similar to those discussed in Section 2.4.2.3.2.2.1 for the overall TSPA. In addition, because GoldSim is used as the human intrusion TSPA integration software (as well as to model various processes at the submodel level, such as unsaturated zone borehole transport) and because many of the DLLs are the same, the verification activities conducted for the GoldSim software and the DLLs in the overall TSPA are applicable to the human intrusion TSPA. The various verification activities conducted specifically for the human intrusion TSPA are documented in *Total System Performance Assessment Model/ Analysis for the License Application* (SNL 2008a, Section 7.2[a])).

4. Model stability testing, including statistical and temporal stability testing, is an important aspect of code verification and confidence building, as described in Section 2.4.2.3.2.2.2. Sections 2.4.3.3.3 and 2.4.3.3.4 describe the model stability testing applied to the human intrusion TSPA.

The various activities described above, along with activities described in Section 2.4.2.3 for the overall TSPA, enhance confidence that the TSPA code is modeling the physical processes of the repository in a manner consistent with the characteristics of the postulated human intrusion event.

2.4.3.4.3 Propagation and Consistency of Uncertainty in the Human Intrusion TSPA

[NUREG-1804, Section 2.2.1.4.2.3: AC 2(4), AC 3(3)]

This section addresses the consistency of uncertainty in the TSPA results with the uncertainty in the underlying input parameters and characteristics of the human intrusion event. As with the overall TSPA, the uncertainty and sensitivity analyses used to address this requirement are primarily applied to the propagation of epistemic uncertainty in the TSPA, since the aleatory uncertainties are averaged over. Thus, the 300 expected annual dose curves used to analyze uncertainty propagation represent the range of epistemic uncertainty in the TPSA model, both for the overall TSPA and the human intrusion TSPA. This concept is explained in Section 2.4.2.3.3 with regards to the overall TSPA model. The discussion of the sources of uncertainty, the framework of the TSPA, and the methodology used for the uncertainty and sensitivity analyses applies equally to the human intrusion TSPA. The three types of aleatory uncertainty in the human intrusion TSPA, as described in Section 2.4.3.1.4, are integrated to produce the expected annual dose curves analyzed here. PRCCs, stepwise rank regression, and scatterplots are used here, as with the overall TSPA model, to demonstrate how uncertainty in the inputs propagates to uncertainty in the dose, and how the various cause-effect relationships make sense from the perspective of the underlying physics of the models.

Uncertainty and sensitivity analysis results for a human intrusion event at 200,000 years are presented in two sets (SNL 2008a, Section K10[a]). The first set is for expected dose to the RMEI (*EXPDOSE*, mrem) over the time period (200,000, 220,000 yr) (Figures 2.4-173 and 2.4-174). The second set is for expected dose to the RMEI (*EXPDOSE*, mrem) over the time period (220,000, 1,000,000 yr) (Figures 2.4-175 and 2.4-176). This division is made because of the relatively rapid (on a 1,000,000-year time scale) changes in EXPDOSE that occur in the first 20,000 years after a drilling intrusion.

As examination of Figure 2.4-173a and b shows that *EXPDOSE* increases for the first 1000 to 2000 years after a drilling intrusion at 200,000 years and then decreases monotonically out to 220,000 years. The individual sample elements produce peak values for *EXPDOSE* between approximately 0.003 and 0.1 mrem. The monotonic decrease in *EXPDOSE* after 220,000 years can be seen in Figure 2.4-175a and b to continue out to approximately 400,000 years, after which *EXPDOSE* remains approximately constant. For the time period (200,000, 300,000 yr), ^{99}Tc and ^{129}I are the dominant radionuclides contributing to *EXPDOSE*, while for the time period (300,000, 1,000,000 yr), ^{242}Pu is the dominant radionuclide contributing to *EXPDOSE* (Figure 2.4-164).

Sensitivity analysis results for the (200,000, 220,000 yr) time period are presented in Figures 2.4-173c and 2.4-174b, c, d, e, f, and g. As indicated by the partial rank correlation coefficients in Figure 2.4-173c, the most important variables affecting *EXPDOSE* for the first 5,000 years after the intrusion are *INFIL* (infiltration scenario), *CSSPECSA* (effective specific surface area of the commercial SNF waste, m^2/mg; as sampled, *CSSPECSA* is actually the logarithm of the indicated surface area), *SZGWSPDM* (groundwater specific discharge multiplier; as sampled, *SZGWSPDM* is actually the logarithm of the indicated multiplier), *SZFIPOVO* (flowing interval porosity in the volcanic unit of the saturated zone), *MICTC99* (dose conversion factor for ^{99}Tc, (rem/yr)/(pCi/L)), and *EBSDIFCF* (scale factor used to represent uncertainty in the EBS diffusion coefficient; as sampled, *EBSDIFCF* is actually the logarithm of the indicated scale factor). For the first 5,000 years after the intrusion, *INFIL*, *CSSPECSA*, *SZGWSPDM*, *MICTC99* and *EBSDIFCF* have positive effects on *EXPDOSE*, and *SZFIPOVO* has a negative effect on *EXPDOSE*. These effects result because (1) increasing *INFIL* increases water flow in the EBS and unsaturated zone, (2) increasing *CSSPECSA* increases the dissolution rate of degrading commercial SNF waste, (3) increasing *SZGWSPDM* increases water flux in the saturated zone, (4) increasing *MICTC99* increases the dose received from a unit concentration of ^{99}Tc in groundwater, and (5) increasing *EBSDIFCF* increases the diffusive transport of radionuclides from the EBS. In contrast, *SZFIPOVO* has an early inverse effect on *EXPDOSE* related to the early transient peak of ^{99}Tc releases. This is a dilution effect related to the storage of ^{99}Tc in the saturated zone pore space. The higher the flowing interval porosity, the lower the peak concentration in the saturated zone. This effect disappears when the sharp release peak subsides.

After approximately 5,000 years, *INFIL*, *CSSPECSA*, *SZGWSPDM* and *EBSDIFCF* have a small negative effect on *EXPDOSE* (Figure 2.4-173c). This reversal in effects results from the high mobility of ^{99}Tc and ^{129}I, which are the dominant radionuclides contributing to *EXPDOSE* prior to 300,000 years. Because of this mobility, variables that increase the release of ^{99}Tc and ^{129}I at early times (i.e., in the first 5,000 years after intrusion) also decrease the releases of ^{99}Tc and ^{129}I at later times. As a result, *INFIL*, *CSSPECSA*, *SZGWSPDM* and *EBSDIFCF* have a positive effect on *EXPDOSE* in the first 5,000 years after intrusion and a negative effect on *EXPDOSE* at later times. In contrast, *MICTC99* continues to have a positive effect on *EXPDOSE* with increasing time, since there is a positive linear relationship between the two quantities.

More detailed analyses for *EXPDOSE* for the time period (200,000, 205,000 yr) are provided by the stepwise regression analyses and scatterplots in Figure 2.4-174. An examination of the regression analyses and associated scatterplots shows that many individual variables affect *EXPDOSE*, but no single variable has a dominant effect on the uncertainty in *EXPDOSE*. Further, many variables having small effects, reflecting complex interactions between processes represented by these variables and the radionuclides that they affect but with no single interaction dominating radionuclide release and transport, which results in regression models with small R^2 values (i.e., 0.75, 0.53 and 0.41).

As indicated by the partial rank correlation coefficients in Figure 2.4-175c, the most important variables affecting *EXPDOSE* after approximately 300,000 years are *SZGWSPDM*, *GOESITED* (density of sorption sites on goethite, sites/nm^2), *COLFEOSS* (iron oxide colloid concentration when degraded stainless steel is present but no degrading carbon steel is present, mg/L), *EP1LOWPU* (scale factor used to incorporate uncertainty into plutonium solubility under low ionic strength conditions; as sampled, *EP1LOWPU* is actually the logarithm of the indicated scale factor), and *SZFISPVO* (flowing interval spacing in volcanic unit of saturated zone, m). The variables *SZGWSPDM*, *COLFEOSS*, *EP1LOWPU*, and *SZFISPVO* have positive effects on *EXPDOSE*; in contrast, *GOESITED* has a negative effect. The positive effects associated with *SZGWSPDM*, *COLFEOSS*, *EP1LOWPU*, and *SZFISPVO* result because (1) increasing *SZGWSPDM* increases water flux in the saturated zone, (2) increasing *COLFEOSS* increases the attachment of radionuclides to mobile colloids, (3) increasing *EP1LOWPU* increases the solubility of plutonium, and (4) increasing *SZFISPVO* decreases the diffusion of radionuclides from fractures in the volcanic unit of the saturated zone into the surrounding rock matrix. The negative effect associated with *GOESITED* results from increasing the sorption of radionuclides onto corrosion products inside the waste package. The effect of *COLFEOSS* is related to the fact that ^{242}Pu dose dominates late time total dose for the human intrusion case and this ^{242}Pu dose is due to the irreversible transport of ^{242}Pu on iron oxyhydroxide colloids, as shown in Figure 2.4-172 for a single realization of the human intrusion modeling case.

More detailed analyses for *EXPDOSE* for the time period (220,000, 1,000,000 yr) are provided by the stepwise regression analyses and scatterplots in Figure 2.4-176. Similarly to Figure 2.4-174, an examination of the regression analyses and associated scatterplots shows that many individual variables affect *EXPDOSE*, but no single variable has a dominant effect on the uncertainty in *EXPDOSE*. Further, many variables having small effects, reflecting complex interactions between processes represented by these variables and the radionuclides that they affect but with no single interaction dominating radionuclide release and transport, which results in regression models with small R^2 values (i.e., 0.50, 0.55 and 0.63).

2.4.3.4.4 Parameters Sampled across Their Ranges of Uncertainty in the Human Intrusion TSPA

[NUREG-1804, Section 2.2.1.4.2.3: AC 3(4)]

This section demonstrates that the parameters in the human intrusion TSPA have been adequately sampled across their ranges of uncertainty. The discussion of this subject in the context of the overall TSPA in Section 2.4.2.3.4 is applicable. In particular, NUREG-1804, Section 2.2.1.4.2.3, Acceptance Criterion 3(4) is shown to be addressed in Sections 2.4.3.3.2 and 2.4.3.3.3, which demonstrates statistical and numerical stability across both the aleatory uncertainty and the epistemic uncertainty in the underlying parameter distributions. In the human intrusion TSPA, Latin hypercube sampling was used for both epistemic and aleatory parameters, although separate samples were generated for each type of uncertainty. The demonstration of statistical stability involved showing that the sample size for computing the mean (or other statistic, such as median) is sufficient or, of equal importance, that the confidence interval about the mean is reasonably narrow (SNL 2008a, Section 7.3.1.2[a]). The demonstration of numerical accuracy involved showing that the sampling of aleatory parameters was sufficient for computing the expected value over aleatory uncertainty (SNL 2008a, Section 7.3.2.8). The demonstration of statistical stability and numerical accuracy indicates that the sampled parameters are adequately sampled across their range of uncertainty. Furthermore, the discussion in Section 2.4.2.3.4 about the efficient stratification properties of Latin hypercube sampling is equally applicable to the human intrusion TSPA.

2.4.4 Analysis of Repository Performance that Demonstrates Compliance with the Separate Standards for the Protection of Groundwater

[NUREG-1804, Section 2.2.1.4.3.3: AC 1, AC 2, AC 3]

The information presented in Section 2.4.4 addresses the requirements that must be met to demonstrate compliance with the separate standards for protection of groundwater at 10 CFR 63.331, considering the characteristics of the representative volume at 10 CFR 63.332. Section 2.4.4 also addresses acceptance criteria contained in NUREG-1804, Section 2.2.1.4.3.3.

10 CFR 63.113(c) requires that the following postclosure performance objective is met:

> The engineered barrier system must be designed so that, working in combination with natural barriers, releases of radionuclides into the accessible environment are within the limits specified at § 63.331 of subpart L of this part. Compliance with this paragraph must be demonstrated through a performance assessment that meets the requirements specified at § 63.114 of this subpart and §§ 63.303, 63.332 and 63.342 of subpart L of this part.

10 CFR 63.331 includes groundwater protection limits for radionuclides in the representative volume of groundwater for 10,000 years after disposal for the following quantities:

- Combined ^{226}Ra and ^{228}Ra concentration, including natural background
- Gross alpha activity concentration (including ^{226}Ra but excluding radon and uranium), including natural background
- Annual beta-photon dose to the whole body or any organ from drinking 2 liters of water per day, excluding natural background.

The values of these limits are provided in Table 2.4-13. The separate standards for protection of groundwater in 10 CFR 63.331 have been met (Section 2.4.4.1.1.4).

The concentrations of radionuclides released from the Yucca Mountain disposal system and captured in the representative volume were estimated using performance assessment, as required by 10 CFR 63.113(c), and found to support a finding of reasonable expectation that the Yucca Mountain disposal system complies with the standards specified in 10 CFR 63.331, as required by 10 CFR 63.332(a). 10 CFR 63.332(a) also includes the specific provisions for the representative volume of groundwater. These requirements and assumptions have been met, in that:

- The representative volume of groundwater is within an aquifer containing less than 10,000 mg of total dissolved solids per liter of water to supply a given water demand
- It includes the highest concentration level in the plume of contamination in the accessible environment
- Its position and dimensions in the aquifer are determined using average hydrologic characteristics that have cautious, but reasonable, values representative of the aquifers along the radionuclide migration path from the Yucca Mountain repository to the accessible environment as determined by site characterization
- It contains 3,000 acre-feet of water (about 3,714,450,000 liters or 977,486,000 gallons).

The position and dimensions of the groundwater aquifers are determined using average hydrologic characteristics of the aquifers along the radionuclide migration path from the Yucca Mountain repository to the accessible environment, in accordance with the methods specified in 10 CFR 63.332 (Section 2.4.4.3). The representative volume of groundwater that would be withdrawn annually from an aquifer includes the highest concentration in the plume of contamination in the accessible environment. The average radionuclide concentrations in the representative volume is used for demonstration of compliance with the individual protection standards (proposed 10 CFR 63.311 and proposed 10 CFR 63.321). The groundwater concentrations for the radionuclides, as specified in Table 2.4-13, are analyzed in the plume at the compliance location, where the postclosure plume crosses the southernmost boundary of the controlled area (at a latitude of 36° 40′ 13.6661″ North) and reaches the accessible environment approximately 18 km from the repository footprint.

The NRC requires excluding unlikely natural processes and events in the performance assessment evaluation for the groundwater protection standard. Unlikely events are those with less than 1 chance in 10 and at least 1 chance in 10,000 of occurring within 10,000 years of disposal. Likely events are those with a 10% or greater chance of occurring in the next 10,000 years. The seismic ground motion modeling case of the seismic scenario class extends across the likely-unlikely boundary. That is, ground motions potentially relevant to evaluating groundwater protection occur with recurrence frequencies both above and below 1 chance in 10 in the next 10,000 years. Therefore, this modeling case is included in the assessment of groundwater protection, but was restricted to consider only the likely seismic events. The following modeling cases, described in more detail in Section 2.4.1.2, are thus included in the performance assessment for the consideration of compliance with the groundwater protection standards: nominal modeling case, waste package early failure modeling case, drip shield early failure modeling case, and seismic ground motion modeling case, but only including seismic events with mean exceedance frequencies in the range from 10^{-5} to 4.3×10^{-4} per year (i.e., seismic events with a horizontal PGV greater than about 1 m/s) (SNL 2008a, Section 8.1.2) and subject to the same approximations as described in Sections 2.4.2.1.5.4 and 2.4.2.2.2.3 with respect to the degradation processes included in the 10,000-year calculations. Although the mean probability of one or more early-failed drip shields is 0.0166 (Section 2.4.2.2.1.2.4) (i.e., it could be considered an unlikely event) this modeling case was conservatively included without restriction on the probability of early failure of a drip shield. This is because the uncertain rate (per drip shield) of drip shield early failures is represented by a log-normal distribution (SNL 2008a, Section 6.4.1.2); thus for a small part of this distribution, the probability of early failure of a drip shield is greater than 0.1. The radionuclide concentrations in groundwater in the performance assessment for demonstration of compliance with the groundwater protection standards were calculated as expected values (i.e., were weighted by the probability of their occurrence). The calculation of mean groundwater concentrations is analogous to the calculation of total mean annual dose (Section 2.4.2.1), and averages over both aleatory uncertainty in the occurrence of events as well as epistemic uncertainty in the repository system.

2.4.4.1 Demonstration that the Groundwater Radioactivity and Doses at Any Year During the Compliance Period Do Not Exceed the Limits in the Groundwater Protection Standards

[NUREG-1804, Section 2.2.1.4.3.3: AC 1, AC 2, AC 3]

The final results of the TSPA analysis of repository performance with respect to the groundwater protection standards are shown in Table 2.4-4.

2.4.4.1.1 Methods Used to Estimate the Level of Radioactivity in the Groundwater

The separate standards for protection of groundwater during the period within 10,000 years after disposal, defined in 10 CFR 63.331, include the limits on radionuclides in the representative volume, which are provided in Table 2.4-13. The DOE must demonstrate there is a reasonable expectation that, for 10,000 years of undisturbed performance after disposal, releases of radionuclides from waste in the Yucca Mountain disposal system into the accessible environment will not cause the level of radioactivity in the representative volume of groundwater to exceed these limits. Demonstration of compliance with these limits is achieved through a performance assessment (TSPA).

2.4.4.1.1.1 Performance Assessment

The level of radioactivity in the representative volume of groundwater is calculated using performance assessment methods, assumptions, models, and data consistent with the repository performance assessment calculations for the undisturbed case for the 10,000 year period after disposal (SNL 2008a, Section 8.1.2). The basis for the TSPA model used to analyze the system is outlined in Section 2.4.1. Performance assessment conducted to show compliance with the groundwater protection standards excludes the unlikely features, events, and processes, i.e., those that are estimated to have less than one chance in 10 and at least one chance in 10,000 of occurring within 10,000 years of disposal (proposed 10 CFR 63.342(b)). Compliance with the groundwater protection standards in 10 CFR 63.331 is based upon the arithmetic means of the projected radionuclide concentrations and doses.

The TSPA used to demonstrate compliance with the groundwater protection standards is based upon FEPs that were screened in (included) for this performance assessment. The effects of these included FEPs on performance of natural and engineered barriers are assessed using abstraction models. Section 2.3 describes how the included FEPs that will affect the performance of the repository are combined in conceptual and numerical models. Section 2.3 also presents the technical basis for each of the abstraction models associated with the Upper Natural Barrier, the EBS, and the Lower Natural Barrier. These abstraction models reproduce, or bound, the essential elements of the more detailed process models.

Data and model uncertainty were propagated into the TSPA model throughout its development and implementation (SNL 2008a, Sections 6.3, 6.3[a], 6.4, 6.6, and 6.6[a]). Uncertainty is captured by the probabilistic TSPA, which calculates future outcomes for multiple realizations using distributions of values for uncertain parameters that may be important to performance. Each of the combinations of parameter values is representative of a subset of the full range of potential outcomes. These probabilistic analyses thus reflect an appropriate range of process behaviors or parameter values (SNL 2008a, Section ES3.3).

The mean of all the realizations for each year during the 10,000 years after closure is used to compare repository performance to postclosure regulatory standards (SNL 2008a, Sections 6.1.2 and 6.1.2[a]). Annual average mass radionuclide concentrations in groundwater are calculated by dividing the annual mass flux of individual radionuclides reaching the accessible environment boundary by the representative volume (SNL 2008a, Section 6.3.11.2). The mass concentrations are then converted into activity concentrations (in curies per liter of groundwater). Activity concentrations are used for demonstration of compliance with the combined ^{226}Ra and ^{228}Ra activity concentration and gross alpha activity concentration limits. For the combined beta and photon dose limit, the whole body and organ doses are calculated assuming consumption of 2 liters of water per day

2.4.4.1.1.2 Quantities Calculated for Evaluating Compliance with the Groundwater Protection Standards

The separate standards for protection of groundwater (10 CFR 63.331) require calculating the predicted concentrations of combined ^{226}Ra and ^{228}Ra and gross alpha activity in a representative volume of 3,000 acre-ft of groundwater. They also require calculating the annual dose to the whole body and any organ from beta- and photon-emitting radionuclides resulting from drinking 2 L of water per day (10 CFR 63.331, Table 1).

^{226}Ra and ^{228}Ra Activity Concentration—To evaluate compliance with the limit for ^{226}Ra and ^{228}Ra, the combined activity concentration of ^{226}Ra and ^{228}Ra in the groundwater is calculated based on the annual mass flux of these radionuclides at the controlled area boundary and the representative volume. The natural background concentrations of ^{226}Ra and ^{228}Ra in groundwater are included with the calculated activity (10 CFR 63.331, Table 1) for comparison with the limit of 5 pCi/L.

Gross Alpha Activity Concentration—Radionuclides classified in Federal Guidance Report 12 (Eckerman and Ryman 1993, Table A1) as alpha emitters were included in the analysis of total alpha activity concentration in groundwater (SNL 2007y, Section 6.15.1.1; Table 6.15-2). Alpha activity concentration of a radionuclide considered in the TSPA model includes the total alpha emissions from the concentration of that radionuclide in the groundwater and from the associated decay products (SNL 2007y, Section 6.15.1.1). Consistent with the approach used in the biosphere model (SNL 2007y, Section 6.3.1.4), short-lived decay products of a long-lived radionuclide tracked in the TSPA model were modeled to be in secular equilibrium with that radionuclide. After the activity concentration of a long-lived radionuclide in the groundwater is calculated, the value is multiplied by the number of alpha particles included in the decay chain to determine the total number of alpha particles associated with the decay of that radionuclide. The natural background concentrations of alpha emitters in groundwater (including ^{226}Ra, but excluding radon and uranium) (10 CFR 63.331, Table 1) must then be added to calculate the gross alpha activity concentration compared with the appropriate groundwater protection standard.

The alpha particle activity concentration in water is calculated as:

$$C_\alpha = \sum_i Cw_i N_{\alpha,i} \tag{Eq. 2.4-44}$$

where

C_α = total alpha particle activity concentration in groundwater (pCi/L)

Cw_i = activity concentration of a primary radionuclide i in groundwater (pCi/L)

$N_{\alpha,i}$ = number of alpha particles attributed to one decay of a long-lived radionuclide i tracked in the TSPA model (SNL 2007y, Table 6.15-3).

Annual Drinking Water Dose from Beta and Photon Emitting Radionuclides—The annual dose limit for beta- and photon-emitting radionuclides to the whole body or any organ is based on water consumption of 2 liters per day (10 CFR 63.331, Table 1). This limit applies to radionuclides other than alpha emitters. Alpha emitters are covered under the gross alpha limit of the groundwater protection standards. If a radionuclide decays with emissions of alpha and beta radiation, this radionuclide is considered for both gross alpha and annual beta-photon dose. Such an approach is conservative and ensures that all types of radiation emitted from a radionuclide are considered. Radionuclides classified as beta emitters and alpha-beta emitters with more than 1% beta decays were included in the predictions of the whole-body and organ doses from beta- and photon-emitting radionuclides (SNL 2007y, Section 6.15.1.2, Table 6.15-2). For these radionuclides, conversion factors were developed that represent annual beta-photon dose to the whole body and organs from daily consumption of 2 liters of water containing a unit activity concentration of a long-lived radionuclide tracked in the TSPA model and its associated short-lived decay products (SNL 2007y, Section 6.15.1.2). Those conversion factors were used to calculate the annual dose resulting from drinking of water containing a predicted concentration of radionuclides and are presented in Table 2.4-14.

Ingestion dose coefficients for organs and the whole body used to calculate the conversion factors were obtained from Federal Guidance Report 13 (EPA 2002). The ingestion dose coefficients include contributions from all emissions (including alpha emissions) for each radionuclide. Thus, the dose contribution is overestimated for the few radionuclides (^{227}Ac, ^{212}Bi, and ^{213}Bi) whose dose coefficients include a contribution from alpha particles (SNL 2007y, Section 6.15.1.2; Table 6.15-2). The use of dose coefficients from Federal Guidance Report 13 (EPA 2002) for the groundwater protection standards is consistent with the methods used to calculate the annual dose for the individual protection standard (Section 2.3.10.2.2) and compliant with the required methods described in 40 CFR Part 197, Appendix A. Values in Appendix A of proposed 40 CFR Part 197 are used per the definition of weighting factor in proposed 10 CFR 63.2.

To evaluate compliance with the separate standards for protection of groundwater (10 CFR 63.331), the beta-photon dose to the whole body or any organ, *D*, is calculated in the TSPA using the conversion factors described above and the following equation (SNL 2007y, Equation 6.15-4):

$$D = \sum_i D_i = \sum_i Cw_i CF_i \qquad \text{(Eq. 2.4-45)}$$

where

D_i = annual beta-photon dose (committed effective dose for the whole body or committed equivalent dose for an organ) from intake of radionuclide *i* by ingestion resulting from daily consumption of 2 liters of water (mrem/yr)

Cw_i = activity concentration of radionuclide *i* in groundwater (pCi/L)

CF_i = conversion factor for calculating beta-photon dose from radionuclide *i* as a result of drinking 2 L/day of water (mrem/yr per pCi/L).

In the source reference (SNL 2007y, Section 6.15.1.2), Equation 2.4-45, including the conversion factors, is provided in SI units (the values in Table 2.4-14 are also in SI units). However, GoldSim, which is used for the TSPA model, is dimensionally aware and data can be entered and displayed in any units, as long as they are dimensionally consistent.

2.4.4.1.1.3 Natural Background Levels of Gross Alpha-Emitting Radionuclides and ^{226}Ra and ^{228}Ra

The quantities calculated to evaluate compliance with the combined ^{226}Ra and ^{228}Ra, as well as the gross alpha activity concentration limits of the groundwater protection standards, require that the contribution from the natural background be included. A summary of the relevant background radiation data collected at the site is provided below. The testing data, including the location and analysis, as well as corroborating data, are presented.

Gross alpha concentration data in groundwater from several locations in the vicinity of the compliance point have been collected as a part of the Yucca Mountain Site Characterization Project. Additional data from the Nevada Test Site Environmental Monitoring Program are also available. The data from the locations identified as being in the Alkali Flat-Furnace Creek groundwater subbasin that contains Yucca Mountain and different sampling times are presented in Table 2.4-15. These data are combined to estimate the background gross alpha concentrations in the groundwater. Some of the reported values of gross alpha activity concentration exclude contributions of radon and uranium, while some values are corrected for the contribution of uranium. This is done because these measured quantities included contributions from radon and uranium, while the groundwater protection limit for gross alpha concentration excludes radon and uranium (SNL 2008f, Section 6.8.6).

Combining data on the gross alpha concentration in groundwater near Yucca Mountain from a variety of sources has several advantages. Stochastic fluctuations in the radioactive decay process and measurement methods can be averaged over a larger number of measurements, leading to a more representative average value and greater precision. Potential variations in groundwater concentrations as a function of time would also be more effectively averaged over several data sets collected during different years. Most importantly, because there are variations in sampling and analytical methods, using data on gross alpha concentration from several studies is a more representative estimate of the average value (SNL 2008f, Section 6.8.6).

Histograms of the 79 estimated values of gross alpha concentration in groundwater near Yucca Mountain are plotted in Figure 2.4-177. The upper plot in Figure 2.4-177 shows the values of gross alpha concentration corrected for uranium concentration. The upper plot in Figure 2.4-177 also shows the values of gross alpha concentration that have not been corrected for uranium concentration in blue. The upper plot in Figure 2.4-177 shows that the uncorrected values of gross alpha concentration are on the higher side of the distribution, as expected. The lower plot in Figure 2.4-177 shows the values of gross alpha concentration from all sources, corrected for uranium concentration. The low concentrations of alpha emitters (a few pCi/L) in groundwater produce only a few decays per liter every hundred seconds. This, coupled with the stochastic nature of the sample counting processes, makes it possible for a gross alpha activity concentration measurement ([activity + background count] – [background count]) to give rise to an unphysical negative value. Furthermore, making the correction to exclude the uranium concentration can result in a corrected value of an even lower value. Thus it is conceivable that some individual measurements can result in negative best estimate concentrations for the uranium-corrected gross alpha activity concentration of a water sample. When multiple estimates of concentrations (including negative values) are pooled to arrive at global average activities over all samples, the stochastic nature of these fluctuations cancels in the statistical sense. If the individual, apparently unphysical, negative concentrations are truncated to zero, an unwanted statistical bias is introduced into the global mean value. Retention of all individual measurement values (positive and negative) allows compensation for the stochastically overestimated and underestimated individual measurements, and results in an unbiased mean value of activity concentration (SNL 2008f, Section 6.8.2.2). Thus it is appropriate, and a common practice, to use individual activity measurements even if some are negative. Including negative measurement values is also recommended by the EPA (Watson 1980, Chapter 6).

The calculated background gross alpha mean activity values and the estimated standard deviation are shown in Table 2.4-15. The measurements of gross alpha concentrations on these groundwater samples are for all alpha emitters, excluding uranium.

The values presented in Table 2.4-16 show that the estimate for the mean background gross alpha concentration in groundwater is 0.50 pCi/L, with a 95% confidence that the concentration will not exceed 0.71 pCi/L (SNL 2008f, Table 6-20).

In the absence of data on the combined concentrations of ^{226}Ra and ^{228}Ra, it is assumed for the standards involving these radionuclides that they are responsible for all gross alpha activity (SNL 2008f, Section 6.8.5). For ^{226}Ra and ^{228}Ra, the mean background concentration is therefore 0.50 pCi/L, with a 95% confidence that the concentration will not exceed 0.71 pCi/L (SNL 2008f, Section 6.8.6).

2.4.4.1.1.4 Results

^{226}Ra and ^{228}Ra Activity Concentration—Figure 2.4-12 shows the probabilistic projections of combined activity concentration of ^{226}Ra and ^{228}Ra in representative volume of groundwater for 10,000 years after disposal, excluding their background concentration (SNL 2008a, Figure 8.1-9[a]). The curves shown in this figure include the projected mean and 95th percentile activity concentrations of combined radium species, the estimated background level, as well as the combined ^{226}Ra and ^{228}Ra activity concentration limit for the groundwater protection standards. The mean concentration curve is greater than the 95th percentile curve because only a very small number of realizations results in non-zero radium concentrations; these results significantly affect the mean. The highest concentration for the combined activity concentration of ^{226}Ra and ^{228}Ra in groundwater for the 10,000-year period following repository closure, along with the background level, is summarized in Table 2.4-4.

^{226}Ra and ^{228}Ra have relatively short half-lives so the activity of these radionuclides reaching the compliance location is created almost entirely by ingrowth from other longer-lived radionuclides released from the repository. Figure 2.4-12 shows that the highest calculated mean activity concentration of combined ^{226}Ra and ^{228}Ra in the representative volume of groundwater resulting from repository releases is less than 10^{-6} pCi/L during the 10,000 years after disposal (SNL 2008a, Table 8.1-2[a] and Figure 8.1-9[a]).

The background level of the combined ^{226}Ra and ^{228}Ra activity concentration in groundwater is 0.50 pCi/L (Section 2.4.4.1). This measured background concentration must be added to the calculated activity concentration of combined ^{226}Ra and ^{228}Ra released from the repository for comparison with the postclosure groundwater protection standard. The highest mean concentration of combined ^{226}Ra and ^{228}Ra released from the repository during the 10,000 yeas after disposal, is estimated to be about 1.3×10^{-7} pCi/L (SNL 2008a, Section 8.1.2.1[a]), and is therefore almost 7 orders of magnitude lower than the measured background levels. Therefore, the total combined ^{226}Ra and ^{228}Ra activity concentration, including background, is considered to be equal to the measured background level of 0.50 pCi/L. This is below the regulatory limit of 5 pCi/L. Thus, these results support a finding of reasonable expectation that, for 10,000 years of undisturbed performance after disposal, releases of ^{226}Ra and ^{228}Ra from waste in the Yucca Mountain disposal system into the accessible environment will not cause the level of radioactivity in the representative volume of groundwater to exceed the limit for combined ^{226}Ra and ^{228}Ra set in 10 CFR 63.331 (Table 1).

Figure 2.4-178 shows the contributions of the modeling cases to the projected mean of combined ^{226}Ra and ^{228}Ra activity concentration in groundwater, excluding natural background, for 10,000 years after disposal (with the natural background level included in the graph) (SNL 2008a, Figure 8.1-10[a]). From the curves in this figure, it is evident that the mean of the combined radium concentration is dominated by the contribution from the waste package early failure modeling case until 4,500 years, after which the contribution from the seismic ground motion modeling case dominates. At 10,000 years, when the mean radium concentration obtains its maximum value, approximately 90% of the mean radium concentration is attributable to the seismic ground motion modeling case. The contributions to the mean radium concentration from each modeling case parallel the importance of these modeling cases to the total mean annual dose (Section 2.4.2.2.1.1.2).

Gross Alpha Activity Concentration—Figure 2.4-13 shows the probabilistic projections of gross alpha activity concentration (including ^{226}Ra, but excluding radon and uranium) in the representative volume of groundwater for 10,000 years after disposal, excluding its background concentration (SNL 2008a, Figure 8.1-11[a]). The curves shown in this figure include the projected mean and 95th percentile of gross alpha activity concentrations, the estimated background level, as well as the gross alpha activity concentration limit for the groundwater protection standards. The highest gross alpha activity concentration in groundwater for the 10,000-year period following disposal, along with its background level, is included in a summary in Table 2.4-4. Radionuclides included in this calculation are ^{210}Pb, ^{226}Ra, ^{227}Ac, ^{228}Th, ^{229}Th, ^{230}Th, ^{232}Th, ^{231}Pa, ^{237}Np, ^{238}Pu, ^{239}Pu, ^{240}Pu, ^{242}Pu, ^{241}Am, and ^{243}Am (SNL 2008a, Section 8.1.2.2[a]). The highest calculated annual mean total alpha activity concentration, resulting from repository releases is less than 10^{-4} pCi/L during the first 10,000 years after disposal (SNL 2008a, Table 8.1-2[a] and Figure 8.1-11[a]).

The measured background concentration of gross alpha activity in the groundwater is 0.50 pCi/L (Section 2.4.4.1). Because the calculated concentration of gross alpha activity (including ^{226}Ra but excluding radon and uranium) is much lower than the measured background levels, the total gross alpha activity concentration is considered to be equal to the measured background level of 0.50 pCi/L. The combined alpha concentration is less than the gross alpha activity limit of 15 pCi/L by more than an order of magnitude. Thus, these results support a finding of reasonable expectation that, for the first 10,000 years of undisturbed performance after disposal, the release of alpha-emitting radionuclides (excluding radon and uranium) from waste in the Yucca Mountain disposal system into the accessible environment will not cause the level of radioactivity in the representative volume of groundwater to exceed the limit for gross alpha activity concentration (including ^{226}Ra but excluding radon and uranium) set in 10 CFR 63.331 (Table 1).

Figure 2.4-179 shows the contributions of the modeling cases to the mean projected gross alpha activity concentration (including ^{226}Ra but excluding radon and uranium) in groundwater for the first 10,000 years after disposal (with the background line included separately in the graph) (SNL 2008a, Figure 8.1-12[a]). This figure shows that the mean gross alpha activity concentration is dominated by the drip shield early failure modeling case until approximately 7,000 years after disposal. From 7,000 to 8,000 years, the waste package early failure, the drip shield early failure, and seismic ground motion modeling cases contribute approximately equally to the projected gross alpha activity concentration. Over the remaining 2,000 years, the releases from the seismic ground motion modeling case become the dominant factor in the projected gross alpha activity concentration (SNL 2008a, Section 8.1.2.2[a]).

Annual Drinking Water Dose from Beta and Photon Emitting Radionuclides—Figure 2.4-180 shows the mean annual dose to the whole body and 23 organs from combined beta- and photon-emitting radionuclides resulting from drinking 2 liters of water per day from representative volume for the first 10,000 years after disposal, excluding the natural background dose (SNL 2008a, Figure 8.1-13[a]). The thyroid is the organ receiving the highest dose; the dose to the lower large intestine is a close second highest (SNL 2008a, Section 8.1.2.3[a]). Figure 2.4-14 shows the mean and the 95th percentile of annual drinking water doses to the whole body and the thyroid for combined beta- and photon-emitting radionuclides for the first 10,000 years after disposal (SNL 2008a, Figure 8.1-14[a]), as well as the combined beta and photon dose limit for the groundwater protection standards. The highest values of the whole body and organ (thyroid) doses are summarized in Table 2.4-4 (SNL 2008a, Table 8.1-2[a]).

Some of the more prominent beta or beta-photon emitters are: ^{14}C, ^{36}Cl, ^{79}Se, ^{90}Sr, ^{99}Tc, ^{129}I, ^{135}Cs, and ^{137}Cs; of this set, only ^{90}Sr and ^{137}Cs have short half-lives (~ 30 years) relative to the 10,000-year time period. Some of the beta-photon emitters that are decay products of alpha and beta emitters are ^{137m}Ba, ^{228}Ac, ^{212}Pb, and ^{208}Tl; this group of radionuclides has half-lives ranging from minutes to several hours (SNL 2008a, Section 8.1.2.3[a]).

The annual doses were calculated by summing all the annual doses from those beta- and photon-emitting radionuclides included in the TSPA model for demonstrating compliance with the groundwater protection standards (SNL 2008a, Section 8.1.2.3[a]). The concentrations of these radionuclides in the groundwater were calculated with exclusion of unlikely features, events, and processes, or sequences of events and processes, as required by proposed 10 CFR 63.342(b).

The highest mean annual drinking water organ doses from beta and photon emitting radionuclides are to the thyroid and the lower large intestine and are estimated to be about 0.26 mrem and 0.25 mrem, respectively (SNL 2008a, Section 8.1.2.3[a]). The dose curves for these organs largely overlay, as shown in Figure 2.4-180 (SNL 2008a, Figure 8.1-13[a]). The whole body dose takes into account the differences in radiation sensitivity of various organs and tissues to the induction of stochastic effects, such as cancer. The maximum mean annual drinking water dose from beta- and photon-emitting radionuclides to the whole body is estimated to be about 6×10^{-2} mrem (SNL 2008a, Table 8.1-2[a] and Figure 8.1-13[a]). Dose to the thyroid is largely attributable to ^{129}I, while ^{99}Tc contributes primarily to the alimentary tract organs, with the lower large intestine and the stomach receiving the highest doses (EPA 2002, CD-ROM, ingestion dose coefficients for ^{99}Tc and ^{129}I). Whole body dose is calculated as a weighted sum of doses to the individual organs. In this calculation, the alimentary tract organs, in particular the colon (lower large intestine) and the stomach, have large tissue weighting factors relative to other organs (proposed 40 CFR Part 197 (70 FR 49014, Appendix A, Table A.2)). The ingestion of ^{99}Tc largely contributes to the dose to these organs (EPA 2002, CD-ROM, ingestion dose coefficient for ^{99}Tc). Thus, most of the whole body dose can be attributed to the dose from ^{99}Tc to the lower large intestine and the stomach, and to the dose from ^{129}I to the thyroid (SNL 2008a, Section 8.1.2.3[a]).

The calculated maximum whole body and organ doses from drinking water from combined beta and photon emitting radionuclides, for the 10,000-year period after disposal, are lower than the limit of 4 mrem per year (SNL 2008a, Section 8.1.2.3[a]). Thus, these results support a finding of reasonable expectation that, for 10,000 years of undisturbed performance after disposal, releases of beta- and photon-emitting radionuclides from waste in the Yucca Mountain disposal system into the accessible environment will not cause the level of radioactivity in the representative volume of groundwater to exceed the combined beta- and photon-emitting radionuclide limit set in 10 CFR 63.331 (Table 1).

Contributions of the modeling cases to the whole body and the thyroid beta-photon doses from drinking water are represented in Figure 2.4-181 (SNL 2008a, Figure 8.1-15[a]). As can be seen on this figure, the largest contributions to mean annual doses to the thyroid and whole body are attributable to the seismic ground motion modeling case. The dominance of this modeling case for the mean annual doses to the thyroid and whole body is similar to its dominance in the total mean annual dose to the RMEI and is explained by the fact that the seismic ground motion modeling case represents a larger expected number of breached waste packages and therefore larger radionuclide releases (SNL 2008a, Section 8.1.2.3[a]).

2.4.4.2 Evaluation of Total Dissolved Solids in the Aquifer
[NUREG-1804, Section 2.2.1.4.3.3: AC 3(1)]

Groundwater quality data collected to measure total dissolved solids indicate the aquifer at the compliance location contains significantly less than 10,000 mg/L of total dissolved solids. Water samples collected from a Nevada Department of Transportation (NDOT) well (BSC 2005d, Figure 1) near the intersection of U.S. Highway 95 and Nevada State Route 373 (approximate location of the hypothetical community) have been measured to have 385 mg/L of total dissolved solids (DTN: GS971000012847.004).

In addition, water quality data from the Alluvial Testing Complex have been measured for major ion concentrations during pump tests and tracer tests conducted at borehole NC-EWDP-19D, which is approximately located at the boundary of the accessible environment (Figure 2.3.9-4). It is one of three wells located at the complex that makes up part of the Nye County Early Warning Drilling Program. The well is screened at different intervals. The total dissolved solids from these samples, estimated as the sum of the major ion concentrations, are also less than 500 mg/L (SNL 2007af,

Table B4-2). Based on these data, the representative volume of groundwater is within an aquifer containing significantly less than 10,000 mg of total dissolved solids per liter of water.

2.4.4.3 Physical Dimensions of the Representative Volume of Groundwater *[NUREG-1804, Section 2.2.1.4.3.3: AC 1, AC 2, AC 3]*

This section provides the methods and assumptions used to determine the location and shape of the representative volume of groundwater. The representative volume is the volume of groundwater that would be withdrawn annually from aquifer to supply a given water demand (10 CFR 63.332(a)). The groundwater protection analysis is based on the assumption that all radionuclides in the simulated plume of contamination are captured in the 3,000 acre-ft representative volume (SNL 2008a, Sections 6.3.10 and 8.1.2). This assumption ensures that the radionuclide concentration in 3,000 acre-ft is conservative regardless of the dimensions of the representative volume.

2.4.4.3.1 Methods and Assumptions Used to Determine the Physical Dimensions of the Representative Volume of Groundwater

The NRC requires that the representative volume includes the highest concentration level in the simulated plume of contamination in the accessible environment (10 CFR 63.332(a)(1)). The plume of contamination is that volume of groundwater in the predominant direction of groundwater flow that contains radioactive contamination from repository releases (10 CFR 63.302). The plume of contamination is transported along the radionuclide migration path from the repository to the accessible environment. Thus, the representative volume is located along the radionuclide migration path from the repository to the accessible environment, and includes the highest concentration level in the radionuclide migration path. The assumption in the TSPA of total radionuclide capture in the 3,000-acre-ft representative volume ensures that the highest concentration is included in the simulated plume (SNL 2008a, Section 8.1.2).

Calculations of radionuclide transport from the repository to the accessible environment to evaluate compliance with the groundwater protection standards use the same model as that for the individual protection standards. A suite of saturated zone models (SNL 2007af, Section 6.3, Section 6.5.2.4, and Figure 6-17; SNL 2008h, Sections 5 and 6.3) is used to determine the location of the representative volume along the radionuclide migration path from the repository to the accessible environment. Section 2.3.9.3.4 describes how these various saturated zone models are linked together to support the performance assessment of the repository. Some discussion of the models is presented here, with more detail found in Section 2.3.9. The location of the plume is determined using hydrologic characteristics, which have cautious but reasonable values representative of the aquifers along the radionuclide migration path from the repository to the accessible environment, as determined by site characterization.

Saturated Zone Flow and Transport Modeling—The saturated zone flow and transport component model of the TSPA is used to evaluate the migration of radionuclides from their introduction at the water table below the repository to the point of release to the accessible environment. Several numerical models are used to support this model. The saturated zone site-scale flow model provides the three-dimensional groundwater flow field from the repository to the accessible environment. The site-scale saturated zone flow model forms the basis of the site-scale saturated zone transport model, which adds the simulation of radionuclide transport. The site-scale saturated zone transport model is the basis for two abstraction models that feed directly into the TSPA analyses: the saturated zone flow and transport abstraction model, and the saturated zone one-dimensional transport model, which provides the transport simulation capability for radionuclide decay products resulting from decay and ingrowth during transport.

The results of these abstraction models incorporate both the conceptual model and parameter uncertainty. The uncertainty is represented through a series of Monte Carlo simulations used to evaluate the impact of the range of values for each parameter. The general approach to modeling radionuclide migration and the assessment of uncertainty in the saturated zone is described in Section 2.3.9.

The saturated zone flow and transport abstraction model provides the TSPA with a set of radionuclide unit mass breakthrough curves at the accessible environment and the methodology for coupling these results into the TSPA simulations of radionuclide releases to the biosphere. The convolution integral method is then used in the TSPA model to determine the radionuclide mass flux at the accessible environment as a function of the transient radionuclide mass flux at the water table beneath the repository (SNL 2008f, Section 6.5.1.1). It combines information about the response of the saturated zone to the input of one unit per year of radionuclide mass, as simulated by the saturated zone flow and transport abstraction model, with the radionuclide source history from the unsaturated zone to calculate transient system behavior. The output is the time-varying radionuclide mass release at the accessible environment (SNL 2008f, Section 6.5). The saturated zone one-dimensional transport model is based upon the full three-dimensional model, but relies on a simplified representation of groundwater flow to simulate transport of radioactive decay and ingrowth products originating during transport (Section 2.3.9.1).

Predicted Flow Paths—The analysis of the groundwater flow system and its flow paths requires properly capturing the location and dynamics of the potential flow paths. The particle-tracking capability of the finite element heat- and mass-transfer software code illustrates flow paths simulated by the calibrated site-scale saturated zone flow model. One hundred particles were distributed randomly over the area beneath the repository, and were allowed to migrate subject to advection only (nondispersive) until they reached the saturated zone site-scale model boundary (Figure 2.3.9-14). The pathways generally leave the area beneath the repository and travel in a south-southeasterly direction to the southern part of the postclosure controlled area boundary. From the postclosure controlled area boundary to the end of the model domain, the flow paths trend to the south-southwest and generally follow Fortymile Wash. Some of the pathways follow fault zones along Fortymile Wash (Figure 2.3.9-11). At the compliance boundary, the predicted pathways extend over a width of about 3,000 m and a depth of about 200 m (Figure 2.3.9-14). The hydrogeologic units through which the flow below the repository passes consist of the Crater Flat group (Bullfrog, Tram, and Prow Pass) with most of the flow in the Bullfrog unit, the upper volcanic aquifer, the upper volcanic confining unit, the valley fill unit, and the undifferentiated valley-fill unit. Figure 2.3.9-14 includes a vertical cross section of the path lines. Evident in the figure is the shallow depth of the path lines relative to the water table along most of the pathways in the vicinity of the southern end of the postclosure controlled area boundary, which is consistent with data supporting an upward head gradient (Section 2.3.9.2.3.3).

2.4.4.3.2 Determination of Physical Dimensions of the Representative Volume

The representative volume, described in 10 CFR 63.332(a)(3), is 3,000 acre-ft of groundwater that would be withdrawn annually from the aquifer at the accessible environment. The representative volume is used to calculate the concentration of radionuclides in groundwater for evaluating compliance with the postclosure performance standards. 10 CFR 63.332(b) states that the DOE must use one of two alternative methods for determining the dimensions of the representative volume: a well capture zone method (10 CFR 63.332(b)(1)), or a slice of the plume method (10 CFR 63.332(b)(2)). The TSPA model uses the slice of the plume method, in which the edge of the plume is effectively selected to be where the concentration of radionuclides is zero (10 CFR 63.332(b)(2)(i)). In this approach, the radionuclides released from the repository and crossing the boundary of accessible environment in a year are collected in the representative volume, regardless of the physical extent of the contamination plume. This is a conservative, bounding assumption with regard to calculating radionuclide concentration in the groundwater. As a result of this conservative approximation, the dimensions of the representative volume are not directly used in calculating radionuclide concentration or in the TSPA analyses, because all of the transported mass crossing the boundary of the accessible environment is captured in the TSPA model.

Although not directly used in the TSPA, calculating the dimensions of the representative volume is required by 10 CFR 63.332(b). The physical dimensions of the representative volume can be approximated by analyzing the spatial distribution of the simulated groundwater flow paths predicted by the saturated zone model. The slice of the plume is perpendicular to the prevalent direction of flow of groundwater in the shallow alluvial aquifer, where the simulated contaminant plume is located, as required by 10 CFR 63.332(b)(2)(ii). The orientation of the slice is approximately east-west, consistent with the simulated flow paths in the saturated zone site-scale flow model being in an approximately north-south orientation of this location (Figure 2.3.9-14). Based on saturated zone groundwater flow modeling results presented in Figure 2.3.9-14 (SNL 2007af, Figure 6-17), a reasonable length (transverse to flow) of the slice is about 3,000 m. This is based on capturing the simulated flow paths crossing the boundary of the accessible environment. Based on the groundwater flow model results presented in Figure 2.3.9-14 (SNL 2007af, Figure 6-17), 200 m is a reasonable estimate of the plume depth. The estimated average groundwater flow rate is about 6 m/yr along the flow path in this area (SNL 2008f, Table 6-5[a]; flow rate in the alluvium at 13 to 18 km for the horizontal anisotropy of 5), and thus the calculated width of the groundwater plume slice, parallel to the direction of flow, is about 6 m.

The estimated dimensions of the slice of the plume can also be compared with the size of the representative volume of 3,000 acre-ft, as follows:

$$3{,}000 \text{ acre-ft} \approx 3.714 \times 10^6 \text{ m}^3 \approx (3{,}000 \text{ m}) \times (6 \text{ m}) \times (200 \text{ m}) \qquad \text{(Eq. 2.4-46)}$$

Assuming that the volume of groundwater contained within the slice of the plume equals the representative volume, as required by 10 CFR 63.332 (b)(2)(iii), the physical dimensions of the representative volume of groundwater are thus, approximately, 3,000 m horizontally transverse to the flow, 6 m in the direction of flow, and 200 m in depth, rounded to one significant figure. Based on the expected value of the alluvium flow porosity of about 0.18 (Table 2.3.9-2; SNL 2007x,

Table 6.5-5), the physical dimensions of the aquifer containing this representative volume of groundwater are about 3,000 m horizontally, 30 m in the direction of flow, and 200 m in depth, where the values were rounded to one significant figure.

In summary, TSPA analyses assume that all radionuclide mass transported by groundwater across the boundary of the accessible environment is contained in the representative volume of the groundwater. This is a conservative, bounding assumption with regard to calculating radionuclide concentration in the groundwater. Consequently, the dimensions of the representative volume are not used directly in the calculation of radionuclide concentration or in the TSPA analyses, but rather all of the transported mass is captured in the TSPA model.

2.4.5 General References

70 FR 49014. Public Health and Environmental Radiation Protection Standards for Yucca Mountain, NV.

70 FR 53313. Implementation of a Dose Standard After 10,000 Years.

Apted, M. 2006. *Program on Technology Innovation: Effects of Multiple Seismic Events and Rockfall on Long-Term Performance of the Yucca Mountain Repository.* EPRI TR 1013444. Palo Alto, California: Electric Power Research Institute. TIC: 259559.

Apted, M. and Kessler, M. 2005. *Program on Technology Innovation: Effects of Seismicity and Rockfall on Long-Term Performance of the Yucca Mountain Repository, 2005 Progress Report.* EPRI TR 1011812. Palo Alto, California: Electric Power Research Institute. TIC: 259560.

Apted, M. and Ross, A. 2005. *Program on Technology Innovation: Evaluation of a Spent Fuel Repository at Yucca Mountain, Nevada, 2005 Progress Report.* EPRI TR 1010074. Palo Alto, California: Electric Power Research Institute. TIC: 259561.

Apted, M.; Ross, A.; and Kessler, J. 2006. *Program on Technology Innovation: EPRI Yucca Mountain Spent Fuel Repository Evaluation, 2006 Progress Report.* EPRI TR 1013445. Palo Alto, California: Electric Power Research Institute. TIC: 259562.

Barnard, R.W.; Wilson, M.L.; Dockery, H.A.; Gauthier, J.H.; Kaplan, P.G.; Eaton, R.R.; Bingham, F.W.; and Robey, T.H. 1992. *TSPA 1991: An Initial Total-System Performance Assessment for Yucca Mountain.* SAND91-2795. Albuquerque, New Mexico: Sandia National Laboratories. ACC: NNA.19920630.0033.

Bourgoyne, A.T., Jr.; Millheim, K.K.; Chenevert, M.E.; and Young, F.S., Jr. 1986. "Rotary Drilling Bits." *Applied Drilling Engineering.* SPE Textbook Series Volume 2. Pages 190–245. Richardson, Texas: Society of Petroleum Engineers. TIC: 250085.

BSC (Bechtel SAIC Company) 2004a. *Characterize Framework for Igneous Activity at Yucca Mountain, Nevada.* ANL-MGR-GS-000001 REV 02. Las Vegas, Nevada: Bechtel SAIC Company. ACC: DOC.20041015.0002.

BSC 2004b. *UZ Flow Models and Submodels*. MDL-NBS-HS-000006 REV 02. Las Vegas, Nevada: Bechtel SAIC Company. ACC: DOC.20041101.0004.

BSC 2004c. *Future Climate Analysis.* ANL-NBS-GS-000008 REV 01. Las Vegas, Nevada: Bechtel SAIC Company. ACC: DOC.20040908.0005.

BSC 2004d. *Seepage Model for PA Including Drift Collapse.* MDL-NBS-HS-000002 REV 03. Las Vegas, Nevada: Bechtel SAIC Company. ACC: DOC.20040922.0008.

BSC 2004e. *CSNF Waste Form Degradation: Summary Abstraction.* ANL-EBS-MD-000015 REV 02. Las Vegas, Nevada: Bechtel SAIC Company. ACC: DOC.20040908.0001.

BSC 2004f. *DSNF and Other Waste Form Degradation Abstraction.* ANL-WIS-MD-000004 REV 04. Las Vegas, Nevada: Bechtel SAIC Company. ACC: DOC.20041201.0007.

BSC 2004g. *Defense HLW Glass Degradation Model.* ANL-EBS-MD-000016 REV 02. Las Vegas, Nevada: Bechtel SAIC Company. ACC: DOC.20041020.0015.

BSC 2004h. *Natural Analogue Synthesis Report.* TDR-NBS-GS-000027 REV 01. Las Vegas, Nevada: Bechtel SAIC Company. ACC: DOC.20040524.0008.

BSC 2004i. *Yucca Mountain Site Description.* TDR-CRW-GS-000001 REV 02 ICN 01. Two volumes. Las Vegas, Nevada: Bechtel SAIC Company. ACC: DOC.20040504.0008.

BSC 2004j. *Drift Degradation Analysis.* ANL-EBS-MD-000027 REV 03. Las Vegas, Nevada: Bechtel SAIC Company. ACC: DOC.20040915.0010.

BSC 2005a. *Parameter Sensitivity Analysis for Unsaturated Zone Flow.* ANL-NBS-HS-000049 REV 00. Las Vegas, Nevada: Bechtel SAIC Company. ACC: DOC.20050808.0005.

BSC 2005b. *Characteristics of the Receptor for the Biosphere Model.* ANL-MGR-MD-000005 REV 04. Las Vegas, Nevada: Bechtel SAIC Company. ACC: DOC.20050405.0005.

BSC 2005c. *Drift-Scale Coupled Processes (DST and TH Seepage) Models.* MDL-NBS-HS-000015 REV 02. Las Vegas, Nevada: Bechtel SAIC Company. ACC: DOC.20050114.0004.

BSC 2005d. *Radioactivity in FY 1998 Groundwater Samples from Wells and Springs Near Yucca Mountain.* BA0000000-01717-5705-00029 REV 01. Las Vegas, Nevada: Bechtel SAIC Company. ACC: DOC.20050114.0003.

BSC 2006. *Impacts of Solubility and Other Geochemical Processes on Radionuclide Retardation in the Natural System - Rev 01.* Las Vegas, Nevada: Bechtel SAIC Company. ACC: MOL.20060105.0022.

BSC 2008. *Thermal Loading Study of the TAD Waste Package.* 000-00C-WIS0-03100-000-00B. Las Vegas, Nevada: Bechtel SAIC Company. ACC: ENG.20080228.0004.

Bureau of the Census. 2002. "2000 Summary File 3 (SF 3) Sample Data, Amargosa Valley CCD, Nye County, Nevada." Washington, D.C.: U.S. Department of Commerce, Bureau of the Census. Accessed August 28, 2002. TIC: 253098.

Budnitz, B.; Ewing, R.C.; Moeller, D.W.; Payer, J.; Whipple, C.; and Witherspoon, P.A. 1999. *Peer Review of the Total System Performance Assessment–Viability Assessment Final Report.* Las Vegas, Nevada: Total System Performance Assessment Peer Review Panel. ACC: MOL.19990317.0328.

Cranwell, R.M.; Guzowski, R.V.; Campbell, J.E.; and Ortiz, N.R. 1990. *Risk Methodology for Geologic Disposal of Radioactive Waste: Scenario Selection Procedure.* NUREG/CR-1667. Washington, D.C.: U.S. Nuclear Regulatory Commission. ACC: NNA.19900611.0073.

CRWMS M&O (Civilian Radioactive Waste Management System Management and Operating Contractor) 1995. *Total System Performance Assessment—1995: An Evaluation of the Potential Yucca Mountain Repository.* B00000000-01717-2200-00136 REV 01. Las Vegas, Nevada: Civilian Radioactive Management System Management and Operating Contractor. ACC: MOL.19960724.0188.

CRWMS M&O 1998. *Probabilistic Seismic Hazard Analyses for Fault Displacement and Vibratory Ground Motion at Yucca Mountain, Nevada.* Milestone SP32IM3, September 23, 1998. Three volumes. Las Vegas, Nevada: Civilian Radioactive Waste Management System Management and Operating Contractor. ACC: MOL.19981207.0393.

CRWMS M&O 2000a. *Total System Performance Assessment for the Site Recommendation.* TDR-WIS-PA-000001 REV 00 ICN 01. Las Vegas, Nevada: Civilian Radioactive Waste Management System Management and Operating Contractor. ACC: MOL.20001220.0045.

CRWMS M&O 2000b. *Waste Packages and Source Terms for the Commercial 1999 Design Basis Waste Streams.* CAL-MGR-MD-000001 REV 00. Las Vegas, Nevada: Civilian Radioactive Waste Management System Management and Operating Contractor. ACC: MOL.20000214.0479.

Cullen, A.C. and Frey, H.C. 1999. *Probabilistic Techniques in Exposure Assessment: A Handbook for Dealing with Variability and Uncertainty in Models and Inputs.* New York, New York: Plenum Press. TIC: 242815.

D'Agnese, F.A.; O'Brien, G.M.; Faunt, C.C.; and San Juan, C.A. 1999. *Simulated Effects of Climate Change on the Death Valley Regional Ground-Water Flow System, Nevada and California.* Water-Resources Investigations Report 98-4041. Denver, Colorado: U.S. Geological Survey. TIC: 243555.

Dobson, P.F.; Cook, P.J.; Ghezzehei, T.; Rodriguez, J.A.; and de la Garza, R. 2008. *Heterogeneous Seepage at the Nopal I Uranium Mine, Chihuahua, Mexico.* LBNL-34E. Berkeley, California: Ernest Orlando Lawrence Berkeley National Laboratory. ACC: LLR.20080225.0081.

DOE (U.S. Department of Energy) 1998. *Total System Performance Assessment.* Volume 3 of *Viability Assessment of a Repository at Yucca Mountain.* DOE/RW-0508. Washington, D.C.: U.S.

Department of Energy, Office of Civilian Radioactive Waste Management. ACC: MOL.19981007.0030.

DOE 2000. *DOE Spent Nuclear Fuel Grouping in Support of Criticality, DBE, TSPA-LA.* DOE/SNF/REP-046, Rev. 0. Idaho Falls, Idaho: U.S. Department of Energy, Idaho Operations Office. ACC: DOC.20030905.0021.

DOE 2002. *Final Environmental Impact Statement for a Geologic Repository for the Disposal of Spent Nuclear Fuel and High-Level Radioactive Waste at Yucca Mountain, Nye County, Nevada.* DOE/EIS-0250. Washington, D.C.: U.S. Department of Energy, Office of Civilian Radioactive Waste Management. ACC: MOL.20020524.0314 through MOL.20020524.0320.

DOE 2003. *Source Term Estimates for DOE Spent Nuclear Fuels.* DOE/SNF/REP-078, Rev. 0. Idaho Falls, Idaho: U.S. Department of Energy, Idaho Operations Office. TIC: 254275.

DOE 2004. *Source Term Estimates for DOE Spent Nuclear Fuels.* DOE/SNF/REP-078, Rev. 1. Three volumes. Idaho Falls, Idaho: U.S. Department of Energy, Idaho Operations Office. ACC: MOL.20040524.0451.

DOE 2005. *Management and Technical Support Peak Dose Sensitivity Analysis.* Las Vegas, Nevada: U.S. Department of Energy, Office of Civilian Radioactive Waste Management. ACC: MOL.20060320.0141.

DOE 2007a. *Design Document for: EXDOC_LA Version 2.0.* Document ID: 11193-DD-2.0-01. Las Vegas, Nevada: U. S. Department of Energy, Office of Repository Development. ACC: MOL.20070723.0262.

DOE 2007b. *Quality Assurance Requirements and Description.* DOE/RW-0333P, Rev. 19. Washington, D. C.: U.S. Department of Energy, Office of Civilian Radioactive Waste Management. ACC: DOC.20070717.0006.

DOE 2007c. *Design Document for: GoldSim v9.60.* Document ID: 10344-DD-9.60-01. Las Vegas, Nevada: U.S. Department of Energy, Office of Repository Development. ACC: MOL.20070416.0338.

DOE 2007d. *Requirements Document for: GoldSim v9.60.* Document ID: 10344-RD-9.60-00. Las Vegas, Nevada: U.S. Department of Energy, Office of Repository Development. ACC: MOL.20070416.0330.

DOE 2007e. *Software Validation Report for: GoldSim v9.60 on Windows 2000.* Document ID: 10344-SVR-9.60-00-WIN2000. Las Vegas, Nevada: U.S. Department of Energy, Office of Repository Development. ACC: MOL.20070416.0341.

DOE 2007f. *Software Validation Report for: EXDOC_LA Version 2.0.* Document ID: 11193-SVR-2.0-00-WINXP. Las Vegas, Nevada: U. S. Department of Energy, Office of Repository Development. ACC: MOL.20070723.0270.

DOE 2007g. *Requirements Document for: EXDOC_LA Version 2.0.* Document ID: 11193-RD-2.0-01. Las Vegas, Nevada: U. S. Department of Energy, Office of Repository Development. ACC: MOL.20070723.0260.

Eckerman, K.F. and Ryman, J.C. 1993. *External Exposure to Radionuclides in Air, Water, and Soil, Exposure-to-Dose Coefficients for General Application, Based on the 1987 Federal Radiation Protection Guidance.* EPA 402-R-93-081. Federal Guidance Report No. 12. Washington, D.C.: U.S. Environmental Protection Agency, Office of Radiation and Indoor Air. TIC: 225472.

Eisenberg, N.A.; Lee, M.P.; Federline, M.V.; Wingefors, S.; Andersson, J.; Norrby, S.; Sagar, B.; and Wittmeyer, G.W. 1999. *Regulatory Perspectives on Model Validation in High-Level Radioactive Waste Management Programs: A Joint NRC/SKI White Paper.* NUREG-1636. Washington, D.C.: U.S. Nuclear Regulatory Commission. TIC: 246310.

EPA (U.S. Environmental Protection Agency) 1997. *Activity Factors.* Volume III of *Exposure Factors Handbook.* EPA/600/P-95/002Fc. Washington, D.C.: U.S. Environmental Protection Agency. TIC: 241062.

EPA 2002. *Federal Guidance Report 13, CD Supplement, Cancer Risk Coefficients for Environmental Exposure to Radionuclides, EPA.* EPA-402-C-99-001, Rev. 1. Washington, D.C.: U.S. Environmental Protection Agency. ACC: MOL.20051013.0016.

EPRI (Electric Power Research Institute) 2002. *Evaluation of the Proposed High-Level Radioactive Waste Repository at Yucca Mountain Using Total System Performance Assessment, Phase 6.* EPRI TR-1003031. Palo Alto, California: Electric Power Research Institute. TIC: 252239.

Fillmore, D.L. 1998. *Parameter Selection for Department of Energy Spent Nuclear Fuel to be Used in the Yucca Mountain Viability Assessment.* INEEL/EXT-98-00666. Idaho Falls, Idaho: Idaho National Engineering and Environmental Laboratory. ACC: MOL.19990511.0296.

GoldSim Technology Group 2007a. *GoldSim Contaminant Transport Module*. Version 4.20. Issaquah, Washington: GoldSim Technology Group. TIC: 259223.

GoldSim Technology Group 2007b. *Radioactive and Hazardous Waste Management Applications using Goldsim*. White Paper. Issaquah, Washington: GoldSim Technology Group. TIC: 260020.

Goldstein, S.J.; Murrell, M.T.; Simmons, A.M.; Oliver, R.D.; Dobson, P.F.; Reyes, I.A.; and de la Garza, R. 2003. “Evidence for Radium Mobility at the Nopal I Uranium Deposit, Peña Blanca, Mexico.” *Abstracts with Programs—Geological Society of America, 35* (6), 436. Boulder, Colorado: Geological Society of America. TIC: 254862.

Gordon, S.J. and Brady, P.V. 2002. “In Situ Determination of Long-Term Basaltic Glass Dissolution in the Unsaturated Zone.” *Chemical Geology, 190* (1–4), 113–122. New York, New York: Elsevier. TIC: 258314.

GS971000012847.004. Water Quality Data Collected from Springs and Wells in the Yucca Mountain Region from May 6, 1997 to May 15, 1997. Submittal date: 10/23/1997.

Guimerà, J. and Carrera, J. 2000. "A Comparison of Hydraulic and Transport Parameters Measured in Low-Permeability Fractured Media." *Journal of Contaminant Hydrology, 41* (3–4), 261–281. New York, New York: Elsevier. TIC: 251013.

Helton, J.C. 1999. "Uncertainty and Sensitivity Analysis in Performance Assessment for the Waste Isolation Pilot Plant." *Computer Physics Communications, 117* (1–2), 156–180. New York, New York: Elsevier. TIC: 253133.

Helton, J.C. and Davis, F.J. 2000. *Sampling-Based Methods for Uncertainty and Sensitivity Analysis.* SAND99-2240. Albuquerque, New Mexico: Sandia National Laboratories. TIC: 251256.

Helton, J.C. and Davis, F.J. 2002. *Latin Hypercube Sampling and the Propagation of Uncertainty in Analyses of Complex Systems.* SAND2001-0417. Albuquerque, New Mexico: Sandia National Laboratories. TIC: 254367.

Helton, J.C. and Davis, F.J. 2003. "Latin Hypercube Sampling and the Propagation of Uncertainty in Analyses of Complex Systems." *Reliability Engineering & System Safety, 81* (1), 23–69. New York, New York: Elsevier. TIC: 256239.

Helton, J.C.; Johnson, J.D.; McKay, M.D.; Shiver, A.W.; and Sprung, J.L. 1995. "Robustness of an Uncertainty and Sensitivity Analysis of Early Exposure Results with the MACCS Reactor Accident Consequence Model." *Reliability Engineering & System Safety, 48* (2), 129–148. New York, New York: Elsevier. TIC: 253092.

Helton, J.C.; Johnson, J.D.; Sallaberry, C.J.; and Storlie, C.B. 2006. "Survey of Sampling-Based Methods for Uncertainty and Sensitivity Analysis." *Reliability Engineering and System Safety, 91* (2006), 1175–1209. New York, New York: Elsevier. TIC: 259831.

Hill, B.E.; Connor, C.B.; Jarzemba, M.S.; La Femina, P.C.; Navarro, M.; and Strauch, W. 1998. "1995 Eruptions of Cerro Negro Volcano, Nicaragua, and Risk Assessment for Future Eruptions." *Geological Society of America Bulletin, 110* (10), 1231–1241. Boulder, Colorado: Geological Society of America. TIC: 245102.

ICRP (International Commission on Radiological Protection) 1991. *1990 Recommendations of the International Commission on Radiological Protection*. Volume 21, Nos. 1–3 of *Annals of the ICRP.* ICRP Publication 60. New York, New York: Pergamon Press. TIC: 235864.

ICRP 1994. *Human Respiratory Tract Model for Radiological Protection.* Volume 24, Nos. 1–3 of *Annals of the ICRP.* Smith, H., ed. ICRP Publication 66. New York, New York: Pergamon. TIC: 249223.

Iman, R.L. 1982. "Statistical Methods for Including Uncertainties Associated with the Geologic Isolation of Radioactive Waste Which Allow for a Comparison with Licensing Criteria." *Proceedings of the Symposium on Uncertainties Associated with the Regulation of the Geologic Disposal of High-Level Radioactive Waste, Gatlinburg, Tennessee, March 9–13, 1981.* Kocher, D.C., ed. NUREG/CP-0022. 145–157. Washington, D.C.: U.S. Nuclear Regulatory Commission. TIC: 213069.

Iman, R.L. 1992. “Uncertainty and Sensitivity Analysis for Computer Modeling Applications.” *Reliability Technology, 1992, Presented at the Winter Annual Meeting of the American Society of Mechanical Engineers, Anaheim, California, November 8-13, 1992.* Cruse, T.A., ed. AD-Vol. 28. Pages 153–168. New York, New York: American Society of Mechanical Engineers. TIC: 252828.

Iman, R.L. and Helton, J.C. 1988. “An Investigation of Uncertainty and Sensitivity Analysis Techniques for Computer Models.” *Risk Analysis, 8* (1), 71–90. New York, New York: Plenum Press. TIC: 252831.

Iman, R.L. and Helton, J.C. 1991. “The Repeatability of Uncertainty and Sensitivity Analyses for Complex Probabilistic Risk Assessments.” *Risk Analysis, 11* (4), 591–606. New York, New York: Plenum Press. TIC: 252830.

Jarzemba, M.S.; LaPlante, P.A.; and Poor, K.J. 1997. *ASHPLUME Version 1.0—A Code for Contaminated Ash Dispersal and Deposition, Technical Description and User’s Guide.* CNWRA 97-004, Rev. 1. San Antonio, Texas: Center for Nuclear Waste Regulatory Analyses. ACC: MOL.20010727.0162.

Kozak, M. and Kessler, J. 2005. *Program on Technology Innovation: EPRI Yucca Mountain Total System Performance Assessment Code (IMARC) Version 8, Model Description.* 1011813. Palo Alto, California: Electric Power Research Institute. TIC: 259558.

Liu, H.H.; Doughty, C.; and Bodvarsson, G.S. 1998. “An Active Fracture Model for Unsaturated Flow and Transport in Fractured Rocks.” *Water Resources Research, 34* (10), 2633–2646. Washington, D.C.: American Geophysical Union. TIC: 243012.

Loo, H.H.; MacKay, N.S.; and Wheatley, P.D. 2004. *Additional DOE Spent Nuclear Fuel Information in Support of TSPA-LA Analysis.* DOE/SNF/REP-081, Rev. 0. Idaho Falls, Idaho: U.S. Department of Energy, DOE Idaho Operations Office. ACC: DOC.20040202.0007.

McKay, M.D.; Beckman, R.J.; and Conover, W.J. 1979. “A Comparison of Three Methods for Selecting Values of Input Variables in the Analysis of Output from a Computer Code.” *Technometrics, 21* (2), 239–245. Alexandria, Virginia: American Statistical Association. TIC: 221741.

McKnight, S.B. and Williams, S.W. 1997. “Old Cinder Cone or Young Composite Volcano?: The Nature of Cerro Negro, Nicaragua.” *Geology, 25* (4), 339–342. Boulder, Colorado: Geological Society of America. TIC: 254104.

MO0708TSPAPOST.000. TSPA-LA Model Post Implementation Verification Tests. Submittal date: 08/08/2007.

MO0803TSPAPSAR.000. TSPA Supplemental Plots for Use in the SAR. Submittal date: 03/17/2008.

Murphy, W.M. 1995. “Contributions of Thermodynamic and Mass Transport Modeling to Evaluation of Groundwater Flow and Groundwater Travel Time at Yucca Mountain, Nevada.”

Scientific Basis for Nuclear Waste Management XVIII, Symposium held October 23–27, 1994, Kyoto, Japan. Murakami, T. and Ewing, R.C., eds. *353*, 419-426. Pittsburgh, Pennsylvania: Materials Research Society. TIC: 216341.

Murphy, W.M. and Codell, R.B. 1999. “Alternate Source Term Models for Yucca Mountain Performance Assessment Based on Natural Analog Data and Secondary Mineral Solubility.” *Scientific Basis for Nuclear Waste Management XXII, Symposium held November 30–December 4, 1998, Boston, Massachusetts.* Wronkiewicz, D.J. and Lee, J.H., eds. 556, 551–558. Warrendale, Pennsylvania: Materials Research Society. TIC: 246426.

Murphy, W.M.; Pearcy, E.C.; and Goodell, P.C. 1991. “Possible Analog Research Sites for the Proposed High-Level Nuclear Waste Repository in Hydrologically Unsaturated Tuff at Yucca Mountain, Nevada.” *Nuclear Science and Technology, Fourth Natural Analogue Working Group Meeting and Pocos de Caldas Project Final Workshop, Pitlochry, 18 to 22 June 1990, Scotland, Final Report.* Come, B. and Chapman N.A., eds. EUR 13014 EN. Pages 267–276. Brussels, Belgium: Commission of European Communities. TIC: 248757.

National Research Council 1990. *Rethinking High-Level Radioactive Waste Disposal, A Position Statement of the Board on Radioactive Waste Management.* Washington, D.C.: National Academy Press. TIC: 205153.

Nuclear Waste Policy Amendments Act of 1987. Public Law No. 100-203, 101 Stat. 1330.

OECD (Organisation for Economic Co-operation and Development) and IAEA (International Atomic Energy Agency) 2002. *An International Peer Review of the Yucca Mountain Project TSPA-SR: Total System Performance Assessment for the Site Recommendation (TSPA-SR).* Paris, France: Organisation for Economic Co-operation and Development, Nuclear Energy Agency. TIC: 252385.

Owen, A.B. 1992. “A Central Limit Theorem for Latin Hypercube Sampling.” *Journal of the Royal Statistical Society: Series B, Statistical Methodology, 54* (2), 541–551. London, England: Royal Statistical Society. TIC: 253131.

Pearcy, E.C. 1994. *Fracture Transport of Uranium at the Nopal I Natural Analog Site.* CNWRA 94-011. San Antonio, Texas: Center for Nuclear Waste Regulatory Analyses. TIC: 247808.

Pearcy, E.C.; Prikryl, J.D.; Murphy, W.M.; and Leslie, B.W. 1993. *Uranium Mineralogy of the Nopal I Natural Analog Site, Chihuahua, Mexico.* CNWRA 93-012. San Antonio, Texas: Center for Nuclear Waste Regulatory Analyses. TIC: 246628.

Pickett, D.A. and Murphy, W.M. 1997. “Isotopic Constraints on Radionuclide Transport at Pena Blanca.” *Seventh EC Natural Analogue Working Group Meeting: Proceedings of an International Workshop held in Stein am Rhein, Switzerland from 28 to 30 October 1996.* von Maravic, H. and Smellie, J., eds. EUR 17851 EN. Pages 113–122. Luxembourg, Luxembourg: Office for Official Publications of the European Communities. TIC: 247461.

Putot, C.J.M.; Guesnon, J.; Perreau, P.J.; and Constantinescu, A. 2000. "Quantifying Drilling Efficiency and Disruption: Field Data vs. Theoretical Model." *SPE Drilling & Completion, 15* (2), 118–125. Richardson, Texas: Society of Petroleum Engineers. TIC: 255897.

Reimus, P.W.; Callahan, T.J.; Ware, S.D.; Haga, M.J.; and Counce, D.A. 2007. "Matrix Diffusion Coefficients in Volcanic Rocks at the Nevada Test Site: Influence of Matrix Porosity, Matrix Permeability, and Fracture Coating Minerals." *Journal of Contaminant Hydrology, 93* (1–4), 85–95. New York, New York: Elsevier. TIC: 259673.

Robinson, B.A.; Wolfsberg, A.V.; Viswanathan, H.S.; and Reimus, P.W. 2007. "A Colloid-Facilitated Transport Model with Variable Colloid Transport Properties." *Geophysical Research Letters, 34*, 1–5. Washington, D.C.: American Geophysical Union. TIC: 259346.

SN0703PAEBSRTA.001. Inputs Used in the Engineered Barrier System (EBS) Radionuclide Transport Abstraction. Submittal date: 08/28/2007.

SNL (Sandia National Laboratories) 2007a. *Analysis of Mechanisms for Early Waste Package/Drip Shield Failure.* ANL-EBS-MD-000076 REV 00. Las Vegas, Nevada: Sandia National Laboratories. ACC: DOC.20070629.0002.

SNL 2007b. *UZ Flow Models and Submodels.* MDL-NBS-HS-000006 REV 03 ADD 01. Las Vegas, Nevada: Sandia National Laboratories. ACC: DOC.20080108.0003.

SNL 2007c. *Seismic Consequence Abstraction.* MDL-WIS-PA-000003 REV 03. Las Vegas, Nevada: Sandia National Laboratories. ACC: DOC.20070928.0011.

SNL 2007d. *Total System Performance Assessment Data Input Package for Requirements Analysis for Engineered Barrier System In-Drift Configuration.* TDR-TDIP-ES-000010 REV 00. Las Vegas, Nevada: Sandia National Laboratories. ACC: DOC.20070921.0008.

SNL 2007e. *Stress Corrosion Cracking of Waste Package Outer Barrier and Drip Shield Materials.* ANL-EBS-MD-000005 REV 04. Las Vegas, Nevada: Sandia National Laboratories. ACC: DOC.20070913.0001.

SNL 2007f. *In-Drift Natural Convection and Condensation.* MDL-EBS-MD-000001 REV 00 ADD 01. Las Vegas, Nevada: Sandia National Laboratories. ACC: DOC.20070907.0004.

SNL 2007g. *Abstraction of Drift Seepage.* MDL-NBS-HS-000019 REV 01 ADD 01. Las Vegas, Nevada: Sandia National Laboratories. ACC: DOC.20070807.0001.

SNL 2007h. *In-Package Chemistry Abstraction.* ANL-EBS-MD-000037 REV 04 ADD 01. Las Vegas, Nevada: Sandia National Laboratories. ACC: DOC.20070816.0004.

SNL 2007i. *Engineered Barrier System: Physical and Chemical Environment.* ANL-EBS-MD-000033 REV 06. Las Vegas, Nevada: Sandia National Laboratories. ACC: DOC.20070907.0003.

SNL 2007j. *In-Drift Precipitates/Salts Model.* ANL-EBS-MD-000045 REV 03. Las Vegas, Nevada: Sandia National Laboratories. ACC: DOC.20070306.0037.

SNL 2007k. *EBS Radionuclide Transport Abstraction.* ANL-WIS-PA-000001 REV 03. Las Vegas, Nevada: Sandia National Laboratories. ACC: DOC.20071004.0001.

SNL 2007l. *Calibrated Unsaturated Zone Properties.* ANL-NBS-HS-000058 REV 00. Las Vegas, Nevada: Sandia National Laboratories. ACC: DOC.20070530.0013.

SNL 2007m. *Atmospheric Dispersal and Deposition of Tephra from a Potential Volcanic Eruption at Yucca Mountain, Nevada.* MDL-MGR-GS-000002 REV 03. Las Vegas, Nevada: Sandia National Laboratories. ACC: DOC.20071010.0003.

SNL 2007n. *Total System Performance Assessment Data Input Package for Requirements Analysis for Transportation Aging and Disposal Canister and Related Waste Package Physical Attributes Basis for Performance Assessment.* TDR-TDIP-ES-000006 REV 00. Las Vegas, Nevada: Sandia National Laboratories. ACC: DOC.20070918.0005.

SNL 2007o. *General Corrosion and Localized Corrosion of Waste Package Outer Barrier.* ANL-EBS-MD-000003 REV 03. Las Vegas, Nevada: Sandia National Laboratories. ACC: DOC.20070730.0003; DOC.20070807.0007.

SNL 2007p. *General Corrosion and Localized Corrosion of the Drip Shield.* ANL-EBS-MD-000004 REV 02 ADD 01. Las Vegas, Nevada: Sandia National Laboratories. ACC: DOC.20070807.0004.

SNL 2007q. *Analysis of Dust Deliquescence for FEP Screening.* ANL-EBS-MD-000074 REV 01 ADD 01. Las Vegas, Nevada: Sandia National Laboratories. ACC: DOC.20070911.0004.

SNL 2007r. *Cladding Degradation Summary for LA.* ANL-WIS-MD-000021 REV 03 ADD 01. Las Vegas, Nevada: Sandia National Laboratories. ACC: DOC.20070614.0002.

SNL 2007s. *Radionuclide Screening.* ANL-WIS-MD-000006 REV 02. Las Vegas, Nevada: Sandia National Laboratories. ACC: DOC.20070326.0003.

SNL 2007t. *Initial Radionuclide Inventories.* ANL-WIS-MD-000020 REV 01 ADD 01. Las Vegas, Nevada: Sandia National Laboratories. ACC: DOC.20070801.0001.

SNL 2007u. *Dissolved Concentration Limits of Elements with Radioactive Isotopes.* ANL-WIS-MD-000010 REV 06. Las Vegas, Nevada: Sandia National Laboratory. ACC: DOC.20070918.0010.

SNL 2007v. *Waste Form and In-Drift Colloids-Associated Radionuclide Concentrations: Abstraction and Summary.* MDL-EBS-PA-000004 REV 03. Las Vegas, Nevada: Sandia National Laboratories. ACC: DOC.20071018.0019.

SNL 2007w. *Radionuclide Transport Models Under Ambient Conditions.* MDL-NBS-HS-000008 REV 02 ADD 01. Las Vegas, Nevada: Sandia National Laboratories. ACC: DOC.20070718.0003.

SNL 2007x. *Saturated Zone In-Situ Testing.* ANL-NBS-HS-000039 REV 02. Las Vegas, Nevada: Sandia National Laboratories. ACC: DOC.20070608.0004.

SNL 2007y. *Biosphere Model Report.* MDL-MGR-MD-000001 REV 02. Las Vegas, Nevada: Sandia National Laboratories. ACC: DOC.20070830.0007.

SNL 2007z. *Dike/Drift Interactions.* MDL-MGR-GS-000005 REV 02. Las Vegas, Nevada: Sandia National Laboratories. ACC: DOC.20071009.0015.

SNL 2007aa. *Number of Waste Packages Hit by Igneous Events.* ANL-MGR-GS-000003 REV 03. Las Vegas, Nevada: Sandia National Laboratories. ACC: DOC.20071002.0001.

SNL 2007ab. *Redistribution of Tephra and Waste by Geomorphic Processes Following a Potential Volcanic Eruption at Yucca Mountain, Nevada.* MDL-MGR-GS-000006 REV 00. Las Vegas, Nevada: Sandia National Laboratories. ACC: DOC.20071220.0004.

SNL 2007ac. *Mechanical Assessment of Degraded Waste Packages and Drip Shields Subject to Vibratory Ground Motion.* MDL-WIS-AC-000001 REV 00. Las Vegas, Nevada: Sandia National Laboratories. ACC: DOC.20070917.0006.

SNL 2007ad. *Characterize Eruptive Processes at Yucca Mountain, Nevada.* ANL-MGR-GS-000002 REV 03. Las Vegas, Nevada: Sandia National Laboratories. ACC: DOC.20070301.0001.

SNL 2007ae. *Total System Performance Assessment Data Input Package for Requirements Analysis for Subsurface Facilities.* TDR-TDIP-PA-000001 REV 00. Las Vegas, Nevada: Sandia National Laboratories. ACC: DOC.20070921.0007.

SNL 2007af. *Saturated Zone Site-Scale Flow Model.* MDL-NBS-HS-000011 REV 03. Las Vegas, Nevada: Sandia National Laboratories. ACC: DOC.20070626.0004.

SNL 2007ag. *MOX Spent Nuclear Fuel and LaBS Glass for TSPA-LA.* ANL-WIS-MD-000022 REV 01. Las Vegas, Nevada: Sandia National Laboratories. ACC: DOC.20070220.0007.

SNL 2008a. *Total System Performance Assessment Model/Analysis for the License Application.* MDL-WIS-PA-000005 REV 00 ADD 01. Las Vegas, Nevada: Sandia National Laboratories. ACC: DOC.20080312.0001.

SNL 2008b. *Features, Events, and Processes for the Total System Performance Assessment: Methods.* ANL-WIS-MD-000026 REV 00. Las Vegas, Nevada: Sandia National Laboratories. ACC: DOC.20080211.0010.

SNL 2008c. *Features, Events, and Processes for the Total System Performance Assessment: Analyses.* ANL-WIS-MD-000027 REV 00. Las Vegas, Nevada: Sandia National Laboratories. ACC: DOC.20080307.0003.

SNL 2008d. *Multiscale Thermohydrologic Model.* ANL-EBS-MD-000049 REV 03 ADD 02. Las Vegas, Nevada: Sandia National Laboratories. ACC: DOC.20080201.0003.

SNL 2008e. *Particle Tracking Model and Abstraction of Transport Processes.* MDL-NBS-HS-000020 REV 02 ADD 02. Las Vegas, Nevada: Sandia National Laboratories. ACC: DOC.20080129.0008.

SNL 2008f. *Saturated Zone Flow and Transport Model Abstraction.* MDL-NBS-HS-000021 REV 03 ADD 02. Las Vegas, Nevada: Sandia National Laboratories. ACC: DOC.20080107.0006.

SNL 2008g. *Simulation of Net Infiltration for Present-Day and Potential Future Climates.* MDL-NBS-HS-000023 REV 01 ADD 01. Las Vegas, Nevada: Sandia National Laboratories. ACC: DOC.20080201.0002.

SNL 2008h. *Site-Scale Saturated Zone Transport*. MDL-NBS-HS-000010 REV 03 ADD 01. Las Vegas, Nevada: Sandia National Laboratories. ACC: DOC.20080121.0003.

SNL 2008i. *Technical Work Plan for: Total System Performance Assessment FY 07–08 Activities.* TWP-MGR-PA-000045 REV 01 ICN 02. Las Vegas, Nevada: Sandia National Laboratories. ACC: DOC.20080131.0048.

Stein, M. 1987. "Large Sample Properties of Simulations Using Latin Hypercube Sampling." *Technometrics, 29* (2), 143–151. Alexandria, Virginia: American Statistical Association. TIC: 253129.

Suzuki, T. 1983. "A Theoretical Model for Dispersion of Tephra." *Arc Volcanism: Physics and Tectonics, Proceedings of a 1981 IAVCEI Symposium, August-September, 1981, Tokyo and Hakone.* Shimozuru, D. and Yokoyama, I., eds. 95–113. Tokyo, Japan: Terra Scientific Publishing Company. TIC: 238307.

USDA (U.S. Department of Agriculture) 2000. *Food and Nutrient Intakes by Individuals in the United States, 1994–1996.* Nationwide Food Surveys Report No. 96-3. Two volumes. Washington, D.C.: U.S. Department of Agriculture. TIC: 249498.

Watson, J.E., Jr. 1980. *Upgrading Environmental Radiation Data.* EPA 520/1-80-012. Washington, D.C.: U.S. Environmental Protection Agency, Office of Radiation Programs. TIC: 228385.

Williams, N.H. 2001. "Contract No. DE-AC08-01RW12101—Total System Performance Assessment—Analyses for Disposal of Commercial and DOE Waste Inventories at Yucca Mountain—Input to Final Environmental Impact Statement and Site Suitability Evaluation REV 00 ICN 02." Letter from N.H. Williams (BSC) to J.R. Summerson (DOE/YMSCO), December 11, 2001, RWA:cs-1204010670, with enclosure. ACC: MOL.20011213.0056.

Wilson, M.L.; Gauthier, J.H.; Barnard, R.W.; Barr, G.E.; Dockery, H.A.; Dunn, E.; Eaton, R.R.; Guerin, D.C.; Lu, N.; Martinez, M.J.; Nilson, R.; Rautman, C.A.; Robey, T.H.; Ross, B.; Ryder, E.E.; Schenker, A.R.; Shannon, S.A.; Skinner, L.H.; Halsey, W.G.; Gansemer, J.D.; Lewis, L.C.; Lamont, A.D.; Triay, I.R.; Meijer, A.; and Morris, D.E. 1994. *Total-System Performance Assessment for Yucca Mountain—SNL Second Iteration (TSPA-1993).* SAND93-2675. Executive Summary and two volumes. Albuquerque, New Mexico: Sandia National Laboratories. ACC: NNA.19940112.0123.

Zyvoloski, G.A.; Robinson, B.A.; Dash, Z.V.; and Trease, L.L. 1997. *User's Manual for the FEHM Application—A Finite-Element Heat- and Mass-Transfer Code.* LA-13306-M. Los Alamos, New Mexico: Los Alamos National Laboratory. TIC: 235999.

Table 2.4-1. TSPA Model Discretization

TSPA Principal Model Components	Submodel for TSPA	SAR Section	Abstraction/Process Model(s)/Analysis(es)	Reference
Unsaturated Zone Flow Model Component	UZ Flow Fields Abstraction	2.3.2	UZ Flow Fields Abstraction	UZ *Flow Models and Submodels* (SNL 2007b).
			Site-Scale UZ Flow Process Model	
			Active Fracture Model	
			Dual-Permeability UZ Flow Model	
	Infiltration Submodel	2.3.1	Infiltration Model Abstraction	*Simulation of Net Infiltration for Present-Day and Potential Future Climates* (SNL 2008g).
			Infiltration Process Model	
	Climate Submodel		Future Climate Analysis	*Future Climate Analysis* (BSC 2004c).
	Drift Seepage Submodel	2.3.3	Drift Seepage Abstraction	*Abstraction of Drift Seepage* (SNL 2007g).
			Drift Seepage Abstraction including Drift Collapse	*Seepage Model for PA Including Drift Collapse* (BSC 2004d).
			TH Seepage Process Model	
	Drift Wall Condensation Submodel	2.3.5	In-Drift Natural Convection and Condensation Process Model	*In-Drift Natural Convection and Condensation* (SNL 2007f).
			Drift Wall Condensation Abstraction	
EBS Environment Model Component	EBS TH Environment Submodel	2.3.5	MSTHM Process Model	*Multiscale Thermohydrologic Model* (SNL 2008d).
			MSTHM Abstraction	
	EBS Chemical Environment Submodel		EBS P&CE Abstraction	*Engineered Barrier System: Physical and Chemical Environment* (SNL 2007i).
			IDPS Process Model	*In Drift Precipitates/Salts Model* (SNL 2007j).

Table 2.4-1. TSPA Model Discretization (Continued)

TSPA Principal Model Components	Submodel for TSPA	SAR Section	Abstraction/Process Model(s)/Analysis(es)	Reference
WP and DS Degradation Model Component	WP and DS Degradation Submodel	2.3.6	WP General Corrosion Abstraction	*General Corrosion and Localized Corrosion of Waste Package Outer Barrier* (SNL 2007o). *Stress Corrosion Cracking of Waste Package Outer Barrier and Drip Shield Materials* (SNL 2007e). *General Corrosion and Localized Corrosion of the Drip Shield* (SNL 2007p).
			WP MIC Abstraction	
			WP SCC Abstraction	
			DS General Corrosion Abstraction	
			Localized Corrosion Initiation Abstraction	
			Localized Corrosion Penetration Rate Abstraction	
Waste Form Degradation and Mobilization Model Component	Radionuclide Inventory Submodel	2.3.7	Initial Radionuclide Inventory Screening Analysis	*Initial Radionuclides Inventory* (SNL 2007t). *MOX Spent Nuclear Fuel and LaBS Glass for TSPA-LA* (SNL 2007ag).
			Initial Radionuclide Inventory Abstraction	*Initial Radionuclides Inventory* (SNL 2007t). *MOX Spent Nuclear Fuel and LaBS Glass for TSPA-LA* (SNL 2007ag).
	In-Package Chemistry Submodel		In-Package Chemistry Abstraction	*In-Package Chemistry Abstraction* (SNL 2007h).
	Cladding Degradation		Cladding Degradation Abstraction	*Cladding Degradation Summary for LA* (SNL 2007r).
	Waste Form Degradation Submodel		CSNF WF Degradation Abstraction	*CSNF Waste Form Degradation: Summary Abstraction* (BSC 2004e).
			DSNF WF Degradation Abstraction	*DSNF and Other Waste Form Degradation Abstraction* (BSC 2004f).
			HLW Glass Degradation Abstraction	*Defense HLW Glass Degradation Model* (BSC 2004g).

Table 2.4-1. TSPA Model Discretization (Continued)

TSPA Principal Model Components	Submodel for TSPA	SAR Section	Abstraction/Process Model(s)/Analysis(es)	Reference
Waste Form Degradation and Mobilization Model Component (Continued)	Dissolved Concentration Limits Submodel	2.3.7	Dissolved Concentration Limits Abstraction	*Dissolved Concentration Limits of Elements with Radioactive Isotopes* (SNL 2007u).
	Engineered Barrier System Colloids Submodel		WF and In-Drift Colloid Concentration Abstraction	*Waste Form and In-Drift Colloids-Associated Radionuclide Concentrations: Abstraction and Summary* (SNL 2007v).
EBS Flow and Transport Model Component	EBS Flow Submodel	2.3.7	EBS Flow Abstraction	*EBS Radionuclide Transport Abstraction* (SNL 2007k).
	EBS Transport Submodel		EBS Transport Abstraction	
			Single Continuum Invert Abstraction	
			Mass of Corrosion Products Abstraction	
			Waste Form Water Volume Abstraction	*Cladding Degradation Summary for LA* (SNL 2007r). *Defense HLW Glass Degradation Model* (BSC 2004g).
	EBS-UZ Interface Submodel		EBS-UZ Interface Abstraction	*EBS Radionuclide Transport Abstraction* (SNL 2007k).
Unsaturated Zone Transport Model Component	UZ Transport Submodel	2.3.8	Active Fracture Model Abstraction	*Particle Tracking Model and Abstraction of Transport Processes* (SNL 2008e).
			Particle Tracking Model Abstraction	
			Dual-Continuum Transport Model Abstraction	
			UZ Transport Abstraction	

Table 2.4-1. TSPA Model Discretization (Continued)

TSPA Principal Model Components	Submodel for TSPA	SAR Section	Abstraction/Process Model(s)/Analysis(es)	Reference
SZ Flow and Transport Model Component	SZ Flow and Transport Submodel	2.3.9	3-D SZ Flow and Transport Process Model	*Saturated Zone Site-Scale Flow Model* (SNL 2007af). *Site-Scale Saturated Zone Transport* (SNL 2008h).
			3-D SZ Flow and Transport Abstraction	*Saturated Zone Flow and Transport Model Abstraction* (SNL 2008f).
			SZ Convolute Abstraction	
			1-D SZ Flow and Transport Abstraction	
Biosphere Model Component	Biosphere Submodel	2.3.10	Biosphere Process Model	*Biosphere Model Report* (SNL 2007y).
			Groundwater Exposure Case Abstraction	
			Volcanic Ash Exposure Case Abstraction	
Events	DS Early Failure Submodel	2.3.6	Abstraction of DS Failures from Undetected Defects	*Analysis of Mechanisms for Early Waste Package/Drip Shield Failures* (SNL 2007a).
	WP Early Failure Submodel		Abstraction of WP Failures from Undetected Defects	
	Igneous Intrusion Submodel	2.3.11	Igneous Activity Analysis	*Characterize Framework for Igneous Activity at Yucca Mountain, Nevada* (BSC 2004a).
	Igneous Event Time and Probability Submodel		Annual Frequency Abstraction	
	Igneous Intrusion EBS Damage Submodel		Number of WP Hit by Igneous Events Abstraction	*Number of Waste Packages Hit by Igneous Events* (SNL 2007aa).

Table 2.4-1. TSPA Model Discretization (Continued)

TSPA Principal Model Components	Submodel for TSPA	SAR Section	Abstraction/Process Model(s)/Analysis(es)	Reference
Events (Continued)	EBS TH Environment Submodel Modifications for Igneous Intrusion	2.3.11	Dike Drift Interactions Analysis	*Dike/Drift Interactions* (SNL 2007z).
	EBS Chemical Environment Submodel Modifications for Igneous Intrusion		Unevaporated Seepage Chemistry Abstraction	
			Basalt Chemistry Abstraction	
	Volcanic Eruption Submodel		Eruptive Processes Analysis	*Characterize Eruptive Processes at Yucca Mountain, Nevada* (SNL 2007ad). *Atmospheric Dispersal and Deposition of Tephra from a Potential Volcanic Eruption at Yucca Mountain, Nevada* (SNL 2007m).
	Volcanic Interaction with the Repository Submodel		Number of WP Hit by Eruptive Conduits Analysis	*Number of Waste Packages Hit by Igneous Events* (SNL 2007aa).
	Atmospheric Transport Submodel		Atmospheric Dispersal and Deposition of Tephra Analysis	*Atmospheric Dispersal and Deposition of Tephra from a Potential Volcanic Eruption at Yucca Mountain, Nevada* (SNL 2007m). *Redistribution of Tephra and Waste by Geomorphic Processes Following a Potential Volcanic Eruption at Yucca Mountain, Nevada* (SNL 2007ab).
			ASHPLUME Model Abstraction	
	Tephra Redistribution Submodel		Redistributed Tephra Abstraction	
	Volcanic Ash Exposure Submodel	2.3.10	Mean Annual Dose for Volcanic Eruption Abstraction	*Biosphere Model Report* (SNL 2007y).
	Ground Motion Damage	2.3.4	Seismic Damage Abstraction	*Seismic Consequence Abstraction* (SNL 2007c).
	Fault Displacement Damage			
	Drift Seepage Submodel for Seismic Disruption	2.3.3	Drift Seepage Abstraction including Drift Collapse	*Abstraction of Drift Seepage* (SNL 2007g). *Seepage Model for PA Including Drift Collapse* (BSC 2004d).

Table 2.4-1. TSPA Model Discretization (Continued)

TSPA Principal Model Components	Submodel for TSPA	SAR Section	Abstraction/Process Model(s)/Analysis(es)	Reference
Events (Continued)	EBS TH Environment Submodel Modifications for Seismic Disruption	2.3.4	Collapsed Drift TH Abstraction	*Multiscale Thermohydrologic Model* (SNL 2008d).
	WP and DS Degradation Submodel Modifications for Seismic Disruption		WP and DS Degradation Submodel	*General Corrosion and Localized Corrosion of Waste Package Outer Barrier* (SNL 2007o). *Stress Corrosion Cracking of Waste Package Outer Barrier and Drip Shield Materials* (SNL 2007e). *General Corrosion and Localized Corrosion of the Drip Shield* (SNL 2007p).
	Human Intrusion Submodel	2.4.3	10 CFR Part 63.322 & 63.321	*Total System Performance Assessment Model/Analysis for the License Application* (SNL 2008a, Section 6.7).

Table 2.4-2. Performance Results for Individual Protection Standard

Time Period After Closure (yrs)	**Projected Maximum Mean Annual Dose (mrem)**	**Time of Maximum Mean Annual Dose (yr)**	**Projected Maximum Median Annual Dose (mrem)**	**Time of Maximum Median Annual Dose (yr)**	**Limit for Annual Dose (mrem)**
10,000	0.24	10,000	NA	NA	15 (mean)
1,000,000	NA	NA	0.96	~ 720,000	350 (median)

NOTE: Numerical Limits from proposed 10 CFR 63.311(a).

Source: SNL 2008a, Table 8.1-1[a].

Table 2.4-3. Performance Results for Human Intrusion Standard with Drilling Event at 200,000 years After Closure

Time Period After Closure (yrs)	**Projected Maximum Median Annual Dose (mrem)**	**Limit for Annual Dose (mrem)**
10,000	0	15 (mean)
1,000,000	0.01	350 (median)

NOTE: Numerical Limits from proposed 10 CFR 63.321(b)).

Source: SNL 2008a, Table 8.1-3[a].

Table 2.4-4. Performance Results for Groundwater Protection Standard During First 10,000 Years After Disposal

Type of Limit	**Projected Maximum Mean Activity Concentration or Annual Dose**	**Natural Background Level**	**Limit for Activity Concentration or Annual Dose**
Combined ^{226}Ra and ^{228}Ra	$<10^{-6}$ pCi/L	0.5 pCi/L	5 pCi/L
Gross Alpha Activity	$<10^{-4}$ pCi/L	0.5 pCi/L	15 pCi/L
Dose from Combined Beta and Photon Emitting Radionuclides	Whole Body ~ 0.06 mrem Thyroid ~ 0.26 mrem	Background level excluded in regulatory requirement	4 mrem

NOTE: Numerical Limits from 10 CFR 63.331.

Source: SNL 2008a, Table 8.1-2[a].

Table 2.4-5. Aleatory Uncertainties in the TSPA Model

Scenario Class	**Aleatory Uncertainties**
Nominal	Time and location of general corrosion failures for each type of waste package
Early Failure	Number of early failed waste packages
	Type and location of each early failed waste package
	Number of early failed drip shields
	Type of waste package under each early failed drip shield
	Location of each early failed drip shield
Igneous	Number of igneous events
	Time of each igneous event
	Number of waste packages affected by eruption
	Eruptive power, height, and duration of each eruption
	Wind speed and wind direction during eruption
Seismic	Number of seismic events
	Type of each seismic event: ground motion or fault displacement
	Time of each seismic event
	Peak ground velocity of each ground motion seismic event
	Occurrence and extent of damage to each type of waste package caused by ground motion
	Occurrence and extent of rupture or puncture of each type of waste package caused by ground motion
	Volume of rockfall caused by ground motion for lithophysal and non-lithophysal zones
	Occurrence of failure of drip shield framework caused by ground motion and accumulated rockfall
	Occurrence of failure of drip shield plates caused by ground motion and accumulated rockfall
	Number of waste packages of each type affected by fault displacement
	Failed area on each type of waste package caused by fault displacement

Source: SNL 2008a, Table 6.1.3-1.

Table 2.4-6. Examples of Epistemic Uncertainties in the TSPA Model

Model Component	**Epistemic Uncertainties**
Unsaturated Zone Flow	Infiltration Submodel: • Infiltration scenario Unsaturated Zone Flow Fields Abstraction: • Hydrologic properties • Ratio of porosity to fracture aperture Drift Seepage Submodel: • Permeability and capillary strength parameters • Factor accounting for local heterogeneity in flow-focusing and permeability Drift Wall Condensation Submodel: • Correlation parameters for abstraction for fraction of waste package locations with dripping condensation and condensation water flow rate
EBS Environment	EBS Thermal-Hydrologic Environment: • Thermal conductivity of surrounding rock EBS Chemical Environment Submodel: • Ambient water composition • $p\mathrm{CO}_2$, ionic strength, and pH of in-drift seepage water • Water-rock interaction for seepage water
Waste Package and Drip Shield Degradation	Waste Package and Drip Shield Degradation Submodel: • Corrosion rates of Alloy 22 and drip shield components • Temperature and relative humidity at drip shield and waste package • pH, NO_3^-, and Cl^- of crown seepage
Waste Form Degradation and Mobilization	Waste Form Degradation and Mobilization: • Radionuclide inventory for commercial SNF, DOE SNF, and HLW • Temperature and relative humidity at waste package • $p\mathrm{CO}_2$, ionic strength, and pH in waste package • Waste form degradation rates • Radionuclide solubility • Colloid concentrations • Mass of Pu and Am embedded in waste form colloids from HLW glass • Forward rate constant for kinetic sorption of radionuclides onto iron oxyhydroxide surfaces • Coefficient for sorption onto colloids for each radionuclide
EBS Flow and Transport	EBS Flow Submodel: • Drip shield and waste package flux splitting factors • Representative subregion typical liquid saturation in invert • Representative subregion typical imbibition flux in invert • Representative subregion typical liquid saturation and flux through the EBS-unsaturated zone interface

Table 2.4-6. Examples of Epistemic Uncertainties in the TSPA Model (Continued)

Model Component	Epistemic Uncertainties
EBS Flow and Transport	EBS Transport Submodel: • Steel corrosion rates • Specific surface area of steel corrosion products • Adsorption isotherm for water vapor sorption onto degraded waste form and onto steel corrosion products • Density of radionuclide sorption sites in steel corrosion products
Unsaturated Zone Transport	Unsaturated Zone Transport Submodel: • Fracture aperture • Active Fracture Model gamma parameter • Tortuosity • Rock Matrix K_ds for each radionuclide • Coefficient for sorption onto colloids for each radionuclide • Colloid retardation factors
Saturated Zone Flow and Transport	Saturated Zone Flow and Transport Submodel: • Groundwater specific discharge multiplier • Flowing interval spacing in volcanic units • Colloid retardation in alluvium
Biosphere	Biosphere Submodel: • Biosphere dose conversion factors for groundwater modeling cases • Biosphere dose conversion factors for volcanic eruption modeling case
Events	DS Early Failure Submodel: • Probability of early failure for a single drip shield WP Early Failure Submodel: • Probability of early failure for a single waste package Igneous Activity, Igneous Intrusion Submodel: • Igneous event probability (event frequency) Igneous Activity, Volcanic Eruption Submodel: • Igneous event probability (event frequency) • Ash and waste particle size • Radionuclide diffusivity in soils Seismic Activity, GM Damage Submodel): • Residual stress threshold for Alloy 22

NOTE: Additional information concerning uncertainty and the distribution of TSPA model parameters and parameter values can be found in the GoldSim model file and in SNL 2008a, Appendix K.

Source: SNL 2008a, Table 6.1.3-2.

Table 2.4-7. Effect of Combinations of Scenario Classes on Total Mean Annual Dose

Later Disruptive Event				
Preceding Event	**Igneous Intrusion**	**Volcanic Eruption**	**Seismic Ground Motion**	**Seismic Fault Displacement**
Early Failure Waste Package	Very minor (~0.02%) overcounting of inventory. Negligible effect on total mean annual dose.	Overcounting of inventory in waste packages affected by the eruption event. Negligible effect on total mean annual dose.	Very minor (~0.02%) overcounting of inventory. Negligible effect on total mean annual dose.	Overcounting of inventory in waste packages affected by the fault displacement event. Negligible effect on total mean annual dose.
Early Failure Drip Shield	Very minor (~0.01%) overcounting of inventory. Negligible effect on total mean annual dose.	Overcounting of inventory in waste packages affected by the eruption event. Negligible effect on total mean annual dose.	Very minor (~0.01%) overcounting of inventory. Negligible effect on total mean annual dose.	Overcounting of inventory in waste packages affected by the fault displacement event. Negligible effect on total mean annual dose.
Igneous Intrusion	Included in calculation of mean dose for the Igneous Scenario Class $\overline{\overline{D}}_I(\tau)$.	Overstatement of the consequences of the igneous eruption event. Negligible effect on total mean annual dose.	Overstatement of the consequences of the seismic ground motion event. Minor effect on total mean annual dose.	Overstatement of the consequences of the seismic fault displacement event. Negligible effect on total mean annual dose.
Volcanic Eruption	Very minor (~0.03%) overcounting of inventory. Negligible effect on total mean annual dose.	Included in calculation of mean dose for the Igneous Scenario Class $\overline{\overline{D}}_I(\tau)$.	Very minor (~0.03%) overcounting of inventory. Negligible effect on total mean annual dose.	Very minor (~0.03%) overcounting of inventory in waste packages affected by the fault displacement event. Negligible effect on total mean annual dose.
Seismic Ground Motion	Overcounting of inventory and consequences of an intrusion. Minor effect on total mean annual dose.	Overcounting of inventory in waste packages affected by the eruption event. Negligible effect on total mean annual dose.	Included in calculation of mean dose for the Seismic Scenario Class $\overline{\overline{D}}_I(\tau)$.	Overcounting of inventory in waste packages affected by the fault displacement event. Negligible effect on total mean annual dose.
Seismic Fault Displacement	Very minor (~2%) overcounting of inventory. Negligible effect on total mean annual dose.	Overcounting of inventory in waste packages affected by the eruption event. Negligible effect on total mean annual dose.	Very minor (~2%) overcounting of inventory. Negligible effect on total mean annual dose.	Included in calculation of mean dose for the Seismic Scenario Class $\overline{\overline{D}}_I(\tau)$.

Source: SNL 2008a, Table 6.1.2-1.

Table 2.4-8. TSPA Model Validation Analyses

Activity Category/Subcategory	Purpose	Activity Description	Section of TSPA Model Report
During-Development Validation Activities (Technical Work Plan Validation (SNL 2008i, Section 2.3.5.1))			
Computer Code and Input Verification (Section 2.4.2.3.2.2.1)			
Model Testing and Verification	Testing of software that is the basis for the TSPA model.	Verify GoldSim software.	7.2.1 and 7.2.1[a]
	Checking to determine whether the correct input parameters are used.	Verify input parameters.	7.2.3 and 7.2.3[a]
	Test cases to determine whether the model is working correctly, saving appropriate results, interfacing with DLLs, feeding the correct information among model components, and not exceeding the applicable range of model components.	Includes verification of DLLs, submodels, model components, and coupling among submodels and model components; and comparison with other models (e.g., stand-alone models from analysis model reports). In addition, the verification of coupling among submodels and model components includes subsystem analyses of annual release across model interfaces, drift-wall condensation, and localized corrosion initiation.	7.2.2, 7.2.4 and 7.2.4[a], 7.2.5, 7.2.6[a]; Tables 7.2-1 and 7.2-2
Model Stability Testing (Section 2.4.2.3.2.2.2)			
Statistical Stability of Mean Annual Dose	Determine confidence interval around total mean annual dose and mean annual dose for each modeling case using three replicates.	TSPA model v5.000: Generate total mean annual dose and mean annual dose for each modeling case using three replicates with different random seeds. Determine a confidence interval around the estimate of the overall mean with a t-test. TSPA model v5.005: Determine stability by comparison with results from TSPA model v5.000. Determine a confidence interval around the estimate of the overall mean with a bootstrap procedure.	7.3.1, 7.3.1[a]

Table 2.4-8. TSPA Model Validation Analyses (Continued)

Activity Category/Subcategory	Purpose	Activity Description	Section of TSPA Model Report
Model Stability Testing (Section 2.4.2.3.2.2.2) (Continued)			
Numerical Accuracy of Expected Annual Dose Calculation—Igneous Scenario Class	Demonstrate accuracy of calculation of expected annual dose for the modeling cases of the igneous scenario class.	For the igneous intrusion modeling case, demonstrate accuracy of the quadrature integration technique by increasing the discretization used in the integral. Increase the number of specified event times from 10 to 50. Calculate expected annual dose for five epistemic realizations for both 10,000 and 1,000,000 years. For the volcanic eruption modeling case for 10,000 years, demonstrate accuracy of the combined Monte Carlo and quadrature integration techniques by increasing the sample size used in the Monte Carlo integration and the discretization used in the quadrature integration. Calculate expected annual dose for 10,000 years for five epistemic realizations, increasing the aleatory LHS sample size from 40 to 120, and the number of specified event times from 10 to 20. Conclusions for 10,000 years apply to the 1,000,000 year calculations.	7.3.2
Numerical Accuracy of Expected Annual Dose Calculation—Seismic Scenario Class	Demonstrate accuracy of calculation of expected annual dose for the modeling cases of the seismic scenario class.	For the seismic ground motion modeling case for 1,000,000 years, demonstrate the accuracy of the Monte Carlo integration technique by means of increased sample size. Repeat Replicate 1 (300 epistemic realizations) with a different aleatory seed to generate a second set of 9,000 dose histories (30 independent aleatory samples for each epistemic realization). Pool the two sets of 9,000 dose histories and generate expected annual dose based on the pooled set of 60 independent aleatory samples per epistemic realization, and compare to expected annual dose for the base case of 30 independent aleatory samples per epistemic realization. For the seismic ground motion modeling case for 10,000 years, demonstrate accuracy of the quadrature integration technique by increasing the discretization used in each integral. Increase the number of specified event times from 6 to 12 and the number of specified damage levels from 5 to 8. Calculate expected annual dose for 5 epistemic realizations. For the seismic fault displacement modeling case, demonstrate accuracy of the quadrature integration technique by increasing the discretization used in each integral. Increase the number of specified event times from 6 to 12 and the number of specified damaged areas from 3 to 6. Calculate expected annual dose for 5 epistemic realizations for both 10,000 and 1,000,000 years.	7.3.2 and 7.3.2[a]

Table 2.4-8. TSPA Model Validation Analyses (Continued)

Activity Category/Subcategory	Purpose	Activity Description	Section of TSPA Model Report
Model Stability Testing (Section 2.4.2.3.2.2.2) (Continued)			
Justification of Simplifications for the Seismic Ground Motion Modeling Case for 10,000 Years	For the seismic ground motion modeling case for 10,000 years, demonstrate that simplifications of the Seismic Consequences Abstraction used in the calculation of expected annual dose are reasonable.	Estimate the effect on mean annual dose of drip shield plate rupture and of framework failure. Estimate the effect on mean annual dose of accounting for drift collapse effects on temperature and seepage entering the drift Estimate the contribution to mean annual dose from waste package rupture and puncture Estimate the contribution to mean annual dose from damage to commercial SNF waste packages	7.3.2
Temporal Stability	Demonstrate stability of expected annual dose for temporal discretization in GoldSim.	Comparison of expected annual dose histories for five epistemic vectors for the following modeling cases: waste package early failure; seismic ground motion (10,000 years); igneous intrusion (10,000 and 1,000,000 years); and drip shield early failure (10,000 years). Compare expected annual dose histories for different temporal discretizations. Assess the temporal stability for the Human Intrusion modeling case.	7.3.3 and 7.3.3[a]; Table 7.3.3-2[a]
Spatial Discretization	Evaluate the impact due to the spatial discretizations inherited by the TSPA model from the supporting natural and engineered-barrier process models.	Evaluate the appropriateness of use of the inherited spatial discretization schemes of the process model abstractions that feed the TSPA. These abstractions include the process models: Mountain-Scale UZ Flow, EBS TH Environment, UZ Transport, and SZ Flow and Transport abstractions.	7.3.4.1
	Evaluate the impact due to the spatial discretizations created within the TSPA model.	Describe the spatial discretization of the repository on the basis of percolation subregions and the binning of the percolation subregions by quantiles (0.0 to 0.05, 0.05 to 0.3, 0.3 to 0.7, 0.7 to 0.95, and 0.95 to 1.0).	7.3.4.2
		Demonstrate the appropriateness and validity of using the representative TH histories as inputs to the EBS Thermal-Hydrologic Environments Submodel of the TSPA, as opposed to using the comprehensive data set available from the MSTHM.	7.3.4.3

Table 2.4-8. TSPA Model Validation Analyses (Continued)

Activity Category/Subcategory	Purpose	Activity Description	Section of TSPA Model Report
Model Stability Testing (Section 2.4.2.3.2.2.2) (Continued)			
Stability of UZ Transport Modeling for the Igneous Intrusion Modeling Case	Evaluate the stability of results in reference to the maximum number of particles allowed per species for the igneous intrusion modeling case for 1,000,000 years.	Analyze the differences in UZ releases of ^{99}Tc, ^{233}U, ^{234}U, ^{237}Np, and ^{239}Pu, and in cumulative dose for three cases (500,000; 750,000; and 900,000 particles).	7.3.5
Stability of UZ Transport Modeling for the Seismic Ground Motion Modeling Case	Evaluate the stability of results in reference to the maximum number of particles allowed per species for the seismic ground motion modeling case for 10,000 years.	Analyze the differences in UZ releases of ^{99}Tc, ^{233}U, ^{234}U, ^{237}Np, and ^{239}Pu and in cumulative dose for three cases (500,000; 750,000; and 900,000 particles.).	7.3.5
Stability of UZ Transport Modeling for the Drip Shield Early Failure Modeling Case	Evaluate the stability of results in reference to the maximum number of particles allowed per species for the drip shield early failure modeling case for 1,000,000 years.	Analyze the differences in UZ releases of ^{99}Tc, ^{233}U, ^{234}U, ^{237}Np, and ^{239}Pu, and in cumulative dose for three cases (500,000; 750,000; and 900,000 particles).	7.3.5
Uncertainty Characterization Reviews (Section 2.4.2.3.2.2.3)			
Ranking of Scenario Classes	Prioritize scenario classes of higher significance to dose.	Develop a risk-based ranking of TSPA scenario classes and modeling cases in order to focus the uncertainty characterization reviews of the most important component model abstractions.	7.4.2
Key Uncertain Parameters	Identify the key uncertain parameters that are important to dose.	Select the key uncertain parameters that are important to dose in the seismic, igneous, and nominal modeling cases for characterization review based on both importance rankings from past TSPA scoping studies and recommendations provided by model abstraction developers and experienced TSPA analysts.	7.4.3
Uncertainty-Characterization Review Findings and their Implementation	Review uncertainty characterization and address findings.	Perform uncertainty characterization of the selected key parameters impacting dose for the seismic, igneous, and nominal modeling cases and implement corrective actions for observed deficiencies.	7.4.4

Table 2.4-8. TSPA Model Validation Analyses (Continued)

Activity Category/Subcategory	Purpose	Activity Description	Section of TSPA Model Report
Surrogate Waste Form Validation (Section 2.4.2.3.2.2.4)			
Spent Fuel Categories	Comparison of naval surrogate fuel to naval fuel (Category 1).	Perform probabilistic runs to compare the naval surrogate (Zircaloy-clad commercial fuel) with naval fuel for drip shield early failure and igneous intrusion modeling cases.	7.5.3 and 7.5.3[a]
	Comparison of the DOE surrogate fuel to each DOE spent fuel category (Category 2 through Category 11).	Perform probabilistic run using drip shield early failure modeling case to compare the DOE surrogate with plutonium/uranium alloy spent fuel (Category 2), plutonium/uranium-carbide spent fuel (Category 3), mixed-oxide spent fuel (Category 4), uranium/thorium-carbide spent fuel (Category 5), uranium/thorium-oxide spent fuel (Category 6), uranium-metal spent fuel (Category 7), uranium-oxide spent fuel (Category 8), aluminum-based spent fuel (Category 9), miscellaneous spent fuel (Category 10) for two inventories, and uranium-zirconium hydride spent fuel (Category 11).	7.5.4
	Justification of the DOE surrogate dissolution model.	Perform probabilistic comparison of fuel degradation models for Category 2 through Category 11 and air alteration rates for Category 5 and Category 7.	7.5.5
	Justification of the DOE surrogate dissolution model.	Perform comparison of uranium-metal dissolution model, uranium-metal dissolution model with air alteration, and instantaneous dissolution (Category 7). Perform similar comparison for the uranium/thorium-carbide dissolution model (Category 5).	7.5.5
	Effects of fuel surface area and free inventory and uncertainty of radionuclide inventory.	Perform probabilistic comparison of uranium-metal nominal surface area with bounding surface area and free inventory and comparison of nominal inventory with the bounding inventory (Category 7).	7.5.5
	Uncertainty in number of waste packages.	Perform probabilistic comparison of aluminum-based spent fuel for nominal and bounding number of waste packages (Category 9).	7.5.5

Table 2.4-8. TSPA Model Validation Analyses (Continued)

Activity Category/Subcategory	**Purpose**	**Activity Description**	**Section of TSPA Model Report**
Surrogate Waste Form Validation (Section 2.4.2.3.2.2.4) (Continued)			
Spent Fuel Categories (Continued)	Comparison of radionuclides that contribute to annual dose from surrogate DOE spent fuel, HLW, uranium-metal spent fuel (Category 7), uranium/thorium-carbide spent fuel (Category 5), and uranium/thorium-oxide spent fuel (Category 6).	Analyze plots of key radionuclides that contribute to total annual dose for the DOE surrogate spent fuel only, HLW only, Category 7 only, Category 5 only, and Category 6 only.	7.5.5
	Justification of the DOE surrogate fuel.	Compare of the weighted sum of Category 2 through Category 11 spent fuel with a single WP of the DOE surrogate spent fuel.	7.5.5
Post–Development Validation Activities (Technical Work Plan Validation (SNL 2008i, Section 2.3.5.2))			
Corroboration of Direct Input Abstraction Results with Validated Process Models (Section 2.4.2.3.2.3.1)			
Corroboration of Abstraction Results with Underlying Process Models	Evaluate consistency of the abstraction results with the underlying validated key natural system environment models.	Perform quantitative and qualitative evaluation of how well the direct input abstraction results corroborate with the underlying validated key natural system environment models. Provide the evidence that builds confidence in the direct inputs.	7.6. 4.1
	Evaluate consistency of the abstraction results with the underlying validated key engineered barrier system models.	Perform quantitative and qualitative evaluation of how well direct input abstraction results corroborate the underlying validated key EBS models. Provide the evidence that builds confidence in the direct inputs.	7.6.4.2
	Evaluate consistency of the abstraction results with the underlying validated key DS, WP, and waste form degradation and mobilization models.	Perform quantitative and qualitative evaluation of how well the direct input abstraction results corroborate the underlying validated key DS, WP, and waste form degradation and mobilization models. Provide the evidence that builds confidence in the direct inputs.	7.6.4.3

Table 2.4-8. TSPA Model Validation Analyses (Continued)

Activity Category/Subcategory	Purpose	Activity Description	Section of TSPA Model Report
Corroboration of Direct Input Abstraction Results with Validated Process Models (Section 2.4.2.3.2.3.1) (Continued)			
Corroboration of Abstraction Results with Underlying Process Models	Evaluate consistency of the abstraction results with the underlying validated key disruptive events models.	Perform quantitative and qualitative evaluation of how well the direct input abstraction results corroborate the underlying validated key seismic and igneous disruptive events models. Provide the evidence that builds confidence in the direct inputs.	7.6.4.4
	Evaluate consistency of the abstraction results with the underlying validated biosphere model.	Provide the evidences that build confidence in the direct inputs from the biosphere model to the TSPA model.	7.6.4.5
Corroboration of Results with Auxiliary Analyses (Section 2.4.2.3.2.3.2)			
Analysis of Single Realizations	Evaluate the realization that contributes significantly to mean annual dose for the Early Failure modeling cases.	Select a realization each from the waste package early failure modeling case and drip shield early failure modeling case and analyze it to examine how the transport of key radionuclides is affected by coupling various components of the EBS, UZ, and SZ domains following the WP failure under varying physical-chemical-thermal-mechanical conditions.	7.7.1 and 7.7.1[a]
	Evaluate the realization that contributes significantly to mean annual dose for the igneous intrusion modeling case.	Select a realization from the igneous intrusion modeling case and analyze it to examine how the transport of key radionuclides is affected by coupling various components of the EBS, UZ, and SZ domains following the waste package failure under varying physical-chemical-thermal-mechanical conditions	7.7.1 and 7.7.1[a]
	Evaluate the realization that contributes significantly to mean annual dose for the seismic ground motion modeling case.	Select a realization from the seismic ground motion modeling case and analyze it to examine how the transport of key radionuclides is affected by coupling various components of the EBS, UZ, and SZ domains following the WP failure under varying physical-chemical-thermal-mechanical conditions. Both the 1,000,000 year and 10,000 year modeling cases were examined.	7.7.1 and 7.7.1[a]

Table 2.4-8. TSPA Model Validation Analyses (Continued)

Activity Category/Subcategory	Purpose	Activity Description	Section of TSPA Model Report
Corroboration of Results with Auxiliary Analyses (Section 2.4.2.3.2.3.2) (Continued)			
Analysis of Single Realizations (Continued)	Evaluate the realization that contributes significantly to mean annual dose for the nominal modeling case.	Select a realization from the nominal modeling case and analyze it to examine how the transport of key radionuclides is affected by coupling various components of the EBS, UZ, and SZ domains. Also evaluate statistical outlier for this modeling case.	7.7.1[a]
	Evaluate the realization that contributes significantly to mean annual dose for the Human Intrusion Scenario modeling case.	Select a realization from the Human Intrusion Scenario modeling case and analyze it to examine how the transport of key radionuclides is affected by coupling various components of the EBS, UZ borehole, and SZ domains following the human intrusion event.	7.7.1[a]
Comparison with Other Simple Models	Compare the TSPA model component results with a simplified analysis.	Perform a Simplified TSPA Analysis and compare the results with those of the TSPA model.	7.7.2 and 7.7.2[a]
	Compare with the EPRI TSPA Analysis.	Develop a comparison of the approach and results of the TSPA independently conducted by EPRI using its code IMARC for the postclosure performance of the Yucca Mountain repository.	7.7.3 and 7.7.3[a]
Performance Margin Analyses	Provide objective evidence for assessing performance margin and degree of conservatism or non conservatism in the TSPA model.	Conduct several auxiliary analyses (see Section 7.7.4 of the parent document for a list) utilizing revisions to selected component models in the TSPA model, including conceptual or uncertainty alternatives, to assess the performance margin in the TSPA model and to evaluate whether the TSPA model dose is underestimated. The analyses include both individual component revisions as well as a combined analysis that incorporates all of the selected component revisions.	7.7.4 and 7.7.4[a]
Corroboration of Results with Natural Analogues (Section 2.4.2.3.2.3.3)			
Cerro Negro	Validation of ASHPLUME for the volcanic eruption modeling case.	Compare of Cerro Negro ash-fall measurements to the results from ASHPLUME.	7.8.1
Peña Blanca, Nopal I Uranium Deposit	Validation of the UZ and SZ Transport Model.	Evaluation of geochemical data collected from rock and water samples with respect to distance from the Nopal I ore deposit.	7.8.2

Table 2.4-8. TSPA Model Validation Analyses (Continued)

Activity Category/Subcategory	Purpose	Activity Description	Section of TSPA Model Report
Independent Technical Reviews Performed in Preparation of TSPA model (Section 2.4.2.3.2.3.4)			
TSPA-VA Peer Review	Evaluate the TSPA-VA methodology and prediction of the future behavior of the total system.	Performed peer review of the TSPA-VA and the supporting process models. The review was conducted by an independent group of external experts. 1997 -1999	7.9.1
TSPA-SR Peer Review	Evaluation of the TSPA-SR for methodology and ability to meet the needs for SR and future LA compliance.	Performed peer review of the TSPA-SR and selected supporting documents to evaluate the approach used in the performance assessment, and how well the TSPA-SR and the future TSPA needs were addressed. The review was conducted by an international panel of experts managed by the OECD/NEA in 2002.	7.9.2
Draft TSPA-LA Technical Review	Evaluate the earlier draft iterations of the TSPA model as they were being drafted as to the degree of validation of the model for its intended purpose.	Performed technical review on the evaluation of the degree to which the draft TSPA model was valid for its intended purpose for the 10,000 years compliance period for which the model was prepared. The review was conducted by a team of experts during 2004, 2005, and early part of 2006.	7.9.3

NOTE: LA = license application; MSTHM = multiscale thermal-hydrologic model; SR = site recommendation; VA = viability assessment.

Source: Modified from SNL 2008a, Table 7.1-1[a].

Table 2.4-9. Verification of Dynamically-Linked Libraries and Model Abstractions Used in the TSPA Model

Model Component	Submodel	Analysis Description	Status
Unsaturated Zone Flow	Drift Seepage	Verification of seepage DLL by comparison of the TSPA model results with a stand-alone GoldSim-based implementation	Verified
	Drift Wall Condensation	Comparison of drift-wall condensation rates and probability data to that supplied in supporting data tracking numbers	Verified
Engineered Environment	EBS Chemical Environment	Verification of TSPA model file to accurately estimate (under both evaporative and condensation conditions) pH and ionic strength for a set of controlled inputs of temperature, relative humidity, $P\text{co}_2$, and percolation bin number	Verified
Waste Package and Drip Shield Degradation	Integrated Waste Package and Drip Shield Degradation	Verification of the WAPDEG, CWD, and SCCD DLLs through comparison of the results of TSPA model implementation with the results of a stand-alone implementation	Verified
Waste Form Degradation and Mobilization	Waste Rind Degradation	Comparison of the rind volume and thickness in a commercial SNF waste package using a Microsoft Excel spreadsheet and the TSPA model file	Verified
		Comparison of the rind volume and thickness in a codisposal waste package using a Microsoft Excel spreadsheet and the TSPA model file	Verified
	Commercial SNF Waste Form Degradation	Comparison of waste form degradation rate in a commercial SNF waste package using a Microsoft Excel spreadsheet and the TSPA model file	Verified
	HLW Glass Degradation	Comparison of TSPA model file results with a spreadsheet implementing the source analysis model report equations for acidic and alkaline conditions with relative humidity less and greater than 0.44	Verified
	Dissolved Concentration Limits	Nominal scenario: Comparison of TSPA model file results with a spreadsheet implementing the calculation of radionuclide solubilities using lookup tables and applying epistemic uncertainty	Verified
		Igneous scenario (igneous intrusion modeling case): Comparison of TSPA model file results with a spreadsheet implementing the calculation of uranium solubilities using lookup tables and applying epistemic uncertainty	Verified[a]
	In-Package Chemistry	Comparison of pH, ionic strength, and total carbonate in the waste packages using a Microsoft Excel spreadsheet and the TSPA model file	Verified

Table 2.4-9. Verification of Dynamically-Linked Libraries and Model Abstractions Used in the TSPA Model (Continued)

Model Component	Submodel	Analysis Description	Status
Engineered Barrier System Flow and Transport	EBS Transport Submodel	Comparison of results of plutonium transport and colloidal transport for both reversible and irreversible sorption on iron oxyhydroxide colloids using a Microsoft Excel implemented finite-difference approximation and the TSPA model file transport submodel	Verified
Unsaturated Zone Transport	FEHM Particle Tracking for the Unsaturated Zone Transport	Comparison of results from the TSPA model (FEHM DLL) with that of a test case developed from the base case FEHM model	Verified
Saturated Zone Flow and Transport	Saturated Zone Flow and Transport	Comparison of TSPA model results with the site-scale saturated zone transport base case for ^{99}Tc	Verified
		Comparison of a one-dimensional stand-alone model that was used for validation of the site-scale model with the TSPA model for ^{14}C	Verified
Biosphere	Groundwater Source Term to Dose	Comparison of calculated dose using a Microsoft Excel spreadsheet and the TSPA model file	Verified
Igneous Scenario Class Modeling Cases	Volcanic Eruption Modeling Case	Comparison of TSPA model results with the stand-alone model used for validation of the ASHPLUME DLL	Verified
		Comparison of TSPA model results with a Microsoft Excel spreadsheet based on the FAR model	Verified
	Igneous Intrusion Modeling Case	Comparison of TSPA model with a stand-alone GoldSim-based model file showing the impact of an igneous intrusion event on the EBS thermal-hydrologic properties	Verified
Seismic Scenario Class Modeling Cases	Seismic Damage Abstraction	Comparison of TSPA model calculated ground motion and fault displacement damage with that of stand-alone GoldSim-based models developed based on the source report	Verified
Verification of Coupling Between Model Components	EBS Transport and EBS-Unsaturated Zone Interface	Transport through the EBS-unsaturated zone interface to demonstrate proper placement of the effective zero-concentration boundary	Verified
	Unsaturated Zone—Saturated Zone Interface	Included in results presented for Verification of saturated zone flow and transport in which a radionuclide source term was specified at the base of the unsaturated zone submodel domain and passed across the interface for use in the saturated zone submodel.	Verified

NOTE: [a] Verification was confirmed in a TSPA model impact analysis (DTN: MO0708TSPAPOST.000, *22_DCL_Igneous.zip*).

Source: Modified from SNL 2008a, Table 7.2-2.

Table 2.4-10. U.S. Department of Energy Spent Nuclear Fuel Categories Analyzed for the TSPA Model

Category	Fuel Category/Fuel Matrix	Typical Fuel in Category	Mass (MTHM)[a]	Percent of Total
1	Naval nuclear fuel	Naval Nuclear Fuel	65[b]	2.88
2	Plutonium/uranium alloy	Enrico Fermi Reactor (FERMI) Core 1 and 2 (standard fuel subassembly)	4.58	0.19
3	Plutonium/uranium carbide	Fast Flux Test Facility Test Fuel Assembly (FFTF-TFA-FC-1)	0.0765	0.003
4	Mixed oxide fuel (plutonium/ uranium oxide and plutonium oxide)	Fast Flux Test Facility Driver Fuel Assembly (FFTF-DFA/TDFA)	12.0	0.49
5	Uranium/thorium carbide	Fort St. Vrain Reactor	26.3	1.08
6	Uranium/thorium oxide	Shippingport Light Water Breeder Reactor (Reflect. IV)	50.2	2.06
7	Uranium metal	N Reactor	2,110	86.77
8	Uranium oxide	Three Mile Island (TMI-2) Core Debris	134	5.51
9	Aluminum based (UAlx, U_3Si_2, uranium oxide in aluminum)	Foreign Research Reactor Pin Cluster (Canada)	22.3	0.92
10	Miscellaneous	Miscellaneous Radioactive Scrap Waste Facility Fuel	0.438	0.02
11	Uranium-zirconium hydride	Training Research Isotopes General Atomics (TRIGA)	1.95	0.08

NOTE: [a] MTHM from *Source Term Estimates for DOE Spent Nuclear Fuels* (DOE 2004, Appendix D, pp. D 3 through D 567). Summed heavy metal mass end of life values from each worksheet for TSPA Categories 2 to 11, excluding uncanistered fuel transfers.
[b] Section 1.5.1.4.

Source: Modified from SNL 2008a, Table 7.5-1.

Table 2.4-11. Summary of Epistemically Uncertain Variables Considered in the TSPA

ALPHAL. van Genuchten capillary strength parameter in lithophysal rock units (Pa). *Distribution:* Triangular. *Range:* –105 to 105. *Mean/Median/Mode:* 0. *TSPA-LA Name:* Alpha_Uncert_Lith_a (SNL 2008a, Sections 6.3.3.1.2 and 6.3.3.1.3; Tables 6.3.3-1, 6.3.3-3, and 6.3.5-4).
ALPHANL[a]. van Genuchten capillary strength parameter in nonlithophysal rock units (Pa). *Distribution:* Triangular. *Range:* –105 to 105. *Mean/Median/Mode:* 0. *TSPA-LA Name:* Alpha_Uncert_NonLith_a[a] (SNL 2008a, Section 6.3.3.1.2; Tables 6.3.3-1, 6.3.3-3, and 6.3.5-4).
ASHDENS. Tephra settled density (kg/m^3). *Distribution:* Truncated normal. *Range:* 300 to 1,500. *Mean:* 1,000. *Standard Deviation:* 100. *TSPA-LA Name:* Ash_Density_a (SNL 2008a, Table 6.5-5).
BCKALPHA. Natural background levels of alpha emitters in groundwater (pCi/L). *Distribution:* Truncated normal. *Range:* 0 to 0.71. *Mean/Median/Mode:* 0.5. *TSPA-LA Name:* Background_Alpha_a (SNL 2008a, Sections 6.3.10.2, 6.3.11.2, and Table 6.3.10-6).
BCKRA226. Natural background levels of combined ^{226}Ra and ^{228}Ra in groundwater (pCi/L). *Distribution:* Truncated normal. *Range:* 0 to 0.71. *Mean/Median/Mode:* 0.5. *TSPA-LA Name:* Background_Ra226_Ra228_a (SNL 2008a, Sections 6.3.10.2, 6.3.11.2, and Table 6.3.10-6).
BETA. Column diffusion constant (dimensionless). *Distribution:* Uniform. *Range:* 0.01 to 0.5. *TSPA-LA Name:* Beta_Dist_a (SNL 2008a, Table 6.5-4).
BTILLAGE. Depth of soil within which radionuclides contribute to dose from external exposure (m). *Distribution:* Uniform. *Range:* 0.05 to 0.3. *TSPA-LA Name:* b_Tillage_a (SNL 2008a, Table 6.5-5).
CFLUXOUT. Ratio of radionuclide mass associated with colloids (reversible and irreversible) to radionuclide mass associated with colloids and dissolved radionuclide mass (dimensionless). *Distribution:* Uniform. *Range:* 0.9 to 0.99. *TSPA-LA Name:* Target_Flux_Out_Ratio_a (SNL 2008a, Table 6.3.7-65).
COLFEOCS. FeOx colloid concentration when carbon steel is corroding (mg/L). *Distribution:* Truncated log normal. *Range:* 0.3 to 30. *Mean:* 3.69. *Standard Deviation:* 2.79. *TSPA-LA Name:* Conc_Col_FeOx_CS_Sampled_a (SNL 2008a, Table 6.3.7-65).
COLFEOSS. FeOx colloid concentration when degraded stainless steel is present, but no degrading carbon steel is present (mg/L). *Distribution:* Piecewise uniform. *Range:* 1.00×10^{-3} to 3.00×10^{1}. *TSPA-LA Name:* Conc_Col_FeOx_SS_Sampled_a (SNL 2008a, Table 6.3.7-65).
COLGW. Concentration of groundwater colloids when colloids are stable (mg/L). *Distribution:* Piecewise uniform. *Range:* 0.001 to 200. Median: 0.1. *TSPA-LA Name:* Conc_Col_Gw_Sampled_a (SNL 2008a, Table 6.3.7-66).
COLU. Concentration of uranophane colloids when colloids are stable (mg/L). *Distribution:* Piecewise uniform. *Range:* 0.001 to 200. *Median:* 0.1. *TSPA-LA Name:* Conc_Col_U_Sampled_a (SNL 2008a, Table 6.3.7-64).
CORRATSS. Stainless steel corrosion rate (mm/yr). *Distribution:* Truncated log normal. *Range:* 0.01 to 0.51. *Mean/Median/Mode:* 0.267. *Standard Deviation:* 0.209. *TSPA-LA Name:* SS_Corrosion_Rate_a (SNL 2008a, Tables 6.3.8-1 and 6.3.8-4).
CPUCOLCS. Concentration of irreversibly attached plutonium on commercial SNF colloids when colloids are stable (mol/L). *Distribution:* Piecewise uniform. *Range:* 1.00×10^{-10} to 5.00×10^{-6}. *Median:* 1.00×10^{-7}. *TSPA-LA Name:* CPu_Col_CSNF_Sampled_a (SNL 2008a, Section 6.3.7.6.2 and Table 6.3.7-63).
CPUCOLWF. Concentration of irreversibly attached plutonium on glass/waste form colloids when colloids are stable (mol/L). *Distribution:* Uniform. *Range:* 1.00×10^{-11} to 1.00×10^{-8}. *TSPA-LA Name:* CPu_Col_Wf_Embed_Sampled_a (SNL 2008a, Section 6.3.7.6.2 and Table 6.3.7-62).
CPUPERCS. Concentration of irreversibly attached plutonium per concentration of commercial SNF colloids ((mol/L)/(mg/L)). *Distribution:* Uniform. *Range:* 5.00×10^{-7} to 1.00×10^{-6}. *TSPA-LA Name:* CPu_Per_CSNF_Embed_Col_a (SNL 2008a, Section 6.3.7.6.2 and Table 6.3.7-63).

Table 2.4-11. Summary of Epistemically Uncertain Variables Considered in the TSPA (Continued)

CPUPERWF. Concentration of irreversibly attached plutonium per concentration of waste form colloids ((mol/L)/(mg/L)). *Distribution:* Triangular. *Range:* 5.00×10^{-9} to 2.5×10^{-8}. *Most Likely:* 2.00×10^{-8}. *TSPA-LA Name:* CPu_Per_WF_Embed_Col_a (SNL 2008a, Section 6.3.7.6.2 and Table 6.3.7-62).
CR2O3SA. Specific surface area of Cr_2O_3 (m^2/g). *Distribution:* Uniform. *Range:* 1 to 20. *TSPA-LA Name:* Cr2O3_SA_a (SNL 2008a, Table 6.3.8-4 and SCP in Equation 6.3.8-19).
CRITSLOP. Critical gradient for tephra mobilization from hillslopes (dimensionless). *Distribution:* Uniform. *Range:* 0.21 to 0.47. *TSPA-LA Name:* Critical_Slope_a (SNL 2008a, Table 6.5-5).
CSCORRAT. Carbon steel corrosion rate (mm/yr). *Distribution:* Truncated log normal. *Range:* 25 to 135. *Mean:* 78.5. *Standard Deviation:* 25. *TSPA-LA Name:* CS_Corrosion_Rate_a (SNL 2008a, Tables 6.3.8-1 and 6.3.8-4).
CSNFMASS. Scale factor used to characterize uncertainty in radionuclide content of commercial SNF (dimensionless). *Distribution:* Uniform. *Range:* 0.85 to 1.4. *TSPA-LA Name:* CSNF_Mass_Uncert_a (SNL 2008a, Sections 6.3.7.1.2, 6.3.7.1.3, and Table 6.3.7-7).
CSRINDDN. Grain density of commercial SNF rind (kg/m^3). *Distribution:* Uniform. *Range:* 5600 to 11500. *TSPA-LA Name:* Density_CSNF_Rind_a (SNL 2008a, Table 6.3.8-4).
CSRINDPO. Porosity in commercial SNF rind (dimensionless). *Distribution:* Uniform. *Range:* 0.05 to 0.3. *TSPA-LA Name:* Rind_Porosity_CSNF_a (SNL 2008a, Section 6.3.8.2.1 and Table 6.3.8-6).
CSRINDSA. Specific surface area of commercial SNF degradation rind (m^2/g). *Distribution:* Uniform. *Range:* 0.5 to 60. *TSPA-LA Name:* CSNF_Rind_SA_a. (SNL 2008a, Tables 6.3.8-2 and 6.3.8-4).
CSSPECSA. Logarithm of the effective specific surface area (m^2/mg) of the representative commercial SNF waste form (dimensionless). *Distribution:* Triangular. *Range:* –7.3 to –5.4. *Most Likely:* –6.7. *TSPA-LA Name:* Log_Specific_SA_CSNF_a. (SNL 2008a, Sections 6.3.7.4.1.2 and 6.3.7.4.1.3; Tables 6.3.7-30 and 6.3.7-31; and Equations 6.3.7-5 and 6.3.7-6).
CSWFA0AC. Correlated regression coefficient a0 in the abstracted rate model under acidic conditions (dimensionless). *Distribution:* Normal. *Mean/Median/Mode:* 0. *Standard Deviation:* 1. *TSPA-LA Name:* CSNF_WF_Uncert_a0_Acid_a. (SNL 2008a, Section 6.3.7.4.1.2; Equation 6.3.7-6).
CSWFA0AK. Correlated coefficient a0 in the abstracted rate model under alkaline conditions (dimensionless). *Distribution:* Normal. *Mean/Median/Mode:* 0. *Standard Deviation:* 1. *TSPA-LA Name:* CSNF_WF_Uncert_a0_Alk_a (SNL 2008a, Section 6.3.7.4.1.2; Equation 6.3.7-5).
CSWFA1AK. Correlated coefficient a1 in the abstracted rate model under alkaline conditions (dimensionless). *Distribution:* Normal. *Mean/Median/Mode:* 0. *Standard Deviation:* 1. *TSPA-LA Name:* CSNF_WF_Uncert_a1_Alk_a (SNL 2008a, Section 6.3.7.4.1.2 and Equation 6.3.7-5).
CSWFA2AK. Correlated coefficient a2 in the abstracted rate model under alkaline conditions (dimensionless). *Distribution:* Normal. *Mean/Median/Mode:* 0. *Standard Deviation:* 1. *TSPA-LA Name:* CSNF_WF_Uncert_a2_Alk_a (SNL 2008a, Section 6.3.7.4.1.2 and Equation 6.3.7-5).
CSWFA3AK. Correlated coefficient a3 in the abstracted rate model under alkaline conditions (dimensionless). *Distribution:* Normal. *Mean/Median/Mode:* 0. *Standard Deviation:* 1. *TSPA-LA Name:* CSNF_WF_Uncert_a3_Alk_a (SNL 2008a, Section 6.3.7.4.1.2 and Equation 6.3.7-5).
CSWFA4AC. Correlated coefficient a4 in the abstracted rate model under acid conditions (dimensionless). *Distribution:* Normal. *Mean/Median/Mode:* 0. *Standard Deviation:* 1. *TSPA-LA Name:* CSNF_WF_Uncert_a4_Acid_a (SNL 2008a, Section 6.3.7.4.1.2 and Equation 6.3.7-6).
DASHAVG. Mass median ash particle diameter (cm). *Distribution:* Log triangular. *Range:* 0.001 to 0.1. Mode: 0.01. *TSPA-LA Name:* Dash_mean_a (SNL 2008a, Table 6.5-4).

Table 2.4-11. Summary of Epistemically Uncertain Variables Considered in the TSPA (Continued)

DASHSIG. Ash particle diameter standard deviation (log (cm)). *Distribution:* Uniform. *Range:* 0.301 to 0.903. *TSPA-LA Name:* Dash_sigma_a (SNL 2008a, Table 6.5-4).
DCHANL. Diffusivity of radionuclides in channels of the Fortymile Wash fan (RMEI location) (cm^2/yr). *Distribution:* Uniform. *Range:* 0.035 to 0.266. *Mean:* 0.1505. *TSPA-LA Name:* D_Channels_a (SNL 2008a, Table 6.5-5).
DDIVIDE. Diffusivity of radionuclides in divides of the Fortymile Wash fan (RMEI location) (cm^2/yr). *Distribution:* Uniform. *Range:* 0.001 to 0.095. *Mean:* 0.048. *TSPA-LA Name:* D_Divides_a (SNL 2008a, Table 6.5-5).
DELPPCO2. Selector variable for partial pressure of CO_2 (dimensionless). *Distribution:* Uniform. *Range:* –1 to 1. *TSPA-LA Name:* PCE_Delta_pCO2_a (SNL 2008a, Sections 6.3.4.2 and 6.3.5.2.3; Table 6.3.5-4).
DIAMCOLL. Diameter of colloid particle (nm). *Distribution:* Uniform. *Range:* 50 to 300. *TSPA-LA Name:* Diameter_Colloid_a (SNL 2008a, Tables 6.3.8-1 and 6.3.8-4).
DIFPATHL. Diffusive path length from waste package outer corrosion barrier to mid-point of invert (m). *Distribution:* Uniform. *Range:* 0.3 to 1.24. *TSPA-LA Name:* Diff_Path_Length_Invert_Top_a (SNL 2008a, Section 6.3.8.2.4; Table 6.3.8-4).
DRAINDNS. Average drainage density for the Fortymile Wash drainage basin (1/km). *Distribution:* Uniform. *Range:* 20 to 33. *TSPA-LA Name:* Drainage_Density_a. (SNL 2008a, Table 6.5-5).
DSFLUX. Drip shield flux splitting factor (dimensionless). *Distribution:* Uniform. *Range:* 0 to 0.85. *TSPA-LA Name:* DS_Flux_Uncertainty_a (SNL 2008a, Tables 6.3.6-1, 6.3.6-2, and 6.3.8-4; Sections 6.3.6.2 and 6.3.6.4.1; Equation 6.3.6-5).
DSNFMASS. Scale factor used to characterize uncertainty in radionuclide content of DOE SNF (dimensionless). *Distribution:* Triangular. *Range:* 0.45 to 2.9. *Most Likely:* 0.62. *TSPA-LA Name:* DSNF_Mass_Uncert_a (SNL 2008a, Sections 6.3.7.1.2 and 6.3.7.1.3; Table 6.3.7-7).
DTDRHUNC. Selector variable used to determine the collapsed drift rubble thermal conductivity (dimensionless). *Distribution:* Discrete. *Range:* 1 to 2. *TSPA-LA Name:* dt_dRh_uncertainty (SNL 2008a, Section 6.6.2.2).
DWCDISP. Selector variable used to determine the axial dispersion modeling case (dimensionless). *Distribution:* Discrete. *Range:* 0 to 1. *TSPA-LA Name:* DWC_Dispersivity_Cond_a (SNL 2008a, Section 6.3.3.2.2; Table 6.3.3-5).
DWCSTERA. Multiplier for the standard deviation on the slope coefficient for determining the probability of condensation from percolation rate (dimensionless). *Distribution:* Normal. *Mean/Median/Mode:* 0. *Standard Deviation:* 1. *TSPA-LA Name:* DWC_Std_Error_a_a (SNL 2008a, Section 6.3.3.2.2; Tables 6.3.3-4 and 6.3.3-5).
DWCSTERB. Multiplier for the standard deviation on the y-intercept coefficient for determining the probability of condensation from percolation rate (dimensionless). *Distribution:* Normal. *Mean/Median/Mode:* 0. *Standard Deviation:* 1. *TSPA-LA Name:* DWC_Std_Error_b_a (SNL 2008a, Section 6.3.3.2.2; Tables 6.3.3-4 and 6.3.3-5).
DWCSTERC. Multiplier for the standard deviation on the slope coefficient for determining condensation rate from percolation rate (dimensionless). *Distribution:* Normal. *Mean/Median/Mode:* 0. *Standard Deviation:* 1. *TSPA-LA Name:* DWC_Std_Error_c_a (SNL 2008a, Section 6.3.3.2.2; Tables 6.3.3-4 and 6.3.3-5).
DWCSTERD. Multiplier for the standard deviation on the y-intercept coefficient for determining the condensation rate from percolation rate (dimensionless). *Distribution:* Normal. *Mean/Median/Mode:* 0. *Standard Deviation:* 1. *TSPA-LA Name:* DWC_Std_Error_d_a (SNL 2008a, Section 6.3.3.2.2; Tables 6.3.3-4 and 6.3.3-5).
DWCVENT. Selector variable specifying whether the ventilated or unventilated drip shield DWC modeling case is performed (dimensionless). *Distribution:* Discrete. *Range:* 0, 1. *TSPA-LA Name:* DWC_Ventilated_Cond_a (SNL 2008a, Section 6.3.3.2.2 and Table 6.3.3-5).

Table 2.4-11. Summary of Epistemically Uncertain Variables Considered in the TSPA (Continued)

EBSDIFCF. Exponential term representing uncertainty in the invert diffusion coefficient (dimensionless). *Distribution:* Truncated normal. *Range:* –0.621 to 0.687. *Mean:* 0.033. *Standard Deviation:* 0.218. *TSPA-LA Name:* Invert_Diff_Coeff_Uncert_a (SNL 2008a, Section 6.3.8.2.4; Table 6.3.8-4; Equation 6.3.8-24).
EP1HINP2[a]. Logarithm of the scale factor used to characterize uncertainty in Np_2O_5 solubility for ionic strength values between 1 and 3 molal (dimensionless). *Distribution:* Truncated normal. *Range:* –1.7 to 1.7. *Mean:* 0. *Standard Deviation:* 0.85. *TSPA-LA Name:* Np2O5_Eps_1_high_a[a] (SNL 2008a, Sections 6.3.7.5.1 and 6.3.7.5.2; Table 6.3.7-42; Equation 6.3.7-13a).
EP1HINPO2[a]. Logarithm of the scale factor used to characterize uncertainty in NpO_2 solubility at an ionic strength between 1 and 3 molal (dimensionless). *Distribution:* Truncated normal. *Range:* –1.34 to 1.34. *Mean:* 0. *Standard Deviation:* 0.67. *TSPA-LA Name:* NpO2_Eps_1_high_a[a] (SNL 2008a, Sections 6.3.7.5.1, 6.3.7.5.2, and 6.3.7.5.3; Table 6.3.7-43; Equation 6.3.7-13a).
EP1HINU[a]. Logarithm of the scale factor used to characterize uncertainty in uranium solubility under nominal or seismic conditions at an ionic strength between 1and 3 molal (dimensionless). *Distribution:* Truncated normal. *Range:* –1.2 to 1.2. *Mean:* 0. *Standard Deviation:* 0.6. *TSPA-LA Name:* U_Eps_1_high_Nominal_a[a] (SNL 2008a, Section 6.3.7.5.1, 6.3.7.5.2, and 6.3.7.5.3; Table 6.3.7-54; Equation 6.3.7-13a).
EP1HIOU[a]. Logarithm of the scale factor used to characterize uncertainty in uranium solubility under conditions other than nominal and seismic at an ionic strength between 1and 3 molal (dimensionless). *Distribution:* Truncated normal. *Range:* –1.2 to 1.2. *Mean:* 0. *Standard Deviation:* 0.6. *TSPA-LA Name:* U_Eps_1_high_Other_a[a] (SNL 2008a, Sections 6.3.7.5.1, 6.3.7.5.2, and 6.3.7.5.3; Table 6.3.7-58; Equation 6.3.7-13a).
EP1HIPU[a]. Logarithm of the scale factor used to characterize uncertainty in plutonium solubility for ionic strength between 1 and 3 molal (dimensionless). *Distribution:* Truncated normal. *Range:* –1.52 to 1.52. *Mean:* 0. *Standard Deviation:* 0.76. *TSPA-LA Name:* Pu_Eps_1_high_a[a] (SNL 2008a, Sections 6.3.7.5.1, 6.3.7.5.2, and 6.3.7.5.3; Table 6.3.7-44; Equation 6.3.7-13a).
EP1HISN[a]. Logarithm of the scale factor used to characterize uncertainty in tin solubility for high ionic strength conditions (dimensionless). *Distribution:* Truncated normal. *Range:* –1.08 to 1.08. *Mean:* 0. *Standard Deviation:* 0.54. *TSPA-LA Name:* Sn_Eps_high_a[a] (SNL 2008a, Sections 6.3.7.5.2 and 6.3.7.5.3; Table 6.3.7-47; Equation 6.3.7-13a).
EP1HITH[a]. Logarithm of the scale factor used to characterize uncertainty in thorium solubility at ionic strength between 1 and 3 molal (dimensionless). *Distribution:* Truncated normal. *Range:* –1.52 to 1.52. *Mean:* 0. *Standard Deviation:* 0.76. *TSPA-LA Name:* Th_Eps_1_high_a[a] (SNL 2008a, Sections 6.3.7.5.1, 6.3.7.5.2, and 6.3.7.5.3; Table 6.3.7-46; Equation 6.3.7-13a).
EP1LOWAM. Logarithm of the scale factor used to characterize uncertainty in americium solubility at an ionic strength below 1 molal (dimensionless). *Distribution:* Truncated normal. *Range:* –2 to 2. *Mean:* 0. *Standard Deviation:* 1. *TSPA-LA Name:* Am_Eps_1_low_a (SNL 2008a, Sections 6.3.7.5.1, 6.3.7.5.2, and 6.3.7.5.3; Table 6.3.7-41; Equation 6.3.7-13a).
EP1LOWNU. Logarithm of the scale factor used to characterize uncertainty in uranium solubility under nominal or seismic conditions at an ionic strength below 1 molal (dimensionless). *Distribution:* Truncated normal. *Range:* –1 to 1. *Mean/Median/Mode:* 0. *Standard Deviation:* 0.5. *TSPA-LA Name:* U_Eps_1_low_Nominal_a (SNL 2008a, Section 6.3.7.5.1, 6.3.7.5.2, and 6.3.7.5.3; Table 6.3.7-54; Equation 6.3.7-13a).
EP1LOWOU. Logarithm of the scale factor used to characterize uncertainty in uranium solubility under conditions other than nominal and seismic at an ionic strength below 1 molal (dimensionless). *Distribution:* Truncated normal. *Range:* –1 to 1. *Mean/Median/Mode:* 0. *Standard Deviation:* 0.5. *TSPA-LA Name:* U_Eps_1_low_Other_a (SNL 2008a, Sections 6.3.7.5.1, 6.3.7.5.2, and 6.3.7.5.3; Table 6.3.7-58; Equation 6.3.7-13a).
EP1LOWPU. Logarithm of the scale factor used to characterize uncertainty in plutonium solubility at an ionic strength below 1 molal (dimensionless). *Distribution:* Truncated normal. *Range:* –1.4 to 1.4. *Mean/Median/Mode:* 0. *Standard Deviation:* 0.7. *TSPA-LA Name:* Pu_Eps_1_low_a (SNL 2008a, Sections 6.3.7.5.1, 6.3.7.5.2, and 6.3.7.5.3; Table 6.3.7-44; Equation 6.3.7-13a).

Table 2.4-11. Summary of Epistemically Uncertain Variables Considered in the TSPA (Continued)

EP1LOWSN. Logarithm of the scale factor used to characterize uncertainty in tin solubility for low ionic strength conditions (dimensionless). *Distribution:* Truncated normal. *Range:* –0.9 to 0.9. *Mean/Median/Mode:* 0. *Standard Deviation:* 0.45. *TSPA-LA Name:* Sn_Eps_low_a (SNL 2008a, Sections 6.3.7.5.2 and 6.3.7.5.3; Table 6.3.7-47; Equation 6.3.7-13a).
EP1LOWTH. Logarithm of the scale factor used to characterize uncertainty in thorium solubility at an ionic strength below 1 molal (dimensionless). *Distribution:* Truncated normal. *Range:* –1.4 to 1.4. *Mean:* 0. *Standard Deviation:* 0.7. *TSPA-LA Name:* Th_Eps_1_low_a (SNL 2008a, Sections 6.3.7.5.1, 6.3.7.5.2, and 6.3.7.5.3; Table 6.3.7-46; Equation 6.3.7-13a).
EP1NP2O5. Logarithm of the scale factor used to characterize uncertainty in Np_2O_5 solubility at an ionic strength below 1 molal (dimensionless). *Distribution:* Truncated normal. *Range:* –1.6 to 1.6. *Mean:* 0. *Standard Deviation:* 0.8. *TSPA-LA Name:* Np2O5_Eps_1_low_a (SNL 2008a, Sections 6.3.7.5.1 and 6.3.7.5.2; Table 6.3.7-42; Equation 6.3.7-13a).
EP1NPO2. Logarithm of the scale factor used to characterize uncertainty in NpO_2 solubility at an ionic strength below 1 molal (dimensionless). *Distribution:* Truncated normal. *Range:* –1.2 to 1.2. *Mean:* 0. *Standard Deviation:* 0.6. *TSPA-LA Name:* NpO2_Eps_1_low_a (SNL 2008a, Sections 6.3.7.5.1, 6.3.7.5.2, and 6.3.7.5.3; Table 6.3.7-43; Equation 6.3.7-13a).
EP1PA. Logarithm of the scale factor used to characterize uncertainty in protactinium solubility (dimensionless). *Distribution:* Uniform. *Range:* –4.42 to –0.05. *TSPA-LA Name:* Pa_Eps_1_a (SNL 2008a, Sections 6.3.7.5.2 and 6.3.7.5.3; Table 6.3.7-45; Equation 6.3.7-13b).
EP2BCDHU[a]**.** Term associated with uncertainty in uranium solubility (controlled by boldwoodite saturation) due to variations in fluoride concentration for CDSP waste packages when ionic strength is greater than or equal to 0.004 molal and for the invert below CDSP waste packages (mg/L). *Distribution:* Triangular. *Range:* 0 to 272.3. *Most Likely:* 0. *TSPA-LA Name:* U_Eps_2_Boltwoodite_CDSP_Hig_a[a] (SNL 2008a, Sections 6.3.7.5.1, 6.3.7.5.2, and 6.3.7.5.3; Table 6.3.7-58; Equation 6.3.7-13a).
EP2BCSHU[a]**.** Term associated with uncertainty in uranium solubility (controlled by boldwoodite saturation) due to variations in fluoride concentration for commercial SNF waste packages when ionic strength is greater than or equal to 0.2 molal and for the invert below commercial SNF waste packages (mg/L). *Distribution:* Triangular. *Range:* 0 to 57.01. *Most Likely:* 0. *TSPA-LA Name:* U_Eps_2_Boltwoodite_CSNF_Hig_a[a] (SNL 2008a, Sections 6.3.7.5.1, 6.3.7.5.2, and 6.3.7.5.3; Table 6.3.7-58; Equation 6.3.7-13a).
EP2BLOWU[a]**.** Term associated with uncertainty in uranium solubility (controlled by boldwoodite saturation) due to variations in fluoride concentration for CDSP waste packages Cell 1a, Cell 1b when ionic strength is less than 0.004 molal, and commercial SNF waste packages when ionic strength is less than 0.2 molal (mg/L). *Distribution:* Triangular. *Range:* 0 to 6.13. *Most Likely:* 0. *TSPA-LA Name:* U_Eps_2_Boltwoodite_Glass_Lo_a[a] (SNL 2008a, Sections 6.3.7.5.1, 6.3.7.5.2, and 6.3.7.5.3; Table 6.3.7-58; Equation 6.3.7-13a).
EP2CDNP2[a]**.** Term associated with uncertainty in Np_2O_5 solubility due to variations in fluoride concentration for CDSP waste packages when ionic strength is greater than or equal to 0.004 molal and for the invert below CDSP waste packages (mg/L). *Distribution:* Triangular. *Range:* 0 to 853. *Most Likely:* 0. *TSPA-LA Name:* Np2O5_Eps_2_CDSP_High_a[a] (SNL 2008a, Sections 6.3.7.5.1 and 6.3.7.5.2; Table 6.3.7-42; Equation 6.3.7-13a).
EP2CDNPO2[a]**.** Term associated with uncertainty in NpO_2 solubility due to variations in fluoride concentration for CDSP waste packages when ionic strength is greater than or equal to 0.004 molal and for the invert below CDSP waste packages (mg/L). *Distribution:* Triangular. *Range:* 0 to 1093.5. *Most Likely:* 0. *TSPA-LA Name:* NpO2_Eps_2_CDSP_High_a[a] (SNL 2008a, Sections 6.3.7.5.1, 6.3.7.5.2, and 6.3.7.5.3; Table 6.3.7-43; Equation 6.3.7-13a).
EP2CDPA[a]**.** Term associated with uncertainty in protactinium solubility due to variations in fluoride concentration for CDSP waste packages when ionic strength is greater than or equal to 0.004 molal and for the invert below CDSP waste packages (mg/L). *Distribution:* Triangular. *Range:* 0 to 853. *Most Likely:* 0. *TSPA-LA Name:* Pa_Eps_2_CDSP_High_a[a] (SNL 2008a, Sections 6.3.7.5.2 and 6.3.7.5.3; Table 6.3.7-45; Equation 6.3.7-13b).

Table 2.4-11. Summary of Epistemically Uncertain Variables Considered in the TSPA (Continued)

EP2CDPU[a]. Term associated with uncertainty in plutonium solubility due to variations in fluoride concentration for CDSP waste packages when ionic strength is greater than or equal to 0.004 molal and for the invert below CDSP waste packages (mg/L). *Distribution:* Triangular. *Range:* 0 to 5460. *Most Likely:* 0. *TSPA-LA Name:* Pu_Eps_2_CDSP_High_a[a] (SNL 2008a, Sections 6.3.7.5.1, 6.3.7.5.2, and 6.3.7.5.3; Table 6.3.7-44; Equation 6.3.7-13a).
EP2CDTH[a]. Term associated with uncertainty in thorium solubility due to variations in fluoride concentration for CDSP waste packages when ionic strength is greater than or equal to 0.004 molal and for the invert below CDSP waste packages (mg/L). *Distribution:* Triangular. *Range:* 0 to 23723.2. *Most Likely:* 0. *TSPA-LA Name:* Th_Eps_2_CDSP_High_a[a] (SNL 2008a, Sections 6.3.7.5.1, 6.3.7.5.2, and 6.3.7.5.3; Table 6.3.7-46; Equation 6.3.7-13a).
EP2CSHNU[a]. Term associated with uncertainty in uranium solubility (under nominal or seismic conditions) due to variations in fluoride concentration for commercial SNF waste packages when ionic strength is greater than or equal to 0.2 molal and for the invert below commercial SNF waste packages (mg/L). *Distribution:* Triangular. *Range:* 0 to 1361. *Most Likely:* 0. *TSPA-LA Name:* U_Eps_2_CSNF_High_Nominal_a[a] (SNL 2008a, Section 6.3.7.5.1, 6.3.7.5.2, and 6.3.7.5.3; Table 6.3.7-54; Equation 6.3.7-13a).
EP2CSLNU[a]. Term associated with uncertainty in uranium solubility (under nominal or seismic conditions) due to variations in fluoride concentration for commercial SNF waste packages when ionic strength is less than 0.2 molal and for the invert below commercial SNF waste packages (mg/L). *Distribution:* Triangular. *Range:* 0 to 78. *Most Likely:* 0. *TSPA-LA Name:* U_Eps_2_CSNF_Low_Nominal_a[a] (SNL 2008a, Section 6.3.7.5.1, 6.3.7.5.2, and 6.3.7.5.3; Table 6.3.7-54; Equation 6.3.7-13a).
EP2CSNP2[a]. Term associated with uncertainty in Np_2O_5 solubility due to variations in fluoride concentration for commercial SNF waste packages when ionic strength is greater than or equal to 0.2 molal and for the invert below commercial SNF waste packages (mg/L). *Distribution:* Triangular. *Range:* 0 to 197. *Most Likely:* 0. *TSPA-LA Name:* Np2O5_Eps_2_CSNF_High_a[a] (SNL 2008a, Sections 6.3.7.5.1 and 6.3.7.5.2; Table 6.3.7-42; Equation 6.3.7-13a).
EP2CSNPO2[a]. Term associated with uncertainty in NpO_2 solubility due to variations in fluoride concentration for commercial SNF waste packages when ionic strength is greater than or equal to 0.2 molal and for the invert below commercial SNF waste packages (mg/L). *Distribution:* Triangular. *Range:* 0 to 255.8. *Most Likely:* 0. *TSPA-LA Name:* NpO2_Eps_2_CSNF_High_a[a] (SNL 2008a, Sections 6.3.7.5.1, 6.3.7.5.2, and 6.3.7.5.3; Table 6.3.7-43; Equation 6.3.7-13a).
EP2CSPA[a]. Term associated with uncertainty in protactinium solubility due to variations in fluoride concentration for commercial SNF waste packages when ionic strength is greater than or equal to 0.2 molal and for the invert below commercial SNF waste packages (mg/L). *Distribution:* Triangular. *Range:* 0 to 197. *Most Likely:* 0. *TSPA-LA Name:* Pa_Eps_2_CSNF_High_a[a] (SNL 2008a, Sections 6.3.7.5.2 and 6.3.7.5.3; Table 6.3.7-45; Equation 6.3.7-13b).
EP2CSPU[a]. Term associated with uncertainty in plutonium solubility due to variations in fluoride concentration for commercial SNF waste packages when ionic strength is greater than or equal to 0.2 molal and for the invert below commercial SNF waste packages (mg/L). *Distribution:* Triangular. *Range:* 0 to 1374. *Most Likely:* 0. *TSPA-LA Name:* Pu_Eps_2_CSNF_High_a[a] (SNL 2008a, Sections 6.3.7.5.1, 6.3.7.5.2 and 6.3.7.5.3; Table 6.3.7-44; Equation 6.3.7-13a).
EP2CSTH[a]. Term associated with uncertainty in thorium solubility due to variations in fluoride concentration for commercial SNF waste packages when ionic strength is greater than or equal to 0.2 molal and for the invert below commercial SNF waste packages (mg/L). *Distribution:* Triangular. *Range:* 0 to 7848.3. *Most Likely:* 0. *TSPA-LA Name:* Th_Eps_2_CSNF_High_a[a] (SNL 2008a, Sections 6.3.7.5.1, 6.3.7.5.2, and 6.3.7.5.3; Table 6.3.7-46; Equation 6.3.7-13a).
EP2HIAM[a]. Logarithm of the scale factor used to characterize uncertainty in americium solubility at ionic strength values between 1 and 3 molal (dimensionless). *Distribution:* Truncated normal. *Range:* –2.08 to 2.08. *Mean:* 0. *Standard Deviation:* 1.04. *TSPA-LA Name:* Am_Eps_1_high_a[a] (SNL 2008a, Sections 6.3.7.5.1, 6.3.7.5.2, and 6.3.7.5.3; Equation 6.3.7-13a; Table 6.3.7-41).

Table 2.4-11. Summary of Epistemically Uncertain Variables Considered in the TSPA (Continued)

EP2HICAM. Term associated with uncertainty in americium solubility due to variations in fluoride concentration for commercial SNF waste packages when ionic strength is greater than or equal to 0.2 molal and for the invert below commercial SNF waste packages (mg/L). *Distribution:* Triangular. *Range:* 0 to 109.03. *Most Likely:* 0. *TSPA-LA Name:* Am_Eps_2_CSNF_High_a (SNL 2008a, Sections 6.3.7.5.2 and 6.3.7.5.3; Table 6.3.7-41; Equation 6.3.7-13a).
EP2HICDAM[a]. Term associated with uncertainty in americium solubility due to variations in fluoride concentration for CDSP waste packages when ionic strength is greater than or equal to 0.004 molal and for the invert below CDSP waste packages (mg/L). *Distribution:* Triangular. *Range:* 0 to 688.6. *Most Likely:* 0. *TSPA-LA Name:* Am_Eps_2_CDSP_High_a[a] (SNL 2008a, Sections 6.3.7.5.2 and 6.3.7.5.3; Table 6.3.7-41; Equation 6.3.7-13a).
EP2LONP2[a]. Term associated with uncertainty in Np_2O_5 solubility due to variations in fluoride concentration for CDSP waste packages Cell 1a, Cell 1b when ionic strength is less than 0.004 molal, and commercial SNF waste packages when ionic strength is less than 0.2 molal (mg/L). *Distribution:* Triangular. *Range:* 0 to 11. *Most Likely:* 0. *TSPA-LA Name:* Np2O5_Eps_2_Glass_Low_a[a] (SNL 2008a, Sections 6.3.7.5.1 and 6.3.7.5.2; Table 6.3.7-42; Equation 6.3.7-13a).
EP2LONPO2[a]. Term associated with uncertainty in NpO_2 solubility due to variations in fluoride concentration for CDSP waste packages Cell 1a, Cell 1b when ionic strength is less than 0.004 molal, and commercial SNF waste packages when ionic strength is less than 0.2 molal (mg/L). *Distribution:* Triangular. *Range:* 0 to 14.1. *Most Likely:* 0. *TSPA-LA Name:* NpO2_Eps_2_Glass_Low_a[a] (SNL 2008a, Sections 6.3.7.5.1, 6.3.7.5.2, and 6.3.7.5.3; Table 6.3.7-43; Equation 6.3.7-13a).
EP2LOPA[a]. Term associated with uncertainty in protactinium solubility due to variations in fluoride concentration for CDSP waste packages Cell 1a, Cell 1b when ionic strength is less than 0.004 molal, and commercial SNF waste packages when ionic strength is less than 0.2 molal (mg/L). *Distribution:* Triangular. *Range:* 0 to 11. *Most Likely:* 0. *TSPA-LA Name:* Pa_Eps_2_Glass_Low_a[a] (SNL 2008a, Sections 6.3.7.5.2 and 6.3.7.5.3; Table 6.3.7-45; Equation 6.3.7-13b).
EP2LOWAM[a]. Term associated with uncertainty in americium solubility due to variations in fluoride concentration for CDSP waste packages Cell 1a, Cell 1b when ionic strength is less than 0.004 molal, and commercial SNF waste packages when ionic strength is less than 0.2 molal (mg/L). *Distribution:* Triangular. *Range:* 0 to 4.42. *Most Likely:* 0. *TSPA-LA Name:* Am_Eps_2_Glass_Low_a[a]. (SNL 2008a, Sections 6.3.7.5.2 and 6.3.7.5.3; Table 6.3.7-41; Equation 6.3.7-13a).
EP2LOWPU[a]. Term associated with uncertainty in plutonium solubility due to variations in fluoride concentration for CDSP waste packages Cell 1a, Cell 1b when ionic strength is less than 0.004 molal, and commercial SNF waste packages when ionic strength is less than 0.2 molal (mg/L). *Distribution:* Triangular. *Range:* 0 to 79. *Most Likely:* 0. *TSPA-LA Name:* Pu_Eps_2_Glass_Low_a[a] (SNL 2008a, Sections 6.3.7.5.1, 6.3.7.5.2, and 6.3.7.5.3; Table 6.3.7-44; Equation 6.3.7-13a).
EP2LOWTH[a]. Term associated with uncertainty in thorium solubility due to variations in fluoride concentration for CDSP waste packages Cell 1a, Cell 1b when ionic strength is less than 0.004 molal, and commercial SNF waste packages when ionic strength is less than 0.2 molal (mg/L). *Distribution:* Triangular. *Range:* 0 to 626.2. *Most Likely:* 0. *TSPA-LA Name:* Th_Eps_2_Glass_Low_a[a] (SNL 2008a, Sections 6.3.7.5.1, 6.3.7.5.2, and 6.3.7.5.3; Table 6.3.7-46; Equation 6.3.7-13a).
EP2SCDHU[a]. Term associated with uncertainty in uranium solubility (controlled by schoepite saturation) due to variations in fluoride concentration for CDSP waste packages when ionic strength is greater than or equal to 0.004 molal and for the invert below CDSP waste packages (mg/L). *Distribution:* Triangular. *Range:* 0 to 5385. *Most Likely:* 0. *TSPA-LA Name:* U_Eps_2_Schoepite_CDSP_High_a[a] (SNL 2008a, Sections 6.3.7.5.1, 6.3.7.5.2, and 6.3.7.5.3; Table 6.3.7-58; Equation 6.3.7-13a.)
EP2SCSHU[a]. Term associated with uncertainty in uranium solubility (controlled by schoepite saturation) due to variations in fluoride concentration for commercial SNF waste packages when ionic strength is greater than or equal to 0.2 molal and for the invert below commercial SNF waste packages (mg/L). *Distribution:* Triangular. *Range:* 0 to 1361. *Most Likely:* 0. *TSPA-LA Name:* U_Eps_2_Schoepite_CSNF_High_a[a] (SNL 2008a, Sections 6.3.7.5.1, 6.3.7.5.2, and 6.3.7.5.3; Table 6.3.7-58; Equation 6.3.7-13a).

Table 2.4-11. Summary of Epistemically Uncertain Variables Considered in the TSPA (Continued)

EP2SLOWU[a]**.** Term associated with uncertainty in uranium solubility (controlled by schoepite saturation) due to variations in fluoride concentration for CDSP waste packages Cell 1a, Cell 1b when ionic strength is less than 0.004 molal, and commercial SNF waste packages when ionic strength is less than 0.2 molal (mg/L). *Distribution:* Triangular. *Range:* 0 to 78. *Most Likely:* 0. *TSPA-LA Name:* U_Eps_2_Schoepite_Glass_Low_a[a] (SNL 2008a, Sections 6.3.7.5.1, 6.3.7.5.2, and 6.3.7.5.3; Table 6.3.7-58; Equation 6.3.7-13a).
FHHISKCP. Frenkel Halsey Hill water vapor adsorption isotherm parameter, *k*, for corrosion products (dimensionless). *Distribution:* Uniform. *Range:* 1.048 to 1.370 (see additional information). *TSPA-LA Name:* FHH_Isotherm_k_CP_a (SNL 2008a, Table 6.3.8-4).
FHHISKCS. Frenkel Halsey Hill water vapor adsorption isotherm parameter, *k*, for commercial SNF rind (dimensionless). *Distribution:* Uniform. *Range:* 1.606 to 8.215. *TSPA-LA Name:* FHH_Isotherm_k_CSNF_Rind_a (SNL 2008a, Table 6.3.8-4).
FHHISSCP. Frenkel Halsey Hill water vapor adsorption isotherm parameter, *s*, for corrosion products (dimensionless). *Distribution:* Uniform. *Range:* 1.525 to 1.852 (see additional information). *TSPA-LA Name:* FHH_Isotherm_s_CP_a (SNL 2008a, Table 6.3.8-4).
FHHISSCS. Frenkel Halsey Hill water vapor adsorption isotherm parameter, *s*, for commercial SNF rind (dimensionless). *Distribution:* Uniform. *Range:* 1.656 to 3.038. *TSPA-LA Name:* FHH_Isotherm_s_CSNF_Rind_a (SNL 2008a, Table 6.3.8-4)
FRACCHNL. Fraction of the RMEI location subject to fluvial deposition (dimensionless). *Distribution:* Uniform. *Range:* 0.09 to 0.54. *TSPA-LA Name:* Fraction_Channel_a (SNL 2008a, Table 6.5-5).
FWDRAT. Default forward rate constant for irreversible sorption of plutonium and americium ($m^3/m^2/yr$). *Distribution:* Log uniform. *Range:* 0.002 to 0.05. *TSPA-LA Name:* Default_Fwd_Rate_Const_a (SNL 2008a, Table 6.3.7-65).
GOERELAB. Fraction of total iron oxide that is goethite (dimensionless). *Distribution:* Uniform. *Range:* 0.45 to 0.8. *TSPA-LA Name:* Relative_Abundance_Goethite_a (SNL 2008a, Section 6.3.8.2.3; Table 6.3.8-4).
GOESA. Specific surface area of goethite (m^2/g). *Distribution:* Truncated log normal. *Range:* 14.7 to 110. *Mean:* 51.42. *Standard Deviation:* 30.09. *TSPA-LA Name:* Goethite_SA_a (SNL 2008a, Table 6.3.8-4; SCP in Equation 6.3.8-19).
GOESITED. Density of sorption sites on goethite ($1/nm^2$). *Distribution:* Discrete. *Range:* 1.02 to 8.59. *TSPA-LA Name:* Goethite_Site_Density_a (SNL 2008a, Table 6.3.8-3).
GP1NO3. Ratio of Cl to NO_3 (Cl:N) in Group 1 pore waters (dimensionless). *Distribution:* Discrete. *Range:* 0.783 to 6.1213. *TSPA-LA Name:* PCE_Gp1_Cl_NO3_CDF_a (SNL 2008a, Section 6.3.4.3.2).
GP2NO3. Ratio of Cl to NO_3 (Cl:N) in Group 2 pore waters (dimensionless). *Distribution:* Discrete. *Range:* 2.359 to 3.187. *TSPA-LA Name:* PCE_Gp2_Cl_NO3_CDF_a (SNL 2008a, Section 6.3.4.3.2).
GP3NO3. Ratio of Cl to NO_3 (Cl:N) in Group 3 pore waters (dimensionless). *Distribution:* Discrete. *Range:* 9.7782 to 64.128. *TSPA-LA Name:* PCE_Gp3_Cl_NO3_CDF_a (SNL 2008a, Section 6.3.4.3.2).
GP4NO3. Ratio of Cl to NO_3 (Cl:N) in Group 4 pore waters (dimensionless). *Distribution:* Discrete. *Range:* 4.4485 to 8.2119. *TSPA-LA Name:* PCE_Gp4_Cl_NO3_CDF_a (SNL 2008a, Section 6.3.4.3.2).
HFOSA. Hydrous ferric oxide (HFO) surface area (m^2/g). *Distribution:* Truncated log normal. *Range:* 68 to 600. *Mean:* 275.6. *Standard Deviation:* 113.4. *TSPA-LA Name:* HFO_SA_a (SNL 2008a, Table 6.3.8-4; SCP in Equation 6.3.8-19).
HFOSITED. Sorption site density for hydrous ferric oxide (HFO) ($1/nm^2$). *Distribution:* Discrete. *Range:* 0.56 to 5.65. *TSPA-LA Name:* HFO_Site_Density_a (SNL 2008a, Table 6.3.8-3).

Table 2.4-11. Summary of Epistemically Uncertain Variables Considered in the TSPA (Continued)

HLWDRACD. Effective rate coefficient (affinity term) for the dissolution of HLW glass in CDSP waste packages under low pH conditions (g/(m^{2}d)). *Distribution:* Triangular. *Range:* 8.41×10^{3} to 1.15×10^{7}. Mode: 8.41×10^{3}. *TSPA-LA Name:* HLW_Diss_kE_Acidic_a (SNL 2008a, Sections 6.3.7.4.3.2 and 6.3.7.4.3.3; Table 6.3.7-32; Equation 6.3.7-8).
HLWDRALK. Effective rate coefficient (affinity term) for the dissolution of HLW glass in CDSP waste packages under high pH conditions (g/(m^{2}d)). *Distribution:* Triangular. *Range:* 2.82×10^{1} to 3.47×10^{4}. *Mode:* 2.82×10^{1}. *TSPA-LA Name:* HLW_Diss_kE_Alkaline_a (SNL 2008a, Sections 6.3.7.4.3.2 and 6.3.7.4.3.3; Table 6.3.7-32; Equation 6.3.7-8).
HLWGRNDS. Specific surface area of HLWG degradation rind (m^2/g). *Distribution:* Uniform. *Range:* 10 to 38. *TSPA-LA Name:* HLWG_Rind_SA_a (SNL 2008a, Table 6.3.8-4).
HLWMASS. Scale factor used to characterize uncertainty in radionuclide content of HLW glass (dimensionless). *Distribution:* Triangular. *Range:* 0.7 to 1.5. *Most Likely:* 1. *TSPA-LA Name:* HLW_Mass_Uncert_a (SNL 2008a, Sections 6.3.7.1.2 and 6.3.7.1.3; Table 6.3.7-7).
IGERATE. Frequency of occurrence of volcanic eruptive events per year. *Calculated by:* Igneous_Event_Prob_a x 0.083. *Range:* 0 to 6.44×10^{-8}. *TSPA-LA Name:* IGERATE (SNL 2008a, Section 6.5.2.1.1; Appendix J; Equation J7.5-3).
IGRATE. Frequency of intersection of the repository footprint by a volcanic event per year. *Distribution:* Piecewise uniform. *Range:* 0 to 7.76×10^{-7}. *TSPA-LA Name:* Igneous_Event_Prob_a (SNL 2008a, Table 6.5-2).
ILTAC227. Volcanic Biosphere Dose Conversion Factor (BDCF) component for long-term inhalation of ^{227}Ac in modern interglacial climate ((Sv/yr)/(Bq/kg)). *Distribution:* Discrete. *Range:* 1.53×10^{-7} to 4.5×10^{-6}. *Mean:* 9.0×10^{-7}. *Standard Deviation:* 5.75×10^{-7}. *TSPA-LA Name:* DE_BDCF_Inh_LT_Ac227 (SNL 2008a, Sections 6.3.11.1 and 6.3.11.2; Equation 6.3.11-4).
ILTAM241. Volcanic Biosphere Dose Conversion Factor (BDCF) component for long-term inhalation of ^{241}Am in modern interglacial climate ((Sv/yr)/(Bq/kg)). *Distribution:* Discrete. *Range:* 8.45×10^{-8} to 2.48×10^{-6}. *Mean:* 4.96×10^{-7}. *Standard Deviation:* 3.17×10^{-7}. *TSPA-LA Name:* DE_BDCF_Inh_LT_Am241(SNL 2008a, Sections 6.3.11.1 and 6.3.11.2; Equation 6.3.11-4).
ILTAM243. Volcanic Biosphere Dose Conversion Factor (BDCF) component for long-term inhalation of ^{243}Am in modern interglacial climate ((Sv/yr)/(Bq/kg)). *Distribution:* Discrete. *Range:* 8.38×10^{-8} to 2.46×10^{-6}. *Mean:* 4.93×10^{-7}. *Standard Deviation:* 3.15×10^{-7}. *TSPA-LA Name:* DE_BDCF_Inh_LT_Am243 (SNL 2008a, Sections 6.3.11.1 and 6.3.11.2; Equation 6.3.11-4).
ILTCS137. Volcanic Biosphere Dose Conversion Factor (BDCF) component for long-term inhalation of ^{137}Cs in modern interglacial climate ((Sv/yr)/(Bq/kg)). *Distribution:* Discrete. *Range:* 3.43×10^{-11} to 1.01×10^{-9}. *Mean:* 2.02×10^{-10}. *Standard Deviation:* 1.29×10^{-10}. *TSPA-LA Name:* DE_BDCF_Inh_LT_Cs137 (SNL 2008a, Sections 6.3.11.1 and 6.3.11.2; Equation 6.3.11-4).
ILTI129. Volcanic Biosphere Dose Conversion Factor (BDCF) component for long-term inhalation of ^{129}I in modern interglacial climate ((Sv/yr)/(Bq/kg)). *Distribution:* Discrete. *Range:* 3.15×10^{-11} to 9.23×10^{-10}. *Mean:* 1.85×10^{-10}. *Standard Deviation:* 1.18×10^{-10}. *TSPA-LA Name:* DE_BDCF_Inh_LT_I129 (SNL 2008a, Sections 6.3.11.1 and 6.3.11.2; Equation 6.3.11-4).
ILTNP237. Volcanic Biosphere Dose Conversion Factor (BDCF) component for long-term inhalation of ^{237}Np in modern interglacial climate ((Sv/yr)/(Bq/kg)). *Distribution:* Discrete. *Range:* 4.35×10^{-8} to 1.28×10^{-6}. *Mean:* 2.56×10^{-7}. *Standard Deviation:* 1.63×10^{-7}. *TSPA-LA Name:* DE_BDCF_Inh_LT_Np237 (SNL 2008a, Sections 6.3.11.1 and 6.3.11.2; Equation 6.3.11-4).
ILTPA231. Volcanic Biosphere Dose Conversion Factor (BDCF) component for long-term inhalation of ^{231}Pa in modern interglacial climate ((Sv/yr)/(Bq/kg)). *Distribution:* Discrete. *Range:* 2.02×10^{-7} to 5.92×10^{-6}. *Mean:* 1.18×10^{-6}. *Standard Deviation:* 7.56×10^{-7}. *TSPA-LA Name:* DE_BDCF_Inh_LT_Pa231 (SNL 2008a, Sections 6.3.11.1 and 6.3.11.2; Equation 6.3.11-4).

Table 2.4-11. Summary of Epistemically Uncertain Variables Considered in the TSPA (Continued)

ILTPU238. Volcanic Biosphere Dose Conversion Factor (BDCF) component for long-term inhalation of ^{238}Pu in modern interglacial climate ((Sv/yr)/(Bq/kg)). *Distribution:* Discrete. *Range:* 9.46×10^{-8} to 2.78×10^{-6}. *Mean:* 5.56×10^{-7}. *Standard Deviation:* 3.55×10^{-7}. *TSPA-LA Name:* DE_BDCF_Inh_LT_Pu238 (SNL 2008a, Sections 6.3.11.1 and 6.3.11.2; Equation 6.3.11-4).
ILTPU239. Volcanic Biosphere Dose Conversion Factor (BDCF) component for long-term inhalation of ^{239}Pu in modern interglacial climate ((Sv/yr)/(Bq/kg)). *Distribution:* Discrete. *Range:* 1.04×10^{-7} to 3.06×10^{-6}. *Mean:* 6.12×10^{-7}. *Standard Deviation:* 3.91×10^{-7}. *TSPA-LA Name:* DE_BDCF_Inh_LT_Pu239 (SNL 2008a, Sections 6.3.11.1 and 6.3.11.2; Equation 6.3.11-4).
ILTPU240. Volcanic Biosphere Dose Conversion Factor (BDCF) component for long-term inhalation of ^{240}Pu in modern interglacial climate ((Sv/yr)/(Bq/kg)). *Distribution:* Discrete. *Range:* 1.04×10^{-7} to 3.06×10^{-6}. *Mean:* 6.12×10^{-7}. *Standard Deviation:* 3.91×10^{-7}. *TSPA-LA Name:* DE_BDCF_Inh_LT_Pu240 (SNL 2008a, Sections 6.3.11.1 and 6.3.11.2; Equation 6.3.11-4).
ILTPU242. Volcanic Biosphere Dose Conversion Factor (BDCF) component for long-term inhalation of ^{242}Pu in modern interglacial climate ((Sv/yr)/(Bq/kg)). *Distribution:* Discrete. *Range:* 9.90×10^{-8} to 2.91×10^{-6}. *Mean:* 5.82×10^{-7}. *Standard Deviation:* 3.72×10^{-7}. *TSPA-LA Name:* DE_BDCF_Inh_LT_Pu242 (SNL 2008a, Sections 6.3.11.1 and 6.3.11.2; Equation 6.3.11-4).
ILTRA226. Volcanic Biosphere Dose Conversion Factor (BDCF) component for long-term inhalation of ^{226}Ra and ^{210}Pb in modern interglacial climate ((Sv/yr)/(Bq/kg)). *Distribution:* Discrete. *Range:* 1.71×10^{-8} to 5.03×10^{-7}. *Mean:* 1.01×10^{-7}. *Standard Deviation:* 6.43×10^{-8}. *TSPA-LA Name:* DE_BDCF_ILT_Ra226_Pb210 (SNL 2008a, Sections 6.3.11.1 and 6.3.11.2; Equation 6.3.11-4).
ILTRA228. Volcanic Biosphere Dose Conversion Factor (BDCF) component for long-term inhalation of ^{228}Ra in modern interglacial climate ((Sv/yr)/(Bq/kg)). *Distribution:* Discrete. *Range:* 1.40×10^{-8} to 4.12×10^{-7}. *Mean:* 8.24×10^{-8}. *Standard Deviation:* 5.27×10^{-8}. *TSPA-LA Name:* DE_BDCF_Inh_LT_Ra228 (SNL 2008a, Sections 6.3.11.1 and 6.3.11.2; Equation 6.3.11-4).
ILTSN126. Volcanic Biosphere Dose Conversion Factor (BDCF) component for long-term inhalation of ^{126}Sn in modern interglacial climate ((Sv/yr)/(Bq/kg)). *Distribution:* Discrete. *Range:* 1.36×10^{-10} to 4.00×10^{-9}. *Mean:* 8.0×10^{-10}. *Standard Deviation:* 5.11×10^{-10}. *TSPA-LA Name:* DE_BDCF_Inh_LT_Sn126 (SNL 2008a, Sections 6.3.11.1 and 6.3.11.2; Equation 6.3.11-4).
ILTSR90. Volcanic Biosphere Dose Conversion Factor (BDCF) component for long-term inhalation of ^{90}Sr in modern interglacial climate ((Sv/yr)/(Bq/kg)). *Distribution:* Discrete. *Range:* 1.39×10^{-10} to 4.08×10^{-9}. *Mean:* 8.16×10^{-10}. *Standard Deviation:* 5.21×10^{-10}. *TSPA-LA Name:* DE_BDCF_Inh_LT_Sr90 (SNL 2008a, Sections 6.3.11.1 and 6.3.11.2; Equation 6.3.11-4).
ILTTC99. Volcanic Biosphere Dose Conversion Factor (BDCF) component for long-term inhalation of ^{99}Tc in modern interglacial climate ((Sv/yr)/(Bq/kg)). *Distribution:* Discrete. *Range:* 1.17×10^{-11} to 3.42×10^{-10}. *Mean:* 6.84×10^{-11}. *Standard Deviation:* 4.37×10^{-11}. *TSPA-LA Name:* DE_BDCF_Inh_LT_Tc99 (SNL 2008a, Sections 6.3.11.1 and 6.3.11.2; Equation 6.3.11-4).
ILTTH229. Volcanic Biosphere Dose Conversion Factor (BDCF) component for long-term inhalation of ^{229}Th in modern interglacial climate ((Sv/yr)/(Bq/kg)). *Distribution:* Discrete. *Range:* 2.24×10^{-7} to 6.57×10^{-6}. *Mean:* 1.31×10^{-6}. *Standard Deviation:* 8.39×10^{-7}. *TSPA-LA Name:* DE_BDCF_Inh_LT_Th229 (SNL 2008a, Sections 6.3.11.1 and 6.3.11.2; Equation 6.3.11-4).
ILTTH230. Volcanic Biosphere Dose Conversion Factor (BDCF) component for long-term inhalation of ^{230}Th in modern interglacial climate ((Sv/yr)/(Bq/kg)). *Distribution:* Discrete. *Range:* 8.94×10^{-8} to 2.62×10^{-6}. *Mean:* 5.25×10^{-7}. *Standard Deviation:* 3.35×10^{-7}. *TSPA-LA Name:* DE_BDCF_Inh_LT_Th230 (SNL 2008a, Sections 6.3.11.1 and 6.3.11.2; Equation 6.3.11-4).
ILTTH232. Volcanic Biosphere Dose Conversion Factor (BDCF) component for long-term inhalation of ^{232}Th in modern interglacial climate ((Sv/yr)/(Bq/kg)). *Distribution:* Discrete. *Range:* 9.64×10^{-8} to 2.83×10^{-6}. *Mean:* 5.66×10^{-7}. *Standard Deviation:* 3.62×10^{-7}. *TSPA-LA Name:* DE_BDCF_Inh_LT_Th232 (SNL 2008a, Sections 6.3.11.1 and 6.3.11.2; Equation 6.3.11-4).

Table 2.4-11. Summary of Epistemically Uncertain Variables Considered in the TSPA (Continued)

ILTU233. Volcanic Biosphere Dose Conversion Factor (BDCF) component for long-term inhalation of ^{233}U in modern interglacial climate ((Sv/yr)/(Bq/kg)). *Distribution:* Discrete. *Range:* 8.40×10^{-9} to 2.47×10^{-7}. *Mean:* 4.94×10^{-8}. *Standard Deviation:* 3.15×10^{-8}. *TSPA-LA Name:* DE_BDCF_Inh_LT_U233 (SNL 2008a, Sections 6.3.11.1 and 6.3.11.2; Equation 6.3.11-4).
ILTU234. Volcanic Biosphere Dose Conversion Factor (BDCF) component for long-term inhalation of ^{234}U in modern interglacial climate ((Sv/yr)/(Bq/kg)). *Distribution:* Discrete. *Range:* 8.23×10^{-9} to 2.42×10^{-7}. *Mean:* 4.84×10^{-8}. *Standard Deviation:* 3.09×10^{-8}. *TSPA-LA Name:* DE_BDCF_Inh_LT_U234 (SNL 2008a, Sections 6.3.11.1 and 6.3.11.2; Equation 6.3.11-4).
ILTU238. Volcanic Biosphere Dose Conversion Factor (BDCF) component for long-term inhalation of ^{238}U in modern interglacial climate ((Sv/yr)/(Bq/kg)). *Distribution:* Discrete. *Range:* 7.05×10^{-9} to 2.07×10^{-7}. *Mean:* 4.14×10^{-8}. *Standard Deviation:* 2.65×10^{-8}. *TSPA-LA Name:* DE_BDCF_Inh_LT_U238 (SNL 2008a, Sections 6.3.11.1 and 6.3.11.2; Equation 6.3.11-4).
INFIL. Pointer variable for determining infiltration conditions: 10th, 30th, 50th or 90th percentile infiltration scenario (dimensionless). *Distribution:* Discrete. *Range:* 1 to 4. *TSPA-LA Name:* Infiltration_Scenario_a (SNL 2008a, Section 6.3.1.2; Tables 6.3.1-2 and 6.3.5-4).
INGAC227. Volcanic Biosphere Dose Conversion Factor (BDCF) component for radon, external exposure and ingestion of ^{227}Ac in modern interglacial climate ((Sv/yr)/(Bq/m^2)). *Distribution:* Discrete. *Range:* 5.78×10^{-9} to 7.76E-09. *Mean:* 6.16×10^{-9}. *Standard Deviation:* 1.8×10^{-10}. *TSPA-LA Name:* DE_BDCF_Ing_Exp_Radon_Ac227 (SNL 2008a, Sections 6.3.11.1 and 6.3.11.2; Equation 6.3.11-4).
INGAM241. Volcanic Biosphere Dose Conversion Factor (BDCF) component for radon, external exposure and ingestion of ^{241}Am in modern interglacial climate ((Sv/yr)/(Bq/m^2)). *Distribution:* Discrete. *Range:* 1.86×10^{-10} to 1.00E-09. *Mean:* 2.51×10^{-10}. *Standard Deviation:* 7.00×10^{-11}. *TSPA-LA Name:* DE_BDCF_Ing_Exp_Radon_Am241 (SNL 2008a, Sections 6.3.11.1 and 6.3.11.2; Equation 6.3.11-4).
INGAM243. Volcanic Biosphere Dose Conversion Factor (BDCF) component for radon, external exposure and ingestion of ^{243}Am in modern interglacial climate ((Sv/yr)/(Bq/m^2)). *Distribution:* Discrete. *Range:* 2.51×10^{-9} to 3.42×10^{-9}. *Mean:* 2.67×10^{-9}. *Standard Deviation:* 8.02×10^{-11}. *TSPA-LA Name:* DE_BDCF_Ing_Exp_Radon_Am243 (SNL 2008a, Sections 6.3.11.1 and 6.3.11.2; Equation 6.3.11-4).
INGCS137. Volcanic Biosphere Dose Conversion Factor (BDCF) component for radon, external exposure and ingestion of ^{137}Cs in modern interglacial climate ((Sv/yr)/(Bq/m^2)). *Distribution:* Discrete. *Range:* 6.75×10^{-9} to 8.48×10^{-9}. *Mean:* 7.17×10^{-9}. *Standard Deviation:* 1.55×10^{-10}. *TSPA-LA Name:* DE_BDCF_Ing_Exp_Radon_Cs137 (SNL 2008a, Sections 6.3.11.1 and 6.3.11.2; Equation 6.3.11-4).
INGI129. Volcanic Biosphere Dose Conversion Factor (BDCF) component for radon, external exposure and ingestion of ^{129}I in modern interglacial climate ((Sv/yr)/(Bq/m^2)). *Distribution:* Discrete. *Range:* 1.39×10^{-10} to 2.86×10^{-8}. *Mean:* 1.26×10^{-9}. *Standard Deviation:* 2.59×10^{-9}. *TSPA-LA Name:* DE_BDCF_Ing_Exp_Radon_I129 (SNL 2008a, Sections 6.3.11.1 and 6.3.11.2; Equation 6.3.11-4).
INGNP237. Volcanic Biosphere Dose Conversion Factor (BDCF) component for radon, external exposure and ingestion of ^{237}Np in modern interglacial climate ((Sv/yr)/(Bq/m^2)). *Distribution:* Discrete. *Range:* 2.62×10^{-9} to 1.2×10^{-8}. *Mean:* 2.98×10^{-9}. *Standard Deviation:* 6.36×10^{-10}. *TSPA-LA Name:* DE_BDCF_Ing_Exp_Radon_Np237 (SNL 2008a, Sections 6.3.11.1 and 6.3.11.2; Equation 6.3.11-4).
INGPA231. Volcanic Biosphere Dose Conversion Factor (BDCF) component for radon, external exposure and ingestion of ^{231}Pa in modern interglacial climate ((Sv/yr)/(Bq/m^2)). *Distribution:* Discrete. *Range:* 5.02×10^{-10} to 4.56×10^{-9}. *Mean:* 7.14×10^{-10}. *Standard Deviation:* 2.92×10^{-10}. *TSPA-LA Name:* DE_BDCF_Ing_Exp_Radon_Pa231 (SNL 2008a, Sections 6.3.11.1 and 6.3.11.2; Equation 6.3.11-4).
INGPU238. Volcanic Biosphere Dose Conversion Factor (BDCF) component for radon, external exposure and ingestion of ^{238}Pu in modern interglacial climate ((Sv/yr)/(Bq/m^2)). *Distribution:* Discrete. *Range:* 1.33×10^{-11} to 9.18×10^{-10}. *Mean:* 7.78×10^{-11}. *Standard Deviation:* 7.72×10^{-11}. *TSPA-LA Name:* DE_BDCF_Ing_Exp_Radon_Pu238 (SNL 2008a, Sections 6.3.11.1 and 6.3.11.2; Equation 6.3.11-4).

Table 2.4-11. Summary of Epistemically Uncertain Variables Considered in the TSPA (Continued)

INGPU239. Volcanic Biosphere Dose Conversion Factor (BDCF) component for radon, external exposure and ingestion of ^{239}Pu in modern interglacial climate ((Sv/yr)/(Bq/m^2)). *Distribution:* Discrete. *Range:* 1.40 × 10^{-11} to 1.01 × 10^{-9}. *Mean:* 8.49 × 10^{-11}. *Standard Deviation:* 8.5 × 10^{-11}. *TSPA-LA Name:* DE_BDCF_Ing_Exp_Radon_Pu239 (SNL 2008a, Sections 6.3.11.1 and 6.3.11.2; Equation 6.3.11-4).

INGPU240. Volcanic Biosphere Dose Conversion Factor (BDCF) component for radon, external exposure and ingestion of ^{240}Pu in modern interglacial climate ((Sv/yr)/(Bq/m^2)). *Distribution:* Discrete. *Range:* 1.42 × 10^{-11} to 1.01 × 10^{-9}. *Mean:* 8.52 × 10^{-11}. *Standard Deviation:* 8.5 × 10^{-11}. *TSPA-LA Name:* DE_BDCF_Ing_Exp_Radon_Pu240 (SNL 2008a, Sections 6.3.11.1 and 6.3.11.2; Equation 6.3.11-4).

INGPU242. Volcanic Biosphere Dose Conversion Factor (BDCF) component for radon, external exposure and ingestion of ^{242}Pu in modern interglacial climate ((Sv/yr)/(Bq/m^2)). *Distribution:* Discrete. *Range:* 1.31 × 10^{-11} to 9.57 × 10^{-10}. *Mean:* 8.04 × 10^{-11}. *Standard Deviation:* 8.06 × 10^{-11}. *TSPA-LA Name:* DE_BDCF_Ing_Exp_Radon_Pu242 (SNL 2008a, Sections 6.3.11.1 and 6.3.11.2; Equation 6.3.11-4).

INGRA226. Volcanic Biosphere Dose Conversion Factor (BDCF) component for radon, external exposure and ingestion of ^{226}Ra and ^{210}Pb in modern interglacial climate ((Sv/yr)/(Bq/m^2)). *Distribution:* Discrete. *Range:* 3.07 × 10^{-8} to 9.43 × 10^{-8}. *Mean:* 3.52 × 10^{-8}. *Standard Deviation:* 3.45 × 10^{-9}. *TSPA-LA Name:* DE_BDCF_IER_Ra226_Pb210 (SNL 2008a, Sections 6.3.11.1 and 6.3.11.2; Equation 6.3.11-4).

INGRA228. Volcanic Biosphere Dose Conversion Factor (BDCF) component for radon, external exposure and ingestion of ^{228}Ra in modern interglacial climate ((Sv/yr)/(Bq/m^2)). *Distribution:* Discrete. *Range:* 1.17 × 10^{-8} to 2.62 × 10^{-8}. *Mean:* 1.27 × 10^{-8}. *Standard Deviation:* 7.44 × 10^{-10}. *TSPA-LA Name:* DE_BDCF_Ing_Exp_Radon_Ra228 (SNL 2008a, Sections 6.3.11.1 and 6.3.11.2; Equation 6.3.11-4).

INGSN126. Volcanic Biosphere Dose Conversion Factor (BDCF) component for radon, external exposure and ingestion of ^{126}Sn in modern interglacial climate ((Sv/yr)/(Bq/m^2)). *Distribution:* Discrete. *Range:* 2.38 × 10^{-8} to 2.79 × 10^{-8}. *Mean:* 2.54 × 10^{-8}. *Standard Deviation:* 4.41 × 10^{-10}. *TSPA-LA Name:* DE_BDCF_Ing_Exp_Radon_Sn126 (SNL 2008a, Sections 6.3.11.1 and 6.3.11.2; Equation 6.3.11-4).

INGSR90. Volcanic Biosphere Dose Conversion Factor (BDCF) component for radon, external exposure and ingestion of ^{90}Sr in modern interglacial climate ((Sv/yr)/(Bq/m^2)). *Distribution:* Discrete. *Range:* 1.44 × 10^{-9} to 6.10 × 10^{-9}. *Mean:* 1.81 × 10^{-9}. *Standard Deviation:* 3.67 × 10^{-10}. *TSPA-LA Name:* DE_BDCF_Ing_Exp_Radon_Sr90 (SNL 2008a, Sections 6.3.11.1 and 6.3.11.2; Equation 6.3.11-4).

INGTC99. Volcanic Biosphere Dose Conversion Factor (BDCF) component for radon, external exposure and ingestion of ^{99}Tc in modern interglacial climate ((Sv/yr)/(Bq/m^2)). *Distribution:* Discrete. *Range:* 5.08 × 10^{-12} to 8.95 × 10^{-9}. *Mean:* 2.72 × 10^{-10}. *Standard Deviation:* 5.16 × 10^{-10}. *TSPA-LA Name:* DE_BDCF_Ing_Exp_Radon_Tc99 (SNL 2008a, Sections 6.3.11.1 and 6.3.11.2; Equation 6.3.11-4).

INGTH229. Volcanic Biosphere Dose Conversion Factor (BDCF) component for radon, external exposure and ingestion of ^{229}Th in modern interglacial climate ((Sv/yr)/(Bq/m^2)). *Distribution:* Discrete. *Range:* 4.33 × 10^{-9} to 7.02 × 10^{-9}. *Mean:* 4.69 × 10^{-9}. *Standard Deviation:* 2.4 × 10^{-10}. *TSPA-LA Name:* DE_BDCF_Ing_Exp_Radon_Th229 (SNL 2008a, Sections 6.3.11.1 and 6.3.11.2; Equation 6.3.11-4).

INGTH230. Volcanic Biosphere Dose Conversion Factor (BDCF) component for radon, external exposure and ingestion of ^{230}Th in modern interglacial climate ((Sv/yr)/(Bq/m^2)). *Distribution:* Discrete. *Range:* 1.92 × 10^{-11} to 8.68 × 10^{-10}. *Mean:* 8.51 × 10^{-11}. *Standard Deviation:* 7.82 × 10^{-11}. *TSPA-LA Name:* DE_BDCF_Ing_Exp_Radon_Th230 (SNL 2008a, Sections 6.3.11.1 and 6.3.11.2; Equation 6.3.11-4).

INGTH232. Volcanic Biosphere Dose Conversion Factor (BDCF) component for radon, external exposure and ingestion of ^{232}Th in modern interglacial climate ((Sv/yr)/(Bq/m^2)). *Distribution:* Discrete. *Range:* 1.72 × 10^{-11} to 9.34 × 10^{-10}. *Mean:* 8.83 × 10^{-11}. *Standard Deviation:* 8.44 × 10^{-11}. *TSPA-LA Name:* DE_BDCF_Ing_Exp_Radon_Th232 (SNL 2008a, Sections 6.3.11.1 and 6.3.11.2; Equation 6.3.11-4).

INGU233. Volcanic Biosphere Dose Conversion Factor (BDCF) component for radon, external exposure and ingestion of ^{233}U in modern interglacial climate ((Sv/yr)/(Bq/m^2)). *Distribution:* Discrete. *Range:* 1.31 × 10^{-11} to 9.04 × 10^{-10}. *Mean:* 6.48 × 10^{-11}. *Standard Deviation:* 6.12 × 10^{-11}. *TSPA-LA Name:* DE_BDCF_Ing_Exp_Radon_U233 (SNL 2008a, Sections 6.3.11.1 and 6.3.11.2; Equation 6.3.11-4).

Table 2.4-11. Summary of Epistemically Uncertain Variables Considered in the TSPA (Continued)

INGU234. Volcanic Biosphere Dose Conversion Factor (BDCF) component for radon, external exposure and ingestion of ^{234}U in modern interglacial climate ((Sv/yr)/(Bq/m^2)). *Distribution:* Discrete. *Range:* 9.60×10^{-12} to 8.7×10^{-10}. *Mean:* 5.96×10^{-11}. *Standard Deviation:* 5.9×10^{-11}. *TSPA-LA Name:* DE_BDCF_Ing_Exp_Radon_U234 (SNL 2008a, Sections 6.3.11.1 and 6.3.11.2; Equation 6.3.11-4).
INGU238. Volcanic Biosphere Dose Conversion Factor (BDCF) component for radon, external exposure and ingestion of ^{238}U in modern interglacial climate ((Sv/yr)/(Bq/m^2)). *Distribution:* Discrete. *Range:* 1.52×10^{-9} to 2.41×10^{-9}. *Mean:* 1.62×10^{-9}. *Standard Deviation:* 6.16×10^{-11}. *TSPA-LA Name:* DE_BDCF_Ing_Exp_Radon_U238 (SNL 2008a, Sections 6.3.11.1 and 6.3.11.2; Equation 6.3.11-4).
INHLTPV. Pointer variable for long-term inhalation dose conversion factor for volcanic ash exposure (dimensionless). *Distribution:* Discrete. *Range:* 1 to 300. *TSPA-LA Name:* BDCF_Inh_LT (SNL 2008a, Section 6.3.11; Equation 6.3.11-4).
INHSTPV. Pointer variable for short-term inhalation dose conversion factor for volcanic ash exposure (dimensionless). *Distribution:* Discrete. *Range:* 1 to 300. *TSPA-LA Name:* BDCF_Inh_ShT (SNL 2008a, Section 6.3.11; Equation 6.3.11-4).
INRFRCCS. The initial release fraction of ^{137}Cs in a commercial SNF waste package (dimensionless). *Distribution:* Triangular. *Range:* 0.0039 to 0.1106. *Mode:* 0.0363. *TSPA-LA Name:* Initial_Release_Frac_Cs_a (SNL 2008a, Sections 6.3.7.4.1.2 and 6.3.7.4.1.3; Table 6.3.7-29).
INRFRCI. The initial release fraction of ^{129}I in a commercial SNF waste package (dimensionless). *Distribution:* Triangular. *Range:* 0.0204 to 0.2675. *Mode:* 0.1124. *TSPA-LA Name:* Initial_Release_Frac_I_a (SNL 2008a, Sections 6.3.7.4.1.2 and 6.3.7.4.1.3; Table 6.3.7-29).
INRFRCSR. The initial release fraction of ^{90}Sr in a commercial SNF waste package (dimensionless). *Distribution:* Triangular. *Range:* 0.0002 to 0.0025. *Mode:* 0.0009. *TSPA-LA Name:* Initial_Release_Frac_Sr_a (SNL 2008a, Sections 6.3.7.4.1.2 and 6.3.7.4.1.3; Table 6.3.7-29).
INRFRCTC. The initial release fraction of ^{99}Tc in a commercial SNF waste package (dimensionless). *Distribution:* Triangular. *Range:* 0.0001 to 0.0026. *Mode:* 0.001. *TSPA-LA Name:* Initial_Release_Frac_Tc_a (SNL 2008a, Sections 6.3.7.4.1.2 and 6.3.7.4.1.3; Table 6.3.7-29).
IS2DHLNS. Pointer variable used to determine ionic strength for 2DHLW Cell (Cell 1a) of CDSP waste packages under vapor influx conditions (dimensionless). *Distribution:* Uniform. *Range:* 0 to 1. *TSPA-LA Name:* Inpkg_IStr_2DHLW_NS_Rand_a (SNL 2008a, Section 6.3.7.2.2 Part III).
IS2DHLS. Pointer variable used to determine ionic strength for 2DHLW Cell (Cell 1a) of CDSP waste packages under liquid influx conditions (dimensionless). *Distribution:* Uniform. *Range:* 0 to 1. *TSPA-LA Name:* Inpkg_IStr_2DHLW_S_Rand_a (SNL 2008a, Section 6.3.7.2.2 Part III).
IS2MCONS. Pointer variable used to determine ionic strength for 2MCO Cell (Cell 1b) of CDSP waste packages under vapor influx conditions (dimensionless). *Distribution:* Uniform. *Range:* 0 to 1. *TSPA-LA Name:* Inpkg_IStr_2MCO_NS_Rand_a (SNL 2008a, Section 6.3.7.2.2 Part III).
IS2MCOS. Pointer variable used to determine ionic strength for 2MCO Cell (Cell 1b) of CDSP waste packages under liquid influx conditions (dimensionless). *Distribution:* Uniform. *Range:* 0 to 1. *TSPA-LA Name:* Inpkg_IStr_2MCO_S_Rand_a (SNL 2008a, Section 6.3.7.2.2 Part III).
ISCSNS. Pointer variable used to determine ionic strength for commercial SNF Cell under vapor influx conditions (dimensionless). *Distribution:* Uniform. *Range:* 0 to 1. *TSPA-LA Name:* Inpkg_IStr_CSNF_NS_Rand_a (SNL 2008a, Section 6.3.7.2.2 Part III).
ISCSS. Pointer variable used to determine ionic strength for commercial SNF Cell under liquid influx conditions (dimensionless). *Distribution:* Uniform. *Range:* 0 to 1. *TSPA-LA Name:* Inpkg_IStr_CSNF_S_Rand_a (SNL 2008a, Section 6.3.7.2.2 Part III).

Table 2.4-11. Summary of Epistemically Uncertain Variables Considered in the TSPA (Continued)

ISTAC227. Volcanic Biosphere Dose Conversion Factor (BDCF) component for short-term inhalation of ^{227}Ac in modern interglacial climate ((Sv/yr)/(Bq/kg)). *Distribution:* Discrete. *Range:* 8.47×10^{-8} to 2.14×10^{-6}. *Mean:* 5.85×10^{-7}. *Standard Deviation:* 3.32×10^{-7}. *TSPA-LA Name:* DE_BDCF_Inh_ShT_Ac227 (SNL 2008a, Sections 6.3.11.1 and 6.3.11.2; Equation 6.3.11-4).
ISTAM241. Volcanic Biosphere Dose Conversion Factor (BDCF) component for short-term inhalation of ^{241}Am in modern interglacial climate ((Sv/yr)/(Bq/kg)). *Distribution:* Discrete. *Range:* 4.67×10^{-8} to 1.18×10^{-6}. *Mean:* 3.23×10^{-7}. *Standard Deviation:* 1.83×10^{-7}. *TSPA-LA Name:* DE_BDCF_Inh_ShT_Am241 (SNL 2008a, Sections 6.3.11.1 and 6.3.11.2; Equation 6.3.11-4).
ISTAM243. Volcanic Biosphere Dose Conversion Factor (BDCF) component for short-term inhalation of ^{243}Am in modern interglacial climate ((Sv/yr)/(Bq/kg)). *Distribution:* Discrete. *Range:* 4.64×10^{-8} to 1.17×10^{-6}. *Mean:* 3.2×10^{-7}. *Standard Deviation:* 1.82×10^{-7}. *TSPA-LA Name:* DE_BDCF_Inh_ShT_Am243 (SNL 2008a, Sections 6.3.11.1 and 6.3.11.2; Equation 6.3.11-4).
ISTCS137. Volcanic Biosphere Dose Conversion Factor (BDCF) component for short-term inhalation of ^{137}Cs in modern interglacial climate ((Sv/yr)/(Bq/kg)). *Distribution:* Discrete. *Range:* 1.90×10^{-11} to 4.80×10^{-10}. *Mean:* 1.31×10^{-10}. *Standard Deviation:* 7.44×10^{-11}. *TSPA-LA Name:* DE_BDCF_Inh_ShT_Cs137 (SNL 2008a, Sections 6.3.11.1 and 6.3.11.2; Equation 6.3.11-4).
ISTI129. Volcanic Biosphere Dose Conversion Factor (BDCF) component for short-term inhalation of ^{129}I in modern interglacial climate ((Sv/yr)/(Bq/kg)). *Distribution:* Discrete. *Range:* 1.74×10^{-11} to 4.40×10^{-10}. *Mean:* 1.2×10^{-10}. *Standard Deviation:* 6.81×10^{-11}. *TSPA-LA Name:* DE_BDCF_Inh_ShT_I129 (SNL 2008a, Sections 6.3.11.1 and 6.3.11.2; Equation 6.3.11-4).
ISTNP237. Volcanic Biosphere Dose Conversion Factor (BDCF) component for short-term inhalation of ^{237}Np in modern interglacial climate ((Sv/yr)/(Bq/kg)). *Distribution:* Discrete. *Range:* 2.41×10^{-8} to 6.08×10^{-7}. *Mean:* 1.66×10^{-7}. *Standard Deviation:* 9.43×10^{-8}. *TSPA-LA Name:* DE_BDCF_Inh_ShT_Np237 (SNL 2008a, Sections 6.3.11.1 and 6.3.11.2; Equation 6.3.11-4).
ISTPA231. Volcanic Biosphere Dose Conversion Factor (BDCF) component for short-term inhalation of ^{231}Pa in modern interglacial climate ((Sv/yr)/(Bq/kg)). *Distribution:* Discrete. *Range:* 1.11×10^{-7} to 2.82×10^{-6}. *Mean:* 7.7×10^{-7}. *Standard Deviation:* 4.37×10^{-7}. *TSPA-LA Name:* DE_BDCF_Inh_ShT_Pa231 (SNL 2008a, Sections 6.3.11.1 and 6.3.11.2; Equation 6.3.11-4).
ISTPU238. Volcanic Biosphere Dose Conversion Factor (BDCF) component for short-term inhalation of ^{238}Pu in modern interglacial climate ((Sv/yr)/(Bq/kg)). *Distribution:* Discrete. *Range:* 5.23×10^{-8} to 1.32×10^{-6}. *Mean:* 3.61×10^{-7}. *Standard Deviation:* 2.05×10^{-7}. *TSPA-LA Name:* DE_BDCF_Inh_ShT_Pu238 (SNL 2008a, Sections 6.3.11.1 and 6.3.11.2; Equation 6.3.11-4).
ISTPU239. Volcanic Biosphere Dose Conversion Factor (BDCF) component for short-term inhalation of ^{239}Pu in modern interglacial climate ((Sv/yr)/(Bq/kg)). *Distribution:* Discrete. *Range:* 5.76×10^{-8} to 1.46×10^{-6}. *Mean:* 3.98×10^{-7}. *Standard Deviation:* 2.26×10^{-7}. *TSPA-LA Name:* DE_BDCF_Inh_ShT_Pu239 (SNL 2008a, Sections 6.3.11.1 and 6.3.11.2; Equation 6.3.11-4).
ISTPU240. Volcanic Biosphere Dose Conversion Factor (BDCF) component for short-term inhalation of ^{240}Pu in modern interglacial climate ((Sv/yr)/(Bq/kg)). *Distribution:* Discrete. *Range:* 5.76×10^{-8} to 1.46×10^{-6}. *Mean:* 3.98×10^{-7}. *Standard Deviation:* 2.26×10^{-7}. *TSPA-LA Name:* DE_BDCF_Inh_ShT_Pu240 (SNL 2008a, Sections 6.3.11.1 and 6.3.11.2; Equation 6.3.11-4).
ISTPU242. Volcanic Biosphere Dose Conversion Factor (BDCF) component for short-term inhalation of ^{242}Pu in modern interglacial climate ((Sv/yr)/(Bq/kg)). *Distribution:* Discrete. *Range:* 5.47×10^{-8} to 1.38×10^{-6}. *Mean:* 3.78×10^{-7}. *Standard Deviation:* 2.14×10^{-7}. *TSPA-LA Name:* DE_BDCF_Inh_ShT_Pu242 (SNL 2008a, Sections 6.3.11.1 and 6.3.11.2; Equation 6.3.11-4).
ISTRA226. Volcanic Biosphere Dose Conversion Factor (BDCF) component for short-term inhalation of ^{226}Ra and ^{210}Pb in modern interglacial climate ((Sv/yr)/(Bq/kg)). *Distribution:* Discrete. *Range:* 9.47×10^{-9} to 2.39×10^{-7}. *Mean:* 6.54×10^{-8}. *Standard Deviation:* 3.71×10^{-8}. *TSPA-LA Name:* DE_BDCF_IST_Ra226_Pb210 (SNL 2008a, Sections 6.3.11.1 and 6.3.11.2; Equation 6.3.11-4).

Table 2.4-11. Summary of Epistemically Uncertain Variables Considered in the TSPA (Continued)

ISTRA228. Volcanic Biosphere Dose Conversion Factor (BDCF) component for short-term inhalation of ^{228}Ra in modern interglacial climate ((Sv/yr)/(Bq/kg)). *Distribution:* Discrete. *Range:* 7.76×10^{-9} to 1.96×10^{-7}. *Mean:* 5.36×10^{-8}. *Standard Deviation:* 3.04×10^{-8}. *TSPA-LA Name:* DE_BDCF_Inh_ShT_Ra228 (SNL 2008a, Sections 6.3.11.1 and 6.3.11.2; Equation 6.3.11-4).
ISTSN126. Volcanic Biosphere Dose Conversion Factor (BDCF) component for short-term inhalation of ^{126}Sn in modern interglacial climate ((Sv/yr)/(Bq/kg)). *Distribution:* Discrete. *Range:* 7.53×10^{-11} to 1.90×10^{-9}. *Mean:* 5.2×10^{-10}. *Standard Deviation:* 2.95×10^{-10}. *TSPA-LA Name:* DE_BDCF_Inh_ShT_Sn126 (SNL 2008a, Sections 6.3.11.1 and 6.3.11.2; Equation 6.3.11-4.
ISTSR90. Volcanic Biosphere Dose Conversion Factor (BDCF) component for short-term inhalation of ^{90}Sr in modern interglacial climate ((Sv/yr)/(Bq/kg)). *Distribution:* Discrete. *Range:* 7.68×10^{-11} to 1.94×10^{-9}. *Mean:* 5.3×10^{-10}. *Standard Deviation:* 3.01×10^{-10}. *TSPA-LA Name:* DE_BDCF_Inh_ShT_Sr90 (SNL 2008a, Sections 6.3.11.1 and 6.3.11.2; Equation 6.3.11-4).
ISTTC99. Volcanic Biosphere Dose Conversion Factor (BDCF) component for short-term inhalation of ^{99}Tc in modern interglacial climate ((Sv/yr)/(Bq/kg)). *Distribution:* Discrete. *Range:* 6.44×10^{-12} to 1.63×10^{-10}. *Mean:* 4.45×10^{-11}. *Standard Deviation:* 2.52×10^{-11}. *TSPA-LA Name:* DE_BDCF_Inh_ShT_Tc99 (SNL 2008a, Sections 6.3.11.1 and 6.3.11.2; Equation 6.3.11-4).
ISTTH229. Volcanic Biosphere Dose Conversion Factor (BDCF) component for short-term inhalation of ^{229}Th in modern interglacial climate ((Sv/yr)/(Bq/kg)). *Distribution:* Discrete. *Range:* 1.24×10^{-7} to 3.13×10^{-6}. *Mean:* 8.54×10^{-7}. *Standard Deviation:* 4.84×10^{-7}. *TSPA-LA Name:* DE_BDCF_Inh_ShT_Th229 (SNL 2008a, Sections 6.3.11.1 and 6.3.11.2; Equation 6.3.11-4).
ISTTH230. Volcanic Biosphere Dose Conversion Factor (BDCF) component for short-term inhalation of ^{230}Th in modern interglacial climate ((Sv/yr)/(Bq/kg)). *Distribution:* Discrete. *Range:* 4.94×10^{-8} to 1.25×10^{-6}. *Mean:* 3.41×10^{-7}. *Standard Deviation:* 1.94×10^{-7}. *TSPA-LA Name:* DE_BDCF_Inh_ShT_Th230 (SNL 2008a, Sections 6.3.11.1 and 6.3.11.2; Equation 6.3.11-4.
ISTTH232. Volcanic Biosphere Dose Conversion Factor (BDCF) component for short-term inhalation of ^{232}Th in modern interglacial climate ((Sv/yr)/(Bq/kg)). *Distribution:* Discrete. *Range:* 5.33×10^{-8} to 1.35×10^{-6}. *Mean:* 3.68×10^{-7}. *Standard Deviation:* 2.09×10^{-7}. *TSPA-LA Name:* DE_BDCF_Inh_ShT_Th232 (SNL 2008a, Sections 6.3.11.1 and 6.3.11.2; Equation 6.3.11-4).
ISTU233. Volcanic Biosphere Dose Conversion Factor (BDCF) component for short-term inhalation of ^{233}U in modern interglacial climate ((Sv/yr)/(Bq/kg)). *Distribution:* Discrete. *Range:* 4.65×10^{-9} to 1.17×10^{-7}. *Mean:* 3.21×10^{-8}. *Standard Deviation:* 1.82×10^{-8}. *TSPA-LA Name:* DE_BDCF_Inh_ShT_U233. (SNL 2008a, Sections 6.3.11.1 and 6.3.11.2; Equation 6.3.11-4).
ISTU234. Volcanic Biosphere Dose Conversion Factor (BDCF) component for short-term inhalation of ^{234}U in modern interglacial climate ((Sv/yr)/(Bq/kg)). *Distribution:* Discrete. *Range:* 4.55×10^{-9} to 1.15×10^{-7}. *Mean:* 3.15×10^{-8}. *Standard Deviation:* 1.78×10^{-8}. *TSPA-LA Name:* DE_BDCF_Inh_ShT_U234 (SNL 2008a, Sections 6.3.11.1 and 6.3.11.2; Equation 6.3.11-4).
ISTU238. Volcanic Biosphere Dose Conversion Factor (BDCF) component for short-term inhalation of ^{238}U in modern interglacial climate ((Sv/yr)/(Bq/kg)). *Distribution:* Discrete. *Range:* 3.90×10^{-9} to 9.85×10^{-8}. *Mean:* 2.69×10^{-8}. *Standard Deviation:* 1.53×10^{-8}. *TSPA-LA Name:* DE_BDCF_Inh_ShT_U238 (SNL 2008a, Sections 6.3.11.1 and 6.3.11.2; Equation 6.3.11-4).
KDAMCOL. Distribution coefficient for reversible sorption of americium onto uranophane colloids (mL/g). *Distribution:* Log uniform. *Range:* 5 to 1.00×10^{4}. *TSPA-LA Name:* Kd_Am_Rev_U_Col_a (SNL 2008a, Sections 6.3.7.6.2 and 6.3.7.6.3; Equation 6.3.7-20; Table 6.3.7-64).
KDAMSMEC. Distribution coefficient for reversible sorption of americium to waste form (smectite) colloids (mL/g). *Distribution:* Piecewise uniform. *Range:* 1.00×10^{4} to 1.00×10^{7}. *TSPA-LA Name:* Kd_Am_Rev_Smectite_a (SNL 2008a, Sections 6.3.7.6.2 and 6.3.7.6.3; Equation 6.3.7-20; Tables 6.3.7-62 and 6.3.7-66).

Table 2.4-11. Summary of Epistemically Uncertain Variables Considered in the TSPA (Continued)

KDCSCOL. Distribution coefficient for reversible sorption of cesium onto uranophane colloids (mL/g). *Distribution:* Log uniform. *Range:* 10 to 1000. *TSPA-LA Name:* Kd_Cs_Rev_U_Col_a (SNL 2008a, Sections 6.3.7.6.2 and 6.3.7.6.3; Equation 6.3.7-20; Table 6.3.7-64).
KDCSSMEC. Distribution coefficient for reversible sorption of cesium to waste form (smectite) colloids (mL/g). *Distribution:* Piecewise uniform. *Range:* 50 to 5000. *TSPA-LA Name:* Kd_Cs_Rev_Smectite_a (SNL 2008a, Sections 6.3.7.6.2 and 6.3.7.6.3; Equation 6.3.7-20; Tables 6.3.7-62 and 6.3.7-66).
KDNPCOL. Distribution coefficient for reversible sorption of neptunium onto uranophane colloids (mL/g). *Distribution:* Log uniform. *Range:* 10 to 500 for v5.005 of the TSPA model. *TSPA-LA Name:* Kd_Np_Rev_U_Col_a (SNL 2008a, Sections 6.3.7.6.2 and 6.3.7.6.3; Equation 6.3.7-20; Table 6.3.7-64; Table P-6[a]).
KDNPSMEC. Distribution coefficient for reversible sorption of neptunium to waste form (smectite) colloids (mL/g). *Distribution:* Log uniform. *Range:* 10 to 500. *TSPA-LA Name:* Kd_Np_Rev_Smectite_a (SNL 2008a, Sections 6.3.7.6.2 and 6.3.7.6.3; Equation 6.3.7-20; Tables 6.3.7-62 and 6.3.7-66).
KDPACOL. Distribution coefficient for reversible sorption of protactinium onto uranophane colloids (mL/g). *Distribution:* Log uniform. *Range:* 5 to 1.00×10^4. *TSPA-LA Name:* Kd_Pa_Rev_U_Col_a (SNL 2008a, Sections 6.3.7.6.2 and 6.3.7.6.3; Equation 6.3.7-20; Table 6.3.7-64).
KDPASMEC. Distribution coefficient for reversible sorption of protactinium to waste form (smectite) colloids (mL/g). *Distribution:* Piecewise uniform. *Range:* 1.00×10^4 to 1.00×10^7. *TSPA-LA Name:* Kd_Pa_Rev_Smectite_a (SNL 2008a, Sections 6.3.7.6.2 and 6.3.7.6.3; Equation 6.3.7-20; Tables 6.3.7-62 and 6.3.7-66).
KDPUCOL. Distribution coefficient for reversible sorption of plutonium onto uranophane colloids (mL/g). *Distribution:* Log uniform. *Range:* 5 to 1.00×10^4. *TSPA-LA Name:* Kd_Pu_Rev_U_Col_a (SNL 2008a, Sections 6.3.7.6.2 and 6.3.7.6.3; Equation 6.3.7-20; Table 6.3.7-64).
KDPUSMEC. Distribution coefficient for reversible sorption of plutonium to waste form (smectite) colloids (mL/g). *Distribution:* Piecewise uniform. *Range:* 1.00×10^3 to 1.00×10^5. *TSPA-LA Name:* Kd_Pu_Rev_Smectite_a (SNL 2008a, Sections 6.3.7.6.2 and 6.3.7.6.3; Equation 6.3.7-20; Tables 6.3.7-62 and 6.3.7-66).
KDRACOL. Distribution coefficient for reversible sorption of radium onto uranophane colloids (mL/g). *Distribution:* Log uniform. *Range:* 10 to 1000. *TSPA-LA Name:* Kd_Ra_Rev_U_Col_a (SNL 2008a, Sections 6.3.7.6.2 and 6.3.7.6.3; Equation 6.3.7-20; Table 6.3.7-64).
KDRASMEC. Distribution coefficient for reversible sorption of radium to waste form (smectite) colloids (mL/g). *Distribution:* Log uniform. *Range:* 100 to 5000. *TSPA-LA Name:* Kd_Ra_Rev_Smectite_a (SNL 2008a, Sections 6.3.7.6.2 and 6.3.7.6.3; Equation 6.3.7-20; Tables 6.3.7-62 and 6.3.7-66).
KDSNCOL. Distribution coefficient for reversible sorption of tin onto uranophane colloids (mL/g). *Distribution:* Log uniform. *Range:* 1 to 100. *TSPA-LA Name:* Kd_Sn_Rev_U_Col_a (SNL 2008a, Sections 6.3.7.6.2 and 6.3.7.6.3; Equation 6.3.7-20; Table 6.3.7-64).
KDSNSMEC. Distribution coefficient for reversible sorption of tin to waste form (smectite) colloids (mL/g). *Distribution:* Log uniform. *Range:* 1.00×10^5 to 1.00×10^6. *TSPA-LA Name:* Kd_Sn_Rev_Smectite_a (SNL 2008a, Sections 6.3.7.6.2 and 6.3.7.6.3; Equation 6.3.7-20; Tables 6.3.7-62 and 6.3.7-66).
KDTHCOL. Distribution coefficient for reversible sorption of thorium onto uranophane colloids (mL/g). *Distribution:* Log uniform. *Range:* 5 to 1.00×10^4. *TSPA-LA Name:* Kd_Th_Rev_U_Col_a (SNL 2008a, Sections 6.3.7.6.2 and 6.3.7.6.3; Equation 6.3.7-20; Table 6.3.7-64)
KDTHSMEC. Distribution coefficient for reversible sorption of thorium to waste form (smectite) colloids (mL/g). *Distribution:* Piecewise uniform. *Range:* 1.00×10^4 to 1.00×10^7. *TSPA-LA Name:* Kd_Th_Rev_Smectite_a (SNL 2008a, Sections 6.3.7.6.2 and 6.3.7.6.3; Equation 6.3.7-20; Tables 6.3.7-62 and 6.3.7-66).
KDUSMEC. Distribution coefficient for reversible sorption of uranium to waste form (smectite) colloids (mL/g). *Distribution:* Log uniform. *Range:* 5.00×10^2 to 5.00×10^4. *TSPA-LA Name:* Kd_U_Rev_Smectite_a (SNL 2008a, Sections 6.3.7.6.2 and 6.3.7.6.3; Equation 6.3.7-20; Tables 6.3.7-62 and 6.3.7-66).

Table 2.4-11. Summary of Epistemically Uncertain Variables Considered in the TSPA (Continued)

LDIVIDE. Depth of permeable soil on divides of the Fortymile Wash fan (RMEI location) (cm). *Distribution:* Uniform. *Range:* 102 to 140. *TSPA-LA Name:* L_Divides_a (SNL 2008a, Table 6.5-5).
MASSDCRS. Mass loading decrease rate constant (1/yr). *Distribution:* Triangular. *Range:* 0.125 to 1. *Mode:* 0.2. *TSPA-LA Name:* Mass_Decrease_Const_GE10_a (SNL 2008a, Equation 6.3.11-5).
MICAC227. Groundwater Biosphere Dose Conversion Factor (BDCF) for ^{227}Ac in modern interglacial climate ((Sv/year)/(Bq/m^3)). *Distribution:* Discrete. *Range:* 4.08×10^{-7} to 4.32×10^{-6}. *Mean:* 1.3×10^{-6}. *Standard Deviation:* 5.28×10^{-7}. *TSPA-LA Name:* GW_BDCF_MIC_Ac227 (SNL 2008a, Sections 6.3.11.2 and 6.3.11.3; Table 6.3.11-3).
MICAM241. Groundwater Biosphere Dose Conversion Factor (BDCF) for ^{241}Am in modern interglacial climate ((Sv/year)/(Bq/m^3)). *Distribution:* Discrete. *Range:* 2.16×10^{-7} to 3.30×10^{-6}. *Mean:* 8.34×10^{-7}. *Standard Deviation:* 4.03×10^{-7}. *TSPA-LA Name:* GW_BDCF_MIC_Am241 (SNL 2008a, Sections 6.3.11.2 and 6.3.11.3; Table 6.3.11-3).
MICAM243. Groundwater Biosphere Dose Conversion Factor (BDCF) for ^{243}Am in modern interglacial climate ((Sv/year)/(Bq/m^3)). *Distribution:* Discrete. *Range:* 2.21×10^{-7} to 3.37×10^{-6}. *Mean:* 8.88×10^{-7}. *Standard Deviation:* 4.12×10^{-7}. *TSPA-LA Name:* GW_BDCF_MIC_Am243 (SNL 2008a, Sections 6.3.11.2 and 6.3.11.3; Table 6.3.11-3).
MICC14. Groundwater Biosphere Dose Conversion Factor (BDCF) for ^{14}C in modern interglacial climate ((Sv/year)/(Bq/m^3)). *Distribution:* Discrete. *Range:* 7.18×10^{-10} to 2.56×10^{-8}. *Mean:* 1.93×10^{-9}. *Standard Deviation:* 1.85×10^{-9}. *TSPA-LA Name:* GW_BDCF_MIC_C14 (SNL 2008a, Sections 6.3.11.2 and 6.3.11.3; Table 6.3.11-3).
MICCl36. Groundwater Biosphere Dose Conversion Factor (BDCF) for ^{36}Cl in modern interglacial climate ((Sv/year)/(Bq/m^3)). *Distribution:* Discrete. *Range:* 1.28×10^{-9} to 3.00×10^{-7}. *Mean:* 8.09×10^{-9}. *Standard Deviation:* 1.41×10^{-8}. *TSPA-LA Name:* GW_BDCF_MIC_Cl36 (SNL 2008a, Sections 6.3.11.2 and 6.3.11.3; Table 6.3.11-3).
MICCS135. Groundwater Biosphere Dose Conversion Factor (BDCF) for ^{135}Cs in modern interglacial climate ((Sv/year)/(Bq/m^3)). *Distribution:* Discrete. *Range:* 3.1×10^{-9} to 8.48×10^{-8}. *Mean:* 1.45×10^{-8}. *Standard Deviation:* 1.02×10^{-8}. *TSPA-LA Name:* GW_BDCF_MIC_Cs135 (SNL 2008a, Sections 6.3.11.2 and 6.3.11.3; Table 6.3.11-3).
MICCS137. Groundwater Biosphere Dose Conversion Factor (BDCF) for ^{137}Cs in modern interglacial climate ((Sv/year)/(Bq/m^3)). *Distribution:* Discrete. *Range:* 3.87×10^{-8} to 4.56×10^{-7}. *Mean:* 1.30×10^{-7}. *Standard Deviation:* 6.33×10^{-8}. *TSPA-LA Name:* GW_BDCF_MIC_Cs137 (SNL 2008a, Sections 6.3.11.2 and 6.3.11.3; Table 6.3.11-3).
MICI129. Groundwater Biosphere Dose Conversion Factor (BDCF) for ^{129}I in modern interglacial climate ((Sv/year)/(Bq/m^3)). *Distribution:* Discrete. *Range:* 8.59×10^{-8} to 1.13×10^{-6}. *Mean:* 1.29×10^{-7}. *Standard Deviation:* 5.28×10^{-8}. *TSPA-LA Name:* GW_BDCF_MIC_I129 (SNL 2008a, Sections 6.3.11.2 and 6.3.11.3; Table 6.3.11-3).
MICNP237. Groundwater Biosphere Dose Conversion Factor (BDCF) for ^{237}Np in modern interglacial climate ((Sv/year)/(Bq/m^3)). *Distribution:* Discrete. *Range:* 1.06×10^{-7} to 8.05×10^{-7}. *Mean:* 2.74×10^{-7}. *Standard Deviation:* 9.70×10^{-8}. *TSPA-LA Name:* GW_BDCF_MIC_Np237 (SNL 2008a, Sections 6.3.11.2 and 6.3.11.3; Table 6.3.11-3).
MICPA231. Groundwater Biosphere Dose Conversion Factor (BDCF) for ^{231}Pa in modern interglacial climate ((Sv/year)/(Bq/m^3)). *Distribution:* Discrete. *Range:* 6.58×10^{-7} to 8.56×10^{-6}. *Mean:* 2.44×10^{-6}. *Standard Deviation:* 1.02×10^{-6}. *TSPA-LA Name:* GW_BDCF_MIC_Pa231 (SNL 2008a, Sections 6.3.11.2 and 6.3.11.3; Table 6.3.11-3).
MICPU238. Groundwater Biosphere Dose Conversion Factor (BDCF) for ^{238}Pu in modern interglacial climate ((Sv/year)/(Bq/m^3)). *Distribution:* Discrete. *Range:* 2.61×10^{-7} to $2.09 \times {}^{-6}$. *Mean:* 7.61×10^{-7}. *Standard Deviation:* 2.78×10^{-7}. *TSPA-LA Name:* GW_BDCF_MIC_Pu238 (SNL 2008a, Sections 6.3.11.2 and 6.3.11.3; Table 6.3.11-3).

Table 2.4-11. Summary of Epistemically Uncertain Variables Considered in the TSPA (Continued)

MICPU239. Groundwater Biosphere Dose Conversion Factor (BDCF) for ^{239}Pu in modern interglacial climate ((Sv/year)/(Bq/m^3)). *Distribution:* Discrete. *Range:* 3.49×10^{-7} to 2.93×10^{-6}. *Mean:* 9.55×10^{-7}. *Standard Deviation:* 3.37×10^{-7}. *TSPA-LA Name:* GW_BDCF_MIC_Pu239 (SNL 2008a, Sections 6.3.11.2 and 6.3.11.3; Table 6.3.11-3).
MICPU240. Groundwater Biosphere Dose Conversion Factor (BDCF) for ^{240}Pu in modern interglacial climate ((Sv/year)/(Bq/m^3)). *Distribution:* Discrete. *Range:* 3.47×10^{-7} to 2.90×10^{-6}. *Mean:* 9.51×10^{-7}. *Standard Deviation:* 3.35×10^{-7}. *TSPA-LA Name:* GW_BDCF_MIC_Pu240 (SNL 2008a, Sections 6.3.11.2 and 6.3.11.3; Table 6.3.11-3).
MICPU242a. Groundwater Biosphere Dose Conversion Factor (BDCF) for ^{242}Pu in modern interglacial climate ((Sv/year)/(Bq/m^3)). *Distribution:* Discrete. *Range:* 3.31×10^{-7} to 2.79×10^{-6}. *Mean:* 9.07×10^{-7}. *Standard Deviation:* 3.20×10^{-7}. *TSPA-LA Name:* GW_BDCF_MIC_Pu242 (SNL 2008a, Sections 6.3.11.2 and 6.3.11.3; Table 6.3.11-3).
MICRA226. Groundwater Biosphere Dose Conversion Factor (BDCF) for ^{210}Pb summed into ^{226}Ra in modern interglacial climate ((Sv/year)/(Bq/m^3)). *Distribution:* Discrete. *Range:* 2.90×10^{-6} to 2.82×10^{-5}. *Mean:* 6.52×10^{-6}. *Standard Deviation:* 2.58×10^{-6}. *TSPA-LA Name:* GW_BDCF_MIC_Ra226_Pb210 (SNL 2008a, Sections 6.3.11.2 and 6.3.11.3; Table 6.3.11-3).
MICRA228a. Groundwater Biosphere Dose Conversion Factor (BDCF) for ^{228}Ra in modern interglacial climate ((Sv/year)/(Bq/m^3)). *Distribution:* Discrete. *Range:* 6.14×10^{-7} to 1.53×10^{-6}. *Mean:* 9.05×10^{-7}. *Standard Deviation:* 1.40×10^{-7}. *TSPA-LA Name:* GW_BDCF_MIC_Ra228 (SNL 2008a, Sections 6.3.11.2 and 6.3.11.3; Table 6.3.11-3).
MICSE79. Groundwater Biosphere Dose Conversion Factor (BDCF) for ^{79}Se in modern interglacial climate. ((Sv/year)/(Bq/m^3)). *Distribution:* Discrete. *Range:* 3.62×10^{-9} to 1.51×10^{-6}. *Mean:* 2.42×10^{-8}. *Standard Deviation:* 7.48×10^{-8}. *TSPA-LA Name:* GW_BDCF_MIC_Se79 (SNL 2008a, Sections 6.3.11.2 and 6.3.11.3; Table 6.3.11-3).
MICSN126. Groundwater Biosphere Dose Conversion Factor (BDCF) for ^{126}Sn in modern interglacial climate ((Sv/year)/(Bq/m^3)). *Distribution:* Discrete. *Range:* 8.92×10^{-8} to 1.68×10^{-6}. *Mean:* 4.33×10^{-7}. *Standard Deviation:* 2.39×10^{-7}. *TSPA-LA Name:* GW_BDCF_MIC_Sn126 (SNL 2008a, Sections 6.3.11.2 and 6.3.11.3; Table 6.3.11-3).
MICSR90. Groundwater Biosphere Dose Conversion Factor (BDCF) for ^{90}Sr in modern interglacial climate ((Sv/year)/(Bq/m^3)). *Distribution:* Discrete. *Range:* 2.51×10^{-8} to 8.60×10^{-8}. *Mean:* 3.43×10^{-8}. *Standard Deviation:* 6.59×10^{-9}. *TSPA-LA Name:* GW_BDCF_MIC_Sr90 (SNL 2008a, Sections 6.3.11.2 and 6.3.11.3; Table 6.3.11-3).
MICTC99. Groundwater Biosphere Dose Conversion Factor (BDCF) for ^{99}Tc in modern interglacial climate ((Sv/year)/(Bq/m^3)). *Distribution:* Discrete. *Range:* 5.28×10^{-10} to 2.85×10^{-8}. *Mean:* 1.12×10^{-9}. *Standard Deviation:* 1.26×10^{-9}. *TSPA-LA Name:* GW_BDCF_MIC_Tc99 (SNL 2008a, Sections 6.3.11.2 and 6.3.11.3; Table 6.3.11-3).
MICTH229. Groundwater Biosphere Dose Conversion Factor (BDCF) for ^{229}Th in modern interglacial climate ((Sv/year)/(Bq/m^3)). *Distribution:* Discrete. *Range:* 7.43×10^{-7} to 8.05×10^{-6}. *Mean:* 2.58×10^{-6}. *Standard Deviation:* 1.03×10^{-6}. *TSPA-LA Name:* GW_BDCF_MIC_Th229 (SNL 2008a, Sections 6.3.11.2 and 6.3.11.3; Table 6.3.11-3).
MICTH230a. Groundwater Biosphere Dose Conversion Factor (BDCF) for ^{230}Th in modern interglacial climate ((Sv/year)/(Bq/m^3)). *Distribution:* Discrete. *Range:* 2.74×10^{-7} to 3.27×10^{-6}. *Mean:* 1.08×10^{-6}. *Standard Deviation:* 4.34×10^{-7}. *TSPA-LA Name:* GW_BDCF_MIC_Th230 (SNL 2008a, Sections 6.3.11.2 and 6.3.11.3; Table 6.3.11-3).
MICU232. Groundwater Biosphere Dose Conversion Factor (BDCF) for ^{232}U in modern interglacial climate ((Sv/year)/(Bq/m^3)). *Distribution:* Discrete. *Range:* 2.87×10^{-7} to 1.86×10^{-6}. *Mean:* 6.04×10^{-7}. *Standard Deviation:* 2.17×10^{-7}. *TSPA-LA Name:* GW_BDCF_MIC_U232 (SNL 2008a, Sections 6.3.11.2 and 6.3.11.3; Table 6.3.11-3).

Table 2.4-11. Summary of Epistemically Uncertain Variables Considered in the TSPA (Continued)

MICTH232a. Groundwater Biosphere Dose Conversion Factor (BDCF) for ^{232}Th in modern interglacial climate ((Sv/year)/(Bq/m^3)). *Distribution:* Discrete. *Range:* 5.05×10^{-7} to 5.26×10^{-6}. *Mean:* 1.85×10^{-6}. *Standard Deviation:* 7.33×10^{-7}. *TSPA-LA Name:* GW_BDCF_MIC_Th232 (SNL 2008a, Sections 6.3.11.2 and 6.3.11.3; Table 6.3.11-3).
MICU233. Groundwater Biosphere Dose Conversion Factor (BDCF) for ^{233}U in modern interglacial climate ((Sv/year)/(Bq/m^3)). *Distribution:* Discrete. *Range:* 4.13×10^{-8} to 3.13×10^{-7}. *Mean:* 8.97×10^{-8}. *Standard Deviation:* 3.35×10^{-8}. *TSPA-LA Name:* GW_BDCF_MIC_U233 (SNL 2008a, Sections 6.3.11.2 and 6.3.11.3; Table 6.3.11-3).
MICU234. Groundwater Biosphere Dose Conversion Factor (BDCF) for ^{234}U in modern interglacial climate ((Sv/year)/(Bq/m^3)). *Distribution:* Discrete. *Range:* 3.96×10^{-8} to 2.20×10^{-7}. *Mean:* 8.19×10^{-8}. *Standard Deviation:* 2.81×10^{-8}. *TSPA-LA Name:* GW_BDCF_MIC_U234 (SNL 2008a, Sections 6.3.11.2 and 6.3.11.3; Table 6.3.11-3).
MICU235a. Groundwater Biosphere Dose Conversion Factor (BDCF) for ^{235}U in modern interglacial climate ((Sv/year)/(Bq/m^3)). *Distribution:* Discrete. *Range:* 3.91×10^{-8} to 2.97×10^{-7}. *Mean:* 9.41×10^{-8}. *Standard Deviation:* 3.67×10^{-8}. *TSPA-LA Name:* GW_BDCF_MIC_U235 (SNL 2008a, Sections 6.3.11.2 and 6.3.11.3; Table 6.3.11-3).
MICU236a. Groundwater Biosphere Dose Conversion Factor (BDCF) for ^{236}U in modern interglacial climate ((Sv/year)/(Bq/m^3)). *Distribution:* Discrete. *Range:* 3.75×10^{-8} to 2.02×10^{-7}. *Mean:* 7.67×10^{-8}. *Standard Deviation:* 2.60×10^{-8}. *TSPA-LA Name:* GW_BDCF_MIC_U236 (SNL 2008a, Sections 6.3.11.2 and 6.3.11.3; Table 6.3.11-3).
MICU238. Groundwater Biosphere Dose Conversion Factor (BDCF) for ^{238}U in modern interglacial climate ((Sv/year)/(Bq/m^3)). *Distribution:* Discrete. *Range:* 3.85×10^{-8} to 2.07×10^{-7}. *Mean:* 7.87×10^{-8}. *Standard Deviation:* 2.62×10^{-8}. *TSPA-LA Name:* GW_BDCF_MIC_U238 (SNL 2008a, Sections 6.3.11.2 and 6.3.11.3; Table 6.3.11-3).
NIOSA. Specific surface area of NiO (m^2/g). *Distribution:* Uniform. *Range:* 1 to 30. *TSPA-LA Name:* NiO_SA_a (SNL 2008a, Table 6.3.8-4; SCP in Equation 6.3.8-19).
PH2DHLNS. Pointer variable used to determine pH in 2DHLW Cell (Cell 1a) of CDSP waste packages under vapor influx conditions (dimensionless). *Distribution:* Uniform. *Range:* 0 to 1. *TSPA-LA Name:* Inpkg_pH_2DHLW_NS_Rand_a (SNL 2008a, Section 6.3.7.2.2, Part IV).
PH2DHLS. Pointer variable used to determine pH in 2DHLW Cell (Cell 1a) of CDSP waste packages under liquid influx conditions (dimensionless). *Distribution:* Uniform. *Range:* 0 to 1. *TSPA-LA Name:* Inpkg_pH_2DHLW_S_Rand_a (SNL 2008a, Section 6.3.7.2.2, Part IV).
PH2MCONS. Pointer variable used to determine pH in 2MCO Cell (Cell 1b) of CDSP waste packages under vapor influx conditions (dimensionless). *Distribution:* Uniform. *Range:* 0 to 1. *TSPA-LA Name:* Inpkg_pH_2MCO_NS_Rand_a (SNL 2008a, Section 6.3.7.2.2, Part IV).
PH2MCOS. Pointer variable used to determine pH in 2MCO Cell (Cell 1b) of CDSP waste packages under liquid influx conditions (dimensionless). *Distribution:* Uniform. *Range:* 0 to 1. *TSPA-LA Name:* Inpkg_pH_2MCO_S_Rand_a (SNL 2008a, Section 6.3.7.2.2, Part IV).
PH2RGER. Error term in regression equation for pH of corrosion products domain (dimensionless). *Distribution:* Truncated normal. *Range:* –0.64 to 0.64. *Mean/Median/Mode:* 0. *Standard Deviation:* 0.32. *TSPA-LA Name:* pH_Cell2_Regression_Error_a (SNL 2008a, Equation 6.3.8-27).
PHCSNS. Pointer variable used to determine pH in commercial SNF Cell1 under vapor influx conditions (dimensionless). *Distribution:* Uniform. *Range:* 0 to 1. *TSPA-LA Name:* Inpkg_pH_CSNF_NS_Rand_a (SNL 2008a, Section 6.3.7.2.2, Part IV).

Table 2.4-11. Summary of Epistemically Uncertain Variables Considered in the TSPA (Continued)

PHCSS. Pointer variable used to determine pH in commercial SNF Cell1 under liquid influx conditions (dimensionless). *Distribution:* Uniform. *Range:* 0 to 1. *TSPA-LA Name:* Inpkg_pH_CSNF_S_Rand_a(SNL 2008a, Section 6.3.7.2.2, Part IV).
PROBDSEF. Probability for undetected defects in drip shields (dimensionless). *Distribution:* Log-normal. *Median:* 4.3×10^{-7}. *Error Factor:* 14. *TSPA-LA Name:* UNC_DS_EF_conv_from_ln (SNL 2008a, Section 6.4.1; Tables 6.4-1 and 6.4-2).
PROBWPEF. Probability for the undetected defects in waste packages (dimensionless). *Distribution:* Log-normal. *Median:* 4.14×10^{-5}. *Error Factor:* 8.17. *TSPA-LA Name:* UNC_WP_EF_conv_from_ln (SNL 2008a, Section 6.4.2; Tables 6.4-1 and 6.4-2).
RHI85. The in-drift precipitated/salts (IDPS) process model uncertainty factor for the logarithm of the ionic strength of the in-drift waters at high relative humidity (≥85%) (log molal). *Distribution:* Triangular. *Range:* –0.1 to 0.1. *Mean/Median/Mode:* 0. *TSPA-LA Name:* PCE_I_Uncert_RH_85_100_a (SNL 2008a, Section 6.3.4.1; Table 6.3.4-3).
RHMU0. The IDPS process model uncertainty factor for the logarithm of the chloride concentration of the in-drift waters at relative humidity ≤20% (dimensionless). *Distribution:* Triangular. *Range:* –0.7 to 0.7. *Most Likely:* 0. *TSPA-LA Name:* PCE_Cl_MU_RH_0_20_a (SNL 2008a, Sections 6.3.4, 6.3.4.2, 6.3.4.3.1, 6.3.4.3.2, and 6.3.5.2.3; Tables 6.3.4-2, 6.3.4-3 and 6.3.5-4).
RHMU20. The IDPS process model uncertainty factor for the logarithm of the chloride concentration of the in-drift waters at relative humidity >20 and ≤40% (dimensionless). *Distribution:* Triangular. *Range:* –0.5 to 0.5. *Most Likely:* 0. *TSPA-LA Name:* PCE_Cl_MU_RH_20_40_a (SNL 2008a, Sections 6.3.4, 6.3.4.2, 6.3.4.3.1, 6.3.4.3.2, and 6.3.5.2.3; Tables 6.3.4-2, 6.3.4-3 and 6.3.5-4).
RHMU40. The IDPS process model uncertainty factor for the logarithm of the chloride concentration of the in-drift waters at relative humidity >40 and ≤65% (dimensionless). *Distribution:* Triangular. *Range:* –0.4 to 0.4. *Most Likely:* 0. *TSPA-LA Name:* PCE_Cl_MU_RH_40_65_a (SNL 2008a, Sections 6.3.4, 6.3.4.2, 6.3.4.3.1, 6.3.4.3.2, and 6.3.5.2.3; Tables 6.3.4-2, 6.3.4-3, and 6.3.5-4).
RHMU65. The IDPS process model uncertainty factor for the logarithm of the chloride concentration of the in-drift waters at relative humidity >65 and ≤85% (dimensionless). *Distribution:* Triangular. *Range:* –0.1 to 0.1. *Most Likely:* 0. *TSPA-LA Name:* PCE_Cl_MU_RH_65_85_a (SNL 2008a, Sections 6.3.4, 6.3.4.2, 6.3.4.3.1, 6.3.4.3.2, and 6.3.5.2.3; Tables 6.3.4-2, 6.3.4-3 and 6.3.5-4).
RHMU85[a]**.** The IDPS process model uncertainty factor for the logarithm of the chloride concentration of the in-drift waters at relative humidity >85% (dimensionless). *Distribution:* Triangular. *Range:* 0 to 0. *Most Likely:* 0. *TSPA-LA Name:* PCE_Cl_MU_RH_85_100_a[a] (SNL 2008a, Sections 6.3.4, 6.3.4.2, 6.3.4.3.1, 6.3.4.3.2, and 6.3.5.2.3; Tables 6.3.4-2, 6.3.4-3, and 6.3.5-4).
RHMUN40. The IDPS process model uncertainty factor for the logarithm of the chloride + nitrate concentration of the in-drift waters at relative humidity >40% and ≤65% (dimensionless). *Distribution:* Triangular. *Range:* –0.57 to 0.57. *Most Likely:* 0. *TSPA-LA Name:* PCE_Cl_N_MU_RH_40_65_a (SNL 2008a, Sections 6.3.4.3.2 and 6.3.5.2.3; Tables 6.3.4-2, 6.3.4-3, and 6.3.5-4).
RHMUN65. The IDPS process model uncertainty factor for the logarithm of the chloride + nitrate concentration of the in-drift waters at relative humidity >65% and ≤85% (dimensionless). *Distribution:* Triangular. *Range:* –0.22 to 0.22. *Most Likely:* 0. *TSPA-LA Name:* PCE_Cl_N_MU_RH_65_85_a (SNL 2008a, Sections 6.3.4.3.2 and 6.3.5.2.3; Tables 6.3.4-2, 6.3.4-3, and 6.3.5-4).
RHMUN85[a]**.** The IDPS process model uncertainty factor for the logarithm of the chloride + nitrate concentration of the in-drift waters at relative humidity >85% (dimensionless). *Distribution:* Triangular. *Range:* 0 to 0. *Most Likely:* 0. *TSPA-LA Name:* PCE_Cl_N_MU_RH_85_100_a[a] (SNL 2008a, Sections 6.3.4.3.2 and 6.3.5.2.3; Tables 6.3.4-2, 6.3.4-3, and 6.3.5-4).

Table 2.4-11. Summary of Epistemically Uncertain Variables Considered in the TSPA (Continued)

RHMUNO0. The IDPS process model uncertainty factor for the logarithm of the chloride to nitrate ratio of the in-drift waters at relative humidity ≤20% (dimensionless). *Distribution:* Triangular. *Range:* –1.4 to 1.4. *Most Likely:* 0. *TSPA-LA Name:* PCE_Cl_NO3_MU_RH_0_20_a (SNL 2008a, Sections 6.3.4.3.1, 6.3.4.3.2, and 6.3.5.2.3; Tables 6.3.4-2, 6.3.4-3, and 6.3.5-4).
RHMUNO20. The IDPS process model uncertainty factor for the logarithm of the chloride to nitrate ratio of the in-drift waters at relative humidity >20% and ≤65% (dimensionless). *Distribution:* Triangular. *Range:* –0.5 to 0.5. *Most Likely:* 0. *TSPA-LA Name:* PCE_Cl_NO3_MU_RH_20_65_a (SNL 2008a, Sections 6.3.4.3.1, 6.3.4.3.2, and 6.3.5.2.3; Tables 6.3.4-2, 6.3.4-3, and 6.3.5-4).
RHMUNO65. The IDPS process model uncertainty factor for the logarithm of the chloride to nitrate ratio of the in-drift waters at relative humidity >65% and ≤85% (dimensionless). *Distribution:* Triangular. *Range:* –0.2 to 0.2. *Most Likely:* 0. *TSPA-LA Name:* PCE_Cl_NO3_MU_RH_65_85_a (SNL 2008a, Sections 6.3.4.3.1, 6.3.4.3.2, and 6.3.5.2.3; Tables 6.3.4-2, 6.3.4-3, and 6.3.5-4.
RHMUNO85[a]**.** The IDPS process model uncertainty factor for the logarithm of the chloride to nitrate ratio of the in-drift waters at low relative humidity >85% (dimensionless). *Distribution:* Triangular. *Range:* 0 to 0. *Most Likely:* 0. *TSPA-LA Name:* PCE_Cl_NO3_MU_RH_85_100_a[a] (SNL 2008a, Sections 6.3.4.3.1, 6.3.4.3.2, and 6.3.5.2.3; Tables 6.3.4-2, 6.3.4-3, and 6.3.5-4.
RHPH0. The IDPS process model uncertainty factor for the pH of the in-drift waters at relative humidity ≤65% (dimensionless). *Distribution:* Triangular. *Range:* –2 to 2. *Most Likely:* 0. *TSPA-LA Name:* PCE_pH_Uncert_RH_0_65_a (SNL 2008a, Table 6.3.5-4).
RHPH65. The IDPS process model uncertainty factor for the pH of the in-drift waters at relative humidity >65 and ≤75% (dimensionless). *Distribution:* Triangular. *Range:* –1 to 1. *Most Likely:* 0. *TSPA-LA Name:* PCE_pH_Uncert_RH_65_75_a (SNL 2008a, Table 6.3.5-4).
RHPH75. The IDPS process model uncertainty factor for the pH of the in-drift waters at relative humidity >75% (dimensionless). *Distribution:* Discrete. *Range:* –0.3123 to 0.4288. *TSPA-LA Name:* PCE_pH_Uncert_RH_75_100_a (SNL 2008a, Table 6.3.5-4).
RSUSTHIK. Thickness of combined ash/soil mixture available for resuspension (m). *Distribution:* Uniform. *Range:* 0.001 to 0.003. *Mean/Median/Mode:* 0.002. *TSPA-LA Name:* Resuspension_Thickness_a (SNL 2008a, Equation 6.3.11-6).
RUBMAXL. Volume of lithophysal rock that must fall to fill the drift (m^3/m). *Distribution:* Uniform. *Range:* 30 to 120. *TSPA-LA Name:* Vol_Rubble_Max_Lith_a (SNL 2008a, Sections 6.3.5.2.3 and 6.6.3.1; Tables 6.3.5-4 and 6.6-2).
RUBMAXNL. Volume of nonlithophysal rock that must fall to fill the drift (m^3/m). *Distribution:* Uniform. *Range:* 30 to 120. *TSPA-LA Name:* Vol_Rubble_Max_NonLith_a (SNL 2008a, Section 6.3.5.2.3 and 6.6.3.1; Tables 6.3.5-4 and 6.6-2).
SC_DPTH. Scour depth in Fortymile Wash at the fan apex (cm). *Distribution:* Uniform. *Range:* 73 to 122. *TSPA-LA Name:* Scour_Depth_a (SNL 2008a, Table 6.5-5).
SCCTHR. Stress threshold for stress corrosion cracking (MPa). *Distribution:* Uniform. *Range:* 315.9 to 368.55. *TSPA-LA Name:* Stress_Thresh_SCC_a (SNL 2008a, Table 6.3.5-3).
SCCTHRP. Residual stress threshold for SCC nucleation of Alloy 22 (as a percentage of yield strength in MPa) (dimensionless). *Distribution:* Uniform. *Range:* 90 to 105. *TSPA-LA Name:* Stress_Thresh_A22_a (SNL 2008a, Section 6.6.1.3.7; Table 6.6-2).
SCHOBOLT. Fractional value used to interpolate between Schoepite and Boltwoodite lookup tables (dimensionless). *Distribution:* Uniform. *Range:* 0 to 1. *TSPA-LA Name:* Schoepite_Boltwoodite_Interp_a (SNL 2008a, Table 6.3.7-58).

Table 2.4-11. Summary of Epistemically Uncertain Variables Considered in the TSPA (Continued)

SEEPCOND. Pointer variable to determine the seepage/condensation regime for the first failed waste package in a percolation subregion (dimensionless). *Distribution:* Uniform. *Range:* 0 to 1. *TSPA-LA Name:* Seepage_Condensation_Prob_a (SNL 2008a, Section 6.3.3.2.2; Table 6.3.3-5).
SEEPPRM. Logarithm of the mean fracture permeability in lithophysal rock units (dimensionless). *Distribution:* Triangular. *Range:* –0.92 to 0.92. *Mode:* 0. *TSPA-LA Name:* LogK_Uncert_Lith_a (SNL 2008a, Sections 6.3.5.2.3, 6.3.3.1.2, and 6.3.3.1.3; Tables 6.3.5-4, 6.3.3-2, and 6.3.3-3).
SEEPPRMN. Logarithm of the mean fracture permeability in non-lithophysal rock units (dimensionless). *Distribution:* Triangular. *Range:* –0.68 to 0.68. *Mode:* 0. *TSPA-LA Name:* LogK_Uncert_NonLith_a (SNL 2008a, Sections 6.3.5.2.3, 6.3.3.1.2, and 6.3.3.1.3; Tables 6.3.5-4, 6.3.3-2, and 6.3.3-3).
SEEPUNC. Uncertainty factor to account for small-scale heterogeneity in fracture permeability (dimensionless). *Distribution:* Uniform. *Range:* 0 to 1. *TSPA-LA Name:* Seepage_Uncertainty_a (SNL 2008a, Section 6.3.3.1.2; Tables 6.3.3-3, and 6.3.5-4).
SEEPWAT. Pointer variable used to select which seepage water type in used in the physical and chemical environment (P&CE) submodel calculations (dimensionless). *Distribution:* Discrete. *Range:* 1 to 4. *TSPA-LA Name:* Seepage_Water_Type_a (SNL 2008a, Table 6.3.5-4).
SMECSA. Specific surface area for smectite colloids (m^2/g). *Distribution:* Uniform. *Range:* 10 to 100. *TSPA-LA Name:* Specific_SA_Smectite_Col_a (SNL 2008a, Table 6.3.7-62).
SOILDENS. Density of surface soil correlated with the volcanic BDCFs (kg/m^3). *Distribution:* Triangular. *Range:* 1300 to 1700. *Mean/Median/Mode:* 1500. *TSPA-LA Name:* Soil_Density_a (SNL 2008a, Equation 6.3.11-6.)
SZCOLRAL. Logarithm of colloid retardation factor in alluvium (dimensionless). *Distribution:* Piecewise uniform. *Range:* 0.903 to 3.715. *TSPA-LA Name:* CORAL (SNL 2008a, Sections 6.3.10.1, 6.3.10.2, and 6.3.10.4.2; Table 6.3.10-2).
SZCOLRVO. Logarithm of colloid retardation factor in volcanic units (dimensionless). *Distribution:* Piecewise uniform. *Range:* 0.778 to 2.903. *TSPA-LA Name:* CORVO (SNL 2008a, Sections 6.3.10.1, 6.3.10.2, and 6.3.10.4.2; Table 6.3.10-2).
SZCONCOL. Logarithm of ambient concentration of colloids in groundwater (g/mL). *Distribution:* Piecewise uniform. *Range:* –9 to –3.6. *TSPA-LA Name:* Conc_Col (SNL 2008a, Table 6.3.10-2).
SZDENAL. Bulk density of alluvium (kg/m^3). *Distribution:* Normal. *Mean/Median/Mode:* 1910. *Standard Deviation:* 78. *TSPA-LA Name:* Alluvium_Density (SNL 2008a, Table 6.3.10-2).
SZDIFCVO. Logarithm of effective diffusion coefficient in fractured volcanic units (m^2/s). *Distribution:* Piecewise uniform. *Range:* –11.3 to –9.3. *TSPA-LA Name:* DCVO (SNL 2008a, Sections 6.3.10.2 and 6.3.10.5; Table 6.3.10-2).
SZFIPOVO. Logarithm of flowing interval porosity in volcanic units (dimensionless). *Distribution:* Piecewise uniform. *Range:* –5 to –1. *Mean/Median/Mode:* –3. *TSPA-LA Name:* FPVO (SNL 2008a, Table 6.3.10-2).
SZFISPVO. Flowing interval spacing in fractured volcanic units (m). *Distribution:* Piecewise uniform. *Range:* 1.86 to 80. *TSPA-LA Name:* FISVO (SNL 2008a, Section 6.3.10.5; Table 6.3.10-2).
SZGWSPDM. Logarithm of the scale factor used to characterize uncertainty in groundwater specific discharge (dimensionless). *Distribution:* Piecewise uniform. *Range:* –0.951 to 0.951. *TSPA-LA Name:* GWSPD (SNL 2008a, Section 6.3.10.2; Table 6.3.10-2).
SZKDAMAL. Americium sorption coefficient in alluvium (mL/g). *Distribution:* Truncated normal. *Range:* 1000 to 10000. *Mean/Median/Mode:* 5500. *Standard Deviation:* 1500. *TSPA-LA Name:* Kd_Am_Al (SNL 2008a, Section 6.3.10.2; Table 6.3.10-2).
SZKDAMCO. Americium sorption coefficient onto smectite colloids (mL/g). *Distribution:* Piecewise uniform. *Range:* 1.00×10^4 to 1.00×10^7. *TSPA-LA Name:* Kd_Am_Col (SNL 2008a, Section 6.3.10.2; Table 6.3.10-2).

Table 2.4-11. Summary of Epistemically Uncertain Variables Considered in the TSPA (Continued)

SZKDAMVO. Americium sorption coefficient in volcanic units (mL/g). *Distribution:* Truncated normal. *Range:* 1000 to 10000. *Mean/Median/Mode:* 5500. *Standard Deviation:* 1500. *TSPA-LA Name:* Kd_Am_Vo (SNL 2008a, Section 6.3.10.2; Table 6.3.10-2).
SZKDCSAL. Cesium sorption coefficient in alluvium (mL/g). *Distribution:* Truncated normal. *Range:* 100 to 1000. *Mean/Median/Mode:* 728. *Standard Deviation:* 464. *TSPA-LA Name:* Kd_Cs_Al (SNL 2008a, Section 6.3.10.2; Table 6.3.10-2).
SZKDCSCO. Cesium sorption coefficient onto smectite colloids (mL/g). *Distribution:* Piecewise uniform. *Range:* 50 to 5000. *TSPA-LA Name:* Kd_Cs_Col (SNL 2008a, Section 6.3.10.2; Table 6.3.10-2).
SZKDCSVO. Cesium sorption coefficient in volcanic units (mL/g). *Distribution:* Piecewise uniform. *Range:* 100 to 6783. *TSPA-LA Name:* Kd_Cs_Vo (SNL 2008a, Section 6.3.10.2; Table 6.3.10-2).
SZKDNPAL. Neptunium sorption coefficient in alluvium (mL/g). *Distribution:* Piecewise uniform. *Range:* 1.8 to 13. *TSPA-LA Name:* Kd_Np_Al (SNL 2008a, Section 6.3.10.2; Table 6.3.10-2).
SZKDNPVO. Neptunium sorption coefficient in volcanic units (mL/g). *Distribution:* Piecewise uniform. *Range:* 0 to 6. *TSPA-LA Name:* Kd_Np_Vo (SNL 2008a, Section 6.3.10.2; Table 6.3.10-2).
SZKDPUAL. Plutonium sorption coefficient in alluvium (mL/g). *Distribution:* Beta. *Range:* 50 to 300. *Mean/Median/Mode:* 100. *Standard Deviation:* 15. *TSPA-LA Name:* Kd_Pu_Al (SNL 2008a, Section 6.3.10.2; Table 6.3.10-2).
SZKDPUCO. Plutonium sorption coefficient onto smectite colloids (mL/g). *Distribution:* Piecewise uniform. *Range:* 1.00×10^3 to 1.00×10^5. *TSPA-LA Name:* Kd_Pu_Col (SNL 2008a, Section 6.3.10.2; Table 6.3.10-2).
SZKDPUVO. Plutonium sorption coefficient in volcanic units (mL/g). *Distribution:* Piecewise uniform. *Range:* 10 to 300. *TSPA-LA Name:* Kd_Pu_Vo (SNL 2008a, Section 6.3.10.2; Table 6.3.10-2).
SZKDRAAL. Radium sorption coefficient in alluvium (mL/g). *Distribution:* Uniform. *Range:* 100 to 1000. *TSPA-LA Name:* Kd_Ra_Al (SNL 2008a, Section 6.3.10.2; Table 6.3.10-2).
SZKDRAVO[a]**.** Radium sorption coefficient in volcanic units (mL/g). *Distribution:* Uniform. *Range:* 100 to 1000. *TSPA-LA Name:* Kd_Ra_Vo[a] (SNL 2008a, Section 6.3.10.2; Table 6.3.10-2).
SZKDSEAL. Selenium sorption coefficient in alluvium (mL/g). *Distribution:* Truncated log normal. *Range:* 1 to 50. *Mean/Median/Mode:* 14. *Standard Deviation:* 11.2. *TSPA-LA Name:* Kd_Se_Al (SNL 2008a, Section 6.3.10.2; Table 6.3.10-2).
SZKDSEVO. Selenium sorption coefficient in volcanic units (mL/g). *Distribution:* Truncated log normal. *Range:* 1 to 50. *Mean/Median/Mode:* 14. *Standard Deviation:* 11.2. *TSPA-LA Name:* Kd_Se_Vo (SNL 2008a, Section 6.3.10.2; Table 6.3.10-2).
SZKDSNAL. Tin sorption coefficient in alluvium (mL/g). *Distribution:* Log uniform. *Range:* 1.00×10^2 to 1.00×10^5. *TSPA-LA Name:* Kd_Sn_Al (SNL 2008a, Section 6.3.10.2; Table 6.3.10-2).
SZKDSNCO. Tin sorption coefficient onto smectite colloids (mL/g). *Distribution:* Log uniform. *Range:* 1.00×10^5 to 1.00×10^6. *TSPA-LA Name:* Kd_Sn_Col (SNL 2008a, Section 6.3.10.2; Table 6.3.10-2).
SZKDSNVO. Tin sorption coefficient in volcanic units (mL/g). *Distribution:* Log uniform. *Range:* 1.00×10^2 to 1.00×10^5. *TSPA-LA Name:* Kd_Sn_Vo (SNL 2008a, Section 6.3.10.2; Table 6.3.10-2).
SZKDSRAL. Strontium sorption coefficient in alluvium (mL/g). *Distribution:* Uniform. *Range:* 20 to 400. *TSPA-LA Name:* Kd_Sr_Al (SNL 2008a, Section 6.3.10.2; Table 6.3.10-2).
SZKDSRVO. Strontium sorption coefficient in volcanic units (mL/g). *Distribution:* Uniform. *Range:* 20 to 400. *TSPA-LA Name:* Kd_Sr_Vo (SNL 2008a, Section 6.3.10.2; Table 6.3.10-2).

Table 2.4-11. Summary of Epistemically Uncertain Variables Considered in the TSPA (Continued)

SZKDUAL. Uranium sorption coefficient in alluvium (mL/g). *Distribution:* Piecewise uniform. *Range:* 1.7 to 8.9. *TSPA-LA Name:* Kd_U_Al (SNL 2008a, Section 6.3.10.2; Table 6.3.10-2).
SZKDUVO. Uranium sorption coefficient in volcanic units (mL/g). *Distribution:* Piecewise uniform. *Range:* 0 to 20. *TSPA-LA Name:* Kd_U_Vo (SNL 2008a, Section 6.3.10.2; Table 6.3.10-2).
SZLODISP. Logarithm of longitudinal dispersivity (m). *Distribution:* Right-truncated normal. *Range:* $-\infty$ to 3.5. *Mean:* 2.0. *Standard Deviation:* 0.75. *TSPA-LA Name:* LDISP (SNL 2008a, Section 6.3.10.2; Table 6.3.10-2).
SZPORSAL. Effective porosity in shallow alluvium (dimensionless). *Distribution:* Truncated normal. *Range:* 0 to 0.3. *Mean:* 0.18. *Standard Deviation:* 0.051. *TSPA-LA Name:* NVF26 (SNL 2008a, Table 6.3.10-2).
SZPORUAL. Effective porosity in undifferentiated alluvium (valley fill) (dimensionless). *Distribution:* Truncated normal. *Range:* 0 to 0.3. *Mean:* 0.18. *Standard Deviation:* 0.051. *TSPA-LA Name:* NVF11 (SNL 2008a, Table 6.3.10-2).
SZRAHAVO. Ratio of horizontal anisotropy (north-south over east-west) in the permeability of the SZ volcanic units (dimensionless). *Distribution:* Piecewise uniform. *Range:* 0.05 to 20. *TSPA-LA Name:* HAVO (SNL 2008a, Sections 6.3.10.2 and 6.3.10.5; Table 6.3.10-2).
SZSREG1X. Relative x location of point source in source region 1 (dimensionless). *Distribution:* Uniform. *Range:* 0 to 1. *TSPA-LA Name:* SRC1X (SNL 2008a, Section 6.3.10.2; Table 6.3.10-2).
SZSREG1Y. Relative y location of point source in source region 1 (dimensionless). *Distribution:* Uniform. *Range:* 0 to 1. *TSPA-LA Name:* SRC1Y (SNL 2008a, Section 6.3.10.2; Table 6.3.10-2).
SZSREG2X. Relative x location of point source in source region 2 (dimensionless). *Distribution:* Uniform. *Range:* 0 to 1. *TSPA-LA Name:* SRC2X (SNL 2008a, Section 6.3.10.2; Table 6.3.10-2).
SZSREG2Y. Relative y location of point source in source region 2 (dimensionless). *Distribution:* Uniform. *Range:* 0 to 1. *TSPA-LA Name:* SRC2Y (SNL 2008a, Section 6.3.10.2; Table 6.3.10-2).
SZSREG3X. Relative x location of point source in source region 3 (dimensionless). *Distribution:* Uniform. *Range:* 0 to 1. *TSPA-LA Name:* SRC3X (SNL 2008a, Section 6.3.10.2; Table 6.3.10-2).
SZSREG3Y. Relative y location of point source in source region 3 (dimensionless). *Distribution:* Uniform. *Range:* 0 to 1. *TSPA-LA Name:* SRC3Y (SNL 2008a, Section 6.3.10.2; Table 6.3.10-2).
SZSREG4X. Relative x location of point source in source region 4 (dimensionless). *Distribution:* Uniform. *Range:* 0 to 1. *TSPA-LA Name:* SRC4X (SNL 2008a, Section 6.3.10.2; Table 6.3.10-2).
SZSREG4Y. Relative y location of point source in source region 4 (dimensionless). *Distribution:* Uniform. *Range:* 0 to 1. *TSPA-LA Name:* SRC4Y (SNL 2008a, Section 6.3.10.2; Table 6.3.10-2).
SZWBNDAL. Northwestern boundary of alluvial uncertainty zone (dimensionless). *Distribution:* Uniform. *Range:* 0 to 1. *TSPA-LA Name:* FPLANW (SNL 2008a, Section 6.3.10.2; Table 6.3.10-2).
THERMCON. Selector variable for one of three host-rock thermal conductivity scenarios (low, mean, and high) (dimensionless). *Distribution:* Discrete. *Range:* 1 to 3. *TSPA-LA Name:* Thermal_Conductivity_Uncert_a (SNL 2008a, Sections 6.3.2.2, 6.3.2.3, 6.3.5.1.3, 6.3.5.2.3, and 6.6.2.2; Tables 6.3.2-1, 6.3.2-3, and 6.3.5-4).
UZCOKDAM. Colloid sorption coefficient for americium (mg/mg). *Calculated by:* Colloidal_Kd_Am_uz^{a}Colloidal_Concentration_uz. *TSPA-LA Name:* Colloidal_Kc_Am_UZP (SNL 2008a, Section 6.3.9.2).
UZCOKDCS. Colloid sorption coefficient for cesium (mg/mg). *Calculated by:* Colloidal_Kd_Cs_uz^{a}Colloidal_Concentration_uz. *TSPA-LA Name:* Colloidal_Kc_Cs_UZP (SNL 2008a, Section 6.3.9.2).

Table 2.4-11. Summary of Epistemically Uncertain Variables Considered in the TSPA (Continued)

UZCOKDPA. Colloid sorption coefficient for protactinium (mg/mg). *Calculated by:* Colloidal_Kd_Am_uz[a]Colloidal_Concentration_uz. *TSPA-LA Name:* Colloidal_Kc_Pa_UZP (SNL 2008a, Section 6.3.9.2).
UZCOKDPU. Colloid sorption coefficient for plutonium (mg/mg). *Calculated by:* Colloidal_Kd_Pu_uz[a]Colloidal_Concentration_uz. *TSPA-LA Name:* Colloidal_Kc_Pu_UZP (SNL 2008a, Section 6.3.9.2).
UZCOKDSN. Colloid sorption coefficient for tin (mg/mg). *Calculated by:* Colloidal_Kd_Sn_uz[a]Colloidal_Concentration_uz. *TSPA-LA Name:* Colloidal_Kc_Sn_UZP (SNL 2008a, Section 6.3.9.2).
UZCOKDTH. Colloid sorption coefficient for thorium (mg/mg). *Calculated by:* Colloidal_Kd_Am_uz[a]Colloidal_Concentration_uz. *TSPA-LA Name:* Colloidal_Kc_Th_UZP (SNL 2008a, Section 6.3.9.2).
UZFAG1. Fracture aperture for group 1 rock unit (chnf) (m). *Calculated by:* Por_group1_a/ff_group1_a. *TSPA-LA Name:* fa_group1_a (SNL 2008a, Section 6.3.9.2; Equation 6.3.9-2; Fracture porosity values and frequency values are shown in Tables 6.3.9-6 and 6.3.9-7).
UZFAG2. Fracture aperture for group 2 rock unit (tswf) (m). *Calculated by:* Por_group2_a/ff_group2_a. *TSPA-LA Name:* fa_group2_a (SNL 2008a, Section 6.3.9.2; Equation 6.3.9-2; Fracture porosity values and frequency values are shown in Tables 6.3.9-6 and 6.3.9-7).
UZFAG3. Fracture aperture for group 3 rock units (ch[2,3,4,5]fz, pcf[2,5]z, pp4fz, pp1fz, bf2fz, tr2fz) (m). *Calculated by:* Por_group3_a/ff_group3_a. *TSPA-LA Name:* fa_group3_a (SNL 2008a, Section 6.3.9.2; Equation 6.3.9-2; Fracture porosity values and frequency values are shown in Tables 6.3.9-6 and 6.3.9-7).
UZFAG4. Fracture aperture for group 4 rock units (pp3fd, pp2fd, bf3fd, tr3fd) (m). *Calculated by:* Por_group4_a/ff_group4_a. *TSPA-LA Name:* fa_group4_a (SNL 2008a, Section 6.3.9.2; Equation 6.3.9-2; Fracture porosity values and frequency values are shown in Tables 6.3.9-6 and 6.3.9-7).
UZFAG5. Fracture aperture for group 5 rock units (ch1fz, pcf1z, ch6fz, pcf6z) (m). *Calculated by:* Por_group5_a/ff_group5_a. *TSPA-LA Name:* fa_group5_a (SNL 2008a, Section 6.3.9.2; Equation 6.3.9-2; Fracture porosity values and frequency values are shown in Tables 6.3.9-6 and 6.3.9-7).
UZFAG6. Fracture aperture for group 6 rock units (ch[1,2,3,4,5,6]fv) (m). *Calculated by:* Por_group6_a/ff_group6_a. *TSPA-LA Name:* fa_group6_a (SNL 2008a, Section 6.3.9.2; Equation 6.3.9-2; Fracture porosity values and frequency values are shown in Tables 6.3.9-6 and 6.3.9-7).
UZFAG7. Fracture aperture for group 7 rock units (tswf9, pcf39, tswfv, tswfz) (m). *Calculated by:* Por_group7_a/ff_group7_a. *TSPA-LA Name:* fa_group7_a (SNL 2008a, Section 6.3.9.2; Equation 6.3.9-2; Fracture porosity values and frequency values are shown in Tables 6.3.9-6 and 6.3.9-7).
UZFAG8. Fracture aperture for group 8 rock units (tswf[4,5], tswf[6,7], tswf8, pcf38) (m). *Calculated by:* Por_group8_a/ff_group8_a. *TSPA-LA Name:* fa_group8_a (SNL 2008a, Section 6.3.9.2; Equation 6.3.9-2; Fracture porosity values and frequency values are shown in Tables 6.3.9-6 and 6.3.9-7).
UZFAG9. Fracture aperture for group 9 rock units (tswf3) (m). *Calculated by:* Por_group9_a/ff_group9_a. *TSPA-LA Name:* fa_group9_a (SNL 2008a, Section 6.3.9.2; Equation 6.3.9-2; Fracture porosity values and frequency values are shown in Tables 6.3.9-6 and 6.3.9-7).
UZGAM. Active fracture model (AFM) Gamma parameter (dimensionless). *Distribution:* Uniform. *Range:* 0.2 to 0.6. *TSPA-LA Name:* Gamma_AFM_a (SNL 2008a, Sections 6.3.9.2, 6.3.9.3 and 6.3.9.4.1; Table 6.3.9-5).
UZKDAMDT. Sorption coefficient of americium in devitrified tuff units of UZ (mL/g). *Distribution:* Truncated normal. *Range:* 1000 to 10000. *Mean:* 5500. *Standard Deviation:* 1500. *TSPA-LA Name:* KdAm_Devit_a (SNL 2008a, Sections 6.3.9.2 and 6.3.9.3; Equation 6.3.9-3; Table 6.3.9-2).

Table 2.4-11. Summary of Epistemically Uncertain Variables Considered in the TSPA (Continued)

UZKDAMVT[a]. Sorption coefficient of americium in vitrified tuff units of UZ (mL/g). *Distribution:* Piecewise uniform. *Range:* 100 to 1000. *Median:* 400. *TSPA-LA Name:* KdAm_Vit_a[a] (SNL 2008a, Sections 6.3.9.2 and 6.3.9.3; Equation 6.3.9-3; Table 6.3.9-2).
UZKDAMZT[a]. Sorption coefficient of americium in zeolitic tuff units of UZ (mL/g). *Distribution:* Truncated normal. *Range:* 1000 to 10000. *Mean:* 5500. *Standard Deviation:* 1500. *TSPA-LA Name:* KdAm_Zeo_a[a] (SNL 2008a, Sections 6.3.9.2 and 6.3.9.3; Equation 6.3.9-3; Table 6.3.9-2).
UZKDCSDT. Sorption coefficient of cesium in devitrified tuff units of UZ (mL/g). *Distribution:* Uniform. *Range:* 1 to 15. *TSPA-LA Name:* KdCs_Devit_a (SNL 2008a, Sections 6.3.9.2 and 6.3.9.3; Equation 6.3.9-3; Table 6.3.9-2).
UZKDCSVT[a]. Sorption coefficient of cesium in vitrified tuff units of UZ (mL/g). *Distribution:* Piecewise uniform. *Range:* 0 to 100. *Median:* 2. *TSPA-LA Name:* KdCs_Vit_a[a] (SNL 2008a, Sections 6.3.9.2 and 6.3.9.3; Equation 6.3.9-3; Table 6.3.9-2).
UZKDCSZT. Sorption coefficient for cesium in zeolitic tuff units of UZ (mL/g). *Distribution:* Piecewise uniform. *Range:* 425 to 20000. *Median:* 5,000. *TSPA-LA Name:* KdCs_Zeo_a (SNL 2008a, Sections 6.3.9.2 and 6.3.9.3; Equation 6.3.9-3; Table 6.3.9-2).
UZKDNPDT. Sorption coefficient for neptunium in devitrified tuff units of UZ (mL/g). *Distribution:* Piecewise uniform. *Range:* 0 to 6. *Median:* 0.5. *TSPA-LA Name:* KdNp_Devit_a (SNL 2008a, Sections 6.3.9.2 and 6.3.9.3; Equation 6.3.9-3; Table 6.3.9-2).
UZKDNPVT[a]. Sorption coefficient for neptunium in vitrified tuff units of UZ (mL/g). *Distribution:* Piecewise uniform. *Range:* 0 to 3. *Median:* 1. *TSPA-LA Name:* KdNp_Vit_a[a] (SNL 2008a, Sections 6.3.9.2 and 6.3.9.3; Equation 6.3.9-3; Table 6.3.9-2).
UZKDNPZT[a]. Sorption coefficient for neptunium in zeolitic tuff units of UZ (mL/g). *Distribution:* Piecewise uniform. *Range:* 0 to 6. *Median:* 0.5. *TSPA-LA Name:* KdNp_Zeo_a[a] (SNL 2008a, Sections 6.3.9.2 and 6.3.9.3; Equation 6.3.9-3; Table 6.3.9-2).
UZKDPADT. Sorption coefficient for protactinium in devitrified tuff units of UZ (mL/g). *Distribution:* Truncated normal. *Range:* 1000 to 10000. *Mean:* 5500. *Standard Deviation:* 1500. *TSPA-LA Name:* KdPa_Devit_a (SNL 2008a, Sections 6.3.9.2 and 6.3.9.3; Equation 6.3.9-3; Table 6.3.9-2).
UZKDPAVT[a]. Sorption coefficient for protactinium in vitrified tuff units of UZ (mL/g). *Distribution:* Truncated normal. *Range:* 1000 to 10000. *Mean:* 5500. *Standard Deviation:* 1500. *TSPA-LA Name:* KdPa_Vit_a[a] (SNL 2008a, Sections 6.3.9.2 and 6.3.9.3; Equation 6.3.9-3; Table 6.3.9-2).
UZKDPAZT[a]. Sorption coefficient for protactinium in zeolitic tuff units of UZ (mL/g). *Distribution:* Truncated normal. *Range:* 1000 to 10000. *Mean:* 5500. *Standard Deviation:* 1500. *TSPA-LA Name:* KdPa_Zeo_a[a] (SNL 2008a, Sections 6.3.9.2 and 6.3.9.3; Equation 6.3.9-3; Table 6.3.9-2).
UZKDPUDT. Sorption coefficient for plutonium in devitrified tuff units of UZ (mL/g). *Distribution:* Piecewise uniform. *Range:* 10 to 200. *Median:* 70. *TSPA-LA Name:* KdPu_Devit_a (SNL 2008a, Sections 6.3.9.2 and 6.3.9.3; Equation 6.3.9-3; Table 6.3.9-2).
UZKDPUVT[a]. Sorption coefficient for plutonium in vitrified tuff units of UZ (mL/g). *Distribution:* Piecewise uniform. *Range:* 10 to 200. *Median:* 100. *TSPA-LA Name:* KdPu_Vit_a[a] (SNL 2008a, Sections 6.3.9.2 and 6.3.9.3; Equation 6.3.9-3; Table 6.3.9-2).
UZKDPUZT[a]. Sorption coefficient for plutonium in zeolitic tuff units of UZ (mL/g). *Distribution:* Piecewise uniform. *Range:* 10 to 200. *Median:* 100. *TSPA-LA Name:* KdPu_Zeo_a[a] (SNL 2008a, Sections 6.3.9.2 and 6.3.9.3; Equation 6.3.9-3; Table 6.3.9-2).
UZKDRADT[a]. Sorption coefficient for radium in devitrified tuff units of UZ (mL/g). *Distribution:* Uniform. *Range:* 100 to 1000. *TSPA-LA Name:* KdRa_Devit_a[a] (SNL 2008a, Sections 6.3.9.2 and 6.3.9.3; Equation 6.3.9-3; Table 6.3.9-2).

Table 2.4-11. Summary of Epistemically Uncertain Variables Considered in the TSPA (Continued)

UZKDRAVT[a]. Sorption coefficient for radium in vitrified tuff units of UZ (mL/g). *Distribution:* Uniform. *Range:* 50 to 600. *TSPA-LA Name:* KdRa_Vit_a[a] (SNL 2008a, Sections 6.3.9.2 and 6.3.9.3; Equation 6.3.9-3; Table 6.3.9-2).

UZKDRAZT[a]. Sorption coefficient for radium in zeolitic tuff units of UZ (mL/g). *Distribution:* Uniform. *Range:* 1000 to 5000. *TSPA-LA Name:* KdRa_Zeo_a[a] (SNL 2008a, Sections 6.3.9.2 and 6.3.9.3; Equation 6.3.9-3; Table 6.3.9-2).

UZKDSEDT. Sorption coefficient for selenium in devitrified tuff units of UZ (mL/g). *Distribution:* Truncated log normal. *Range:* 1 to 50. *Mean:* 14. *Standard Deviation:* 11.2. *TSPA-LA Name:* KdSe_Devit_a (SNL 2008a, Sections 6.3.9.2 and 6.3.9.3; Equation 6.3.9-3; Table 6.3.9-2).

UZKDSEVT[a]. Sorption coefficient for selenium in vitrified tuff units of UZ (mL/g). *Distribution:* Truncated log normal. *Range:* 0 to 25. *Mean:* 8.6. *Standard Deviation:* 7.9. *TSPA-LA Name:* KdSe_Vit_a[a] (SNL 2008a, Sections 6.3.9.2 and 6.3.9.3; Equation 6.3.9-3; Table 6.3.9-2.)

UZKDSEZT[a]. Sorption coefficient for selenium in zeolitic tuff units of UZ (mL/g). *Distribution:* Truncated log normal. *Range:* 1 to 35. *Mean:* 14.3. *Standard Deviation:* 7.9. *TSPA-LA Name:* KdSe_Zeo_a[a] (SNL 2008a, Sections 6.3.9.2 and 6.3.9.3; Equation 6.3.9-3; Table 6.3.9-2).

UZKDSNDT. Sorption coefficient for tin in devitrified tuff units of UZ (mL/g). *Distribution:* Log-uniform. *Range:* 100 to 100000. *TSPA-LA Name:* KdSn_Devit_a (SNL 2008a, Sections 6.3.9.2 and 6.3.9.3; Equation 6.3.9-3; Table 6.3.9-2).

UZKDSNVT[a]. Sorption coefficient for tin in vitrified tuff units of UZ (mL/g). *Distribution:* Log-uniform. *Range:* 100 to 5000. *TSPA-LA Name:* KdSn_Vit_a[a] (SNL 2008a, Sections 6.3.9.2 and 6.3.9.3; Equation 6.3.9-3; Table 6.3.9-2).

UZKDSNZT[a]. Sorption coefficient for tin in zeolitic tuff units of UZ (mL/g). *Distribution:* Log-uniform. *Range:* 100 to 5000. *TSPA-LA Name:* KdSn_Zeo_a[a] (SNL 2008a, Sections 6.3.9.2 and 6.3.9.3; Equation 6.3.9-3; Table 6.3.9-2).

UZKDSRDT. Sorption coefficient for strontium in devitrified tuff units of UZ (mL/g). *Distribution:* Uniform. *Range:* 10 to 70. *TSPA-LA Name:* KdSr_Devit_a (SNL 2008a, Sections 6.3.9.2 and 6.3.9.3; Equation 6.3.9-3; Table 6.3.9-2).

UZKDSRVT[a]. Sorption coefficient for strontium in vitrified tuff units of UZ (mL/g). *Distribution:* Uniform. *Range:* 0 to 50. *TSPA-LA Name:* KdSr_Vit_a[a] (SNL 2008a, Sections 6.3.9.2 and 6.3.9.3; Equation 6.3.9-3; Table 6.3.9-2).

UZKDSRZT[a]. Sorption coefficient for strontium in zeolitic tuff units of UZ (mL/g). *Distribution:* Uniform. *Range:* 50 to 2000. *TSPA-LA Name:* KdSr_Zeo_a[a] (SNL 2008a, Sections 6.3.9.2 and 6.3.9.3; Equation 6.3.9-3; Table 6.3.9-2).

UZKDTHDT. Sorption coefficient for thorium in devitrified tuff units of UZ (mL/g). *Distribution:* Uniform. *Range:* 1000 to 10000. *TSPA-LA Name:* KdTh_Devit_a (SNL 2008a, Sections 6.3.9.2 and 6.3.9.3; Equation 6.3.9-3; Table 6.3.9-2).

UZKDTHVT[a]. Sorption coefficient for thorium in vitrified tuff units of UZ (mL/g). *Distribution:* Uniform. *Range:* 1000 to 10000. *TSPA-LA Name:* KdTh_Vit_a[a] (SNL 2008a, Sections 6.3.9.2 and 6.3.9.3; Equation 6.3.9-3; Table 6.3.9-2).

UZKDTHZT[a]. Sorption coefficient for thorium in zeolitic tuff units of UZ (mL/g). *Distribution:* Uniform. *Range:* 1000 to 30000. *TSPA-LA Name:* KdTh_Zeo_a[a] (SNL 2008a, Sections 6.3.9.2 and 6.3.9.3; Equation 6.3.9-3; Table 6.3.9-2).

UZKDUDT. Sorption coefficient for uranium in devitrified tuff units of UZ (mL/g). *Distribution:* Piecewise uniform. *Range:* 0 to 4. *Median:* 0.2. *TSPA-LA Name:* KdU_Devit_a (SNL 2008a, Sections 6.3.9.2 and 6.3.9.3; Equation 6.3.9-3; Table 6.3.9-2).

UZKDUVT[a]. Sorption coefficient for uranium in vitrified tuff units of UZ (mL/g). *Distribution:* Piecewise uniform. *Range:* 0 to 3. *Median:* 0.2. *TSPA-LA Name:* KdU_Vit_a[a] (SNL 2008a, Sections 6.3.9.2 and 6.3.9.3; Equation 6.3.9-3; Table 6.3.9-2).

UZKDUZT[a]. Sorption coefficient for uranium in zeolitic tuff units of UZ (mL/g). *Distribution:* Piecewise uniform. *Range:* 0 to 30. *Median:* 0.5. *TSPA-LA Name:* KdU_Zeo_a[a]. *Location in TSPA-LA:* Sections 6.3.9.2 and 6.3.9.3; Equation 6.3.9-3; Table 6.3.9-2).

Table 2.4-11. Summary of Epistemically Uncertain Variables Considered in the TSPA (Continued)

UZRCOL. Colloid retardation factor (dimensionless). *Distribution:* Piecewise uniform. *Range:* 6 to 799.83. *TSPA-LA Name:* Colloidal_Retard_Factor_dist_a (SNL 2008a,Sections 6.3.9.2 and 6.3.9.3; Table 6.3.9-12).
UZTORRG1. Logarithm of the tortuosity in rock group 1 (dimensionless). *Distribution:* Left truncated normal. *Range:* 0 to ∞ . *Mean:* –1.15. *Standard Deviation:* 0.29. *TSPA-LA Name:* UZ_Tortuosity_RG1 (SNL 2008a, Section 6.3.9.2; Table 6.3.9-4).
UZTORRG2. Logarithm of the tortuosity in rock group 2 (dimensionless). *Distribution:* Left truncated normal. *Range:* 0 to ∞ . *Mean:* –3.62. *Standard Deviation:* 0.29. *TSPA-LA Name:* UZ_Tortuosity_RG2. (SNL 2008a, Section 6.3.9.2; Table 6.3.9-4).
UZTORRG3. Logarithm of the tortuosity in rock group 3 (dimensionless). *Distribution:* Left truncated normal. *Range:* 0 to ∞ . *Mean:* –1.84. *Standard Deviation:* 0.29. *TSPA-LA Name:* UZ_Tortuosity_RG3. Section 6.3.9.2; Table 6.3.9-4).
WATRCKIN. Parameter used to correlate WRIP_beta so that it resamples at the same probability level throughout a realization (dimensionless). *Distribution:* Uniform. *Range:* 0 to 1. *TSPA-LA Name:* WRIP_beta_rand_a (SNL 2008a, Section 6.3.4.2; Table 6.3.4-1).
WDCRCDEN. Ratio of SCC area to unit of seismic damaged area for a waste package (dimensionless). *Distribution:* Uniform. *Range:* 0.00327 to 0.0131. *TSPA-LA Name:* WP_Crack_Area_Density_a (SNL 2008a,Table 6.6-2).
WDDEFCNT. Flaw density parameter (flaws per mm^3 of weld) (dimensionless). *Distribution:* Gamma. *Mean:* 4.529×10^{-7}. *Standard Deviation:* 1.654×10^{-7}. *TSPA-LA Name:* Defect_Count_a (SNL 2008a, Section 6.3.5.1.2; Table 6.3.5-3).
WDDEFSZE. Flaw size parameter (flaw size per mm of weld) (dimensionless). *Distribution:* Gamma. *Mean:* 0.2205. *Standard Deviation:* 0.0833. *TSPA-LA Name:* Defect_Size_a (SNL 2008a, Section 6.3.5.1.2; Table 6.3.5-3; Equation 6.3.5-10).
WDDSAGGC. Topside general corrosion rate of the drip shield (nm/yr). *Distribution:* Student-t with 5 degrees of freedom. *Mean:* 46.1. *Standard Deviation:* 1.19. *TSPA-LA Name:* WDDSAggrGC_Mean_a (SNL 2008a, Sections 6.3.5.1.2 and 6.3.5.1.3; Table 6.3.5-3).
WDDSBEGC. Underside general corrosion rate of the drip shield (mm/yr). *Distribution:* Normal. *Mean:* 5.15×10^{-6}. *Standard Deviation:* 8.31×10^{-7}. *TSPA-LA Name:* WDDSBenignGC_Mean_a (SNL 2008a, Sections 6.3.5.1.2 and 6.3.5.1.3; Table 6.3.5-3).
WDDSGC29. General corrosion rate ratio for drip shield support material (ratio of Titanium Grade 29 to Titanium Grade 7) (dimensionless). *Distribution:* Discrete. *Range:* 1 to 6.6786. *TSPA-LA Name:* WDDSGC_29_a (SNL 2008a, Section 6.3.5.1.2).
WDGCA22. Temperature dependent slope term of Alloy 22 general corrosion rate (K). *Distribution:* Truncated normal. *Range:* 666 to 7731. *Mean:* 4905. *Standard Deviation:* 1413. *TSPA-LA Name:* C1_GenCorr_A22_a (SNL 2008a, Sections 6.3.5.1.2 and 6.3.5.1.3; Tables 6.3.5-3 and 6.3.5-4; Equation 6.3.5-4).
WDGCUA22. Variable for selecting distribution for general corrosion rate (low, medium, or high) (dimensionless). *Distribution:* Discrete. *Range:* 1 to 3. *TSPA-LA Name:* GC_ULevel_A22_a (SNL 2008a,Table 6.3.5-4).
WDLCRATE. Crevice corrosion (localized corrosion) propagation rate (mm/yr). *Distribution:* Log uniform. *Range:* 0.0127 to 1.27. *TSPA-LA Name:* LC_rate_a (SNL 2008a, Sections 6.3.5.2.1, 6.3.5.2.2, 6.3.5.2.3, 6.3.5.3.2 and 6.3.5.4; Table 6.3.5-4).
WDMICRHT. Relative humidity threshold for initiating microbially induced corrosion (dimensionless). *Distribution:* Uniform. *Range:* 0.75 to 0.9. *TSPA-LA Name:* MIC_RHThresh_a (SNL 2008a,Sections 6.3.5.1.2 and 6.3.5.1.3; Tables 6.3.5-3 and 6.3.5-4).

Table 2.4-11. Summary of Epistemically Uncertain Variables Considered in the TSPA (Continued)

WDNSCC. Stress corrosion cracking growth rate exponent (repassivation slope) (dimensionless). *Distribution:* Truncated normal. *Range:* 0.935 to 1.395. *Mean:* 1.165. *Standard Deviation:* 0.115. *TSPA-LA Name:* n_SCC_a (SNL 2008a, Sections 6.3.5.1.2 and 6.3.5.4; Table 6.3.5-3; Equations 6.3.5-13 and 6.3.5-14).
WDZOLID. Deviation from median yield strength range for outer lid (dimensionless). *Distribution:* Truncated normal. *Range:* –3 to 3. *Mean/Median/Mode:* 0. *Standard Deviation:* 1. *TSPA-LA Name:* z_OL_a (SNL 2008a, Sections 6.3.5.1.2 and 6.3.5.1.3; Table 6.3.5-3).
WFDEGEXF. The surface area exposure factor for the amount of HLW glass contacted by water (dimensionless). *Distribution:* Triangular. *Range:* 4 to 17. *Mode:* 4. *TSPA-LA Name:* Exposure_Factor_a (SNL 2008a, Sections 6.3.7.4.3.2 and 6.3.7.4.3.3; Equation 6.3.7-9; Table 6.3.7-32).
WPFLUX. Waste package flux splitting factor (dimensionless). *Distribution:* Uniform. *Range:* 0 to 2.41. *TSPA-LA Name:* WP_Flux_Uncertainty_a (SNL 2008a, Sections 6.3.6.1, 6.3.6.2 and 6.3.6.3; Tables 6.3.6-1, 6.3.6-2 and 6.3.8-4; Equation 6.3.6-6).

NOTE: [a]Indicates variable not considered in sensitivity analysis due to correlations.

Source: SNL 2008a, Table K3-1.

Table 2.4-12. Summary of Selected Sensitivity Analysis Results

Scenario Class	TSPA Model Output (time of maximum mean value)	Key Uncertain Inputs
Total System	Total expected dose 0 to 10,000 years (10,000 years)	Residual stress threshold for SCC (*SCCTHRP*) (Section 2.3.4.5.1, Section 2.3.6.5.3) Frequency of occurrence of igneous events (*IGRATE*) (Section 2.2.2.2, Section 2.3.11.2.2) Logarithm of scale factor in ground water specific discharge (*SZGWSPDM*) (Section 2.3.9.2.3)
	Total expected dose 10,000 to 1,000,000 years (1,000,000 years)	Frequency of occurrence of igneous events (*IGRATE*) (Section 2.2.2.2, Section 2.3.11.2.2) General corrosion rate (Alloy 22) temperature dependence (*WDGCA22*) (Section 2.3.6.3.3) Logarithm of scale factor in ground water specific discharge (*SZGWSPDM*) (Section 2.3.9.2.3)
Nominal	Expected dose resulting from corrosion processes (720,000 years)	General corrosion rate (Alloy 22) temperature dependence (*WDGCA22*) (Section 2.3.6.3.3) Deviation from median yield strength range for outer lid (*WDZOLID*) (Section 2.3.6.5.2)
Early Failure Drip Shield	Expected dose resulting from early failure of drip shields over 20,000 years (2,000 years)	Probability of early failure per drip shield (*PROBDSEF*) (Section 2.2.2.3.3, Section 2.3.6.8.4) Uncertainty factor accounting for small-scale heterogeneity in fracture permeability (*SEEPUNC*) (Section 2.3.3.2.3) Logarithm of mean fracture permeability in lithophysal rock units (*SEEPRM*) (Section 2.3.3.2.3)
Early Failure Waste Package	Expected dose resulting from early failure of waste packages over 20,000 years (12,000 years)	Probability of early failure per waste package (*PROBWPEF*) (Section 2.2.2.3.2, Section 2.3.6.6) Pointer variable for infiltration scenario (*INFIL*) (Section 2.3.2.4) Selector for host-rock thermal conductivity scenario (*THERMCON*) (Section 2.3.5.3)
Igneous Intrusive	Expected dose resulting from igneous intrusion over 20,000 years (20,000 years)	Frequency of occurrence of igneous events (*IGRATE*) (Section 2.2.2.2, Section 2.3.11.2.2) Logarithm of scale factor in ground water specific discharge (*SZGWSPDM*) (Section 2.3.9.2.3) Pointer variable for infiltration scenario (*INFIL*) (Section 2.3.2.4)
	Expected dose resulting from igneous intrusion over 1,000,000 years (1,000,000 years)	Frequency of occurrence of igneous events (*IGRATE*) (Section 2.2.2.2, Section 2.3.11.2.2) Logarithm of scale factor in ground water specific discharge (*SZGWSPDM*) (Section 2.3.9.2.3) Pointer variable for infiltration scenario (*INFIL*) (Section 2.3.2.4)

Table 2.4-12. Summary of Selected Sensitivity Analysis Results (Continued)

Scenario Class	**TSPA Model Output (time of maximum mean value)**	**Key Uncertain Inputs**
Igneous Eruptive	Expected dose resulting from volcanic eruption over 20,000 years (20,000 years)	Frequency of occurrence of volcanic eruptions (*IGERATE*) (Section 2.3.11.4.5) Pointer variable for long-term inhalation dose conversation factors for exposure to volcanic ash (*INHLTPV*) (Section 2.3.10.2) Diffusivity of radionuclides in divides (*DDIVIDE*) (Section 2.3.11.4.2)
	Expected dose resulting from volcanic eruption over 1,000,000 years (1,000,000 years)	Frequency of occurrence of volcanic eruptions (*IGERATE*) (Section 2.3.11.4.5) Depth of soil within which radionuclides affect the biosphere (*BTILLAGE*) (Section 2.3.11.4)
Seismic Ground Motion	Expected dose resulting from seismic ground motion over 20,000 years (20,000 years)	Residual stress threshold for SCC (*SCCTHRP*) (Section 2.3.4.5.1, Section 2.3.6.5.3)
	Expected dose resulting from combination of seismic ground motion and corrosion processes over 1,000,000 years (1,000,000 years)	General corrosion rate (Alloy 22) temperature dependence (*WDGCA22*) (Section 2.3.6.3.3) Residual stress threshold (*SCCTHRP*) (Section 2.3.4.5.1, Section 2.3.6.5.3)
Seismic Fault Displacement	Expected dose resulting from fault displacement over 20,000 years (20,000 years)	Groundwater biosphere dose conversion factor for ^{99}Tc (*MICTC99*) (Section 2.3.10.5) Pointer variable for infiltration scenario (*INFIL*) (Section 2.3.2.4) Logarithm of scale factor in ground water specific discharge (*SZGWSPDM*) (Section 2.3.9.2.3) Selector variable determining the collapsed drift rubble thermal conductivity (*DTDRHUNC*) (Section 2.3.5.4)
	Expected dose resulting from fault displacement over 1,000,000 years (1,000,000 years)	Pointer variable for infiltration scenario (*INFIL*) (Section 2.3.2.4) Logarithm of scale factor for uncertainty in plutonium solubility at ionic strength below 1 molal (*EP1LOWPU*) (Section 2.3.7.10.3) Logarithm of scale factor in ground water specific discharge (*SZGWSPDM*) (Section 2.3.9.2.3) Waste package flux splitting factor (*WPFLUX*) (Section 2.3.7.13)

NOTE: Name in parentheses is the variable name used in the sensitivity analyses (see Table 2.4-11).

Source: SNL 2008a, Table K9-1[a].

Table 2.4-13. Limits on Radionuclides in the Representative Volume

Radionuclide or Type of Radiation Emitted	Limit	Is Natural Background Included?
Combined ^{226}Ra and ^{228}Ra	5 pCi/L	Yes
Gross Alpha Activity (including ^{226}Ra but excluding radon and uranium)	15 pCi/L	Yes
Combined beta- and photon-emitting radionuclides	0.04 mSv (4 mrem) per year to the whole body or any organ, based on drinking 2 L of water per day from the representative volume	No

Table 2.4-14. Conversion Factors (Sv/yr per Bq/m3) for Calculating Annual Beta-Gamma Dose from Drinking 2 Liters of Water per Day

Organ or Tissue	^{14}C	^{36}Cl	^{79}Se	^{90}Sr	^{99}Tc	^{126}Sn	^{129}I	^{135}Cs	^{137}Cs	^{228}Ra	^{228}Th
Adrenals	4.18×10^{-10}	5.89×10^{-10}	7.06×10^{-10}	4.85×10^{-10}	2.83×10^{-11}	7.21×10^{-10}	8.99×10^{-11}	1.40×10^{-9}	1.02×10^{-8}	1.13×10^{-7}	1.57×10^{-9}
Bone Surface	4.18×10^{-10}	5.89×10^{-10}	7.06×10^{-10}	2.99×10^{-7}	2.83×10^{-11}	4.07×10^{-9}	2.91×10^{-10}	1.40×10^{-9}	1.01×10^{-8}	1.64×10^{-5}	3.81×10^{-8}
Brain	4.18×10^{-10}	5.89×10^{-10}	7.06×10^{-10}	4.85×10^{-10}	2.83×10^{-11}	5.31×10^{-10}	1.04×10^{-10}	1.40×10^{-9}	8.62×10^{-9}	1.12×10^{-7}	1.53×10^{-9}
Breast	4.18×10^{-10}	5.89×10^{-10}	7.06×10^{-10}	4.85×10^{-10}	2.83×10^{-11}	3.52×10^{-10}	8.33×10^{-11}	1.40×10^{-9}	8.18×10^{-9}	1.11×10^{-7}	1.54×10^{-9}
Stomach Wall	4.59×10^{-10}	8.18×10^{-10}	7.52×10^{-10}	1.44×10^{-9}	1.59×10^{-9}	1.50×10^{-9}	1.45×10^{-10}	1.46×10^{-9}	9.79×10^{-9}	1.12×10^{-7}	3.65×10^{-9}
Small Intestine Wall	4.19×10^{-10}	5.95×10^{-10}	7.30×10^{-10}	2.70×10^{-9}	1.35×10^{-10}	3.51×10^{-9}	9.20×10^{-11}	1.41×10^{-9}	1.02×10^{-8}	1.14×10^{-7}	5.22×10^{-9}
Upper Large Intestine Wall	4.24×10^{-10}	6.57×10^{-10}	1.04×10^{-9}	1.41×10^{-8}	1.00×10^{-9}	1.27×10^{-8}	1.64×10^{-10}	1.59×10^{-9}	1.05×10^{-8}	1.30×10^{-7}	1.34×10^{-8}
Lower Large Intestine Wall	4.36×10^{-10}	7.89×10^{-10}	1.68×10^{-9}	3.90×10^{-8}	2.87×10^{-9}	3.40×10^{-8}	3.15×10^{-10}	1.93×10^{-9}	1.22×10^{-8}	1.63×10^{-7}	1.49×10^{-8}
Kidneys	4.18×10^{-10}	5.89×10^{-10}	2.36×10^{-8}	4.85×10^{-10}	2.83×10^{-11}	7.02×10^{-10}	8.84×10^{-11}	1.40×10^{-9}	9.86×10^{-9}	3.16×10^{-7}	3.30×10^{-8}
Liver	4.18×10^{-10}	5.89×10^{-10}	1.02×10^{-8}	4.85×10^{-10}	3.76×10^{-11}	5.76×10^{-10}	8.91×10^{-11}	1.40×10^{-9}	9.93×10^{-9}	7.60×10^{-7}	1.00×10^{-8}
Extrathoracic Airways	4.18×10^{-10}	5.89×10^{-10}	7.06×10^{-10}	4.85×10^{-10}	2.83×10^{-11}	4.67×10^{-10}	1.04×10^{-10}	1.40×10^{-9}	9.57×10^{-9}	1.12×10^{-7}	1.53×10^{-9}
Lung	4.18×10^{-10}	5.89×10^{-10}	7.06×10^{-10}	4.85×10^{-10}	2.83×10^{-11}	4.79×10^{-10}	1.12×10^{-10}	1.40×10^{-9}	9.28×10^{-9}	1.12×10^{-7}	1.54×10^{-9}
Muscle	4.18×10^{-10}	5.89×10^{-10}	7.06×10^{-10}	4.85×10^{-10}	2.83×10^{-11}	6.36×10^{-10}	2.20×10^{-10}	1.40×10^{-9}	9.13×10^{-9}	1.12×10^{-7}	1.56×10^{-9}
Ovaries	4.18×10^{-10}	5.89×10^{-10}	1.33×10^{-9}	4.85×10^{-10}	2.83×10^{-11}	2.13×10^{-9}	9.35×10^{-11}	1.40×10^{-9}	1.04×10^{-8}	1.57×10^{-7}	1.77×10^{-9}
Pancreas	4.18×10^{-10}	5.89×10^{-10}	3.66×10^{-9}	4.85×10^{-10}	2.83×10^{-11}	6.86×10^{-10}	9.13×10^{-11}	1.40×10^{-9}	1.05×10^{-8}	1.12×10^{-7}	1.59×10^{-9}

Table 2.4-14. Conversion Factors (Sv/yr per Bq/m3) for Calculating Annual Beta-Gamma Dose from Drinking 2 Liters of Water per Day (Continued)

Organ or Tissue	**^{14}C**	**^{36}Cl**	**^{79}Se**	**^{90}Sr**	**^{99}Tc**	**^{126}Sn**	**^{129}I**	**^{135}Cs**	**^{137}Cs**	**^{228}Ra**	**^{228}Th**
Red Bone Marrow	4.18×10^{-10}	5.89×10^{-10}	7.06×10^{-10}	1.31×10^{-7}	2.83×10^{-11}	2.15×10^{-9}	1.02×10^{-10}	1.40×10^{-9}	9.57×10^{-9}	1.69×10^{-6}	4.86×10^{-9}
Skin	4.18×10^{-10}	5.89×10^{-10}	7.06×10^{-10}	4.85×10^{-10}	2.83×10^{-11}	4.25×10^{-10}	1.04×10^{-10}	1.40×10^{-9}	7.82×10^{-9}	1.12×10^{-7}	1.54×10^{-9}
Spleen	4.18×10^{-10}	5.89×10^{-10}	4.07×10^{-9}	4.85×10^{-10}	2.83×10^{-11}	5.71×10^{-10}	8.99×10^{-11}	1.40×10^{-9}	9.86×10^{-9}	1.13×10^{-7}	1.58×10^{-9}
Testes	4.18×10^{-10}	5.89×10^{-10}	2.09×10^{-9}	4.85×10^{-10}	2.83×10^{-11}	5.23×10^{-10}	8.47×10^{-11}	1.40×10^{-9}	9.20×10^{-9}	1.56×10^{-7}	1.55×10^{-9}
Thymus	4.18×10^{-10}	5.89×10^{-10}	7.06×10^{-10}	4.85×10^{-10}	2.83×10^{-11}	4.21×10^{-10}	1.26×10^{-10}	1.40×10^{-9}	9.57×10^{-9}	1.12×10^{-7}	1.54×10^{-9}
Thyroid	4.18×10^{-10}	5.89×10^{-10}	7.06×10^{-10}	4.85×10^{-10}	7.38×10^{-10}	4.67×10^{-10}	1.54×10^{-6}	1.40×10^{-9}	9.57×10^{-9}	1.12×10^{-7}	1.53×10^{-9}
Uterus	4.18×10^{-10}	5.89×10^{-10}	7.06×10^{-10}	4.85×10^{-10}	2.83×10^{-11}	1.17×10^{-9}	9.20×10^{-11}	1.40×10^{-9}	1.06×10^{-8}	1.12×10^{-7}	1.65×10^{-9}
Urinary Bladder Wall	4.18×10^{-10}	1.53×10^{-9}	8.11×10^{-10}	1.08×10^{-9}	1.17×10^{-10}	9.43×10^{-10}	3.14×10^{-10}	1.59×10^{-9}	1.06×10^{-8}	1.12×10^{-7}	1.71×10^{-9}
Whole Body	4.24×10^{-10}	6.79×10^{-10}	2.11×10^{-9}	2.22×10^{-8}	4.69×10^{-10}	3.76×10^{-9}	7.74×10^{-8}	1.46×10^{-9}	9.93×10^{-9}	5.09×10^{-7}	4.56×10^{-9}

Table 2.4-14. Conversion Factors (Sv/yr per Bq/m3) for Calculating Annual Beta-Gamma Dose from Drinking 2 Liters of Water per Day (Continued)

Organ or Tissue	**^{232}Th = ^{228}Ra + ^{228}Th**	**^{232}U = ^{228}Th**	**^{237}Np**	**^{229}Th**	**^{228}U**	**^{226}Ra**	**^{210}Pb**	**^{226}Ra + ^{210}Pb**	**^{243}Am**	**^{235}U**	**^{227}Ac**
Adrenals	1.15×10^{-7}	1.57×10^{-9}	9.86×10^{-12}	8.26×10^{-9}	1.65×10^{-12}	1.35×10^{-11}	6.45×10^{-8}	6.45×10^{-8}	6.57×10^{-12}	3.54×10^{-13}	3.46×10^{-8}
Bone Surface	1.65×10^{-5}	3.81×10^{-8}	6.57×10^{-11}	2.63×10^{-6}	3.46×10^{-11}	1.41×10^{-10}	1.65×10^{-5}	1.65×10^{-5}	1.88×10^{-11}	4.25×10^{-12}	6.84×10^{-6}
Brain	1.13×10^{-7}	1.53×10^{-9}	2.97×10^{-13}	8.19×10^{-9}	4.75×10^{-13}	7.50×10^{-12}	6.45×10^{-8}	6.45×10^{-8}	3.75×10^{-14}	1.31×10^{-14}	3.46×10^{-8}
Breast	1.13×10^{-7}	1.54×10^{-9}	1.52×10^{-12}	8.19×10^{-9}	6.66×10^{-13}	9.04×10^{-12}	6.45×10^{-8}	6.45×10^{-8}	7.96×10^{-13}	4.38×10^{-14}	3.46×10^{-8}
Stomach Wall	1.16×10^{-7}	3.65×10^{-9}	2.13×10^{-10}	9.42×10^{-9}	7.32×10^{-10}	1.27×10^{-9}	6.49×10^{-8}	6.62×10^{-8}	2.52×10^{-10}	1.42×10^{-10}	3.54×10^{-8}
Small Intestine Wall	1.19×10^{-7}	5.22×10^{-9}	5.65×10^{-10}	9.18×10^{-9}	1.87×10^{-9}	5.66×10^{-10}	6.54×10^{-8}	6.59×10^{-8}	6.22×10^{-10}	3.21×10^{-10}	3.51×10^{-8}
Upper Large Intestine Wall	1.43×10^{-7}	1.34×10^{-8}	2.70×10^{-9}	1.37×10^{-8}	1.10×10^{-8}	2.17×10^{-10}	7.11×10^{-8}	7.13×10^{-8}	2.87×10^{-9}	1.41×10^{-9}	4.10×10^{-8}
Lower Large Intestine Wall	1.78×10^{-7}	1.49×10^{-8}	7.45×10^{-9}	3.51×10^{-8}	3.15×10^{-8}	3.28×10^{-11}	8.39×10^{-8}	8.39×10^{-8}	6.36×10^{-9}	2.48×10^{-9}	5.49×10^{-8}
Kidneys	3.49×10^{-7}	3.30×10^{-8}	2.54×10^{-11}	2.75×10^{-8}	1.40×10^{-11}	2.89×10^{-10}	2.74×10^{-6}	2.74×10^{-6}	1.53×10^{-11}	9.93×10^{-13}	5.22×10^{-8}
Liver	7.70×10^{-7}	1.00×10^{-8}	1.53×10^{-11}	1.42×10^{-7}	5.92×10^{-12}	3.20×10^{-11}	1.41×10^{-6}	1.41×10^{-6}	1.00×10^{-11}	7.20×10^{-13}	1.48×10^{-6}
Extrathoracic Airways	1.13×10^{-7}	1.53×10^{-9}	4.14×10^{-13}	8.19×10^{-9}	5.01×10^{-13}	7.65×10^{-12}	6.45×10^{-8}	6.45×10^{-8}	1.04×10^{-13}	1.45×10^{-14}	3.46×10^{-8}
Lung	1.13×10^{-7}	1.54×10^{-9}	2.58×10^{-12}	8.19×10^{-9}	7.91×10^{-13}	9.82×10^{-12}	6.45×10^{-8}	6.45×10^{-8}	1.52×10^{-12}	9.06×10^{-14}	3.46×10^{-8}
Muscle	1.13×10^{-7}	1.56×10^{-9}	1.94×10^{-11}	8.26×10^{-9}	2.94×10^{-12}	1.09×10^{-11}	6.45×10^{-8}	6.45×10^{-8}	1.21×10^{-11}	1.00×10^{-12}	3.46×10^{-8}
Ovaries	1.59×10^{-7}	1.77×10^{-9}	1.72×10^{-10}	9.79×10^{-9}	2.49×10^{-11}	2.09×10^{-11}	6.45×10^{-8}	6.45×10^{-8}	1.09×10^{-10}	1.37×10^{-11}	1.37×10^{-7}
Pancreas	1.13×10^{-7}	1.59×10^{-9}	2.01×10^{-11}	8.26×10^{-9}	3.00×10^{-12}	2.85×10^{-11}	6.45×10^{-8}	6.45×10^{-8}	1.45×10^{-11}	1.12×10^{-12}	3.46×10^{-8}

Table 2.4-14. Conversion Factors (Sv/yr per Bq/m3) for Calculating Annual Beta-Gamma Dose from Drinking 2 Liters of Water per Day (Continued)

Organ or Tissue	**^{232}Th = ^{228}Ra + ^{228}Th**	**^{232}U = ^{228}Th**	**^{237}Np**	**^{229}Th**	**^{228}U**	**^{226}Ra**	**^{210}Pb**	**^{226}Ra + ^{210}Pb**	**^{243}Am**	**^{235}U**	**^{227}Ac**
Red Bone Marrow	1.69×10^{-6}	4.86×10^{-9}	3.52×10^{-11}	2.54×10^{-7}	2.14×10^{-11}	2.38×10^{-11}	1.82×10^{-6}	1.82×10^{-6}	1.89×10^{-11}	1.35×10^{-12}	3.59×10^{-7}
Skin	1.13×10^{-7}	1.54×10^{-9}	6.15×10^{-12}	8.19×10^{-9}	1.27×10^{-12}	8.88×10^{-12}	6.45×10^{-8}	6.45×10^{-8}	3.60×10^{-12}	2.11×10^{-13}	3.46×10^{-8}
Spleen	1.14×10^{-7}	1.58×10^{-9}	1.59×10^{-11}	8.26×10^{-9}	2.41×10^{-12}	2.52×10^{-11}	2.06×10^{-6}	2.06×10^{-6}	1.10×10^{-11}	7.02×10^{-13}	3.47×10^{-8}
Testes	1.58×10^{-7}	1.55×10^{-9}	1.58×10^{-11}	9.79×10^{-9}	3.44×10^{-12}	8.28×10^{-12}	6.45×10^{-8}	6.45×10^{-8}	8.47×10^{-12}	4.13×10^{-13}	1.36×10^{-7}
Thymus	1.13×10^{-7}	1.54×10^{-9}	1.23×10^{-12}	8.19×10^{-9}	6.13×10^{-13}	8.65×10^{-12}	6.45×10^{-8}	6.45×10^{-8}	5.83×10^{-13}	3.16×10^{-14}	3.46×10^{-8}
Thyroid	1.13×10^{-7}	1.53×10^{-9}	4.14×10^{-13}	8.19×10^{-9}	5.01×10^{-13}	7.65×10^{-12}	6.45×10^{-8}	6.45×10^{-8}	1.04×10^{-13}	1.45×10^{-14}	3.46×10^{-8}
Uterus	1.13×10^{-7}	1.65×10^{-9}	7.82×10^{-11}	8.26×10^{-9}	1.03×10^{-11}	1.86×10^{-11}	6.45×10^{-8}	6.45×10^{-8}	5.14×10^{-11}	3.55×10^{-12}	3.46×10^{-8}
Urinary Bladder Wall	1.14×10^{-7}	1.71×10^{-9}	5.60×10^{-11}	8.26×10^{-9}	7.47×10^{-12}	1.44×10^{-11}	6.51×10^{-8}	6.51×10^{-8}	3.43×10^{-11}	2.09×10^{-12}	3.47×10^{-8}
Whole Body	5.14×10^{-7}	4.56×10^{-9}	6.41×10^{-10}	7.29×10^{-8}	2.48×10^{-9}	1.83×10^{-10}	5.09×10^{-7}	5.10×10^{-7}	5.84×10^{-10}	2.45×10^{-10}	2.36×10^{-7}

Source: SNL 2007y, Table 6.15-6.

Table 2.4-15. Data Table Showing Calculation of Mean and Standard Deviation of Gross Alpha Concentration

Location	Date	Gross Alpha (x_i) (pCi/L)	Uncertainty[a] ($2\sigma_i$) (pCi/L)	Sigma (σ_i) (pCi/L)	σ_i^2 $(pCi/L)^2$
NDOT Well	24-Jun-98	-0.08	1.56	0.780	0.608
NDOT Well	29-Jul-98	0.32	1.1	0.550	0.303
NDOT Well	23-Sep-98	-1.40	0.79	0.395	0.156
Gilgan's South Well	24-Jun-98	-0.63	0.86	0.430	0.185
Gilgan’s South Well	29-Jul-98	0.64	0.86	0.430	0.185
Gilgan's South Well	23-Sep-98	-0.74	0.69	0.345	0.119
UE-25 J-12	23-Jun-98	0.06	0.96	0.480	0.230
UE-25 J-12	28-Jul-98	0.27	0.72	0.360	0.130
UE-25 J-12	22-Sep-98	0.27	0.8	0.400	0.160
UE-25 J-13	23-Jun-98	0.05	0.94	0.470	0.221
UE-25 J-13	28-Jul-98	0.50	0.73	0.365	0.133
UE-25 J-13	22-Sep-98	-0.18	1.2	0.600	0.360
UE-25 c#2	23-Jun-98	1.20	1.33	0.665	0.442
UE-25 c#2	28-Jul-98	1.49	0.94	0.470	0.221
UE-25 c#2	22-Sep-98	0.73	1.67	0.835	0.697
Crystal Pool	22-Jun-98	1.04	1.27	0.635	0.403
Crystal Pool	27-Jul-98	1.75	1.64	0.820	0.672
Crystal Pool	25-Sep-98	-0.85	1.21	0.605	0.366
NDOT Well	FY 1997 first quarter	-0.14	2.63	1.315	1.729
NDOT Well	FY 1997 first quarter	-0.67	2.17	1.085	1.177
NDOT Well	FY 1997 third quarter	-2.61	2.14	1.070	1.145
NDOT Well	FY 1997 fourth quarter	1.26	2.57	1.285	1.651
Gilgan's South Well	FY 1997 first quarter	-0.94	1.36	0.680	0.462
Gilgan's South Well	FY 1997 second quarter	-1.05	1.29	0.645	0.416

Table 2.4-15. Data Table Showing Calculation of Mean and Standard Deviation of Gross Alpha Concentration (Continued)

Location	Date	Gross Alpha (x_i) (pCi/L)	Uncertainty[a] ($2\sigma_i$) (pCi/L)	Sigma (σ_i) (pCi/L)	σ_i^2 $(\text{pCi/L})^2$
Gilgan's South Well	FY 1997 Third quarter	0.96	2.18	1.090	1.188
Gilgan's South Well	FY 1997 fourth quarter	1.40	2.00	1.000	1.000
Crystal Pool	FY 1997 first quarter	-1.56	2.91	1.455	2.117
Crystal Pool	FY 1997 second quarter	-0.57	2.89	1.445	2.088
Crystal Pool	FY 1997 third quarter	0.49	3.48	1.740	3.028
Crystal Pool	FY 1997 fourth quarter	-1.01	2.70	1.350	1.823
UE-25 c#3	FY 1997 first quarter	-2.67	1.67	0.835	0.697
UE-25 c#3	FY 1997 second quarter	1.43	1.87	0.935	0.874
UE-25 c#3	FY 1997 third quarter	4.57	2.71	1.355	1.836
UE-25 c#3	FY 1997 fourth quarter	2.02	2.02	1.010	1.020
UE-25 J-12	FY 1997 first quarter	-0.79	1.47	0.735	0.540
UE-25 J-12	FY 1997 second quarter	0.13	1.49	0.745	0.555
UE-25 J-12	FY 1997 third quarter	-4.52	15.6	7.800	60.840
UE-25 J-12	FY 1997 fourth quarter	-0.51	1.39	0.695	0.483
UE-25 J-13	FY 1997 first quarter	-1.06	1.55	0.775	0.601
UE-25 J-13	FY 1997 second quarter	0.00	1.52	0.760	0.578
UE-25 J-13	FY 1997 third quarter	-0.36	1.72	0.860	0.740
UE-25 J-13	FY 1997 fourth quarter	0.98	1.80	0.900	0.810

Table 2.4-15. Data Table Showing Calculation of Mean and Standard Deviation of Gross Alpha Concentration (Continued)

Location	Date	Gross Alpha (x_i) (pCi/L)	Uncertainty[a] ($2\sigma_i$) (pCi/L)	Sigma (σ_i) (pCi/L)	σ_i^2 $(pCi/L)^2$
UE-25 J-12[b]	26-Jan-00	3.02	1.11	0.555	0.308
UE-25 J-12[b]	19-Apr-00	1.64	1.00	0.500	0.250
UE-25 J-12[b]	19-Apr-00	2.13	0.98	0.490	0.240
UE-25 J-12[b]	25-Jul-00	1.12	0.96	0.480	0.230
UE-25 J-12[b]	24-Oct-00	0.57	0.38	0.190	0.036
UE-25 J-13[b]	26-Jan-00	3.34	1.13	0.565	0.319
UE-25 J-13[b]	25-Jul-00	1.94	1.04	0.520	0.270
UE-25 J-13[b]	24-Oct-00	0.53	0.85	0.425	0.181
Amargosa Valley RV Park[b]	14-Nov-00	-0.99	0.50	0.250	0.063
Crystal Pool[b]	16-Jun-00	2.76	2.22	1.110	1.232
Crystal Pool[b]	16-Nov-00	3.03	0.90	0.450	0.203
UE-25 J-12[b]	7-Feb-01	0.81	1.01	0.505	0.255
UE-25 J-12[b]	4-Apr-01	0.55	0.946	0.473	0.224
UE-25 J-12[b]	1-Aug-01	-0.10	1.03	0.515	0.265
UE-25 J-12[b]	31-Oct-01	1.56	0.84	0.420	0.176
UE-25 J-13[b]	7-Feb-01	1.02	1.08	0.540	0.292
UE-25 J-13[b]	4-Apr-01	0.18	0.976	0.488	0.238
UE-25 J-13[b]	1-Aug-01	0.92	0.936	0.468	0.219
UE-25 J-13[b]	31-Oct-01	0.60	0.9	0.450	0.203
Crystal Pool[b]	23-Jul-01	1.83	2.13	1.065	1.134
UE-25 J-12[b]	20-Feb-02	1.36	1.58	0.790	0.624
UE-25 J-12[b]	24-Apr-02	1.09	1.08	0.540	0.292
UE-25 J-12[b]	17-Jul-02	-0.33	1.12	0.560	0.314
UE-25 J-12[b]	16-Oct-02	0.41	1.56	0.780	0.608
UE-25 J-13[b]	20-Feb-02	1.62	1.82	0.910	0.828
UE-25 J-13[b]	24-Apr-02	2.20	1.45	0.725	0.526
UE-25 J-13[b]	17-Jul-02	0.64	1.80	0.900	0.810
UE-25 J-13[b]	16-Oct-02	1.63	1.73	0.865	0.748

Table 2.4-15. Data Table Showing Calculation of Mean and Standard Deviation of Gross Alpha Concentration (Continued)

Location	**Date**	**Gross Alpha (x_i) (pCi/L)**	**Uncertainty[a] ($2\sigma_i$) (pCi/L)**	**Sigma (σ_i) (pCi/L)**	**σ_i^2 $(pCi/L)^2$**
Crystal Pool[b]	18-Apr-02	2.83	2.22	1.110	1.232
Amargosa Valley RV Park[b]	20-Aug-03	-1.15	0.873	0.437	0.191
Crystal Pool[b]	13-Aug-03	0.21	0.673	0.337	0.113
UE-25 J-12[b]	29-Jan-03	1.33	0.730	0.365	0.133
UE-25 J-12[b]	30-Apr-03	0.30	0.642	0.321	0.103
UE-25 J-12[b]	2-Jul-03	-0.33	0.424	0.212	0.045
UE-25 J-12[b]	8-Oct-03	0.04	0.753	0.377	0.142
UE-25 J-13[b]	29-Jan-03	1.62	1.17	0.585	0.342
UE-25 J-13[b]	8-Oct-03	0.27	0.710	0.355	0.126
Average of all sources		Mean Gross Alpha, $\bar{x}$ = 0.50 pCi/L Standard Deviation, $\sigma_{\bar{x}}$ = 0.13 pCi/L			

NOTE: [a] Uncertainty is defined as being two standard deviations (sigma).
[b] Estimated values of gross alpha concentration have been approximately corrected for uranium concentration, as described in SNL (2008f, Section 6.8.6).

Source: SNL 2008f, Table 6-19.

Table 2.4-16. Summary of Alpha Concentration Results in Amargosa Valley Groundwater

Parameter	Expected Value (pCi/L)	Upper (95%) Limit (pCi/L)
Gross Alpha Concentration	0.50	0.71
Combined Concentration of ^{226}Ra and ^{228}Ra	0.50	0.71

Source: SNL 2008f, Table 6-20.

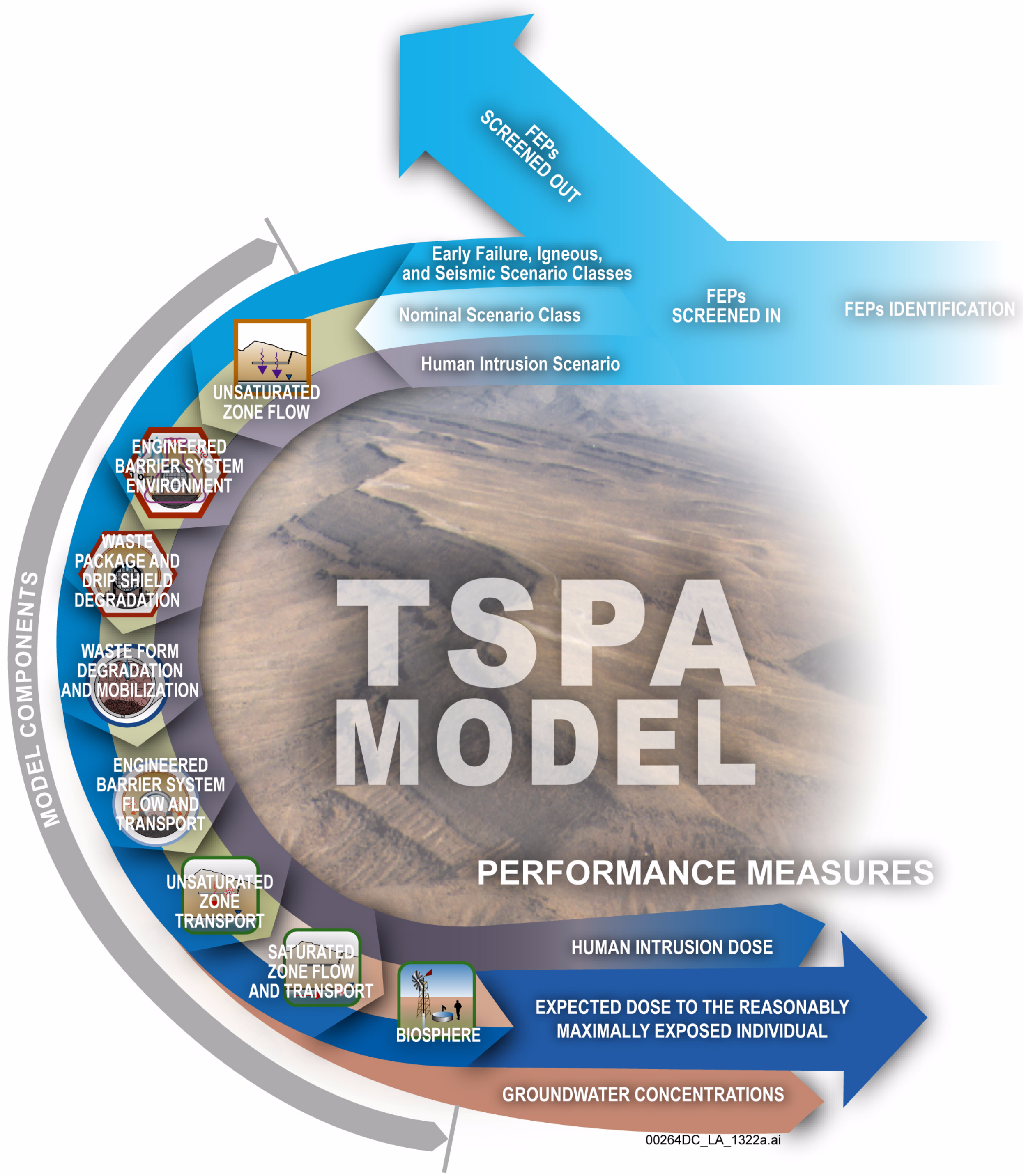

Figure 2.4-1. Schematic Representation of the Development of the TSPA Model, Including the Nominal, Early Failure, Igneous, and Seismic Scenario Classes, as Well as the Human Intrusion Scenario

NOTE: FEPs = features, events, and processes; TSPA = total system performance assessment.

Source: Modified from SNL 2008a, Figure 1-3.

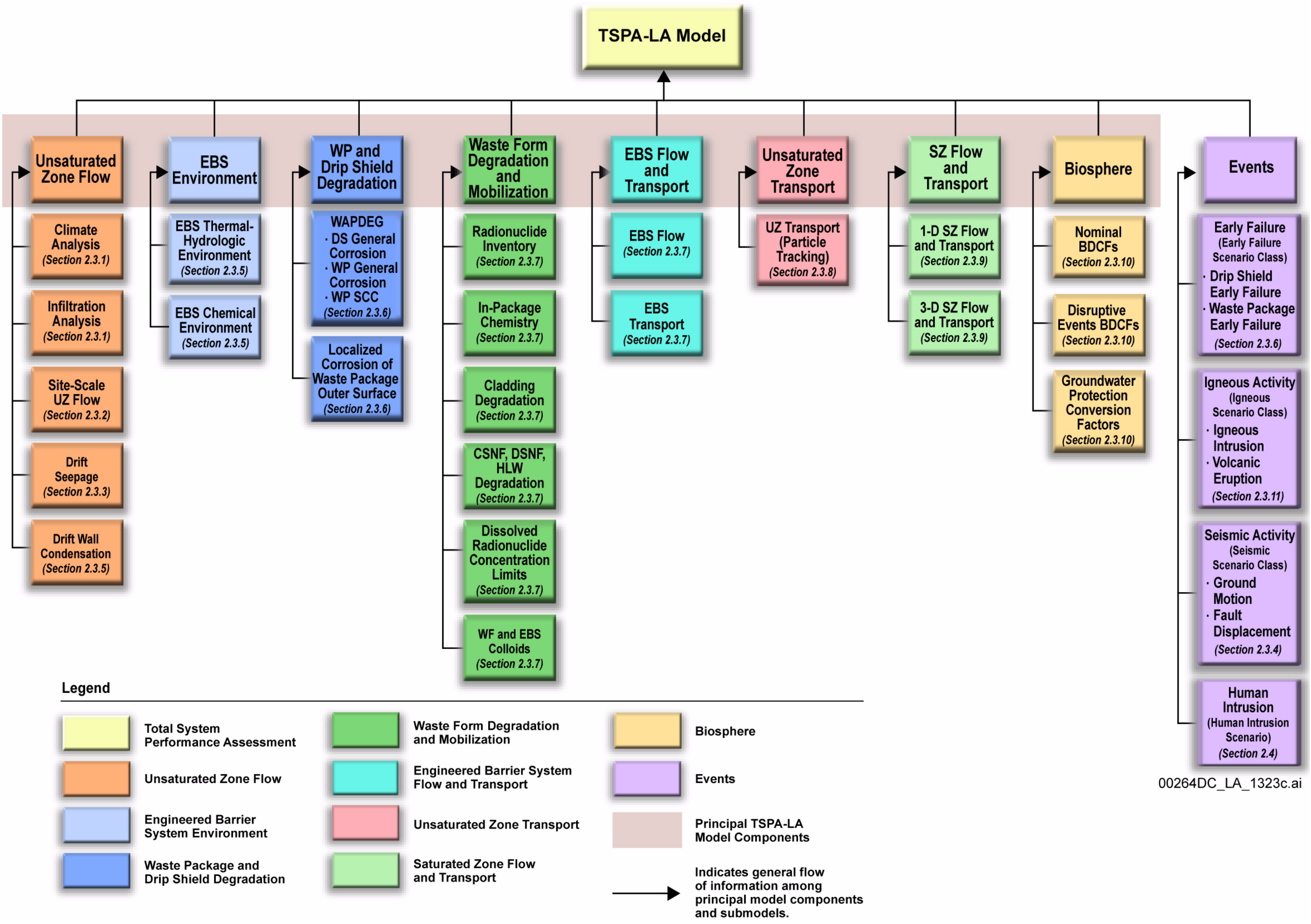

00264DC_LA_1323c.ai

Figure 2.4-2. TSPA Principal Model Components and Submodels

NOTE: DS = drip shield; LC = localized corrosion; MSTHM = multiscale thermal-hydrologic model; PA = performance assessment; RH = relative humidity; SZ = saturated zone; TH = thermal-hydrologic; THC = thermal-hydrologic-chemical; UZ = unsaturated zone; WF = waste form; WP = waste package.

Source: Modified from SNL 2008a, Figure 6-1.

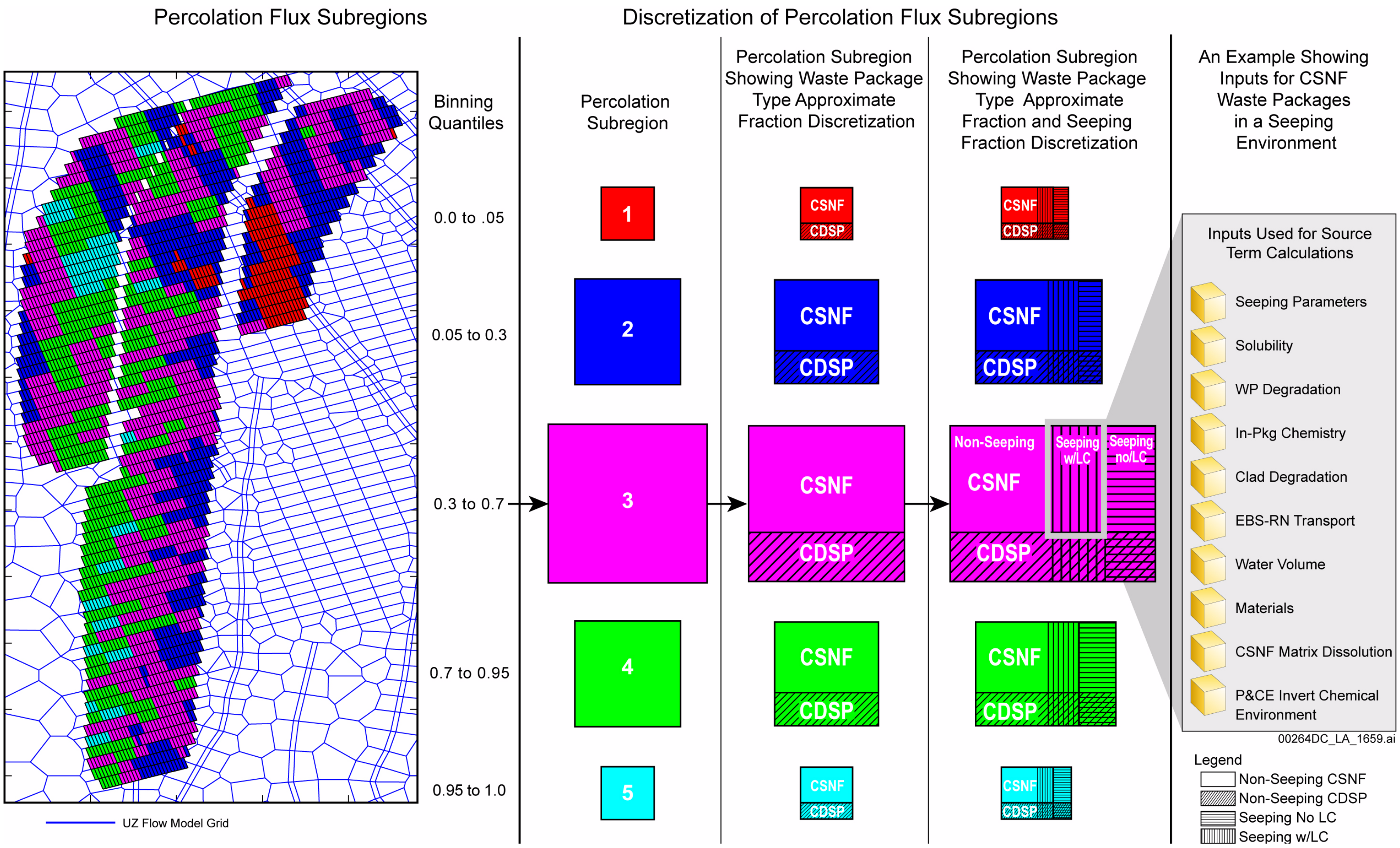

Figure 2.4-3. Schematic of the Five Repository Percolation Subregions and the Implementation of the Engineered Barrier System Representation in the TSPA Model Involving Discretizations of the Submodels by Waste Type, Percolation Subregion, and Seepage Environment

NOTE: CDSP = codisposal waste package; CSNF = commercial spent nuclear fuel; EBS-RN = engineered barrier system-radionuclide; LC= localized corrosion; P & CE = physical and chemical environment; WP = waste package.

Source: SNL 2008a, Figure 6.1.5-11.

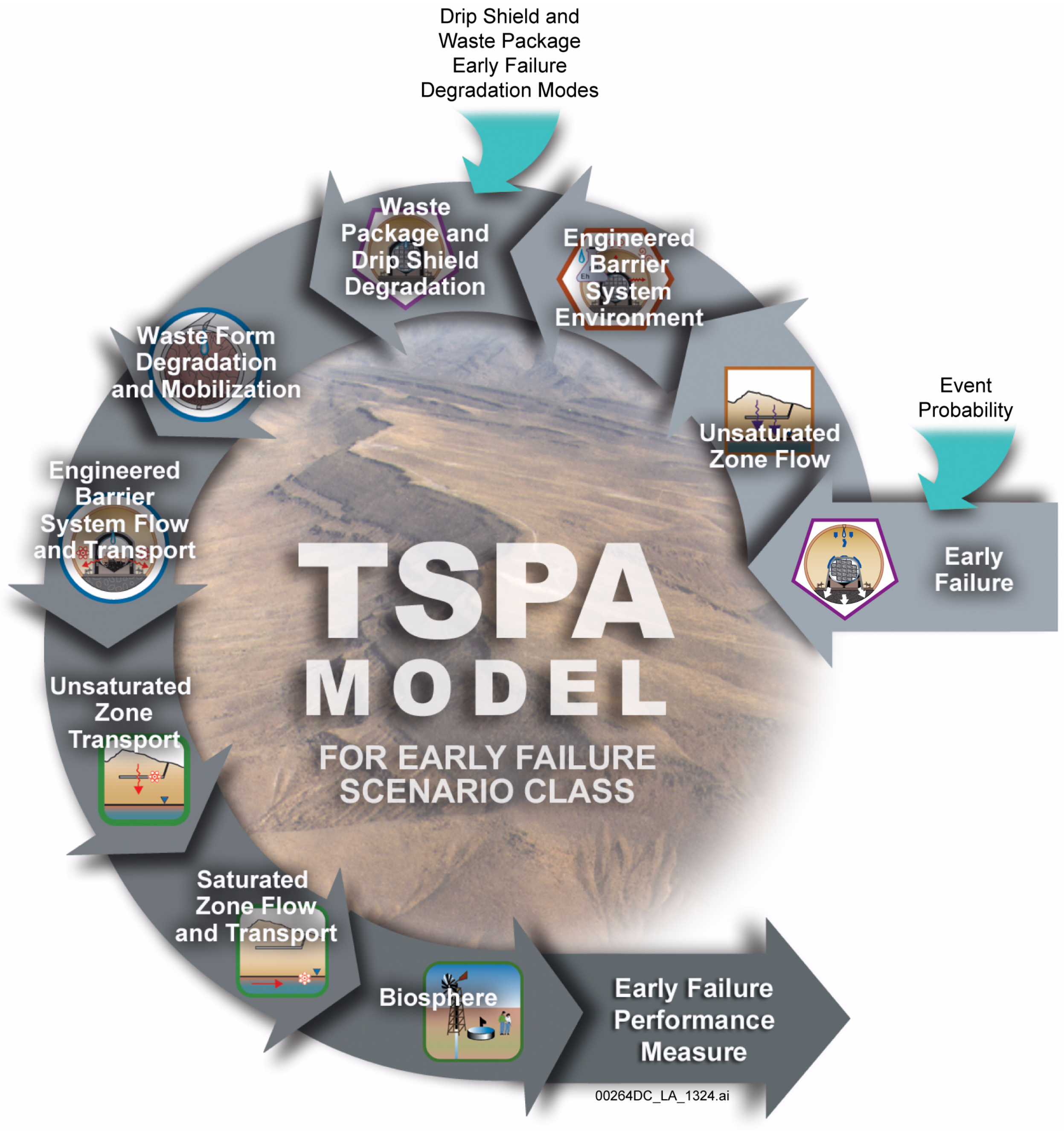

Figure 2.4-4. TSPA Model Components for the Early Failure Scenario Case

Source: Modified from SNL 2008a, Figure 6.4-1

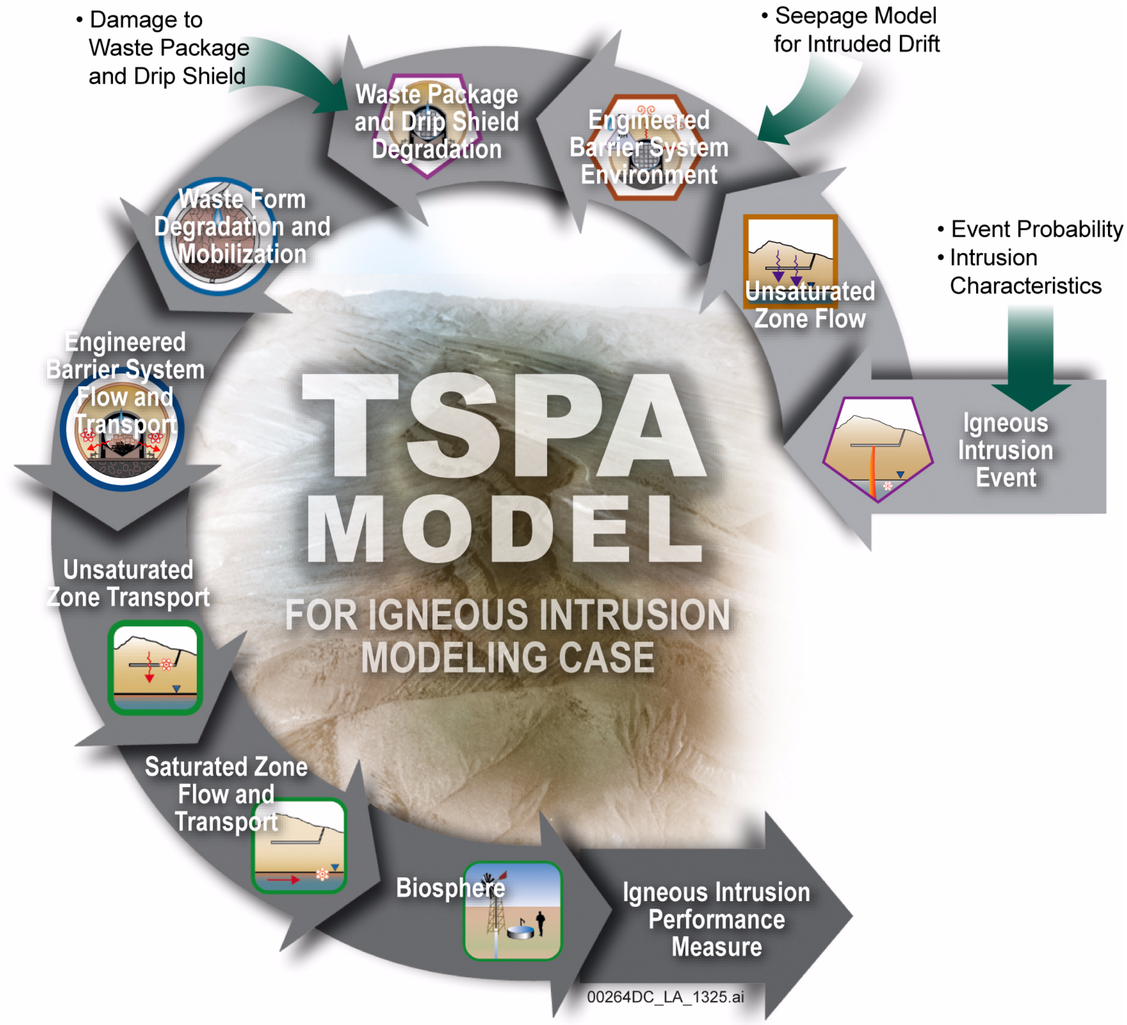

Figure 2.4-5. TSPA Model Components for the Igneous Intrusion Modeling Case

Source: SNL 2008a, Figure 6.1.1-5.

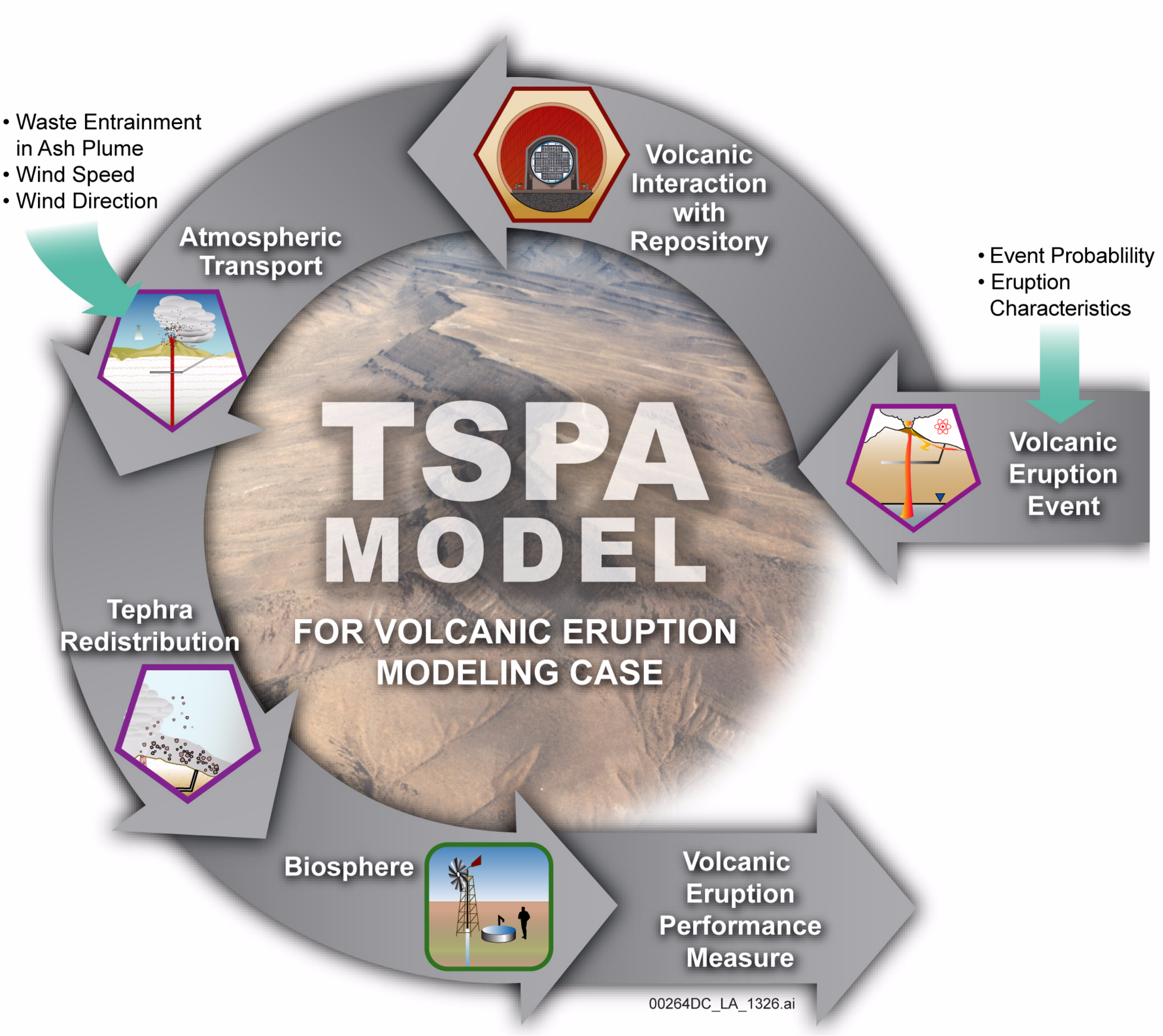

Figure 2.4-6. TSPA Model Components for the Volcanic Eruption Modeling Case

Source: SNL 2008a, Figure 6.1.1-6.

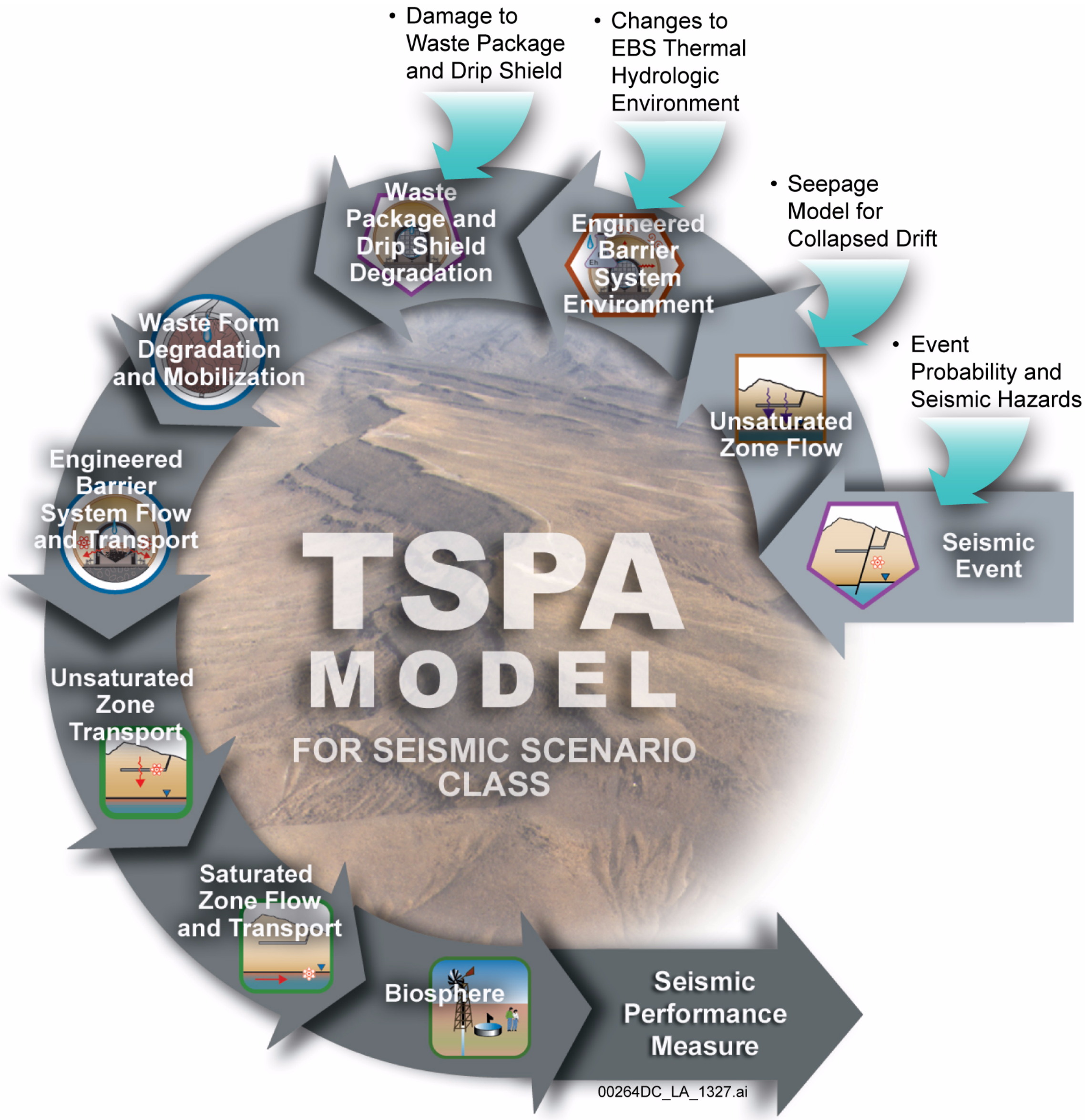

Figure 2.4-7. TSPA Model Components for the Seismic Scenario Class

Source: SNL 2008a, Figure 6.1.1-7.

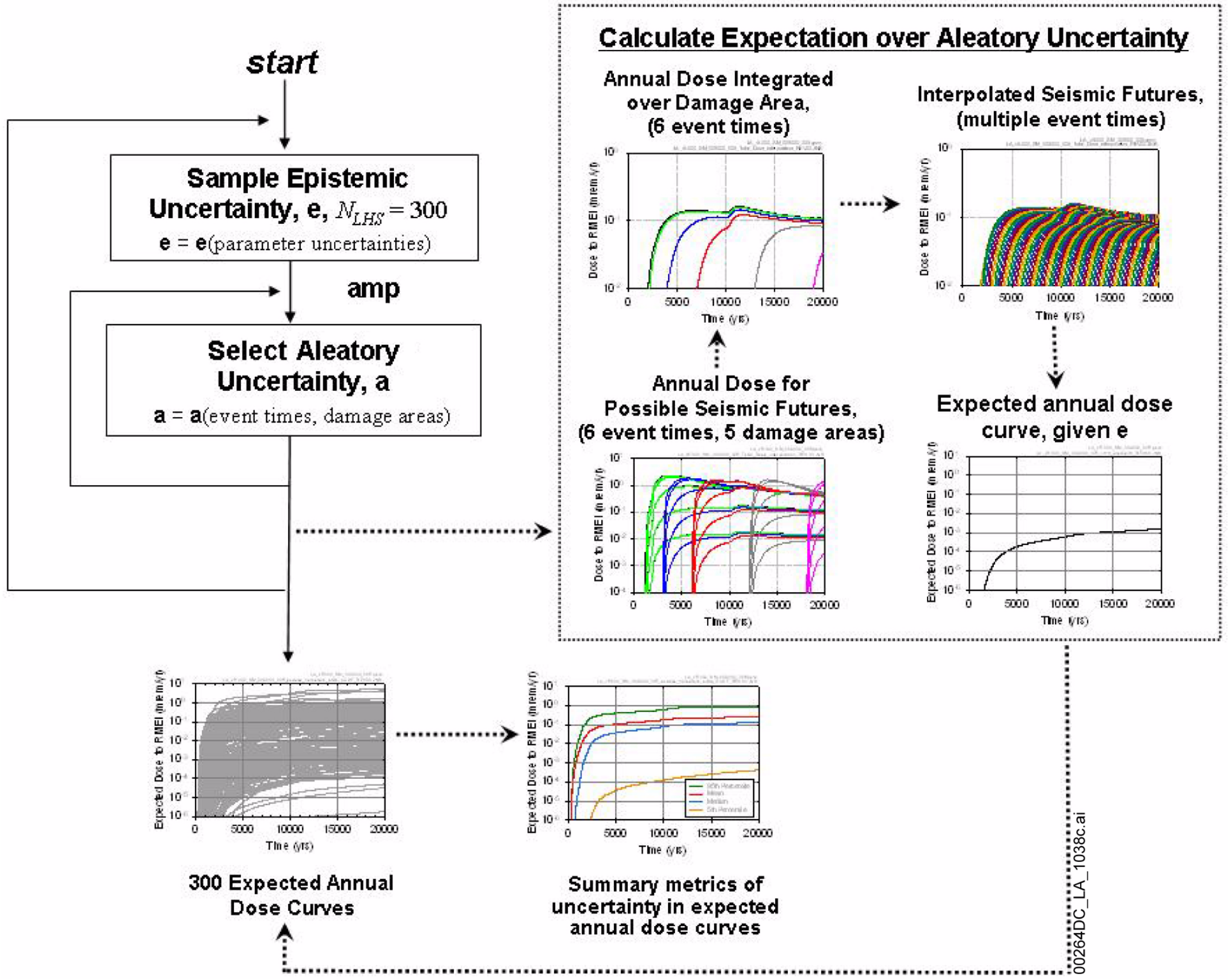

Figure 2.4-8. Computational Strategy for Computing the Expected Annual Dose and Associated Summary Metrics for the 10,000-Year Seismic Ground Motion Modeling Case

NOTE: Methodology and results shown out to 20,000 years (SNL 2008a, Appendix J8.3).

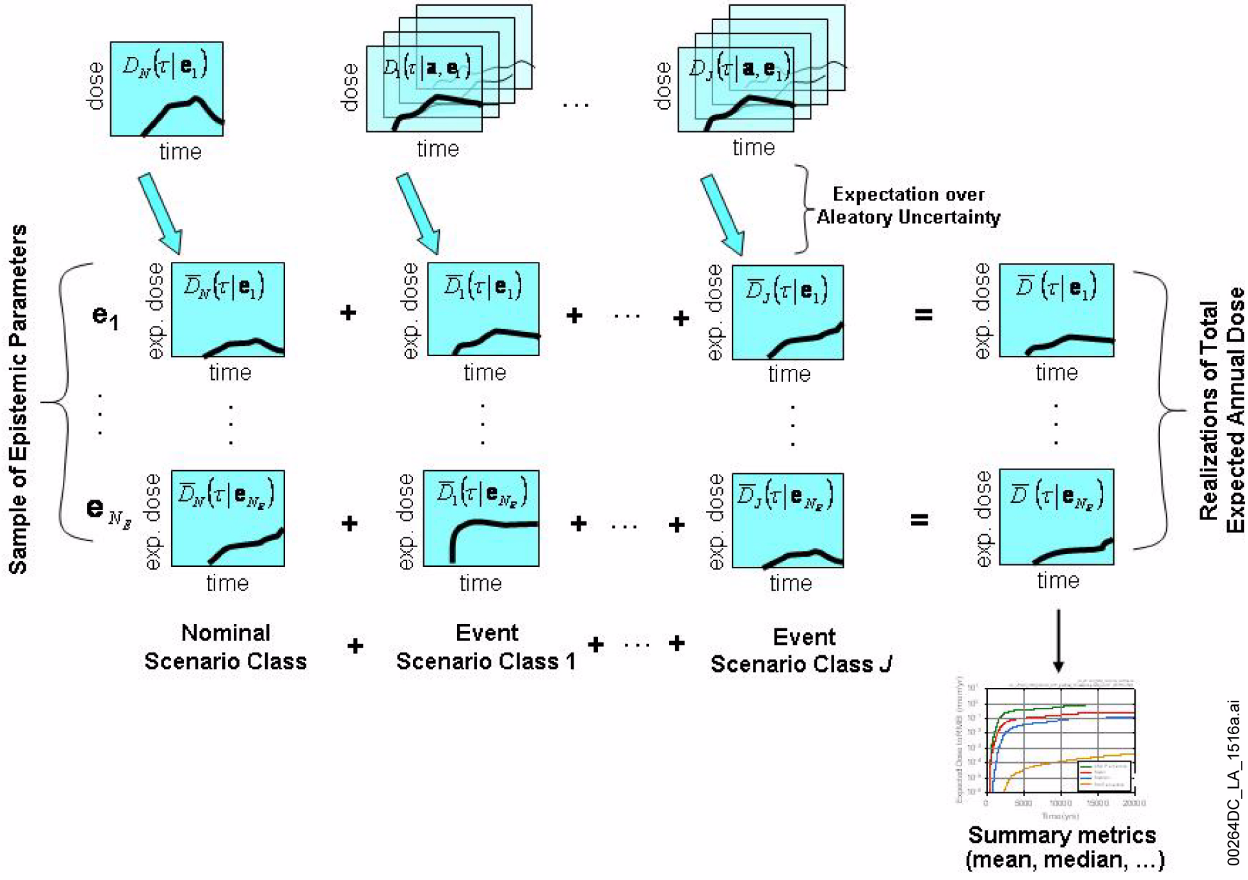

Figure 2.4-9. Computational Strategy for Computing The Total Expected Annual Dose (Expectation Over Aleatory Uncertainty) as a Sum of Expected Annual Doses for Each Event Scenario Class (or Each Modeling Case)

NOTE: $\bar{D}(\tau, \mathbf{e}_i)$ = total expected annual dose at time t, for epistemic sample $\mathbf{e}_i$. $D_J(\tau, \mathbf{a}, \mathbf{e}_i)$ = annual dose for event scenario class *J* (or modeling case *J*), for epistemic sample $\mathbf{e}_i$ and aleatory vector $\mathbf{a}$.

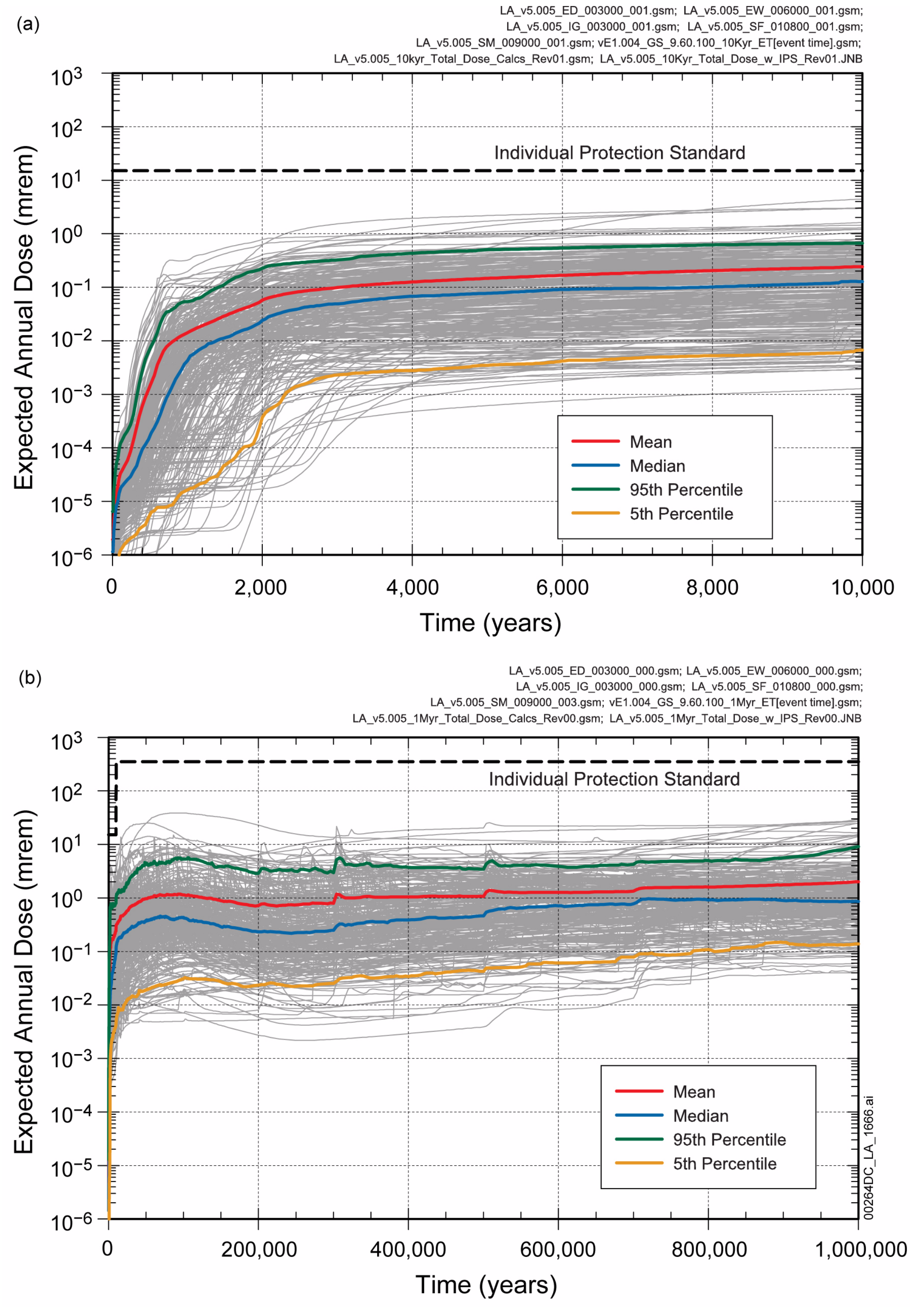

Figure 2.4-10. Distribution of Total Expected Annual Dose for (a) 10,000 Years and (b) 1 Million Years after Repository Closure

NOTE: The individual protection standard in Figure 2.4-10b is based on proposed 10 CFR 63.311.

Source: Modified from SNL 2008a, Figures 8.1-1[a] and 8.1-2[a].

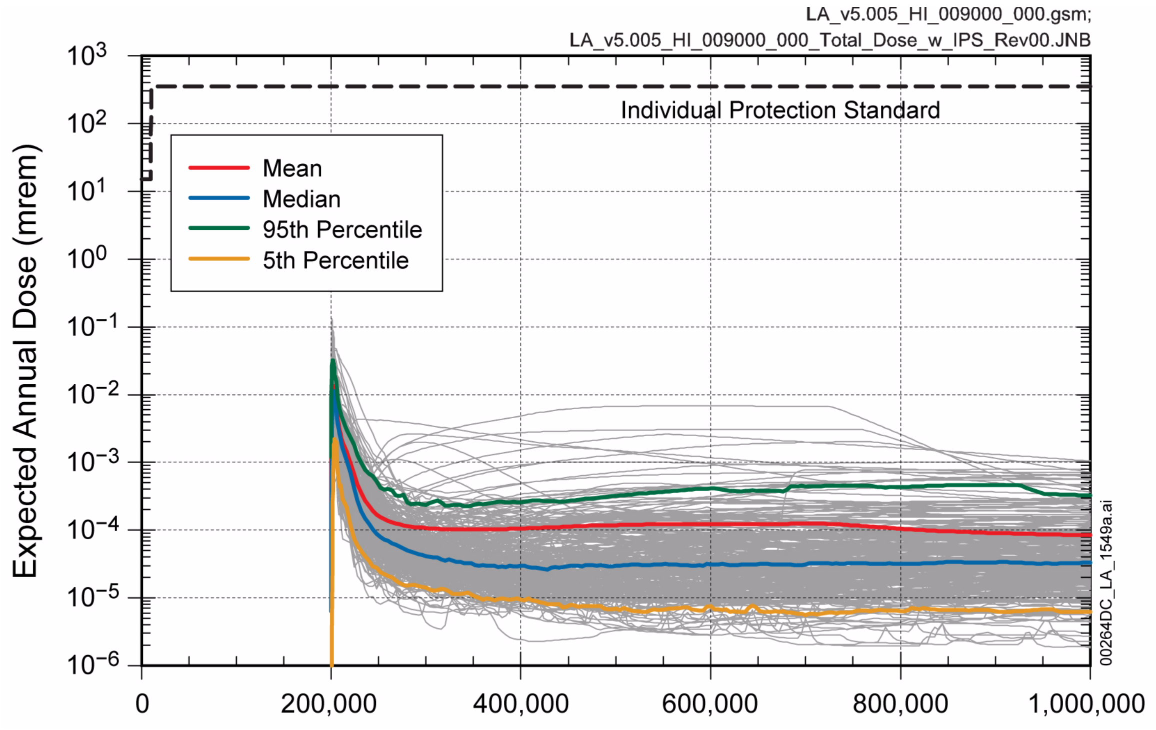

Figure 2.4-11. Distribution of Expected Annual Dose for the Human Intrusion Modeling Case for the Post-10,000 Year Period after Permanent Closure, with Drilling Intrusion Event at 200,00 Years

NOTE: The individual protection standard in this figure is based on proposed 10 CFR 63.321.

Source: Modified from SNL 2008a, Figure 8.1-16[a].

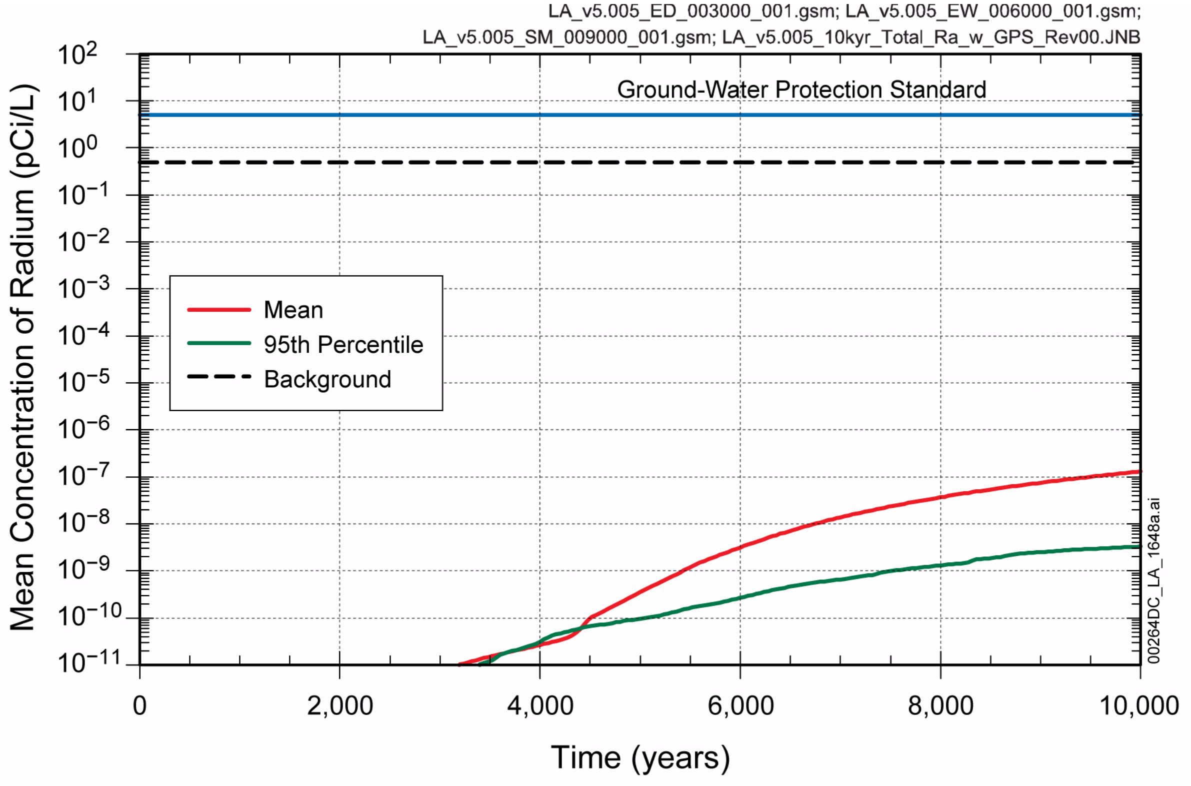

Figure 2.4-12. Activity Concentrations for Total Radium (^{226}Ra and ^{228}Ra) in Groundwater, Excluding Natural Background, for 10,000 Years after Repository Closure

Source: Modified from SNL 2008a,Figure 8.1-9[a].

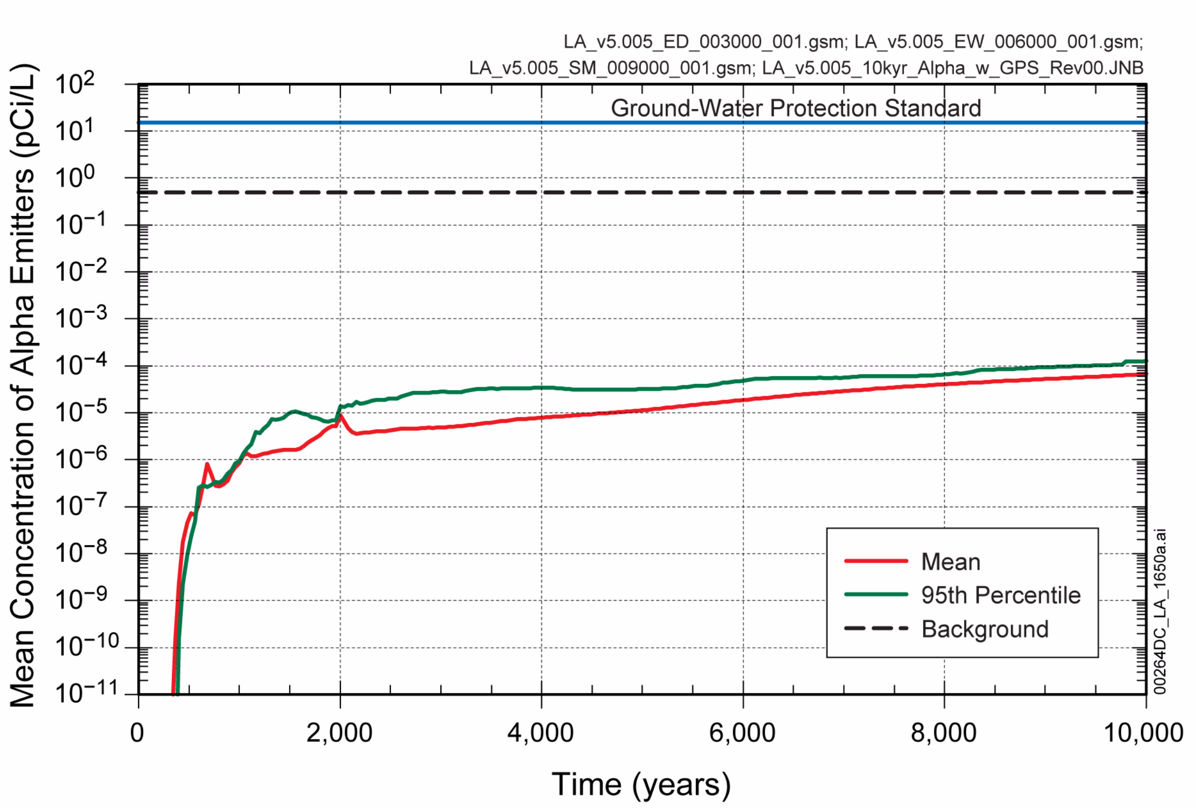

Figure 2.4-13. Summary Statistics for Activity Concentration of Gross Alpha (Including ^{226}Ra but Excluding Radon and Uranium) in Groundwater for 10,000 Years after Repository Closure

Source: Modified from SNL 2008a, 8.1-11[a].

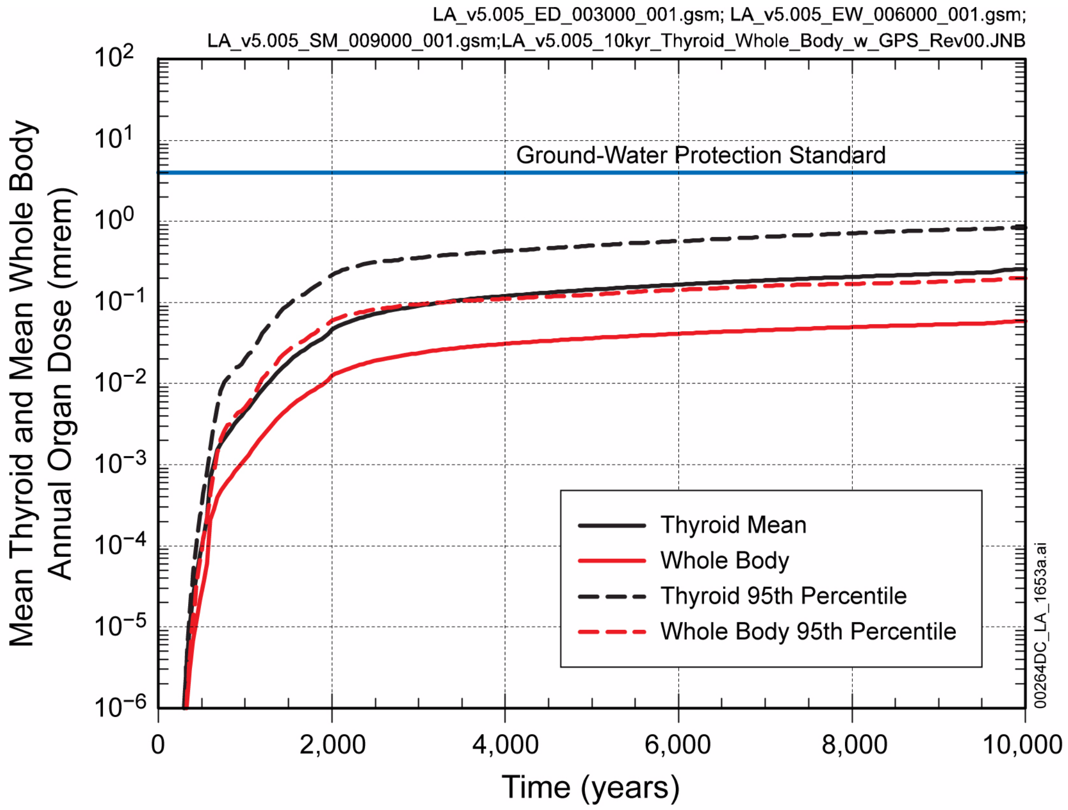

Figure 2.4-14. Summary Statistics for Annual Drinking Water Doses for Combined Beta and Photon Emitting Radionuclides for 10,000 Years after Repository Closure

Source: Modified from SNL 2008a, 8.1-14[a].

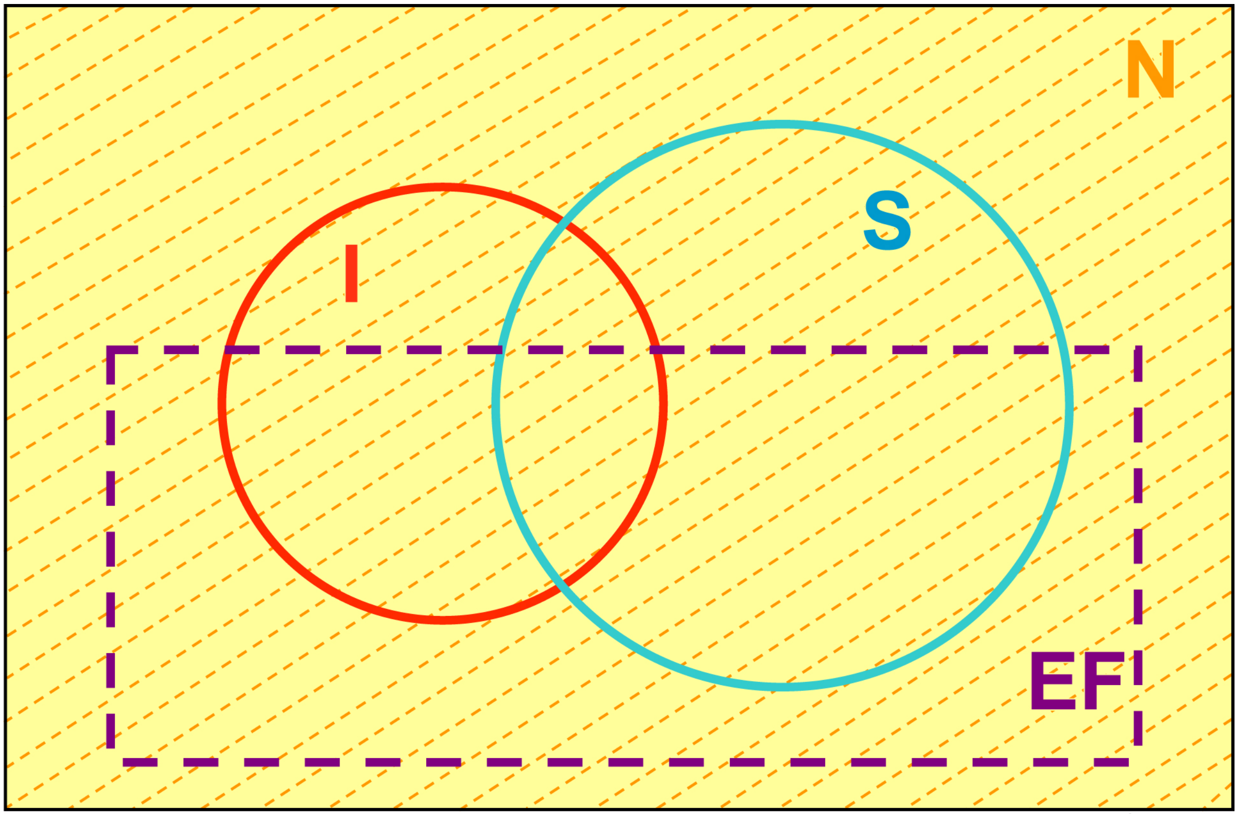

Figure 2.4-15. Sets of Futures or Event Classes Associated with Disruptive Events: Igneous (Red), Seismic (Blue), and Early Failure (Purple) Event Classes

NOTE: The cross-hatching indicates that nominal processes occur in each event class.
N = nominal event class; I = igneous event class; S = seismic event class; EF = early failure event class.

Source: SNL 2008b, Figure 6-2.

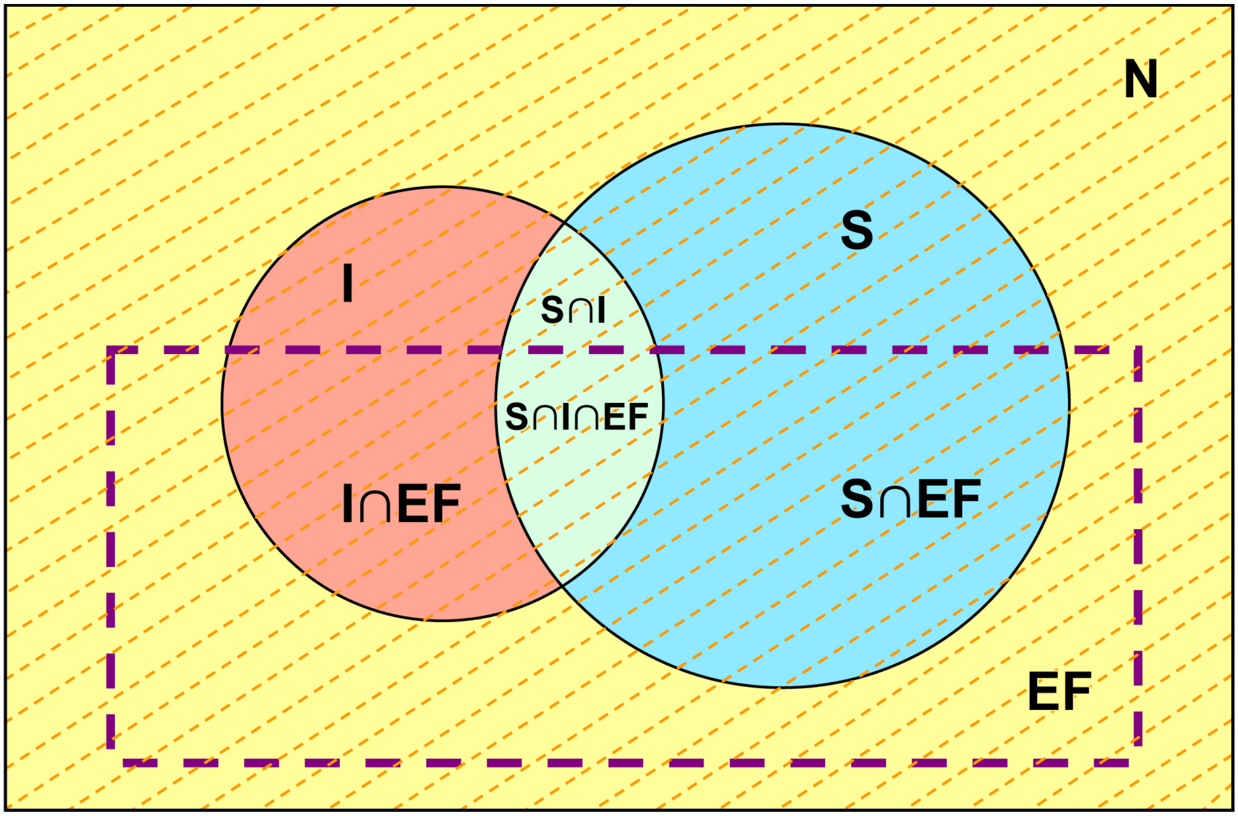

00264DC_LA_1453.ai

Figure 2.4-16. Sets of Disjoint Scenario Classes or Subsets Associated with Igneous, Seismic, and Early-Failure Events for the 10,000-Year Postclosure Period: Nominal, Seismic, Igneous, Early-Failure, Seismic/Igneous, Seismic/Early-Failure, Igneous/Early-Failure, and Seismic/Igneous/Early-Failure

NOTE: The cross-hatching indicates that nominal processes occur in each scenario class.
N = nominal event class; I = igneous event class; S = seismic event class; EF = early failure event class.

Source: SNL 2008b, Figure 6-3.

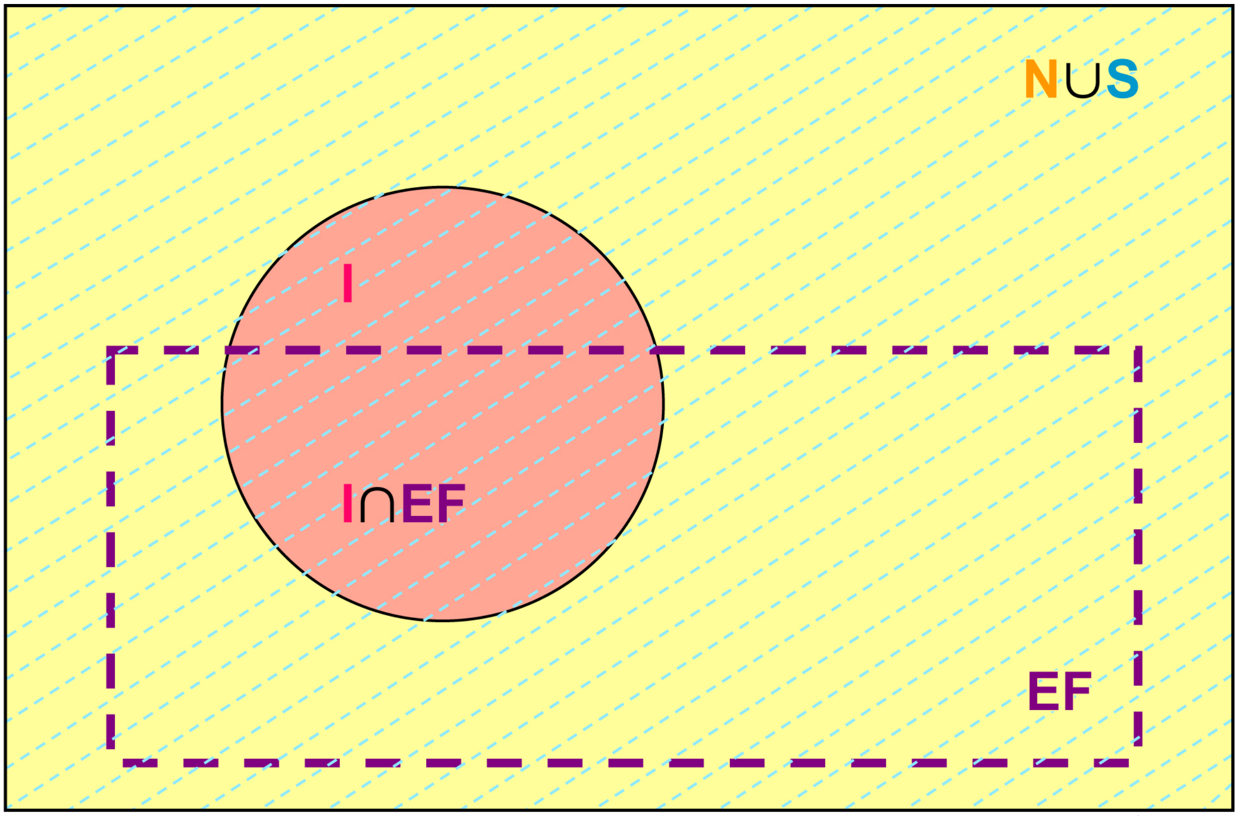

00264DC_LA_1454.ai

Figure 2.4-17. Sets of Disjoint Scenario Classes or Subsets Associated with Igneous, Seismic, and Early-Failure Events for the Post-10,000-Year Period: Nominal-Seismic, Igneous, Early-Failure, and Igneous/Early-Failure Scenario Classes

NOTE: The cross-hatching indicates that nominal processes and seismic events occur in each scenario class. N = nominal event class; I = igneous event class; S = seismic event class; EF = early failure event class.

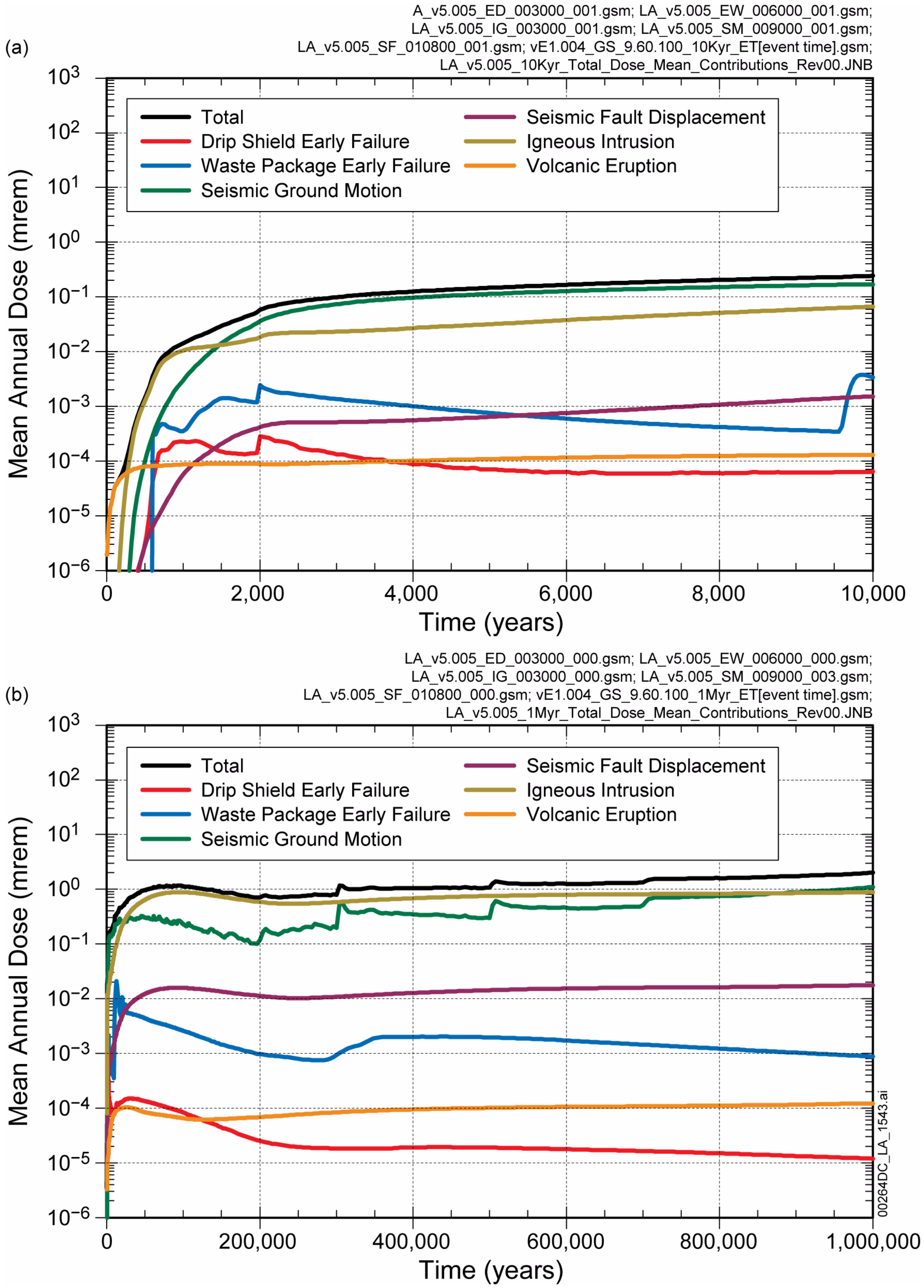

Figure 2.4-18. Relative Contributions of Modeling Cases to Total Mean Annual Dose for (a) 10,000 Years and (b) 1 Million Years after Repository Closure

Source: SNL 2008a, Figure 8.1-3[a].

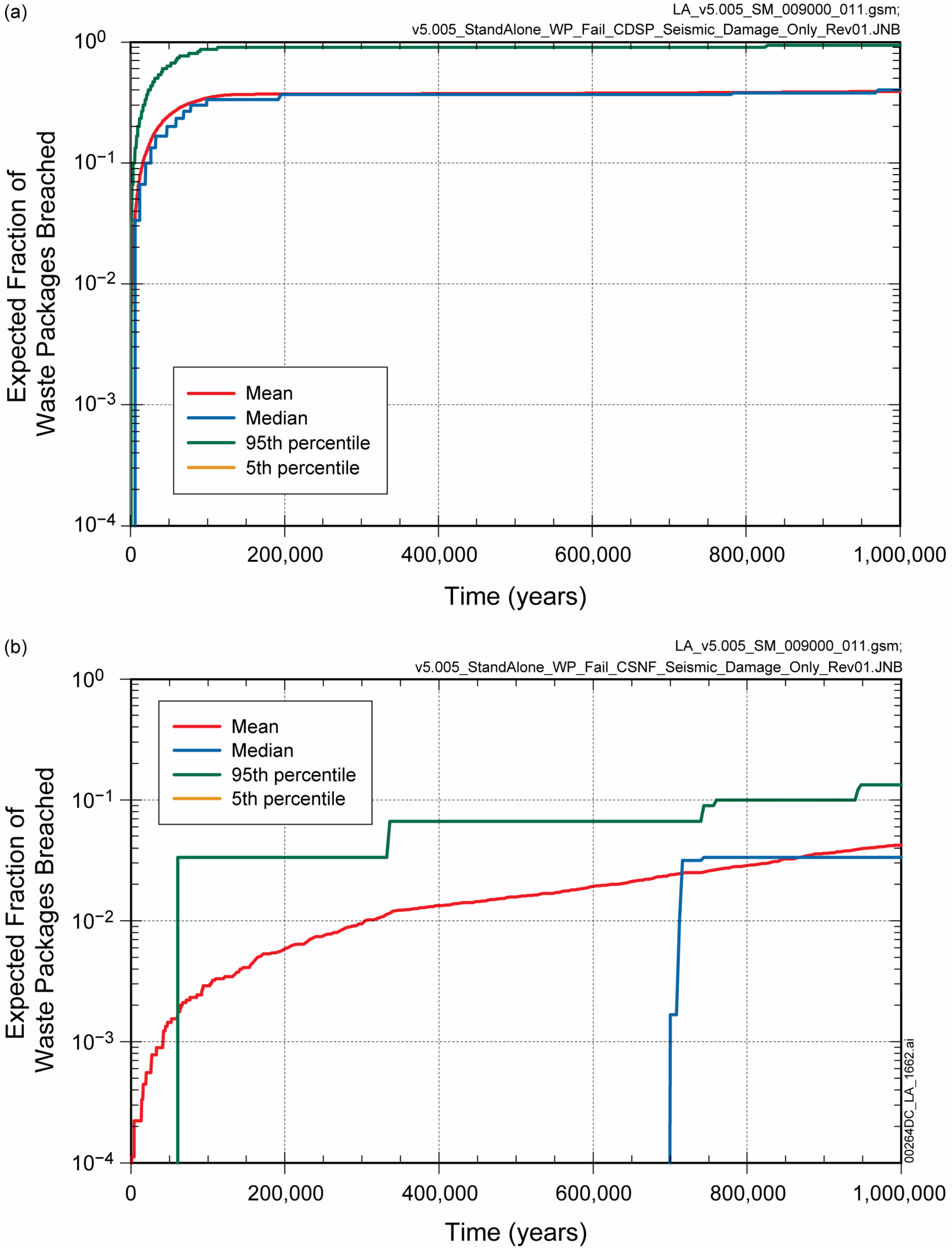

Figure 2.4-19. Expected Fraction of (a) Codisposal Waste Packages Failed and (b) Commercial SNF Waste Packages Failed by Seismic Damage for Percolation Subregion 3

Source: SNL 2008a, Figure 8.1-5[a].

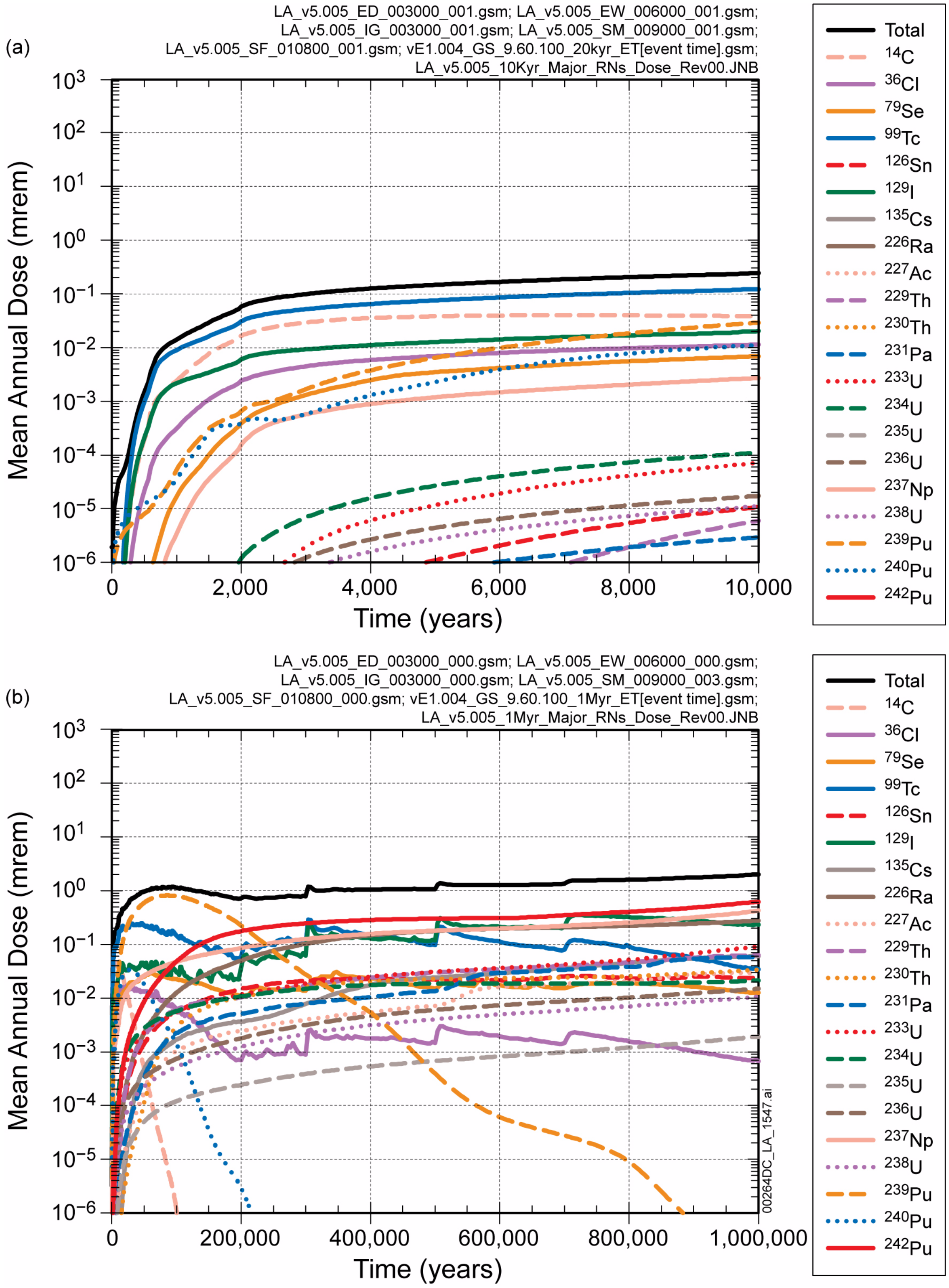

Figure 2.4-20. Contribution of Individual Radionuclides to Total Mean Annual Dose for (a) 10,000 Years and (b) 1 Million Years after Repository Closure

Source: SNL 2008a, Figures 8.1-6[a] and 8.1-7[a].

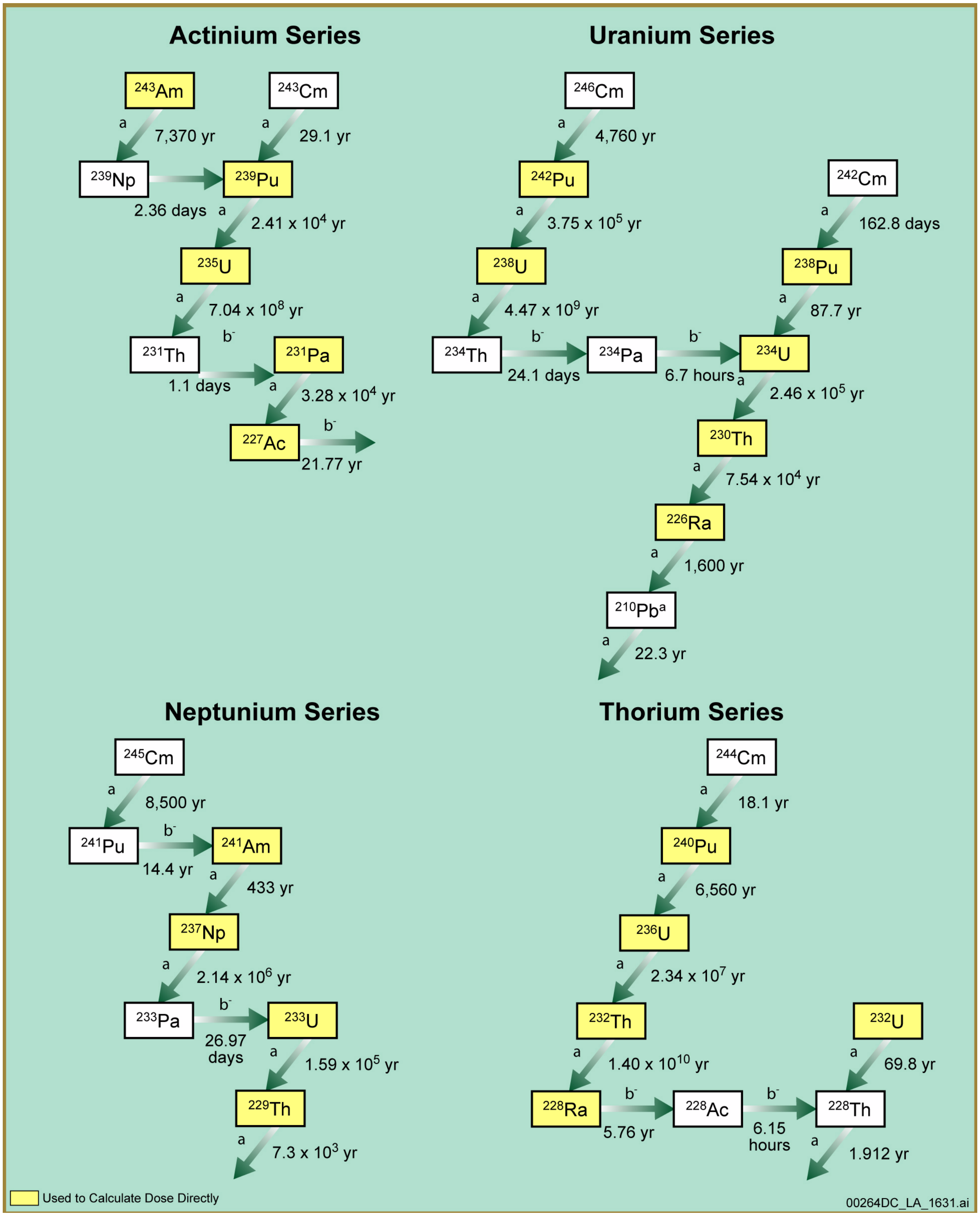

Figure 2.4-21. Radioactive Decay Series of the Actinide Elements

Source: SNL 2008a, Figure 6.3.7-4.

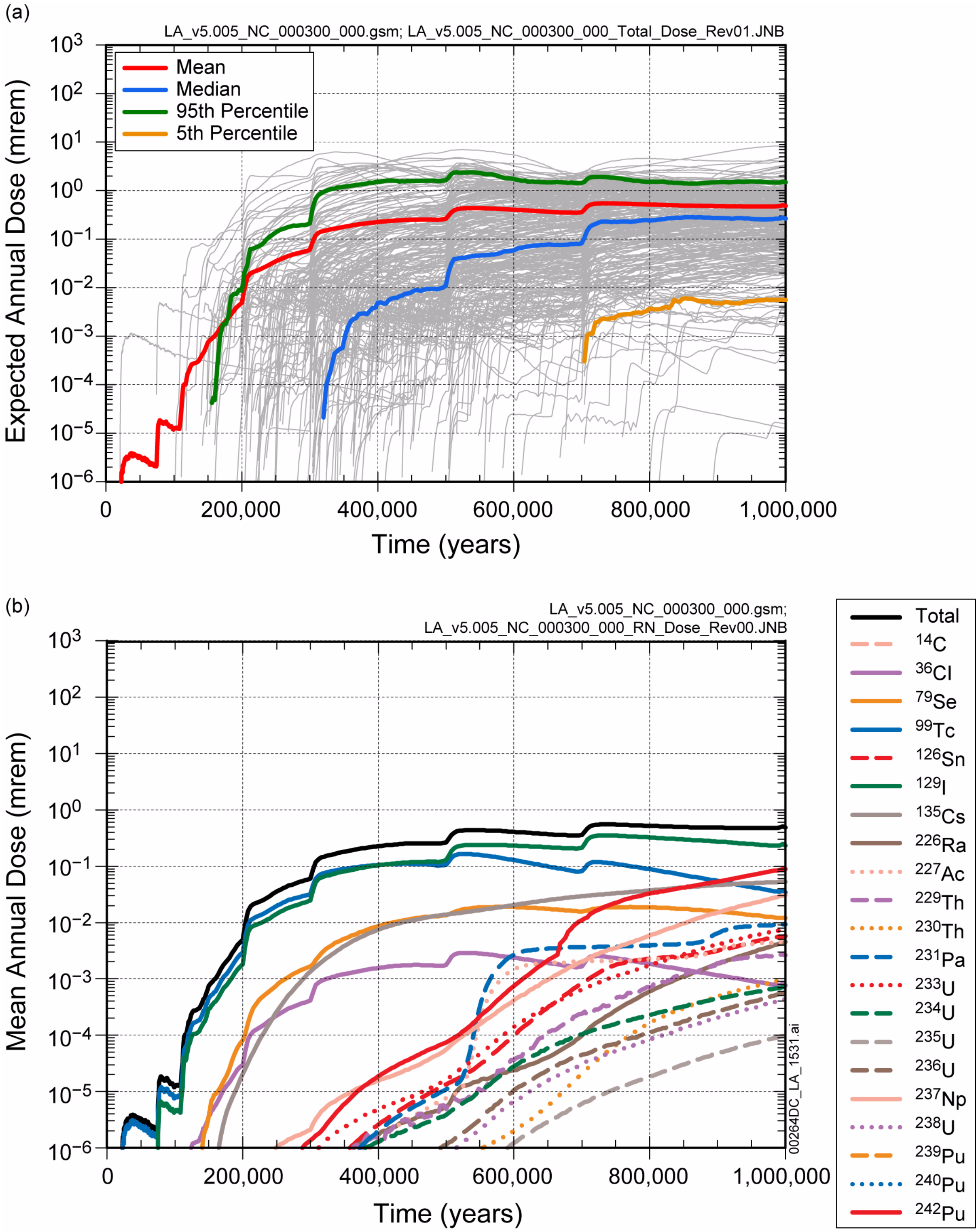

Figure 2.4-22. (a) Distribution of Expected Annual Dose for the Nominal Modeling Case for 1 Million Years after Repository Closure and (b) Contribution of Individual Radionuclides to Mean Annual Dose for the Nominal Modeling Case for 1 Million Years after Repository Closure

Source: SNL 2008a, Figures 8.2-1[a] and 8.2-2[a].

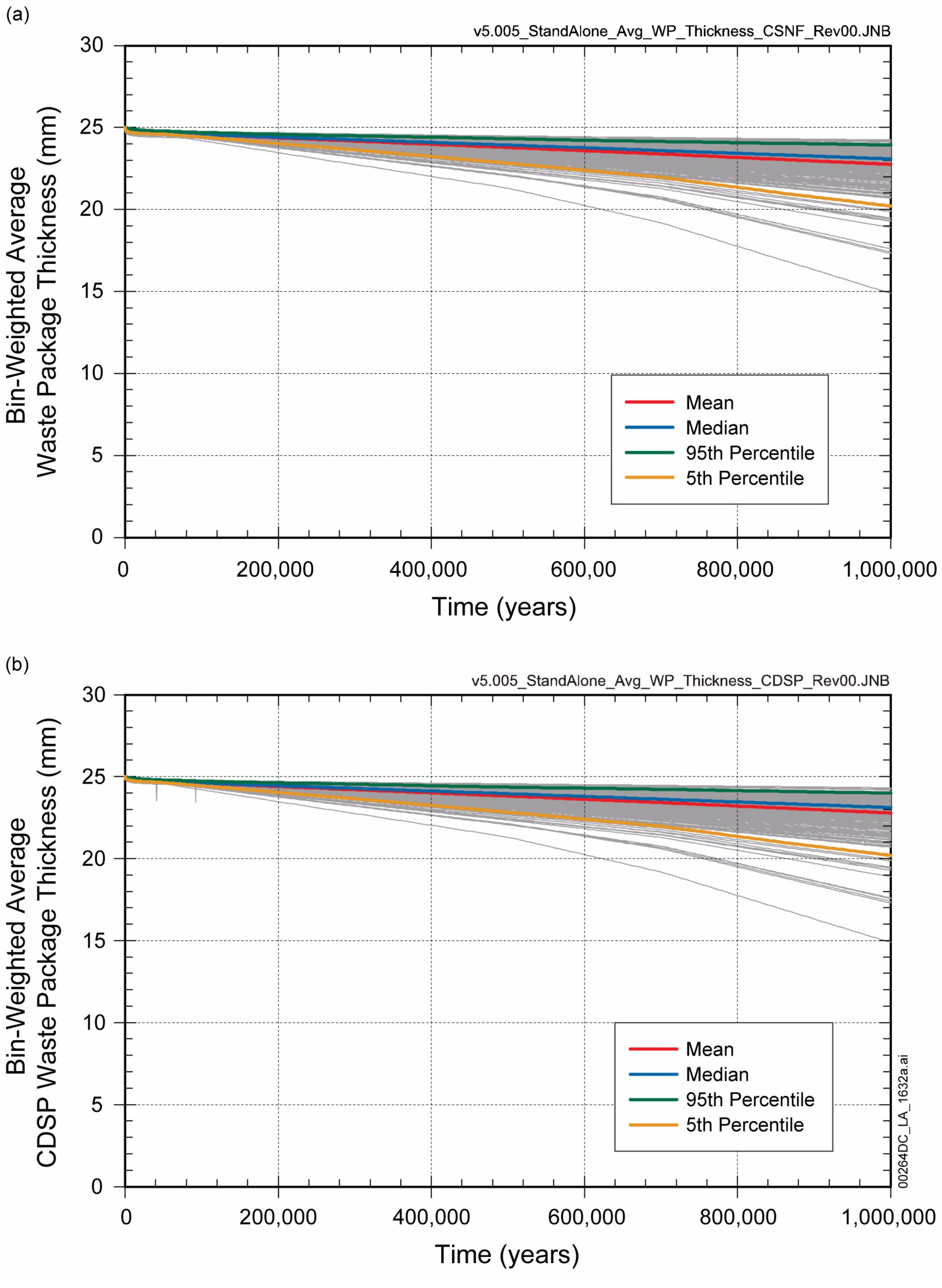

Figure 2.4-23. Spatially Averaged Waste Package Outer Barrier Thicknesses for 1 Million Years for (a) Commercial SNF Waste Packages and (b) Codisposal Waste Packages

NOTE: These plots shows epistemic uncertainty in average waste package thickness, where "average thickness" represents a triple average over (1) all patches on a individual waste package, (2) all waste packages in a percolation subregion or "bin", and (3) all percolation subregions.

Source: DTN: MO0803TSPAPSAR.000.

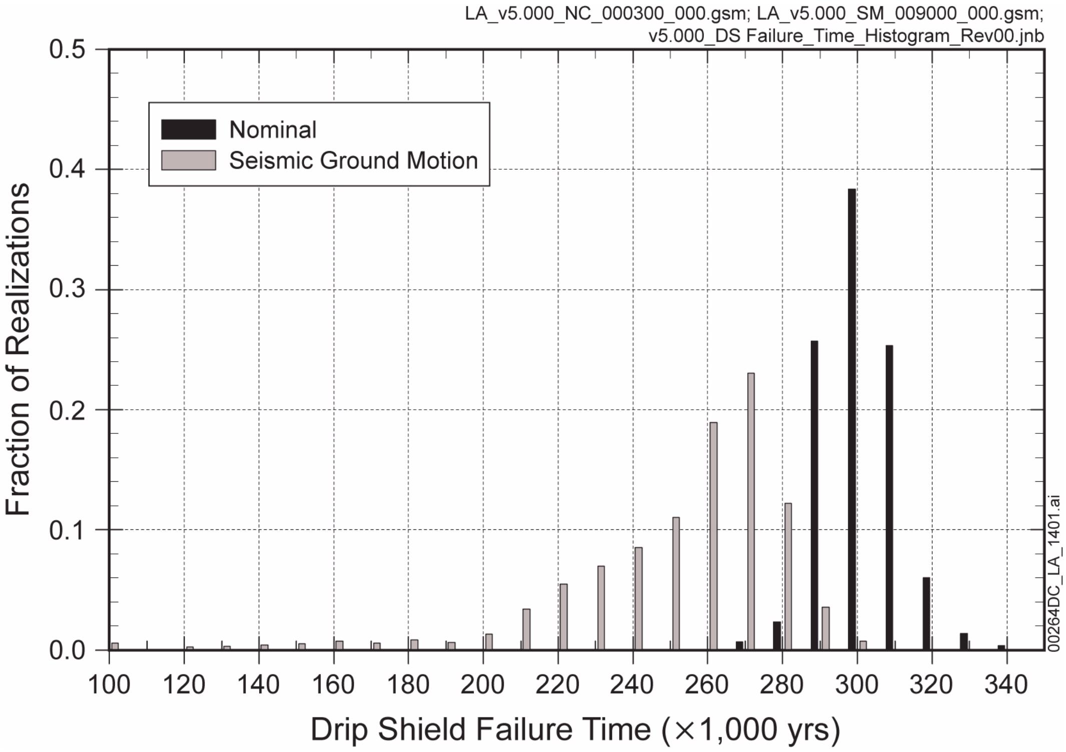

Figure 2.4-24. Histogram of Drip Shield Failure for the Nominal and Seismic Ground Motion Modeling Cases

Source: SNL 2008a, Figure 8.1-4[a].

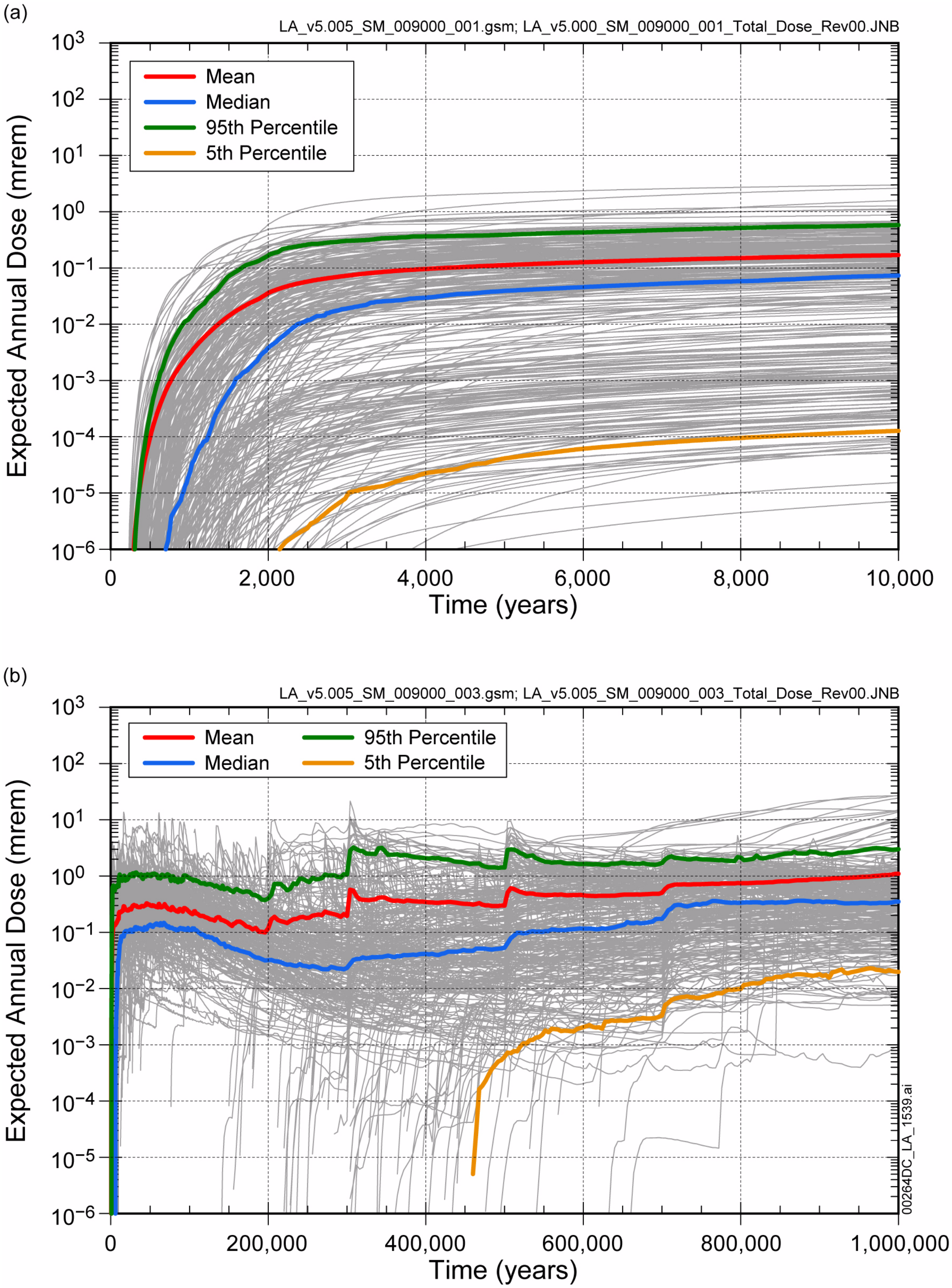

Figure 2.4-25. Distribution of Expected Annual Dose for the Seismic Ground Motion Modeling Case for (a) 10,000 Years and (b) 1 Million Years after Repository Closure

Source: SNL 2008a, Figure 8.2-11[a].

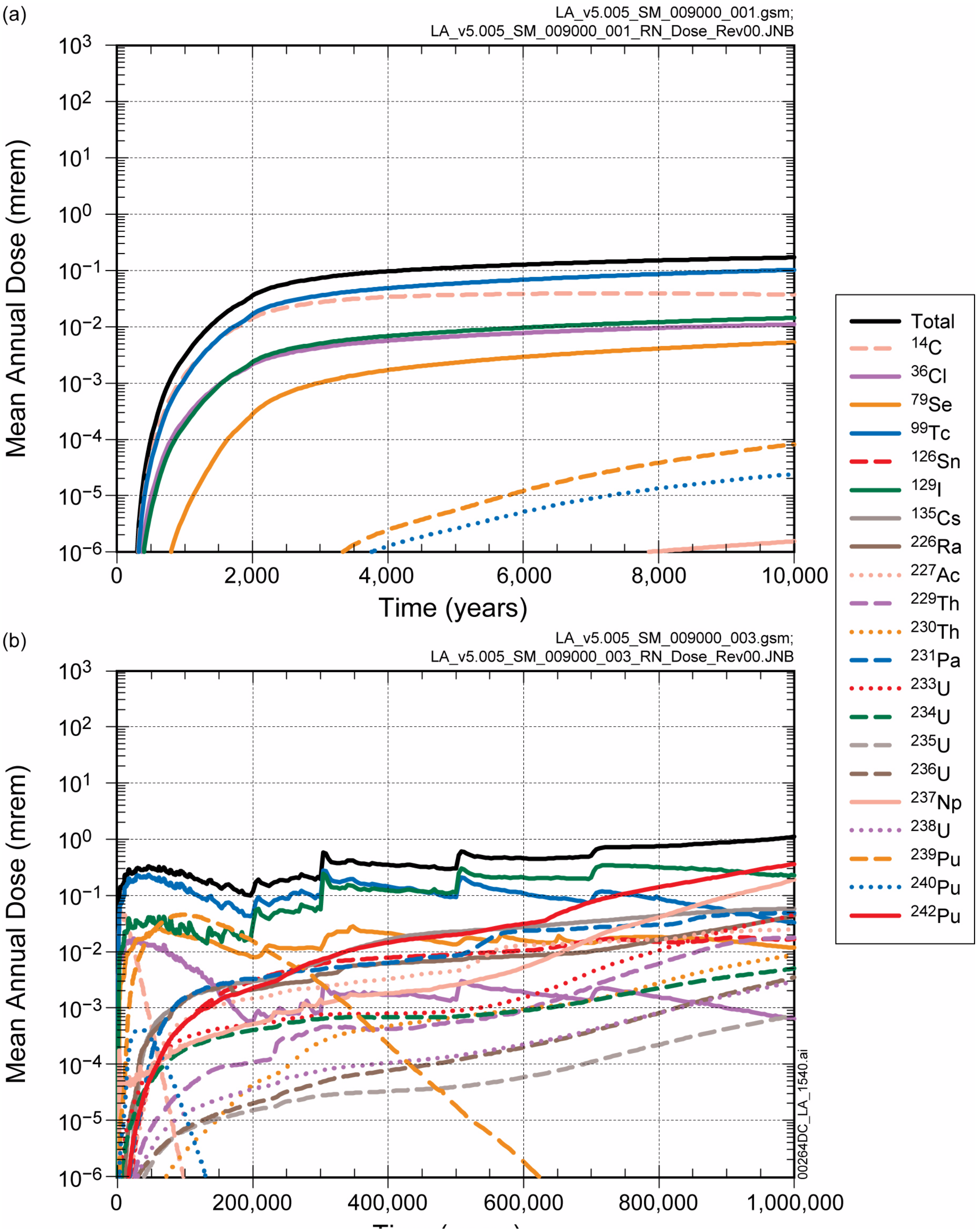

Figure 2.4-26. Contribution of Individual Radionuclides to Mean Annual Dose for the Seismic Ground Motion Modeling Case for (a) 10,000 Years and (b) 1 Million Years after Repository Closure

Source: SNL 2008a, Figure 8.2-12[a].

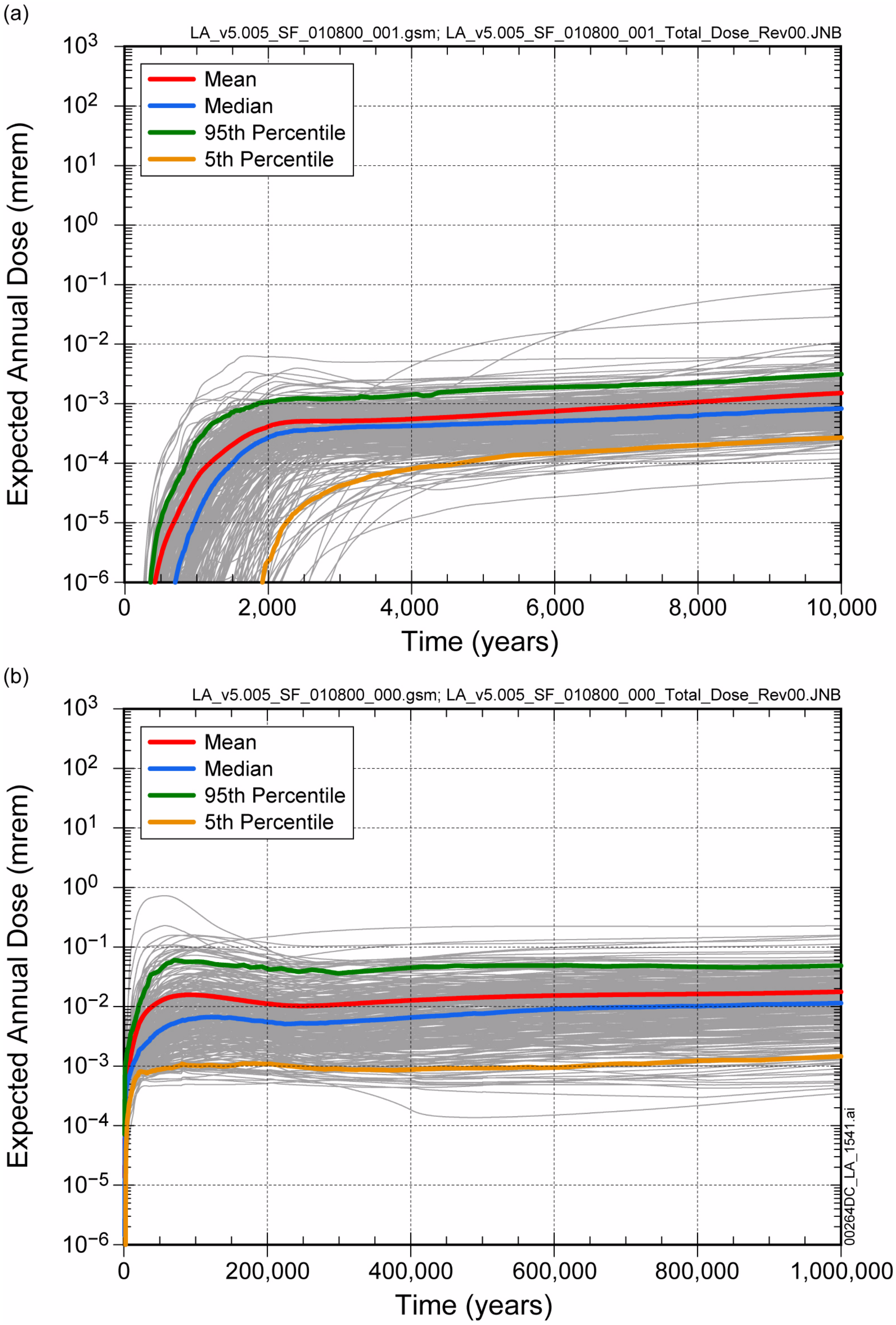

Figure 2.4-27. Distribution of Expected Annual Dose for the Seismic Fault Displacement Modeling Case for (a) 10,000 Years and (b) 1 Million Years after Repository Closure

Source: SNL 2008a, Figure 8.2-13[a].

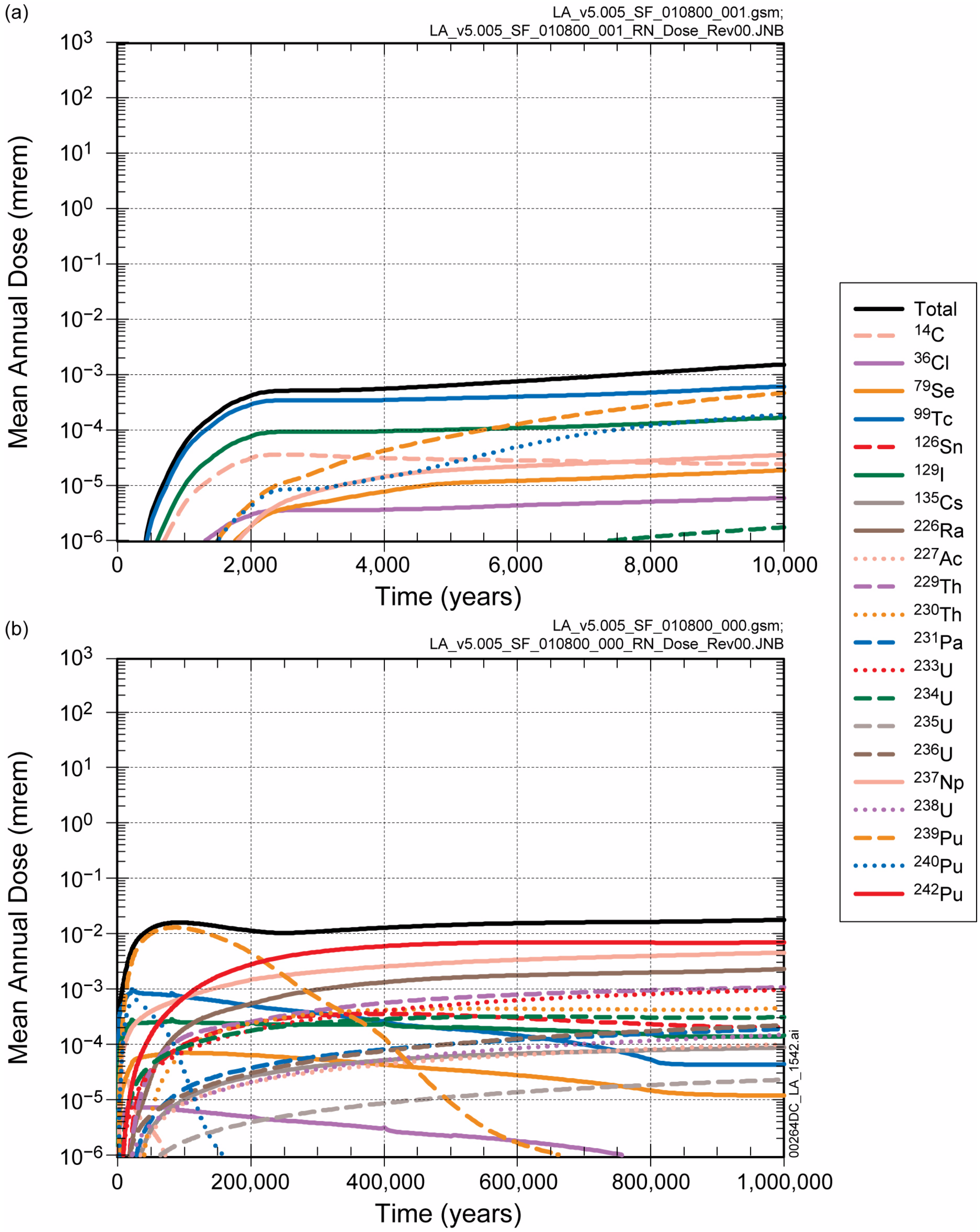

Figure 2.4-28. Contribution of Individual Radionuclides to Mean Annual Dose for the Seismic Fault Displacement Modeling Case for (a) 10,000 Years and (b) 1 Million Years after Repository Closure

Source: SNL 2008a, Figure 8.2-14[a].

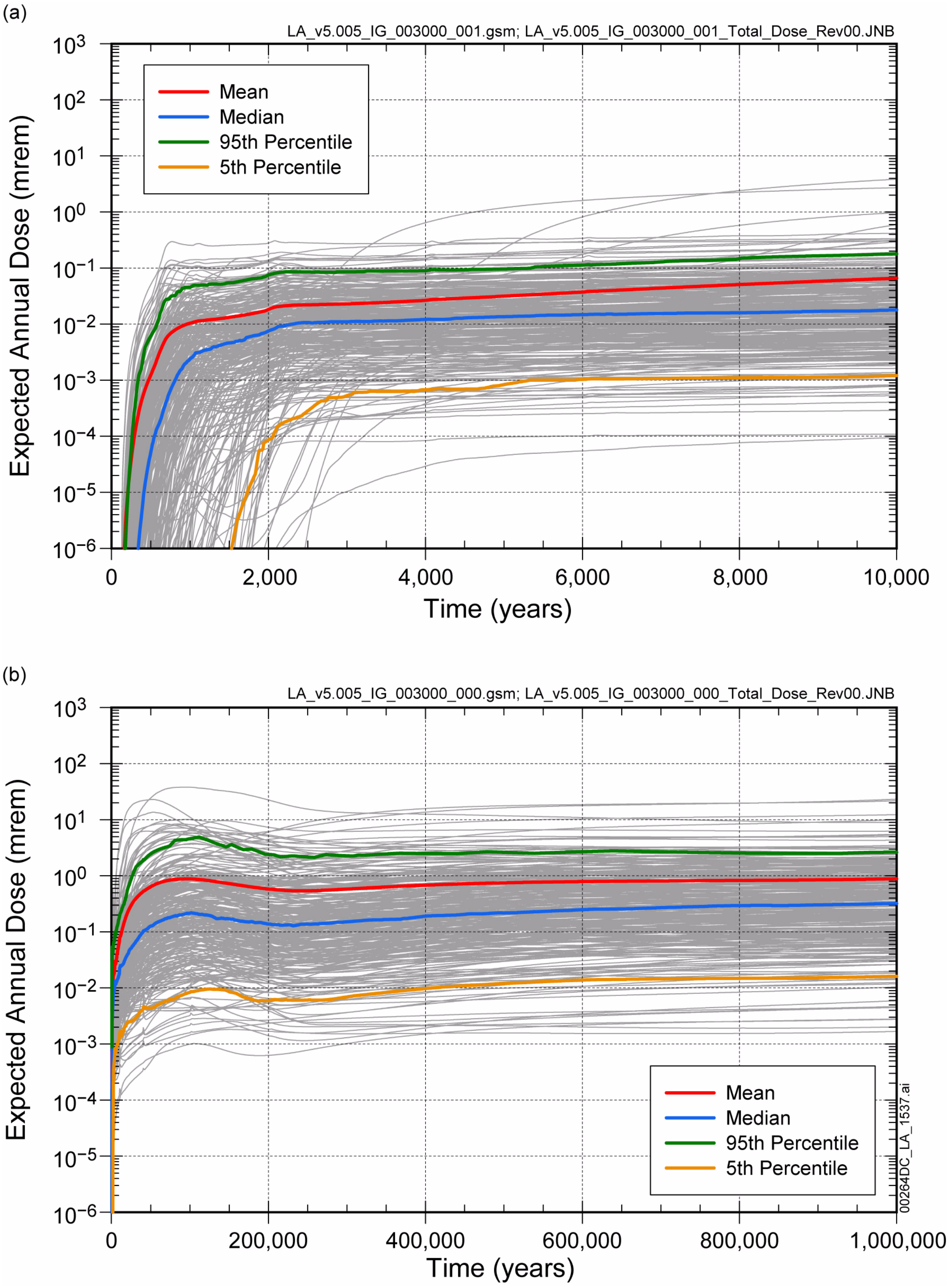

Figure 2.4-29. Distribution of Expected Annual Dose for the Igneous Intrusion Modeling Case for (a) 10,000 Years and (b) 1 Million Years after Repository Closure

Source: SNL 2008a, Figure 8.2-7[a].

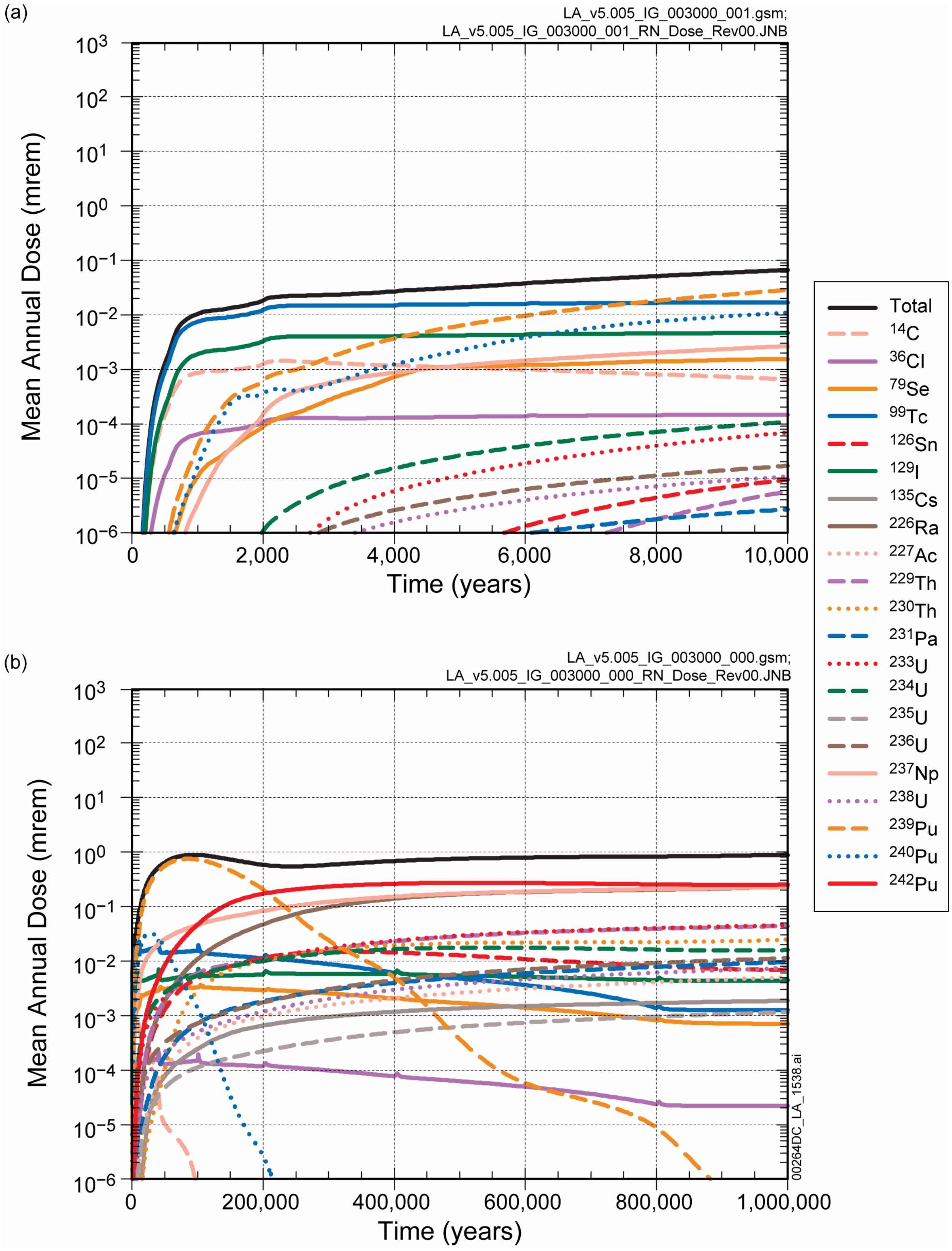

Figure 2.4-30. Contribution of Individual Radionuclides to Mean Annual Dose for the Igneous Intrusion Modeling Case for (a) 10,000 Years and (b) 1 Million Years after Repository Closure

Source: SNL 2008a, Figure 8.2-8[a].

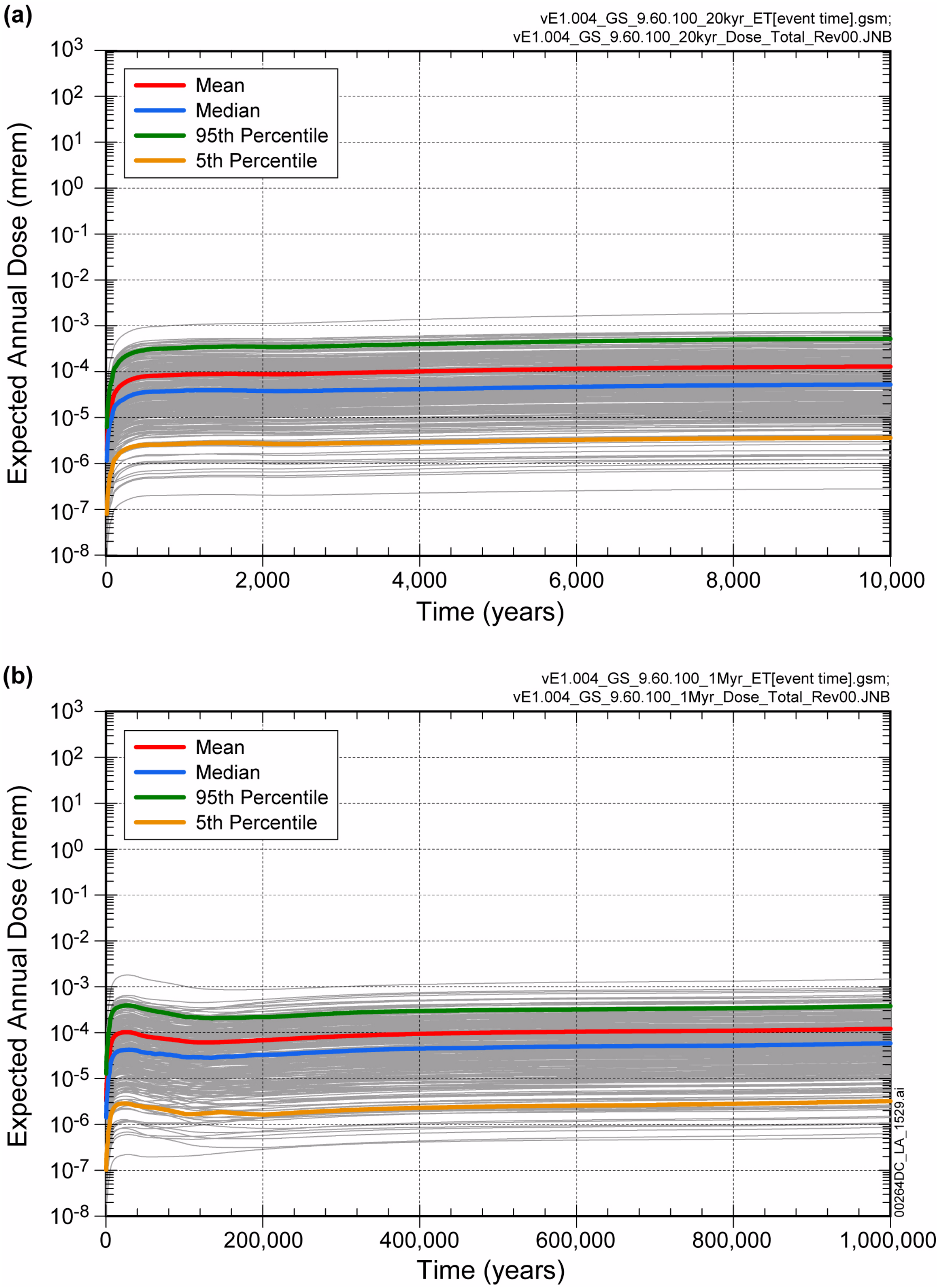

Figure 2.4-31. Distribution of Expected Annual Dose for the Volcanic Eruption Modeling Case for (a) 10,000 Years and (b) 1 Million Years after Repository Closure

Source: SNL 2008a, Figure 8.2-9.

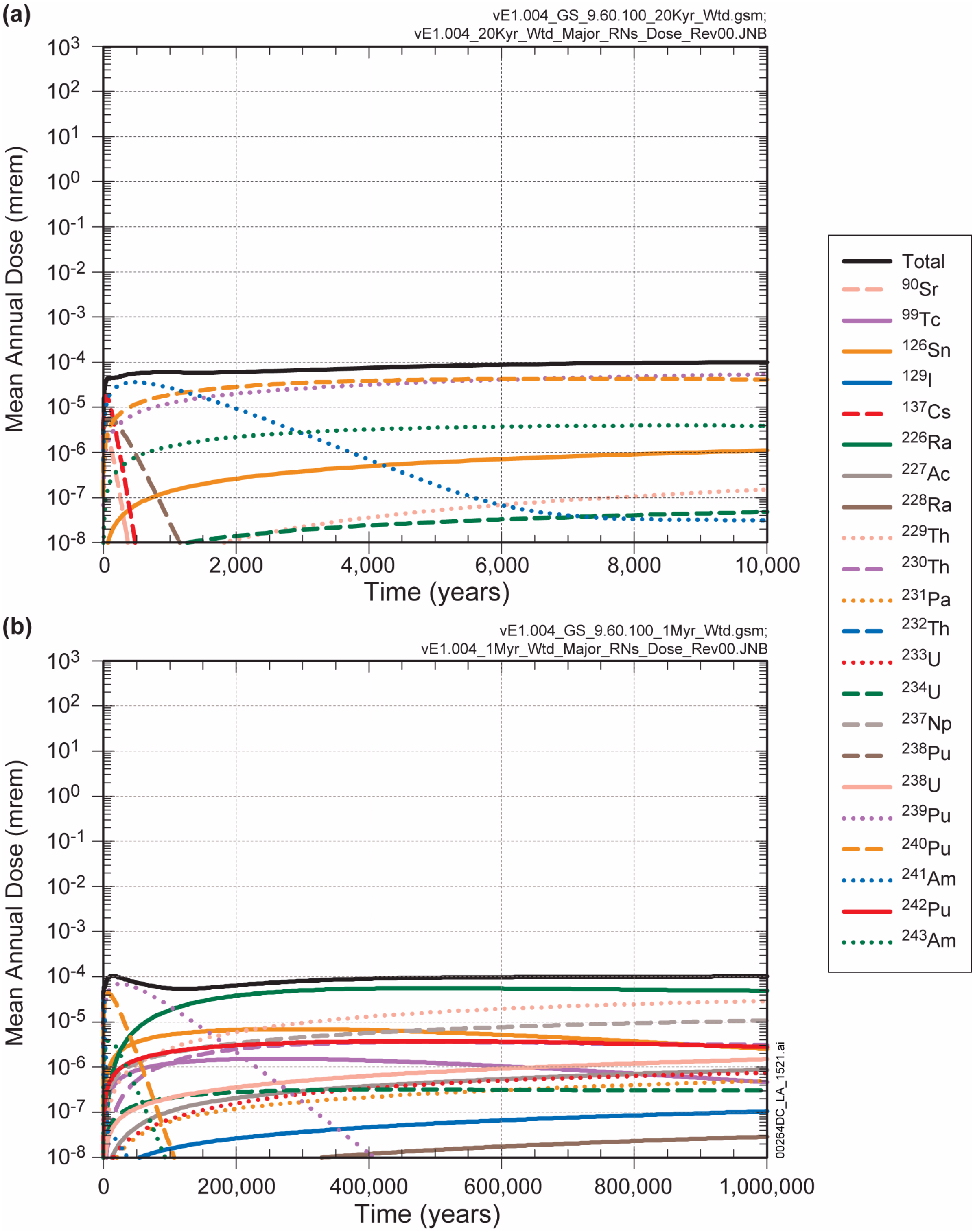

Figure 2.4-32. Contribution of Individual Radionuclides to Mean Annual Dose for the Volcanic Eruption Modeling Case for (a) 10,000 Years and (b) 1 Million Years after Repository Closure

Source: SNL 2008a, Figure 8.2-10.